Structure-based development of nonpeptidic fluorescent probes, PET tracers and homobivalent neuropeptide Y Y_1 receptor ligands with picomolar binding affinities

Dissertation

zur Erlangung des Doktorgrades der Naturwissenschaften (Dr. rer. nat.)
an der Fakultät für Chemie und Pharmazie
der Universität Regensburg

vorgelegt von
Christoph Müller
aus Straubing
2022

Die vorliegende Arbeit entstand in der Zeit von Juni 2017 bis November 2022 unter der Anleitung von Herrn PD Dr. Max Keller an der Fakultät für Chemie und Pharmazie der Universität Regensburg.

Das Promotionsgesuch wurde eingereicht im:	November 2022
Tag der mündlichen Prüfung:	19.12.2022
Vorsitzender des Prüfungsausschusses:	Prof. Dr. Werner Kunz
Erstgutachter:	PD Dr. Max Keller
Zweigutachter:	Prof. Dr. Pierre Koch
Drittprüfer:	Prof. Dr. Joachim Wegener

Acknowledgements

An dieser Stelle möchte ich mich bedanken bei:

Herrn Dr. Max Keller für die umfangreiche Betreuung der Arbeit in Form von wissenschaftlichen Ratschlägen zu Fragestellungen sowohl bezüglich Synthese als auch zellbiologischer Testung, für die Unterstützung bei der Vorbereitung des Manuskripts (Kapitel 2), sowie dem konstruktiven Durchsehen der Arbeit. Weiterhin bedanke ich mich für ein stets offenes Ohr, auch abseits des Laborgeschehens,

Herrn Prof. Dr. Armin Buschauer, der leider viel zu früh verstarb, für die ursprüngliche Bereitstellung des interessanten Themas,

Herrn Prof. Dr. Pierre Koch für wertvolle Ratschläge beim Verfassen des Manuskripts (Kapitel 2) und für die von ihm vermittelte Kollaboration mit Dr. Dieter Schollmeyer, dessen strukturelle Aufklärung der Verbindung (*R*)-**2.16** ausschlaggebend war für die eindeutige Stereodiskriminierung aller charakterisierten Endverbindungen in dieser Arbeit,

Herrn Prof. Dr. Günther Bernhardt, der durch sein ausgeprägtes Fachwissen besonders im Bezug auf zellbiologische Testung wertvolle Ratschläge vermitteln konnte,

Herrn Prof. Dr. Ago Rinken für die Ermöglichung und Betreuung meines Forschungsaufenthalts an der Universität Tartu in Estland, sowie der darauf aufbauenden, anschließenden wissenschaftlichen Zusammenarbeit,

dem Graduiertenkolleg 1910 „Medicinal chemistry of selective GPCR ligands“, gefördert durch die Deutsche Forschungsgemeinschaft (DFG), für die Finanzierung des Forschungsaufenthalts,

Herrn Prof. Dr. Olaf Prante und Frau Dr. Simone Maschauer von der Abteilung für Nuklearmedizin an der Friedrich-Alexander-Universität Erlangen-Nürnberg für die

Durchführung von Radiosynthesen der Verbindungen [^{18}F]**3.11**, [^{18}F]**3.12** und [^{68}Ga]**3.25**, sowie für die *in vivo*- und *in vitro*-Charakterisierung dieser PET Liganden,

Herrn Prof. Dr. Dirk Hellwig von der Abteilung für Nuklearmedizin am Universitätsklinikum Regensburg für die Bereitstellung der benötigten Geräte und Räumlichkeiten für die Synthese von Verbindung [^{68}Ga]**3.25**, sowie Frau Dr. Jutta Moosbauer für die Durchführung der Radiosynthesen,

meinen Laborkollegen Herrn Dr. Jonas Buschmann und Herrn Jakob Gleixner für die produktive Arbeitsatmosphäre, Letzterem im Besonderen für die Unterstützung nicht nur bei der Anreicherung von enantiomerenreinem (*R*)-**2.16**, sondern auch bei einigen Syntheseschritten,

Frau Maria Beer-Krön, Frau Susanne Bollwein und Frau Brigitte Wenzl für die exzellente Durchführung von Radioligand-Kompetitionsbindungsassays, Bindungsassays am Durchflusszytometer und des Calcein-AM Assays, sowie für die Unterstützung bei der Zellkultur, und Frau Lydia Schneider für die exzellente Durchführung des Fura-2 Calcium Assays,

Herrn Franz Wiesenmayer für die Injektion von MCF-7-Y_1-Zellsuspensionen in Nacktmäuse sowie das Vermessen der Tumore,

Herrn Fritz Kastner, Herrn Josef Kiermaier und Herrn Wolfgang Söllner für die fachlichen Ratschläge bezüglich der Auswertung von NMR- und Massenspektren, sowie für die stets zügige und einwandfreie Bearbeitung der Messaufträge,

Herrn Peter Richthammer für die Unterstützung bei technischen Angelegenheiten sowie für erheiternde Gespräche und Frau Silvia Heinrich für die zuverlässige Unterstützung bei organisatorischen und bürokratischen Angelegenheiten,

allen Mitgliedern des Arbeitskreises, im Besonderen Frau Lisa Schindler, für das angenehme Arbeitsklima und die stets selbstverständliche Hilfsbereitschaft,

sowie meiner Mutter Edeltraud, meiner Schwester Simone und meinem Vater Siegfried, solange er bis zu seinem frühen Tod noch dazu beitragen konnte, für unbedingten familiären Rückhalt.

Publications

(peer-reviewed articles published prior to the submission of the thesis)

Gruber, C. G.; Pegoli, A.; Müller, C.; Grätz, L.; She, X.; Keller, M. Differently fluorescence-labeled dibenzodiazepinone-type muscarinic acetylcholine receptor ligands with high M_2R affinity. *RSC Med. Chem.* **2020**, 11, 823-832, doi: 10.1039/D0MD00137F.

Grätz, L.; Tropmann, K.; Bresinsky, M.; Müller, C.; Bernhardt, G.; Pockes, S. NanoBRET binding assay for histamine H_2 receptor ligands using live recombinant HEK293T cells. *Sci. Rep.* **2020**, 10, doi: 10.1038/s41598-020-70332-3.

Müller, C.; Gleixner, J.; Tahk, M.-J.; Kopanchuk, S.; Laasfeld, T.; Weinhart, M.; Schollmeyer, D.; Betschart, M. U.; Lüdeke, S.; Koch, P.; Rinken, A.; Keller, M. Structure-based design of high-affinity fluorescent probes for the neuropeptide Y Y_1 receptor. *J. Med. Chem.* **2022**, 65, 5, 4832-4853, doi: 10.1021/acs.jmedchem.1c02033.

Tahk, M.-J.; Torp, J.; Ali, A. S. M.; Fishman, D.; Parts, L.; Grätz, L.; Müller, C.; Keller, M.; Veiksina, S.; Laasfeld, T.; Rinken, A. Live-cell microscopy or fluorescence anisotropy with budded baculoviruses – which way to go with measuring ligand binding M_4 muscarinic receptors? *Open Biol.* **2022**, 12, doi: 10.1098/rsob.220019.

Grätz, L.; Müller, C.; Pegoli, A.; Schindler, L.; Bernhardt, G.; Littmann, T. Insertion of Nanoluc into the extracellular loops as a complementary method to establish BRET-based binding assays for GPCRs. *ACS Pharmacol. Transl. Sci.* **2022**, 5, 1142-1155, doi: 10.1021/acsptsci.2c00162.

Poster presentations

Müller, C.; Keller, M.; Littmann, T.; Bernhardt, G.; Buschauer, A. UR-MK299-Derived red-emitting fluorescent NPY Y_1 receptor ligands with picomolar binding constants. *Frontiers in Medicinal Chemistry*, **2018**, Jena, Germany.

Müller, C.; Buschmann, J.; Littmann, T.; Wifling, A.; Buschauer, A.; Bernhardt, G.; Keller, M. Red-emitting fluorescent neuropeptide Y Y_1 antagonists with picomolar binding constants: Design, synthesis and characterization. *9th International Summerschool "Medicinal Chemistry"* **2018**, Regensburg, Germany.

Professional training

Since 2018 member of the research training group (Graduiertenkolleg 1910) “Medicinal chemistry of selective GPCR ligands“.

Table of contents

Chapter 1

General introduction

1.1 The neuropeptide Y peptide family

1.1.1 General information

With over 100 identified and characterized variants, neuropeptides represent the most diverse group among endogenous neurochemically active molecules compared to the group of "gasotransmitters" (NO, CO and H_2S) and the group of small molecule (classical) neurotransmitters, which include biogenic amines (dopamine, adrenaline, noradrenaline, serotonin, acetylcholine, histamine), amino acids (glycine, glutamate, GABA), endocannabinoids (anandamide, 2-arachidonoylglycerol), and ATP.[1-3] Neuropeptides regulate a myriad of physiological processes by exerting neurotransmitter-like interneuronal signaling, controlling the synaptic activity of neurotransmitters or effecting the endocrine system as peptide hormones.[1, 4-6] Thus, they are – in a state of regulatory imbalance – considered key role players in the pathogenesis of many diseases.

Based on structural homologies, neuropeptides can be subgrouped into families.[7] Neuropeptide Y (NPY) belongs to the neuropeptide Y family of peptide hormones together with peptide YY (PYY) and the pancreatic polypeptide (PP), which are each composed of 36 amino acids, featuring a characteristic amidated C-terminal tyrosine and significant sequential homology in humans (Figure 1.1).[8, 9] NPY in particular also shows remarkable homology between many species among not only mammals, but vertebrates in general (at least 61% among investigated species), which is why it is considered a "phylogenetically ancient" neuropeptide.[10, 11]

	1	10	20	30	36
NPY	H_2N	YPSKPDNPGE	DAPAEDMARY	YSALRHYINL	ITRQRY $CONH_2$
PYY	H_2N	YPIKPEAPRE	DASPEELNRY	YASLRHYLNL	VTRQRY $CONH_2$
PP	H_2N	APLEPVYPGD	NATPEQMAQY	AADLRRYINM	LTRPRY $CONH_2$

Figure 1.1. Primary sequences of NPY, PYY and PP in humans, displaying homologies of 64% (PYY) and 50% (PP) compared to NPY.

Whereas the gut hormones PYY and PP are mainly produced in and secreted by gastrointestinal epithelial cells and PP cells of the pancreas, respectively,[12] and show – in the case of PYY – only moderate expression rates in few brain regions,[13] NPY is abundantly present in the mammalian CNS and PNS.[14, 15] Centrally, high NPY expression levels were found in hypothalamic nuclei, hippocampus, neocortex, striatum, amygdala and thalamus.[11, 13, 16, 17] In the periphery, NPY is expressed in postganglionic, sympathetic nerve fibers innervating organs and surrounding blood vessels, in chromaffin cells of the adrenal gland and in platelets.[14, 18, 19]

1.1.2 The NPY receptors

1.1.2.1 Signal transduction and binding profile of NPY, PYY and PP

In humans, NPY, PYY and PP, as endogenous agonists, address four class-A rhodopsin-like GPCRs, Y_1R, Y_2R, Y_4R and Y_5R, which convey a multitude of physiological functions depending on their expression site in the body.[20] Throughout all subtypes, receptor activation by agonist binding predominantly induces the stimulation of pertussis toxin-sensitive $G_{i/o}$-type G proteins and subsequently a decrease in intracellular cAMP levels by inhibition of adenylyl cyclase activity.[21-23] Depending on cell type and receptor subtype, G protein activation may also lead to intracellular mobilization of Ca^{2+} independent,[24] or dependent on G_q-mediated synthesis of inositol trisphosphate (IP_3),[25-27] modulation of Ca^{2+} channels,[28, 29] and activation of G protein-coupled inwardly rectifying K^+ channels (GIRKs).[30, 31] A fifth NPY receptor, the y_6R, has been identified as a functional GPCR in mice and rabbits, however with so far no or unknown function in primates.[23, 32-34]

Generally, NPY and PYY bind to the NPY receptors with comparable affinities, although some receptor binding studies suggest a slight preference of NPY for the Y_1R and lowest affinity for the Y_4R, and a preference of PYY for the Y_2R (Table 1.1). PP on the other hand shows clear selectivity for the Y_4R (Table 1.1). In addition to the three 36 residue endogenous peptides, certain metabolites, most notably the N-terminally truncated versions of NPY and PYY, NPY(3-36) and PYY(3-36), also display significant pharmacological activity with an altered selectivity profile. The N-terminal truncation of NPY and PYY is catalyzed by the ubiquitously present membrane-bound dipeptidylpeptidase IV (DPP4), resulting in decreased Y_1R affinity, but retained or increased Y_2R binding (Table 1.1).[35-38]

Table 1.1. NPY receptor affinity and selectivity profiles of endogenous agonists; pK_i values suggesting selectivity for a particular receptor subtype are highlighted.

endogenous agonist	pK_i[a]			
	hY_1R	hY_2R	hY_4R	hY_5R
NPY	10.1[b] 9.3[c]	9.3[b] 8.9[c]	8.7[d] 8.2[c]	9.1[e] 8.9[b]
PYY	9.8[b] 8.9[f]	9.5[b] **10.9**[f]	9.1[d] 9.0[f]	9.0[g] 9.2[f]
PP	6.3[h] 7.3[f]	<6[b,f,h]	**9.3**[h] **11.1**[f]	7.8[h] 8.1[f]
PYY(3-36)	7.3[b]	**9.2**[b]	7.9[d]	8.1[g]
NPY(3-36)[f]	7.3	**9.7**	6.6	7.9

[a]Data, previously reported as K_i, were converted to pK_i values. [b]Gerald *et al.*;[39] [c]Parker *et al.*;[40] [d]Bard *et al.*;[41] [e]Hu *et al.*;[42] [f]McCrea *et al.*;[43] [g]Borowski *et al.*;[44] [h]Berlicki *et al.*[45]

1.1.2.2 Physiological effects mediated by NPY receptors and therapeutic potential as drug targets

Whereas the Y_1R, Y_2R and Y_5R are expressed in many areas of the brain and in peripheral tissues, central Y_4R expression is limited to few brain regions as hypothalamic nuclei, the postrema region and the nucleus solitary tract, but is high in peripheral tissues as in the gastrointestinal tract and the pancreas.[20, 46-53] Hence, the importance of the Y_4R in centrally regulated physiological processes is still subject to investigation.[54-56]

NPY receptors play an imperative role in regulation of food intake and energy homeostasis, originating from the hypothalamic “feeding center”, where food intake is strongly promoted by activation of Y_1Rs and Y_5Rs. Thus, they are considered important mediators in the pathogenesis of diseases like obesity and diabetes, increasingly prevalent in “westernized” societies and thus rendering Y_1R and Y_5R antagonists potential drugs to reduce food intake.[57] Recent studies however revealed that NPY only exerts a complementary role in a complex neuroendocrine circuit controlling appetite and metabolism, involving centrally released peptide hormones like the stress-related hormone corticotropin, but also peripherally released metabolism-related peptide hormones like leptin, insulin, ghrelin and PYY(3-36).[58-61]

As part of the HPA-axis (hypothalamic-pituitary-adrenal axis), the central control system for stress, NPY regulates stress signaling by increasing the activity of CRH (corticotropin-releasing hormone), a peptide hormone initially released from the hypothalamic paraventricular nucleus as a biological stress response, and eventually leading to increased glucocorticoid plasma levels.[62-64] Interestingly, these elevated glucocorticoid levels are in turn capable of upregulating hypothalamic NPY expression, thus potentiating the stimulatory effect of NPY on the HPA-axis.[65] On the other hand, NPY also attenuates the anxiogenic effect of CRH in the limbic system, presumably independent on HPA-axis activity, by activation of Y_1Rs and Y_5Rs, whereas Y_2R activation leads to anxiogenesis.[66-71] As the orexigenic effects of NPY are also originating from the hypothalamus, participation of NPY in developing obesity as a consequence of stress-induced “emotional eating” was suggested.[72-74] In combat veterans suffering from PTSD, baseline NPY levels both in plasma and cerebrospinal fluid were consistently low compared to unaffected control groups, indicating that high NPY levels correlate with stress resilience.[75-77]

Whereas NPY through its anxiolytic effects generally functions as a "brake" against stressors in the CNS, it is released in the PNS from postganglionic sympathetic neurons projecting towards vascular smooth muscle cells in various tissues, including the myocardium. Following a central stress response, postsynaptic Y_1Rs induce vasoconstriction through activation of postsynaptic Y_1Rs and successive release of noradrenaline and ATP, promoting the

sympathetic “fight-or-flight” response.[78-80] In this context, specific single nucleotid polymorphisms (SNPs) in the NPY gene, causing a slight increase of NPY production in peripheral neurons, were recently associated with early onset arteriosclerosis, which could be reduced in mice models by administration of Y_1R antagonists.[81]

NPY also stimulates neurogenesis from neural precursors in the subventricular zone, the olfactory epithelium and in hippocampal areas, predominantly *via* the Y_1R, and additionally upregulates levels of brain-derived neurotrophic factor (BDNF), a protein essential for survival and development of newly formed neurons.[82, 83] Hence, NPY can induce neuron proliferation and is involved in the development of spatial memory, but can also provide trophic support for neurons in neurodegenerative diseases as Alzheimer’s and Huntington’s, where BDNF is pathologically downregulated.[84-86]

The anxiolytic properties of NPY may be used to control comorbidities often associated with chronic stress, PTSD, and neurodegenerative diseases, which are anxiety, fear, and depression. Therefore, Y_1R agonists and Y_2R antagonists have been suggested as modulators for psychological disorders.[87, 88]

In some hippocampal regions, Y_2R expression was found to be enriched presynaptically in glutamatergic and GABAergic terminals and the activation of the Y_2R inhibited the Ca^{2+}-dependent synaptic release of glutamate, decreasing the excitatory firing rate of these neurons.[89-91] Therefore, Y_2R selective agonists could support the suppression of epileptic seizures.[92]

Other pathological CNS-related conditions where NPY is involved are chronic pain,[93] migraine,[94] bone diseases,[95] and addictions,[96] all associated to at least two NPY receptors (comprising Y_1R, Y_2R and/or Y_5R) and linked to different brain areas, emphasizing the quantity of physiological processes where the NPY system is involved.

1.1.2.3 Selective NPY Y_1 receptor ligands

The use of receptor-specific agonists and antagonists in *in vitro* and *in vivo* models constitutes a common approach to identify the physiological functions of individual receptors.

A frequently pursued strategy to gain access to agonists selective towards not only the Y_1R, but each of the respective subtypes was the modification of residues and truncation of the endogenous peptides NPY, PP and PYY. As it proved to be crucial for receptor binding throughout all NPY receptor subtypes, the amidated C-terminal segment -Arg^{35}-Tyr^{36}-NH_2 was conserved throughout.[97, 98] The porcine NPY (pNPY) analogue [Phe^7,Pro^{34}]pPNY[99] was presented as one of the first NPY analogues with excellent Y_1R selectivity over the Y_2R and the Y_5R, while maintaining subnanomolar Y_1R affinity (Table 1.2) (note: porcine NPY contains residue Leu^{17} instead of Met^{17} in hNPY).[99] A modified C-terminal fragment of NPY,

[Pro^{30},Nle^{31},Bpa^{32},Leu^{34}]NPY(28–36),[100] displaying slight preference for the Y_1R, was presented as a Y_1R agonist with significantly decreased molecular weight, however at the cost of a drastic decrease in affinity (Table 1.2). So far, nonpeptidic Y_1R-selective agonists, considered advantageous over peptidic ligands in terms of molecular weight and proteolytic stability, have not been reported.

Concerning antagonists, a number of peptidic and nonpeptidic Y_1R selective ligands have been developed: The heterodimeric peptidic Y_1R antagonist 1229U91[101] (Figure 1.2, panel A), derived from the C-terminal region of NPY, presents an interesting pharmacological profile, as it shows high Y_1R binding affinity and subtype selectivity, but also functions as a weak partial agonist at the Y_4R (pEC_{50} = 7.43[102]) (Table 1.2). As the Y_1R represents an attractive target due to its regulatory role in controlling food intake, pharmaceutical companies were in search for nonpeptidic small molecule (MW < 600 Da) antagonists featuring a suitable bioavailability profile for oral application. As such, dihydropyridine BMS-193885[103] and pyrazolopyrimidine CP-671906[104] were developed by Bristol-Myers-Squib (BMS) and Pfizer, respectively, representing Y_1R antagonists with binding affinities in the one-digit nanomolar range and no significant binding to the other subtypes (Table 1.2). However, even though the compounds were able to penetrate across the blood-brain barrier, none of the antagonists were considered as a candidate for clinical studies, mainly due to insufficient gastrointestinal absorption and therefore, bioavailability.[57] A ^{18}F-labeled analogue of the 2,4-diaminopyridine Y1-973[105] (Figure 1.2, panel B) with a promising selectivity profile was developed by Merck (previously Banyu Pharmaceuticals, Japan) and has been successfully applied to visualize Y_1R expression in rhesus monkey brain in PET experiments upon intravenous administration (Table 1.2).[57, 106]

By mimicking the C-terminal dipeptide of NPY, -Arg^{35}-Tyr^{36}-NH_2, and inverting the stereoconfiguration at the arginine, BIBP3226 (Figure 1.2, panel C) was developed as the first argininamide-type Y_1R antagonist exhibiting one-digit nanomolar binding affinity and excellent subtype selectivity (Table 1.2).[107] The introduction of a short N^{ω}-carbamoyl substituent, an approach initially pursued to decrease the basicity of the guanidino group potentially resulting in improved bioavailability of argininamide-type compounds,[108] led to compounds with unprecedented subnanomolar binding affinity, e.g. UR-MK299 (Table 1.2).[109]

The therapeutical potential of N^{ω}-carbamoylated argininamide-type Y_1R ligands such as UR-MK299 to combat Y_1R-related disorders originating from the CNS remains unclear due to the lack of data on blood-brain permeability and bioavailability. However, due to the resulting high Y_1R affinity, subtype selectivity and high stability, N^{ω}-carbamoylation enabled the development of several tool compounds for the Y_1R, e.g. radioligands, fluorescent ligands and PET-tracers.[110-115]

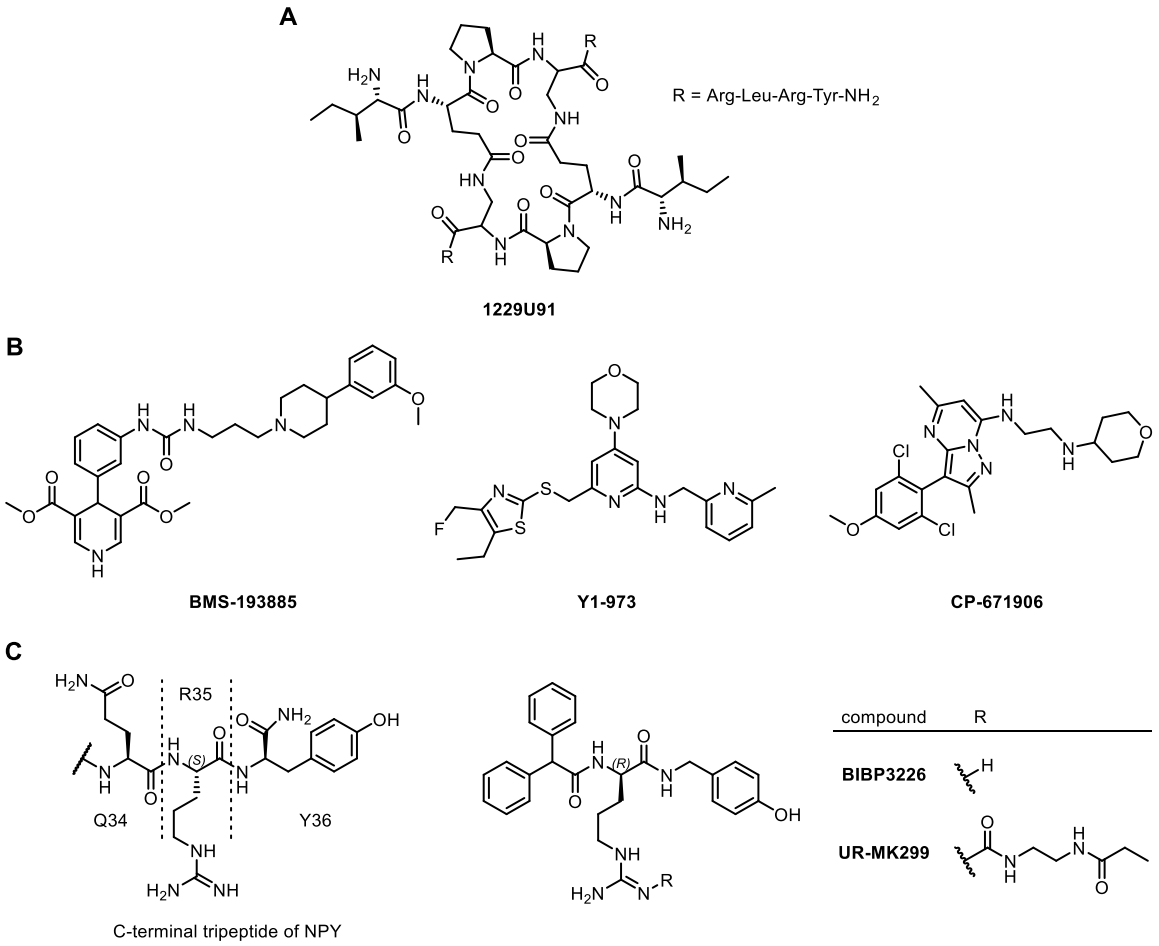

Figure 1.2. (A) Structure of the peptidic Y_1R antagonist 1229U91. (B) Structures of nonpeptidic Y_1R antagonists: dihydropyridine BMS-193885, 2,4-diaminopyridine Y1-973 and triazaindene CP-671906. (C) Structures of the argininamide-type Y_1R antagonists BIBP3226 and UR-MK299, and their structural analogy to the C-terminus of NPY.

Table 1.2. NPY receptor binding data of described Y_1R-selective agonists and antagonists.

agonist	pK_i (pIC_{50})[a]			
	hY_1R	hY_2R	hY_4R	hY_5R
[Phe^7,Pro^{34}]pNPY[b]	11.05	7.49	nd[c]	7.47
[Pro^{30},Nle^{31},Bpa^{32},Leu^{34}]NPY(28-36)[d,e]	(7.53)	(<6)	(<6)	(<6)
antagonist				
1229U91	8.99[f]	6.15[g]	7.05[f]	<6[h]
BMS193885	8.48[i]	<6[j]	<6[j]	<6[j]
Y1-973[k]	(9.89)	(<5)	(<5)	(<5)
CP-671906[l]	8.82	<5	nd[c]	<5
BIBP3226	8.80[m]	<5[n]	<5.3[o]	<6[p]
UR-MK299[q]	10.27	<5.5	<5	<5

[a]Data, previously reported as K_i and IC_{50}, were converted to pK_i and pIC_{50} values, respectively. [b]Söll *et al.*;[99] [c]not determined. [d]Nle: norleucine ((2*S*)-2-aminohexanoic acid); Bpa: (*S*)-4-benzoyl-phenylalanine. [e]Zwanziger *et al.*;[100] [f]Richardson *et al.*;[102] [g]Kanatani *et al.*;[116] [h]Balasubramaniam *et al.*;[117] [i]Poindexter *et al.*;[103] [j]Antal-Zimanyi *et al.*;[118] [k]Hostetler *et al.*;[106] [l]Griffith *et al.*; [104] [m]Keller *et al.*;[112] [n]Rudolf *et al.*;[107] [o]Keller *et al.*;[119] [p]Hu *et al.*;[42] [q]Keller *et al.*[109]

1.1.2.4 Structural insights on NPY Y_1 receptor-ligand binding interactions

Elucidation of Y_1R structures by X-ray crystallography was achieved in collaborative research projects led by the working group of Prof. Beili Wu (Yang *et al*., 2018)[120] in complex with the argininamide-type Y_1R antagonist UR-MK299 (PDB ID: 5ZBQ, Figure 1.3, bottom right) and the 1,4-dihydropyridine-type Y_1R antagonist BMS-193885 (PDB ID: 5ZBH, data not shown), respectively. The crystal structure of the Y_2R (Tang *et al*., 2021)[121] was resolved in complex with the Y_2R antagonist JNJ-31020028 (PDB ID: 7DDZ). Very recently, Tang *et al*. provided cryo-EM structures of the Y_1R, the Y_2R and the Y_4R in complex with the respective endogenous ligand, i.e. NPY for the Y_1R (Figure 1.3, top left, G_{i1} protein not shown, PDB ID: 7X9A) and the Y_2R (PDB ID: 7X9B) or PP for the Y_4R (PDB ID: 7X9C), and the coupled trimeric G_{i1} protein.[122] This enables the direct comparison of the Y_1R binding modes of the endogenous agonist NPY and the argininamide-type antagonist UR-MK299 (Figure 1.3).

The C-terminal tetrapeptide of the hairpin-like folded NPY, -Arg^{33}-Gln^{34}-Arg^{35}-Tyr^{36}-NH_2, occupies the orthosteric binding pocket, which is formed by residues from all transmembrane helices, except for helix I (Figure 1.3, top left). Amidated C-terminal Tyr^{36}, which was identified pivotal for ligand binding throughout all NPY receptor subtypes,[97] is stabilized by interactions with residues from helices II, III, V and VII: The terminal amido group makes polar contacts to $T97^{2.61}$, $Q120^{3.32}$ and $H306^{7.39}$, which are complemented by an additional polar contact of the phenolic hydroxyl group to $Q219^{5.46}$ (Figure 1.3, top right) (superscripts on receptor residues represent Ballesteros–Weinstein nomenclature[123]). Arg^{35} is oriented towards helices V and VI and associates to residues $N283^{6.55}$, $D287^{6.59}$ and $T212^{5.39}$ *via* its highly polar guanidino group. Furthermore, the carbonyl group of Arg^{35} contributes a polar contact to $N283^{6.55}$. The amido group in Gln^{34} interacts with $T97^{2.61}$ and Arg^{33} is stabilized by a polar contact to $N283^{6.55}$, which is supported by a π–cation-π complex formed between the charged guanidinium group and the aromatic side chains of $F302^{7.35}$ and $F286^{6.58}$. A characteristic feature of NPY binding to the Y_1R compared to the Y_2R is the strong involvement of the N-terminal tyrosine, which is bound to a cavity in the extracellular region formed by residues of helices V and VI as well as extracellular loop 2 (ECL2). These stabilizing interactions are not as pronounced in the Y_2R-NPY complex and provide an explanation for the decreased Y_1R binding affinity observed for N-terminally truncated peptides, e.g. NPY(3-36), while the Y_2R affinity remains largely unaffected (Table 1.1).[122] The interaction of protonated N-terminal Tyr^1 of NPY with $D205^{5.32}$ is demonstrated in Figure 1.3 (top right).

In the case of the Y_1R-UR-MK299 complex (Figure 1.3, bottom right), in particular the N^{ω}-carbamoylated arginine side chain displays a strikingly similar orientation in the binding pocket compared to amino acid Arg^{35} of NPY in the Y_1R-NPY complex. In analogy to Arg^{35} in NPY, the N^{ω}-carbamoylguanidino group undergoes multiple polar interactions with residues $D287^{6.59}$

and T212$^{5.39}$ and is further stabilized by interaction of the backbone carbonyl group of the *N*$^{\omega}$-carbamoylated arginine with residue N283$^{6.55}$. The carbamoyl substituent of the arginine side chain, i.e. the propionamide moiety, reaches deeper into the binding pocket, finding another polar contact to Q219$^{5.46}$, which, in the Y_1R-NPY complex, interacts with the phenolic hydroxyl group of Tyr^{36} instead. Consequently, the hydroxybenzylamide moiety is pushed away from helices III and V towards helix IV, where it associates to the highly conserved W276$^{6.48}$, which was identified as a pivotal contributor to high affinity binding of UR-MK299 (replacement of W276 by alanine led to a 2000-fold loss in Y_1R affinity). Furthermore, the interaction of W276$^{6.48}$ with the 4-hydroxybenzylamido moiety in UR-MK299 is assumed to stabilize the inactive conformation of the receptor, explaining the antagonistic nature of UR-MK299, and beyond that, possibly of all argininamide-type Y_1R antagonists.[120] This interaction potentially leads to one of the most noticeable conformational differences between the active state (Y_1R-NPY complex) and the inactive state (Y_1R-UR-MK299 complex) Y_1R structures, as helix VI is oriented in a more vertical position in the active state compared to its position in the inactive state (not shown in Figure 1.3).

With regard to exploiting the Y_1R-UR-MK299 complex as a structural basis for the synthesis of new Y_1R antagonists bearing e.g. a fluorescent or radioactive tag, the diphenylacetyl moiety in UR-MK299 represents the most promising site for a chemical modification: While one of the phenyl rings is stabilized in a π-π stack with F282$^{6.54}$, the other one projects towards the extracellular region of the receptor (Figure 1.3, bottom left). Addressing this phenyl ring with a spacer of suitable length, the receptor surface can be reached without impairing the key interactions between UR-MK299 and the Y_1R.

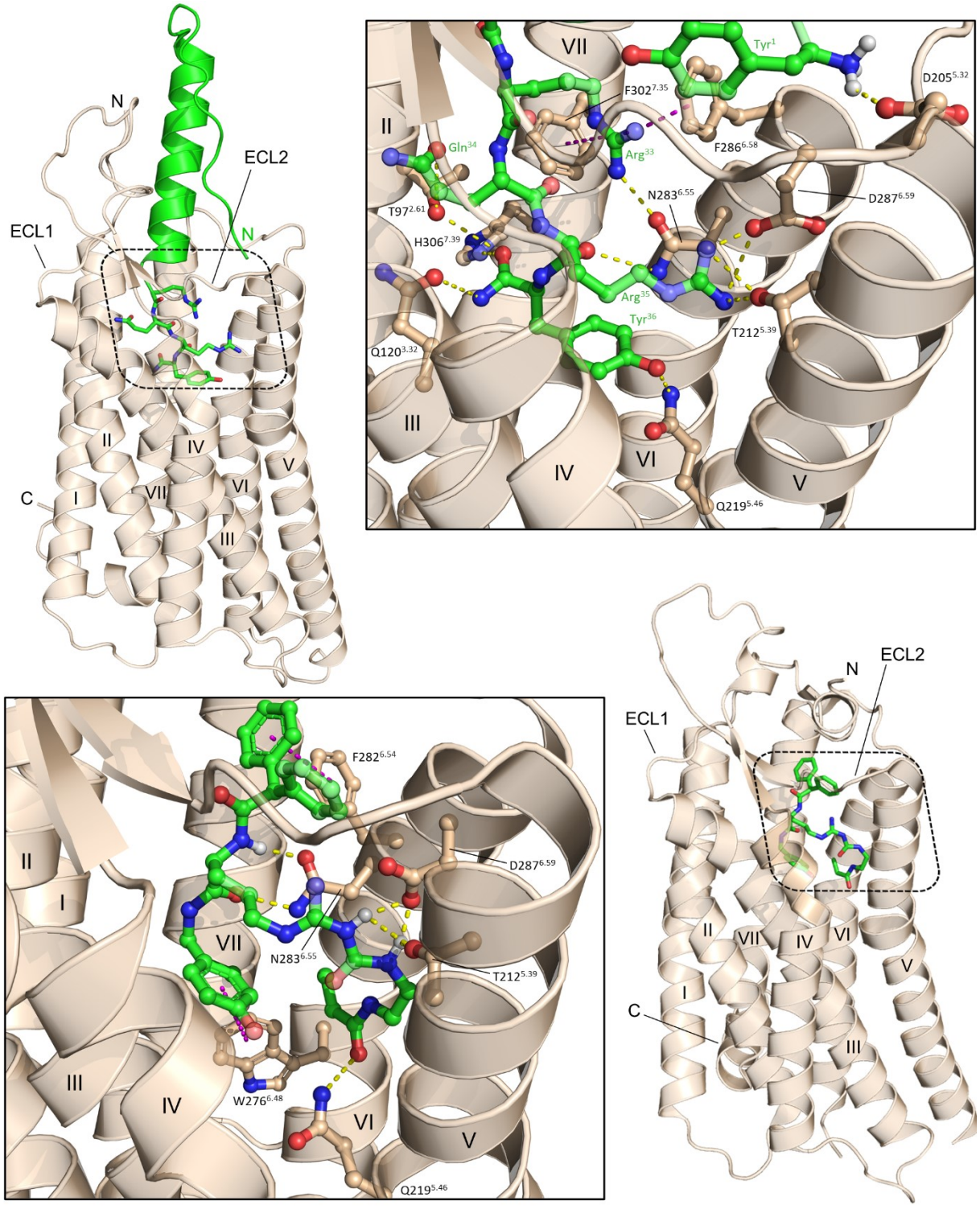

Figure 1.3. Cryo-EM structure of the Y_1R-NPY complex[122] (top, PDB ID: 7X9A) and X-ray crystal structure of the Y_1R-UR-MK299 complex[120] (bottom, PDB ID: 5ZBQ). Contacts between the ligand (green sticks) and the receptor are presented in the boxes. Receptor residues interacting with the ligand are shown as beige sticks. Polar contacts between ligand and receptor residues are shown as yellow dashes, π–π and π–cation interactions are shown as dashes in magenta. For clarity, the G_i proteins are not displayed.

1.1.2.5 NPY receptor dimerization

Among class A rhodopsin-like GPCRs, numerous types have been reported to form homodimers, heterodimers or higher-order oligomers, including neuropeptide receptors, e.g. in Gal_1R-5-HT_{1A} (galanin 1 receptor-serotonin 1A receptor) or NTS_1R-D_2R (neurotensin 1 receptor-dopamine D_2 receptor) heterodimers.[124-126] The formation of dimers or oligomers, which is based on noncovalent allosteric interactions between receptor protomers, can occur already at an ontogenic level in the ER, where dimerization ensures correct folding of the GPCR protomers prior to their transport to the cell membrane.[127-129] It can also occur at the cell surface, for instance as a response to ligand binding, or spontaneously, resulting in receptor protomers toggling between monomeric and multimeric states in rapid succession.[130]

For many GPCRs, functional consequences of dimerization remain elusive, although several observations indicating a (patho)physiological significance have been reported:[131] Among them are κ-δ-opioid receptor heteromers, associated with an attenuated development of drug tolerance,[132, 133] 5-HT_{2A}R-CB_1R (serotonin 2A receptor-cannabinoid 1 receptor) heterodimers, whose dissociation might result in a reduction of short-term memory loss after cannabis consumption,[134] or pathologically decreased levels of TXA2 (thromboxane 2) receptor homodimers, leading to platelet function defects in affected patients.[135]

In principle, NPY receptors are also able to dimerize, as the hY_1R, hY_2R and hY_5R subtypes[136] and also the Y_4R from rhesus macaques (rhY_4R)[137] have been reported to form homodimers *in vitro*, as elucidated in FRET or BRET assays. Inspired by the observed co-localization in certain brain areas and by the overlapping physiological effects, the formation of heterodimers between Y_1Rs and Y_5Rs was examined and demonstrated.[138-140] Altered functions of dimerized NPY receptors regarding receptor internalization or signal transduction could not be observed in homodimers, however, allosteric interactions effecting the structures of the orthosteric binding sites within the Y_1R-Y_5R heterodimer led to altered efficacy of described agonists and significantly delayed the inhibitory effect of antagonists on agonist-stimulated receptor internalization. This indicates that potentially more (hetero)dimers among NPY receptors exist, mediating different physiological effects in comparison to the respective monomers.

1.1.2.6 Overexpression of NPY receptors in endocrine tumors

In the last two centuries, the working group around Prof. Dr. Jean Claude Reubi from the University of Bern made outstanding contributions to the NPY research field by identifying NPY receptor overexpression, in particular of Y_1Rs and Y_2Rs, in various peripheral tumor tissues and tumor tissue-associated blood vessels.[141-146] High receptor incidence and expression levels were found in breast carcinomas,[147] ovarian sex cord-stromal tumors,[148] Ewing's sarcoma[149] and adrenal cortical tumors.[150] Other tumors with moderate and low NPY receptor

density and incidence include neuroblastic tumors,[151] pheochromocytomas, paragangliomas, renal cell carcinomas[150] and gastrointestinal stromal tumors.[152] Localization of high NPY receptor densities in tumor-associated blood vessels by autoradiography is often masked by the respective tumoral receptor overexpression. However, in tumors with low incidence and density as renal carcinomas and gastrointestinal stromal tumors, vascular Y_1R receptor overexpression was consistent and high.[152] These findings suggest Y_1Rs and Y_2Rs as targets for tumor diagnosis and even therapy, as selective high-affinity Y_1R ligands can be labeled with radioisotopes suited for imaging or endoradiotherapy.

Functional autoradiography studies revealed G protein binding of intracellular [^{35}S]GTPγS upon receptor activation by agonist binding in Y_1R- and Y_2R-expressing tumors, indicating an intact machinery for downstream signaling and, therefore, potentially a regulatory role of these receptors in tumor proliferation.[143] It is known that NPY, mainly through Y_1Rs and Y_2Rs, is a positive modulator of cell proliferation, as in vascular smooth muscle cells,[153] in endothelial cells, leading to angiogenesis,[154, 155] and in sympathetic neuroblasts,[156] but also of cell growth, as in cardiomyocytes.[157] In the neuroblastoma cell line SK-N-BE(2), receptor activation by Y_2R selective agonists induced mitogenic effects and the increased constitutive release of NPY in this cell line promoted proliferation of human dermal microvascular endothelial cells, suggesting a key role of Y_2Rs in tumor vascularization.[156] On the other hand, in SK-N-MC cells, a cell line derived from an Ewing's sarcoma family tumor (ESFT) and to some extent also in PC12 cells from pheochromocytoma, NPY was shown to exert antiproliferative and pro-apoptotic effects, presumably *via* Y_1R activation.[147, 156, 158] Additionally, it was demonstrated on PC-3 prostate cancer cells that NPY does not promote cell migration and metastatic spread into reconstituted basement membranes and even inhibited migration of colon adenocarcinoma cells.[159-161] This leads to the conclusion that the functional roles of NPY receptors overexpressed in the respective tumor tissue exhibit similar complexity compared to the manifold physiological functions of NPY in non-tumoral tissue and therefore need to be further explored.[146]

Among the investigated NPY receptor-containing tumor tissues, breast carcinomas, located in the periphery, stand out in terms of Y_1R-targeted tumor imaging as they not only exhibit the highest density and incidence of Y_1R receptors, the Y_1R/Y_2R expression ratio was also found to be shifted from almost exclusively Y_2R-dominated in non-affected healthy mammary tissue to a prevalent Y_1R expression upon neoplastic transformations.[147, 162] This renders the Y_1R a promising marker for abnormal breast tissue growth and therefore, targeting peripheral Y_1R with radiolabeled ligands harbors the potential to detect and monitor breast cancer even in early stages.[142, 163, 164] Remarkably, Y_1R overexpression in breast carcinomas and related lymph node metastases coincides with the overexpression of gastrin-releasing peptide

receptors (GRPRs). This gives rise to the development of heterodimeric radiolabeled ligands targeting GRPRs and Y_1Rs.[162, 165] It should be noted, that the (over)expression of Y_1Rs was demonstrated to be dependent on the presence of estradiol in MCF-7 mammary carcinoma cells and corresponding nude mice xenografts, as the treatment with antiestrogens completely abolished Y_1R expression.[166]

1.2 Fluorescent GPCR ligands as pharmacological tools

A broad portfolio of binding assays is available to determine GPCR-ligand binding affinities and binding kinetics, both on a fluorometric and a radiochemical basis. These assays can be categorized by different characteristics, for example comparing heterogenous assay formats, that require separation of the free from the receptor-bound probe before readout, and homogenous assay formats, where the presence of the free tracer does not impair signal readout. The first category comprises radioligand binding assays, since non-bound radioactive tracer must be removed to enable the quantification of receptor-bound ligand. This separation, however, is not required for most fluorescence-based binding assays, including flow cytometric assays, microscopy-based methods (confocal microscopy, total internal reflection fluorescence (TIRF) microscopy, fluorescence lifetime imaging microscopy (FLIM)), RET-based assays (BRET- and FRET-assays) and fluorescence polarization (FP)- and anisotropy (FA)-based assays, not only facilitating assay performance on a practical level, but also enabling a time-resolved monitoring of binding processes.[167-170]

Fluorometric flow cytometry has been implemented as a tool to examine GPCR ligand binding almost four centuries ago,[171] and has since also been used to characterize NPY receptors.[110, 111, 172-174] Confocal microscopy contributes a unique feature among fluorescence-based methods allowing the localization of GPCRs in membranes of live cells in a visible spatial context, but has also been applied for time-resolved receptor binding studies and compound characterization by high-content imaging.[175-179] The NanoBRET assay format has been successfully utilized to conveniently characterize ligand binding kinetics for several GPCRs, including the histamine receptor family (H_1R,[180] H_2R,[181] H_3R,[182] and H_4R[183]), the adenosine receptor family (A_1R,[184] A_{2B}R[185] and A_3R[186]), the β_2-adrenoceptor,[187] the angiotensin II type 1 receptor, [188] and very recently also the Y_1R.[189] FP-/FA-based assays, measuring orientational changes of a fluorophore in its excited state after irradiation with linearly polarized light, were applied to examine the binding kinetics of fluorescent dopamine D_1 receptor ligands,[190] melanocortin 4 receptor ligands,[191] and histamine H_3 receptor ligands[192] (note: the terms FP and FA describe the same process, but can be interpreted mathematically in two ways, depending on user preferences[193]). Furthermore, a systematic study comparing the NanoBRET and FA method was conducted for the M_2 muscarinic acetylcholine receptor.[194]

While the number of GPCR binding studies involving fluorescence-based assays is steadily rising, the imperative premise for the success of these methods must be pointed out: They require fluorescently labeled receptor ligands with suitable pharmacological properties. Conserving high receptor affinity after introduction of a fluorescent dye to a nonlabeled parent compound is detrimental for several reasons: The amount of fluorescent ligand required for binding assays is reduced, which can be a relevant cost factor owed to the high prices for many of available fluorescent dyes. Also, as nonspecific binding generally rises with increasing concentrations of the applied fluorescent probe, the use of high-affinity fluorescent ligands, requiring low concentrations of the same, can considerably improve the signal-to-noise ratio of the respective fluorescence-based assay. In addition, some of the aforementioned methods, e.g. the ratiometric FP-/FA-based assays, are not at all compatible with low affinity ligands (K_D > 10 nM).[193] However, as fluorescent dyes feature a hydrophobic core element containing an extended π-system, which increases the size of the labeled ligand considerably, the decrease in binding affinity compared to the labeling precursor is unavoidable in most cases.[195, 196] The most effective measure to minimize the expected drop in binding affinity consists in ligand design based on the knowledge of the ligand binding mode, preferably accessible from a crystal or cryo-EM structure of the respective receptor in complex with the parent ligand. This way, time consuming SAR-based screening for the most suitable linker length and attachment site in the parent compound may become obsolete as demonstrated in Chapter 2.

To conclude, fluorescence-based assays excel radiochemical methods in many facets, not only concerning the high safety requirements to prevent radiation exposure and the costs involved in radioactive disposal, but also with respect to the broad applicability of fluorescent ligands and a less time-intensive conduction of fluorescence-based assays. However, for certain situations, radiolabeled ligands are still invaluable tools, e.g. if a suitable fluorescent ligand or the biochemically engineered receptor constructs, required e.g. for RET-based assays, are not available, or for experiments that require the outstanding sensitivity of radioactively labeled ligands such as the autoradiographic detection of a certain receptor in tissues.

1.3 GPCR PET ligands as diagnostic tools in nuclear medicine

1.3.1 The principle of PET and its diagnostic applications

PET (positron-emission tomography), often coupled to CT (computer tomography) to combine functional and anatomic imaging, represents an indispensable, non-invasive diagnostic tool in modern nuclear medicine to visualize biochemical processes throughout the body. It is especially used to identify tissues with abnormal metabolic activity or altered expression of

certain proteins including membrane receptors, which can serve as markers for the detection of tumor tissue or for the diagnosis of neurodegenerative diseases.[197]

PET tracers – in most cases administered intravenously to the patient – bear a “proton-rich” positron-emitting nuclide, which decays into a nuclide with its atomic number reduced by one (Table 1.3[197]). For this type of radioactive decay, a proton dissimilates into an electron neutrino and a positron. The emitted positron dissipates almost all of its kinetic energy by interactions with atoms of the medium it passes through before it is annihilated together with an electron, resulting in the back-to-back emission of two 511 keV photons in opposite directions (note: the mass energies of a positron and an electron correspond to 511 keV each, according to $E = m c^2$). These photons can be detected quasi-simultaneously by circularly arranged PET scanning units, which allows the construction of a three-dimensional image, displaying the amount of radioactivity measured in certain region of interest.[197]

Table 1.3. Decay products, half-lives, and maximum positron kinetic energies (E_{max} β^+) for common nuclides used in PET.

nuclide	decay product	$t_{1/2}$ [min]	E_{max} β^+ [keV]
^{11}C	^{11}Be	20	970
^{13}N	^{13}C	10	1190
^{15}O	^{15}N	2	1720
^{18}F	^{18}O	110	635
^{68}Ga	^{68}Zn	68	1900

Due to their short half-lives, ^{13}N and ^{15}O can only be administered in chemical forms, which are obtained directly from the cyclotron or linac (linear particle accelerator), e.g. $^{13}NH_3$, $H_2{}^{15}O$ and $^{15}O_2$. If chemical transformations need to be carried out, nuclides with higher half-lives are preferred. Among them, ^{18}F is considered advantageous for PET tracers requiring multiple reaction and/or purification steps. ^{68}Ga represents another indispensable positron-emitting nuclide for PET, which however requires a bulky chelator such as DOTA in the target compound, effecting the physicochemical profile and potentially also the bioactivity of the probe. Additionally, positrons emitted by ^{68}Ga exhibit high energy (*cf*. Table 1.3), resulting in decreased image resolution as these positrons travel several millimeters from the site of positron emission before they reach the low energy state required to trigger the annihilation event (Table 1.3). Nevertheless, ^{68}Ga is still the most used PET nuclide, since the nuclide source, a $^{68}Ge/^{68}Ga$-generator, constitutes a highly affordable alternative to cyclotrons or linacs. Moreover, the bifunctional chelators feature flexibility as they can also be used to bind other radiometals, e.g. ^{177}Lu, ^{161}Tb, and ^{90}Y as radiotherapeutic nuclides, or ^{111}In for SPECT (single photon emission computed tomography) imaging.[198]

Whether one of the two most frequently used non-invasive imaging techniques, PET/CT or SPECT, is superior to the other one, largely depends on the infrastructure of the respective nuclear medical department. In SPECT, gamma photons with weaker energy compared to 511 keV are directly emitted from unstable heavy nuclides such as ^{123}I, ^{99m}Tc or ^{111}In. Several comparative studies favor PET/CT over SPECT due to higher spatio-temporal resolution, resulting in higher sensitivity and image quality.[199, 200] On the other hand, SPECT offers a wider range of radiopharmaceuticals with half-lives from several hours to several days, which enables the delivery of SPECT tracers from commercial cyclotron facilities to hospitals. For the next decades, both imaging modalities will be of relevance in the clinic and likely even complemented with the rise of other imaging methods, e.g. magnetic particle imaging using ultra-small superparamagnetic iron oxide nanoparticles (SPIONs).[201-203]

1.3.2 PET ligands based on GPCR ligand-receptor interactions as clinical research tools

Aminergic GPCRs such as dopamine and serotonin receptors, and opioid receptors have been targeted with suitable PET ligands to study the expression of these receptors in individuals suffering from neurodegenerative diseases, e.g. Parkinson's disease, Alzheimer's disease or dementia, or from mental disorders, e.g. schizophrenia, depression, anxieties and drug addictions.[204] These PET ligands usually represent radiolabeled analogues of already characterized receptor subtype selective agonists or antagonists, for example the 5-HT_{2A}R antagonist ^{18}F-altanserin (associated with depression),[205] the D_2R antagonist ^{11}C-raclopride (associated with Parkinson's disease and schizophrenia)[206, 207] or the MOR agonist ^{11}C-carfentanil (associated with depression, addictions, and the social distress and reward system)[208-211] (Figure 1.4, panel A). Regarding the synthesis of the PET ligands, the radionuclides ^{11}C (e.g. as $^{11}CH_3OTf$ or $^{11}CH_3I$ in S_N2 reactions) or ^{18}F (as $K^{18}F$ in S_N2 reactions or as $^{18}F_2$ in aromatic substitutions) are preferably incorporated in the last synthetic step, followed by quick and convenient purification.

As various GPCRs are overexpressed in different types of neoplasia, selective PET ligands targeting these GPCRs can in principle serve as radiopharmaceuticals for tumor diagnosis and therapy. However, only one GPCR PET ligand has been approved for routine tumor diagnosis and monitoring to date: The somatostatin analogue ^{68}Ga-DOTATATE (structure see Figure 5.1, Chapter 5) is used in nuclear medicine for the diagnosis of somatostatin receptor-expressing neuroendocrine tumors.[212] However, other GPCR PET ligands are currently evaluated in clinical studies, for example ^{68}Ga-pentaxifor[213] (Figure 1.4, panel B), a ligand for the chemokine 4 receptor (CXCR4), which is associated with numerous cancer types like multiple myeloma,[214] glioblastoma,[215] and neuroendocrine tumors,[216] or the GRPR ligand ^{68}Ga-RM2[217] (Figure 1.4, panel B), a potential diagnostic agent for prostate cancer.[218, 219] Concerning

NPY receptors, few Y_1R PET ligands have been described as potential radiopharmaceuticals for breast cancer diagnosis and evaluated *in vivo*. These include a ^{18}F-labeled high-molecular-weight glycopeptide derived from NPY,[220] ^{18}F-labeled BIBP3226-derived argininamides,[114, 115] and also a heterobivalent peptidic ligand bearing pharmacophores recognized by the Y_1R and the GRPR.[165] However, many more efforts are required to establish a Y_1R PET ligand approved for tumor imaging in the clinic.

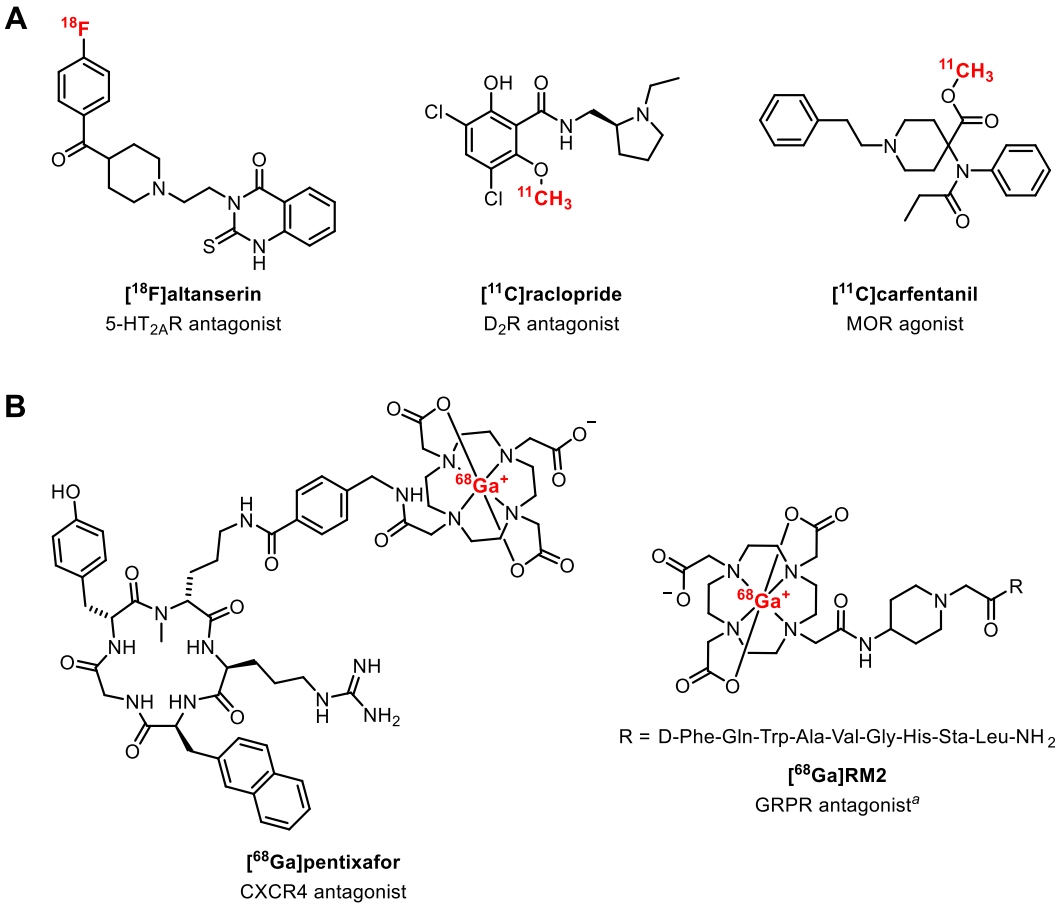

Figure 1.4. (A) GPCR PET ligands used for receptor expression studies in patients suffering from neurodegenerative diseases and mental disorders. (B) GPCR PET ligands evaluated as tools for tumor diagnosis. [a]Sta: statine ((3*S*,4*S*)-4-amino-3-hydroxy-6-methylheptanoic acid).

1.4 Scope of the thesis

The neuropeptide Y Y_1 receptor, a class A GPCR and a member of the NPY receptor family, is involved in the regulation of many physiological processes such as energy homeostasis, stress regulation, anxiolysis and the regulation of blood pressure. Moreover, elevated Y_1R levels were found in various types of cancer tissue. Therefore, the Y_1R represents an interesting drug target and a potential tumor marker, in particular for the diagnosis of mammary carcinoma.

In search for pharmacological tools, argininamide-type Y_1R ligands, representing small molecule peptidomimetics of the C-terminus of NPY, were identified as highly selective Y_1R antagonists. Structural modifications of the lead structure BIBP3226 (pK_i (Y_1R) = 8.80[112]), i.e. the introduction of an N^{ω}-carbamoyl substituent at the guanidino group, resulted in the radiolabeled tool compound [^{3}H]UR-MK299, showing high Y_1R affinity (pK_D = 10.36).[109, 113] However, the attachment of bulky fluorescent dyes at the carbamoylated guanidine moiety caused a marked decrease in binding affinity (pK_i < 8).[109, 111]

This work focused on the structure-based development of fluorescently labeled argininamide-type Y_1R ligands displaying considerably higher Y_1R affinity than previously reported probes. To achieve this aim, the structural information provided by the newly reported crystal structure of the Y_1R in complex with UR-MK299 had to be exploited. As the diphenylacetyl moiety in UR-MK299 was located closest to the receptor surface in the crystal structure, analogues of UR-MK299 had to be synthesized, containing an amine-functionalized linker at one of the phenyl rings of the diphenylacetyl moiety. Subsequently, the amine-functionalized derivatives of UR-MK299 had to be conjugated to different fluorophores yielding fluorescent Y_1R ligands, which had to be pharmacologically characterized with respect to Y_1, Y_2, Y_4 and Y_5 receptor binding (radioligand competition binding studies) and Y_1R antagonism (Fura-2 Ca^{2+} assay). Most importantly, the fluorescent ligands had to be investigated in flow cytometry- and fluorescence anisotropy-based assays, comprising saturation binding, kinetic studies, and competition binding experiments. Moreover, this project included the exploration of the probes by different fluorescence microscopy techniques to visualize and localize Y_1Rs in live MCF-7-Y_1 mammary carcinoma cells.

Using the same amine-functionalized precursor compounds as for the synthesis of the fluorescent ligands, fluorinated and Ga^{3+}-containing potential Y_1R PET ligands had to be synthesized. After the pharmacological evaluation of the PET ligand candidates regarding NPY receptor binding, two selected compounds had to be radiochemically labeled with ^{18}F and one with $^{68}Ga^{3+}$ (collaboration with Prof. O. Prante and Dr. S. Maschauer at the University Hospital in Erlangen, and with Prof. D. Hellwig at the University Hospital in Regensburg). The obtained PET tracers had to be characterized *in vitro*, to examine, e.g. their physicochemical properties, and *in vivo* with respect to their biodistribution and the PET imaging of subcutaneous MCF-7-Y_1 tumors in nude mice.

Additionally, the amine-functionalized precursors had to be used to synthesize a set of homobivalent Y_1R ligands, exhibiting different linker lengths between the two pharmacophoric entities, as potential tools to investigate Y_1R homodimerization.

Finally, a synthetic route towards a fluorinated and chelator-carrying prototypic Y_1R “radiohybrid” ligand, a compound that can be transformed to either a cancer diagnostic tool or a therapeutic agent, had to be developed.

1.5 References

(1) Russo, A. F. Overview of neuropeptides: Awakening the senses? *Headache* **2017**, 57, 37-46.

(2) Paul, B. D.; Snyder, S. H. H_2S: A novel gasotransmitter that signals by sulfhydration. *Trends Biochem. Sci* **2015**, 40, 687-700.

(3) Harilal, S.; Kumar, R.; Mathew, G. E.; Jose, J.; Uddin, M. S.; Mathew, B. Neurochemicals in nervous system and exploring the chemical make-up of human brain in *Principles of neurochemistry*, Mathew, B.; Thomas Parambi, D. G., Eds., Springer: Singapore, **2020**, pp. 19-39.

(4) Hökfelt, T.; Barde, S.; Xu, Z.-Q. D.; Kuteeva, E.; Rüegg, J.; Le Maitre, E.; Risling, M.; Kehr, J.; Ihnatko, R.; Theodorsson, E.; Palkovits, M.; Deakin, W.; Bagdy, G.; Juhasz, G.; Prud’homme, H. J.; Mechawar, N.; Diaz-Heijtz, R.; Ögren, S. O. Neuropeptide and small transmitter coexistence: Fundamental studies and relevance to mental illness. *Front. Neural Circuits* **2018**, 12.

(5) Bhat, U. S.; Shahi, N.; Surendran, S.; Babu, K. Neuropeptides and behaviors: How small peptides regulate nervous system function and behavioral outputs. *Front. Mol. Neurosci.* **2021**, 14.

(6) van den Pol, Anthony N. Neuropeptide transmission in brain circuits. *Neuron* **2012**, 76, 98-115.

(7) Burbach, J.; H., P. Neuropeptides from concept to online database www.neuropeptides.nl. *Eur. J. Pharmacol.* **2010**, 626, 27-48.

(8) D., L.; Söderberg, C.; Blomqvist, A. G. Evolution of neuropeptide Y family of peptides in *The biology of neuropeptide Y and related peptides*, 1st ed.; Colmers, W. F., Wahlestedt, C., Eds., Humana Press: Totowa, N.J., **1993**, pp. 1-41.

(9) Beck-Sickinger, A. G.; Jung, G. Structure-activity relationships of neuropeptide Y analogues with respect to Y_1 and Y_2 receptors. *Biopolymers* **1995**, 37, 123-42.

(10) Hoyle, C. H. V. Neuropeptide families and their receptors: evolutionary perspectives. *Brain Res.* **1999**, 848, 1-25.

(11) Cerdá-Reverter, J. M.; Larhammar, D. Neuropeptide Y family of peptides: Structure, anatomical expression, function, and molecular evolution. *Biochem. Cell Biol.* **2000**, 78, 371-92.

(12) Ekblad, E.; Sundler, F. Distribution of pancreatic polypeptide and peptide YY. *Peptides* **2002**, 23, 251-261.

(13) Morimoto, R.; Satoh, F.; Murakami, O.; Totsune, K.; Saruta, M.; Suzuki, T.; Sasano, H.; Ito, S.; Takahashi, K. Expression of peptide YY in human brain and pituitary tissues. *Nutrition* **2008**, 24, 878-884.

(14) Dumont, Y.; Martel, J.; Fournier, A.; Stpierre, S.; Quirion, R. Neuropeptide Y and neuropeptide Y receptor subtypes in brain and peripheral tissues. *Prog. Neurobiol.* **1992**, 38, 125-167.

(15) Michel, M. C.; Beck-Sickinger, A.; Cox, H.; Doods, H. N.; Herzog, H.; Larhammar, D.; Quirion, R.; Schwartz, T.; Westfall, T. XVI. International union of pharmacology recommendations for the nomenclature of neuropeptide Y, peptide YY, and pancreatic polypeptide receptors. *Pharmacol. Rev.* **1998**, 50, 143-150.

(16) Adrian, T. E.; Allen, J. M.; Bloom, S. R.; Ghatei, M. A.; Rossor, M. N.; Roberts, G. W.; Crow, T. J.; Tatemoto, K.; Polak, J. M. Neuropeptide Y distribution in human brain. *Nature* **1983**, 306, 584-586.

(17) Nagaki, S.; Fukamauchi, F.; Sakamoto, Y.; Higuchi, H.; Miki, N.; Miki, N.; Ono, M.; Sadamatsu, M.; Kato, N.; Osawa, M. Upregulation of brain somatostatin and neuropeptide Y following lidocaine-induced kindling in the rat. *Brain Res.* **2000**, 852, 470-474.

(18) Ericsson, A.; Schalling, M.; McIntyre, K. R.; Lundberg, J. M.; Larhammar, D.; Seroogy, K.; Hökfelt, T.; Persson, H. Detection of neuropeptide Y and its mRNA in megakaryocytes: Enhanced levels in certain autoimmune mice. *Proc. Natl. Acad. Sci. U.S.A.* **1987**, 84, 5585-5589.

(19) Myers, A. K.; Torres Duarte, A. P.; Zukowska-Grojec, Z. Immunoreactive neuropeptide Y (NPY) in plasma and platelets of rat and mouse strains and human volunteers. *Regul. Pept.* **1993**, 47, 239-245.

(20) Dumont, Y.; Jacques, D.; St-Pierre, J. A.; Tong, Y.; Parker, R.; Herzog, H.; Quirion, R. Neuropeptide Y, peptide YY and pancreatic polypeptide receptor proteins and mRNAs in mammalian brains in *Handbook of Chemical Neuroanatomy*, *Vol. 16*, Quirion, R.; Björklund, A.; Hökfelt, T., Eds., Academic Press, Elsevier: Amsterdam, **2000**, pp. 375-475.

(21) Zhu, J.; Li, W.; Toews, M. L.; Hexum, T. D. Neuropeptide Y inhibits forskolin-stimulated adenylate cyclase in bovine adrenal chromaffin cells *via* a pertussis toxin-sensitive process. *J. Pharmacol. Exp. Ther.* **1992**, 263, 1479-86.

(22) Gerald, C.; Walker, M. W.; Criscione, L.; Gustafson, E. L.; Batzl-Hartmann, C.; Smith, K. E.; Vaysse, P.; Durkin, M. M.; Laz, T. M.; Linemeyer, D. L.; Schaffhauser, A. O.; Whitebread, S.; Hofbauer, K. G.; Taber, R. I.; Branchek, T. A.; Weinshank, R. L. A receptor subtype involved in neuropeptide Y-induced food intake. *Nature* **1996**, 382, 168-171.

(23) Weinberg, D. H.; Sirinathsinghji, D. J. S.; Tan, C. P.; Shiao, L.-L.; Morin, N.; Rigby, M. R.; Heavens, R. H.; Rapoport, D. R.; Bayne, M. L.; Cascieri, M. A.; Strader, C. D.; Linemeyer, D. L.; MacNeil, D. J. Cloning and expression of a novel neuropeptide Y receptor. *J. Biol. Chem.* **1996**, 271, 16435-16438.

(24) Motulsky, H. J.; Michel, M. C. Neuropeptide Y mobilizes Ca^{2+} and inhibits adenylate cyclase in human erythroleukemia cells. *Am. J. Physiol. - Endocrinol. Metab.* **1988**, 255, E880-E885.

(25) Drakulich, D. A.; Walls, A. M.; Toews, M. L.; Hexum, T. D. Neuropeptide Y receptor-mediated sensitization of ATP-stimulated inositol phosphate formation. *J. Pharmacol. Exp. Ther.* **2003**, 307, 559-565.

(26) Perney, T. M.; Miller, R. J. Two different G proteins mediate neuropeptide Y and bradykinin-stimulated phospholipid breakdown in cultured rat sensory neurons. *J. Biol. Chem.* **1989**, 264, 7317-7327.

(27) Misra, S.; Murthy, K. S.; Zhou, H.; Grider, J. R. Coexpression of Y_1, Y_2, and Y_4 receptors in smooth muscle coupled to distinct signaling pathways. *J. Pharmacol. Exp. Ther.* **2004**, 311, 1154-1162.

(28) McCullough, L. A.; Egan, T. M.; Westfall, T. C. Neuropeptide Y receptors involved in calcium channel regulation in PC12 cells. *Regul. Pept.* **1998**, 75-76, 101-107.

(29) Walker, M. W.; Ewald, D. A.; Perney, T. M.; Miller, R. J. Neuropeptide Y modulates neurotransmitter release and Ca^{2+} currents in rat sensory neurons. *J. Neurosci.* **1988**, 8, 2438-2446.

(30) Sosulina, L.; Schwesig, G.; Seifert, G.; Pape, H.-C. Neuropeptide Y activates a G protein-coupled inwardly rectifying potassium current and dampens excitability in the lateral amygdala. *Mol. Cell. Neurosci.* **2008**, 39, 491-498.

(31) Sun, Q. Q.; Huguenard, J. R.; Prince, D. A. Neuropeptide Y receptors differentially modulate G-protein-activated inwardly rectifying K^+ channels and high-voltage-activated Ca^{2+} channels in rat thalamic neurons. *J. Physiol.* **2001**, 531, 67-79.

(32) Matsumoto, M.; Nomura, T.; Momose, K.; Ikeda, Y.; Kondou, Y.; Akiho, H.; Togami, J.; Kimura, Y.; Okada, M.; Yamaguchi, T. Inactivation of a novel neuropeptide Y/peptide YY receptor gene in primate species. *J. Biol. Chem.* **1996**, 271, 27217-27220.

(33) Gregor, P.; Feng, Y.; DeCarr, L. B.; Cornfield, L. J.; McCaleb, M. L. Molecular characterization of a second mouse pancreatic polypeptide receptor and its inactivated human homologue. *J. Biol. Chem.* **1996**, 271, 27776-27781.

(34) Rose, P. M.; Lynch, J. S.; Frazier, S. T.; Fisher, S. M.; Chung, W.; Battaglino, P.; Fathi, Z.; Leibel, R.; Fernandes, P. Molecular genetic analysis of a human neuropeptide Y receptor. *J. Biol. Chem.* **1997**, 272, 3622-3627.

(35) Grandt, D.; Schimiczek, M.; Rascher, W.; Feth, F.; Shively, J.; Lee, T. D.; Davis, M. T.; Reeve, J. R.; Michel, M. C. Neuropeptide Y 3–36 is an endogenous ligand selective for Y_2 receptors. *Regul. Pept.* **1996**, 67, 33-37.

(36) Grandt, D.; Schimiczek, M.; Beglinger, C.; Layer, P.; Goebell, H.; Eysselein, V. E.; Reeve, J. R. Two molecular forms of Peptide YY (PYY) are abundant in human blood: Characterization of a radioimmunoassay recognizing PYY 1–36 and PYY 3–36. *Regul. Pept.* **1994**, 51, 151-159.

(37) Mentlein, R.; Dahms, P.; Grandt, D.; Krüger, R. Proteolytic processing of neuropeptide Y and peptide YY by dipeptidyl peptidase IV. *Regul. Pept.* **1993**, 49, 133-144.

(38) Medeiros, M. S.; Turner, A. J. Post-secretory processing of regulatory peptides: The pancreatic polypeptide family as a model example. *Biochimie* **1994**, 76, 283-287.

(39) Gerald, C.; Walker, M. W.; Vaysse, P. J. J.; He, C.; Branchek, T. A.; Weinshank, R. L. Expression cloning and pharmacological characterization of a human hippocampal neuropeptide Y/peptide YY Y_2 receptor subtype. *J. Biol. Chem.* **1995**, 270, 26758-26761.

(40) Parker, E. M.; Balasubramaniam, A.; Guzzi, M.; Mullins, D. E.; Salisbury, B. G.; Sheriff, S.; Witten, M. B.; Hwa, J. J. [D-Trp^{34}] neuropeptide Y is a potent and selective neuropeptide Y Y_5 receptor agonist with dramatic effects on food intake. *Peptides* **2000**, 21, 393-399.

(41) Bard, J. A.; Walker, M. W.; Branchek, T. A.; Weinshank, R. L. Cloning and functional expression of a human Y_4 subtype receptor for pancreatic polypeptide, neuropeptide Y, and peptide YY. *J. Biol. Chem.* **1995**, 270, 26762-26765.

(42) Hu, Y.; Bloomquist, B. T.; Cornfield, L. J.; DeCarr, L. B.; Flores-Riveros, J. R.; Friedman, L.; Jiang, P.; Lewis-Higgins, L.; Sadlowski, Y.; Schaefer, J.; Velazquez, N.; McCaleb, M. L. Identification of a novel hypothalamic neuropeptide Y receptor associated with feeding behavior. *J. Biol. Chem.* **1996**, 271, 26315-26319.

(43) McCrea, K.; Wisialowski, T.; Cabrele, C.; Church, B.; Beck-Sickinger, A.; Kraegen, E.; Herzog, H. 2–36[K^4,RYYSA$^{19–23}$]PP a novel Y_5-receptor preferring ligand with strong stimulatory effect on food intake. *Regul. Pept.* **2000**, 87, 47-58.

(44) Borowsky, B.; Walker, M. W.; Bard, J.; Weinshank, R. L.; Laz, T. M.; Vaysse, P.; Branchek, T. A.; Gerald, C. Molecular biology and pharmacology of multiple NPY Y_5 receptor species homologs. *Regul. Pept.* **1998**, 75-76, 45-53.

(45) Berlicki, Ł.; Kaske, M.; Gutiérrez-Abad, R.; Bernhardt, G.; Illa, O.; Ortuño, R. M.; Cabrele, C.; Buschauer, A.; Reiser, O. Replacement of Thr^{32} and Gln^{34} in the C-terminal neuropeptide Y fragment 25–36 by cis-cyclobutane and cis-cyclopentane β-amino acids shifts selectivity toward the Y_4 receptor. *J. Med. Chem.* **2013**, 56, 8422-8431.

(46) Erondu, N.; Wadden, T.; Gantz, I.; Musser, B.; Nguyen, A. M.; Bays, H.; Bray, G.; O'Neil, P. M.; Basdevant, A.; Kaufman, K. D.; Heymsfield, S. B.; Amatruda, J. M. Effect of NPY Y_5R antagonist MK-0557 on weight regain after very-low-calorie diet-induced weight loss. *Obesity* **2007**, 15, 895-905.

(47) Kask, A.; Harro, J.; von Hörsten, S.; Redrobe, J. P.; Dumont, Y.; Quirion, R. The neurocircuitry and receptor subtypes mediating anxiolytic-like effects of neuropeptide Y. *Neurosci. Biobehav. Rev.* **2002**, 26, 259-283.

(48) Parker, R. M. C.; Herzog, H. Regional distribution of Y-receptor subtype mRNAs in rat brain. *Eur. J. Neurosci.* **1999**, 11, 1431-1448.

(49) Lundell, I.; Statnick, M. A.; Johnson, D.; Schober, D. A.; Starbäck, P.; Gehlert, D. R.; Larhammar, D. The cloned rat pancreatic polypeptide receptor exhibits profound differences to the orthologous receptor. *Proc. Natl. Acad. Sci. U.S.A.* **1996**, 93, 5111-5115.

(50) Dumont, Y.; Jacques, D.; Bouchard, P.; Quirion, R. Species differences in the expression and distribution of the neuropeptide Y Y_1, Y_2, Y_4, and Y_5 receptors in rodents, guinea pig, and primates brains. *J. Comp. Neurol.* **1998**, 402, 372-384.

(51) Kishi, T.; Aschkenasi, C. J.; Choi, B. J.; Lopez, M. E.; Lee, C. E.; Liu, H.; Hollenberg, A. N.; Friedman, J. M.; Elmquist, J. K. Neuropeptide Y Y_1 receptor mRNA in rodent brain: Distribution and colocalization with melanocortin-4 receptor. *J. Comp. Neurol.* **2005**, 482, 217-243.

(52) Jacques, D.; Tong, Y.; Dumont, Y.; Shen, S. H.; Quirion, R. Expression of the neuropeptide Y Y_1 receptor mRNA in the human brain. *Neuroreport* **1996**, 7, 1053-1056.

(53) Wolak, M. L.; deJoseph, M. R.; Cator, A. D.; Mokashi, A. S.; Brownfield, M. S.; Urban, J. H. Comparative distribution of neuropeptide Y Y_1 and Y_5 receptors in the rat brain by using immunohistochemistry. *J. Comp. Neurol.* **2003**, 464, 285-311.

(54) Holzer, P.; Reichmann, F.; Farzi, A. Neuropeptide Y, peptide YY and pancreatic polypeptide in the gut–brain axis. *Neuropeptides* **2012**, 46, 261-274.

(55) Verma, D.; Hörmer, B.; Bellmann-Sickert, K.; Thieme, V.; Beck-Sickinger, A. G.; Herzog, H.; Sperk, G.; Tasan, R. O. Pancreatic polypeptide and its central Y_4 receptors are essential for cued fear extinction and permanent suppression of fear. *Br. J. Pharmacol.* **2016**, 173, 1925-1938.

(56) Khandekar, N.; Berning, B. A.; Sainsbury, A.; Lin, S. The role of pancreatic polypeptide in the regulation of energy homeostasis. *Mol. Cell. Endocrinol.* **2015**, 418, 33-41.

(57) Moreno-Herrera, A.; Garcia, A.; Palos, I.; Rivera, G. Neuropeptide Y_1 and Y_5 receptor antagonists as potential anti-obesity drugs: Current status. *Mini-Rev. Med. Chem.* **2014**, 14, 896-919.

(58) Loh, K.; Herzog, H.; Shi, Y.-C. Regulation of energy homeostasis by the NPY system. *Trends Endocrinol. Metab.* **2015**, 26, 125-135.

(59) Valassi, E.; Scacchi, M.; Cavagnini, F. Neuroendocrine control of food intake. *Nutr. Metab. Cardiovasc. Dis.* **2008**, 18, 158-168.

(60) Vohra, M. S.; Benchoula, K.; Serpell, C. J.; Hwa, W. E. AgRP/NPY and POMC neurons in the arcuate nucleus and their potential role in treatment of obesity. *Eur. J. Pharmacol.* **2022**, 915, 174611.

(61) Herzog, H. Neuropeptide Y and energy homeostasis: Insights from Y receptor knockout models. *Eur. J. Pharmacol.* **2003**, 480, 21-29.

(62) Hanson, E. S.; Dallman, M. F. Neuropeptide Y (NPY) may integrate responses of hypothalamic feeding systems and the hypothalamo-pituitary-adrenal axis. *J. Neuroendocrinol.* **1995**, 7, 273-279.

(63) Sainsbury, A.; Rohner-Jeanrenaud, F.; Grouzmann, E.; Jeanrenaud, B. Acute intracerebroventricular administration of neuropeptide Y stimulates corticosterone output and feeding but not insulin output in normal rats. *Neuroendocrinology* **1996**, 63, 318-326.

(64) Li, C.; Chen, P.; Smith, M. S. Corticotropin releasing hormone neurons in the paraventricular nucleus are direct targets for neuropeptide Y neurons in the arcuate nucleus: An anterograde tracing study. *Brain Res.* **2000**, 854, 122-129.

(65) Shimizu, H.; Arima, H.; Ozawa, Y.; Watanabe, M.; Banno, R.; Sugimura, Y.; Ozaki, N.; Nagasaki, H.; Oiso, Y. Glucocorticoids increase NPY gene expression in the arcuate nucleus by inhibiting mTOR signaling in rat hypothalamic organotypic cultures. *Peptides* **2010**, 31, 145-149.

(66) Sajdyk, T. J.; Johnson, P. L.; Leitermann, R. J.; Fitz, S. D.; Dietrich, A.; Morin, M.; Gehlert, D. R.; Urban, J. H.; Shekhar, A. Neuropeptide Y in the amygdala induces long-term resilience to stress-induced reductions in social responses but not hypothalamic-adrenal-pituitary axis activity or hyperthermia. *J. Neurosci.* **2008**, 28, 893-903.

(67) Sajdyk, T. J.; Schober, D. A.; Smiley, D. L.; Gehlert, D. R. Neuropeptide Y Y_2 receptors mediate anxiety in the amygdala. *Pharmacol. Biochem. Behav.* **2002**, 71, 419-423.

(68) Redrobe, J. P.; Dumont, Y.; Fournier, A.; Quirion, R. The neuropeptide Y (NPY) Y_1 receptor subtype mediates NPY-induced antidepressant-like activity in the mouse forced swimming test. *Neuropsychopharmacology* **2002**, 26, 615-624.

(69) Stogner, K. A.; Holmes, P. V. Neuropeptide Y exerts antidepressant-like effects in the forced swim test in rats. *Eur. J. Pharmacol.* **2000**, 387, R9-R10.

(70) Ishida, H.; Shirayama, Y.; Iwata, M.; Katayama, S.; Yamamoto, A.; Kawahara, R.; Nakagome, K. Infusion of neuropeptide Y into CA3 region of hippocampus produces antidepressant-like effect *via* Y_1 receptor. *Hippocampus* **2007**, 17, 271-280.

(71) Redrobe, J. P.; Dumont, Y.; Herzog, H.; Quirion, R. Neuropeptide Y (NPY) Y_2 receptors mediate behaviour in two animal models of anxiety: Evidence from Y_2 receptor knockout mice. *Behav. Brain Res.* **2003**, 141, 251-255.

(72) Adam, T. C.; Epel, E. S. Stress, eating and the reward system. *Physiol. Behav.* **2007**, 91, 449-458.

(73) Maniam, J.; Morris, M. J. The link between stress and feeding behaviour. *Neuropharmacology* **2012**, 63, 97-110.

(74) Kuo, L. E.; Kitlinska, J. B.; Tilan, J. U.; Li, L.; Baker, S. B.; Johnson, M. D.; Lee, E. W.; Burnett, M. S.; Fricke, S. T.; Kvetnansky, R.; Herzog, H.; Zukowska, Z. Neuropeptide Y acts directly in the periphery on fat tissue and mediates stress-induced obesity and metabolic syndrome. *Nat. Med.* **2007**, 13, 803-811.

(75) Rasmusson, A. M.; Hauger, R. L.; Morgan, C. A.; Bremner, J. D.; Charney, D. S.; Southwick, S. M. Low baseline and yohimbine-stimulated plasma neuropeptide Y (NPY) levels in combat-related PTSD. *Biol. Psychiatry* **2000**, 47, 526-539.

(76) Sah, R.; Ekhator, N. N.; Jefferson-Wilson, L.; Horn, P. S.; Geracioti, T. D. Cerebrospinal fluid neuropeptide Y in combat veterans with and without posttraumatic stress disorder. *Psychoneuroendocrinology* **2014**, 40, 277-283.

(77) Yehuda, R.; Brand, S.; Yang, R.-K. Plasma neuropeptide Y concentrations in combat exposed veterans: Relationship to trauma exposure, recovery from PTSD, and coping. *Biol. Psychiatry* **2006**, 59, 660-663.

(78) You, J.; Edvinsson, L.; Bryan, R. M. Neuropeptide Y-mediated constriction and dilation in rat middle cerebral arteries. *J. Cereb. Blood Flow Metab.* **2016**, 21, 77-84.

(79) Boric, M. P.; Martínez, A.; Donoso, M. V.; Huidobro-Toro, J. P. Neuropeptide Y is a vasoconstrictor and adrenergic modulator in the hamster microcirculation by acting on neuropeptide Y_1 and Y_2 receptors. *Eur. J. Pharmacol.* **1995**, 294, 391-401.

(80) Donoso, M. V.; Brown, N.; Carrasco, C.; Cortes, V.; Fournier, A.; Huidobro-Toro, J. P. Stimulation of the sympathetic perimesenteric arterial nerves releases neuropeptide Y potentiating the vasomotor activity of noradrenaline: Involvement of neuropeptide Y Y_1 receptors. *J. Neurochem.* **2002**, 69, 1048-1059.

(81) Shah, S. H.; Freedman, N. J.; Zhang, L.; Crosslin, D. R.; Stone, D. H.; Haynes, C.; Johnson, J.; Nelson, S.; Wang, L.; Connelly, J. J.; Muehlbauer, M.; Ginsburg, G. S.; Crossman, D. C.; Jones, C. J.; Vance, J.; Sketch, M. H.; Granger, C. B.; Newgard, C. B.; Gregory, S. G.; Goldschmidt-Clermont, P. J.; Kraus, W. E.; Hauser, E. R. Neuropeptide Y gene polymorphisms confer risk of early-onset atherosclerosis. *PLoS Genet.* **2009**, 5, e1000318.

(82) Decressac, M.; Prestoz, L.; Veran, J.; Cantereau, A.; Jaber, M.; Gaillard, A. Neuropeptide Y stimulates proliferation, migration and differentiation of neural

precursors from the subventricular zone in adult mice. *Neurobiol. Dis.* **2009**, 34, 441-449.

(83) Duarte-Neves, J.; Gonçalves, N.; Cunha-Santos, J.; Simões, A. T.; den Dunnen, W. F. A.; Hirai, H.; Kügler, S.; Cavadas, C.; Pereira de Almeida, L. Neuropeptide Y mitigates neuropathology and motor deficits in mouse models of Machado–Joseph disease. *Hum. Mol. Genet.* **2015**, 24, 5451-5463.

(84) Hock, C.; Heese, K.; Hulette, C.; Rosenberg, C.; Otten, U. Region-specific neurotrophin imbalances in Alzheimer disease. *Arch. Neurol.* **2000**, 57, 846.

(85) Ferrer, I.; Goutan, E.; Marín, C.; Rey, M. J.; Ribalta, T. Brain-derived neurotrophic factor in Huntington disease. *Brain Res.* **2000**, 866, 257-261.

(86) Lu, B.; Nagappan, G.; Lu, Y. BDNF and synaptic plasticity, cognitive function, and dysfunction. *Handb. Exp. Pharmacol.* **2014**, 220, 223-250.

(87) Rimondini, R.; Thorsell, A.; Heilig, M. Suppression of ethanol self-administration by the neuropeptide Y (NPY) Y_2 receptor antagonist BIIE0246: Evidence for sensitization in rats with a history of dependence. *Neurosci. Lett.* **2005**, 375, 129-133.

(88) Brothers, S. P.; Wahlestedt, C. Therapeutic potential of neuropeptide Y (NPY) receptor ligands. *EMBO Mol. Med.* **2010**, 2, 429-439.

(89) Bahh, B. E.; Cao, J. Q.; Beck-Sickinger, A. G.; Colmers, W. F. Blockade of neuropeptide Y_2 receptors and suppression of NPY's anti-epileptic actions in the rat hippocampal slice by BIIE0246. *Br. J. Pharmacol.* **2002**, 136, 502-509.

(90) Bahh, B. E.; Balosso, S.; Hamilton, T.; Herzog, H.; Beck-Sickinger, A. G.; Sperk, G.; Gehlert, D. R.; Vezzani, A.; Colmers, W. F. The anti-epileptic actions of neuropeptide Y in the hippocampus are mediated by Y_2 and not Y_5 receptors. *Eur. J. Neurosci.* **2005**, 22, 1417-1430.

(91) Klapstein, G. J.; Colmers, W. F. On the sites of presynaptic inhibition by neuropeptide Y in rat hippocampus *in vitro*. *Hippocampus* **1993**, 3, 103-111.

(92) Green, B. R.; White, K. L.; McDougle, D. R.; Zhang, L.; Klein, B.; Scholl, E. A.; Pruess, T. H.; White, H. S.; Bulaj, G. Introduction of lipidization-cationization motifs affords systemically bioavailable neuropeptide Y and neurotensin analogs with anticonvulsant activities. *J. Pept. Sci.* **2010**, 16, 486-495.

(93) Diaz del Castillo, M.; Woldbye, D. P. D.; Heegaard, A. M. Neuropeptide Y and its involvement in chronic pain. *Neuroscience* **2018**, 387, 162-169.

(94) Oliveira, M.-M.; Akerman, S.; Tavares, I.; Goadsby, P. J. Neuropeptide Y inhibits the trigeminovascular pathway through NPY Y_1 receptor: Implications for migraine. *Pain* **2016**, 157, 1666-1673.

(95) Chen, Q.-C.; Zhang, Y. The role of NPY in the regulation of bone metabolism. *Front. Endocrinol.* **2022**, 13.

(96) Thorsell, A.; Mathé, A. A. Neuropeptide Y in alcohol addiction and affective disorders. *Front. Endocrinol.* **2017**, 8.

(97) Merten, N.; Beck-Sickinger, A. G. Molecular ligand-receptor interaction of the NPY/PP peptide family in *NPY family of peptides in neurobiology, cardiovascular and metabolic disorders: From genes to therapeutics*, *Vol. 95*, Zukowska, Z. F., G., Eds., Springer: Basel, **2006**, pp. 35-62.

(98) Lindner, D.; Stichel, J.; Beck-Sickinger, A. G. Molecular recognition of the NPY hormone family by their receptors. *Nutrition* **2008**, 24, 907-917.

(99) Söll, R. M.; Dinger, M. C.; Lundell, I.; Larhammer, D.; Beck-Sickinger, A. G. Novel analogues of neuropeptide Y with a preference for the Y_1 receptor. *Eur. J. Biochem.* **2001**, 268, 2828-2837.

(100) Zwanziger, D.; Böhme, I.; Lindner, D.; Beck-Sickinger, A. G. First selective agonist of the neuropeptide Y_1 receptor with reduced size. *J. Pept. Sci.* **2009**, 15, 856-866.

(101) Daniels, A. J.; Matthews, J. E.; Slepetis, R. J.; Jansen, M.; Viveros, O. H.; Tadepalli, A.; Harrington, W.; Heyer, D.; Landavazo, A.; Leban, J. J. High-affinity neuropeptide Y receptor antagonists. *Proc. Natl. Acad. Sci. U.S.A.* **1995**, 92, 9067-9071.

(102) Richardson, R. R.; Groenen, M.; Liu, M.; Mountford, S. J.; Briddon, S. J.; Holliday, N. D.; Thompson, P. E. Heterodimeric analogues of the potent Y_1R antagonist 1229U91, lacking one of the pharmacophoric C-terminal structures, retain potent Y_1R affinity and show improved selectivity over Y_4R. *J. Med. Chem.* **2020**, 63, 5274-5286.

(103) Poindexter, G. S.; Bruce, M. A.; LeBoulluec, K. L.; Monkovic, I.; Martin, S. W.; Parker, E. M.; Iben, L. G.; McGovern, R. T.; Ortiz, A. A.; Stanley, J. A.; Mattson, G. K.; Kozlowski, M.; Arcuri, M.; Antal-Zimanyi, I. Dihydropyridine neuropeptide Y Y_1 receptor antagonists. *Bioorg. Med. Chem. Lett.* **2002**, 12, 379-382.

(104) Griffith, D. A.; Hargrove, D. M.; Maurer, T. S.; Blum, C. A.; De Lombaert, S.; Inthavongsay, J. K.; Klade, L. E.; Mack, C. M.; Rose, C. R.; Sanders, M. J.; Carpino, P. A. Discovery and evaluation of pyrazolo[1,5-*a*]pyrimidines as neuropeptide Y_1 receptor antagonists. *Bioorg. Med. Chem. Lett.* **2011**, 21, 2641-2645.

(105) Kameda, M.; Ando, M.; Nakama, C.; Kobayashi, K.; Kawamoto, H.; Ito, S.; Suzuki, T.; Tani, T.; Ozaki, S.; Tokita, S.; Sato, N. Synthesis and evaluation of a series of 2,4-diaminopyridine derivatives as potential positron emission tomography tracers for neuropeptide Y Y_1 receptors. *Bioorg. Med. Chem. Lett.* **2009**, 19, 5124-5127.

(106) Hostetler, E. D.; Sanabria-Bohórquez, S.; Fan, H.; Zeng, Z.; Gantert, L.; Williams, M.; Miller, P.; O'Malley, S.; Kameda, M.; Ando, M.; Sato, N.; Ozaki, S.; Tokita, S.; Ohta, H.; Williams, D.; Sur, C.; Cook, J. J.; Burns, H. D.; Hargreaves, R. Synthesis, characterization, and monkey positron emission tomography (PET) studies of [^{18}F]Y1-

973, a PET tracer for the neuropeptide Y Y_1 receptor. *NeuroImage* **2011**, 54, 2635-2642.

(107) Rudolf, K.; Eberlein, W.; Engel, W.; Wieland, H. A.; Willim, K. D.; Entzeroth, M.; Wienen, W.; Beck-Sickinger, A. G.; Doods, H. N. The first highly potent and selective nonpeptide neuropeptide Y Y_1 receptor antagonist: BIBP3226. *Eur. J. Pharmacol.* **1994**, 271, R11-R13.

(108) Hutzler, C. Synthese und pharmakologische Aktivität neuer Neuropeptid-Y-Rezeptorliganden: Von N,N-disubstituierten Alkanamiden zu hochpotenten Y_1-Antagonisten der Argininamid-Reihe. Doctoral Thesis. University of Regensburg, Regensburg, **2001**.

(109) Keller, M.; Weiss, S.; Hutzler, C.; Kuhn, K. K.; Mollereau, C.; Dukorn, S.; Schindler, L.; Bernhardt, G.; König, B.; Buschauer, A. N^{ω}-Carbamoylation of the argininamide moiety: An avenue to insurmountable NPY Y_1 receptor antagonists and a radiolabeled selective high-affinity molecular tool ([^{3}H]UR-MK299) with extended residence time. *J. Med. Chem.* **2015**, 58, 8834-8849.

(110) Schneider, E.; Keller, M.; Brennauer, A.; Hoefelschweiger, B. K.; Gross, D.; Wolfbeis, O. S.; Bernhardt, G.; Buschauer, A. Synthesis and characterization of the first fluorescent nonpeptide NPY Y_1 receptor antagonist. *ChemBioChem* **2007**, 8, 1981-1988.

(111) Keller, M.; Erdmann, D.; Pop, N.; Pluym, N.; Teng, S.; Bernhardt, G.; Buschauer, A. Red-fluorescent argininamide-type NPY Y_1 receptor antagonists as pharmacological tools. *Biorg. Med. Chem.* **2011**, 19, 2859-2878.

(112) Keller, M.; Pop, N.; Hutzler, C.; Beck-Sickinger, A. G.; Bernhardt, G.; Buschauer, A. Guanidine−acylguanidine bioisosteric approach in the design of radioligands: synthesis of a tritium-labeled N^G-propionylargininamide ([^{3}H]-UR-MK114) as a highly potent and selective neuropeptide Y Y_1 receptor antagonist. *J. Med. Chem.* **2008**, 51, 8168-8172.

(113) Keller, M.; Bernhardt, G.; Buschauer, A. [^{3}H]UR-MK136: A highly potent and selective radioligand for neuropeptide Y Y_1 receptors. *ChemMedChem* **2011**, 6, 1566-1571.

(114) Keller, M.; Maschauer, S.; Brennauer, A.; Tripal, P.; Koglin, N.; Dittrich, R.; Bernhardt, G.; Kuwert, T.; Wester, H.-J.; Buschauer, A.; Prante, O. Prototypic ^{18}F-labeled argininamide-type neuropeptide Y Y_1R antagonists as tracers for PET imaging of mammary carcinoma. *ACS Med. Chem. Lett.* **2017**, 8, 304-309.

(115) Maschauer, S.; Ott, J. J.; Bernhardt, G.; Kuwert, T.; Keller, M.; Prante, O. ^{18}F-Labelled triazolyl-linked argininamides targeting the neuropeptide Y Y_1R for PET imaging of mammary carcinoma. *Sci. Rep.* **2019**, 9.

(116) Kanatani, A.; Ishihara, A.; Asahi, S.; Tanaka, T.; Ozaki, S.; Ihara, M. Potent neuropeptide Y Y_1 receptor antagonist, 1229U91: Blockade of neuropeptide Y-induced and physiological food intake. *Endocrinology* **1996**, 137, 3177-3182.

(117) Balasubramaniam, A.; Dhawan, V. C.; Mullins, D. E.; Chance, W. T.; Sheriff, S.; Guzzi, M.; Prabhakaran, M.; Parker, E. M. Highly selective and potent neuropeptide Y (NPY) Y_1 receptor antagonists based on [Pro^{30}, Tyr^{32}, Leu^{34}]NPY(28-36)-NH_2 (BW1911U90). *J. Med. Chem.* **2001**, 44, 1479-1482.

(118) Antal-Zimanyi, I.; Bruce, M. A.; LeBoulluec, K. L.; Iben, L. G.; Mattson, G. K.; McGovern, R. T.; Hogan, J. B.; Leahy, C. L.; Flowers, S. C.; Stanley, J. A.; Ortiz, A. A.; Poindexter, G. S. Pharmacological characterization and appetite suppressive properties of BMS-193885, a novel and selective neuropeptide Y_1 receptor antagonist. *Eur. J. Pharmacol.* **2008**, 590, 224-232.

(119) Keller, M.; Kaske, M.; Holzammer, T.; Bernhardt, G.; Buschauer, A. Dimeric argininamide-type neuropeptide Y receptor antagonists: Chiral discrimination between Y_1 and Y_4 receptors. *Biorg. Med. Chem.* **2013**, 21, 6303-6322.

(120) Yang, Z.; Han, S.; Keller, M.; Kaiser, A.; Bender, B. J.; Bosse, M.; Burkert, K.; Kögler, L. M.; Wifling, D.; Bernhardt, G.; Plank, N.; Littmann, T.; Schmidt, P.; Yi, C.; Li, B.; Ye, S.; Zhang, R.; Xu, B.; Larhammar, D.; Stevens, R. C.; Huster, D.; Meiler, J.; Zhao, Q.; Beck-Sickinger, A. G.; Buschauer, A.; Wu, B. Structural basis of ligand binding modes at the neuropeptide Y Y_1 receptor. *Nature* **2018**, 556, 520-524.

(121) Tang, T.; Hartig, C.; Chen, Q.; Zhao, W.; Kaiser, A.; Zhang, X.; Zhang, H.; Qu, H.; Yi, C.; Ma, L.; Han, S.; Zhao, Q.; Beck-Sickinger, A. G.; Wu, B. Structural basis for ligand recognition of the neuropeptide Y Y_2 receptor. *Nat. Commun.* **2021**, 12.

(122) Tang, T.; Tan, Q.; Han, S.; Diemar, A.; Löbner, K.; Wang, H.; Schüß, C.; Behr, V.; Mörl, K.; Wang, M.; Chu, X.; Yi, C.; Keller, M.; Kofoed, J.; Reedtz-Runge, S.; Kaiser, A.; Beck-Sickinger, A. G.; Zhao, Q.; Wu, B. Receptor-specific recognition of NPY peptides revealed by structures of NPY receptors. *Sci. adv.* **2022**, 8.

(123) Ballesteros, J. A., Weinstein, Harel Integrated methods for the construction of three-dimensional models and computational probing of structure-function relations in G protein-coupled receptors in *Methods in Neurosciences*, Sealfon, S. C., Eds., Academic Press, Elsevier: Amsterdam, **1995**, pp. 366-428.

(124) Faron-Górecka, A.; Szlachta, M.; Kolasa, M.; Solich, J.; Górecki, A.; Kuśmider, M.; Żurawek, D.; Dziedzicka-Wasylewska, M. Understanding GPCR dimerization. *Methods Cell Biol.* **2019**, 149, 155-178.

(125) Hübner, H.; Schellhorn, T.; Gienger, M.; Schaab, C.; Kaindl, J.; Leeb, L.; Clark, T.; Möller, D.; Gmeiner, P. Structure-guided development of heterodimer-selective GPCR ligands. *Nat. Commun.* **2016**, 7.

(126) Borroto-Escuela, D. O.; Narvaez, M.; Marcellino, D.; Parrado, C.; Narvaez, J. A.; Tarakanov, A. O.; Agnati, L. F.; Díaz-Cabiale, Z.; Fuxe, K. Galanin receptor-1 modulates 5-hydroxtryptamine-1A signaling *via* heterodimerization. *Biochem. Biophys. Res. Commun.* **2010**, 393, 767-772.

(127) Chini, B. Expanding neuropeptide signalling by multiplying receptor functional states and sub-cellular locations. *Cell Tissue Res.* **2018**, 375, 49-56.

(128) Sleno, R.; Hébert, T. E. The dynamics of GPCR oligomerization and their functional consequences in *Int. Rev. Cell Mol. Biol.*, *Vol. 338*, K., S. A., Eds., Academic Press, Elsevier: Amsterdam, **2018**, pp. 141-171.

(129) Dupré, D. J.; Hébert, T. E. Biosynthesis and trafficking of seven transmembrane receptor signalling complexes. *Cell. Signal.* **2006**, 18, 1549-1559.

(130) Ward, R. J.; Pediani, J. D.; Godin, A. G.; Milligan, G. Regulation of oligomeric organization of the serotonin 5-hydroxytryptamine 2C (5-HT_{2C}) receptor observed by spatial intensity distribution analysis. *J. Biol. Chem.* **2015**, 290, 12844-12857.

(131) Panetta, R.; Greenwood, M. T. Physiological relevance of GPCR oligomerization and its impact on drug discovery. *Drug Discov. Today* **2008**, 13, 1059-1066.

(132) Gomes, I.; Gupta, A.; Filipovska, J.; Szeto, H. H.; Pintar, J. E.; Devi, L. A. A role for heterodimerization of μ- and δ-opiate receptors in enhancing morphine analgesia. *Proc. Natl. Acad. Sci. U.S.A.* **2004**, 101, 5135-5139.

(133) Gomes, I.; Fujita, W.; Gupta, A.; Saldanha, S. A.; Negri, A.; Pinello, C. E.; Eberhart, C.; Roberts, E.; Filizola, M.; Hodder, P.; Devi, L. A. Identification of a μ-δ opioid receptor heteromer-biased agonist with antinociceptive activity. *Proc. Natl. Acad. Sci. U.S.A.* **2013**, 110, 12072-12077.

(134) Nestler, E. J.; Viñals, X.; Moreno, E.; Lanfumey, L.; Cordomí, A.; Pastor, A.; de La Torre, R.; Gasperini, P.; Navarro, G.; Howell, L. A.; Pardo, L.; Lluís, C.; Canela, E. I.; McCormick, P. J.; Maldonado, R.; Robledo, P. Cognitive impairment induced by Δ^9-tetrahydrocannabinol occurs through heteromers between cannabinoid CB_1 and serotonin 5-HT_{2A} receptors. *PLoS Biol.* **2015**, 13, e1002194.

(135) Capra, V.; Mauri, M.; Guzzi, F.; Busnelli, M.; Accomazzo, M. R.; Gaussem, P.; Nisar, S. P.; Mundell, S. J.; Parenti, M.; Rovati, G. E. Impaired thromboxane receptor dimerization reduces signaling efficiency: A potential mechanism for reduced platelet function *in vivo*. *Biochem. Pharmacol.* **2017**, 124, 43-56.

(136) Dinger, M. C.; Bader, J. E.; Kóbor, A. D.; Kretzschmar, A. K.; Beck-Sickinger, A. G. Homodimerization of neuropeptide Y receptors investigated by fluorescence resonance energy transfer in living cells. *J. Biol. Chem.* **2003**, 278, 10562-10571.

(137) Berglund, M. M.; Schober, D. A.; Esterman, M. A.; Gehlert, D. R. Neuropeptide Y Y_4 receptor homodimers dissociate upon agonist stimulation. *J. Pharmacol. Exp. Ther.* **2003**, 307, 1120-1126.

(138) Kilpatrick, L. E.; Humphrys, L. J.; Holliday, N. D. A G protein–coupled receptor dimer imaging assay reveals selectively modified pharmacology of neuropeptide Y Y_1/Y_5 receptor heterodimers. *Mol. Pharmacol.* **2015**, 87, 718-732.

(139) Gehlert, D. R.; Schober, D. A.; Morin, M.; Berglund, M. M. Co-expression of neuropeptide Y Y_1 and Y_5 receptors results in heterodimerization and altered functional properties. *Biochem. Pharmacol.* **2007**, 74, 1652-1664.

(140) Czarnecka, M.; Lu, C.; Pons, J.; Maheswaran, I.; Ciborowski, P.; Zhang, L.; Cheema, A.; Kitlinska, J. Neuropeptide Y receptor interactions regulate its mitogenic activity. *Neuropeptides* **2019**, 73, 11-24.

(141) Ruscica, M.; Dozio, E.; Motta, M.; Magni, P. NPY family of peptides in endocrine, breast and prostate tumors in *The NPY family of peptides in immune disorders, inflammation, angiogenesis and cancer*, 1st ed.; Zukowska, Z. F. G., Eds., Birkhäuser: Basel, **2005**, pp. 237-248.

(142) Li, J.; Tian, Y.; Wu, A. Neuropeptide Y receptors: a promising target for cancer imaging and therapy. *Regenerative Biomaterials* **2015**, 2, 215-219.

(143) Körner, M.; Reubi, J. C. NPY receptors in human cancer: A review of current knowledge. *Peptides* **2007**, 28, 419-425.

(144) Zhang, L.; Bijker, M. S.; Herzog, H. The neuropeptide Y system: Pathophysiological and therapeutic implications in obesity and cancer. *Pharmacol. Ther.* **2011**, 131, 91-113.

(145) Lin, S.-t.; Li, Y.-z.; Sun, X.-q.; Chen, Q.-q.; Huang, S.-f.; Lin, S.; Cai, S.-q. Update on the role of neuropeptide Y and other related factors in breast cancer and osteoporosis. *Front. Endocrinol.* **2021**, 12.

(146) Ruscica, M.; Dozio, E.; Motta, M.; Magni, P. Relevance of the neuropeptide Y system in the biology of cancer progression. *Curr. Top. Med. Chem.* **2007**, 7, 1682-1691.

(147) Reubi, J. C.; Gugger, M.; Waser, B.; Schaer, J. C. Y_1-mediated effect of neuropeptide Y in cancer: Breast carcinomas as targets. *Cancer Res.* **2001**, 61, 4636-41.

(148) Körner, M.; Waser, B.; Reubi, J. C. Neuropeptide Y receptor expression in human primary ovarian neoplasms. *Lab. Invest.* **2003**, 84, 71-80.

(149) Körner, M.; Waser, B.; Reubi, J. C. High Expression of Neuropeptide Y1 Receptors in Ewing Sarcoma Tumors. *Clin. Cancer. Res.* **2008**, 14, 5043-5049.

(150) Körner, M.; Waser, B.; Reubi, J. C. High Expression of Neuropeptide Y Receptors in Tumors of the Human Adrenal Gland and Extra-Adrenal Paraganglia. *Clin. Cancer. Res.* **2004**, 10, 8426-8433.

(151) Lu, C.; Everhart, L.; Tilan, J.; Kuo, L.; Sun, C. C. J.; Munivenkatappa, R. B.; Jönsson-Rylander, A. C.; Sun, J.; Kuan-Celarier, A.; Li, L.; Abe, K.; Zukowska, Z.; Toretsky, J. A.; Kitlinska, J. Neuropeptide Y and its Y_2 receptor: potential targets in neuroblastoma therapy. *Oncogene* **2010**, 29, 5630-5642.

(152) Reubi, J. C.; Körner, M.; Waser, B.; Mazzucchelli, L.; Guillou, L. High expression of peptide receptors as a novel target in gastrointestinal stromal tumours. *Eur. J. Nucl. Med. Mol. Imag.* **2004**, 31, 803-810.

(153) Zukowska-Grojec, Z.; Karwatowska-Prokopczuk, E.; Fisher, T. A.; Ji, H. Mechanisms of vascular growth-promoting effects of neuropeptide Y: Role of its inducible receptors. *Regul. Pept.* **1998**, 75-76, 231-238.

(154) Ekstrand, A. J.; Cao, R.; Björndahl, M.; Nyström, S.; Jönsson-Rylander, A.-C.; Hassani, H.; Hallberg, B.; Nordlander, M.; Cao, Y. Deletion of neuropeptide Y_2 receptor in mice results in blockage of NPY-induced angiogenesis and delayed wound healing. *Proc. Natl. Acad. Sci. U.S.A.* **2003**, 100, 6033-6038.

(155) Zukowska-Grojec, Z.; Karwatowska-Prokopczuk, E.; Rose, W.; Rone, J.; Movafagh, S.; Ji, H.; Yeh, Y.; Chen, W.-T.; Kleinman, H. K.; Grouzmann, E.; Grant, D. S. Neuropeptide Y. *Circul. Res.* **1998**, 83, 187-195.

(156) Kitlinska, J.; Abe, K.; Kuo, L.; Pons, J.; Yu, M.; Li, L.; Tilan, J.; Everhart, L.; Lee, E. W.; Zukowska, Z.; Toretsky, J. A. Differential effects of neuropeptide Y on the growth and vascularization of neural crest–derived tumors. *Cancer Res.* **2005**, 65, 1719-1728.

(157) McDermott, B.; Bell, D. NPY and cardiac diseases. *Curr. Top. Med. Chem.* **2007**, 7, 1692-1703.

(158) Kitlinska, J.; Kuo, L.; Abe, K.; Pons, J.; Yu, M.; Li, L.; Tilan, J.; Toretsky, J.; Zukowska, Z. Role of neuropeptide Y and dipeptidyl peptidase IV in regulation of Ewing's sarcoma growth. *Adv. Exp. Med. Biol.* **2006**, 575, 223-229.

(159) Nagakawa, O.; Ogasawara, M.; Murata, J.; Fuse, H.; Saiki, I. Effect of prostatic neuropeptides on migration of prostate cancer cell lines. *Int. J. Urol.* **2008**, 8, 65-70.

(160) Nagakawa, O.; Ogasawara, M.; Fujii, H.; Murakami, K.; Murata, J.; Fuse, H.; Saiki, I. Effect of prostatic neuropeptides on invasion and migration of PC-3 prostate cancer cells. *Cancer Lett.* **1998**, 133, 27-33.

(161) Ogasawara, M.; Murata, J.; Ayukawa, K.; Saimi, I. Differential effect of intestinal neuropeptides on invasion and migration of colon carcinoma cells *in vitro*. *Cancer Lett.* **1997**, 116, 111-116.

(162) Reubi, J.; Gugger, M.; Waser, B. Co-expressed peptide receptors in breast cancer as a molecular basis for *in vivo* multireceptor tumour targeting. *Eur. J. Nucl. Med. Mol. Imag.* **2002**, 29, 855-862.

(163) Yu, Z.; Xia, Y.; Xing, J.; Li, Z.; Zhen, J.; Jin, Y.; Tian, Y.; Liu, C.; Jiang, Z.; Li, J.; Wu, A. Y_1-receptor–ligand-functionalized ultrasmall upconversion nanoparticles for tumor-targeted trimodality imaging and photodynamic therapy with low toxicity. *Nanoscale* **2018**, 10, 17038-17052.

(164) Liu, L. E. I.; Xu, Q.; Cheng, L.; Ma, C.; Xiao, L.; Xu, D.; Gao, Y.; Wang, J.; Song, H. NPY Y_1R is a novel peripheral blood marker predictive of metastasis and prognosis in breast cancer patients. *Oncol. Lett.* **2015**, 9, 891-896.

(165) Vall-Sagarra, A.; Litau, S.; Decristoforo, C.; Wängler, B.; Schirrmacher, R.; Fricker, G.; Wängler, C. Design, synthesis, *in vitro*, and initial *in vivo* evaluation of heterobivalent peptidic ligands targeting both NPY Y_1- and GRP-receptors—An improvement for breast cancer imaging? *Pharmaceuticals* **2018**, 11, 65.

(166) Memminger, M.; Keller, M.; Lopuch, M.; Pop, N.; Bernhardt, G.; von Angerer, E.; Buschauer, A. The neuropeptide Y Y receptor: a diagnostic marker? Expression in MCF-7 breast cancer cells is downregulated by antiestrogens *in vitro* and in xenografts. *PLoS One* **2012**, 7, e51032.

(167) Soave, M.; Briddon, S. J.; Hill, S. J.; Stoddart, L. A. Fluorescent ligands: Bringing light to emerging GPCR paradigms. *Br. J. Pharmacol.* **2020**, 177, 978-991.

(168) Stoddart, L. A.; White, C. W.; Nguyen, K.; Hill, S. J.; Pfleger, K. D. G. Fluorescence- and bioluminescence-based approaches to study GPCR ligand binding. *Br. J. Pharmacol.* **2016**, 173, 3028-3037.

(169) Sridharan, R.; Zuber, J.; Connelly, S. M.; Mathew, E.; Dumont, M. E. Fluorescent approaches for understanding interactions of ligands with G protein coupled receptors. *Biochim. Biophys. Acta* **2014**, 1838, 15-33.

(170) Waller, A.; Simons, P.; Prossnitz, E.; Edwards, B.; Sklar, L. High throughput screening of G protein-coupled receptors *via* flow cytometry. *Combinatorial Chem. High Throughput Screening* **2003**, 6, 389-397.

(171) Sklar, L. A.; Sayre, J.; McNeil, V. M.; Finney, D. A. Competitive binding kinetics in ligand-receptor-competitor systems: Rate parameters for unlabeled ligands for the formyl peptide receptor. *Mol. Pharmacol.* **1985**, 28, 323-30.

(172) Schneider, E.; Mayer, M.; Ziemek, R.; Li, L.; Hutzler, C.; Bernhardt, G.; Buschauer, A. A simple and powerful flow cytometric method for the simultaneous determination of multiple parameters at G protein-coupled receptor subtypes. *ChemBioChem* **2006**, 7, 1400-1409.

(173) Ziemek, R.; Brennauer, A.; Schneider, E.; Cabrele, C.; Beck-Sickinger, A. G.; Bernhardt, G.; Buschauer, A. Fluorescence- and luminescence-based methods for the determination of affinity and activity of neuropeptide Y_2 receptor ligands. *Eur. J. Pharmacol.* **2006**, 551, 10-18.

(174) Ziemek, R.; Schneider, E.; Kraus, A.; Cabrele, C.; Beck-Sickinger, A. G.; Bernhardt, G.; Buschauer, A. Determination of affinity and activity of ligands at the human neuropeptide Y Y_4 receptor by flow cytometry and aequorin luminescence. *J. Recept. Signal Transduct.* **2007**, 27, 217-233.

(175) May, L. T.; Self, T. J.; Briddon, S. J.; Hill, S. J. The effect of allosteric modulators on the kinetics of agonist-G protein-coupled receptor interactions in single living cells. *Mol. Pharmacol.* **2010**, 78, 511-523.

(176) May, L. T.; Bridge, L. J.; Stoddart, L. A.; Briddon, S. J.; Hill, S. J. Allosteric interactions across native adenosine-A3 receptor homodimers: quantification using single-cell ligand-binding kinetics. *FASEB J.* **2011**, 25, 3465-3476.

(177) Stoddart, Leigh A.; Vernall, Andrea J.; Denman, Jessica L.; Briddon, Stephen J.; Kellam, B.; Hill, Stephen J. Fragment screening at adenosine-A3 receptors in living cells using a fluorescence-based binding assay. *Chem. Biol.* **2012**, 19, 1105-1115.

(178) Biselli, S.; Alencastre, I.; Tropmann, K.; Erdmann, D.; Chen, M.; Littmann, T.; Maia, A. F.; Gomez-Lazaro, M.; Tanaka, M.; Ozawa, T.; Keller, M.; Lamghari, M.; Buschauer, A.; Bernhardt, G. Fluorescent H_2 receptor squaramide-type antagonists: synthesis, characterization, and applications. *ACS Med. Chem. Lett.* **2020**, 11, 1521-1528.

(179) Keller, M.; Mahuroof, S. A.; Hong Yee, V.; Carpenter, J.; Schindler, L.; Littmann, T.; Pegoli, A.; Hübner, H.; Bernhardt, G.; Gmeiner, P.; Holliday, N. D. Fluorescence labeling of neurotensin(8–13) *via* arginine residues gives molecular tools with high receptor affinity. *ACS Med. Chem. Lett.* **2020**, 11, 16-22.

(180) Stoddart, L. A.; Vernall, A. J.; Bouzo-Lorenzo, M.; Bosma, R.; Kooistra, A. J.; de Graaf, C.; Vischer, H. F.; Leurs, R.; Briddon, S. J.; Kellam, B.; Hill, S. J. Development of novel fluorescent histamine H_1 receptor antagonists to study ligand-binding kinetics in living cells. *Sci. Rep.* **2018**, 8.

(181) Grätz, L.; Tropmann, K.; Bresinsky, M.; Müller, C.; Bernhardt, G.; Pockes, S. NanoBRET binding assay for histamine H_2 receptor ligands using live recombinant HEK293T cells. *Sci. Rep.* **2020**, 10.

(182) Rosier, N.; Grätz, L.; Schihada, H.; Möller, J.; Işbilir, A.; Humphrys, L. J.; Nagl, M.; Seibel, U.; Lohse, M. J.; Pockes, S. A versatile sub-nanomolar fluorescent ligand enables NanoBRET binding studies and single-molecule microscopy at the histamine H_3 receptor. *J. Med. Chem.* **2021**, 64, 11695-11708.

(183) Mocking, T. A. M.; Verweij, E. W. E.; Vischer, H. F.; Leurs, R. Homogeneous, real-time NanoBRET binding assays for the histamine H_3 and H_4 receptors on living cells. *Mol. Pharmacol.* **2018**, 94, 1371-1381.

(184) Stoddart, L. A.; Johnstone, E. K. M.; Wheal, A. J.; Goulding, J.; Robers, M. B.; Machleidt, T.; Wood, K. V.; Hill, S. J.; Pfleger, K. D. G. Application of BRET to monitor ligand binding to GPCRs. *Nat. Methods* **2015**, 12, 661-663.

(185) White, C. W.; Johnstone, E. K. M.; See, H. B.; Pfleger, K. D. G. NanoBRET ligand binding at a GPCR under endogenous promotion facilitated by CRISPR/Cas9 genome editing. *Cell. Signal.* **2019**, 54, 27-34.

(186) Bouzo-Lorenzo, M.; Stoddart, L. A.; Xia, L.; Ijzerman, A. P.; Heitman, L. H.; Briddon, S. J.; Hill, S. J. A live cell NanoBRET binding assay allows the study of ligand-binding kinetics to the adenosine A_3 receptor. *Purinergic Signal.* **2019**, 15, 139-153.

(187) Alcobia, D. C.; Ziegler, A. I.; Kondrashov, A.; Comeo, E.; Mistry, S.; Kellam, B.; Chang, A.; Woolard, J.; Hill, S. J.; Sloan, E. K. Visualizing ligand binding to a GPCR *in vivo* using NanoBRET. *iScience* **2018**, 6, 280-288.

(188) Ali, A.; Johnstone, E. K. M.; Baby, B.; See, H. B.; Song, A.; Rosengren, K. J.; Pfleger, K. D. G.; Ayoub, M. A.; Vijayan, R. Insights into the interaction of LVV-hemorphin-7 with angiotensin II type 1 receptor. *Int. J. Mol. Sci.* **2020**, 22, 209.

(189) Grätz, L.; Müller, C.; Pegoli, A.; Schindler, L.; Bernhardt, G.; Littmann, T. Insertion of Nanoluc into the extracellular loops as a complementary method to establish BRET-based binding assays for GPCRs. *ACS Pharmacol. Transl. Sci.* **2022**.

(190) Allikalt, A.; Kopanchuk, S.; Rinken, A. Implementation of fluorescence anisotropy-based assay for the characterization of ligand binding to dopamine D_1 receptors. *Eur. J. Pharmacol.* **2018**, 839, 40-46.

(191) Link, R.; Veiksina, S.; Rinken, A.; Kopanchuk, S. Characterization of ligand binding to melanocortin 4 receptors using fluorescent peptides with improved kinetic properties. *Eur. J. Pharmacol.* **2017**, 799, 58-66.

(192) Reiner, D.; Stark, H. Ligand binding kinetics at histamine H_3 receptors by fluorescence-polarization with real-time monitoring. *Eur. J. Pharmacol.* **2019**, 848, 112-120.

(193) Rinken, A.; Lavogina, D.; Kopanchuk, S. Assays with detection of fluorescence anisotropy: Challenges and possibilities for characterizing ligand binding to GPCRs. *Trends Pharmacol. Sci.* **2018**, 39, 187-199.

(194) Grätz, L.; Laasfeld, T.; Allikalt, A.; Gruber, C. G.; Pegoli, A.; Tahk, M.-J.; Tsernant, M.-L.; Keller, M.; Rinken, A. BRET- and fluorescence anisotropy-based assays for real-time monitoring of ligand binding to M_2 muscarinic acetylcholine receptors. *Biochim. Biophys. Acta* **2021**, 1868, 118930.

(195) Iliopoulos-Tsoutsouvas, C.; Kulkarni, R. N.; Makriyannis, A.; Nikas, S. P. Fluorescent probes for G protein-coupled receptor drug discovery. *Expert Opin. Drug Discov.* **2018**, 13, 933-947.

(196) Nienhaus, G. U.; Nienhaus, K. Fluorescence Labeling in *Fluorescence microscopy: From principles to biological applications*, *Vol. 12*, 1st ed.; Kubitscheck, U., Eds., Wiley-VCH: Weinheim, **2017**, pp. 133-164.

(197) Salvadori, P. A.; Filidei, E.; Giorgetti, A. Positron-emitting radiopharmaceuticals in *Nuclear Medicine Textbook: Methodology and Clinical Applications*, 1st ed.; Volterrani, D.; Carrió, I.; Mariani, G.; Erba, P. A.; Strauss, H. W., Eds., Springer: Cham, Switzerland, **2019**, pp. 57-98.

(198) Talip, Z.; Favaretto, C.; Geistlich, S.; van der Meulen, N. P. A step-by-step guide for the novel radiometal production for medical applications: Case studies with ^{68}Ga, ^{44}Sc, ^{177}Lu and ^{161}Tb. *Molecules* **2020**, 25, 966.

(199) Werner, R. A.; Chen, X.; Hirano, M.; Rowe, S. P.; Lapa, C.; Javadi, M. S.; Higuchi, T. SPECT vs. PET in cardiac innervation imaging: Clash of the titans. *Clin. Transl. Imaging* **2018**, 6, 293-303.

(200) Davison, C. M.; O'Brien, J. T. A comparison of FDG-PET and blood flow SPECT in the diagnosis of neurodegenerative dementias: A systematic review. *Int. J. Geriatr. Psychiatry* **2014**, 29, 551-561.

(201) Yang, C.-T.; Ghosh, K. K.; Padmanabhan, P.; Langer, O.; Liu, J.; Eng, D. N. C.; Halldin, C.; Gulyás, B. PET-MR and SPECT-MR multimodality probes: Development and challenges. *Theranostics* **2018**, 8, 6210-6232.

(202) Zhang, C.; Yan, Y.; Zou, Q.; Chen, J.; Li, C. Superparamagnetic iron oxide nanoparticles for MR imaging of pancreatic cancer: Potential for early diagnosis through targeted strategies. *Asia Pac. J. Clin. Oncol.* **2016**, 12, 13-21.

(203) Merinopoulos, I.; Gunawardena, T.; Stirrat, C.; Cameron, D.; Eccleshall, S. C.; Dweck, M. R.; Newby, D. E.; Vassiliou, V. S. Diagnostic applications of ultrasmall superparamagnetic particles of iron oxide for imaging myocardial and vascular inflammation. *JACC Cardiovasc. Imaging* **2021**, 14, 1249-1264.

(204) Doot, R. K.; Dubroff, J. G.; Labban, K. J.; Mach, R. H. Selectivity of probes for PET imaging of dopamine D_3 receptors. *Neurosci. Lett.* **2019**, 691, 18-25.

(205) Sheline, Y. I.; Mintun, M. A.; Barch, D. M.; Wilkins, C.; Snyder, A. Z.; Moerlein, S. M. Decreased hippocampal 5-HT_{2A} receptor binding in older depressed patients using [^{18}F]altanserin positron emission tomography. *Neuropsychopharmacology* **2004**, 29, 2235-2241.

(206) Smigielski, L.; Wotruba, D.; Treyer, V.; Rössler, J.; Papiol, S.; Falkai, P.; Grünblatt, E.; Walitza, S.; Rössler, W. The interplay between postsynaptic striatal $D_{2/3}$ receptor availability, adversity exposure and odd beliefs: A [^{11}C]-raclopride PET study. *Schizophr. Bull.* **2021**, 47, 1495-1508.

(207) Tedroff, J.; Pedersen, M.; Aquilonius, S. M.; Hartvig, P.; Jacobsson, G.; Langstrom, B. Levodopa-induced changes in synaptic dopamine in patients with Parkinson's disease as measured by [^{11}C]raclopride displacement and PET. *Neurology* **1996**, 46, 1430-1430.

(208) Domino, E. F.; Hirasawa-Fujita, M.; Ni, L.; Guthrie, S. K.; Zubieta, J. K. Regional brain [^{11}C]carfentanil binding following tobacco smoking. *Prog. Neuro-Psychopharmacol. Biol. Psychiatry* **2015**, 59, 100-104.

(209) Zubieta, J.-K.; Gorelick, D. A.; Stauffer, R.; Ravert, H. T.; Dannals, R. F.; Frost, J. J. Increased μ-opioid receptor binding detected by PET in cocaine–dependent men is associated with cocaine craving. *Nat. Med.* **1996**, 2, 1225-1229.

(210) Hsu, D. T.; Sanford, B. J.; Meyers, K. K.; Love, T. M.; Hazlett, K. E.; Wang, H.; Ni, L.; Walker, S. J.; Mickey, B. J.; Korycinski, S. T.; Koeppe, R. A.; Crocker, J. K.; Langenecker, S. A.; Zubieta, J. K. Response of the μ-opioid system to social rejection and acceptance. *Mol. Psychiatry* **2013**, 18, 1211-1217.

(211) Kennedy, S. E.; Koeppe, R. A.; Young, E. A.; Zubieta, J.-K. Dysregulation of endogenous opioid emotion regulation circuitry in major depression in women. *Arch. Gen. Psychiatry* **2006**, 63, 1199.

(212) Sanli, Y.; Garg, I.; Kandathil, A.; Kendi, T.; Zanetti, M. J. B.; Kuyumcu, S.; Subramaniam, R. M. Neuroendocrine tumor diagnosis and management: ^{68}Ga-DOTATATE PET/CT. *Am. J. Roentgenol.* **2018**, 211, 267-277.

(213) Gourni, E.; Demmer, O.; Schottelius, M.; D'Alessandria, C.; Schulz, S.; Dijkgraaf, I.; Schumacher, U.; Schwaiger, M.; Kessler, H.; Wester, H.-J. PET of CXCR4 expression by a ^{68}Ga-labeled highly specific targeted contrast agent. *J. Nucl. Med.* **2011**, 52, 1803-1810.

(214) Pan, Q.; Cao, X.; Luo, Y.; Li, J.; Feng, J.; Li, F. Chemokine receptor-4 targeted PET/CT with ^{68}Ga-Pentixafor in assessment of newly diagnosed multiple myeloma: comparison to ^{18}F-FDG PET/CT. *Eur. J. Nucl. Med. Mol. Imag.* **2019**, 47, 537-546.

(215) Lapa, C.; Lückerath, K.; Kleinlein, I.; Monoranu, C. M.; Linsenmann, T.; Kessler, A. F.; Rudelius, M.; Kropf, S.; Buck, A. K.; Ernestus, R.-I.; Wester, H.-J.; Löhr, M.; Herrmann, K. ^{68}Ga-Pentixafor-PET/CT for imaging of chemokine receptor 4 expression in glioblastoma. *Theranostics* **2016**, 6, 428-434.

(216) Weich, A.; Werner, R. A.; Buck, A. K.; Hartrampf, P. E.; Serfling, S. E.; Scheurlen, M.; Wester, H.-J.; Meining, A.; Kircher, S.; Higuchi, T.; Pomper, M. G.; Rowe, S. P.; Lapa, C.; Kircher, M. CXCR4-Directed PET/CT in patients with newly diagnosed neuroendocrine carcinomas. *Diagnostics* **2021**, 11, 605.

(217) Mansi, R.; Wang, X.; Forrer, F.; Waser, B.; Cescato, R.; Graham, K.; Borkowski, S.; Reubi, J. C.; Maecke, H. R. Development of a potent DOTA-conjugated bombesin

antagonist for targeting GRPR-positive tumours. *Eur. J. Nucl. Med. Mol. Imag.* **2010**, 38, 97-107.

(218) Schollhammer, R.; de Clermont Gallerande, H.; Robert, G.; Yacoub, M.; Vimont, D.; Hindié, E.; Fernandez, P.; Morgat, C. ^{68}Ga-PSMA-617 compared with ^{68}Ga-RM2 and ^{18}F-F-choline PET/CT for the initial staging of high-risk prostate cancer. *Clin. Nucl. Med.* **2019**, 44, e535-e536.

(219) Hoberück, S.; Michler, E.; Wunderlich, G.; Löck, S.; Hölscher, T.; Froehner, M.; Braune, A.; Ivan, P.; Seppelt, D.; Zöphel, K.; Kotzerke, J. ^{68}Ga-RM2 PET in PSMA- positive and -negative prostate cancer patients. *Nuklearmedizin* **2019**, 58, 352-362.

(220) Hofmann, S.; Maschauer, S.; Kuwert, T.; Beck-Sickinger, A. G.; Prante, O. Synthesis and *in vitro* and *in vivo* evaluation of an ^{18}F-labeled neuropeptide Y analogue for imaging of breast cancer by PET. *Mol. Pharm.* **2015**, 12, 1121-1130.

Chapter 2

Structure-based design of high-affinity fluorescent probes for the neuropeptide Y Y_1 receptor

Note: This chapter (except for the characterization of compound **2.40** in section 2.2.6) was published in collaboration with cooperation partners prior to the submission of this thesis (Figure 2.5 and Table 2.3 differ from the published version due to the addition of flow cytometric binding data of **2.40**):

Müller, C.; Gleixner, J.; Tahk, M.-J.; Kopanchuk, S.; Laasfeld, T.; Weinhart, M.; Schollmeyer, D.; Betschart, M. U.; Lüdeke, S.; Koch, P.; Rinken, A.; Keller, M. Structure-based design of high-affinity fluorescent probes for the neuropeptide Y Y_1 receptor. *J. Med. Chem.* **2022**, 65, 5, 4832-4853. Reused with permission from ACS Medicinal Chemistry Letters. Copyright 2022 American Chemical Society. https://doi.org/10.1021/acs.jmedchem.1c02033

Author contributions: Christoph Müller synthesized and analytically characterized all chemical compounds. Jakob Gleixner performed fractional crystallization to afford (*R*)-**2.16** and measured optical rotation. Michael Weinhart supported compound crystallization. Dieter Schollmeyer performed X-ray diffraction analysis. Martin Ulrich Betschart and Steffen Lüdeke explored stereochemistry by CD spectroscopy. Christoph Müller performed radioligand competition binding assays, Calcium Fura-2 assays, flow cytometry-based binding assays and fluorescence spectroscopy. Christoph Müller, Maris-Johanna Tahk and Tõnis Laasfeld performed fluorescence anisotropy-based assays. Sergei Kopanchuk studied Y_1 receptor binding by confocal microscopy. Max Keller initiated and planned the project. Pierre Koch, Ago Rinken, Steffen Lüdeke and Max Keller supervised the research.

2.1 Introduction

In humans, the neuropeptide Y (NPY) receptor family comprises four subtypes (Y_1R, Y_2R, Y_4R and Y_5R), which are all members of the superfamily of G protein-coupled receptors. NPY receptors are endogenously targeted by the linear 36-amino acid peptides neuropeptide Y, peptide YY (PYY), and pancreatic polypeptide (PP).[1] The regulation of various physiological processes has been attributed to the NPY receptor family. For instance, the Y_1R mediates increased food intake and anxiolytic effects. It is also involved in the regulation of the cardiovascular system, learning and cognitive processes, sexual behavior as well as alcohol and drug addiction.[2-8] The Y_1R and Y_2R are expressed in various malign tumors such as mamma carcinoma (Y_1R) and pancreatic adenocarcinoma (Y_1R, Y_2R). Thus, labeled Y_1 and Y_2 receptor ligands represent potential tools for tumor diagnosis.[9-16] Previous structure-activity relationship studies with (*R*)-argininamide-type Y_1R antagonists derived from BIBP3226 (**2.1**[17], Figure 2.1, panel A), focusing on the modification of the arginine side chain (N^{ω}-acylation and N^{ω}-carbamoylation),[18, 19] yielded the high-affinity Y_1R antagonist UR-MK299 (**2.2**, Figure 2.1, panel A) and its tritiated analogue [^{3}H]UR-MK299.[20] However, the attachment of fluorescent dyes *via* the modified arginine side chain (e.g. **2.3**-**2.5**[20-22]) resulted in fluorescent ligands with markedly lower Y_1R affinity ($pK_i < 8$) compared to **2.1** and **2.2** (Figure 2.1, panel A). Noteworthily, N^{ω}-carbamoylated derivatives of **2.1** are chemically stable in aqueous media in contrast to N^{ω}-acylated argininamides such as **2.3**, which are prone to hydrolytic cleavage (acylguanidine moiety).[19, 21] In addition to the nonpeptidic fluorescent Y_1R ligands derived from antagonist **2.1**,[21, 22] several fluorescence-labeled peptidic Y_1R ligands were reported, typically featuring low receptor subtype selectivity.[23-27]

The recently reported crystal structure of the human Y_1R (hY_1R) in complex with **2.2** (PDB ID: 5ZBQ[28]) provided an explanation for the decrease in Y_1R binding affinity when bulky fluorescent dyes are attached *via* the acylated or carbamoylated guanidine moiety: the N^{ω}-carbamoyl substituent is deeply buried in the binding pocket (Figure 2.1, panel B), revealing that bulky attachments to the guanidino group are incompatible with the binding mode of **2.2**. Taking advantage of this insight, we identified the diphenylacetyl moiety, which is facing the receptor surface according to the crystal structure, as the most beneficial position for the attachment of bulky moieties such as fluorescent dyes (Figure 2.1, panel B). We hypothesized that attachment of a fluorophore *via* a spacer to one of the two phenyl rings in **2.2** should not considerably impair Y_1R binding due to location of the fluorescent label outside of the binding pocket. As this structural modification generated a second chiral center (methine carbon of the diphenylacetyl moiety), the presented approach included the elucidation of the absolute stereochemistry of the new stereocenter and the investigation of (*R,R*)- and (*S,R*)-configured diastereomers with respect to Y_1, Y_2, Y_4 and Y_5 receptor affinity and Y_1R antagonism.

Additionally, Y_1R binding of selected probes was investigated by flow cytometry (FC), widefield and total internal reflection fluorescence (TIRF) microscopy and in fluorescence anisotropy (FA)-based assays.

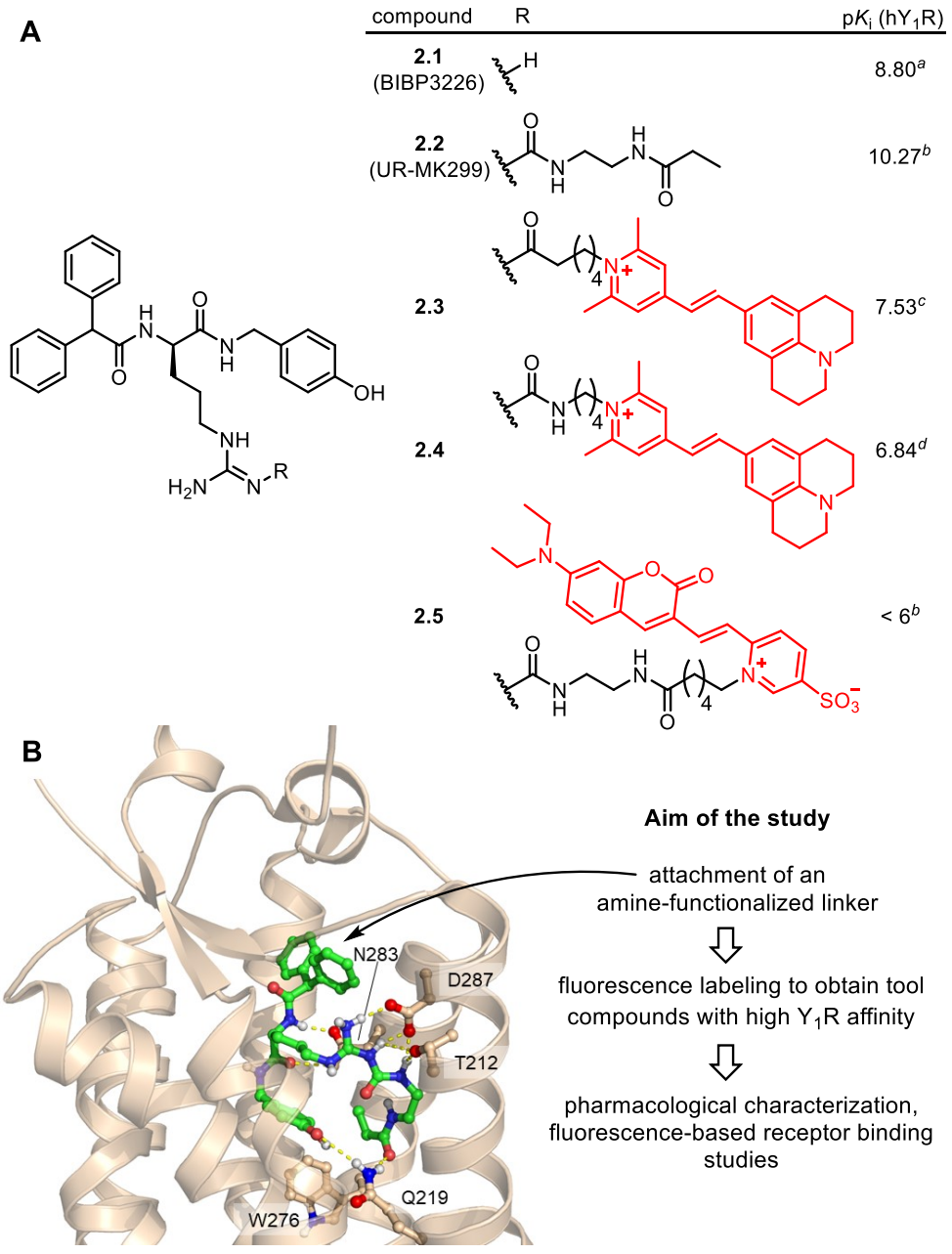

Figure 2.1. (A) Structures and Y_1R affinities (pK_i values) of BIBP3226 (**2.1**[17]), UR-MK299 (**2.2**[20]) and the previously reported fluorescent ligands **2.3**,[22] **2.4**[21] and **2.5**,[20] where the fluorescent dye (pyrylium/pyridinium dye Py1 in **2.3** and **2.4**, Red Mega 480 in **2.5**) was attached to the guanidino group *via* an N^{ω}-acyl (**2.3**) or an N^{ω}-carbamoyl (**2.4**, **2.5**) linker. (B) Binding site of **2.2** in the human Y_1R as identified by crystallization of the Y_1R in complex with **2.2** (PDB ID: 5ZBQ[28]) and rationale of the present study, i.e. the introduction of amine-functionalized substituents in *meta* or *para* position at one of the phenyl rings of **2.2** followed by the preparation and characterization of fluorescent Y_1R ligands. [a]Keller *et al.*;[18] [b]Keller *et al.*;[20] [c]Schneider *et al.*;[22] [d]Keller *et al.*[21] Y_1R binding data of **2.1**-**2.5**, previously reported as K_i, were re-evaluated to obtain the pK_i values.

2.2 Results and discussion

2.2.1 Synthesis and stereochemical discrimination of (*R*)-2.14 and (*S*)-2.14

The synthetic route towards amine-functionalized NPY Y_1 receptor ligands derived from argininamide **2.2**, needed as precursors for fluorescence labeling, included the preparation of two key intermediates: isothiourea derivative **2.10** and (*R*)-configured ornithinamide **2.13**, which were converted to N^{ω}-carbamoylated argininamide **2.14** by a mercury(II)-assisted guanidinylation reaction (Scheme 2.1). For the synthesis of the guanidinylating agent **2.10**, isothiourea derivative **2.6** (*cf*. section A.2.1 and supplementary Scheme A2.1) was deprotected under acidic conditions to obtain amine **2.7**. Subsequent propionylation at the primary amino group using succinimidyl ester **2.8** resulted in propionamide **2.9**, which was Boc-protected to obtain **2.10**. N^{α}-acylation of ornithinamide **2.11** using racemic diphenylacetic acid derivative **2.12** (*cf.* section A.2.1 and supplementary Scheme A2.1) gave a 1:1 mixture of the diastereomers (*S*,*R*)-**2.13** and (*R*,*R*)-**2.13** (Scheme 2.1). Hydrogenolytic cleavage of the Cbz protecting group in **2.13** followed by guanidinylation using **2.10** in the presence of mercury(II) chloride and subsequent treatment with TFA to remove acid-labile protecting groups afforded a mixture of (*S*,*R*)-**2.14** and (*R*,*R*)-**2.14**. The latter were separated by achiral preparative RP-HPLC, at this stage with unknown stereochemistry with respect to the chiral center of the diphenylacetyl moiety.

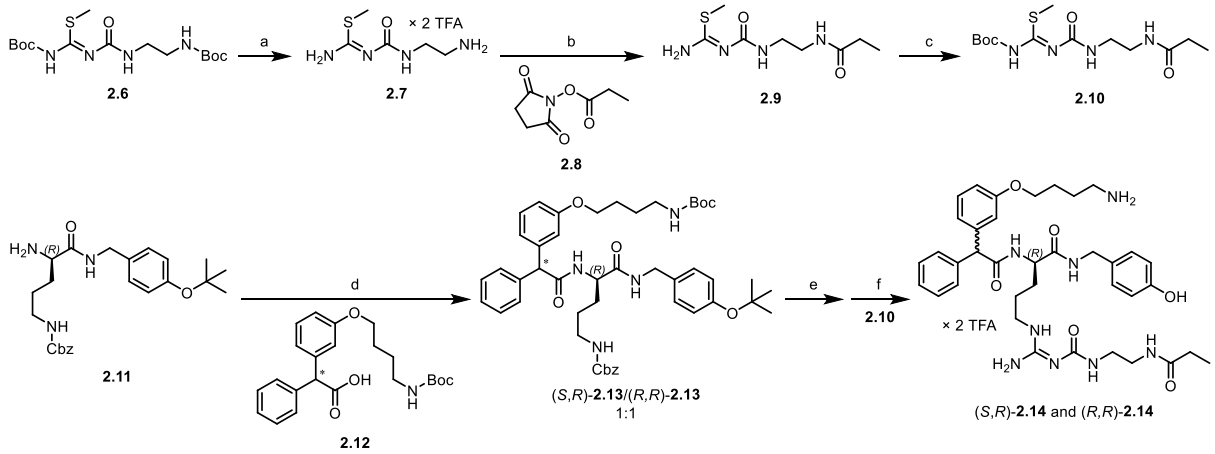

Scheme 2.1. Synthesis of the amine-functionalized argininamide-type Y_1R antagonists (*S,R*)-**2.14** and (*R,R*)-**2.14**. The asterisks in **2.12** and **2.13** indicate racemic and diastereomeric mixtures, respectively. The wavy bond in **2.14** indicates either configuration, *S* or *R*. Reagents and conditions: a) TFA, CH_2Cl_2, 900 mbar, rt, 16 h, 91%; b) Et_3N, CH_2Cl_2, rt, 1 h, 79%; c) di-*tert*-butyldicarbonate, DMAP, Et_3N, CH_2Cl_2, rt, 2 h, 73%; d) HBTU, HOBt, DIPEA, DMF, 0 °C, 15 min, 64%; e) H_2, Pd/C, trifluoroethanol, rt, 3 h; f) (1) mercury(II) chloride, DIPEA, CH_2Cl_2, rt, 30 min; (2) TFA, CH_2Cl_2, 900 mbar, rt, 3 h, 23% ((*S*,*R*)-**2.14**), 8% ((*R*,*R*)-**2.14**). Note: (*S*,*R*)-**2.14** and (*R*,*R*)-**2.14** were separated and isolated by preparative RP-HPLC.

Efforts to obtain crystals of (*S*,*R*)-**2.14** or (*R*,*R*)-**2.14** as well as derivatives of (*S*,*R*)-**2.14** (e.g. conjugates with camphorsulfonic acid and 1-naphtoic acid) suitable for X-ray crystallography

were unsuccessful. Therefore, to explore the stereochemistry of the diphenylacetyl moiety in **2.14**, a racemic mixture of carboxylic acid **2.16** (obtained from nitrile **2.15**) was subjected to repeated fractional crystallization using (*R*)-(+)-1-phenylethylamine as a base to yield (*R*)-**2.16** in 90% *ee* (Scheme 2.2), as determined by ^{1}H-NMR spectroscopy of (*R*)-**2.16** in the presence of (−)-cinchonidine (supplementary Figure A2.1 in section A.2.3). The stereochemistry of (*R*)-**2.16** could be solved by X-ray diffraction analysis of single crystals of the free carboxylic acid obtained after separation from the chiral base by extraction (Figure 2.2, for crystallographic data *cf*. section A.2.4).

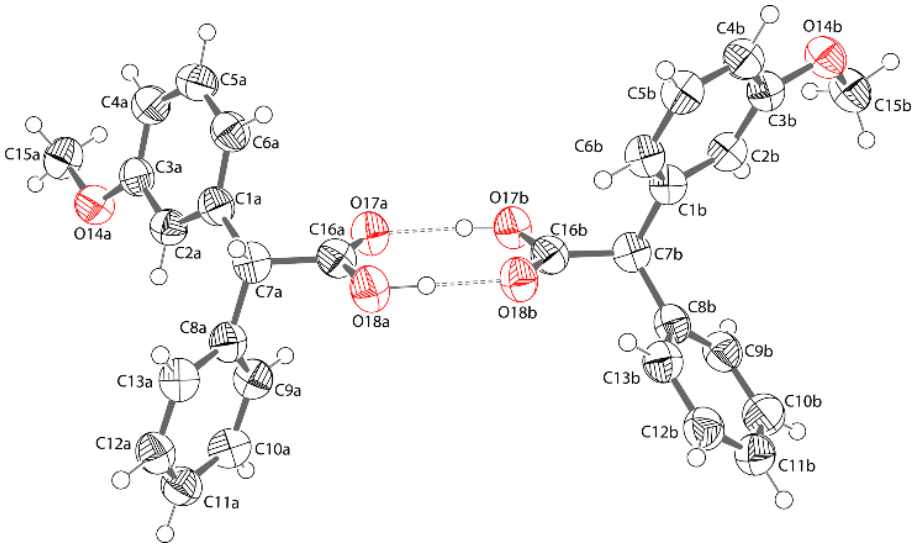

Figure 2.2. Molecular structure of (*R*)-**2.16** (CCDC 2905892) obtained by X-ray crystallography. The unit cell contained two molecules of (*R*)-**2.16** with different conformations. Intermolecular hydrogen bond interactions are shown as dashed lines.

(*R*)-**2.16** (free acid) served as a starting material for the synthesis of diastereomerically enriched (*R*,*R*)-**2.19** (Scheme 2.2). (*R*)-**2.16** was converted to (*R*)-**2.17** by cleavage of the methyl ether using BBr_3. Noteworthily, during this reaction the proton of the methine group in (*R*)-**2.16** was prone to deprotonation/proton exchange, leading to (*R*)-**2.17** with a decreased enantiomeric purity (74% *ee*) compared to that of (*R*)-**2.16** (Scheme 2.2 and supplementary Figure A2.2 in section A.2.3). Likewise, the proton of the methine group in (*R*)-**2.17** was prone to deprotonation/proton exchange during the synthesis of (*R*,*R*)-**2.19** by formation of an amide bond between (*R*)-**2.17** and (*R*)-configured ornithine derivative **2.18** using DCC as an active ester forming coupling reagent. These conditions gave (*R*,*R*)-**2.19** with a diastereomeric excess of 56%. It should be noted that this reaction had to be performed strictly in the absence of base and CH_2Cl_2 had to be used as solvent instead of DMF to preclude a complete loss of stereoinformation with respect to the chiral center of the diphenylacetyl moiety. The synthesis of diastereomerically enriched (*R*,*R*)-**2.19** provided the basis for the assignment of the

stereochemistry to (*R*,*R*)-**2.19** and (*S*,*R*)-**2.19**, separated by achiral RP-HPLC (chromatograms in Scheme 2.2). As the synthesis of (*R*,*R*)-**2.19** and (*S*,*R*)-**2.19** *via* (*R*)-**2.16** was performed only on a small scale (no preparative workup), the two diastereomers of **2.19** were prepared on a larger scale from racemic carboxylic acid **2.17** (obtained from nitrile **2.15**), which was converted to succinimidyl ester **2.20** (Scheme 2.2). Treatment of ornithine derivate **2.21** with **2.20** resulted in an equimolar ratio of (*S*,*R*)-**2.19** and (*R*,*R*)-**2.19**, which were separated by preparative HPLC. To assign the absolute stereochemistry to the two diastereomers of **2.14**, pure (*S*,*R*)-**2.19** (*cf.* supplementary Figure A2.3, panel A in section A.2.3) served as a starting material for the synthesis of (*S*,*R*)-**2.14** following a different route compared to the synthetic strategy shown in Scheme 2.1. (*S*,*R*)-**2.19** was converted to (*S*,*R*)-**2.23** by amidation with **2.22**, using EDC × HCl as a coupling reagent under base-free conditions to minimize epimerization (*cf*. supplementary Figure A2.3, panel B in section A.2.3). Alkylation of (*S*,*R*)-**2.23** using alkyl bromide **2.24** yielded phenol ether (*S*,*R*)-**2.13**. These conditions required the use of a strong base (cesium carbonate) and led to partial epimerization, which became obvious from RP-HPLC monitoring of the reaction (*cf.* supplementary Figure A2.3, panel C in section A.2.3). Conversion of diastereomerically enriched (*S*,*R*)-**2.13** to **2.14** according to the procedure shown in Scheme 2.1 yielded (*S*,*R*)-**2.14** in a diastereomeric excess of 50% over (*R*,*R*)-**2.14** (*cf.* supplementary Figure A2.3, panel D in section A.2.3), allowing the assignment of the absolute stereochemistry to both diastereomers of **2.14**.

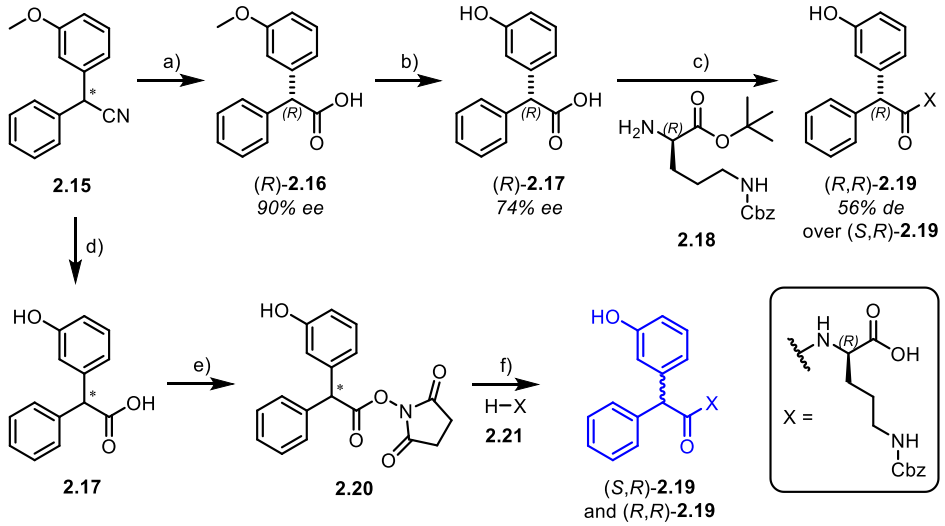
a)
b)
c)
d)
e)
f)
H–X
2.21
2.15
(R)-2.16
90% ee
(R)-2.17
74% ee
2.18
(R,R)-2.19
56% de
over (S,R)-2.19
2.17
2.20
(S,R)-2.19
and (R,R)-2.19
X =

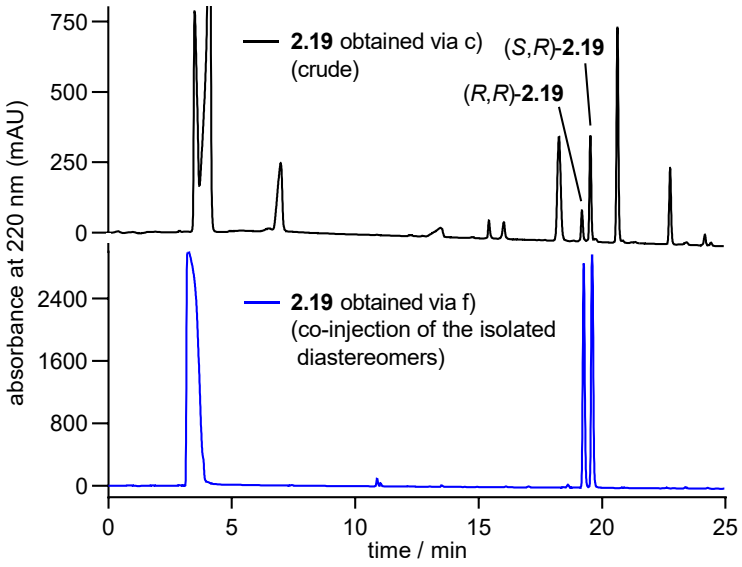
2.19 obtained via c)
(crude)
(S,R)-2.19
(R,R)-2.19
2.19 obtained via f)
(co-injection of the isolated
diastereomers)
absorbance at 220 nm (mAU)
time / min

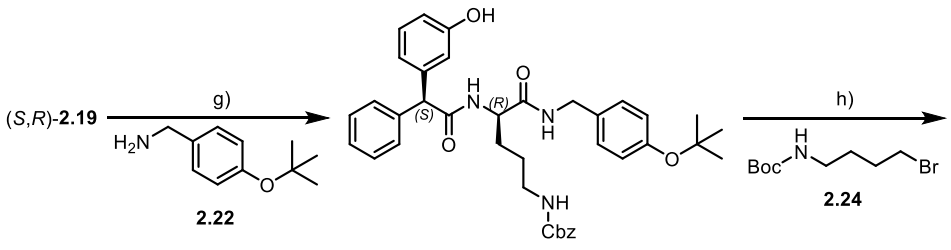
(S,R)-2.19
g)
h)
2.22
(S,R)-2.23
2.24

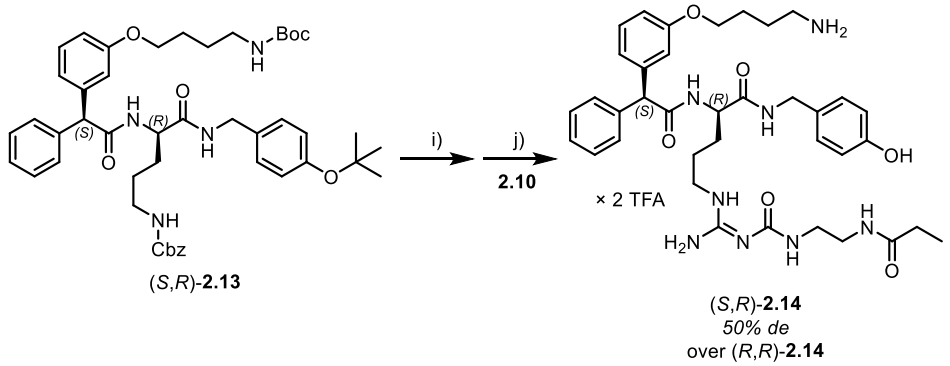
i)
j)
2.10
(S,R)-2.13
× 2 TFA
(S,R)-2.14
50% de
over (R,R)-2.14

Scheme 2.2. Synthesis of the key-intermediates (*S,R*)-**2.19** and (*R,R*)-**2.19** for assignment of the absolute stereochemistry to the (*S,R*)- and (*R,R*)-configured diastereomers of **2.14**. The asterisks in **2.15**, **2.17** and **2.20** indicate racemic mixtures. The wavy bond in **2.19** indicates either configuration, *S* or *R*. Reagents and conditions: a) (1) conc. H_2SO_4, glacial acetic acid, H_2O, 120 °C, 16 h, 76%; (2) repeated fractional crystallization of a diastereomeric salt of **2.16** and (*R*)-(+)-1-phenylethylamine from chloroform/hexane 45:55 v/v, 5%; b) BBr_3, CH_2Cl_2, −84 °C, 1 h, 68%; c) (1) DCC, HOBt, CH_2Cl_2, 4 °C, 3 h; (2) TFA, CH_2Cl_2, 4 °C, 10 min, products not isolated; d) aq. HBr (47%), glacial acetic acid, H_2O, reflux, 16 h, 75%; e) NHS, DCC, THF, 0 °C to rt, 16 h, 37%; f) DIPEA, DMF, rt, 2 h, 17% ((*S,R*)-**2.19**), 15% ((*R,R*)-**2.19**); note: (*S,R*)-**2.19** and (*R,R*)-**2.19** were separated and isolated by preparative RP-HPLC; g) HOBt, EDC × HCl, DMF, 4 °C, 16 h, 57%; h) Cs_2CO_3, DMF, 40 °C, 16 h, 84%; i) H_2, Pd/C, trifluoroethanol, rt, 1 h; j) (1) mercury(II) chloride, DIPEA, CH_2Cl_2, rt, 30 min; (2) TFA, CH_2Cl_2, rt, 24 h, 16%. The inset Figure shows the RP-HPLC chromatograms of crude (*S,R*)-**2.19**/(*R,R*)-**2.19** with a diastereomeric excess of 56% for (*R,R*)-**2.19**, obtained *via* reaction c) (black line) and a co-analysis of equal amounts of (*S,R*)-**2.19** and (*R,R*)-**2.19**, obtained *via* reaction f) (blue line). The synthesis of (*R,R*)-**2.19** from (*R*)-**2.16** (a-c), yielding 56% diastereomeric excess of (*R,R*)-**2.19**, and the subsequent synthesis of (*S,R*)-**2.14** from diastereomerically pure (*S,R*)-**2.19** (g-j), yielding 50% diastereomeric excess of (*S,R*)-**2.14**, served to assign the correct configuration to the diastereomers of **2.14**. The identity of **2.19** was confirmed by HRMS.

2.2.2 Synthesis and stereochemical discrimination of (*R*)-2.30 and (*S*)-2.30

In addition to (*S*,*R*)-**2.14** and (*R*,*R*)-**2.14**, containing a 4-aminobutoxy linker at the *meta* position at the diphenylacetyl moiety, a second pair of diastereomers, (*S*,*R*)-**2.30** and (*R*,*R*)-**2.30**, bearing the 4-aminobutoxy linker at the *para* position, was synthesized (Scheme 2.3). (*S*,*R*)-**2.30** and (*R*,*R*)-**2.30** were synthesized by solid phase synthesis according to the Fmoc strategy starting with the treatment of commercially available 2-chlorotrityl (2-ClTrt) resin (**2.25**) with phenol **2.26** to obtain polymer-bound Fmoc-protected amine **2.27**. After Fmoc deprotection, (*R*)-configured arginine derivative **2.28** (*cf*. section A.2.1 and supplementary Scheme A2.1) was coupled to **2.27** using HBTU/HOBt as coupling reagents, followed by Fmoc deprotection and coupling of *para*-substituted diphenylacetic acid derivative **2.29** (*cf.* section A.2.1 and supplementary Scheme A2.1) to afford the polymer-bound Boc-protected precursor of compound **2.30**. Acidic cleavage from the resin and removal of the protecting groups resulted in a 1:1 mixture of (*S*,*R*)-**2.30** and (*R*,*R*)-**2.30**, which were separated by achiral preparative RP-HPLC (Scheme 2.3).

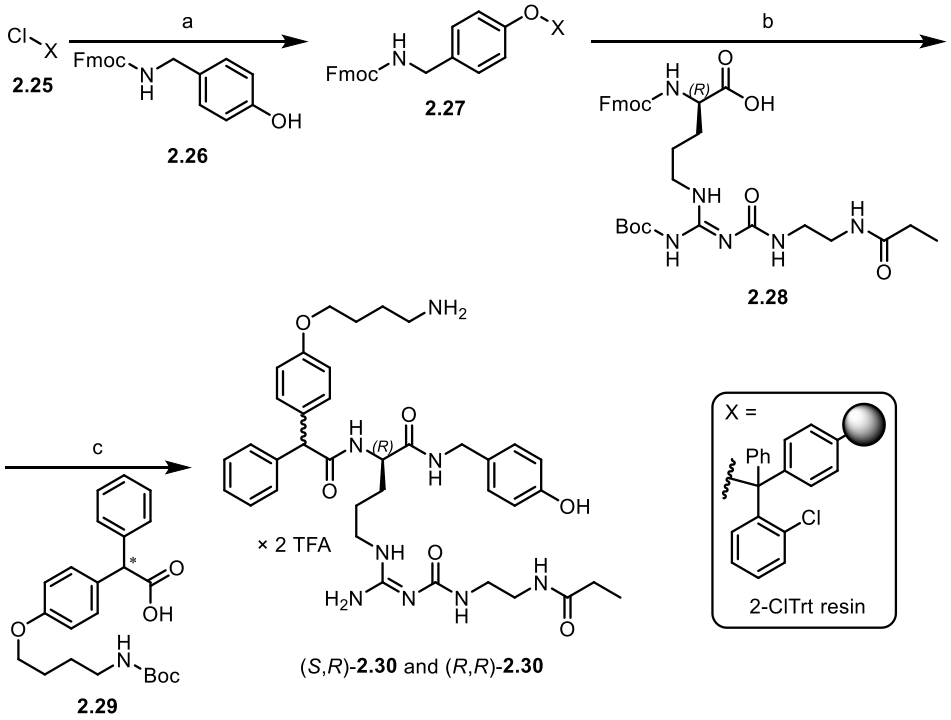

Scheme 2.3. Synthesis of the amine-functionalized argininamide-type Y_1R antagonists (*S,R*)-**2.30** and (*R,R*)-**2.30**. The asterisk in **2.29** indicates a racemic mixture. The wavy bond in **2.30** indicates either configuration, *S* or *R*. Reagents and conditions: a) DMAP, DIPEA, 40 °C, 3 h, 44%; b) (1) piperidine, DMF, 35 °C, 2 h (procedure repeated once), (2) HBTU, HOBt, DIPEA, DMF, 35 °C, 16 h; c) (1) piperidine, DMF, 35 °C, 2 h (procedure repeated once), (2) HBTU, HOBt, DIPEA, DMF, 35 °C, 16 h; (3) TFA, CH_2Cl_2, rt, 20 min; overall yields: 10% ((*R*,*R*)-**2.30**), 13% ((*S*,*R*)-**2.30**). Note: (*S*,*R*)-**2.30** and (*R*,*R*)-**2.30** were separated and purified by preparative RP-HPLC.

The absolute stereochemistry of (*S*,*R*)-**2.30** and (*R*,*R*)-**2.30** was determined by CD spectroscopy employing a combinatorial approach taking advantage of the known stereochemistry of the structurally closely related constitutional isomers (*S*,*R*)-**2.14** and (*R*,*R*)-**2.14**. In brief, the spectra of (*S*,*R*)-**2.14**, (*R*,*R*)-**2.14** and the two diastereomers of **2.30**, preliminarily labeled **2.30a** and **2.30b** (Figure 2.3, panel A), were subjected to singular-value decomposition (SVD), affording three “abstract spectra” that were different from noise (Figure 2.3, panel B). Each of these spectra represents spectral components that are present in all four spectra, irrespective of intensity and sign. Reversion of this deconvolution using only the three SVD components from Figure 2.3 (panel B) and their corresponding coefficients afforded the spectra in Figure 2.3 (panel C). The close resemblance to Figure 2.3 (panel A) demonstrates that each of the four CD spectra can be regarded as a combination of only three linearly independent spectral components, putatively being associated with the stereochemistry of the argininamide moiety, the stereochemistry of the diphenylacetyl moiety, and the regiochemistry (*para* or *meta*) of the amine-functionalized substituent. The contribution of SVD component 1 to each CD spectrum is shown in Figure 2.3 (panel D).

As all four spectra exhibited the same sign, we attributed component 1 to the configuration of the argininamide moiety (*R* for all isomers). The contributions of component 2 (Figure 2.3, panel E) to the spectra of (*S*,*R*)-**2.14** and (*R*,*R*)-**2.14** have the opposite sign. Therefore, a minimum at 234 nm and a maximum at around 210 nm indicate the *S*-configuration at the diphenylacetyl moiety, while an inverse spectrum corresponds to *R*-configuration. This allowed the assignment of **2.30a** to (*S*,*R*)-**2.30** and **2.30b** to (*R*,*R*)-**2.30**. The contributions of component 3 (Figure 2.3, panel F) correlated with the regiochemistry of the amine-functionalized substituent: consistent with the assignments from above, contributions to the CD-spectra of *meta*-substituted isomers and to the spectra of *para*-substituted isomers have the opposite sign.

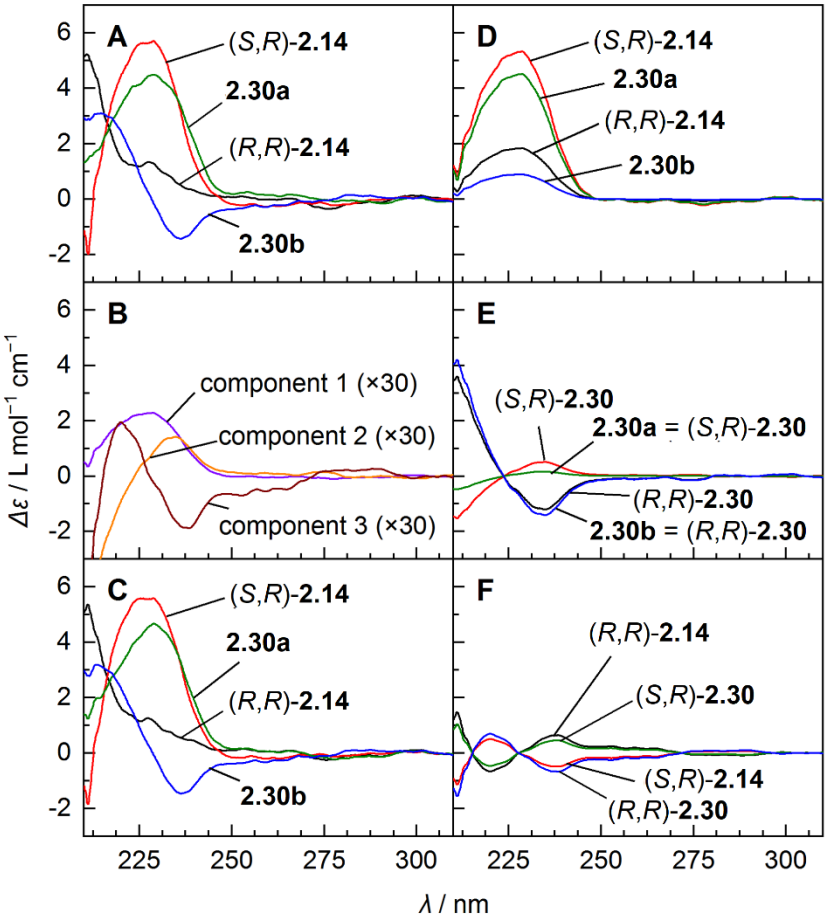

Figure 2.3. Assignment of the absolute configuration to the diastereomers of **2.30** through spectral deconvolution and assignment of linearly independent spectral features to stereo- and regiochemical properties. (A) CD spectra of all four isomers. (B) Linearly independent components ("abstract spectra") from SVD, shared by all 4 isomers (rescaled by a factor of 30 for better comparison). (C) Reconstruction of full spectra from linear combination of the "abstract spectra" in panel B. (D) Contributions of component 1 to the full spectra in panel A or C correlating with the configuration at the argininamide moiety. (E) Contributions of component 2 correlating with the configuration at the diphenylacetyl moiety. (F) Contributions of component 3 correlating with the regiochemistry of the amine-functionalized substituent.

2.2.3 Synthesis of fluorescent ligands 2.35-2.40

Finally, a set of six fluorescent ligands was prepared using four different amine-reactive dyes: the pyridinium cyanine dye Py5 (**2.31**) and succinimidyl esters of the indolinium cyanine dye S0387 (**2.32**), the boron dipyrromethene-type dye BODIPY 630/650 (**2.33**) and the rhodamine dye 5'-TAMRA (**2.34**) (Scheme 2.4). Fluorescent probes **2.35** and **2.37**-**2.39** were prepared by treatment of (*S*,*R*)-**2.14** with **2.31**-**2.34**, respectively. The (*R,R*)-configured counterpart of **2.35**, compound **2.36**, was synthesized from (*R*,*R*)-**2.14** and **2.31**. Fluorescent ligand **2.40**, representing a constitutional isomer of **2.39** (*para* vs. *meta* substitution pattern at the diphenylacetyl moiety) was prepared from (*S*,*R*)-**2.30** and **2.34**. Fluorescence dye coupling to the amines was performed at rt in DMF in the presence of DIPEA throughout, affording the fluorescent ligands in moderate to high yields (21-69%) and high purities (≥ 96%, RP-HPLC analysis at 220 nm) after purification by preparative HPLC. The investigation of the chemical stability in PBS pH 7.4 at 22 °C revealed high chemical stability for compounds **2.35**-**2.37**, **2.39** and **2.40** (≥ 95% purity after 24 h) and a slow decomposition for fluorescent probe **2.38** (90% purity after 24 h) (for RP-HPLC chromatograms see section A.2.5).

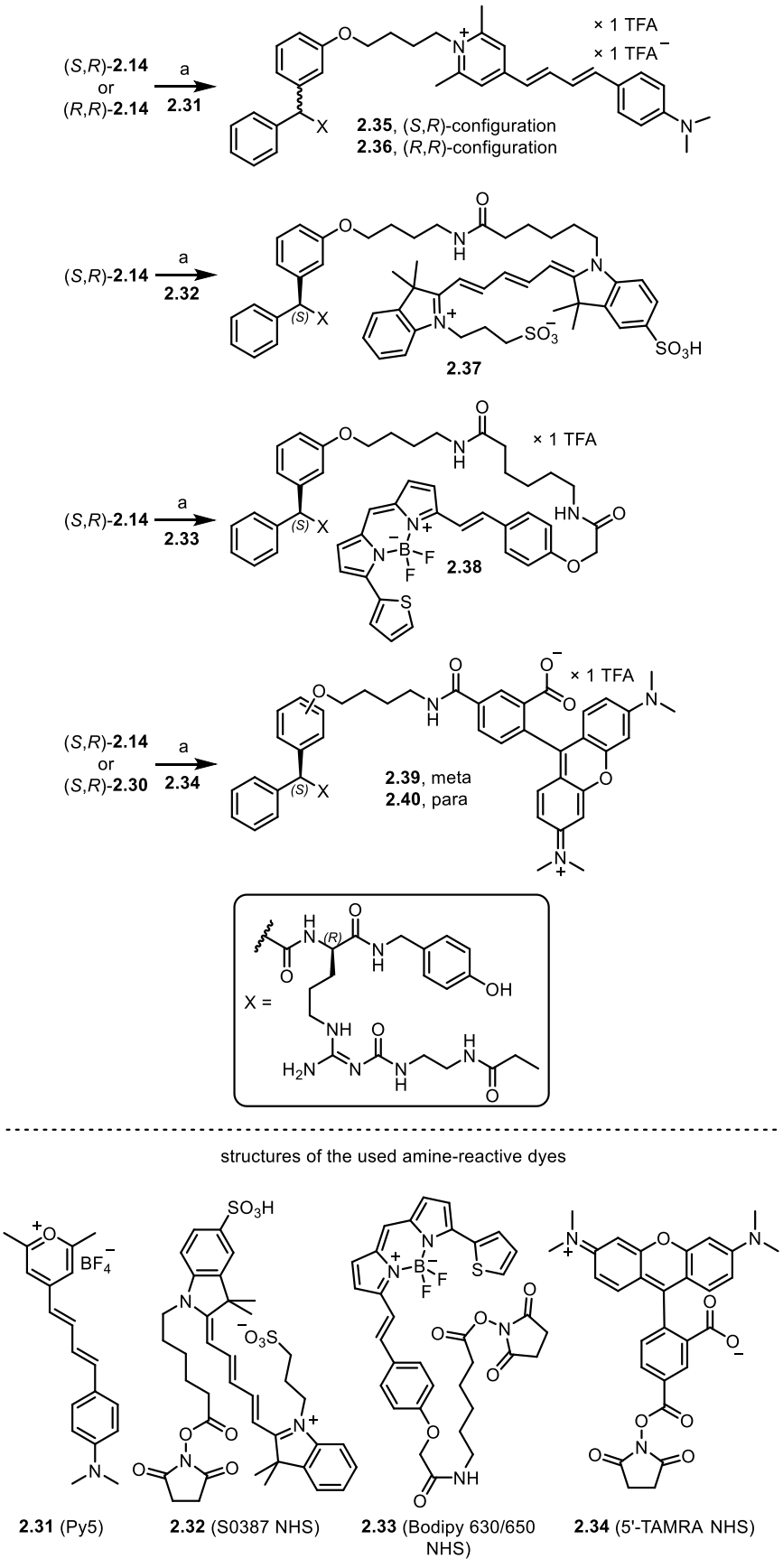

Scheme 2.4. Synthesis of the fluorescent Y_1R ligands **2.35-2.40**. Reagents and conditions: a) DIPEA, DMF, rt, 0.5-4 h, 21-69%.

2.2.4 NPY receptor binding and Y_1R antagonism

Y_1R binding affinities of the amine-functionalized precursor compounds (*S*,*R*)-**2.14**, (*R*,*R*)-**2.14**, (*S*,*R*)-**2.30** and (*R*,*R*)-**2.30**, and fluorescently labeled compounds **2.35**-**2.40** were determined in Y_1R competition binding experiments using [^{3}H]**2.2** as the radioligand. For these experiments, human Y_1R-expressing SK-N-MC neuroblastoma cells, being well established for Y_1R binding studies, were used. The obtained pK_i values are listed in Table 2.1 and for **2.35**-**2.40**, the corresponding radioligand displacement curves are displayed in supplementary Figure A2.4 (section A.2.3). (*S*,*R*)-**2.14**, (*R*,*R*)-**2.14**, (*S*,*R*)-**2.30** and (*R*,*R*)-**2.30** exhibited very high Y_1R affinities (pK_i = 10.30-10.89), in the case of (*R*,*R*)-**2.30** 6-fold higher compared to the parent compound **2.2**. It is rather a matter of speculation, if this increase in affinity is caused by an additional attractive interaction of the primary amino group in **2.14** and **2.30** with the receptor or if it is due to an entropically favored binding process.

Whereas the Y_1R affinities of the two diastereomers of **2.14** were not distinguishable (pK_i = 10.61 and 10.62), the Y_1R affinity of (*R*,*R*)-**2.30** was 4-fold higher compared to (*S*,*R*)-**2.30**. Even though the fluorescently labeled ligands showed lower Y_1R affinities compared to the amine precursor compounds, five of them (**2.35**-**2.39**) exhibited subnanomolar Y_1R affinity (pK_i = 9.36-9.95), a very promising result for fluorescence-tagged nonpeptidic receptor ligands. For the fluorescent ligands derived from (*S*,*R*)-**2.14** (**2.35**, **2.37**-**2.39**), the decrease in Y_1R affinity compared to that of (*S*,*R*)-**2.14** correlated with the molecular weight of the introduced fluorescent dye (**2.31** < **2.34** < **2.33** < **2.32**, *cf.* Scheme 2.4), ranging from 4-fold (**2.35**) to 17-fold (**2.37**). Py5-labeled diastereomers **2.35** and **2.36**, prepared from (*S*,*R*)-**2.14** and (*R*,*R*)-**2.14**, respectively, exhibited comparable Y_1R affinities (pK_i = 9.95 and 9.74, respectively) as also observed for (*S*,*R*)-**2.14** and (*R*,*R*)-**2.14**. This confirmed that the type of stereochemistry at the diphenylacetyl moiety has an insignificant effect on Y_1R binding. For this reason, only (*S*,*R*)-**2.14** was labeled with S0387 (**37**), BODIPY 630/650 (**2.38**) and 5'-TAMRA (**2.39**). Interestingly, the Y_1R affinities of the 5'-TAMRA-labeled derivatives **2.39** and **2.40**, varying only with respect to the position of the 4-aminobutoxy linker (*meta* in **2.39** and *para* in **2.40**, *cf.* Scheme 2.4), differed by a factor of 9 (pK_i = 9.77 and 8.82, respectively). In contrast, the difference in Y_1R binding of the precursor compounds of **2.39** and **2.40**, i.e. (*S*,*R*)-**2.14** and (*S*,*R*)-**2.30**, respectively, was less pronounced (≈ 2-fold, *cf.* Table 2.1). As previously reported for the argininamide-type Y_1R antagonists **2.1** and **2.2**, all synthesized Y_1R ligands showed an excellent preference for the Y_1R (>1000-fold) over the other NPY receptor subtypes (Table 2.1).

Table 2.1. NPY receptor binding data of **2.2**, **2.14**, **2.30** and fluorescent ligands **2.35**-**2.40**.

compound	stereochemistry diphenylacetyl/ argininamide moiety	pK_i ± SEM / K_i [nM][a]	pK_i ± SEM[a]		
		Y_1R[b]	Y_2R[c]	Y_4R[d]	Y_5R[e]
2.2	-/*R*	10.27 ± 0.17 / 0.077[f]	<5.5[f]	<5[f]	<5[f]
(*S*,*R*)-**2.14**	*S*/*R*	10.61 ± 0.08 / 0.026	<5	<5	<5
(*R*,*R*)-**2.14**	*R*/*R*	10.62 ± 0.02 / 0.024	<5	<5	<5
(*S*,*R*)-**2.30**	*S*/*R*	10.30 ± 0.11 / 0.054	<5	<5	<5
(*R*,*R*)-**2.30**	*R*/*R*	10.89 ± 0.08 / 0.013	<5	<5	<5
2.35	*S*/*R*	9.95 ± 0.01 / 0.11	<5.5	<5.5	6.38 ± 0.01
2.36	*R*/*R*	9.74 ± 0.07 / 0.17	<5.5	<5.5	<5.5
2.37	*S*/*R*	9.36 ± 0.06 / 0.44	<5.5	<5.5	<5.5
2.38	*S*/*R*	9.52 ± 0.10 / 0.31	<5.5	<5.5	<5.5
2.39	*S*/*R*	9.77 ± 0.12 / 0.19	<5.5	6.22 ± 0.15	<5.5
2.40	*S*/*R*	8.82 ± 0.07 / 1.6	<5.5	<5.5	<5.5

[a]Data represent mean values ± SEM (pK_i) or mean values (K_i) from at least three independent experiments performed in triplicate. [b]Determined by competition binding with [^{3}H]**2.2** (K_d = 0.044 nM,[22] c = 0.15 nM) at intact SK-N-MC neuroblastoma cells. [c]Determined by competition binding with [^{3}H]propionyl-pNPY (K_d = 0.14 nM,[29] c = 0.5 nM) at intact CHO-hY_2R cells. [d]Determined by competition binding with [^{3}H]UR-KK200 (K_d = 0.67 nM,[30] c = 1 nM) at intact CHO-hY_4-Gqi5-mtAEQ cells. [e]Determined by competition binding with [^{3}H]propionyl-pNPY (K_d = 11 nM,[31] c = 5 nM) at intact HEC-1B-hY_5 cells. [f]Keller *et al*. (data, previously reported as K_i, were re-evaluated to afford the pK_i values).[20]

The Y_1R antagonistic activities of precursor compounds (*S*,*R*)-**2.14**, (*R*,*R*)-**2.14**, (*S*,*R*)-**2.30** and (*R*,*R*)-**2.30** and fluorescently labeled compounds **2.35**-**2.40** were determined in a Fura-2 calcium flux assay using Y_1R-expressing HEL cells[32] and pNPY as the agonist. All compounds were capable of fully inhibiting the pNPY-stimulated cellular response (increase in cytosolic Ca^{2+} concentration) as demonstrated by the sigmoidal inhibition curves displayed in Figure 2.4. The resulting pIC_{50} values, ranging from 9.53 (**2.40**) to 10.77 ((*R*,*R*)-**2.30**), were comparable to the pK_i values obtained from radioligand competition binding. It should be noted that pIC_{50} values were not converted to pK_b values as the Ca^{2+} assay is incompatible with equilibrium conditions.

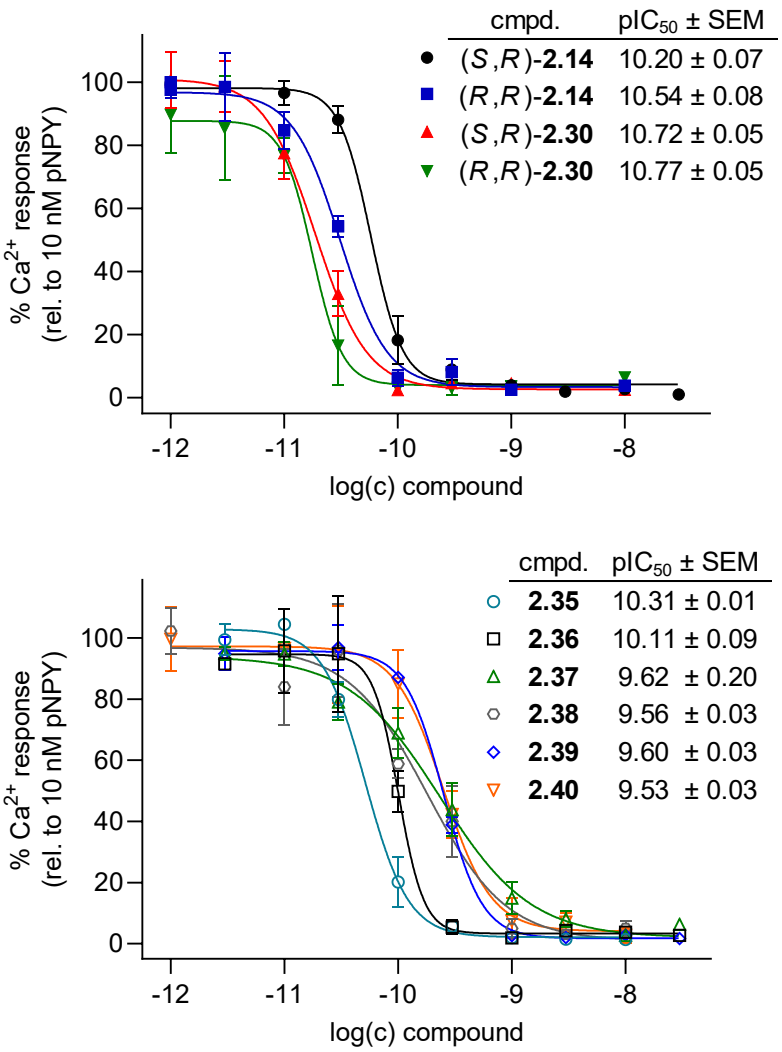

Figure 2.4. Investigation of the nonlabeled Y_1R antagonists **2.14** and **2.30** (top), and fluorescent Y_1R antagonists **2.35-2.40** (bottom) in a Fura-2 Ca^{2+} assay using human erythroleukemia (HEL) cells. The inhibition curves resulted from the inhibition of the pNPY (10 nM)-induced intracellular Ca^{2+} mobilization by the antagonists. Data represent mean values ± SEM from three independent experiments. An impairment of the optical readout of the assay (excitation: 340 and 380 nm, emission: 510 nm)[33] by the indolinium-type cyanine dye present in **2.37** was excluded previously within the used concentration range.[34] Likewise, the pyridinium cyanine dye (present in **2.35** and **2.36**) and the rhodamine dye 5'-TAMRA (present in **2.39** and **2.40**) did not significantly affect the optical readout (*cf.* supplementary Figure A2.5, panels A and C in section A.2.3). Note: the pEC_{50} value of pNPY amounted to 8.29 ± 0.12 (mean ± SEM from three individual experiments; for the concentration-effect curve see supplementary Figure A2.5, panel B in section A.2.3).

2.2.5 Fluorescence spectroscopy

For all fluorescent ligands (**2.35**-**2.40**), excitation and emission spectra were recorded in PBS supplemented with 1% BSA (maxima summarized in Table 2.2). Additionally, excitation and emission spectra of fluorescent probes **2.35**, **2.37** and **2.39** were recorded in the media used for the respective fluorescence-based assay (λ_{max} given in Table 2.2). Excitation and emission spectra are depicted in supplementary Figures A2.6 and A2.7 (section A.2.3). Compounds **2.35** and **2.36**, labeled with the pyrylium/pyridinium dye Py5 (**2.31**) exhibited excitation maxima close to the argon laser line of 488 nm. As reported previously for Py5-labeled fluorescent ligands,[21, 35] the Stokes shift of **2.35** and **2.36** was less pronounced in BSA-containing buffer than in BSA-free media (Table 2.2). The fluorescent ligands **2.37** and **2.38**, labeled with the red-emitting indolinium cyanine dye **2.32** and BODIPY 630/650 **2.33**, respectively, exhibited maxima close to the emission wavelength of red diode lasers (633-640 nm). Therefore, fluorescent probes **2.35**-**2.38** were predestined for flow cytometry-based Y_1R binding studies using flow cytometers equipped with an argon and a red diode laser. 5'-TAMRA labeled compounds **2.39** and **2.40** showed excitation maxima in the range of 556-563 nm (Table 2.2). These probes can still be excited with an argon laser (488 nm), as present in the flow cytometer used in this study, but were mainly prepared for the purpose of FA-based assays as the 5'-TAMRA dye exhibits a fluorescence lifetime ($\tau \approx 2.3$ ns in H_2O) that is ideal for FA measurements in aqueous media.[36, 37]

Fluorescence quantum yields were determined for fluorescent ligands **2.35**-**2.37**, **2.39** and **2.40** in PBS (pH 7.4) and PBS supplemented with 1% BSA. The fluorescence quantum yield in PBS with 1% BSA is supposed to represent the quantum yield of the receptor-bound fluorescent ligand. All investigated fluorescent ligands showed a higher quantum yield in PBS with 1% BSA compared to PBS alone (Table 2.2). This observation can be explained by albumin binding of the fluorescent probe and the resulting rigidization of the fluorophore.[38] This effect was most pronounced for the Py5-labeled ligands **2.35** and **2.36**, being consistent with previous reports on Py5-labeled fluorescent ligands.[21, 35] Interestingly, compound **2.40**, containing a *para* substitution pattern at the diphenylacetyl moiety, exhibited a markedly higher quantum yield in PBS with 1% BSA compared to that of its *meta*-substituted congener **2.39** (37% vs. 23%). This might be attributed to differences in albumin binding between **2.39** and **2.40**. Fluorescent quantum yields of the BODIPY-labeled ligand **2.38** were not determined as **2.38** showed strong adsorption to the cuvette material.

Table 2.2. Fluorescence quantum yields of **2.35**-**2.37**, **2.39** and **2.40** determined in neat PBS pH 7.4 and PBS containing 1% BSA as well as excitation and emission maxima determined in PBS supplemented with 1% BSA (**2.35**-**2.40**) and in the media used for fluorescence-based Y_1R binding studies (**2.35**, **2.37** and **2.39**).

compd.	dye	Φ (%)[a]		$\lambda_{ex}/\lambda_{em}$[b]			
		PBS	PBS + 1% BSA	PBS +1% BSA	L15 (FC)	FA binding buffer[c]	MEMO (microscopy)
2.35	pyridinium cyanine (Py5)	2.1 ± 0.1	29 ± 5	491/661	458/706	459/707	456/708
2.36	pyridinium cyanine (Py5)	2.8 ± 0.2	29 ± 6	495/658	nd[d]	nd[d]	nd[d]
2.37	indolinium cyanine (S0387)	24 ± 5	60 ± 6	657/672	650/667	651/668	650/668
2.38	boron dipyrromethene (BODIPY 630/650)	nd[d]	nd[d]	641/647	nd[d]	nd[d]	nd[d]
2.39	rhodamine (5'-TAMRA)	19 ± 2	23 ± 3	559/581	557/585	557/585	556/586
2.40	rhodamine (5'-TAMRA)	13 ± 2	37 ± 1	563/587	nd[d]	nd[d]	nd[d]

[a]Fluorescence quantum yield. Data represent mean values ± SEM from at least two independent determinations. [b]Wavelengths at the maxima of the excitation and corrected emission spectra. [c]20 mM HEPES buffer (pH 7.4) containing $CaCl_2$ (1 mM), NaCl (135 mM) and 0.1% Pluronic F-127. [d]Not determined.

2.2.6 Flow cytometry-based receptor binding studies

For the characterization of Y_1R binding of fluorescent ligands **2.35**, **2.37**, **2.39** and **2.40** by FC, saturation binding as well as association and dissociation experiments were performed at intact mamma carcinoma MCF-7-Y_1 cells. Compared to SK-N-MC cells, the canonical cell line for radiochemical Y_1R binding assays, MCF-7-Y_1 cells display a higher level of Y_1R expression,[19] a favorable feature for fluorescence-based flow cytometric receptor binding studies. Moreover, MCF-7 cells are useful for xenograft mouse models with respect to Y_1R-mediated *in vivo* tumor imaging.[39]

The BODIPY 630/650 labeled ligand **2.38**, being compatible with a red-laser excitation, was also investigated by flow cytometry (saturation binding). However, as this fluorescent ligand showed strong adsorption to vessel materials (HPLC vial inlets, sample tubes, etc.) and high nonspecific binding at cells, results were not reproducible (data not shown). Saturation binding studies with **2.35**, **2.37**, **2.39** and **2.40**, carried out using a cell density of 1.0×10^6 cells/mL, afforded saturable specific binding of **2.35**, **2.37**, **2.39** and **2.40** to the Y_1R (Figure 2.5, panel A). Data fitting according to an equation describing equilibrium binding of a labeled ligand to a

single receptor population (hyperbolic saturation isotherm, equation 1) yielded the dissociation constants (K_d values), which were converted to pK_d values (negative logarithm of dissociation constants K_d in molar).

$$B = \frac{B_{max}[L]}{K_d + [L]} \quad (1)$$

B: receptor-bound fluorescence (specifically bound fluorescent ligand); B_{max}: maximum of receptor-bound fluorescence, [L]: concentration of nonbound (free) fluorescent ligand at equilibrium; K_d: dissociation constant of the labeled receptor ligand.

The obtained apparent pK_d values of **2.35**, **2.37**, **2.39** and **2.40**, ranging from 8.88 to 9.87, were in good agreement with the respective pK_i values determined in radioligand competition binding experiments (*cf.* Tables 2.1 and 2.3). A requirement for the determination of accurate K_d values by this type of saturation binding experiment is a large excess of labeled ligand over the amount of receptor, assuring a negligible reduction of the free ligand in solution ([L]) upon receptor-ligand binding. However, ligands with high affinities (typically K_d < 1 nM, which is the case for **2.35**, **2.37** and **2.39**) require the use of low ligand concentrations (<< 0.5 nM) for binding experiments, resulting in a marked decrease in the free fluorescent ligand concentration upon binding of the ligand to the receptor, a phenomenon termed ligand depletion.[40, 41] To reduce the extent of ligand depletion, the amount of receptor or receptor source must be reduced relative to the amount of the labeled ligand, or the amount of ligand must be increased relative to the amount of receptor. However, for each method with its technical setup, there is a limit for this kind of optimization. In the case of FC-based binding assays, the amount of receptor is determined by the cellular expression level and the cell density of the cell suspension. The latter must be high enough to enable an adequate sample measurement time and reasonable statistical precision (a cell density of 1.0-2.0 × 10^5 cells per mL is considered the lower limit). Whereas radiochemical binding assays allow a convenient determination of the free radioligand concentration, which can be involved in the data analysis, the quantification of free fluorescent ligand at equilibrium ([L]) is not conveniently feasible within the scope of a FC-based saturation binding experiment. To verify whether the determination of the dissociation constants was affected by ligand depletion, saturation binding experiments with **2.35**, **2.37** and **2.39** were also performed using a 10-fold lower cell density of 1.0 × 10^5 cells/mL (higher excess of fluorescent ligand over Y_1R; saturation isotherms see supplementary Figure A2.8 in section A.2.3). In these experiments, **2.35**, **2.37** and **2.39** showed higher apparent Y_1R affinities (Table 2.3, largest difference found for **2.35**: pK_d = 9.87 (high cell density) vs. 10.38 (low cell density)), suggesting a moderate underestimation of the Y_1R affinity of **2.35**, **2.37** and **2.39** determined by FC-based saturation binding. It should be

noted that, for the aforementioned reasons, the data acquired for the reference experiments with a lower cell density were statistically less precise, particularly in the case of the 5'-TAMRA-labeled derivative **2.39** (supplementary Figure A2.8 in section A.2.3).

The association of **2.35**, **2.37**, **2.39** and **2.40** to the Y_1R was investigated at cell densities of 1.0×10^6 cells/mL and 1.0×10^5 cells/mL, resulting in observed association rate constants (k_{obs}) (data only shown for the higher cell density, Table 2.3). Among the studied fluorescent ligands, **2.35** showed the fastest association to the Y_1R (Figure 2.5 (panel B), Table 2.3).

The analysis of the association binding data by a monophasic fit (yielding $k_{obs(mono)}$) and a biphasic fit ($k_{obs(bi,fast)}$ and $k_{obs(bi,slow)}$) showed a stronger correlation for the biphasic fit for all studied ligands (Figure 2.5, panel B). A biphasic association can be explained, for example, by the presence of more than one receptor state with distinct binding properties. Dissociation experiments with **2.35**, **2.37**, **2.39** and **2.40**, which should not be affected by ligand depletion at all, gave monophasic dissociation curves and suggested a complete dissociation of the fluorescent probes from the Y_1R with half-lives ranging from 0.5 h (**2.40**) to 5.5 h (**2.35**) (Figure 2.5, panel C). Based on the dissociation rate constants (k_{off}), the apparent k_{obs} values from association experiments, and the fluorescent ligand concentrations used in association experiments, the respective association rate constants ($k_{on(mono)}$, $k_{on(bi,fast)}$ and $k_{on(bi,slow)}$) were calculated (Table 2.3). The kinetically derived dissociation constants K_d(kin), defined as k_{off}/k_{on} for systems acting according to the law of mass action, were calculated, as an approximation, from k_{off} and $k_{on(mono)}$. The respective pK_d(kin) values of **2.35**, **2.37**, **2.39** and, notably, also **2.40**, the ligand with the lowest binding affinity, i.e. least affected by ligand depletion, were considerably higher than their pK_d values obtained from saturation binding experiments (Table 2.3). In view of the fact that kinetic binding studies are less affected by ligand depletion due to the use of higher ligand concentrations, this supported the hypothesis that Y_1R affinities of **2.35**, **2.37**, **2.39** and **2.40** were underestimated when determined by FC-based saturation binding experiments.

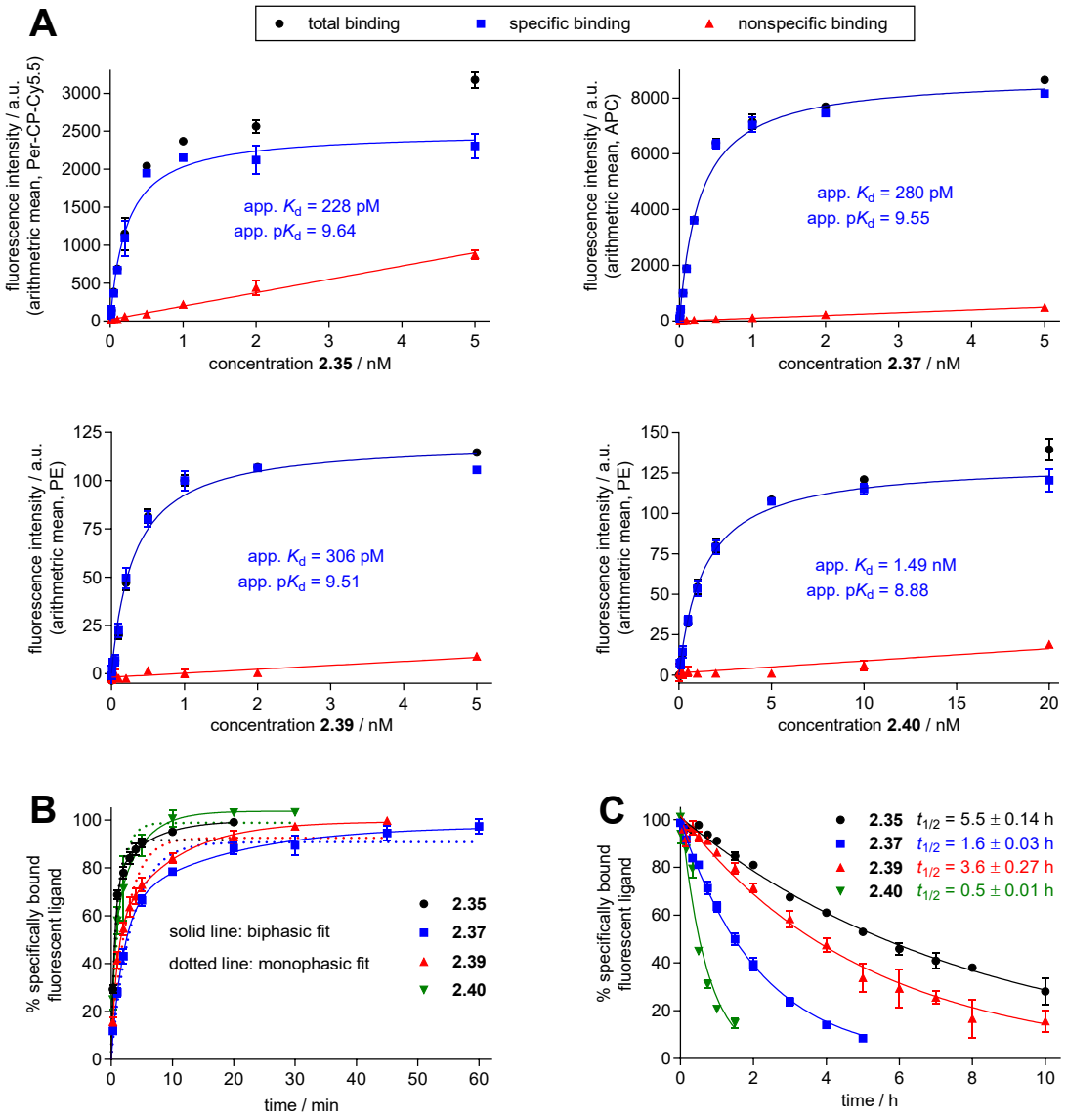

Figure 2.5. Characterization of Y_1R binding of the fluorescent ligands **2.35**, **2.37**, **2.39** and **2.40** in FC-based assays performed with intact human MCF-7-Y_1 mamma carcinoma cells (cell density: 1.0 × 10^6 cells/mL) at 22 °C. (A) Representative hY_1R binding isotherms of fluorescent ligands **2.35**, **2.37**, **2.39** and **2.40** obtained from FC-based saturation binding (performed in duplicate). Nonspecific binding was determined in the presence of **2.1** (10 µM). Total and nonspecific binding data represent mean values ± SEM. Specific binding data represent calculated values ± propagated error. (B) Association of **2.35** (0.25 nM), **2.37** (0.5 nM), **2.39** (0.5 nM) and **2.40** (1 nM) with the hY_1R. Nonspecific binding was determined in the presence of **2.2** (1 µM). Data (means ± SEM from at least three independent experiments performed in duplicate) were analyzed by a two-parameter equation describing a monophasic exponential rise to a maximum (dashed lines) and by a four-parameter equation describing a biphasic exponential rise to a maximum (solid lines). (C) Dissociation of **2.35**, **2.37**, **2.39** and **2.40** from the hY_1R (preincubation at 1 nM (**2.35**, **2.37**, **2.39**) or 2 nM (**2.40**) for 2 h) initiated by the addition of **2.2** (1 µM). Nonspecific binding was determined by the addition of **2.2** (1 µM) already during preincubation. Data (mean values ± SEM from three independent experiments performed in duplicate) were analyzed by a two-parameter equation describing a monophasic exponential decline.

Interestingly, the comparison of **2.39** and **2.40**, only different in the substitution pattern at the diphenylacetyl moiety (*meta* vs. *para*) reveals comparable association rate constants (k_{on}(**2.39**) = 0.81 [nM^{-1} min^{-1}] vs. k_{on}(**2.40**) = 0.58 [nM^{-1} min^{-1}]). Therefore, the lower binding affinity of **2.40** compared to **2.39** (ca. 5-fold, Figure 2.5, panel A) can be attributed to a markedly higher residence time at the Y_1 receptor for **2.39**, as is obvious from the big discrepancy in the dissociation half-lives ($t_{1/2}$ (**2.39**) = 3.6 h, $t_{1/2}$ (**2.40**) = 0.5 h).

The applicability of fluorescent probes **2.35**, **2.37** and **2.39** as molecular tools to determine the affinity of nonlabeled NPY Y_1R ligands was studied by competition binding with the argininamide-type Y_1R antagonists **2.1** and **2.2** and the agonist pNPY (supplementary Figure A2.9 in section A.2.3). To reduce ligand depletion, all displacement experiments were performed at a cell density of 1.0×10^5 cells/mL. As large peptidic NPY receptor agonists such as PP derivatives show comparatively slow binding kinetics,[31] we chose a longer incubation time for the FC-based competition binding experiments with pNPY compared to experiments involving the antagonists **2.1** and **2.2** (4 h vs. 2 h). In the case of antagonists **2.1** and **2.2**, the obtained pK_i values were in good agreement with reported Y_1R binding data. However, the determined Y_1R affinity of pNPY was markedly lower than the literature data (Table 2.4). Noteworthily, the lowest discrepancy (≈ 1 log unit) was observed when fluorescent probe **2.37**, which showed the fastest dissociation from the Y_1R (*cf.* Figure 2.5, panel C), was used. This demonstrated that a labeled probe, which is used for the determination of binding affinities of nonlabeled receptor ligands, should not dissociate too slowly from the receptor, i.e., should not exhibit a long target residence time. Therefore, compound **2.37**, which also displayed the highest signal-to-noise ratio among the investigated set of tracers (Figure 2.5), can be considered the most promising candidate as a potential replacement for radioactively labeled analogues, e.g. [^{3}H]**2.2**, in this specific application.

Table 2.3. Parameters characterizing Y_1R binding of the fluorescent ligands **2.35**, **2.37**, **2.39** and **2.40** determined in FC-based assays at a temperature of 22 °C.

	saturation binding		binding kinetics						
			association					dissociation	
cmpd.	pK_d[a] 1×10^6 cells/mL	pK_d[a] 1×10^5 cells/mL	c [nM]	$k_{obs(mono)}$ [min^{-1}][b]	$k_{obs(bi,fast)}$ $k_{obs(bi,slow)}$ [min^{-1}][b]	$k_{on(mono)}$ [nM^{-1}min^{-1}][c]	$k_{on(bi,fast)}$ $k_{on(bi,slow)}$ [nM^{-1}min^{-1}][c]	k_{off} [min^{-1}][d]	pK_d(kin)[e]
2.35	9.87 ± 0.12	10.38 ± 0.04	0.25	1.2 ± 0.3	1.85 ± 0.13 0.20 ± 0.06	4.9 ± 1.3	7.4 ± 0.5 0.8 ± 0.2	0.0021 ± 0.0001	12.37 ± 0.14
2.37	9.57 ± 0.05	9.81 ± 0.05	0.5	0.31 ± 0.05	0.52 ± 0.01 0.07 ± 0.01	0.60 ± 0.10	1.03 ± 0.08 0.13 ± 0.01	0.0072 ± 0.0001	10.92 ± 0.09
2.39	9.64 ± 0.15	9.93 ± 0.15	0.5	0.41 ± 0.04	1.21 ± 0.08 0.13 ± 0.01	0.81 ± 0.07	2.4 ± 0.2 0.25 ± 0.01	0.0032 ± 0.0002	11.40 ± 0.08
2.40	8.88 ± 0.05	nd[f]	1	0.69 ± 0.14	1.14 ± 0.21 0.13 ± 0.10	0.58 ± 0.08	1.06 ± 0.23 0.14 ± 0.06	0.0257 ± 0.0005	10.34 ± 0.06

[a]Apparent pK_d value determined by FC-based saturation binding at MCF-7-Y_1 cells using the given cell densities. Data represent mean values ± SEM from at least three individual experiments performed in duplicate. [b]Observed association rate constant obtained by monophasic ($k_{obs(mono)}$) or biphasic ($k_{obs(bi,fast)}$ and $k_{obs(bi,slow)}$) fitting; mean values ± SEM from at least three individual experiments performed in duplicate. [c]Association rate constant ± propagated error calculated from $k_{obs(mono)}$, $k_{obs(bi,fast)}$ or $k_{obs(bi,slow)}$, the respective k_{off} value and the applied ligand concentration. [d]Dissociation rate constants obtained from monophasic fits; mean values ± SEM from three individual experiments performed in duplicate; corresponding half-lives $t_{1/2}$ are displayed in Figure 2.5 (panel C). [e]Kinetically derived dissociation constants (expressed as pK_d(kin) ± SEM) calculated from k_{off} and $k_{on(mono)}$. For all association and dissociation experiments, a cell density of 1.0 × 10^6 cells/mL was used. [f]Not determined.

2.2.7 Fluorescence anisotropy-based receptor binding studies

Compound **2.39**, bearing a 5'-TAMRA label, was also investigated in a FA-based Y_1R binding assay using budded baculovirus particles (BBVs) as the Y_1R source (note that BBVs are favorable for FA measurement compared to whole cells and membrane preparations with respect to uniform shape, size, homogenous distribution, and stability[42]). Unlike the FC-based binding assay, requiring a large excess of the labeled ligand relative to the receptor concentration, FA measurements necessitate approximately equal concentrations of the fluorescent ligand and receptor. Consequently, ligand depletion is an unavoidable feature of FA assays. However, the mathematical analysis of the experimental data accounts for the occurring ligand depletion. For a detailed introduction into FA binding assays, see e.g. Rinken *et al.*[37] For FA Y_1R binding studies, **2.39** (used at two fixed concentrations: 0.5 and 3 nM) was incubated with increasing concentrations of Y_1R-displaying BBVs and the FA signal was measured in real time (for ≤ 15 h). In contrast to the FC-based assay setup, the FA assay setup enables the acquisition of kinetic data (association and dissociation rate constants) and equilibrium binding data (dissociation constant K_d) in one experiment. Moreover, this method allows an estimation of the receptor concentration for each experiment. To obtain k_{on}, k_{off} and

pK_d values of **2.39**, data from FA-based Y_1R binding studies were analyzed using a previously reported global model.[42] Both the association and dissociation of **2.39**, analyzed by global fitting, appeared to be monophasic (Figure 2.6 (panel A), for the purpose of illustration, data for only three receptor concentrations and one ligand concentration (0.5 nM) are shown). The obtained k_{on} and k_{off} values (caption of Figure 2.6) were in excellent agreement with $k_{on(mono)}$ and k_{off} from FC-based kinetic binding studies (Table 2.3). Consequently, the corresponding pK_d(kin) values of **2.39** (11.17 (FA) and 11.40 (FC)) were also in good agreement. Extracted FA data after completed association (30 min), representing equilibrium binding (Figure 2.6, panel B), gave a pK_d value of 11.02, which was in good agreement with the kinetically derived pK_d(kin) values of **2.39** obtained from either FA- or FC-based experiments but differed from the pK_d value from FC-based saturation binding experiments (lower cell density) by approximately 1 log unit (Table 2.3). These results suggest that the FA assay, taking into account ligand depletion, is better suited for the investigation of high-affinity probes.

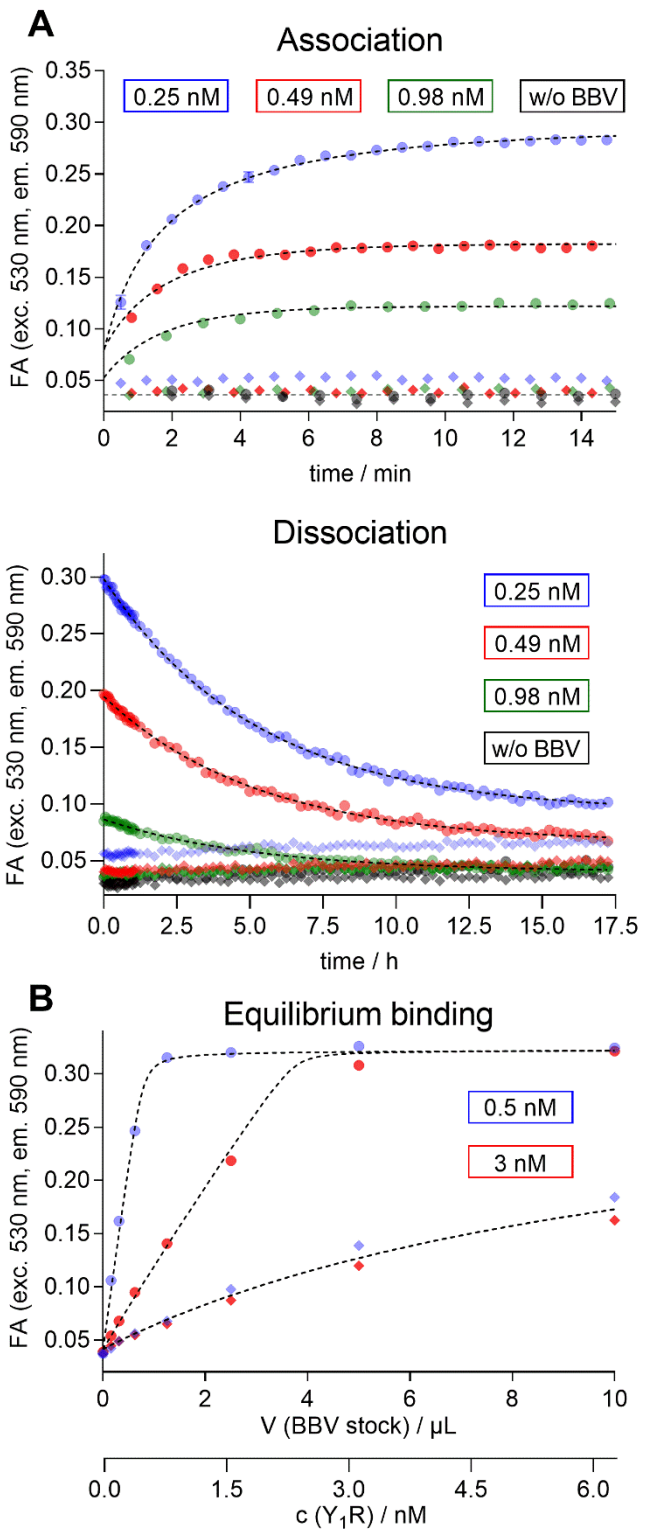

Figure 2.6. Binding of **2.39** to human Y_1 receptors, displayed on BBVs, studied at 27 °C by FA measurement. (A) Association and dissociation of **2.39** (0.5 nM) determined in real time for three different Y_1 receptor concentrations (green, red, and blue symbols). Total binding is represented by circles, and nonspecific binding (determined in the presence of 500 nM **2.2**) is represented by diamonds; data represent mean values ± SEM from one representative experiment performed in duplicate. Global fitting of the data from four individual association and three individual dissociation experiments, each involving six different receptor concentrations and two different concentrations of **2.39** (data not shown), yielded the following kinetic parameters: k_{on} = 0.52 ± 0.09 $min^{-1}nM^{-1}$, k_{off} = 0.0032 ± 0.0001 min^{-1}, $t_{1/2}$ = 3.60 ± 0.05 h, pK_d(kin) = 11.17 ± 0.09 (mean values ± SEM). (B) Binding isotherms of **2.39** obtained from experiments using fixed concentrations of **2.39** (0.5 nM or 3 nM) and increasing amounts of Y_1R. Total binding is represented by circles, and nonspecific binding (determined in the presence of 0.5 µM or 3 µM **2.2**) by diamonds. Depicted data (mean values ± SEM from one representative experiment performed in duplicate) represent snapshots after 30 min incubation from a total monitoring period of 15 h; global fitting of the data from three individual experiments yielded the following parameters: pK_d = 11.02 ± 0.04, c(Y_1R) (estimated binding site concentration of the applied BBV stock) = 63 ± 5 nM (mean values ± SEM). Y_1R concentrations displayed on the abscissa in panel B were calculated after global analysis of the data. Note: the signal cutoff value in panel B of ≈ 0.32 is mainly attributed to the theoretical limit for FA measurements.[43]

The determination of Y_1R binding data of the nonlabeled Y_1R ligands **2.2**, BIBO3304, BVD10 and pNPY in FA-based competition binding experiments using **2.39** as the fluorescent probe yielded Y_1R affinities, which were, except for that of pNPY, in good agreement with both the reported binding data, and the Y_1R affinities determined in FC-based competition binding studies (Table 2.4, supplementary Figure A2.10 in section A.2.3). As also observed in FC-

based competition binding experiments, **2.39** could be displaced by pNPY only at high pNPY concentrations yielding considerably lower Y_1R affinities compared to reported binding data. This indicated that these discrepancies cannot be attributed to the used methods, but rather to peculiarities of ligand-receptor interactions.

Table 2.4. Overview and comparison of Y_1R binding affinities of reported Y_1R ligands determined in FC- and FA-based competition binding assays using **2.35**, **2.37** and **2.39** as fluorescent probes.

compound	pK_i (hY_1R)				
	FC[a]			FA[b]	literature[c]
	2.35	**2.37**	**2.39**	**2.39**	
2.1	8.77 ± 0.14	8.36 ± 0.10	8.55 ± 0.15	7.96 ± 0.10	8.82[d] 8.14[e]
2.2	11.01 ± 0.17	10.23 ± 0.15	10.64 ± 0.03	10.75 ± 0.23	10.27[d]
BIBO3304	nd[h]	nd[h]	nd[h]	8.86 ± 0.07	9.60[f]
BVD10	nd[h]	nd[h]	nd[h]	7.39 ± 0.01	7.59[g]
pNPY	7.58 ± 0.24	8.15 ± 0.09	7.33 ± 0.15	< 6	9.30[d] 9.70[e] [17]

[a]Determined by FC-based competition binding using **2.35**, **2.37** or **2.39** as the fluorescent ligand (incubation period of 4 h (pNPY) or 2 h (**2.1** and **2.2**)). Mean values ± SEM from at least three independent experiments performed in duplicate. [b]Determined in FA-based competition binding assays using **2.39** as the fluorescent ligand (incubation period: 10 h). Mean values ± SEM from at least three independent experiments performed in duplicate. [c]Reported K_i values were converted to pK_i values. [d]Keller *et al*.;[20] [e]Rudolf *et al*.;[17] [f]Wieland *et al*.;[44] [g]Balasubramaniam *et al*.[45] [h]Not determined.

2.2.8 Fluorescence microscopy

Y_1R binding of **2.35**, **2.37** and **2.39** to live MCF-7-Y_1 cells was also studied by fluorescence microscopy (widefield epifluorescence and TIRF). Association of the ligand with the plasma membrane could be visualized with high contrast (Figure 2.7, widefield fluorescence). This membrane-localized fluorescence represented Y_1R binding as it could be abolished by the addition of the selective Y_1R ligand BIBO3304. Unlike the indolinium cyanine (**2.37**)- and 5'-TAMRA (**2.39**)-labeled ligands, the Py5-labeled ligand **2.35** was capable of entering the cells in a Y_1R-independent manner (intracellular fluorescence observed for total and nonspecific binding, Figure 2.7). This might be explained by the unfavorable physicochemical properties of the positively charged pyridinium dye in **2.35**, which was supported by the TIRF images: a strong adsorption of **2.35** to the cover glass was obvious, resulting in depletion and low membrane binding of **2.35** (Figure 2.7, panel C).

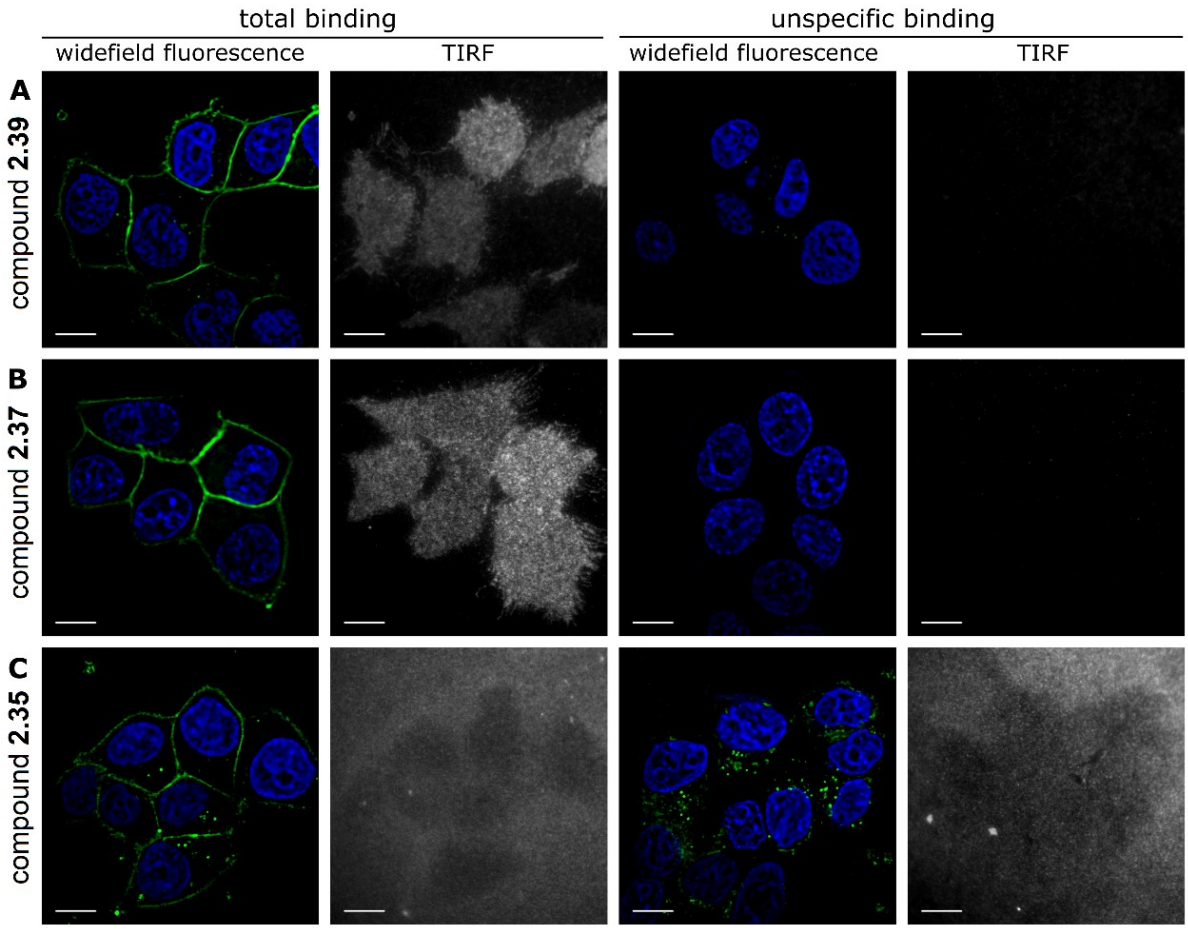

Figure 2.7. Visualization of fluorescent ligand binding to Y_1R-expressing MCF-7 mamma carcinoma cells using widefield fluorescence and TIRF microscopy. Shown are representative images acquired after incubation of the cells with (A) 1 nM **2.35**, (B) 1 nM **2.37**, or (C) 1 nM **2.39** at 37 °C for (B) 30 min or (A and C) 60 min. Nonspecific binding was determined in the presence of 10 µM BIBO3304. In widefield fluorescence images, the two-color composite of individual focal planes after Z-stack deconvolution is shown with green pseudocolor for fluorescent ligand channels (**2.37**: 638 nm excitation; **2.35** and **2.39**: 515 nm excitation) and blue pseudocolor for nuclear stain channels (Hoechst 34580 (B), 405 nm excitation; SiR-DNA (A and C), 638 nm excitation). In TIRF images, fluorescent ligand channels are shown in white pseudocolor. Scale bar of 10 µm.

In contrast, the TIRF images of **2.37** and **2.39** (panels A and B, respectively, of Figure 2.7) revealed clear plasma membrane binding, suggesting **2.37** and **2.39** as suitable tools for more detailed studies also at the single-molecule level, such as single-particle tracking[46, 47] or single-molecule FRET.[48] However, for this kind of experiment, **2.39** is considered more favorable than **2.37**, as indolinium cyanine dye labeled compound **2.37** showed fast photobleaching. This is demonstrated in a TIRF video sequence (recorded and shown at 10 Hz resolution, provided with the online full text of the publication), which displays the interactions of **2.39** (left panel) and **2.37** (right panel) with the basal plasma membrane of adherent MCF-7-Y_1 cells (experimental conditions as described in the caption of Figure 2.7 and under experimental procedures; scale bar of 10 µm).

2.3 Conclusion

We identified a position for linker attachment at the diphenylacetyl moiety in the high-affinity Y_1R antagonist UR-MK299 (**2.2**), which resulted in amine-functionalized labeling precursors with two-digit picomolar binding constants (pK_i (Y_1R) = 10.30-10.89). Conjugation of different fluorophores to the precursors was well tolerated with respect to Y_1R binding, yielding probes with three-digit picomolar binding constants (pK_i (Y_1R) = 9.36-9.95) and pronounced subtype selectivity (at least 1000-fold over the Y_2R, Y_4R and Y_5R). Until now, such a markedly high receptor affinity and selectivity have not been achieved for fluorescent probes targeting NPY receptors. Application of the fluorescent probes in flow cytometry- and fluorescence anisotropy-based receptor binding assays confirmed the high Y_1R affinity and revealed, with the exception of **2.40** ($t_{1/2}$ = 0.5 h), long receptor residence times ($t_{1/2}$ = 1.6-5.5 h). As demonstrated by widefield and, in the case of **2.39**, TIRF microscopy studies, these properties render the fluorescent ligands excellent tools for the imaging of Y_1Rs in live cells. Most importantly, the presented approach suggests that the synthesized amine-functionalized precursors are useful building blocks not only for the preparation of various fluorescent probes, but also for the synthesis of, for instance, radiotracers suitable for *in vivo* imaging of Y_1R-expressing tumors.

2.4 Experimental section

2.4.1 General experimental conditions

Chemicals. Standard chemicals, solvents, and buffer components were purchased from commercial suppliers (Sigma-Aldrich, München, Germany; Merck, Darmstadt, Germany; Fisher Scientific, Schwerte, Germany; TCI, Eschborn, Germany; ABCR, Karlsruhe, Germany; Iris Biotech, Marktredwitz, Germany) and used without further purification. Gradient grade acetonitrile for HPLC was purchased from Sigma Aldrich (München, Germany). (*R*)-(+)-1-phenylethylamine was from Sigma-Aldrich (München, Germany). Fura-2/AM and BSA were from Merck (Darmstadt, Germany) and SERVA (Heidelberg, Germany), respectively. Succinimidyl ester-activated dyes **2.32**, **2.33** and **2.34** were from FEW Chemicals (Wolfen, Germany), Lumiprobe (Hannover, Germany), and ABCR, respectively. Porcine NPY was obtained from SynPeptide (Shanghai, China). BVD10 was from Tocris Bioscience (Bristol, U.K.). Compounds **2.8**,[20] **2.11**,[18] **2.21**,[18] and **2.22**[18] and the pyrylium dye **2.31**[49] were prepared as described previously. The synthesis of BIBO3304 was described elsewhere.[21] [^{3}H]propionyl-pNPY (specific activity of 37.5 Ci/mmol, radiochemical purity of 99%) was prepared according to a previously reported procedure[20] with minor modifications (DMF/NMP/H_2O/DIPEA 45:20:32:3 v/v/v/v (60 µL) as solvent) instead of 0.1 M sodium borate buffer (pH 8.5, 135 µL); propionyl-pNPY was used instead of pNPY for the determination of the molarity and specific

activity; radiochemical yield of 26%). Reactions requiring anhydrous conditions were carried out in oven-dried (24 h at 120 °C) Schlenk flasks under an atmosphere of dry nitrogen using anhydrous solvents. Anhydrous DMF was from Sigma-Aldrich (München, Germany). Anhydrous CH_2Cl_2 and anhydrous benzene were prepared by storage over desiccants (3 Å molecular sieves, 20% m/v) for at least 2 days under an atmosphere of dry nitrogen. The molecular sieves were predried for 4 h at 300 °C immediately before use.[50] Purifications by column chromatography were carried out using technical grade solvents and Geduran Si 60 silica gel (pore size of 60 Å, particle size of 40-63 or 63-200 µm, Merck). Thin layer chromatography (TLC) was performed on ALUGRAM Xtra SIL G/UV254 TLC sheets from Macherey-Nagel GmbH & Co. KG (Düren, Germany).

Optical rotation. The optical rotation of (*R*)-**16** at 589 nm (Na D line) was measured on model P8000-T polarimeter equipped with an electronic Peltier thermostat PT31 (A. KRÜSS Optronic, Hamburg, Germany) using a thermostated (20 °C) microcuvette (layer thickness of 1 dm, volume of 0.9 mL).

NMR spectroscopy. NMR spectra were recorded on a Bruker Avance 300 (^{1}H, 300 MHz, ^{13}C, 75 MHz), an Avance 400 (^{1}H, 400 MHz, ^{13}C, 100 MHz) or an Avance 600 (^{1}H, 600 MHz, ^{13}C, 150 MHz) spectrometer (Bruker, Karlsruhe, Germany). The ^{1}H-NMR spectra of compounds **2.35-2.40** were recorded in 10:1 (v/v) DMSO-d_6/D_2O resulting in a total H-D exchange of the phenolic OH proton and NH protons of the (carbamoylated) guanidino groups and no or a partial H-D exchange of amide NH protons (Note: Spectra were recorded at least 2 h after the preparation of the samples). Because only very small amounts (< 0.5 µmol) of the fluorescent ligands were used for ^{1}H-NMR spectroscopy, characteristic system signals were apparent in the ^{1}H-NMR (0.81-0.87 ppm and 1.20-1.30 ppm), most likely originating from impurities in the solvents used for preparative HPLC (*cf.* supplementary Figure A2.11 in section A.2.3).

Mass spectrometry. Low-resolution mass spectrometry (MS) analysis was performed on an AccuTOF GCX (Jeol, Freising, Germany) (EI-MS, FD-MS), a Finnigan ThermoQuest TSQ 7000 (Thermo Scientific, Waltham, MA) (ESI-MS) or on a Finnigan SSQ 710 A (Thermo Scientific) (EI-MS) instrument. High-resolution mass spectrometry (HRMS) analysis was performed on an Agilent 6540 UHD AccurateMass Q-TOF LC/MS system (Agilent Technologies, Santa Clara, CA) (ESI-MS). LC analyses were performed using the following method: column: ZORBAX RRHD Eclipse Plus C18, 1.8 µm, 50 × 2.1 mm (Agilent Technologies, Santa Clara, CA), column temperature: 40 °C, flow: 0.6 mL/min, solvent/linear gradient: 0-4 min: 0.1% aqueous HCOOH/0.1% HCOOH in MeCN 95:5-2:98, 4-5 min: 2:98 (isocratic).

Analytical RP-HPLC. Reaction controls, purity controls, and investigations of compound stability were carried out by analytical HPLC (RP-HPLC) using an 1100 series system from Agilent Technologies (herein termed system A) consisting of a degasser (G1379A), a binary pump (G1312A), a diode array detector (G1315A), a thermostated column compartment (G1316A), and an autosampler (G1329A), or on an identically composed 1100 series system from Agilent Technologies, except for a variable wavelength detector (G1314A) instead of the diode array detector (herein termed system B). A Phenomenex Kinetex XB-C18 100A (5 µm, 250 mm × 4.6 mm, Phenomenex, Aschaffenburg, Germany) was used as the stationary phase. The flow rate was 0.8 mL min^{-1}, the oven temperature was set to 30 °C, and the injection volume was 40 µL. Mixtures of solvents A (0.05% aqueous TFA) and B (acetonitrile) were used as the mobile phase. The following gradient was applied: 0-30 min: A/B 90:10 to 5:95, 30-40 min: A/B 5:95 (isocratic). For the reaction control of (*R*,*R*)-**2.14** and (*S*,*R*)-**2.14** (*cf*. supplementary Figure A2.3 in section A.2.3), the following gradient was applied: 0-9 min: A/B 90:10 to 75:25, 9-19 min: A/B 75:25 to 65:35, 19-33 min: A/B 65:35 to 5:95, 33-40 min: A/B 5:95 (isocratic). The detection wavelength was set to 220 nm throughout. Retention factor *k* was calculated according to the following equation $k = (t_R\text{-}t_0)/t_0$ (where t_0 is the dead time of 2.6 min for systems A and B). Chromatograms of the RP-HPLC purity controls of the target compounds (*R*,*R*)-**2.14**, (*S*,*R*)-**2.14**, (*R*,*R*)-**2.30**, (*S*,*R*)-**2.30**, and **2.35**-**2.40** are provided in section A.2.6. The purities of these compounds were >95%.

Preparative HPLC. Purifications by preparative HPLC were performed with a system from Knauer (Berlin, Germany), composed of two K-1800 pumps and a K-2001 detector (herein termed system C), or with a Prep 150 LC system from Waters (Eschborn, Germany) consisting of a 2545 binary gradient module, a 2489 UV/visible detector and a Waters Fraction Collector III (herein termed system D). A Kinetex-XB C18 (5 µm, 250 mm × 21 mm, Phenomenex), a Gemini-NX C18 110A (5 µm, 250 mm × 21 mm, Phenomenex) or a YMC-Actus Triart C18 (5 µm, 150 mm × 20 mm, YMC, Dinslaken, Germany) were used as the stationary phase. The mobile phase was composed of the solvents C (0.1% aqueous TFA with 5% acetonitrile) and B (acetonitrile). Lyophilization of the eluates containing the products was performed with a Scanvac CoolSafe 100-9 freeze-drying apparatus (Labogene, Allerød, Denmark) equipped with a RZ 6 rotary vane vacuum pump (Vacuubrand, Wertheim, Germany). Compound **2.38** was purified by analytical HPLC using system A and a semipreparative YMC-Triart C18 column (5 µm, 250 mm × 6.0 mm, YMC) as the stationary phase at a flow rate of 1.5 mL/min.

2.4.2 Experimental synthetic protocols and analytical data

***N*-(2-Aminoethyl)aminocarbonyl-*S*-methylisothiourea bis(hydrotrifluoroacetate) (2.7)**

A solution of TFA (10.0 mL, 130 mmol) in CH_2Cl_2 (10 mL) was added dropwise to a solution of **2.6** (3.3 g, 8.7 mmol) in CH_2Cl_2 (80 mL) at rt over a period of 30 min. The mixture was stirred at rt at 900 mbar for 16 h followed by rotary evaporation of the volatiles. CH_2Cl_2 (50 mL) was added, the volatiles were removed by rotary evaporation, and the process was repeated twice. The resulting oily residue was taken up in H_2O (50 mL) followed by lyophilization yielding **2.7** as a white fluffy solid (3.2 g, 8.1 mmol, 91%), which was used without further purification. ^{1}H-NMR (400 MHz, DMSO-d_6): δ (ppm) 2.28 (s, 3H), 2.96-3.11 (m, 4H), 7.34-7.50 (br s, 1H), 7.74 (br s, 3H), 8.88-9.28 (m, 3H). ^{13}C-NMR (100 MHz, DMSO-d_6): δ (ppm) 13.25, 38.24, 40.12, 157.70, 167.12. MS (LC-HRMS, ESI): *m/z* $[M+H]^+$ calcd for $[C_5H_{13}N_4OS]^+$ 177.0805, found 177.0806. $C_5H_{12}N_4OS \times C_4H_2F_6O_4$ (404.28).

***N*-(2-Propionylaminoethyl)aminocarbonyl-*S*-methylisothiourea (2.9)**

Triethylamine (9.6 mL, 69.5 mmol) and a solution of **2.8** (1.5 g, 8.7 mmol) in CH_2Cl_2 (10 mL) were added to a suspension of **2.7** (3.2 g, 8.1 mmol) in CH_2Cl_2 (150 mL) and the reaction mixture was stirred at rt for 1 h. The white precipitate was filtered off, and the solvent was removed by rotary evaporation. The product was purified by column chromatography (ethyl acetate to ethyl acetate/methanol 4:1 v/v) to yield **2.9** as a white solid (1.5 g, 6.4 mmol, 79%). TLC (ethyl acetate/methanol 6:1 v/v): R_f = 0.45. ^{1}H-NMR (400 MHz, DMSO-d_6): δ (ppm) 0.98 (t, *J* = 7.6 Hz, 3H), 2.05 (q, *J* = 7.6 Hz, 2H), 2.30 (s, 3H), 3.00-3.13 (m, 4H), 6.97 (s, 1H), 7.77 (s, 1H), 8.48 (br s, 2H). ^{13}C-NMR (100 MHz, DMSO-d_6): δ (ppm) 10.34, 13.57, 28.96, 158.29, 165.86, 174.01. Note: the carbon signals of the ethylene group were not apparent due to interference with the solvent residual peak. MS (LC-HRMS, ESI): *m/z* $[M+H]^+$ calcd for $[C_8H_{17}N_4O_2S]^+$ 233.1067, found 233.1068. $C_8H_{16}N_4O_2S$ (232.30).

***N*-*tert*-Butoxycarbonyl-*N'*-(2-propionylaminoethyl)aminocarbonyl-*S*-methylisothiourea (2.10)**

A solution of di-*tert*-butyldicarbonate (3.8 g, 17.2 mmol) in CH_2Cl_2 (30 mL) was added in small portions to a stirred suspension of **2.9** (1.5 g, 6.4 mmol), DMAP (0.78 g, 6.4 mmol) and triethylamine (2.4 mL, 17.2 mmol) in CH_2Cl_2 (100 mL) at rt over a period of 2 h. The mixture was washed with H_2O (2 × 100 mL) and dried over Na_2SO_4, and the solvent was removed by rotary evaporation. The product was purified by column chromatography (light petroleum/ethyl acetate 1:4 v/v to ethyl acetate/methanol 5:1 v/v) to yield **2.10** as a white solid (1.6 g, 4.7 mmol, 73%). TLC (ethyl acetate): R_f = 0.50. ^{1}H-NMR (400 MHz, DMSO-d_6): δ (ppm) 0.98 (t, *J* = 7.6 Hz, 3H), 1.44 (s, 9H), 2.06 (q, *J* = 7.6 Hz, 2H), 2.28 (s, 3H), 3.05-3.15 (m, 4H), 7.72-7.94 (m, 2H), 12.30 (s, 1H). ^{13}C-NMR (100 MHz, DMSO-d_6): δ (ppm) 9.86, 13.58, 27.59, 28.49,

37.93, 39.08, 82.17, 150.18, 161.60, 164.82, 173.07 (the signals at 37.93 and 39.08 ppm, interfering with the solvent residual peak, were identified by ^{1}H-^{13}C HSQC). MS (LC-HRMS, ESI): *m/z* $[M+H]^+$ calcd for $[C_{13}H_{25}N_4O_4S]^+$ 333.1591, found 333.1594. $C_{13}H_{24}N_4O_4S$ (332.42).

N^{δ}-Benzyloxycarbonyl-*N*'-(4-*tert*-butoxybenzyl)-N^{α}-(((*S*)-3-(4-((*tert*-butoxycarbonyl)-amino)butoxy)phenyl)(phenyl)acetyl)-(*R*)-ornithinamide ((*S,R*)-2.13) and N^{δ}-Benzyloxycarbonyl-*N*'-(4-*tert*-butoxybenzyl)-N^{α}-(((*R*)-3-(4-((*tert*-butoxycarbonyl) amino)butoxy)phenyl)(phenyl)acetyl)-(*R*)-ornithinamide ((*R,R*)-2.13)

A solution of **2.12** (1.36 g, 3.4 mmol), HOBt (0.52 g, 13.6 mmol), HBTU (1.29 g, 3.4 mmol) and DIPEA (2.3 mL, 13.6 mmol) in DMF (50 mL) was stirred at 0 °C for 5 min. **2.11** (1.46 g, 3.4 mmol) was added, and stirring was continued at 0 °C for 15 min. H_2O (200 mL) was added, and the mixture was treated with ethyl acetate (100 mL). The organic layer was separated, washed with H_2O (3 × 100 mL), and dried over Na_2SO_4. The solvent was removed by rotary evaporation, and the product was purified by column chromatography (light petroleum/ethyl acetate 5:2 v/v to light petroleum/ethyl acetate 1:1 v/v) to yield **2.13** as a white solid (1.77 g, 2.19 mmol, 64%). Analytical RP-HPLC (system A): t_R = 31.0 min, k = 10.9. Note: the two diastereomers (*S*,*R*)-**2.13** and (*R*,*R*)-**2.13** could not be separated on the used nonchiral HPLC column (*cf*. supplementary Figure A2.3, panel C in section A.2.3). TLC (light petroleum/ethyl acetate 1:1 v/v): R_f = 0.40. ^{1}H-NMR (400 MHz, DMSO-d_6): δ (ppm) 1.26 (s, 9H), 1.30-1.44 (m, 11H), 1.45-1.70 (m, 6H), 2.89-2.99 (m, 4H), 3.85-3.90 (m, 2H), 4.15-4.31 (m, 3H), 4.99 (s, 2H), 5.06 (s, 1H), 6.75-6.89 (m, 6H), 7.06-7.11 (m, 2H), 7.15-7.38 (m, 12H), 8.36-8.46 (m, 2H). ^{13}C-NMR (100 MHz, DMSO-d_6): δ (ppm) 26.00, 26.11, 26.15, 28.27, 28.53, 29.65, 39.47 (two merging carbon signals, as identified by ^{1}H-^{13}C HSQC), 41.48, 52.55, 55.84, 65.13, 66.98, 77.37, 77.73, 112.10, 115.05, 120.70, 123.56, 126.53, 127.66, 127.70, 127.74, 128.11, 128.34, 128.55, 129.19, 133.73, 137.23, 140.25, 141.93, 153.76, 155.62, 156.08 158.46, 170.82, 171.41. MS (LC-HRMS, ESI): *m/z* $[M+H]^+$ calcd for $[C_{47}H_{61}N_4O_8]^+$ 809.4484, found 809.4495. $C_{47}H_{60}N_4O_8$ (809.02).

N^{δ}-Benzyloxycarbonyl-*N*-(4-*tert*-butoxybenzyl)-N^{α}-((*S*)-2-(3-(4-((*tert*-butoxycarbonyl)-amino)butoxy)phenyl)-2-phenylacetyl)-(*R*)-ornithinamide ((*S,R*)-2.13)

A solution of **2.24** (108 mg, 0.42 mmol) in anhydrous DMF (5 mL) was added to a heated (40 °C) stirred suspension of (*S*,*R*)-**2.23** (135 mg, 0.21 mmol) and cesium carbonate (135 mg, 0.42 mmol) in anhydrous DMF (5 mL). Stirring was continued at 40 °C for 16 h. The mixture was diluted with H_2O/acetonitrile 1:1 v/v (15 mL) and subjected to preparative HPLC (system B, column: Actus Triart C18, gradient: 0-20 min: C/B 40:60-5:95, t_R = 12 min) yielding (*S*,*R*)-**2.13** as a white solid (142 mg, 0.18 mmol, 84%). Analytical RP-HPLC (system A): t_R = 31.0 min, k = 10.9. Note: NMR data of **2.13** are provided under the description of the

nondiastereoselective synthesis of **2.13**. As (*S*,*R*)-**2.13** and (*R*,*R*)-**2.13** could not be separated on the used nonchiral HPLC column, the diastereomeric excess of (*S*,*R*)-**2.13** could not be determined. However, the diastereomeric excess of (*S*,*R*)-**2.14** (de = 50%), which was prepared from (*S*,*R*)-**2.13**, revealed that the ratio of (*S*,*R*)-**2.13**/(*R*,*R*)-**2.13** consequently was ≥ 3:1. MS (LC-HRMS, ESI): *m/z* $[M+H]^+$ calcd for $[C_{47}H_{61}N_4O_8]^+$ 809.4484, found 809.4478. $C_{47}H_{60}N_4O_8$ (809.02).

N^{α}-(((*S*)-3-(4-Aminobutoxy)phenyl)(phenyl)acetyl)-N^{ω}-((2-(propionyl)-aminoethyl)aminocarbonyl)-*N*'-(4-hydroxybenzyl)-(*R*)-argininamide bis(hydrotrifluoroacetate) ((*S*,*R*)-2.14) and N^{α}-(((*R*)-3-(4-Aminobutoxy)phenyl)(phenyl)acetyl)-N^{ω}-((2-(propionyl)-aminoethyl)aminocarbonyl)-*N*'-(4-hydroxybenzyl)-(*R*)-argininamide bis(hydrotrifluoroacetate) ((*R*,*R*)-2.14)

Palladium on activated charcoal (10 wt %, 100 mg) was suspended in a stirred solution of **2.13** (0.58 g, 0.72 mmol) in trifluoroethanol (30 mL). The vigorously stirred mixture was set under an atmosphere of hydrogen (1 bar) at rt for 3 h followed by centrifugation. The solvent of the supernatant was removed by rotary evaporation and the residue was dissolved in CH_2Cl_2 (30 mL). **2.10** (0.24 g, 0.72 mmol), mercury(II) chloride (0.29 g, 1.08 mmol) and DIPEA (0.49 mL, 2.87 mmol) were added, and the mixture was stirred at rt for 30 min. The mixture was centrifuged, the supernatant was collected, and the pellet was washed with CH_2Cl_2 (2 × 30 mL, each followed by centrifugation). The supernatants were combined, and the solvent was removed by rotary evaporation. A solution of TFA (2.5 mL) in CH_2Cl_2 (10 mL) was added, the mixture was stirred at rt at 900 mbar for 3 h and the volatiles were removed *in vacuo*. The residue was subjected to preparative HPLC (system C, column: Gemini-NX C18, gradient: 0-15 min: C/B 88:12-83:17, 15-40 min: C/B 83:17, t_R((*R*,*R*)-**2.14**) = 28 min, t_R((*S*,*R*)-**2.14**) = 32 min) yielding (*R*,*R*)-**2.14** (53 mg, 0.06 mmol, 8%) and (*S*,*R*)-**2.14** (152 mg, 0.16 mmol, 23%) as white fluffy, hygroscopic solids. Analytical data of (*R*,*R*)-**2.14**: RP-HPLC (system B, 220 nm): 96%, t_R = 11.8 min, *k* = 3.5. ^{1}H-NMR (600 MHz, DMSO-d_6): δ (ppm) 0.98 (t, *J* = 7.7 Hz, 3H), 1.36-1.58 (m, 3H), 1.63-1.76 (m, 5H), 2.06 (q, *J* = 7.7 Hz, 2H), 2.80-2.87 (m, 2H), 3.13-3.24 (m, 6H), 3.92 (t, *J* = 6.1 Hz, 2H), 4.10-4.18 (m, 2H), 4.29-4.34 (m, 1H), 5.09 (s, 1H), 6.64-6.70 (m, 2H), 6.78-6.82 (m, 1H), 6.83-6.88 (m, 2H), 6.98-7.03 (m, 2H), 7.17-7.24 (m, 2H), 7.26-7.32 (m, 4H), 7.51 (br s, 1H), 7.71-7.91 (m, 4H), 8.34-8.54 (m, 4H), 9.00 (s, 1H), 9.34 (br s, 1H), 10.47 (s, 1H). ^{13}C-NMR (150 MHz, DMSO-d_6): δ (ppm) 9.84, 23.97, 24.62, 25.69, 28.49, 29.43, 38.09, 38.66, 39.10 (interfering with the solvent residual signal, as identified by ^{1}H-^{13}C HSQC), 40.34, 41.65, 52.33, 55.79, 66.63, 112.03, 115.04, 115.14, 115.98 (TFA), 118.95 (TFA), 120.95, 126.65, 128.21, 128.41, 128.47, 129.10, 129.19, 140.32, 141.78, 153.68, 153.95, 156.31, 158.37, 170.94, 171.06, 173.29. MS (LC-HRMS, ESI): *m/z* $[M+H]^+$ calcd for $[C_{37}H_{51}N_8O_6]^+$ 703.3926, found 703.3935. Analytical data of (*S*,*R*)-**2.14**: RP-HPLC

(system B, 220 nm): 99%, t_R = 11.9 min, k = 3.6. ^{1}H-NMR (600 MHz, DMSO-d_6): δ (ppm) 0.98 (t, J = 7.6 Hz, 3H), 1.38-1.58 (m, 3H), 1.64-1.76 (m, 5H), 2.06 (q, J = 7.6 Hz, 2H), 2.81-2.87 (m, 2H), 3.12-3.23 (m, 6H), 3.91 (t, J = 6.1 Hz, 2H), 4.10-4.19 (m, 2H), 4.28-4.34 (m, 1H), 5.08 (s, 1H), 6.66-6.69 (m, 2H), 6.78-6.81 (m, 2H), 6.87-6.90 (m, 1H), 6.98-7.02 (m, 2H), 7.19-7.25 (m, 2H), 7.26-7.31 (m, 4H), 7.51 (br s, 1H), 7.69-7.91 (m, 4H), 8.35 (t, J = 5.8 Hz, 1H), 8.39-8.54 (m, 3H), 9.00 (s, 1H), 9.33 (br s, 1H), 10.46 (s, 1H). ^{13}C-NMR (150 MHz, DMSO-d_6): δ (ppm) 9.81, 23.96, 24.63, 25.69, 28.49, 29.36, 38.08, 38.66, 39.12 (interfering with the solvent residual signal, as identified by ^{1}H-^{13}C HSQC), 40.37, 41.64, 52.40, 55.81, 66.63, 111.96, 115.30, 115.70, 116.65 (q, J = 295 Hz, TFA), 120.86, 126.62, 128.19, 128.42, 128.48, 129.12, 129.25, 140.18, 141.91, 153.69, 153.94, 156.30, 158.37, 158.65 (q, J = 33 Hz, TFA), 170.90, 171.00, 173.30. MS (LC-HRMS, ESI): *m/z* $[M+H]^+$ calcd for $[C_{37}H_{51}N_8O_6]^+$ 703.3926, found 703.3936. $C_{37}H_{50}N_8O_6 \times C_4H_2F_6O_4$ (930.90).

N^{α}-(((*S*)-3-(4-Aminobutoxy)phenyl)(phenyl)acetyl)-N^{ω}-((2-(propionyl)-aminoethyl)aminocarbonyl)-*N'*-(4-hydroxybenzyl)-(*R*)-argininamide bis(hydrotrifluoroacetate) ((*S*,*R*)-2.14, 50% *de*)

The three-step synthesis was carried out in analogy to the nondiastereoselective synthesis of (*S*,*R*)/(*R*,*R*)-**2.14**, but diastereomerically enriched (*S*,*R*)-**2.13** (142 mg, 0.18 mmol) was used as starting material. (*S*,*R*)-**2.14** was obtained in a diastereomeric excess (de) of 50% over (*R*,*R*)-**2.14** (*cf.* supplementary Figure A2.3, panel D in section A.2.3). Separation from (*R*,*R*)-**2.14** by preparative HPLC yielded pure (*S*,*R*)-**2.14** as a white hygroscopic solid (27 mg, 0.03 mmol, 16%). Analytical RP-HPLC (system A, 220 nm, applied gradient see general experimental section): t_R((*R*,*R*)-**2.14**) = 16.2 min, k = 5.2, t_R((*S*,*R*)-**2.14** = 16.7 min, k = 5.4. Note: NMR data of **2.14** are provided under the description of the nondiastereoselective synthesis of (*S*,*R*)-**2.14** and (*R*,*R*)-**2.14**. MS (LC-HRMS, ESI): *m/z* $[M+H]^+$ calcd for $[C_{37}H_{51}N_8O_6]^+$ 703.3926, found 703.3935. $C_{37}H_{50}N_8O_6 \times C_4H_2F_6O_4$ (930.90).

((*R*)-3-Methoxyphenyl)(phenyl)acetic acid ((*R*)-2.16)

Concentrated sulfuric acid (80 mL) was added carefully to a stirred and cooled (0 °C) suspension of **2.15** (7.2 g, 32.2 mmol) in H_2O (100 mL) and glacial acetic acid (30 mL). The reaction mixture was refluxed for 16 h. The cooled mixture (rt) was diluted with H_2O (200 mL) and treated with CH_2Cl_2 (300 mL). The organic layer was separated, and the solvents were removed by rotary evaporation. The product was purified by column chromatography (light petroleum/ethyl acetate 4:1 v/v to light petroleum/ethyl acetate 1:1 v/v) to yield (*rac*)-**2.16** as a yellow solid. A solution of (*rac*)-**2.16** (29.8 g, 123 mmol) and (*R*)-(+)-1-phenylethylamine (15.6 mL, 123 mmol) in chloroform/hexane 45:55 v/v (1.3 L) was heated to reflux and slowly cooled down to rt. After 1 h, the white crystalline precipitate was separated by filtration, dried

in vacuo, and subjected to recrystallization from chloroform/hexane 45:55 v/v. The recrystallization procedure was repeated six times (in each step, the used volume of the solvent was reduced according to the reduction of the feed). The final precipitate was dissolved in ethyl acetate (50 mL) and the mixture was treated with aqueous HCl (0.1 N, 100 mL). The organic layer was separated, and the volatiles were removed *in vacuo* to yield (*R*)-**2.16** as a white crystalline solid (690 mg, 2.8 mmol, 5%, mp 89 °C, *ee* = 90%, as determined by ^{1}H-NMR, *cf.* supplementary Figure A2.1 in section A.2.3). TLC (light petroleum/ethyl acetate 4:1 v/v): R_f = 0.30. $[\alpha]^{20}_D$ −11.2 (*c* 4.9 g/100mL, methanol). ^{1}H-NMR (400 MHz, DMSO-d_6): δ (ppm) 3.71 (s, 3H), 5.04 (s, 1H), 6.81-6.85 (m, 1H), 6.88-6.93 (m, 2H), 7.21-7.27 (m, 2H), 7.29-7.35 (m, 4H), 12.63 (br s, 1H). ^{13}C-NMR (100 MHz, DMSO-d_6): δ (ppm) 54.99. 56.19, 111.91, 114.65, 120.74, 126.88, 128.38, 128.49, 129.46, 139.44, 140.96, 159.23, 173.32. MS (LC-HRMS, ESI): *m/z* $[M+H]^+$ calcd for $[C_{15}H_{15}O_3]^+$ 243.1016, found 243.1012. $C_{15}H_{14}O_3$ (242.70).

((*R*)-3-Hydroxyphenyl)(phenyl)acetic acid ((*R*)-2.17)

Boron tribromide (1 M in hexanes, 590 µL, 0.59 mmol) was added to a stirred cooled (−84 °C) solution of (*R*)-**2.16** (24 mg, 0.10 mmol) in CH_2Cl_2 (5 mL). The mixture was stirred at −84 °C for 1 h, allowed to warm to rt, and stirring was continued for an additional 30 min. The reaction was quenched by the addition of ice-cold aqueous HCl (1 N, 5 mL). The reaction mixture was treated with ethyl acetate (20 mL) and the solvents were removed by rotary evaporation. The crude product was purified by preparative (system D, column: Actus Triart C18, gradient: 0-30 min: C/B 80:20-50:50, t_R((*R*)-**2.17**) = 15 min) to yield (*R*)-**2.17** as a white solid (15 mg, 0.07 mmol, 68%, *ee* = 74%, as determined by ^{1}H-NMR, *cf.* supplementary Figure A2.2 in section A.2.3). Note: NMR and MS data are provided under the description of the synthesis of (*rac*)-**2.17**.

((*rac*)-3-Hydroxyphenyl)(phenyl)acetic acid ((*rac*)-2.17)

A stirred suspension of **2.15** (10.0 g, 44.8 mmol) in glacial acetic acid (20 mL) and aq. hydrobromic acid (47%, 30 mL) was refluxed for 16 h. The mixture was diluted with H_2O (200 mL) and treated with CH_2Cl_2 (2 × 150 mL). The combined organic layers were dried over Na_2SO_4, and the volatiles were removed *in vacuo* to yield (*rac*)-**2.17** as a green solid (7.7 g, 33.7 mmol, 75%), which was used without further purification. TLC (light petroleum/ethyl acetate/acetic acid 66:33:1 v/v/v): R_f = 0.25. ^{1}H-NMR (400 MHz, DMSO-d_6): δ (ppm) 4.94 (s, 1H), 6.61-6.65 (m, 1H), 6.70-6.74 (m, 2H), 7.07-7.12 (m, 1H), 7.21-7.27 (m, 1H), 7.28-7.35 (m, 4H), 9.36 (br s, 1H), 12.64 (br s, 1H). ^{13}C-NMR (100 MHz, DMSO-d_6): δ (ppm) 56.18, 113.85, 115.35, 119.15, 126.81, 128.31, 128.52, 129.31, 139.49, 140.75, 157.31, 173.37. $C_{14}H_{12}O_3$ (228.25). MS (LC-MS, ESI): *m/z* (%) 229.1 (100) $[M+H]^+$. $C_{15}H_{13}NO$ (223.28).

(*R*)-*N*$^{\delta}$-Benzyloxycarbonylornithine *tert*-butyl ester[51] (2.18)

Aq. perchloric acid (72%, 244 µL, 2.9 mmol) was added to a stirred cooled (0 °C) suspension of **2.21** (0.69 g, 2.6 mmol) in *tert*-butyl acetate (50 mL). The mixture was allowed to warm to rt and stirring was continued for 16 h. H_2O (50 mL) and ethyl acetate (50 mL) were added, and the pH value of the aqueous layer was adjusted to 9 by the dropwise addition of saturated aqueous $NaHCO_3$. The organic layer was separated and dried with Na_2SO_4, and the volatiles were removed *in vacuo* to yield **2.18** as a colorless resin (0.82 g, 2.5 mmol, 98%), which was used without further purification. ^{1}H-NMR (400 MHz, DMSO-d_6): δ (ppm) 1.38-1.66 (m, 13H), 2.94-3.06 (m, 2H), 3.40-3.53 (m, 1H), 4.98-5.06 (m, 2H), 7.26-7.40 (m, 5H). Note: NH signals of the amino group and the carbamate protecting group were not apparent. ^{13}C-NMR (100 MHz, DMSO-d_6): δ (ppm) 25.40, 27.62, 30.29, 39.96 (interfering with the solvent residual peak, as identified by ^{1}H-^{13}C HSQC), 53.41, 65.13, 81.06, 127.72, 127.77, 128.35, 137.24, 156.11, 172.04. MS (LC-MS, ESI): *m/z* (%) 323.2 (100) $[M+H]^+$. $C_{17}H_{25}N_2O_4$ (322.41).

N^{α}-(((*R*)-3-Hydroxyphenyl)(phenyl)acetyl)-(*R*)-N^{δ}-benzyloxycarbonylornithine ((*R*,*R*)-2.19, 56% *de*)

DCC (50 µL of a 20 mM solution in CH_2Cl_2, 1 µmol) was added to a cooled (4 °C) mixture of HOBt (50 µL of a 20 mM solution in CH_2Cl_2, 1 µmol), **2.18** (50 µL of a 20 mM solution in CH_2Cl_2, 1 µmol) and (*R*)-**2.17** (200 µL from a 5 mM solution in CH_2Cl_2, 1 µmol, 74% *ee)* in a 1.5-mL polypropylene reaction vessel and the mixture was stirred at 4 °C for 1 h. TFA (200 µL) was added and stirring was continued for 1 h. The mixture was analyzed by analytical RP-HPLC and LC-HRMS, and the target compound (*R*,*R*)-**2.19** and its epimer (*S*,*R*)-**2.19** were identified in a diastereomeric ratio of 78:22 (56% *de* of (*R*,*R*)-**2.19** over (*S*,*R*)-**2.19**, *cf*. Scheme 2.2). Analytical RP-HPLC (system B, 220 nm): t_R((*S*,*R*)-**2.19**) = 19.2 min, k = 6.4, t_R((*R*,*R*)-**2.19**) = 19.6 min, k = 6.5. MS (LC-HRMS, ESI): *m/z* ((*S*,*R*)-**2.19**) $[M+H]^+$ calcd for $[C_{27}H_{29}N_2O_6]^+$ 477.2020, found 477.2024. *m/z* $[M+H]^+$ ((*R*,*R*)-**2.19**) calcd for $[C_{27}H_{29}N_2O_6]^+$ 477.2020, found 477.2028. $C_{27}H_{28}N_2O_6$ (476.53). Note: NMR data of **2.19** are provided under the following description of the nondiastereoselective synthesis of (*R*,*R*)-**2.19** and (*S*,*R*)-**2.19**.

N^{α}-(((*S*)-3-Hydroxyphenyl)(phenyl)acetyl)-(*R*)-N^{δ}-benzyloxycarbonylornithine ((*S*,*R*)-2.19) and N^{α}-(((*R*)-3-Hydroxyphenyl)(phenyl)acetyl)-(*R*)-N^{δ}-benzyloxycarbonylornithine ((*R*,*R*)-2.19)

A suspension of **2.21** (0.39 g, 1.48 mmol) and DIPEA (0.25 mL, 1.48 mmol) in DMF (25 mL) and H_2O (25 mL) was added to a solution of **2.20** (0.48 g, 1.48 mmol) in DMF (50 mL) and the mixture was stirred at rt for 2 h. Aq. HCl (1 N, 100 mL) and ethyl acetate (100 mL) were added, and the mixture was vigorously shaken. The organic layer was separated and washed with H_2O (2 × 100 mL), and the solvent was removed by rotary evaporation. The products were

purified by preparative HPLC (system B, column: Gemini-NX C18, gradient: 0-30 min: C/B 70:30-60:40, t_R((*S*,*R*)-**2.19**) = 21 min, t_R((*R*,*R*)-**2.19**) = 22 min) to yield (*S*,*R*)-**2.19** (122 mg, 0.26 mmol, 17%) and (*R*,*R*)-**2.19** (105 mg, 0.22 mmol, 15%) as white, fluffy hygroscopic solids. Analytical data of (*S*,*R*)-**2.19**: RP-HPLC (system A, 220 nm): 95%, t_R((*S*,*R*)-**2.19**) = 20.3 min, *k* = 6.8 (*cf*. supplementary Figure A2.3, panel A in section A.2.3). RP-HPLC (system B, 220 nm): 95%, t_R((*S*,*R*)-**2.19**) = 19.2 min, *k* = 6.4 (*cf*. Scheme 2.2). ^{1}H-NMR (600 MHz, DMSO-d_6): δ (ppm) 1.36-1.48 (m, 2H), 1.52-1.64 (m, 1H), 1.66-1.77 (m, 1H), 2.93-3.03 (m, 2H), 4.14-4.22 (m, 1H), 4.97 (s, 1H), 5.01 (s, 2H), 6.58-6.63 (m, 1H), 6.67-6.72 (m, 2H), 7.03-7.10 (m, 1H), 7.18-7.39 (m, 11H), 8.53 (d, *J* = 7.5 Hz, 1H), 9.28 (br s, 1H), 12.54 (br s, 1H). ^{13}C-NMR (150 MHz, DMSO-d_6): δ (ppm) 26.52, 28.94, 39.52 (interfering with the solvent residual peak, as identified by ^{1}H-^{13}C HSQC), 52.44, 55.32, 65.60, 114.08, 116.03, 119.68, 126.95, 128.17, 128.21, 128.52, 128.82, 129.01, 129.52, 137.73, 140.82, 142.13, 156.58, 157.62, 171.59, 173.93. MS (LC-HRMS, ESI): *m/z* $[M+H]^+$ calcd for $[C_{27}H_{29}N_2O_6]^+$ 477.2020, found 477.2027. Analytical data of (*R*,*R*)-**2.19**: RP-HPLC (system A, 220 nm): 95%, t_R((*R*,*R*)-**2.19**) = 20.6 min, *k* = 6.9 (*cf*. supplementary Figure A2.3, panel A in section A.2.3). Analytical RP-HPLC (system B, 220 nm): 95%, t_R((*R*,*R*)-**2.19**) = 19.6 min, *k* = 6.5 (*cf*. Scheme 2.2). ^{1}H-NMR (600 MHz, DMSO-d_6): δ (ppm) 1.33-1.46 (m, 2H), 1.50-1.62 (m, 1H), 1.66-1.77 (m, 1H), 2.92-3.02 (m, 2H), 4.14-4.24 (m, 1H), 4.97 (s, 1H), 5.00 (s, 2H), 6.58-6.63 (m, 1H), 6.69-6.75 (m, 2H), 7.04-7.11 (m, 1H), 7.17-7.39 (m, 11H), 8.52 (d, *J* = 7.7 Hz, 1H), 9.27 (br s, 1H), 12.54 (br s, 1H). ^{13}C-NMR (150 MHz, DMSO-d_6): δ (ppm) 26.00, 28.56, 39.53 (interfering with the solvent residual peak, as identified by ^{1}H-^{13}C HSQC), 51.85, 55.86, 65.12, 113.53, 115.62, 119.27, 126.53, 127.69, 127.74, 128.13, 128.35, 129.45, 128.97, 137.26, 140.46, 141.53, 156.09, 157.12, 171.04, 173.42. MS (LC-HRMS, ESI): *m/z* $[M+H]^+$ calcd for $[C_{27}H_{29}N_2O_6]^+$ 477.2020, found 477.2025. $C_{27}H_{28}N_2O_6$ (476.53).

(3-Hydroxyphenyl)(phenyl)acetic acid succinimidyl ester (2.20)

A solution of DCC (0.98 g, 4.7 mmol) in THF (15 mL) was added to a cooled (0 °C) solution of (*rac*)-**2.17** (0.90 g, 3.9 mmol) and *N*-hydroxysuccinimide (0.54 g, 4.7 mmol) in THF (15 mL). The mixture was allowed to warm to rt and stirring was continued for 16 h. The white precipitate was filtered off, and the solvent of the filtrate was removed by rotary evaporation. The product was purified by column chromatography (light petroleum/ethyl acetate 2:1 v/v) to yield **2.20** as a yellow solid (0.48 g, 1.5 mmol, 37%). TLC (light petroleum/ethyl acetate/acetic acid 75:25:1 v/v/v): R_f = 0.25. ^{1}H-NMR (400 MHz, DMSO-d_6): δ (ppm) 2.81 (s, 4H), 5.61 (s, 1H), 6.69 (d, *J* = 8.0 Hz, 1H), 6.74-6.76 (m, 1H), 6.82 (d, *J* = 7.7 Hz, 1H), 7.16 (t, *J* = 7.7 Hz, 1H), 7.28-7.43 (m, 5H), 9.50 (s, 1H). ^{13}C-NMR (100 MHz, DMSO-d_6): δ (ppm) 25.49, 52.36, 114.64, 115.42, 118.99, 127.61, 128.40, 128.69, 129.67, 137.38, 138.52, 157.33, 168.27, 170.10. Note: due to

rapid hydrolysis of **2.20** in diluted aqueous solutions of formic acid or TFA, identification *via* standard LC-MS was unsuccessful. $C_{18}H_{15}NO_5$ (325.32).

N^{δ}-Benzyloxycarbonyl-*N'*-(4-*tert*-butoxybenzyl)-N^{α}-((*S*)-2-(3-hydroxyphenyl)-2-phenylacetyl)-(*R*)-ornithinamide ((*S*,*R*)-2.23)

HOBt (120 mg, 0.40 mmol), **2.22** (70 mg, 0.40 mmol) and a suspension of EDC × HCl (0.15 mg, 0.40 mmol) in anhydrous DMF (1 mL) were added to an ice-cold (0 °C) solution of (*S*,*R*)-**2.19** (190 mg, 0.40 mmol) in anhydrous DMF (8 mL) in an oven-dried Schlenk. The mixture was stirred at 0 °C for 16 h. 0.5% aq. TFA/acetonitrile 80:20 v/v (8 mL) was added, and the mixture was subjected to preparative HPLC (system B, column: Actus Triart C18, gradient: 0-30 min: C/B 50:50-25:75, t_R(**2.23**) = 12 min) yielding **2.23** as a white fluffy solid (142 mg, 0.22 mmol, 57%). Analytical RP-HPLC (system A, 220 nm): t_R(**2.23**) = 26.1 min. Note: (*S*,*R*)-**2.23** could not be isolated from residual (*R*,*R*)-**2.23** formed by epimerization during the synthesis of (*S*,*R*)-**2.23** (*cf.* supplementary Figure A2.3, panel B in section A.2.3). ^{1}H-NMR (400 MHz, DMSO-d_6): δ (ppm) 1.26 (s, 9H), 1.29-1.46 (m, 2H), 1.47-1.59 (m, 1H), 1.60-1.70 (m, 1H), 2.92-3.00 (m, 2H), 4.15-4.34 (m, 3H), 4.98-5.03 (m, 3H), 6.58-6.62 (m, 1H), 6.68-6.72 (m, 2H), 6.84-6.88 (m, 2H), 7.03-7.17 (m, 3H), 7.18-7.38 (m, 11H), 8.34-8.43 (m, 2H), 9.27 (br s, 1H). ^{13}C-NMR (100 MHz, DMSO-d_6): δ (ppm) 26.01, 28.53, 29.67, 39.72 (interfering with the solvent residual peak, as identified by ^{1}H-^{13}C HSQC), 41.47, 52.52, 55.85, 65.13, 77.73, 113.55, 115.53, 119.15, 123.55, 126.45, 127.65, 127.69, 127.74, 128.04, 128.34, 128.58, 129.03, 133.72, 137.23, 140.42, 141.83, 153.75, 156.08, 157.13, 170.90, 171.42. MS (LC-HRMS, ESI): *m/z* $[M+H]^+$ calcd for $[C_{38}H_{44}N_3O_6]^+$ 638.3225, found 638.3237. $C_{38}H_{43}N_3O_6$ (637.78).

4-((*tert*-Butoxycarbonyl)amino)butyl bromide[52] (2.24)

A solution of PPh_3 (6.7 g, 25.4 mmol) in CH_2Cl_2 (50 mL) was added to a stirred solution of NBS (4.5 g, 25.4 mmol) in CH_2Cl_2 (50 mL) at rt. Pyridine (1.0 mL, 12.75 mmol) was added dropwise over a period of 10 min followed by the addition of a solution of 4-((*tert*-butoxycarbonyl)amino)-1-butanol (1.6 g, 8.5 mmol) in CH_2Cl_2 (60 mL) and stirring was continued at rt for 3 h. The mixture was treated with saturated $NaHCO_3$ (100 mL). The organic layer was separated, dried over Na_2SO_4 and the solvent was removed by rotary evaporation. The product was purified by column chromatography (light petroleum/ethyl acetate 4:1 v/v) to yield **2.24** as yellow needles (1.99 g, 7.9 mmol, 93%, mp 30-32 °C (lit.[52] 31-34 °C). TLC (light petroleum/ethyl acetate 4:1 v/v): R_f = 0.50; ^{1}H-NMR (400 MHz, $CDCl_3$): δ (ppm) 1.34 (s, 9H), 1.49-1.58 (m, 2H), 1.74-1.83 (m, 2H), 3.01-3.08 (m, 2H), 3.29-3.36 (m, 2H), 4.43 (br s, 1H). ^{13}C-NMR (100 MHz, $CDCl_3$): δ (ppm) 28.56, 28.94, 30.07, 33.41, 45.39, 77.36, 156.09. MS (LC-HRMS, ESI): *m/z* $[M(^{79}Br)+H-C_4H_8]^+$ calcd for $[C_5H_{11}{}^{79}BrNO_2]^+$ 195.9968, found 195.9969. $C_9H_{18}BrNO_2$ (252.15).

N-Fmoc-4-hydroxybenzylamine (2.26)

A solution of (9*H*-fluoren-9-yl)methyl succinimidyl carbonate (11.3 g, 33.4 mmol) in dioxane (120 mL) was added dropwise to a stirred solution of **2.22** (5.0 g, 27.8 mmol) and Na_2CO_3 (3.0 g, 27.8 mmol) in H_2O/dioxane 2.5:1 v/v (200 mL) over a period of 1 h and the mixture was stirred at rt for 16 h. Dioxane was removed by rotary evaporation and the aqueous residue was treated with diethyl ether (3 × 100 mL). The combined organic layers were dried over $MgSO_4$, and the volatiles were removed *in vacuo* to yield crude *N*-Fmoc-4-*tert*-butoxybenzylamine as a yellow solid, which was suspended in CH_2Cl_2 (225 mL) and the suspension was cooled to 0 °C. HCl (6 N in isopropanol, 225 mL, 1.35 mol) was added dropwise under vigorous stirring over a period of 1 h. The mixture was allowed to warm to rt and stirring was continued for 12 h. After careful addition of ice-cold H_2O (500 mL), the organic layer was separated, washed with saturated brine (2 × 250 mL), and dried over $MgSO_4$. The solvent was removed by rotary evaporation and the product was purified by column chromatography (light petroleum/ethyl acetate 3:1 v/v) to yield **2.26** as an orange solid (7.5 g, 21.6 mmol, 78%). TLC (light petroleum/ethyl acetate 3:1 v/v): R_f = 0.25. ^{1}H-NMR (400 MHz, DMSO-d_6): δ (ppm) 4.06 (d, *J* = 6.0 Hz, 2H), 4.21 (t, *J* = 6.7 Hz, 1H), 4.32 (d, *J* = 6.7 Hz, 2H), 6.68 (d, *J* = 8.4 Hz, 2H), 7.02 (d, *J* = 8.4 Hz, 2H), 7.32 (t, *J* = 7.5 Hz, 2H), 7.41 (t, *J* = 7.5 Hz, 2H), 7.69 (d, *J* = 7.5 Hz, 2H), 7.89 (d, *J* = 7.5 Hz, 2H), 9.25 (s, 1H). Note: the proton signal of the NH group was not apparent. ^{13}C-NMR (100 MHz, DMSO-d_6): 43.33, 46.79, 65.24, 114.95, 120.10, 125.17, 127.02, 127.58, 128.92, 129.93, 140.74, 143.90, 156.22, 156.25. MS (LC-HRMS, ESI): *m/z* $[M+H]^+$ calcd for $[C_{22}H_{20}NO_3]^+$ 346.1438, found 346.1440. $C_{22}H_{19}NO_3$ (345.40).

4-(*N*-Fmoc-aminomethyl)phenoxy-(2-chlorophenyl)-diphenylmethane (polymer bound) (2.27)[53, 54]

2-ClTrt resin **2.25** (4 g, 6.4 mmol, maximal loading of 1.6 mmol/g, 200-400 mesh, 1% divinylbenzene) was allowed to swell in anhydrous CH_2Cl_2 (20 mL, pretreated with K_2CO_3) in a 50-mL polypropylene tube at rt for 10 min. **2.26** (4.4 g, 12.8 mmol), DMAP (50 mg, 0.38 mmol) and DIPEA (6.8 mL, 38.4 mmol) were added, and the tube was shaken at 40 °C for 3 h. The resin was transferred into a 20-mL syringe (BD Discardit II, Becton Dickinson, Heidelberg, Germany) equipped with a polyethylene frit (35 µm), the liquid was removed by filtration and the resin was washed with CH_2Cl_2 and DMF (40 mL each). For end capping, the resin was allowed to swell in CH_2Cl_2 (20 mL) in a 50-mL polypropylene tube and methanol (770 µl, 19.4 mmol) was added. The tube was shaken at 40 °C for 30 min, the resin was transferred to a syringe and the solvent was sucked off. The resin was washed with CH_2Cl_2, DMF and methanol (40 mL each) followed by removal of residual volatiles *in vacuo* to yield 4.2 g of the yellow-colored loaded resin **2.27**. To determine the loading of the resin according to a reported procedure,[54] a small amount of dried resin was treated with piperidine/DMF 1:4

v/v (1 mL) at rt for 1 h. 50 µL of the supernatant were diluted with DMF (950 µL). This solution was further diluted with piperidine/DMF 1:99 v/v (1:100, 1:200, 1:400 and 1:500) and the absorbances of the samples were measured at 301 nm using piperidine/DMF 1:99 v/v as a reference solution. The concentration of the quantitatively formed dibenzofulvene-piperidine adduct was calculated *via* its absorption coefficient and the loading of the resin was determined to be 0.67 mmol/g (2.8 mmol, 44%).

N^{α}-(((*S*)-4-(4-Aminobutoxy)phenyl)(phenyl)acetyl)-N^{ω}-((2-(propionyl)-aminoethyl)aminocarbonyl)-*N'*-(4-hydroxybenzyl)-(*R*)-argininamide bis(hydrotrifluoroacetate) ((*S*,*R*)-2.30) and N^{α}-(((*R*)-4-(4-aminobutoxy)phenyl)(phenyl)acetyl)-N^{ω}-((2-(propionyl)-aminoethyl)aminocarbonyl)-*N'*-(4-hydroxybenzyl)-(*R*)-argininamide bis(hydrotrifluoroacetate) ((*R*,*R*)-2.30)

In a 20 mL syringe (BD Discardit II, Becton Dickinson, Heidelberg, Germany) equipped with a polyethylene frit (35 µm), **2.27** (266 mg, 0.179 mmol) was allowed to swell in anhydrous DMF/NMP 4:1 v/v (2 mL) at rt for 15 min. Fmoc deprotection was carried out by sucking off the solvent, adding piperidine/DMF 1:4 v/v (3 mL) and shaking the reaction vessel at 35 °C for 2 h. This procedure was repeated once. The resin was washed with CH_2Cl_2 and DMF/NMP 4:1 v/v (3 × 3 mL each), and the liquid was sucked off. In a separate vessel, **2.28** (114 mg, 0.179 mmol), HBTU (115 mg, 0.304 mmol) and DIPEA (103 µL, 0.607 mmol) were added to a solution of HOBt (41 mg, 0.304 mmol) in anhydrous DMF/NMP 4:1 v/v (2 mL), the mixture was incubated at rt for 5 min, then added to the resin and the reaction vessel was shaken at 35 °C for 16 h. Fmoc deprotection was carried out as described above followed by washing of the resin and coupling of **2.29** (72 mg, 0.179 mmol) using the same procedure with identical amounts of reagents as for the aforementioned coupling of **2.28**. To cleave off the product, the resin was incubated in CH_2Cl_2/TFA 95:5 v/v (2 mL) at rt for 20 min, the liquid was collected, and the resin was washed with CH_2Cl_2/TFA 99:1 v/v (4 × 2 mL). After removal of the volatiles from the combined filtrates by rotary evaporation, the residue was taken up in CH_2Cl_2, followed by rotary evaporation. TFA/H_2O 95:5 v/v (2 mL) was added, and the mixture was incubated at rt for 3 h. CH_2Cl_2 (30 mL) was added, and the volatiles were removed by rotary evaporation. H_2O (100 mL) was added followed by lyophilization. The product was purified by preparative HPLC (system C, column: Kinetex-XB C18, gradient: 0-20 min: C/B 80:20-70:30, t_R((*S*,*R*)-**2.30**) = 9 min, t_R((*R*,*R*)-**2.30**) = 10 min) to yield (*S*,*R*)-**2.30** (21.8 mg, 0.023 mmol, 13%) and (*R*,*R*)-**2.30** (16.8 mg, 0.018 mmol, 10%) as white fluffy, hygroscopic solids. Analytical data of (*S*,*R*)-**2.30**: RP-HPLC (system B, 220 nm): 98%, t_R = 11.2 min, k = 3.3. ^{1}H-NMR (600 MHz, DMSO-d_6): δ (ppm) 0.98 (t, J = 7.6 Hz, 3H), 1.36-1.50 (m, 2H), 1.50-1.58 (m, 1H), 1.64-1.78 (m, 5H), 2.06 (q, J = 7.6 Hz, 2H), 2.82-2.89 (m, 2H), 3.12-3.25 (m, 6H), 3.95 (t, J = 6.0 Hz, 2H), 4.11-4.18 (m, 2H), 4.29-4.34 (m, 1H), 5.05 (s, 1H), 6.67-6.70 (m, 2H), 6.82-6.86 (m, 2H), 6.99-

7.03 (m, 2H), 7.18-7.22 (m, 3H), 7.24-7.30 (m, 4H), 7.51 (br s, 1H), 7.72-7.90 (m, 4H), 8.35 (t, *J* = 5.7 Hz, 1H), 8.38-8.58 (m, 3H), 9.00 (br s, 1H), 9.35 (br s, 1H), 10.49 (br s, 1H). ^{13}C-NMR (150 MHz, DMSO-d_6): δ (ppm) 9.82, 23.98, 24.60, 25.67, 28.48, 29.44, 38.08, 38.65, 39.10 (interfering with the solvent residual signal, as identified by ^{1}H-^{13}C HSQC), 40.34, 41.64, 52.26, 55.10, 66.78, 114.08, 115.02, 126.49, 128.16, 128.35, 128.44, 129.13, 129.60, 132.32, 140.89, 153.68, 153.94, 156.31, 157.21, 171.04, 171.32, 173.27. MS (LC-HRMS, ESI): MS (LC-HRMS, ESI): *m/z* $[M+H]^+$ calcd for $[C_{37}H_{51}N_8O_6]^+$ 703.3926, found 703.3938. Analytical data of (*R*,*R*)-**2.30**: RP-HPLC (system B, 220 nm): 97%, t_R = 11.8 min, *k* = 3.5. ^{1}H-NMR (600 MHz, DMSO-d_6): δ (ppm) 0.98 (t, *J* = 7.6 Hz, 3H), 1.37-1.58 (m, 3H), 1.63-1.78 (m, 5H), 2.06 (q, *J* = 7.6 Hz, 2H), 2.81-2.88 (m, 2H), 3.11-3.25 (m, 6H), 3.94 (t, *J* = 5.9 Hz, 2H), 4.09-4.19 (m, 2H), 4.29-4.34 (m, 1H), 5.05 (s, 1H), 6.65-6.70 (m, 2H), 6.82-6.87 (m, 2H), 6.98-7.02 (m, 2H), 7.17-7.23 (m, 3H), 7.24-7.30 (m, 4H), 7.51 (br s, 1H), 7.74-7.89 (m, 4H), 8.35 (t, *J* = 5.7 Hz, 1H), 8.37-8.57 (m, 3H), 9.00 (br s, 1H), 9.33 (br s, 1H), 10.44 (br s, 1H). ^{13}C-NMR (150 MHz, DMSO-d_6): δ (ppm) 9.80, 23.96, 24.57, 25.66, 28.46, 29.35, 38.05, 38.65, 39.10 (interfering with the solvent residual signal, as identified by ^{1}H-^{13}C HSQC), 40.34, 41.61, 52.28, 55.08, 66.74, 114.09, 114.99, 126.44, 128.10, 128.36, 128.39, 129.10, 129.56, 132.49, 140.71, 153.66, 153.90, 156.26, 157.23, 170.99, 171.30, 173.27. MS (LC-HRMS, ESI): *m/z* $[M+H]^+$ calcd for $[C_{37}H_{51}N_8O_6]^+$ 703.3926, found 703.3938. $C_{37}H_{50}N_8O_6 \times C_4H_2F_6O_4$ (930.90).

4-((1*E*,3*E*)-4-(4-(Dimethylamino)phenyl)buta-1,3-dien-1-yl)-1-(4-(3-((1*S*,4*R*)-4-((4-hydroxybenzyl)carbamoyl)-9-imino-2,11,16-trioxo-1-phenyl-3,8,10,12,15-pentaazaoctadecyl)phenoxy)butyl)-2,6-dimethylpyridin-1-ium hydrotrifluoroacetate trifluoroacetate (2.35)

DIPEA (3.6 µL, 17.6 µmol) and a solution of **2.31** (2.60 mg, 5.6 µmol) in anhydrous DMF (80 µL) were added to a stirred solution of (*S*,*R*)-**2.14** (3.30 mg, 2.8 µmol) in anhydrous DMF (100 µL) and the mixture was stirred at rt in the dark for 30 min. 10% aqueous TFA (27 µL) was added and the mixture was subjected to preparative HPLC (system C, column: Kinetex-XB C18, gradient: 0-25 min: C/B 70:30-50:50, t_R = 14 min) yielding **2.35** (1.47 mg, 1.23 µmol, 35%) as a dark red fluffy solid, which was stored at −20 °C under protection from light. RP-HPLC (system B, 220 nm): 96%, t_R = 17.6 min, *k* = 5.8. ^{1}H-NMR (600 MHz, DMSO-d_6/D_2O 10:1 v/v): δ (ppm) 0.98 (t, *J* = 7.6 Hz, 3H), 1.36-1.57 (m, 3H), 1.62-1.71 (m, 1H), 1.83-1.93 (m, 4H) 2.06 (q, *J* = 7.6 Hz, 2H), 2.74 (s, 6H), 2.98 (s, 6H), 3.12-3.16 (m, 4H), 3.17-3.22 (m, 2H), 3.96-4.02 (m, 2H), 4.08-4.19 (m, 2H), 4.28-4.33 (m, 1H), 4.35-4.42 (m, 2H), 5.07 (s, 1H), 6.58 (d, *J* = 15.3 Hz, 1H), 6.65-6.68 (m, 2H), 6.71-6.74 (m, 2H), 6.81-6.85 (m, 2H), 6.88-6.91 (m, 1H), 6.94-7.03 (m, 4H), 7.20-7.25 (m, 2H), 7.26-7.32 (m, 4H), 7.44-7.48 (m, 2H), 7.69 (dd, J_1 = 15.3 Hz, J_2 = 10.0 Hz, 1H), 7.83 (s, 2H), 8.35 (t, *J* = 5.7 Hz, 1H), 8.44 (d, *J* = 8.0 Hz, 1H).

MS (LC-HRMS, ESI): *m/z* $[M]^+$ calcd for $[C_{56}H_{70}N_9O_6]^+$ 965.5444, found 965.5457. $C_{56}H_{70}N_9O_6^+ \times C_4HF_6O_4^-$ (1192.27).

4-((1*E*,3*E*)-4-(4-(Dimethylamino)phenyl)buta-1,3-dien-1-yl)-1-(4-(3-((1*R*,4*R*)-4-((4-hydroxybenzyl)carbamoyl)-9-imino-2,11,16-trioxo-1-phenyl-3,8,10,12,15-pentaazaoctadecyl)phenoxy)butyl)-2,6-dimethylpyridin-1-ium hydrotrifluoroacetate trifluoroacetate (2.36)

DIPEA (3.6 µL, 17.6 µmol) and a solution of **2.31** (2.60 mg, 5.6 µmol) in anhydrous DMF (80 µL) were added to a stirred solution of (*R*,*R*)-**2.14** (3.30 mg, 2.8 µmol) in anhydrous DMF (100 µL) and the mixture was stirred at rt in the dark for 30 min. 10% aqueous TFA (27 µL) was added and the mixture was subjected to preparative HPLC (system C, column: Kinetex-XB C18, gradient: 0-25 min: C/B 70:30-50:50, t_R = 14 min) yielding **2.36** (1.82 mg, 1.52 µmol, 43%) as a dark red fluffy solid, which was stored at −20 °C under protection from light. RP-HPLC (system B, 220 nm): 97%, t_R = 17.5 min, k = 5.7. ^{1}H-NMR (600 MHz, DMSO-d_6/D_2O 10:1 v/v): δ (ppm) 0.97 (t, J = 7.6 Hz, 3H), 1.35-1.56 (m, 3H), 1.61-1.69 (m, 1H), 1.81-1.90 (m, 4H) 2.06 (q, J = 7.6 Hz, 2H), 2.70 (s, 6H), 2.96 (s, 6H), 3.11-3.19 (m, 6H), 3.96-4.00 (m, 2H), 4.06-4.17 (m, 2H), 4.25-4.30 (m, 1H), 4.35-4.42 (m, 2H), 5.04 (s, 1H), 6.57 (d, J = 15.3 Hz, 1H), 6.61-6.64 (m, 2H), 6.69-6.74 (m, 2H), 6.80-6.85 (m, 2H), 6.88-6.91 (m, 1H), 6.94-6.99 (m, 4H), 7.18-7.24 (m, 2H), 7.25-7.31 (m, 4H), 7.42-7.46 (m, 2H), 7.67 (dd, J_1 = 15.3 Hz, J_2 = 10.3 Hz, 1H), 7.74-7.77 (m, 2H), 8.35 (t, J = 5.8 Hz, 1H), 8.48 (d, J = 8.0 Hz, 1H). MS (LC-HRMS, ESI): *m/z* $[M]^+$ calcd for $[C_{56}H_{70}N_9O_6]^+$ 965.5444, found: 965.5455. $C_{56}H_{70}N_9O_6^+ \times C_4HF_6O_4^-$ (1192.27).

4-(2-((1*E*,3*E*)-5-((*Z*)-1-(6-((4-(3-((1*S*,4*R*,*Z*)-9-Amino-4-((4-hydroxybenzyl)carbamoyl)-2,11,16-trioxo-1-phenyl-3,8,10,12,15-pentaazaoctadec-9-en-1-yl)phenoxy)butyl)amino)-6-oxohexyl)-3,3-dimethyl-5-sulfoindolin-2-ylidene)penta-1,3-dien-1-yl)-3,3-dimethyl-3*H*-indol-1-ium-1-yl)butane-1-sulfonate hydrotrifluoroacetate (2.37)

DIPEA (3.6 µL, 17.6 µmol) and a solution of **2.32** (2.7 mg, 2.8 µmol) in anhydrous DMF (50 µL) were added to a stirred solution of (*S*,*R*)-**2.14** (3.3 mg, 2.8 µmol) in anhydrous DMF (100 µL) and the mixture was stirred at rt in the dark for 30 min. 10% aqueous TFA (27 µL) was added and the mixture was subjected to preparative HPLC (system C, column: Kinetex-XB C18, gradient: 0-25 min: C/B 80:20-55:45, t_R = 22 min) yielding **2.37** (0.9 mg, 0.58 µmol, 21%) as a blue fluffy solid, which was stored at −20 °C under protection from light. RP-HPLC (system B, 220 nm): 99%, t_R = 16.2 min, k = 5.2. ^{1}H-NMR (600 MHz, DMSO-d_6/D_2O 10:1 v/v): δ (ppm) 0.96 (t, J = 7.6 Hz, 3H), 1.28-1.33 (m, 2H), 1.36-1.56 (m, 8H), 1.61-1.80 (m, 22H), 2.00-2.07 (m, 4H), 3.01-3.05 (m, 2H), 3.08-3.19 (m, 6H), 3.84-3.88 (m, 2H), 3.98-4.17 (m, 6H), 4.27-4.32 (m, 1H), 5.06 (s, 1H), 6.24 (d, J = 14.1 Hz, 1H), 6.37 (d, J = 14.1 Hz, 1H), 6.52-6.60 (m, 1H),

6.63-6.67 (m, 2H), 6.73-6.77 (m, 1H), 6.79-6.84 (m, 2H), 7.15 (t, *J* = 7.9 Hz, 1H), 7.17-7.21 (m, 1H), 7.22-7.28 (m, 6H), 7.35-7.43 (m, 2.6H*), 7.59-7.64 (m, 2H), 7.76-7.80 (m, 2H), 7.81-7.86 (m, 1H), 8.27-8.36 (m, 2.3H*), 8.44 (d, *J* = 7.9 Hz, 0.5H*). *Residual NH proton signals due to incomplete deuterium/proton exchange. MS (LC-HRMS, ESI): *m/z* $[M+H]^+$ calcd for $[C_{72}H_{93}N_{10}O_{13}S_2]^+$ 1369.6360, found: 1369.6377. $C_{72}H_{92}N_{10}O_{13}S_2$ (1369.71).

6-(2-(4-((*E*)-2-(5,5-Difluoro-7-(thiophen-2-yl)-5*H*-4λ^4,5λ^4-dipyrrolo[1,2-c:2',1'-f][1,3,2]diazaborinin-3-yl)vinyl)phenoxy)acetamido)-*N*-(4-(3-((1*S*,4*R*)-4-((4-hydroxybenzyl)carbamoyl)-9-imino-2,11,16-trioxo-1-phenyl-3,8,10,12,15-pentaazaoctadecyl)phenoxy)butyl)hexanamide hydrotrifluoroacetate (2.38)

DIPEA (3.5 µL, 20.4 µmol) and a solution of **2.33** (2.25 mg, 3.4 µmol) in DMF (50 µL) were added to a stirred solution of (*S*,*R*)-**2.14** (3.2 mg, 3.40 µmol) in DMF (50 µL) and the mixture was stirred at rt in the dark for 1 h. 10% aqueous TFA (40 µL) was added and the product was subjected to semipreparative HPLC (system A, gradient: 0-20 min: A/B 55:45-32:68, t_R = 17 min) to yield **2.38** (3.17 mg, 2.33 µmol, 68%) as a dark blue fluffy solid, which was stored at −20 °C under protection from light. RP-HPLC (system B, 220 nm): 96%, t_R = 22.2 min, *k* = 7.5. ^{1}H-NMR (600 MHz, DMSO-d_6/D_2O 10:1 v/v): δ (ppm) 0.97 (t, *J* = 7.6 Hz, 3H), 1.17-1.21 (m, 2H), 1.37-1.54 (m, 9H), 1.62-1.69 (m, 3H), 2.00-2.08 (m, 4H), 3.03-3.06 (m, 2H), 3.08-3.14 (m, 6H), 3.16-3.20 (m, 2H), 3.86 (t, *J* = 6.3 Hz, 2H), 4.08-4.18 (m, 2H), 4.28-4.33 (m, 1H), 4.52 (s, 2H), 5.05 (s, 1H), 6.64-6.67 (m, 2H), 6.75-6.77 (m, 1H), 6.79-6.80 (m, 1H), 6.84 (d, *J* = 7.8 Hz, 1H), 6.94 (d, *J* = 4.2 Hz, 1H), 6.97-7.00 (m, 2H), 7.04-7.07 (m, 2H), 7.18 (t, *J* = 8.0 Hz, 1H), 7.20-7.23 (m, 1H), 7.24-7.29 (m, 7H), 7.35-7.38 (m, 1.4H*), 7.39-7.41 (m, 0.5H*), 7.58-7.61 (m, 3H), 7.72 (d, *J* = 16.4 Hz, 1H), 7.75-7.78 (m, 0.3H*), 7.80-7.82 (m, 1H), 7.83-7.86 (m, 0.6H*), 8.00-8.03 (m, 1H), 8.12 (t, *J* = 5.5 Hz, 1H), 8.34 (t, *J* = 6.0 Hz, 1H), 8.44 (d, *J* = 7.9 Hz, 1H). *Residual NH proton signals due to incomplete deuterium/proton exchange. MS (LC-HRMS, ESI): *m/z* $[M+H]^+$ calcd for $[C_{66}H_{77}{}^{10}BF_2N_{11}O_9S]^+$ 1247.5718, found: 1247.5727. $C_{66}H_{76}BF_2N_{11}O_9S \times C_2HF_3O_2$ (1362.29).

5-((4-(3-((1*S*,4*R*,*Z*)-9-Amino-4-((4-hydroxybenzyl)carbamoyl)-2,11,16-trioxo-1-phenyl-3,8,10,12,15-pentaazaoctadec-9-en-1-yl)phenoxy)butyl)carbamoyl)-2-(6-(dimethylamino)-3-(dimethyliminio)-3*H*-xanthen-9-yl)benzoate hydrotrifluoroacetate (2.39)

DIPEA (4.1 µL, 23.8 µmol) and a solution of **2.34** (1.74 mg, 3.3 µmol) in DMF (100 µL) were added to a stirred solution of (*S*,*R*)-**2.14** (3.1 mg, 3.30 µmol) in DMF (100 µL) and the mixture was stirred at rt in the dark for 1 h. 10% aqueous TFA (40 µL) was added and the mixture was subjected to preparative HPLC (system D, column: Kinetex-XB C18, gradient: 0-20 min: C/B 82:18-55:45, t_R = 18 min) yielding **2.39** (1.92 mg, 1.56 µmol, 43%) as a pink fluffy solid, which

was stored at −20 °C under protection from light. RP-HPLC (system B, 220 nm): 99%, t_R = 16.6 min, k = 5.4. ^{1}H-NMR (600 MHz, DMSO-d_6): δ (ppm) (600 MHz, DMSO-d_6/D_2O 10:1 v/v): δ (ppm) 0.98 (t, J = 7.6 Hz, 3H), 1.38-1.57 (m, 3H), 1.64-1.80 (m, 5H), 2.06 (q, J = 7.6 Hz, 2H), 2.90-3.04 (m, 2H), 3.12-3.16 (m, 4H), 3.17-3.22 (m, 2H), 3.23-3.32 (br s, 12H), 3.95 (t, J = 6.1 Hz, 2H), 4.09-4.19 (m, 2H), 4.29-4.34 (m, 1H), 5.07 (s, 1H), 6.53 (br s, 1H) 6.65-6.68 (m, 2H), 6.80-6.84 (m, 2H), 6.87 (d, J = 7.8 Hz, 1H), 6.94-7.10 (m, 7H), 7.19-7.24 (m, 2H), 7.26-7.30 (m, 4H), 7.55-7.60 (m, 1H), 7.82-7.88 (m, 0.6H*), 8.25-8.32 (m, 1H), 8.35 (t, J = 5.7 Hz, 1H), 8.45 (d, J = 7.9 Hz, 1H), 8.64-8.72 (m, 1H), 8.87-8.94 (m, 1H). *Residual NH proton signals due to incomplete deuterium/proton exchange. MS (LC-HRMS, ESI): *m/z* $[M+H]^+$ calcd for $[C_{62}H_{71}N_{10}O_{10}]^+$ 1115.5349, found: 1115.5367. $C_{62}H_{70}N_{10}O_{10} \times C_2HF_3O_2$ (1229.32).

5-((4-(4-((1*R*,4*R*,*Z*)-9-Amino-4-((4-hydroxybenzyl)carbamoyl)-2,11,16-trioxo-1-phenyl-3,8,10,12,15-pentaazaoctadec-9-en-1-yl)phenoxy)butyl)carbamoyl)-2-(6-(dimethylamino)-3-(dimethyliminio)-3*H*-xanthen-9-yl)benzoate hydrotrifluoroacetate (2.40)

DIPEA (4.3 µL, 25.2 µmol) and a solution of **2.34** (2.2 mg, 4.2 µmol) in DMF (50 µL) were added to a stirred solution of (*R*,*R*)-**2.30** (4.30 mg, 4.6 µmol) in DMF (100 µL) and the mixture was stirred at rt in the dark for 4 h. 10% aqueous TFA (40 µL) was added and the product was isolated by preparative HPLC (system C, column: Kinetex-XB C18, gradient: 0-25 min: C/B 75:25-40:60 t_R = 18 min) to yield **2.40** (3.53 mg, 2.90 µmol, 69%) as a pink fluffy solid, which was stored at −20 °C under protection from light. RP-HPLC (system B, 220 nm): 98%, t_R = 16.5 min, k = 5.3. ^{1}H-NMR (600 MHz, DMSO-d_6/D_2O 10:1 v/v): δ (ppm) 0.98 (t, J = 7.6 Hz, 3H), 1.36-1.56 (m, 3H), 1.63-1.82 (m, 5H), 2.06 (q, J = 7.6 Hz, 2H), 2.86-3.04 (m, 2H), 3.13-3.16 (m, 4H), 3.17-3.21 (m, 2H), 3.22-3.32 (br s, 12H), 3.99 (t, J = 6.4 Hz, 2H), 4.10-4.18 (m, 2H), 4.29-4.35 (m, 1H), 5.04 (s, 1H), 6.51 (br s, 1H) 6.66-6.70 (m, 2H), 6.83-6.88 (m, 2H), 6.94-7.11 (m, 7H), 7.17-7.22 (m, 3H), 7.24-7.30 (m, 4H), 7.54-7.61 (m, 1H), 7.84-7.88 (m, 0.2H*), 8.26-8.31 (m, 1H), 8.34 (t, J = 5.6 Hz, 1H), 8.43 (d, J = 8.1 Hz, 1H), 8.66-8.72 (m, 1H), 8.88-8.95 (m, 1H). *Residual NH proton signals due to incomplete deuterium/proton exchange. MS (LC-HRMS, ESI): *m/z* $[M+H]^+$ calcd for $[C_{62}H_{71}N_{10}O_{10}]^+$ 1115.5349, found: 1115.5352. $C_{62}H_{70}N_{10}O_{10} \times C_2HF_3O_2$ (1229.32).

2.4.3 X-ray crystallographic analysis of (*R*)-2.16

A single crystal of **2.16** was mounted using a nylon loop on a STOE STADI VARI Diffractometer with EIGER 2 CdTe Detector (STOE & CIE GmbH, Darmstadt, Germany). Assuming a noncentrosymmetric space group, the necessary Friedel Pairs were collected with CuKα radiation. The absolute configuration was proofed by Flack parameter and Bayesian statistic.

The unit cell contained two independent molecules. During refinement of the crystal structure, the hydrogen atom of the carboxyl group was refined and assigned to the respective oxygen atom without constrains and/or restraints applying isotropic displacement parameters.

2.4.4 Circular dichroism analysis

CD spectra of 0.2 mM solutions of the *S*,*R*- and *R*,*R*-configured diastereomers of **2.14** and **2.30** in methanol were recorded in a 2 mm path length cuvette at 20 °C with a Jasco J-810 spectropolarimeter (Jasco, Tokyo, Japan) equipped with a PTC-423S Peltier temperature controller (Jasco). Instrumental parameters: spectral range of 200–500 nm, bandwidth of 1 nm, scanning speed of 500 nm/min. The CD spectra shown in Figure 2.3 (panel A) represent the average of five measurements after solvent subtraction. The "economy-size" singular-value decomposition (SVD) of the spectra in Figure 2.3 (panel B) (matrix **A**) was calculated in MATLAB (MathWorks, Natick, MA) as $\mathbf{A} = \mathbf{U} \times \mathbf{S} \times \mathbf{V}^{\mathbf{T}}$, where **U** is a matrix in which columns 1 to 3 represent the "abstract spectra" shown in Figure 2.3 (panel B), **S** is a diagonal matrix containing the singular values, and $\mathbf{V}^{\mathbf{T}}$ is the transpose of matrix **V**, which contains the linear coefficients associated with the columns of **U**. The spectra in Figure 2.3 (panel C) were obtained from $\mathbf{U} \times \mathbf{S} \times \mathbf{V}^{\mathbf{T}}$ considering only the first 3 columns of **U** and **V** and the corresponding singular values, respectively. For panels D-F of Figure 2.3, either the first, the second, or the third column of **U** and **V** was combined with the corresponding singular values.

2.4.5 Investigation of the chemical stability of compounds 2.35-2.40

The chemical stability of **2.35**-**2.40** was investigated in PBS (pH 7.4) at 22 °C. Incubation was started by the addition of 2.5 µL of a 2 mM stock solution (in DMSO) of each investigated compound to 47.5 µL of PBS to give a final concentration of 100 µM. For each compound, this sample was prepared three times. In the case of **2.35-2.37**, **2.39** and **2.40**, incubation was stopped by the addition of 50 µL 1% aq. TFA/acetonitrile 1:1 v/v after 0 min, 4 h and 24 h. 80 µL of the resulting solutions were analyzed by analytical RP-HPLC (system A). As **2.38** showed strong adsorption to the sample tube, a different solvent composition was used (addition of 50 µL of 1% TFA in acetonitrile).

2.4.6 Cell culture

Cells were cultured in 75-cm^2 or 175-cm^2 flasks (Sarstedt, Nümbrecht, Germany) in a humidified atmosphere (95% air, 5% CO_2) at 37 °C. SK-N-MC neuroblastoma cells (obtained from the American Type Culture Collection, ATCC HTB-10) were maintained in Eagle's minimum essential medium (EMEM) (Sigma-Aldrich) containing 10% fetal calf serum (FCS) (Sigma-Aldrich). Human erythroleukemia (HEL) cells (HEL 92.1.7 from the American Type Culture Collection, ATCC TIB-180) were maintained in RPMI (Sigma) supplemented with 6.5% FCS. MCF-7-Y_1 cells[19] were cultivated in EMEM containing 5% FCS. CHO-hY_2R cells

(PerkinElmer, Rodgau, Germany) were cultured in Ham's F12 medium (Sigma Aldrich, München, Germany) supplemented with 5% FCS and G418 (400 µg/mL) (Fisher Scientific). CHO-hY_4-Gqi5-mtAEQ cells[55] were cultured in Ham's F12 medium containing 10% FCS, G418 (400 µg/mL) (Sigma-Aldrich), hygromycin (400 µg/mL) (A.G. Scientific Inc, San Diego, CA, USA) and zeocin (250 µg/mL) (InvivoGen, San Diego, CA). HEC-1B-hY_5R cells[56] were maintained in EMEM containing 7.5% FCS and G418 (400 µg/mL).

2.4.7 Radioligand competition binding

Y_1R binding: radioligand competition binding experiments at the hY_1R were performed at intact hY_1R-expressing SK-N-MC neuroblastoma cells at 22 ± 1 °C as previously described, using [^{3}H]**2.2** (K_d = 0.044 nM, c = 0.15 nM) as radioligand.[20] Nonspecific binding was determined in the presence of BIBO3304 (75 nM). Y_2R binding: radioligand competition binding experiments at the hY_2R were performed at CHO-hY_2R cells (purchased from PerkinElmer, product no. ES352-C, lot no. 460-167-A) at 22 ± 1 °C as previously described, using [^{3}H]propionyl-pNPY (K_d = 0.14 nM, c = 0.5 nM) as radioligand.[29] Nonspecific binding was determined in the presence of BIIE0246 and JNJ31020028 (5 µM each). Y_4R binding: radioligand competition binding experiments at the hY_4R were performed at CHO-hY_4RG_{qi5}-mtAEQ cells at 22 ± 1 °C as previously described, using [^{3}H]UR-KK200 (K_d = 0.67 nM,[30] c = 1 nM) as radioligand.[57] Nonspecific binding was determined in the presence of hPP (1 µM). Y_5R binding: radioligand competition binding at the hY_5R was performed at intact HEC-1B-hY_5R cells at 22 ± 1 °C as previously described, using [^{3}H]propionyl-pNPY (K_d = 11 nM,[31] c = 5 nM) as radioligand.[30] Nonspecific binding was determined in presence of pNPY (2 µM). For each compound and each receptor subtype, at least three individual experiments were performed in triplicate. For Y_1R binding, specific binding data (nonspecific binding subtracted from total binding) were normalized (100% = specifically bound radioligand in the absence of competitor), plotted as % over log(concentration of competitor) and analyzed by a four-parameter logistic equation (log(inhibitor) vs. response - variable slope, GraphPad Prism 9, GraphPad Software, San Diego, CA) to obtain pIC_{50} values, which were converted into pK_i values according to the Cheng-Prusoff equation (logarithmic form).[58] In the case of compound **2.35** (Y_5R) and compound **2.39** (Y_4R), radioligand displacement at the highest concentration of **2.35** or **2.39** amounted to 60-80%. To obtain pIC_{50} values, log(B/(B_0 − B)) (Hill plot; B denotes specifically bound radioligand in the presence of competitor (values between 10 and 90%), B_0 = specifically bound radioligand in the absence of competitor (B_0 = 100%)) was plotted against log(competitor concentration) followed by linear regression (pIC_{50} corresponds to the intercept with the x-axis, log(B/(B_0 – B)) = 0). For the other compounds, investigated with respect to Y_2R, Y_4R and Y_5R binding, radioligand displacement was < 50% for the highest competitor concentration (3 or 10 µM), i.e. pIC_{50} values could not be determined.

2.4.8 Fura-2 Ca^{2+} assay

The Y_1R Fura-2 Ca^{2+} assay was performed at hY_1R-expressing HEL cells at 22 ± 1 °C as previously described.[33] In antagonist mode, Ca^{2+} mobilization was induced by the addition of pNPY (10 nM) after preincubation of the cells with the antagonists for 15 min. At least three independent experiments were performed in a singlet. In the case of the fluorescent dummy ligands **2.57** and **2.58** (*cf*. supplementary Figure A2.5 in section A.2.3), the preincubation period was 2 min and six individual determinations were performed in a singlet. Cytosolic Ca^{2+} concentrations obtained from the investigation of pNPY in agonist mode (concentration-effect curves) were plotted against log(concentration of pNPY) and analyzed by a four-parameter logistic equation (log(agonist) vs response−variable slope, GraphPad Prism 9). Subsequently, data were normalized (100% = "top" of the four-parameter logistic fit, 0% = "bottom" of the four-parameter logistic fit) followed by plotting of the normalized data against log(concentration of pNPY) and analysis according to a four-parameter logistic equation (log(agonist) vs response − variable slope, GraphPad Prism 9) to obtain pEC_{50} values. Net Ca^{2+} responses (basal cytosolic Ca^{2+} concentration subtracted from the measured peak Ca^{2+} concentration) obtained from the investigation of the antagonists **2.14**, **2.30**, and **2.35**-**2.40** in antagonist mode (inhibition of the effect elicited by 10 nM pNPY) were normalized (100% = Ca^{2+} response induced by 10 nM pNPY) and plotted against log(concentration of antagonist) followed by analysis according to a four-parameter logistic equation (log(inhibitor) vs response − variable slope, GraphPad Prism 9) to obtain pIC50 values.

2.4.9 Fluorescence excitation and emission spectra

Excitation and emission spectra were recorded with a Cary Eclipse spectrofluorimeter (Varian Inc., Mulgrave, Victoria, Australia) using acryl cuvettes (10 mm × 10 mm, Ref. 67.755, Sarstedt). Sample solutions (2 mL) were prepared in the cuvettes. Spectra in PBS (pH 7.4) supplemented with 1% BSA were obtained for all fluorescent ligands (**2.35**-**2.40**) using the following concentrations: 6 µM for **2.35** and **2.36** and 2 µM for **2.37**-**2.40**. Excitation spectra (*cf.* supplementary Figure A2.6 in section A.2.3) were recorded with a slit adjustment of 10/10 nm (excitation/emission) (**2.37**) or 5/10 nm (**2.35**, **2.36**, **2.38**-**2.40**). The slit adjustments applied for the emission spectra were 10/10 nm (excitation/emission) for **2.37** and 10/5 nm for **2.35**, **2.36** and **2.38**-**2.40**. Spectra in Leibovitz's L15 medium (Gibco/Fisher Scientific), HEPES buffer (pH 7.4) (20 mM HEPES, 1 mM $CaCl_2$, 135 mM NaCl and 0.1% Pluronic F-127) and MEMO (Cell Guidance Systems, UK) were recorded for compounds **2.35** (6 µM), **2.37** (2 µM) and **2.39** (8 µM) (*cf.* supplementary Figure A2.7 in section A.2.3). A slit adjustment of 10/10 (excitation/emission) was applied for both excitation and emission spectra. Net spectra were obtained by subtracting the respective vehicle reference spectrum, and corrected emission

spectra were calculated by multiplying the net emission spectra with the respective lamp correction spectrum.

2.4.10 Determination of fluorescent quantum yields

The quantum yields (compounds **2.35**-**2.37**, **2.39** and **2.40**) were determined with the aforementioned Cary Eclipse spectrofluorimeter (emission spectra) and a Lambda 650 UV/vis spectrophotometer (PerkinElmer) (absorption spectra) according to a described procedure with minor modifications.[21] The following compound concentrations, resulting in absorbances between 0.08 and 0.12 at the respective excitation wavelength, were applied: 6 µM for **2.35** and **2.36**, 2 µM for **2.37** and cresyl violet perchlorate (Acros Organics, Geel, Belgium) and 8 µM for **2.39** and **2.40**. The excitation wavelength was set close to the absorption maximum (**2.35** and **2.36**) or at the shoulder to the left of the absorption maximum (**2.37**, **2.39** and **2.40**) enabling recording of full emission spectra. Emission spectra of cresyl violet perchlorate in EtOH were recorded at an excitation wavelength of 575 nm. Sample solutions (2 mL) were prepared in polystyrene cuvettes (10 mm × 10 mm, Ref. 67.742, Sarstedt), immediately followed by measurement of the absorption spectra, transfer of the solutions into acryl cuvettes (10 mm × 10 mm, Ref. 67.755, Sarstedt) and measurement of the emission spectra. At least two independent determinations were performed each comprising fluorescence spectra at the slit adjustments (excitation/emission) 5/10, 10/5 nm and 10/10 nm. The obtained quantum yields were averaged (slit adjustments, independent determinations).

2.4.11 Flow cytometry-based binding experiments

Flow cytometry (FC)-based Y_1R binding studies with the fluorescent ligands **2.35**, **2.37**, **2.39** and **2.40** were performed at intact MCF-7-Y_1 mamma carcinoma cells[19] with a FACSCantoII flow cytometer (Becton Dickinson, Heidelberg, Germany), equipped with an argon laser (488 nm) and a red diode laser (640 nm). All experiments were performed in duplicate. The following gain settings for forward and sideward scatter were applied throughout: FSC: 0 V, SSC: 252 V. Fluorescence was recorded using the following settings: compound **2.35**: excitation: 488 nm, emission: >670 nm (PerCP-Cy5.5 channel), gain: 390-490 V, compound **2.37**: excitation: 640 nm, emission: 660 ± 10 nm (APC channel), gain: 525-555 V, compounds **2.39** and **2.40**: excitation: 488 nm, emission: 585 ± 21 nm (PE channel), gain: 300-370 V. For all measurements, the medium flow rate was used. Measurements for saturation binding and competition binding experiments were stopped after counting of 5000-10000 (cell density: 1.0 × 10^6 cells/mL) or 500-1000 (cell density: 1.0 × 10^5 cells/mL) gated events. Measurements for kinetic binding studies (association and dissociation) were stopped after counting of at least 1000 (cell density: 1.0 × 10^6 cells/mL) or 200 (cell density: 1.0 × 10^5 cells/mL) gated events, but latest after 10 seconds of data acquisition.

Two to three days prior to the experiment, cells were seeded in 75-cm^2 or 175-cm^2 culture flasks and 24-48 h prior to the experiment, estradiol (1 nM) was added to the culture medium (added to stimulate Y_1R expression[18, 19]). On the day of the experiment, cells were detached by trypsinization, suspended in culture medium and centrifuged. The cell pellet was resuspended in phenol red-free Leibovitz's L15 medium and the cell density was adjusted to 1.0×10^5 or 1.0×10^6 cells/mL. All samples were prepared and incubated in 1.5-mL or 2-mL polypropylene reaction vessels (Sarstedt) and were transferred into 75 mm × 12 mm polystyrene sample tubes (Sarstedt) shortly before the measurement. Solutions of fluorescent and nonlabeled ligands were prepared in DMSO/H_2O 1:1 v/v. For saturation binding experiments, reaction vessels were prefilled with 2.5 µL of a 100-fold concentrated (compared to the final concentration) solution of the fluorescent ligand and 2.5 µL of DMSO/H_2O 1:1 v/v (total binding) or were prefilled with 2.5 µL of the same fluorescent ligand solution and 2.5 µL of a 100-fold concentrated solution of **2.1** (nonspecific binding). The final concentration of **2.1** was 10 µM throughout. The incubation was started by the addition of 245 µL of cell suspension followed by gentle shaking of the reaction vessels under protection from light at 22 ± 2 °C for 2 h and subsequent data acquisition. For association experiments with **2.37**, **2.39** and **2.40**, 2-mL reaction vessels were prefilled with 1780 µL of cell suspension (adjusted to the respective cell density) and association was started by the addition of DMSO/H_2O 1:1 v/v (1.8 µL) and 18 µL of a 50 nM solution (**2.37** or **2.39**, final concentrations: 0.5 nM each) or 18 µL of a 100 nM solution (**2.40**, final concentration: 1 nM) to the cell suspension, followed by short mixing and gentle shaking under protection from light at 22 ± 2 °C. To determine nonspecific binding, 1.8 µL of a 1 mM solution of **2.2** were added instead of 1.8 µL of the vehicle (final concentration of **2.2**: 1 µM). After different periods of time (**2.37**: 0.5-45 min, **2.39**: 0.5-60 min, **2.40**: 0.5-30 min) aliquots (100 µL) were withdrawn and subjected to measurement. For association experiments with **2.35**, the cell suspension (495 µL) was placed directly into a polystyrene sample tube and the experiment was started by the addition of 5 µL of a 25 nM solution of **2.35** (final concentration: 0.25 nM), followed by short mixing and immediate data acquisition (after approximately 5 s). Additional measurements were conducted after different periods of time (0-20 min) using the same sample tube. To determine nonspecific binding, 0.5 µL of a 1 mM solution of **2.2** were added to the cell suspension (final concentration of **2.2**: 1 µM) shortly before the addition of **2.35**. For dissociation experiments, 2-mL reaction vessels were prefilled with 1778 µL of cell suspension. Pre-incubation was started by the addition of DMSO/H_2O 1:1 v/v (1.8 µL) and 18 µL of a 100 nM solution (**2.35**, **2.37** or **2.39**, final concentrations: 1 nM each) or 18 µL of a 200 nM solution (**2.40**, final concentration: 2 nM). The samples were gently shaken in the dark at 22 ± 2 °C for 2 h. For the determination of nonspecific binding, 1.8 µL of a 1 mM solution of **2.2** were added instead of 1.8 µL of the vehicle (final concentration of **2.2**: 1 µM). Dissociation was initiated by the addition of 1.8 µL of a 1 mM solution of **2.2**. After

different periods of time (**2.35** and **2.39**: 5-600 min, **2.37**: 1-300 min, **2.40**: 1-90 min), aliquots (100 µL) were withdrawn and subjected to measurement. In contrast to saturation binding and association experiments, dissociation experiments were only performed at a cell density of 1.0 × 10^6 cells/mL. For competition binding experiments, reactions vessels were prefilled with cell suspension (245 µL) followed by the addition of 2.5 µL of a 100-fold concentrated solution of the competing (nonlabeled) ligand and gentle shaking in the dark. After 10 min (**2.1** and **2.2**) or 1 h (pNPY) of pre-incubation, 2.5 µL of the fluorescent ligand solution (100-fold concentrated) were added and shaking under protection from light at 22 ± 2 °C was continued for 2 h (**2.1** and **2.2**) or 4 h (pNPY). The final concentrations of the fluorescent ligands were 0.25 nM (**2.35**) or 0.5 nM (**2.37** and **2.39**). For the determination of nonspecific and total binding, 2.5 µL of a 0.5 mM solution of BIBO3304 (final concentration: 5 µM) and 2.5 µL of DMSO/H_2O 1:1 v/v, respectively, were initially added, followed by the addition of fluorescent ligand after the pre-incubation period as described above. Competition binding experiments were only performed at a cell density of 1.0 × 10^5 cells/mL.

Specific binding data were obtained by subtracting nonspecific binding from total binding. Nonspecific binding data, depicted in Figure 2.5 (panel A) and supplementary Figure A2.8 (section A.2.3), are autofluorescence corrected. Specific binding data from saturation binding experiments were analyzed by an equation describing a hyperbolic isotherm (Binding - Saturation: One site - Specific binding, GraphPad Prism 9) yielding K_d values, which were converted to pK_d values (*cf*. Table 2.3). Specific binding data from association experiments were analyzed by a two-parameter equation describing a monophasic exponential rise to a maximum (yielding $k_{obs(mono)}$) and by a four-parameter equation describing a biphasic exponential rise to a maximum (yielding $k_{obs(bi,fast)}$ and $k_{obs(bi,slow)}$) (GraphPad Prism 9) (*cf*. Table 2.3).

Specific binding data from FC-based dissociation experiments were analyzed by a two-parameter equation describing a monophasic exponential decline (GraphPad Prism 9) yielding k_{off} . The association rate constants $k_{on(mono)}$, $k_{on(bi,fast)}$ and $k_{on(bi,slow)}$ were calculated from the individually determined observed association rate constants $k_{obs(mono)}$, $k_{obs(bi,fast)}$ and $k_{obs(bi,slow)}$, respectively (three independent experiments for each fluorescent ligand), the mean values of the corresponding dissociation rate constants k_{off} (*cf*. Table 2.3) and the fluorescent ligand concentrations used for the association experiments (**2.35**: 0.25 nM, **2.37**: 0.5 nM, **2.39**: 0.5 nM, **2.40**: 1 nM) according to $k_{on} = (k_{obs} - k_{off})/[\text{fluorescent ligand}]$. The kinetically derived dissociation constants K_d(kin) were calculated from individual $k_{on(mono)}$ values and the mean value of the dissociation rate constants k_{off} (*cf*. Table 2.3) according to $K_d(\text{kin}) = k_{off}/k_{on}$. K_d(kin) values were converted to pK_d(kin) values, which were averaged to obtain mean pK_d(kin) values

± SEM. Error propagation for the calculation of k_{on} values and K_d(kin) values was performed as described previously.[34]

Specific binding data from competition binding experiments were normalized (100% = specifically bound fluorescent ligand in the absence of competitor), plotted as % over log(competitor concentration) and analyzed by a four-parameter logistic equation (log(inhibitor) vs response−variable slope, GraphPad Prism 9) to obtain pIC_{50} values, which were converted to pK_i values according to the Cheng-Prusoff equation[58] (logarithmic form) using the following K_d values of the fluorescent ligands: **2.35**: K_d = 0.042 nM, **2.37**: K_d = 0.159 nM, **2.39**: K_d = 0.138 nM (mean K_d values from three individual saturation binding experiments performed with a cell density of 1.0 × 10^5 cells/mL).

2.4.12 Fluorescence anisotropy-based Y_1R binding assays

Fluorescence anisotropy-based (FA-based) Y_1R binding studies with fluorescent ligand **39** were performed at hY_1R displaying budded baculovirus particles (termed BBVs below), which were prepared as described previously.[59] The obtained viruses were collected by centrifugation at 1600 g for 10 min and the virus titer was determined with an image-based cell-size estimation assay as described elsewhere.[60] The viruses were amplified using a multiplicity of infection (MOI) between 0.01-0.1 until a high titer baculovirus stock (virus concentration of at least 1.0 × 10^8 infectious viral particles/mL) was acquired. To produce BBV preparations with high receptor density, Sf9 cells with a density of 1.9 × 10^6 cells/mL were infected with a MOI of 3 and the BBVs were collected by centrifugation 63 h after the infection, when the cell viability was below 30%. The BBVs were concentrated 40-fold by centrifugation at 48,000 g for 40 min at 4 °C, washed with ice-cold buffer (consisting of 0.1% Pluronic F-127, 20 mM HEPES, 1 mM $CaCl_2$, 135 mM NaCl and cOmplete EDTA-free Protease Inhibitor Cocktail (used according to manufacturer's protocol), pH 7.4), resuspended and homogenized. Aliquots of the BBV preparations were stored at −90 °C until use.

FA measurements were carried out using a Synergy NEO multimode plate reader (BioTek, Winooski, VT) and black, half-area, flat bottom polystyrene NBS (non-binding surface) 96-well plates (Corning, Corning, NY, product no. 3993). Polarizing excitation (530 ± 15 nm) and dual emission (590 ± 17.5 nm) filters with a dichroic mirror were used, allowing the simultaneous detection of parallelly and perpendicularly polarized fluorescence emission. All measurements were performed at 27 °C. For extended measurements (>3 h), the 96-well plates were covered with a custom-made glass lid to avoid excessive evaporation. Saturation binding experiments, association and dissociation experiments as well as competition binding experiments were performed in duplicate, following a previously described protocol with minor modifications.[61] All ligand dilutions were prepared in binding buffer (20 mM Na-HEPES, 1 mM $CaCl_2$, 135 mM

NaCl, 0.1% Pluronic F-127 and cOmplete EDTA-free Protease Inhibitor Cocktail (pH 7.4)). The final total volume per well was 100 µL. Frozen preparations of hY_1R displaying BBVs were thawed and thoroughly resuspended using a 1 mL syringe (Norm-Ject-F, B. Braun Melsungen AG) with a 0.3 mm diameter needle (Sterican, Braun Melsungen AG). For association experiments, 30 µL of a 3.33-fold concentrated (compared to the final concentration) solution of **2.39** (used at final concentrations of 0.5 nM and 3 nM) and 20 µL of binding buffer were premixed in the 96-well plate followed by the addition of 50 µL of BBV suspension (used at at least 6 different dilutions) to initiate total binding. To determine nonspecific binding, the procedure was the same, but instead of neat binding buffer, 20 µL of a five-fold concentrated solution of **2.2** (final concentration: 1000-fold compared to the concentration of **2.39**) were added. For blank measurement, 50 µL of BBV suspension were added to 50 µL of neat binding buffer. Note: Due to the very fast association of **2.39** with the Y_1R (most pronounced for the combination of high receptor concentrations with the lower concentration of **2.39**), measurements were not performed simultaneously for all BBV dilutions. Instead, to enable short time intervals between the readout cycles, separate measurements (for at least 7 min) were performed for the high BBV concentrations combined with the lower concentration of **2.39** (0.5 nM). For each combination of receptor and ligand concentration, binding equilibrium was reached within less than 30 min. Therefore, FA signals for each combination of BBV and fluorescent ligand concentration, acquired after 30 min, were used to analyze equilibrium binding (see below). For dissociation experiments, the preincubation was set up as the association experiments (final concentrations of **2.39**: 0.5 nM or 3 nM) and started by the addition of the BBV suspensions to the wells. After the preincubation period (1 h), dissociation was initiated by the addition of 2 µL of a 50-fold concentrated solution of **2.2** (final concentration: 1000-fold compared to the concentration of **2.39**) and the FA signal was measured for 15 h. An incubation period of 30 min was sufficient for each receptor:ligand ratio to reach binding equilibrium. Note: In principle, association, equilibrium binding and dissociation experiments can be performed consecutively in one plate. However, to enable a quasi-simultaneous readout for all combinations of BBV and fluorescent ligand concentrations without the time delay as required for association experiments (see above), equilibrium binding and dissociation experiments were performed separately.

For competition binding experiments, 20 µL of a 5-fold concentrated (compared to the final concentration) solution of the competitive ligand (used at varying concentrations) and 20 µL of a 5-fold concentrated solution of **2.39** (final concentrations: 0.1 nM or 0.2 nM) were premixed in the 96-well plate followed by the addition of 60 µL of the BBV suspension (used at one fixed dilution) to initiate total binding. To determine total binding in the absence of competitor and nonspecific binding, the same procedure was used, but instead of the addition of competing

ligand, neat binding buffer (20 µL) and 20 µL of a 5-fold concentrated solution of **2.2** (final concentration: 1 µM), respectively, were added. FA signals were measured for 15 h.

Data processing for FA binding assays was assisted by the software Aparecium 2.0.20 developed in house (http://www.gpcr.ut.ee/software.html). Before the calculation of FA using equation 2 as previously described,[42] the measured parallel ($I_{\parallel}(t)$) and perpendicular ($I_{\perp}(t)$) fluorescence intensities were blank corrected on the basis of values obtained from wells containing BBVs but no receptor ligand.

$$FA(t) = \frac{I_{\parallel}(t) - I_{\perp}(t)}{I_{\parallel}(t) + 2I_{\perp}(t)} \quad (2)$$

$I_{\parallel}(t)$, $I_{\perp}(t)$: blank corrected parallel and perpendicular fluorescence intensities, respectively, measured at the time t; FA(t): calculated fluorescence anisotropy at the time t

FA association binding data were globally fitted to obtain association rate constants k_{on} and pK_d values using a previously presented user-defined GraphPad Prism-compatible binding model, which takes ligand depletion into account (k_{off} constrained to 5.35 × 10^5 s^{-1}).[42] Association rate constant k_{on} and the pK_d value presented in Figure 2.6 were calculated as mean values ± SEM from individual k_{on} and pK_d values, respectively, obtained from at least three individual FA association binding experiments using six different BBV concentrations and two different concentrations of **2.39**. The kinetically derived dissociation constant $K_{d(kin)}$ was calculated from individual (n = 7) k_{on} values and the corresponding k_{off} value (k_{off} = 5.35 × 10^5 s^{-1}) according to the equation $K_{d(kin)} = k_{off}/k_{on}$. The obtained $K_{d(kin)}$ values were converted to p$K_{d(kin)}$ values, which were averaged to obtain the mean p$K_{d(kin)}$ value ± SEM. The mean value ± SEM of the dissociation rate constant k_{off} was calculated from individual k_{off} values obtained from three independent FA dissociation experiments each using six different BBV concentrations and two different concentrations of **2.39** (GraphPad Prism 9). Data from FA competition binding experiments using **2.39** as the fluorescent probe (K_d = 0.010 nM, mean value from three individual FA equilibrium binding experiments) were analyzed using a previously presented user-defined GraphPad Prism-compatible binding model, which takes into account fluorescent ligand depletion and includes the calculation of pK_i values of the competing, nonlabeled ligands (GraphPad Prism 9).[42]

2.4.13 Fluorescence microscopy

For fluorescence ligand binding imaging experiments, human MCF-7-Y_1 mamma carcinoma cells[19] were seeded at a density of 20,000 cells per well into eight-well CG imaging chambers (Zell Kontakt GmbH, Nörten-Hardenberg, Germany). After incubation for 24 h in EMEM (Sigma) supplemented with 1 nM estradiol, FCS (Sigma) and a solution containing penicillin

(100 units/mL), streptomycin (0,1 mg/mL), amphotericin B (0,25 µg/mL) (Sigma) and nuclear stains (5 µg/ml Hoechst 34580 (Chemodex Ltd., St. Gallen, Switzerland) or 1 µM SiR-DNA (Spirochrome AG, Stein am Rhein, Switzerland)) were added and incubation was continued for 1 h. The culture medium was replaced by LiveLight MEMO imaging medium (Cell Guidance Systems, Cambridge, U.K.) (200 µL, supplemented with Supplement A according to the manufacturer's protocol). After incubation for 2 h at 37 °C in a humidified atmosphere containing 5% CO_2, compounds **2.35**, **2.37** or **2.39** (1 nM final concentrations) were added and cells were imaged for up to 60 min (37 °C, atmosphere with 5% CO_2). Imaging was carried out with the TIRF microscopy setup as described previously.[62] Briefly, widefield epifluorescence and TIRF imaging was conducted using an inverted microscope connected to a Till iMIC body (Till Photonics/FEI, Munich, Germany), equipped with a TIRF APON 60× oil (NA 1.49) objective (Olympus Corp., Tokyo, Japan). The samples were sequentially excited using PhoxX laser diodes (Omicron-Laserage) combined with the SOLE-6 light engine (Omicron-Laserage): 515 nm (80 mW) (compounds **2.35** and **2.39**) and 638 nm (150 mW) (SiR-DNA); or 405 nm (120 mW) (Hoechst 34580) and 638 nm (150 mW) (**2.37**). Excitation light was launched into a Yanus scan head, which, along with a Polytrope galvanometric mirror (Till Photonics/FEI), was used to position the laser for widefield epifluorescence or TIRF (approximately 100 nm depth) illumination. Excitation and emission light were spectrally separated with imaging filter cubes containing a 390/40 BrightLine exciter filter (Semrock, West Henrietta, NY), a zt 405 rdc 2 mm beam splitter (Chroma Technology Corp), and an ET 460/50 emitter filter (Chroma) for Hoechst 34580 or containing a zt 514/640 rpc 2 mm dual-line beam splitter (Chroma) and a 577/690/25 BrightLine dual-band bandpass emission filter (Semrock) for compounds **2.35**, **2.37**, **2.39** or SiR-DNA. Additionally, the brightfield channel was used for the determination of cell borders. The electron multiplying charge-coupled device Ultra 897 camera (Andor Technology, Belfast, U.K.) was mounted to the microscope through a TuCam adapter with 2-fold magnification (Andor Technology). The camera was cooled down to −100 °C with the assistance of a liquid recirculating chiller Oasis 160 (Solid State Cooling Systems, Wappingers Falls, NY). All measurements were performed in the eight-well CG imaging chambers, and at least five selected areas per well were captured as 16-bit OME-TIFF multicolor Z-stacks (100 frames, with 200 nm piezo-focusing increment), with 100 ms exposure time and EM gain 300 in the case of widefield epifluorescence imaging or one-color time-stacks (1000 frames at 10 Hz) in the case of TIRF. For different fluorescent ligands and stains, the laser powers were varied to enable optimal signal levels (the absence of a detectable crosstalk signal in the channels was ensured). The widefield epifluorescence Z-stacks were deconvolved with an EpiDEMIC plugin.[63] For each fluorescent ligand, at least three independent experiments were performed.

2.5 References

(1) Michel, M. C.; Beck-Sickinger, A.; Cox, H.; Doods, H. N.; Herzog, H.; Larhammar, D.; Quirion, R.; Schwartz, T.; Westfall, T. XVI. International union of pharmacology recommendations for the nomenclature of neuropeptide Y, peptide YY, and pancreatic polypeptide receptors. *Pharmacol. Rev.* **1998**, 50, 143-150.

(2) MacNeil, D. NPY Y_1 and Y_5 receptor selective antagonists as anti-obesity drugs. *Curr. Top. Med. Chem.* **2007**, 7, 1721-1733.

(3) Reichmann, F.; Holzer, P. Neuropeptide Y: A stressful review. *Neuropeptides* **2016**, 55, 99-109.

(4) Robinson, S. L.; Thiele, T. E. The role of neuropeptide Y (NPY) in alcohol and drug abuse disorders. *Int. Rev. Neurobiol.* **2017**, 136, 177-197.

(5) Thiele, T. E.; Koh, M. T.; Pedrazzini, T. Voluntary alcohol consumption is controlled *via* the neuropeptide Y Y_1 receptor. *J. Neurosci.* **2002**, 22, RC208.

(6) Crnkovic, S.; Egemnazarov, B.; Jain, P.; Seay, U.; Gattinger, N.; Marsh, L. M.; Bálint, Z.; Kovacs, G.; Ghanim, B.; Klepetko, W.; Schermuly, R. T.; Weissmann, N.; Olschewski, A.; Kwapiszewska, G. NPY Y_1 receptor-mediated vasoconstrictory and proliferative effects in pulmonary hypertension. *Br. J. Pharmacol.* **2014**, 171, 3895-3907.

(7) Bertocchi, I.; Mele, P.; Ferrero, G.; Oberto, A.; Carulli, D.; Eva, C. NPY Y_1 receptor signaling controls spatial learning and perineuronal net expression. *Neuropharmacology* **2021**, 184, 108425.

(8) Inaba, A.; Komori, Y.; Muroi, Y.; Kinoshita, K.; Ishii, T. Neuropeptide Y signaling in the dorsal raphe nucleus inhibits male sexual behavior in mice. *Neuroscience* **2016**, 320, 140-148.

(9) Körner, M.; Reubi, J. C. NPY receptors in human cancer: A review of current knowledge. *Peptides* **2007**, 28, 419-425.

(10) Reubi, J. C.; Maecke, H. R. Peptide-based probes for cancer imaging. *J. Nucl. Med.* **2008**, 49, 1735-1738.

(11) Zwanziger, D.; Beck-Sickinger, A. Radiometal targeted tumor diagnosis and therapy with peptide hormones. *Curr. Pharm. Des.* **2008**, 14, 2385-2400.

(12) Lu, C.; Everhart, L.; Tilan, J.; Kuo, L.; Sun, C. C. J.; Munivenkatappa, R. B.; Jönsson-Rylander, A. C.; Sun, J.; Kuan-Celarier, A.; Li, L.; Abe, K.; Zukowska, Z.; Toretsky, J. A.; Kitlinska, J. Neuropeptide Y and its Y_2 receptor: potential targets in neuroblastoma therapy. *Oncogene* **2010**, 29, 5630-5642.

(13) Morgat, C.; Mishra, A. K.; Varshney, R.; Allard, M.; Fernandez, P.; Hindié, E. Targeting neuropeptide receptors for cancer imaging and therapy: Perspectives with bombesin, neurotensin, and neuropeptide Y receptors. *J. Nucl. Med.* **2014**, 55, 1650-1657.

(14) Ruscica, M.; Dozio, E.; Motta, M.; Magni, P. Role of neuropeptide Y and its receptors in the progression of endocrine-related cancer. *Peptides* **2007**, 28, 426-434.

(15) Körner, M.; Waser, B.; Reubi, J. C. High expression of neuropeptide Y_1 receptors in Ewing sarcoma tumors. *Clin. Cancer. Res.* **2008**, 14, 5043-5049.

(16) Waldmann, J.; Fendrich, V.; Reichert, M.; Hecker, A.; Bartsch, D. K.; Padberg, W.; Holler, J. P. N. Expression of neuropeptide Y and its receptors Y_1 and Y_2 in pancreatic intraepithelial neoplasia and invasive pancreatic cancer in a transgenic mouse model and human samples of pancreatic cancer. *J. Surg. Res.* **2018**, 223, 230-236.

(17) Rudolf, K.; Eberlein, W.; Engel, W.; Wieland, H. A.; Willim, K. D.; Entzeroth, M.; Wienen, W.; Beck-Sickinger, A. G.; Doods, H. N. The first highly potent and selective nonpeptide neuropeptide Y Y_1 receptor antagonist: BIBP3226. *Eur. J. Pharmacol.* **1994**, 271, R11-R13.

(18) Keller, M.; Pop, N.; Hutzler, C.; Beck-Sickinger, A. G.; Bernhardt, G.; Buschauer, A. Guanidine−acylguanidine bioisosteric approach in the design of radioligands: synthesis of a tritium-labeled N^G-propionylargininamide ([^{3}H]-UR-MK114) as a highly potent and selective neuropeptide Y Y_1 receptor antagonist. *J. Med. Chem.* **2008**, 51, 8168-8172.

(19) Keller, M.; Bernhardt, G.; Buschauer, A. [^{3}H]UR-MK136: A highly potent and selective radioligand for neuropeptide Y Y_1 receptors. *ChemMedChem* **2011**, 6, 1566-1571.

(20) Keller, M.; Weiss, S.; Hutzler, C.; Kuhn, K. K.; Mollereau, C.; Dukorn, S.; Schindler, L.; Bernhardt, G.; König, B.; Buschauer, A. N^{ω}-Carbamoylation of the argininamide moiety: An avenue to insurmountable NPY Y_1 receptor antagonists and a radiolabeled selective high-affinity molecular tool ([^{3}H]UR-MK299) with extended residence time. *J. Med. Chem.* **2015**, 58, 8834-8849.

(21) Keller, M.; Erdmann, D.; Pop, N.; Pluym, N.; Teng, S.; Bernhardt, G.; Buschauer, A. Red-fluorescent argininamide-type NPY Y_1 receptor antagonists as pharmacological tools. *Biorg. Med. Chem.* **2011**, 19, 2859-2878.

(22) Schneider, E.; Keller, M.; Brennauer, A.; Hoefelschweiger, B. K.; Gross, D.; Wolfbeis, O. S.; Bernhardt, G.; Buschauer, A. Synthesis and characterization of the first fluorescent nonpeptide NPY Y_1 receptor antagonist. *ChemBioChem* **2007**, 8, 1981-1988.

(23) Ingenhoven, N.; Beck-Sickinger, A. G. Fluorescent labelled analogues of neuropeptide Y for the characterization of cells expressing NPY receptor subtypes. *J. Recept. Signal Transduct.* **1997**, 17, 407-418.

(24) Fabry, M.; Langer, M.; Rothen-Rutishauser, B.; Wunderli-Allenspach, H.; Höcker, H.; Beck-Sickinger, A. G. Monitoring of the internalization of neuropeptide Y on neuroblastoma cell line SK-N-MC. *Eur. J. Biochem.* **2000**, 267, 5631-5637.

(25) Dumont, Y.; Gaudreau, P.; Mazzuferi, M.; Langlois, D.; Chabot, J.-G.; Fournier, A.; Simonato, M.; Quirion, R. BODIPY®-conjugated neuropeptide Y ligands: new fluorescent tools to tag Y_1, Y_2, Y_4 and Y_5 receptor subtypes. *Br. J. Pharmacol.* **2005**, 146, 1069-1081.

(26) Mountford, S. J.; Liu, M.; Zhang, L.; Groenen, M.; Herzog, H.; Holliday, N. D.; Thompson, P. E. Synthetic routes to the Neuropeptide Y Y_1 receptor antagonist 1229U91 and related analogues for SAR studies and cell-based imaging. *Org. Biomol. Chem.* **2014**, 12, 3271-3281.

(27) Liu, M.; Richardson, R. R.; Mountford, S. J.; Zhang, L.; Tempone, M. H.; Herzog, H.; Holliday, N. D.; Thompson, P. E. Identification of a cyanine-dye labeled peptidic ligand for Y_1R and Y_4R, based upon the neuropeptide Y C-terminal analogue, BVD-15. *Bioconjugate Chem.* **2016**, 27, 2166-2175.

(28) Yang, Z.; Han, S.; Keller, M.; Kaiser, A.; Bender, B. J.; Bosse, M.; Burkert, K.; Kögler, L. M.; Wifling, D.; Bernhardt, G.; Plank, N.; Littmann, T.; Schmidt, P.; Yi, C.; Li, B.; Ye, S.; Zhang, R.; Xu, B.; Larhammar, D.; Stevens, R. C.; Huster, D.; Meiler, J.; Zhao, Q.; Beck-Sickinger, A. G.; Buschauer, A.; Wu, B. Structural basis of ligand binding modes at the neuropeptide Y Y_1 receptor. *Nature* **2018**, 556, 520-524.

(29) Konieczny, A.; Braun, D.; Wifling, D.; Bernhardt, G.; Keller, M. Oligopeptides as neuropeptide Y Y_4 receptor ligands: identification of a high-affinity tetrapeptide agonist and a hexapeptide antagonist. *J. Med. Chem.* **2020**, 63, 8198-8215.

(30) Kuhn, K. K.; Ertl, T.; Dukorn, S.; Keller, M.; Bernhardt, G.; Reiser, O.; Buschauer, A. High affinity agonists of the neuropeptide Y (NPY) Y_4 receptor derived from the C-terminal pentapeptide of human pancreatic polypeptide (hPP): Synthesis, stereochemical discrimination, and radiolabeling. *J. Med. Chem.* **2016**, 59, 6045-6058.

(31) Dukorn, S.; Littmann, T.; Keller, M.; Kuhn, K.; Cabrele, C.; Baumeister, P.; Bernhardt, G.; Buschauer, A. Fluorescence- and radiolabeling of [Lys^4,Nle^{17,30}]hPP yields molecular tools for the NPY Y_4 receptor. *Bioconjugate Chem.* **2017**, 28, 1291-1304.

(32) Motulsky, H. J.; Michel, M. C. Neuropeptide Y mobilizes Ca^{2+} and inhibits adenylate cyclase in human erythroleukemia cells. *Am. J. Physiol. - Endocrinol. Metab.* **1988**, 255, E880-E885.

(33) Müller, M.; Knieps, S.; Geßele, K.; Dove, S.; Bernhardt, G.; Buschauer, A. Synthesis and neuropeptide Y Y_1 receptor antagonistic activity of N,N-disubstituted ω-guanidino- and ω-aminoalkanoic acid amides. *Arch. Pharm.* **1997**, 330, 333-342.

(34) Keller, M.; Mahuroof, S. A.; Hong Yee, V.; Carpenter, J.; Schindler, L.; Littmann, T.; Pegoli, A.; Hübner, H.; Bernhardt, G.; Gmeiner, P.; Holliday, N. D. Fluorescence labeling of neurotensin(8–13) *via* arginine residues gives molecular tools with high receptor affinity. *ACS Med. Chem. Lett.* **2020**, 11, 16-22.

(35) She, X.; Pegoli, A.; Gruber, C. G.; Wifling, D.; Carpenter, J.; Hübner, H.; Chen, M.; Wan, J.; Bernhardt, G.; Gmeiner, P.; Holliday, N. D.; Keller, M. Red-emitting dibenzodiazepinone derivatives as fluorescent dualsteric probes for the muscarinic acetylcholine M_2 receptor. *J. Med. Chem.* **2020**, 63, 4133-4154.

(36) Unruh, J. R.; Gokulrangan, G.; Wilson, G. S.; Johnson, C. K. Fluorescence properties of fluorescein, tetramethylrhodamine, and texas red linked to a DNA aptamer. *Photochem. Photobiol.* **2005**, 81, 682-690.

(37) Rinken, A.; Lavogina, D.; Kopanchuk, S. Assays with detection of fluorescence anisotropy: Challenges and possibilities for characterizing ligand binding to GPCRs. *Trends Pharmacol. Sci.* **2018**, 39, 187-199.

(38) Dunn, S. M. J. Fluorescence measurements of receptor-ligand interactions in *Handbook of Neurochemistry and Molecular Neurobiology*, 3rd ed.; Lajtha, A., Baker G., Dunn S., Holt A., Eds., Springer: New York, **2007**, pp. 133-148.

(39) Maschauer, S.; Ott, J. J.; Bernhardt, G.; Kuwert, T.; Keller, M.; Prante, O. ^{18}F-Labelled triazolyl-linked argininamides targeting the neuropeptide Y Y_1R for PET imaging of mammary carcinoma. *Sci. Rep.* **2019**, 9.

(40) Carter, C. M. S.; Leighton-Davies, J. R.; Charlton, S. J. Miniaturized receptor binding assays: Complications arising from ligand depletion. *J. Biomol. Screen.* **2007**, 12, 255-266.

(41) Goldstein, A.; Barrett, R. W. Ligand dissociation constants from competition binding assays: Errors associated with ligand depletion. *Mol. Pharmacol.* **1987**, 31, 603-609.

(42) Veiksina, S.; Kopanchuk, S.; Rinken, A. Budded baculoviruses as a tool for a homogeneous fluorescence anisotropy-based assay of ligand binding to G protein-coupled receptors: The case of melanocortin 4 receptors. *Biochim. Biophys. Acta* **2014**, 1838, 372-381.

(43) Zhang, H.; Wu, Q.; Berezin, M. Y. Fluorescence anisotropy (polarization): From drug screening to precision medicine. *Expert Opin. Drug Discov.* **2015**, 10, 1145-1161.

(44) Wieland, H. A.; Engel, W.; Eberlein, W.; Rudolf, K.; Doods, H. N. Subtype selectivity of the novel nonpeptide neuropeptide Y Y_1 receptor antagonist BIBO3304 and its effect on feeding in rodents. *Br. J. Pharmacol.* **1998**, 125, 549-555.

(45) Balasubramaniam, A.; Dhawan, V. C.; Mullins, D. E.; Chance, W. T.; Sheriff, S.; Guzzi, M.; Prabhakaran, M.; Parker, E. M. Highly selective and potent neuropeptide Y (NPY)

Y_1 receptor antagonists based on [Pro^{30}, Tyr^{32}, Leu^{34}]NPY(28-36)-NH_2 (BW1911U90). *J. Med. Chem.* **2001**, 44, 1479-1482.

(46) Hern, J. A.; Baig, A. H.; Mashanov, G. I.; Birdsall, B.; Corrie, J. E. T.; Lazareno, S.; Molloy, J. E.; Birdsall, N. J. M. Formation and dissociation of M_1 muscarinic receptor dimers seen by total internal reflection fluorescence imaging of single molecules. *Proc. Natl. Acad. Sci. U.S.A.* **2010**, 107, 2693-2698.

(47) Kasai, R. S.; Suzuki, K. G. N.; Prossnitz, E. R.; Koyama-Honda, I.; Nakada, C.; Fujiwara, T. K.; Kusumi, A. Full characterization of GPCR monomer–dimer dynamic equilibrium by single molecule imaging. *J. Cell Biol.* **2011**, 192, 463-480.

(48) Asher, W. B.; Geggier, P.; Holsey, M. D.; Gilmore, G. T.; Pati, A. K.; Meszaros, J.; Terry, D. S.; Mathiasen, S.; Kaliszewski, M. J.; McCauley, M. D.; Govindaraju, A.; Zhou, Z.; Harikumar, K. G.; Jaqaman, K.; Miller, L. J.; Smith, A. W.; Blanchard, S. C.; Javitch, J. A. Single-molecule FRET imaging of GPCR dimers in living cells. *Nat. Methods* **2021**, 18, 397-405.

(49) Höfelschweiger, B. K. The pyrylium dyes: A new class of biolabels. Synthesis, spectroscopy, and application as labels and in general protein assay. Doctoral Thesis. University of Regensburg, Regensburg, **2005**, https://epub.uni-regensburg.de/10331/.

(50) Williams, D. B. G.; Lawton, M. Drying of organic solvents: Quantitative evaluation of the efficiency of several desiccants. *J. Org. Chem.* **2010**, 75, 8351-8354.

(51) Gruber, B.; Balk, S.; Stadlbauer, S.; König, B. Dynamic interface imprinting: High-affinity peptide binding sites assembled by analyte-induced recruiting of membrane receptors. *Angew. Chem. Int. Ed.* **2012**, 51, 10060-10063.

(52) Ciccotosto, S. The preparation and evaluation of N-acetylneuraminic acid derivatives as probes of sialic acid-recognizing proteins. Doctoral Thesis. Monash University, Melbourne, **2004**.

(53) Bernhardt, A.; Drewello, M.; Schutkowski, M. The solid-phase synthesis of side-chain-phosphorylated peptide-4-nitroanilides. *J. Pept. Res.* **1997**, 50, 143-152.

(54) Chan, W. C.; White, P. D. *Fmoc solid phase peptide synthesis: A practical approach*. Oxford University Press: New York, **2000**.

(55) Ziemek, R.; Schneider, E.; Kraus, A.; Cabrele, C.; Beck-Sickinger, A. G.; Bernhardt, G.; Buschauer, A. Determination of affinity and activity of ligands at the human neuropeptide Y Y_4 receptor by flow cytometry and aequorin luminescence. *J. Recept. Signal Transduct.* **2007**, 27, 217-233.

(56) Moser, C.; Bernhardt, G.; Michel, J.; Schwarz, H.; Buschauer, A. Cloning and functional expression of the hNPY Y_5 receptor in human endometrial cancer (HEC-1B) cells. *Can. J. Physiol. Pharmacol.* **2000**, 78, 134-142.

(57) Konieczny, A.; Conrad, M.; Ertl, F. J.; Gleixner, J.; Gattor, A. O.; Grätz, L.; Schmidt, M. F.; Neu, E.; Horn, A. H. C.; Wifling, D.; Gmeiner, P.; Clark, T.; Sticht, H.; Keller, M. N-Terminus to arginine side-chain cyclization of linear peptidic neuropeptide Y Y_4 receptor ligands results in picomolar binding constants. *J. Med. Chem.* **2021**, 64, 16746-16769.

(58) Cheng, Y.-C.; Prusoff, W. H. Relationship between the inhibition constant (K_i) and the concentration of inhibitor which causes 50 per cent inhibition (IC_{50}) of an enzymatic reaction. *Biochem. Pharmacol.* **1973**, 22, 3099-3108.

(59) Laasfeld, T.; Ehrminger, R.; Tahk, M.-J.; Veiksina, S.; Kõlvart, K. R.; Min, M.; Kopanchuk, S.; Rinken, A. Budded baculoviruses as a receptor display system to quantify ligand binding with TIRF microscopy. *Nanoscale* **2021**, 13, 2436-2447.

(60) Laasfeld, T.; Kopanchuk, S.; Rinken, A. Image-based cell-size estimation for baculovirus quantification. *BioTechniques* **2017**, 63, 161-168.

(61) Link, R.; Veiksina, S.; Rinken, A.; Kopanchuk, S. Characterization of ligand binding to melanocortin 4 receptors using fluorescent peptides with improved kinetic properties. *Eur. J. Pharmacol.* **2017**, 799, 58-66.

(62) Nonga, O. E.; Lavogina, D.; Enkvist, E.; Kestav, K.; Chaikuad, A.; Dixon-Clarke, S. E.; Bullock, A. N.; Kopanchuk, S.; Ivan, T.; Ekambaram, R.; Viht, K.; Knapp, S.; Uri, A. Crystal structure-guided design of bisubstrate inhibitors and photoluminescent probes for protein kinases of the PIM family. *Molecules* **2021**, 26, 4353.

(63) Soulez, F.; Denis, L.; Tourneur, Y.; Thiebaut, E. In Blind deconvolution of 3D data in wide field fluorescence microscopy, *IEEE International Symposium on Biomedical Imaging*, **2012**; pp 1735-1738.

Chapter 3

High-affinity ^{18}F- and ^{68}Ga-labeled nonpeptidic neuropeptide Y_1 receptor ligands for PET imaging of mammary carcinomas

Note: The stereochemical discrimination of compounds (*S*,*R*)-**3.6** and (*R*,*R*)-**3.6** by CD-spectroscopy was performed by Dr. Steffen Lüdecke. Compound **3.25** was synthesized by Diana Braun. Radiosynthesis of compounds [^{18}F]**3.11**, [^{18}F]**3.12** and in part [^{68}Ga]**3.25**, PET experiments, biodistribution, and determination of $logD_{7.4}$ values of compounds [^{18}F]**3.11** and [^{18}F]**3.12** were performed by Dr. Simone Maschauer from the Department of Nuclear Medicine at the Friedrich-Alexander-Universität Erlangen-Nürnberg. Dr. Jutta Moosbauer from the Department of Nuclear Medicine at the University Hospital Regensburg assisted with the radiosynthesis of compound [^{68}Ga]**3.25**.

3.1 Introduction

Neuropeptide Y (NPY), a 36 amino acid-residue neuropeptide abundantly found in the CNS and PNS, is involved in the regulation of central processes such as food intake and energy homeostasis, stress response, anxiety, spatial memory and learning, and the addiction-related reward system, but also exerts vasoconstrictive effects in the periphery in response to central stress signals. In humans, the effects of NPY and the other two members of the NPY family, peptide YY (PYY) and pancreatic polypeptide (PP), are mediated by four class A G protein-coupled receptors, designated Y_1R, Y_2R, Y_4R and the Y_5R.[1-5]

In the past two decades, several studies revealed that the Y_1R and Y_2R are (over)expressed in various types of tumors, including ovarian sex cord-stromal tumors,[6] Ewing's sarcoma,[7] adrenal cortical tumors,[8] and mammary carcinoma.[9] Hence, radiolabeled Y_1R and Y_2R ligands can potentially be used as radiopharmaceuticals (e.g. ^{18}F-labeled PET tracers for cancer diagnosis and ^{177}Lu-labeled compounds for radioendotherapy).[10-12] Among the investigated tumors, high incidence and density of Y_1R expression was found in mammary carcinoma, suggesting the Y_1R as a marker for the diagnosis of breast cancer.[9, 13]

Different approaches, based on peptidic or nonpeptidic Y_1R ligands, have been pursued to develop ^{18}F- or ^{68}Ga-labeled Y_1R-specific PET tracers.[14] Concerning peptidic tracers, the difficulties disclosed by the study of a fluoroglycosylated ^{18}F-labeled NPY derivative[15] and a N-terminally truncated ^{68}Ga-labeled NPY analogue,[16] used for the imaging of xenografted Y_1R-positive tumors in nude mice, were a low tumor-to-background ratio and proteolytic degradation.

In contrast to peptidic PET tracers, nonpeptidic Y_1R PET ligands, representing Y_1R antagonists, exhibit lower molecular weight and potentially higher *in vivo* stability. A ^{18}F-labeled 2,4-diaminopyridine-type Y_1R antagonist was used to localize Y_1 receptors in rhesus monkey brains, but an application of this tracer for tumor imaging was not reported so far.[17, 18] Furthermore, ^{18}F-labeled argininamide-type Y_1R antagonists derived from BIBP3226 (**2.1**, Figure 3.1) were investigated with respect to *in vivo* imaging of Y_1R-positive MCF-7 tumors in nude mice ([^{18}F]**3.1**-[^{18}F]**3.4**, Figure 3.1, panel A).[19, 20] Although the [^{18}F]2-fluoropropionylated PET tracer [^{18}F]**3.1**, exhibiting high Y_1R affinity and high *in vivo* stability, enabled the imaging of the subcutaneous tumor, the study also revealed an unfavorable high accumulation of this lipophilic tracer ($logD_{7.4}$ = 2.34) in the hepatobiliary system.[19] In a follow-up study, less lipophilic ^{18}F-labeled Y_1R antagonists [^{18}F]**3.2**-[^{18}F]**3.4** were investigated using the same mouse xenograft model. [^{18}F]**3.2** and [^{18}F]**3.3**, containing a ^{18}F-fluoroethoxy and ^{18}F-fluoro-PEG moiety, respectively, showed displaceable Y_1R binding in the tumor, but tumor-to-background ratios were low due to rapid degradation of these PET tracers.[20] In contrast, imaging of the

tumor was not possible with the low-affinity (pK_i(Y_1R) = 6.55) fluoroglycosylated tracer [^{18}F]**3.4**. Worth mentioning, despite the lower lipophilicity of [^{18}F]**3.2**-[^{18}F]**3.4** compared to [^{18}F]**3.1**, the majority of the injected radioactivity was still present in the bile.[20]

The recent elucidation of the Y_1R binding mode of the high-affinity Y_1R antagonist UR-MK299 (**2.2**, Figure 3.1, panel A), which is structurally closely related to **3.1-3.4**, revealed that the carbamoyl residue attached at the guanidino group is deeply buried in the receptor binding pocket (Figure 3.1, panel B) (PDB ID: 5ZBQ[21]). This provided an explanation for the markedly decreased affinity of **3.3** and **3.4**, which both contain a large N^{ω}-carbamoyl substituent (*cf*. Figure 3.1, panel A) causing, in contrast to **2.2**, a steric clash in the binding pocket, as also recently demonstrated by computational chemistry for a series of N^{ω}-carbamoylated argininamide-type Y_1R antagonists.[22] Taking advantage from the reported crystal structure of the Y_1R in complex with **2.2**, the synthesis of a derivative of **2.2**, compound (*S*,*R*)-**2.14** (Figure 3.1, panel A), which contains an amine-functionalized linker at the receptor surface-facing diphenylacetyl moiety, and the successive attachment of bulky fluorescent dyes yielded fluorescent Y_1R ligands with picomolar binding affinities.[23]

In the present study, we applied this structure-based approach to develop argininamide-type Y_1R PET ligands with considerably higher Y_1R affinity compared to **3.1-3.4**. For this purpose, the amine-functionalized precursor (*S*,*R*)-**2.14** was conjugated to a fluorinated glycosyl moiety or a Ga^{3+}-binding chelator. Additionally, a fluorinated PET ligand derived from **2.1**, not containing a carbamoylated guanidino group, was prepared. After *in vitro* characterization of the respective “cold” ligands, ^{18}F- and ^{68}Ga-labeled derivatives were synthesized and subjected to *in vivo* studies in nude mice bearing subcutaneous MCF-7 breast cancer xenografts.

A

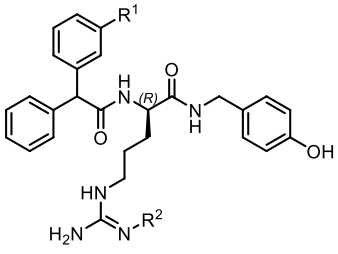

compd.	R^1	R^2	pK_i (hY_1R)	log$D_{7.4}$[a]
2.1 (BIBP3226)			8.80[b]	-
3.1		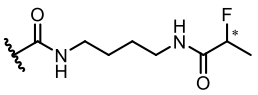	8.89[c]	2.34[c]
3.2		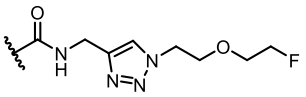	8.55[d]	1.74[d]
3.3		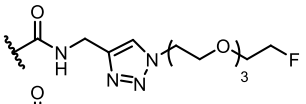	7.54[d]	1.49[d]
3.4		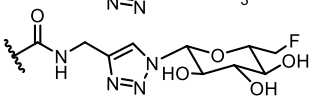	6.55[d]	0.78[d]
2.2 (UR-MK299)		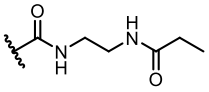	10.27[e]	-
(*S*,*R*)-**2.14**[f]	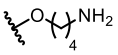	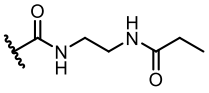	10.61[g]	-

B

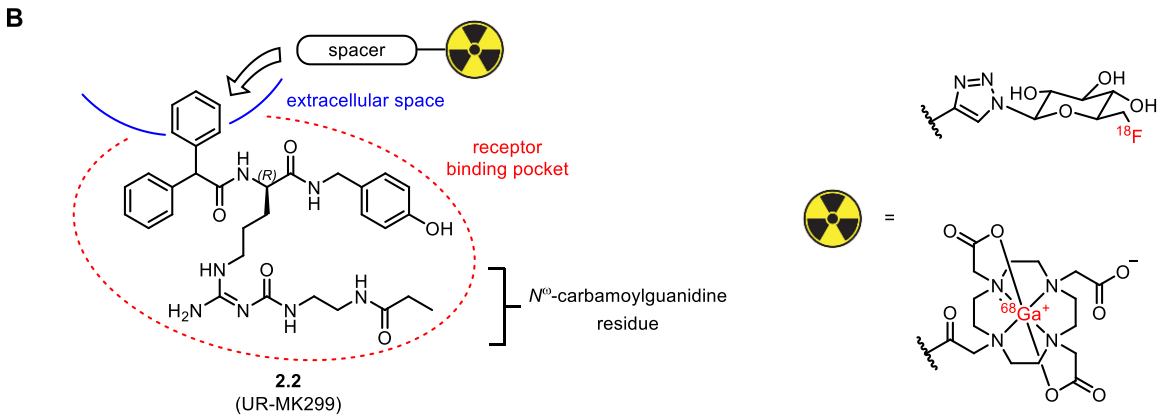

Figure 3.1. (A) Structures and Y_1R affinities (pK_i values) of compounds **2.1**, **3.1**-**3.4**, **2.2** and (*S*,*R*)-**2.14**, and experimental log$D_{7.4}$ values of the potential Y_1R PET ligands **3.1**-**3.4**, where radionuclide-carrying moieties (2-fluoropropionyl in **3.1**, fluoroethoxy in **3.2** and **3.3**, and fluoroglycosyl in **3.4**) were attached to the N^{ω}-carbamoylguanidine residue. (B) Structure of UR-MK299 (**2.2**) positioned in a schematically depicted Y_1R binding pocket. The binding mode of **2.2** suggests an attachment of radionuclide carrying entities to the diphenylacetyl moiety in **3.5**. [a]Log$D_{7.4}$ values were determined using the respective radioactively labeled analogues; [b]Keller *et al.*;[24] [c]Keller *et al.*;[19] [d]Maschauer *et al.*;[20] [e]Keller *et al.*;[25] [f]The additional stereocenter at the diphenyl acetyl moiety in (*S*,*R*)-**2.14** is (*S*)-configured; [g]Mueller *et al.*;[23] Y_1R binding data of **2.1**, **2.2** and **3.1**-**3.4**, previously reported as K_i, were converted to the respective pK_i values.

3.2 Results and discussion

3.2.1 "Cold" synthesis of potential NPY Y_1 PET ligands

In addition to the amine-functionalized precursor (*S*,*R*)-**2.14**[23] (Figure 3.1, panel A), an analogue devoid of a carbamoyl substituent in N^{ω}-position, compound (*S*,*R*)-**3.6**, was synthesized (Scheme 3.1) and used as starting material for the synthesis of fluoroglycosylated PET tracers. 2ClTrt-resin-bound Fmoc-protected hydroxybenzylamine (**2.27**[23]) was deprotected and coupled to commercially available D-arginine derivative **3.5** using HOBt/HBTU, followed by Fmoc deprotection and acylation with racemic carboxylic acid **2.12**.[23] TFA-mediated cleavage from the resin and removal of the acid-labile protecting groups yielded the diastereomers (*S*,*R*)-**3.6** and (*R*,*R*)-**3.6** in a 1:1 ratio, which were separated by preparative HPLC.

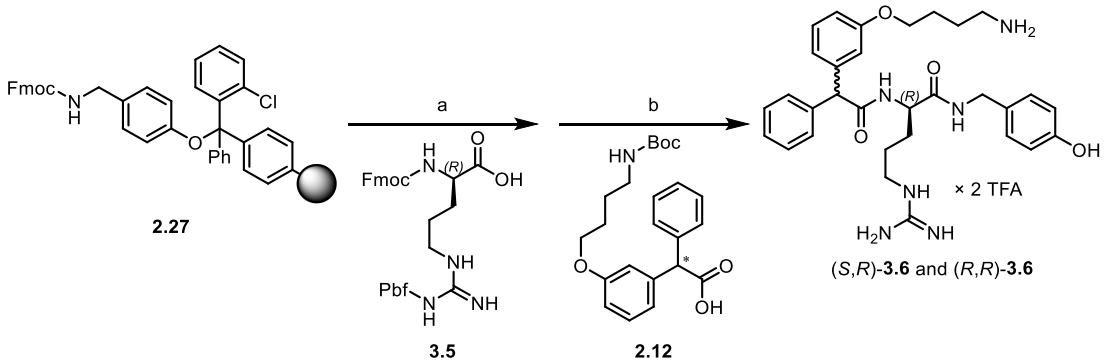

Scheme 3.1. Synthesis of the amine-functionalized argininamide-type Y_1R antagonists (*S,R*)-**3.6** and (*R,R*)-**3.6**. The asterisk in **2.12** indicates a racemic mixture. The wavy bond in **3.6** indicates either configuration, *S* or *R*. Reagents and conditions: a) (1) piperidine, DMF, 35 °C, 2 h (procedure repeated once), (2) HBTU, HOBt, DIPEA, DMF, 35 °C, 16 h; b) (1) piperidine, DMF, 35 °C, 2 h (procedure repeated once), (2) HBTU, HOBt, DIPEA, DMF, 35 °C, 16 h; (3) TFA, CH_2Cl_2, rt, 20 min; (4), TFA, H_2O, rt, 16 h; overall yields: 23% ((*S*,*R*)-**3.6**), 14% ((*R*,*R*)-**3.6**). Note: (*S*,*R*)-**3.6** and (*R*,*R*)-**3.6** were separated and purified by preparative RP-HPLC.

The assignment of the absolute stereochemistry to the methine carbon of the substituted diphenylacetyl moiety in the synthesized diastereomers of **3.6** was achieved by comparison of the ^{1}H-NMR spectra of compounds (*S*,*R*)-**2.14** and (*R*,*R*)-**2.14** (known stereochemistry) with the ^{1}H-NMR spectra of (*S*,*R*)-**3.6** and (*R*,*R*)-**3.6** (Figure 3.2). Characteristic ^{1}H-NMR signal splitting pattern of three aromatic protons of the *meta*-substituted benzene ring (Figure 3.2, red) and the benzylic protons of the 4-hydroxybenzylamide moiety (Figure 3.2, blue), considerably differing between (*S*,*R*)- and (*R*,*R*)-configured compounds, allowed the assignment of the absolute configuration to the diastereomers of **3.6**. The assignment was confirmed by CD-spectrometric analysis using (*S*,*R*)-**2.14** and (*R*,*R*)-**2.14** as reference compounds (Figure 3.3).

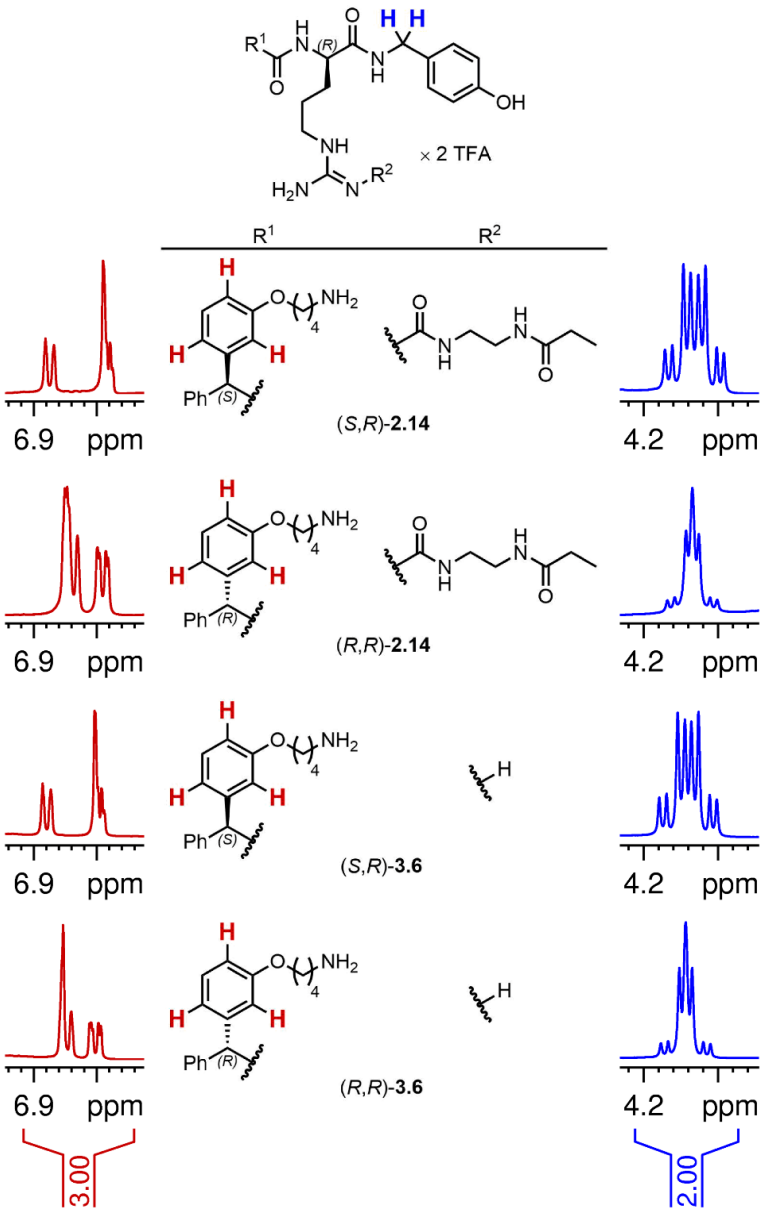

Figure 3.2. Assignment of the absolute stereochemistry to (*S*,*R*)-**3.6** and (*R*,*R*)-**3.6** using ^{1}H-NMR spectroscopy (600 MHz, DMSO-d_6). The ^{1}H-NMR signal splitting patterns of three aromatic protons (highlighted in red) and of the two benzylic protons (highlighted in blue) were coherent for reference compound (*S*,*R*)-**2.14** and (*S*,*R*)-**3.6**, and for reference compound (*R*,*R*)-**2.14** and (*R*,*R*)-**3.6**.

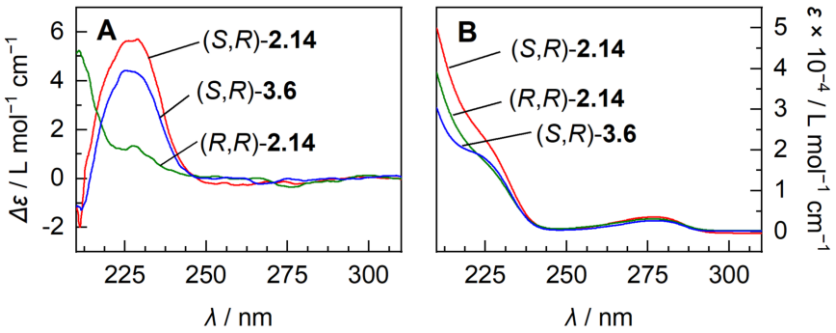

Figure 3.3. CD (A) and parent absorption spectrum (B) of a methanolic solution (0.2 mg/mL) of one of the two diastereomers of **3.6** (blue) in comparison to spectra recorded for (*S*,*R*)-**2.14** (red) and (*R*,*R*)-**2.14** (green). The strong CD-maximum at 226 nm indicates the *S*-configuration at the diphenylated carbon and is absent in the *R*,*R*-diastereomer (*R*,*R*)-**2.14** (*cf*. Mueller *et al*.[23]). As it is obviously not affected by substitution of the guanidino group (demonstrated by the absorption spectra in B), the blue spectrum can be assigned to (*S*,*R*)-**3.6**. All spectra are shown in molar absorptivity units.

Compounds (*S*,*R*)-**3.6** and (*S*,*R*)-**2.14** were treated with succinimidyl ester **3.7** under basic conditions to yield the alkyne precursors **3.8** and **3.9**, respectively. In a Cu(I)-catalyzed azide-alkyne cycloaddition (CuAAC), **3.8** and **3.9** were conjugated to 6-deoxy-6-fluoroglucosyl azide (**3.10**)[26] resulting in the potential Y_1R PET ligands **3.11** and **3.12**, respectively (Scheme 3.2).

For the synthesis of the fluoroglycosylated potential PET ligand **3.16**, containing an extended linker with an ethylene glycol dialkyl ether moiety, (*S*,*R*)-**2.14** was coupled to *N*-Boc,*N*'-succinyl-3,6-dioxaoctane-1,8-diamine (**3.13**) using HBTU/HOBt, followed by acidic removal of the Boc protecting group, resulting in amine **3.14**. The latter was converted to alkyne **3.15** by treatment with **3.7** in the presence of DIPEA. CuAAC-mediated conjugation of **3.10** to **3.15** gave **3.16** (Scheme 3.2).

The synthesis of the potential PET ligand **3.22**, containing, for reasons of increased hydrophilicity, a maltosyl residue in addition to the fluoroglycosyl moiety, started with the CuAAC-mediated conjugation of azide **3.17** to *N*-Boc-propargyl glycine (**3.18**) to afford the Boc-protected amino acid **3.19**. HBTU/HOBt were used to link (*S*,*R*)-**2.14** with **3.19** by amide bond formation yielding Boc-protected amine **3.20**. Removal of the Boc protecting group in **3.20** and treatment with succinimidyl ester **3.7** followed by Zemplén deacetylation of the maltosyl moiety gave alkyne **3.21**, which was finally "clicked" to **3.10** affording compound **3.22** (Scheme 3.2).

The PET ligand candidate **3.25** was synthesized by treatment of (*S*,*R*)-**2.14** with DOTA-succinimidyl ester **3.23**, yielding **3.24**, followed by the incorporation of Ga^{3+} under moderately acidic conditions (pH 4.2) at 100° C (Scheme 3.2).

The chemical stability of the potential Y_1R PET ligands **3.11**, **3.12**, **3.16**, **3.22** and **3.25** was assessed by incubation in PBS pH 7.4 at 22 °C for up to 24 h. Under these conditions, the studied compounds showed no decomposition (*cf.* section A.3.1).

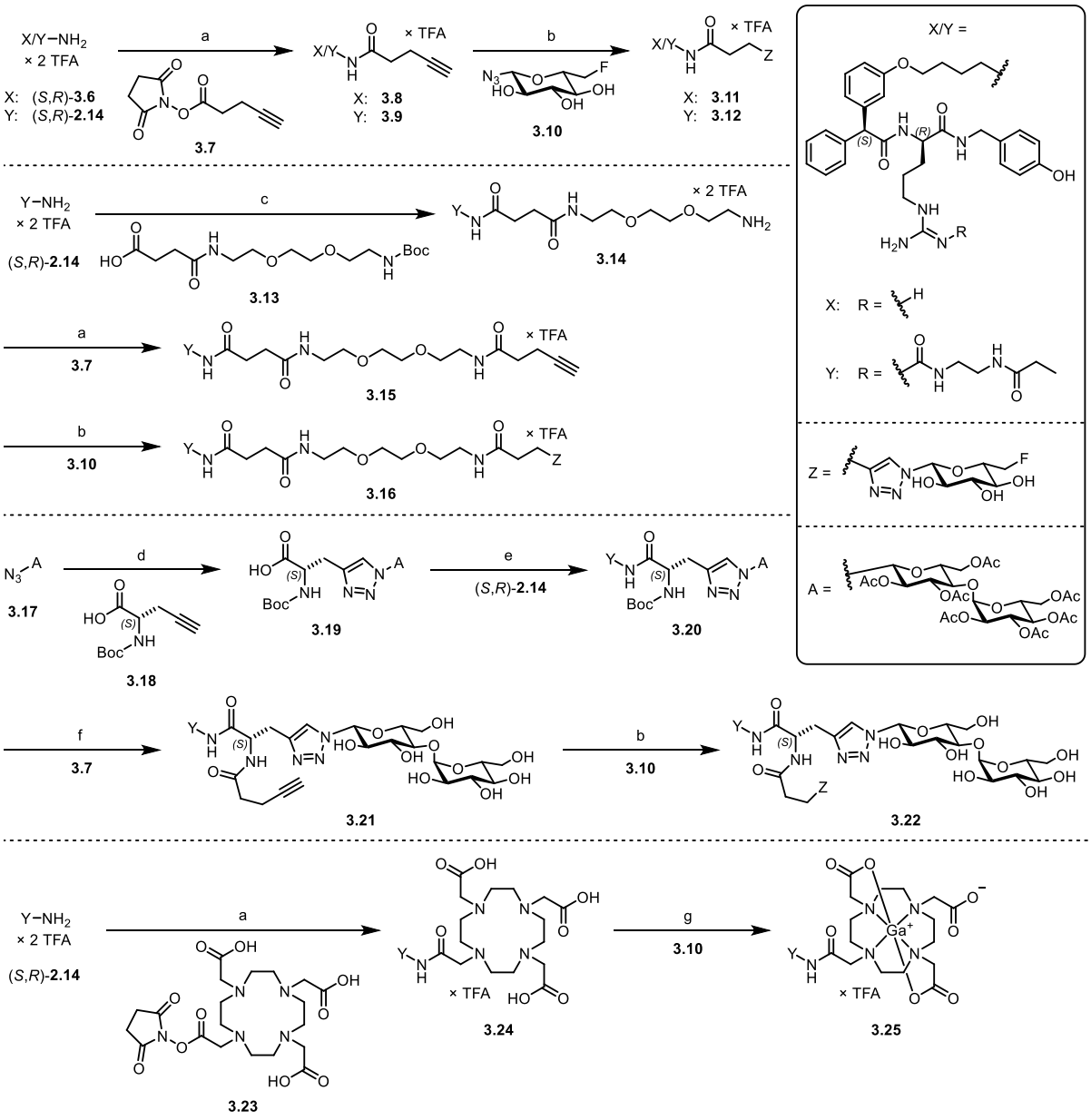

Scheme 3.2. Synthesis of the potential Y_1R PET ligands **3.11**, **3.12**, **3.16**, **3.22** and **3.25**. Reagents and conditions: a) DIPEA, DMF, rt, 1 h, 63% (**3.8**), 64% (**3.9**), 67% (**3.15**), 53% (**3.24**); b) $CuSO_4$ × 5 H_2O, sodium ascorbate, H_2O/ethanol, rt, 30-60 min, 57% (**3.11**), 44% (**3.12**), 62% (**3.16**), 51% (**3.22**); c) (1) HBTU, HOBt, DIPEA, DMF, rt, 5 min; (2) TFA, CH_2Cl_2, rt, 1 h, 51%; d) $CuSO_4$ × 5 H_2O, sodium ascorbate, H_2O/ethanol, rt, 1 h, 25%; e) HBTU, HOBt, DIPEA, DMF, rt, 2 h, 31%; f) (1) TFA, CH_2Cl_2, rt, 16 h; (2) **3.7**, DIPEA, DMF, rt, 1 h; (3) sodium methoxide, methanol, rt, 30 min, 29%; g) $Ga(NO_3)_3$ × H_2O, HEPES pH 4.2, aq. HCl, 100 °C, 10 min, 33%.

3.2.2 NPY receptor binding and Y_1R antagonism

Y_1R binding affinities of the amine-functionalized BIBP3226 (**2.1**)-derived compounds (*S*,*R*)-**3.6** and (*R*,*R*)-**3.6**, and the potential PET ligands **3.11**, **3.12**, **3.16**, **3.22** and **3.25** were determined in Y_1R competition binding experiments using [^{3}H]**2.2** as the radioligand and human Y_1R-expressing SK-N-MC neuroblastoma cells as the receptor source. The obtained pK_i values are listed in Table 3.1. For **3.11**, **3.12**, **3.16**, **3.22** and **3.25**, the corresponding radioligand displacement curves are displayed in Figure 3.4.

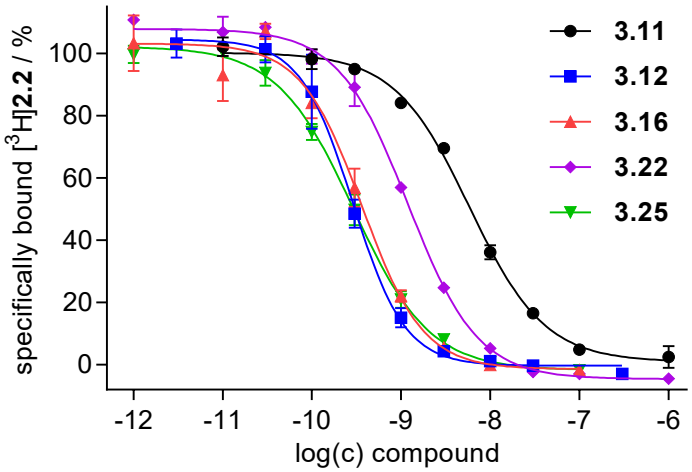

Figure 3.4. Radioligand displacement curves obtained from competition binding studies with [^{3}H]**2.2** (K_D = 0.044 nM, c = 0.15 nM)[25] and compounds **3.11**, **3.12**, **3.16**, **3.22** and **3.25** performed at intact SK-N-MC neuroblastoma cells. Data represent mean values ± SEM from at least three independent experiments performed in triplicate.

Interestingly, (*S*,*R*)-**3.6** and (*R*,*R*)-**3.6** exhibited increased Y_1R affinity compared to parent compound **2.1** (pK_i = 9.95 and 9.41, respectively), 10-fold in the case of (*S*,*R*)-**3.6** (Table 3.1). A similar increase in binding affinity compared to the respective parent compound was also observed for the N^{ω}-carbamoylated congeners of (*S*,*R*)-**3.6** and (*R*,*R*)-**3.6**, i.e. (*S*,*R*)-**2.14** and (*R*,*R*)-**2.14** (pK_i = 10.62 and 10.61, respectively; pK_i of the parent compound **2.2** = 10.27, *cf.* Chapter 2). This suggests beneficial interactions of the primary amine groups in (*S*,*R*)-**2.14**, (*S*,*R*)-**3.6**, (*R*,*R*)-**2.14** and (*R*,*R*)-**3.6** with the Y_1 receptor. The presence of the fluoroglycosyltriazolyl moiety in the (*S*,*R*)-**3.6**-derived compound **3.11** leads to a tenfold decrease in affinity (pK_i = 8.87) compared to (*S*,*R*)-**3.6**. Consequently, **3.11** exhibits a Y_1R affinity comparable to that of parent compound **2.1** (pK_i = 8.80) and the previously reported PET ligand **3.1** (pK_i = 8.89).

The N^{ω}-carbamoylated argininamides **3.12**, **3.16** and **3.25** displayed very high Y_1R affinities in the two-digit picomolar range (pK_i = 10.10-10.20), irrespective of the attached residue at the diphenylacetyl moiety, being either a fluoroglycosyl residue (**3.12** and **3.16**) or a Ga^{3+}-

containing DOTA chelator (**3.25**). The slightly decreased Y_1R binding affinity of **3.22** (pK_i = 9.55), bearing the bulkiest residue at the diphenylacetyl moiety, is in agreement with previous observations made in the case of fluorescently labeled Y_1R ligands derived from (*S*,*R*)-**2.14**, where the size of the attached fluorescent dye correlated inversely with Y_1R binding affinity (*cf.* Chapter 2).

As previously reported for the argininamide-type Y_1R antagonists **2.1** and **2.2**, compounds **3.11**, **3.12**, **3.16**, **3.22** and **3.25** showed an excellent preference for the Y_1R (> 1000-fold) over the other NPY receptor subtypes (Table 3.1).

Table 3.1. NPY receptor binding data of parent compounds **2.1** and **2.2**, amine-functionalized argininamides (*S*,*R*)-**2.14**, (*S*,*R*)-**3.6** and (*R*,*R*)-**3.6**, and potential PET ligands **3.11**, **3.12**, **3.16**, **3.22** and **3.25**.

compd.	pK_i ± SEM / K_i [nM][a]	pK_i ± SEM[a]		
	Y_1R[b]	Y_2R[c]	Y_4R[d]	Y_5R[e]
2.1	8.80 / 1.3[f]	<5[g]	<5.3[h]	<6[i]
2.2	10.27 ± 0.17 / 0.077[i]	<5.5[j]	<5[j]	<5[j]
(*S*,*R*)-**2.14**	10.62 ± 0.02 / 0.024	<5	<5	<5
(*S*,*R*)-**3.6**	9.95 ± 0.01 / 0.11	nd[k]	nd[k]	nd[k]
(*R*,*R*)-**3.6**	9.41 ± 0.06 / 0.39	nd[k]	nd[k]	nd[k]
3.11	8.87 ± 0.02 / 1.3	<5.5	<5.5	<5.5
3.12	10.20 ± 0.06 / 0.065	<5.5	<5.5	<5.5
3.16	10.10 ± 0.10 / 0.083	<5.5	<5.5	<5.5
3.22	9.55 ± 0.02 / 0.28	<5.5	<5.5	<5.5
3.25	10.20 ± 0.05 / 0.060	<5.5	<5.5	<5.5

[a]Data represent mean values ± SEM (pK_i) or mean values (K_i) from at least three independent experiments performed in triplicate. [b]Determined by competition binding with [^{3}H]**2.2** (K_d = 0.044 nM,[22] c = 0.15 nM) at intact SK-N-MC neuroblastoma cells. [c]Determined by competition binding with [^{3}H]propionyl-pNPY (K_d = 0.14 nM,[27] c = 0.5 nM) at intact CHO-hY_2R cells. [d]Determined by competition binding with [^{3}H]UR-KK200 (K_d = 0.67 nM,[28] c = 1 nM) at intact CHO-hY_4-Gqi5-mtAEQ cells. [e]Determined by competition binding with [^{3}H]propionyl-pNPY (K_d = 11 nM,[29] c = 5 nM) at intact HEC-1B-hY_5 cells. [f]Keller *et al.*;[24] [g]Rudolf *et al.*;[30] [h]Keller *et al.*;[31] [i]Hu *et al.*;[32] [j]Keller *et al.*[25] Data, previously reported as K_i, were re-evaluated to afford the pK_i values. [k]Not determined.

As determined in a Fura-2 calcium flux assay using Y_1R-expressing HEL cells, **3.11**, **3.12**, **3.16**, **3.22** and **3.25** exhibited Y_1R antagonistic activities being capable of fully inhibiting the increase in cytosolic Ca^{2+} elicited by pNPY. The resulting pIC_{50} values, ranging from 7.87 (**3.11**) to 9.92 (**3.25**) were in the same range as the pK_i values obtained from radioligand competition binding, except for compound **3.11**, where the pIC_{50} was considerably lower than the respective pK_i value (Figure 3.5 and Table 3.1).

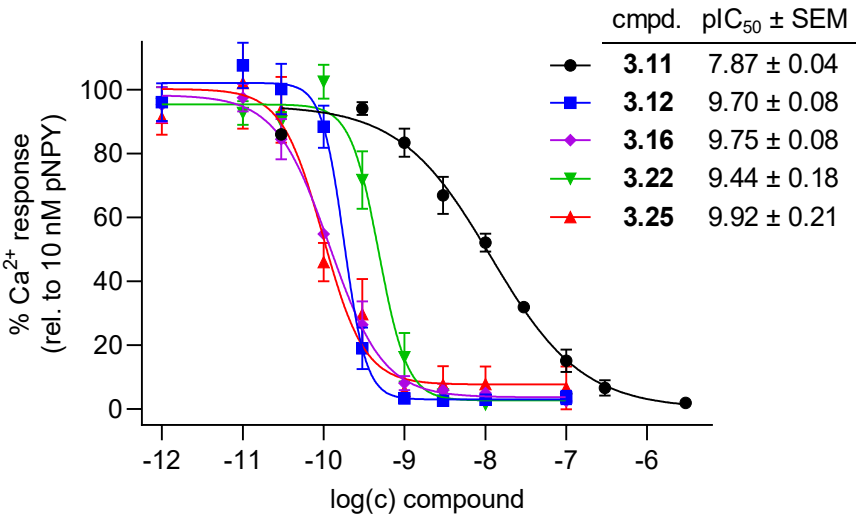

Figure 3.5. Investigation of compounds **3.11**, **3.12**, **3.16**, **3.22** and **3.25** in a Fura-2 Ca^{2+} assay using human erythroleukemia (HEL) cells. The inhibition curves resulted from the inhibition of the pNPY-induced (10 nM) intracellular Ca^{2+} mobilization by the antagonists. Data represent mean values ± SEM from three independent experiments performed in singlet.

The previously reported argininamide-type Y_1R PET ligand [^{18}F]**3.1**,[19] being structurally closely related to e.g. **2.2**, **3.12** and **3.25**, showed strong hepatobiliary clearance in mice. As the ABC transporter P-glycoprotein (P-gp) mediates hepatobiliary excretion, preferentially of cationic, lipophilic compounds,[33, 34] in particular the most lipophilic N^{ω}-carbamoylated compound **3.12** represents a potential substrate of P-gp. Hence, **2.2**, **3.12** and **3.25** were investigated in a flow cytometric calcein efflux assay, developed to indicate whether a compound of interest is capable of (competitively) inhibiting the P-gp mediated efflux of intracellular calcein.[35, 36] As demonstrated in Figure 3.6, none of the studied compounds displayed an inhibitory effect on the P-gp mediated efflux of calcein suggesting that **2.2**, **3.12** and **3.25** are neither substrates nor inhibitors of P-gp. However, the involvement of other hepatobiliary clearance mechanisms independent on the P-gp-mediated efflux, e.g organic anion transporters in the case of **3.25**, cannot be precluded.[37]

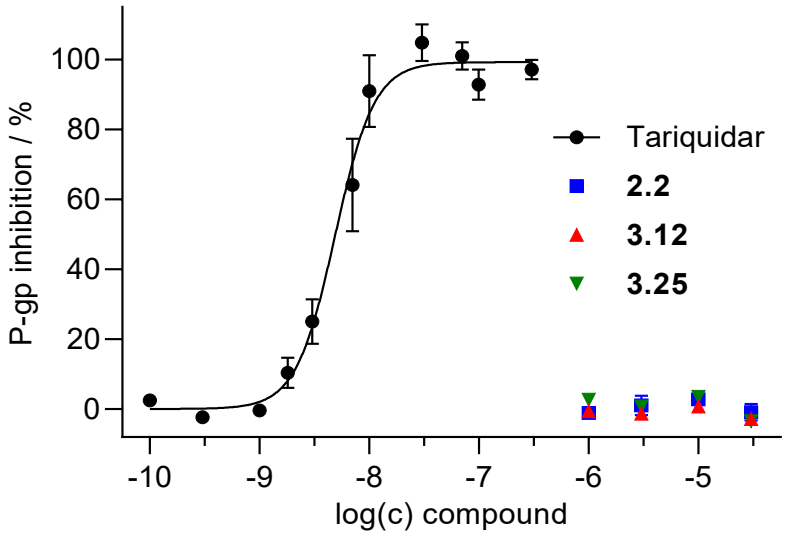

Figure 3.6. Investigation of the Y_1R antagonists **2.2**, **3.12** and **3.25** in a flow cytometric calcein-AM efflux assay using P-gp expressing (induced by doxorubicin) murine P388 leukemia cells.[38] The P-gp inhibitor tariquidar was used as positive control (pIC_{50} = 8,30 ± 0.09, mean ± SEM from four independent determinations performed in triplicate). Compounds **2.2**, **3.12** and **3.25** showed no inhibiting effect up to a concentration of 30 µM. Cells were preincubated with tariquidar, **2.2**, **3.12** or **3.25** for 15 min followed by incubation for 1 min with calcein-AM (1 µM), and flow cytometric analysis. Data represent mean values ± SEM from four independent experiments performed in triplicate.

3.2.3 Synthesis and *in vitro* characterization of the PET ligands [^{18}F]3.11, [^{18}F]3.12 and [^{68}Ga]3.25

From the synthesized set of PET ligand candidates (**3.11**, **3.12**, **3.16**, **3.22**, **3.25**) we chose **3.11**, **3.12** and **3.25** for radiolabeling and *in vivo* studies. The selection included two ^{18}F-labeled ligands ([^{18}F]**3.11** and [^{18}F]**3.12**), differing in the absence or presence of the carbamoyl substituent at the guanidino group (absent in **3.11** and present in **3.12**), and the ^{68}Ga-labeled ligand [^{68}Ga]**3.25**. According to the order of elution obtained from RP-HPLC analysis, **3.22** and **3.25** are the most polar compounds with almost equal retention time, with **3.25** exhibiting higher binding affinity compared to **3.22** (pK_i = 10.20 and 9.55, respectively). On the other hand, **3.12**, exhibiting identical binding affinity compared to **3.25**, constitutes the most lipophilic member within the series of prepared PET ligand candidates (see chromatograms and ligand retention times of the HPLC purity controls, section A.3.3). Thus, with [^{18}F]**3.11**, [^{18}F]**3.12** and [^{68}Ga]**3.25**, the full span of hydrophilicity within the synthesized set of potential PET ligands was covered, and the most commonly used radionuclides for PET, ^{18}F and ^{68}Ga, were included.

The PET ligands [^{18}F]**3.11** and [^{18}F]**3.12** were prepared from the alkyne-functionalized precursors **3.8** and **3.9** and the previously described fluoroglycosyl azide [^{18}F]**3.10**[39] by Cu(I)-mediated alkyne-azide cycloaddition in aqueous solution using the reagents Cu(II) acetate,

sodium ascorbate and THPTA. After purification by semipreparative reversed phase HPLC, [^{18}F]**3.11** and [^{18}F]**3.12** were obtained in activity yields between 250 and 300 MBq (Table 3.2).

[^{68}Ga]**3.25** was prepared by incorporation of $^{68}Ga^{3+}$ into the chelator moiety of **3.24** at elevated temperatures (99-125 °C) using a Scintomics GRP® synthesizer module or applying a manual procedure. In both cases, a ^{68}Ge/^{68}Ga-generator served as source of $^{68}Ga^{3+}$ (obtained as [^{68}Ga]$GaCl_3$ upon elution with 0.1 M HCl). After the incorporation of $^{68}Ga^{3+}$, inorganic components including free $^{68}Ga^{3+}$ were removed by solid phase extraction (C18 cartridge) to afford [^{68}Ga]**3.25** in activity yields between 120-516 MBq (*cf.* Table 3.2).

Table 3.2. Overview of amounts of precursor and activity yields for the radiosynthesis of [^{18}F]**3.11,** [^{18}F]**3.12** and [^{68}Ga]**3.25**.

PET ligand	labeling precursor	amount of precursor	conditions labeling reaction (temp., time)	activity yield [MBq]
[^{18}F]**3.11**	**3.8**	144 µg, 150 nmol	60 °C, 10 min[a]	250-300[b]
[^{18}F]**3.12**	**3.9**	165 µg, 150 nmol	60 °C, 10 min[a]	250-300[b]
[^{68}Ga]**3.25**	**3.24**	24 µg, 18 nmol[c] 5.3 µg, 4 nmol[d]	125 °C, 6 min[c] 99 °C, 5 min[d]	225-516[c] 120-160[d]

[a]Reaction conditions applied for the CuAAC-mediated coupling of priorly synthesized [^{18}F]**3.10** with **3.8** and **3.9**, respectively. [b]Activity yield after two reaction steps (synthesis of [^{18}F[**3.10** and successive CuAAC), starting with the elution of ^{18}F with 1000 MBq activity. [c]Synthesis performed with a Scintomics GRP® synthesizer module using the ABX Hardware Kits SC-01 and SC-01-H. [d]Synthesis performed manually.

To assess the lipophilicity of the PET ligands [^{18}F]**3.11**, [^{18}F]**3.12** and [^{68}Ga]**3.25**, their n-octanol/PBS pH 7.4 distribution coefficients ($logD_{7.4}$) were determined. As expected, compound [^{18}F]**3.12**, containing an N^{ω}-carbamoyl residue, was more lipophilic ($logD_{7.4}$ = –0.10 ± 0.01, mean ± SD from 3 independent determinations) compared to the non-carbamoylated congener [^{18}F]**3.11** ($logD_{7.4}$ = –0.45 ± 0.02, mean ± SD from 3 independent determinations). [^{68}Ga]**3.25**, carrying the highly polar DOTA chelator, represented the least lipophilic PET tracer ($logD_{7.4}$ = –2.60 ± 0.10, mean ± SD from 3 independent determinations). Overall, [^{18}F]**3.11**, [^{18}F]**3.12** and [^{18}F]**3.25** exhibited markedly decreased lipophilicity in comparison to the previously reported PET ligands [^{18}F]**3.1-3.4** ($logD_{7.4}$ values between 0.78 and 2.34), which is considered favorable in terms of shifting biliary towards renal excretion.

For [^{68}Ga]**3.25**, the chemical stability in human plasma was investigated over a period of 3 h revealing that no detectable amounts of radioactive metabolites or degradation products were formed (*cf.* section A.3.2).

Autoradiographic binding experiments using [^{68}Ga]**3.25** as radioligand were performed on cryosections of a human MCF-7 and a human SK-N-MC tumor, subcutaneously grown in nude mice. For MCF-7 tumors, high Y_1R densities were previously confirmed by autoradiography

using tritiated Y_1R ligands.[24, 40] Likewise, the autoradiography with the PET ligand [^{68}Ga]**3.25** revealed high Y_1R expression in the MCF-7 tumor as becomes obvious from the marked difference between total and nonspecific binding (Figure 3.7). Y_1R binding sites could also be detected in the SK-N-MC tumor, however in lower quantity only in the peripheral regions of the tumor, most likely due to necrotic tissue in the tumor center (Figure 3.7).

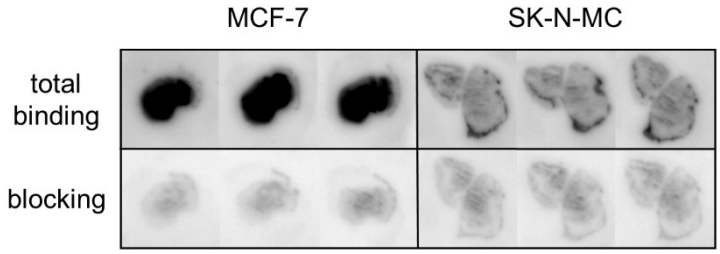

Figure 3.7. *In vitro* autoradiography at MCF-7 (left) and SK-N-MC (right) tumor cryosections (12 µm) using the Y_1R PET ligand [^{68}Ga]**3.25**. The sections were incubated with [^{68}Ga]**3.25** at rt for 50 min. Blocking experiments were performed in presence of **2.1** (15 µM).

3.2.4 Biodistribution studies with [^{18}F]3.11 and [^{18}F]3.12

For the ^{18}F-labeled PET ligands [^{18}F]**3.11** and [^{18}F]**3.12**, differing in structure only with respect to the absence (**3.11**) and presence (**3.12**) of the N^{ω}-carbamoyl substituent, biodistribution studies were performed in nude mice bearing a subcutaneous Y_1R-negative MDA-MB-231 tumor and a subcutaneous Y_1R-expressing MCF-7 tumor.[41] In this xenograft model, the Y_1R-negative tumor serves as a control to verify Y_1R-mediated uptake of the PET ligand in the MCF-7 tumor. When comparing the activities in the tumors, both tracers showed a higher uptake in the MCF-7 tumor compared to the MDA-MB-231 tumor at 90 min p.i. (Figure 3.8, Table 3.3). Whereas this difference was statistically significant for [^{18}F]**3.12** ($p < 0.05$, unpaired t-test), it was statistically insignificant in the case of [^{18}F]**3.11** ($p > 0.05$, unpaired t-test). With PET ligand [^{18}F]**3.12**, exhibiting higher Y_1R affinity than [^{18}F]**3.11** (*cf*. Table 3.1), higher absolute %ID/g values were achieved. Likewise, the retention (30 to 90 min) of [^{18}F]**3.12** in the MCF-7 tumor was more pronounced than for [^{18}F]**3.11**.

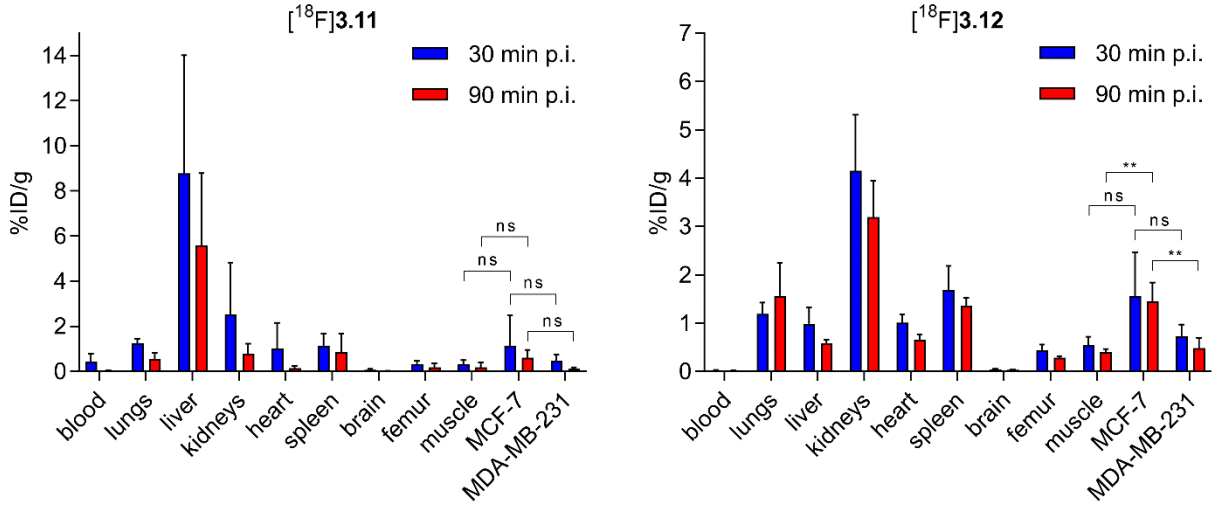

Figure 3.8. Biodistribution of the Y_1R PET ligands [^{18}F]**3.11** and [^{18}F]**12** in mice bearing a subcutaneous Y_1R-negative MDA-MB-231 tumor and a subcutaneous Y_1R-expressing MCF-7 tumor, studied after 30 and 90 min p.i. Data represent mean values ± SD from at least three animals. Statistical analysis of differences between tracer accumulation in the MCF-7 tumor and the MDA-MB-231 tumor, and between the MCF-7 tumor and muscle tissue was performed by an unpaired two-tailed t-test ($p < 0.05$ was considered statistically significant, ** $p < 0.01$, ns: not significant).

Unexpectedly, PET tracer [^{18}F]**3.11**, being more polar compared to [^{18}F]**3.12** ($logD_{7.4}$ = –0.45 vs. –0.10), was primarily eliminated hepatobiliary, while the less polar tracer [^{18}F]**3.12** mainly underwent renal excretion (Figure 3.8, Table 3.3). Possibly, this might be caused by the strong difference in basicity between the carbamoylguanidino group (pK_s ca. 8[42]) in [^{18}F]**3.12** and the unsubstituted guanidino group (pK_s ca. 12.5). The tumor-to-muscle ratios amounted to 9 and 3.7 after 90 min p.i. for [^{18}F]**3.11** and [^{18}F]**3.12**, respectively (Table 3.3), constituting an improvement over the previously reported PET ligand [^{18}F]**3.1**.[19]

Table 3.3. *Ex vivo* biodistribution data and tumor-to-blood ratios of [^{18}F]**3.11** and [^{18}F]**3.12**.[a]

tissue	[^{18}F]**3.11**		[^{18}F]**3.12**	
	uptake (%ID/g)		uptake (%ID/g)	
	30 min p.i.	90 min p.i.	30 min p.i.	90 min p.i.
blood	0.4 ± 0.3	0.044 ± 0.013	0.025 ± 0.008	0.015 ± 0.012
lungs	1.26 ± 0.20	0.55 ± 0.26	1.20 ± 0.23	1.6 ± 0.7
liver	9 ± 5	5.6 ± 3.2	1.0 ± 0.3	0.57 ± 0.09
kidney	2.5 ± 2.3	0.8 ± 0.4	4.1 ± 1.2	3.2 ± 0.8
heart	1.0 ± 1.1	0.15 ± 0.09	1.01 ± 0.17	0.66 ± 0.11
spleen	1.1 ± 0.5	0.9 ± 0.8	1.7 ± 0.5	1.4 ± 0.17
brain	0.07 ± 0.05	0.019 ± 0.018	0.040 ± 0.013	0.031 ± 0.005
femur	0.33 ± 0.14	0.19 ± 0.17	0.44 ± 0.12	0.28 ± 0.03
muscle	0.30 ± 0.21	0.19 ± 0.23	0.54 ± 0.18	0.41 ± 0.06
MCF-7	1.2 ± 1.3	0.6 ± 0.3	1.6 ± 0.9	1.5 ± 0.4
MDA-MB-231	0.47 ± 0.29	0.13 ± 0.04	0.73 ± 0.24	0.48 ± 0.21
MCF-7-to-muscle	4 ± 3	9 ± 8	3.3 ± 2.7	3.7 ± 1.4

[a]Given are mean values ± SD from at least three individual experiments. Organ uptake values were obtained at 30 and 90 min p.i. (intravenous) from mice bearing a subcutaneous Y_1R-negative MDA-MB-231 tumor and a subcutaneous Y_1R-positive MCF-7 tumor.

3.2.5 Small animal PET studies with [^{18}F]3.11, [^{18}F]3.12 and [^{68}Ga]3.25

The PET ligands [^{18}F]**3.11** and [^{18}F]**3.12** were also investigated by PET imaging (60 min PET scans) using the same mouse xenograft model as for the biodistribution studies. PET images for the time frames 25-30 min and 50-60 min and the time-activity curves for both tumors are displayed in Figure 3.9 (panels A and B, respectively). The PET studies confirmed the Y_1R-specific uptake of the tracers in the MCF-7 tumor and the longer retention of [^{18}F]**3.12** in this tumor compared to [^{18}F]**3.11**. In contrast to the biodistribution data, the tumor uptake values of [^{18}F]**3.11** were higher than those of [^{18}F]**3.12**. Moreover, unlike the results of the biodistribution experiments, the PET data suggested a predominant hepatobiliary excretion of [^{18}F]**3.12**. However, the PET data must be interpreted with caution as the used PET scanner was not equipped with a CT modality, hampering the quantitative analysis of the obtained data.

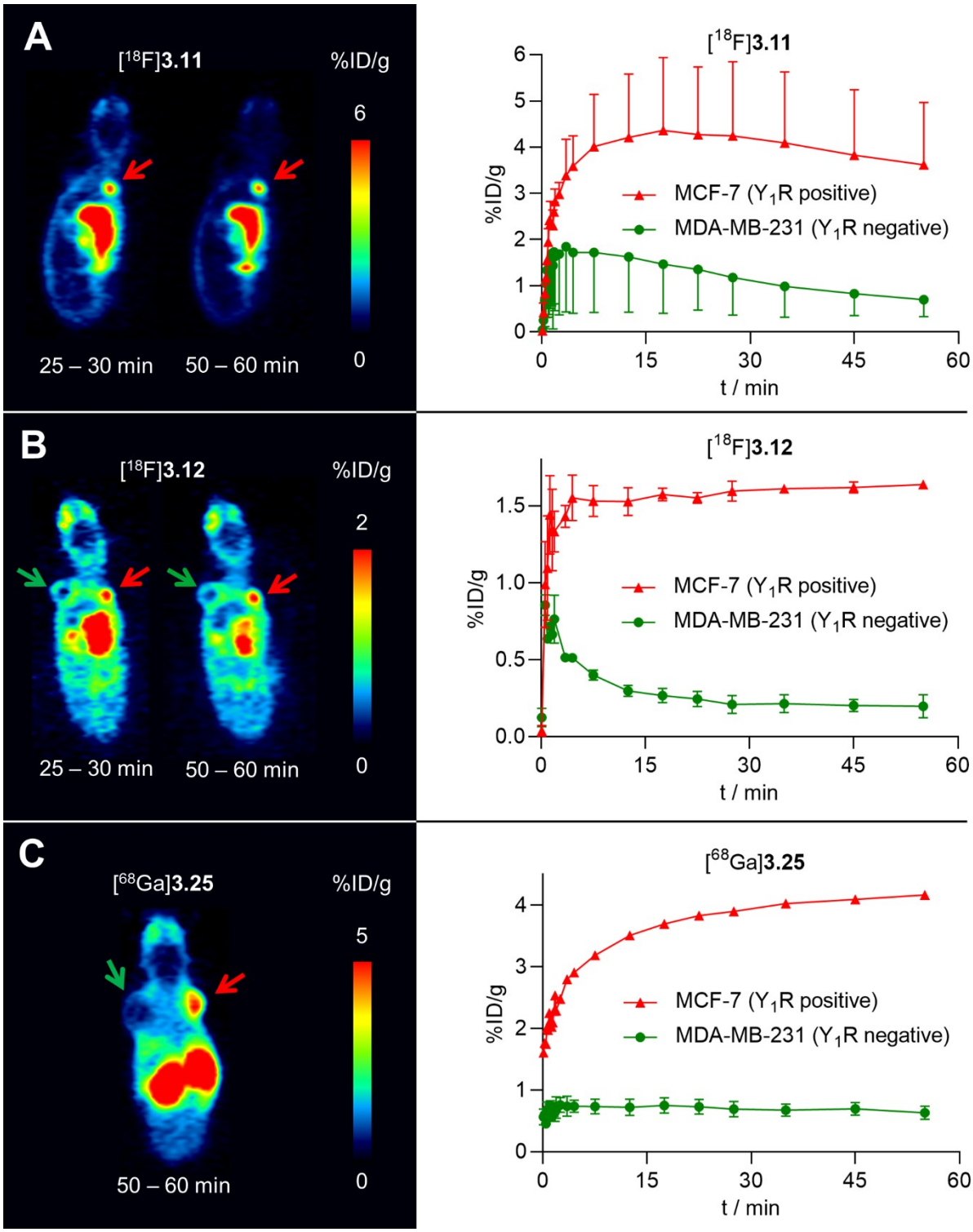

Figure 3.9. Representative PET images of nude mice, bearing MCF-7-Y_1 (red arrows) and MDA-MB-231 (green arrows) tumor xenografts, injected with radioligands (A) [^{18}F]**3.11**, (B) [^{18}F]**3.12** or (C) [^{68}Ga]**3.25** (time frames: 25-30 min and/or 50-60 min post injection), and corresponding time-activity curves of the tumors for the whole PET scan. Radioactivity measures are displayed as injected dose per gram tumor (%ID/g). Data in the time-activity curves represent mean values ± SD from two ([^{18}F]**3.11**, [^{18}F]**3.12**) or three ([^{68}Ga]**3.25)** independent experiments. Note: The MDA-MB-231 tumor in panel A (PET scan) is not visible in the displayed plane.

In addition to the ^{18}F-labeled PET ligands [^{18}F]**3.11** and [^{18}F]**3.12**, the ^{68}Ga-labeled ligand [^{68}Ga]**3.25** was also studied by PET imaging (60 min PET scans) using the same mouse xenograft model. As it is obvious from the obtained PET images and the time-activity curves of the tumors, the uptake of [^{68}Ga]**3.25** in the MCF-7 tumor was high and specific (Y_1R-mediated) (Figure 3.9, panel C). Moreover, [^{68}Ga]**3.25** exhibited an excellent retention in the MCF-7 tumor. Strikingly, the PET studies revealed that [^{68}Ga]**3.25** is predominantly renally excreted being in agreement with the considerably higher hydrophilicity of [^{68}Ga]**3.25** compared to [^{18}F]**3.11** and [^{18}F]**3.12**, and previously reported argininamide-type Y_1R PET ligands such as [^{18}F]**3.1**-[^{18}F]**3.4**.[19, 20]

3.3 Conclusion

Compared to previously reported argininamide-type Y_1R PET ligands derived from **2.1**, which were labeled *via* a carbamoyl residue attached to the guanidino group, the PET ligands presented in this study display considerably higher Y_1R affinity and hydrophilicity (pK_i (Y_1R) = 8.87-10.20, log$D_{7.4}$ = −0.10 to −2.60). This was achieved by attachment of the label to the diphenylacetyl moiety in the parent compound UR-MK299 (**2.2**). The novel PET ligands, [^{18}F]**3.11**, [^{18}F]**3.12**, and [^{68}Ga]**3.25**, representing highly selective Y_1R antagonists, showed an improved uptake and increased retention in subcutaneous Y_1R-expressing MCF-7 tumors. In contrast to previous reports on Y_1R PET ligands studied with respect to tumor imaging, the Y_1R-mediated uptake of the PET tracers was confirmed by a Y_1R-negative tumor (MDA-MB-231) present in the same animal. [^{68}Ga]**3.25**, the most polar PET tracer studied in this work, represents a promising argininamide-type Y_1R PET ligand, that is mainly excreted *via* the kidneys, which is considered a favorable feature of radioactive tumor imaging agents. With this study, we confirmed that the attachment of various bulky moieties to the diphenyl acetyl group in **2.2** is well tolerated in terms of Y_1R binding. Therefore, based on the presented concept, high-affinity Y_1R PET ligands, e.g. with optimized pharmacokinetics can be developed including ^{18}F-labeled tracers that are renally excreted.

3.4 Experimental procedures

3.4.1 General experimental conditions

Chemicals. Standard chemicals, solvents, and buffer components were purchased from commercial suppliers (Sigma-Aldrich, München, Germany; Merck, Darmstadt, Germany; Fisher Scientific, Schwerte, Germany; TCI, Eschborn, Germany; ABCR, Karlsruhe, Germany; Iris Biotech, Marktredwitz, Germany) and used without further purification. Gradient grade acetonitrile for HPLC was purchased from Sigma-Aldrich. **3.5** was from Iris Biotech (Marktredwitz, Germany), **3.23** from CheMatech (Dijon, France) and **3.18** was from TCI (Eschborn, Germany). Fura-2/AM and BSA were from Merck (Darmstadt, Germany) and

SERVA (Heidelberg, Germany), respectively. Ultrapure 4-(2-hydroxyethyl)-1-piperazineethanesulfonic acid (HEPES) was obtained from Gerbu (Heidelberg, Germany). Calcein-AM was from Biotium (Hayward, CA). The syntheses of **2.27**,[23] **2.12**,[23] **3.10**[39] and [^{18}F]**3.10**[20] were described elsewhere. [^{3}H]propionyl-pNPY (specific activity of 37.5 Ci/mmol, radiochemical purity of 99%) was prepared according to a previously reported procedure[25] with minor modifications (DMF/NMP/H_2O/DIPEA 45:20:32:3 v/v/v/v (60 µL) was used as solvent instead of 0.1 M sodium borate buffer (pH 8.5, 135 µL); propionyl-pNPY was used instead of pNPY for the determination of the molarity and specific activity; radiochemical yield: 26%). Reactions requiring anhydrous conditions were carried out in oven-dried (24 h at 120 °C) Schlenk flasks under an atmosphere of dry nitrogen using anhydrous solvents. Anhydrous DMF was from Sigma-Aldrich (München, Germany). Anhydrous NMP and anhydrous methanol was prepared by storage over desiccants (3 Å molecular sieves, 20% m/v) for at least 2 days under an atmosphere of dry nitrogen. The molecular sieves were predried for 4 h at 300 °C immediately before use.[43] Purifications by column chromatography were carried out using technical grade solvents and Geduran Si 60 silica gel (pore size of 60 Å, particle size of 40-63 or 63-200 µm, Merck). Thin layer chromatography (TLC) was performed on ALUGRAM Xtra SIL G/UV254 TLC sheets from Macherey-Nagel GmbH & Co. KG (Düren, Germany).

NMR spectrometry. NMR spectra were recorded on a an Avance 400 (^{1}H, 400 MHz, ^{13}C, 100 MHz) or an Avance 600 (^{1}H, 600 MHz, ^{13}C, 150 MHz) spectrometer (Bruker, Karlsruhe, Germany). NMR spectra of compounds **3.11, 3.12, 3.16, 3.22** and **3.25** were recorded in 10:1 (v/v) DMSO-d_6/D_2O resulting in a total H-D exchange of OH protons and NH protons of the guanidino groups and no or a partial H-D exchange of amide NH protons (Note: Spectra were recorded at least 2 h after the preparation of the samples). Because only very small amounts (< 0.9 µmol) were used for for some of the ligands, characteristic system signals were apparent in the ^{1}H-NMR spectrum (0.81-0.87 ppm and 1.20-1.30 ppm), originating from impurities in the solvents used for preparative HPLC (*cf.* supplementary Figure A2.11 in section A.2.3).[23]

Mass spectrometry. High-resolution mass spectrometry (HRMS) analysis was performed on an Agilent 6540 UHD AccurateMass Q-TOF LC/MS system coupled to an Agilent 1290 HPLC system (Agilent Technologies, Santa Clara, CA), using an ESI source. Analyses were performed using the following LC method: column: ZORBAX RRHD Eclipse Plus C18, 1.8 µm, 50 × 2.1 mm (Agilent Technologies, Santa Clara, CA), column temperature: 40 °C, flow: 0.6 mL/min, solvent/linear gradient: 0-4 min: 0.1% aqueous HCOOH/0.1% HCOOH in MeCN 95:5-2:98, 4-5 min: 2:98.

Analytical RP-HPLC. Reaction controls, purity controls, and investigations on chemical stabilities for non-labeled compounds were carried out using a 1100 series system from Agilent Technologies (Santa Clara, CA) consisting of a degasser (G1379A), a binary pump (G1312A),

a variable wavelength detector (G1314A), a thermostated column compartment (G1316A), and an autosampler (G1329A) (herein termed system A). A Phenomenex Kinetex XB-C18 100A (5 µm, 250 mm × 4.6 mm, Phenomenex, Aschaffenburg, Germany) was used as the stationary phase. The flow rate was 0.8 mL min^{-1}, the oven temperature was set to 30 °C, and the injection volume was 90 µL. Mixtures of solvents A (0.05% aqueous TFA) and B (acetonitrile) were used as the mobile phase. The following gradient was applied: 0-30 min: A/B 90:10 to 5:95, 30-40 min: 5:95 (isocratic). The detection wavelength was set to 220 nm throughout. Retention factors *k* were calculated according to $k = (t_R\text{-}t_0)/t_0$ (where t_0 is the dead time of 2.6 min for system A). Chromatograms of the RP-HPLC purity controls of the target compounds (*S*,*R*)-**3.6**, (*R*,*R*)-**3.6**, **3.11**, **3.12**, **3.16**, **3.22** and **3.25** are provided in section A.2.2. The purities of these compounds were ≥ 95%.

Preparative HPLC. Purifications by preparative HPLC were performed with a system from Knauer (Berlin, Germany), composed of two K-1800 pumps and a K-2001 detector (herein termed system B), or with a Prep 150 LC system from Waters (Eschborn, Germany) consisting of a 2545 binary gradient module, a 2489 UV/visible detector and a Waters Fraction Collector III (herein termed system C). A Kinetex-XB C18 (5 µm, 250 mm × 21 mm, Phenomenex), a Gemini-NX C18 110A (5 µm, 250 mm × 21 mm, Phenomenex) or a YMC-Actus Triart C18 (5 µm, 150 mm × 20 mm, YMC, Dinslaken, Germany) were used as the stationary phase. The mobile phase was composed of the solvents C (0.1% aqueous TFA with 5% acetonitrile) and B (acetonitrile). Lyophilization of the eluates containing the products was performed with a Scanvac CoolSafe 100-9 freeze-drying apparatus (Labogene, Allerød, Denmark) equipped with a RZ 6 rotary vane vacuum pump (Vacuubrand, Wertheim, Germany).

3.4.2 Experimental synthetic protocols and analytical data

(*R*)-2-((*R*)-2-(3-(4-aminobutoxy)phenyl)-2-phenylacetamido)-5-guanidino-*N*-(4-hydroxybenzyl)pentanamide bis(trihydrofluoroacetate) ((*R*,*R*)-3.6) and (*R*)-2-((*S*)-2-(3-(4-aminobutoxy)phenyl)-2-phenylacetamido)-5-guanidino-*N*-(4-hydroxybenzyl)pentanamide bis(trihydrofluoroacetate) ((*S*,*R*)-3.6)

Compounds (*R*,*R*)-**3.6** and (*S*,*R*)-**3.6** were prepared by solid-phase synthesis according to a reported procedure used for the synthesis of structurally related argininamides.[23] In a 20 mL syringe (BD Discardit II, Becton Dickinson, Heidelberg, Germany), equipped with a polyethylene frit (35 µm), **2.27** (266 mg, 0.18 mmol) was allowed to swell in anhydrous DMF/NMP 4:1 v/v (2 mL) at rt for 15 min. Fmoc deprotection was carried out by sucking off the solvent, adding piperidine/DMF 1:4 v/v (3 mL) and shaking at 35 °C for 2 h. This procedure was repeated once. The resin was washed with CH_2Cl_2 and DMF/NMP 4:1 v/v (3 × 3 mL) and the liquid was sucked off. In a separate vessel, **3.5** (116 mg, 0.18 mmol), HBTU (115 mg,

0.30 mmol) and DIPEA (103 µL, 0.61 mmol) were added to a solution of HOBt (41 mg, 0.30 mmol) in anhydrous DMF/NMP 4:1 v/v (2 mL), the mixture was gently shaken at rt for 5 min, then added to the resin follwed by shaking at 35 °C for 16 h. Fmoc deprotection was carried out as described above followed by washing of the resin and coupling of **2.12** (72 mg, 0.18 mmol) using the same procedure and identical amounts of reagents as for the aforementioned coupling of **3.5**. To cleave off the product, the resin was incubated in CH_2Cl_2/TFA 95:5 v/v (2 mL) at rt for 20 min, the liquid (filtrate) was collected, and the resin was washed with CH_2Cl_2/TFA 99:1 v/v (4 × 2 mL). After removal of the volatiles from the combined filtrates by rotary evaporation, the residue was taken up in CH_2Cl_2, followed by rotary evaporation. TFA/H_2O 95:5 v/v (2 mL) was added, and the mixture was incubated at rt for 16 h. CH_2Cl_2 (30 mL) was added, and the volatiles were removed by rotary evaporation. H_2O (100 mL) was added followed by lyophilization. The product was purified by preparative HPLC (system B, column: Kinetex-XB C18, gradient: 0-30 min: C/B 64:36-59:41, t_R ((*R*,*R*)-**3.6**) = 13 min, t_R ((*S*,*R*)-**3.6**) = 15 min) to yield (*R*,*R*)-**3.6** (7 mg, 9 µmol, 14%) and (*S*,*R*)-**3.6** (14 mg, 18 µmol, 23%) as white fluffy, hygroscopic solids. Analytical data of (*R*,*R*)-**3.6**: RP-HPLC (system A, 220 nm): 95%, t_R = 11.4 min, k = 3.4. ^{1}H-NMR (600 MHz, DMSO-d_6): δ (ppm) 1.32-1.46 (m, 2H), 1.48-1.52 (m, 1H), 1.62-1.78 (m, 5H), 2.81-2.89 (m, 2H), 3.01-3.11 (m, 2H), 3.92 (t, J = 6.1 Hz, 2H), 4.11-4.19 (m, 2H), 4.28-4.33 (m, 1H), 5.09 (s, 1H), 6.64-6.71 (m, 2H), 6.78-6.83 (m, 1H), 6.83-6.87 (m, 2H), 6.88-7.48 (m, 12H), 7.63 (t, J = 5.8 Hz, 1H), 7.77 (br s, 3H), 8.36 (t, J = 5.8 Hz, 1H), 8.47 (d, J = 8.1 Hz, 1H), 9.32 (br s, 1H). ^{13}C-NMR (150 MHz, DMSO-d_6): δ (ppm) 23.96, 25.15, 25.67, 29.51, 38.65, 40.28, 41.63, 52.38, 55.76, 66.61, 112.00, 115.03, 115.12, 116.86 (q, J = 298 Hz, TFA), 120.94, 126.64, 128.21, 128.39, 128.46, 129.11, 129.18, 140.32, 141.79, 156.28, 156.70, 158.32 (q, J = 32 Hz, TFA), 158.35, 170.87, 171.07. MS (LC-HRMS, ESI): *m/z* $[M+H]^+$ calcd for $[C_{31}H_{41}N_6O_4]^+$ 561.3184, found 561.3185. Analytical data of (*S*,*R*)-**3.6**: RP-HPLC (system A, 220 nm): 99%, t_R = 11.7 min, k = 3.5. ^{1}H-NMR (600 MHz, DMSO-d_6): δ (ppm) 1.33-1.47 (m, 2H), 1.49-1.57 (m, 1H), 1.63-1.76 (m, 5H), 2.81-2.88 (m, 2H), 3.04-3.09 (m, 2H), 3.91 (t, J = 6.0 Hz, 2H), 4.09-4.19 (m, 2H), 4.27-4.32 (m, 1H), 5.08 (s, 1H), 6.66-6.69 (m, 2H), 6.78-6.82 (m, 2H), 6.86-6.90 (m, 1H), 6.91-7.52 (m, 12H), 7.70 (t, J = 5.7 Hz, 1H), 7.74-7.89 (m, 3H), 8.35 (t, J = 5.8 Hz, 1H), 8.46 (d, J = 7.9 Hz, 1H), 9.33 (br s, 1H). ^{13}C-NMR (150 MHz, DMSO-d_6): δ (ppm) 23.97, 25.18, 25.69, 29.45, 38.65, 40.31, 41.63, 52.47, 55.80, 66.63, 111.98, 115.02, 115.26, 116.74 (q, J = 297 Hz, TFA), 120.87, 126.61, 128.18, 128.42, 128.47, 129.14, 129.26, 140.21, 141.93, 156.29, 156.78, 158.20, 158.51 (q, J = 33 Hz, TFA), 170.86, 171.04. MS (LC-HRMS, ESI): MS (LC-HRMS, ESI): *m/z* $[M+H]^+$ calcd for $[C_{31}H_{41}N_6O_4]^+$ 561.3184, found 561.3184. $C_{31}H_{40}N_6O_4 \times C_4H_2F_6O_4$ (788.75).

4-Pentynoic acid succinimidyl ester[44] (3.7)

DCC (4.2 g, 20.4 mmol) was added to a stirred suspension of 4-pentynoic acid (2.0 g, 20.4 mmol) and *N*-hydroxysuccinimide (2.4 g, 20.4 mmol) in CH_2Cl_2 (200 mL) at 4°C and the suspension was stirred for 1 h. The suspension was allowed to warm up to rt and stirring was continued for 16 h. The white precipitate was separated by filtration and washed with CH_2Cl_2 (100 mL). The filtrates were combined, the solvent was removed by rotary evaporation and the crude product was purified by column chromatography (light petroleum/ethyl acetate 3:1 v/v to light petroleum/ethyl acetate 1:1 v/v) to yield **3.8** as a white solid (3.1 g, 15.9 mmol, 77%). TLC (light petroleum/ethyl acetate 1:1 v/v): R_f = 0.50. ^{1}H-NMR (400 MHz, $CDCl_3$): δ (ppm) 2.04 (t, *J* = 2.7 Hz, 1H), 2.60 (m, 2H), 2.83 (s, 4H), 2.87 (m, 2H). ^{13}C-NMR (100 MHz, $CDCl_3$): δ (ppm) 18.70, 30.68, 34.86, 77.42, 87.23, 172.89, 175.33. MS (LC-HRMS, ESI): *m/z* $[M+H]^+$ calcd for $[C_9H_{10}NO_4]^+$ 196.0604, found 196.0605. $C_9H_9NO_4$ (195.17).

***N*-(4-(3-((*S*)-2-(((*R*)-5-Guanidino-1-((4-hydroxybenzyl)amino)-1-oxopentan-2-yl)amino)-2-oxo-1-phenylethyl)phenoxy)butyl)pent-4-ynamide hydrotrifluoroacetate (3.8)**

A solution of **3.7** (2.0 mg, 10.5 µmol) in anhydrous DMF (50 µL) was added to a stirred solution of (*S*,*R*)-**3.6** (5.5 mg, 7.0 µmol) and DIPEA (7.1 µL, 42 µmol) in anhydrous DMF (150 µL) and the mixture was stirred at rt for 1 h. 0.5% Aq. TFA/acetonitrile 80:20 v/v (1 mL) was added and the mixture was subjected to preparative HPLC (system C, column: Gemini-NX C18, gradient: 0-30 min: C/B 85:15-60:40, t_R = 21 min) to yield **3.8** (3.3 mg, 4.4 µmol, 63%) as a white fluffy solid. ^{1}H-NMR (600 MHz, DMSO-d_6/D_2O 10:1 v/v): δ (ppm) 1.31-1.44 (m, 2H), 1.46-1.54 (m, 3H), 1.60-1.68 (m, 3H), 2.22-2.26 (m, 2H), 2.31-2.35 (m, 2H), 2.66-2.69 (m, 1H), 3.01-3.09 (m, 4H), 3.87 (t, *J* = 6.3 Hz, 2H), 4.07-4.17 (m, 2H), 4.24-4.29 (m, 1H), 5.02 (s, 1H), 6.62-6.66 (m, 2H), 6.75-6.86 (m, 3H), 6.95-7.01 (m, 2H), 7.16-7.31 (m, 6H), 8.33 (t, *J* = 5.9 Hz, 1H), 8.41 (d, *J* = 8.0 Hz, 1H). MS (LC-HRMS, ESI): *m/z* $[M+H]^+$ calcd for $[C_{36}H_{45}N_6O_5]^+$ 641.3446, found: 641.3457. $C_{36}H_{44}N_6O_5 \times C_2HF_3O_2$ (755.81).

***N*-(4-(3-((1*S*,4*R*)-4-((4-Hydroxybenzyl)carbamoyl)-9-imino-2,11,16-trioxo-1-phenyl-3,8,10,12,15-pentaazaoctadecyl)phenoxy)butyl)pent-4-ynamide hydrotrifluoroacetate (3.9)**

A solution of **3.7** (1.4 mg, 7.0 µmol) in anhydrous DMF (50 µL) was added to a stirred solution of (*S*,*R*)-**2.14** (4.3 mg, 4.7 µmol) and DIPEA (4.8 µL, 28.2 µmol) in anhydrous DMF (150 µL) and the mixture was stirred at rt for 1 h. 0.5% Aq. TFA/acetonitrile 80:20 v/v (1 mL) was added and the mixture was subjected to preparative HPLC (system C, column: Gemini-NX C18, gradient: 0-30 min: C/B 85:15-60:40, t_R = 23 min) to yield **3.9** (2.7 mg, 3.0 µmol, 64%) as a white fluffy solid. ^{1}H-NMR (600 MHz, DMSO-d_6/D_2O 10:1 v/v): δ (ppm) 0.97 (t, *J* = 7.6 Hz, 3H), 1.40-1.56 (m, 5H), 1.61-1.69 (m, 3H), 2.06 (q, *J* = 7.6 Hz, 2H), 2.21-2.26 (m, 2H), 2.31-2.36

(m, 2H), 2.66-2.68 (m, 1H), 3.05-3.09 (m, 2H), 3.12-3.19 (m, 6H), 3.86 (t, *J* = 6.4 Hz, 2H), 4.08-4.16 (m, 2H), 4.25-4.29 (m, 1H), 5.02 (s, 1H), 6.64-6.68 (m, 2H), 6.75-6.80 (m, 2H), 6.82-6.86 (m, 1H), 6.96-7.00 (m, 2H), 7.16-7.23 (m, 2H), 7.24-7.29 (m, 4H), 7.52-7.56 (m, 0.4H*), 7.68-7.71 (m, 0.4H*), 7.84-7.87 (m, 0.6H*), 7.93-7.97 (m, 0.3H*). *Residual NH proton signals due to incomplete deuterium/proton exchange. MS (LC-HRMS, ESI): *m/z* $[M+H]^+$ calcd for $[C_{42}H_{55}N_8O_7]^+$ 783.4188, found: 783.4210. $C_{42}H_{54}N_8O_7 \times C_2HF_3O_2$ (896.96).

(*R*)-2-((*S*)-2-(3-(4-(3-(1-(1,6-Bisdeoxy-6-fluoro-β-D-glucopyranos-1-yl)-1*H*-1,2,3-triazol-4-yl)propanamido)butoxy)phenyl)-2-phenylacetamido)-5-guanidino-*N*-(4-hydroxybenzyl)pentanamide hydrotrifluoroacetate (3.11)

6-Deoxy-6-fluoro-β-D-glucopyranosyl azide (**3.10**, 1.3 mg, 6.2 µmol), a solution of $CuSO_4$ pentahydrate (9.3 µL of a 0.2 M solution in H_2O, 1.9 µmol) and a solution of sodium ascorbate (9.4 µL of a 0.6 M solution in H_2O, 5.6 µmol) were added to a solution of **3.8** (1.2 mg, 1.6 µmol) in H_2O/ethanol 1:1 v/v (200 µL) and the mixture was stirred at rt for 30 min. The mixture was subjected to preparative HPLC (system C, column: Actus Triart C18, gradient: 0-30 min: C/B 82:18-71:29, t_R = 21 min) to yield **3.11** (0.9 mg, 0.9 µmol, 57%) as a white fluffy solid. RP-HPLC (system A, 220 nm): 99%, t_R = 13.4 min, *k* = 4.2. ^{1}H-NMR (600 MHz, DMSO-d_6/D_2O 10:1 v/v): δ (ppm) 1.34-1.55 (m, 5H), 1.59-1.69 (m, 3H), 2.41-2.45 (m, 2H), 2.81-2.87 (m, 2H), 3.01-3.09 (m, 4H), 3.25-3.30 (m, 1H), 3.39-3.44 (m, 1H), 3.70-3.75 (m, 2H), 3.87 (t, *J* = 6.4 Hz, 2H), 4.07-4.17 (m, 2H), 4.25-4.30 (m, 1H), 4.45-4.61 (m, 2H), 5.02 (s, 1H), 5.55 (d, *J* = 9.4 Hz, 1H), 6.64-6.67 (m, 2H), 6.76-6.86 (m, 3H), 6.97-7.00 (m, 2H), 7.17-7.28 (m, 6H), 7.95 (s, 1H), 8.33 (t, *J* = 5.9 Hz, 0.7H*), 8.41 (d, *J* = 7.1 Hz, 0.7H*). *Residual NH proton signals due to incomplete deuterium/proton exchange. MS (LC-HRMS, ESI): *m/z* $[M+H]^+$ calcd for $[C_{42}H_{55}FN_9O_9]^+$ 848.4101, found: 848.4117. $C_{42}H_{54}FN_9O_9 \times C_2HF_3O_2$ (961.97).

(2*R*)-2-(2-(3-(4-(3-(1-(1,6-Bisdeoxy-6-fluoro-β-D-glucopyranos-1-yl)-1*H*-1,2,3-triazol-4-yl)propanamido)butoxy)phenyl)-2-phenylacetamido)-*N*-(4-hydroxybenzyl)-5-(3-((2-propionamidoethyl)carbamoyl)guanidino)pentanamide (3.12)

Compound **3.10** (1.2 mg, 5.8 µmol), a solution of $CuSO_4$ pentahydrate (8.7 µL of a 0.2 M solution in H_2O, 1.7 µmol) and a solution of sodium ascorbate (8.8 µL of a 0.6 M solution in H_2O, 5.2 µmol) were added to a solution of **3.9** (1.3 mg, 1.5 µmol) in H_2O/ethanol (100 µL 1:1 v/v) and the mixture was stirred at rt for 30 min. The mixture was subjected to preparative HPLC (system B, column: Gemini-NX C18, gradient: 0-30 min: C/B 84:16-60:40, t_R = 18 min) to yield **3.12** (0.7 mg, 0.6 µmol, 44%) as a white fluffy solid. RP-HPLC (system A, 220 nm): 99%, t_R = 13.7 min, *k* = 4.3. ^{1}H-NMR (600 MHz, DMSO-d_6/D_2O 10:1 v/v): δ (ppm) 0.97 (t, *J* = 7.6 Hz, 3H), 1.37-1.55 (m, 5H), 1.60-1.69 (m, 3H), 2.06 (q, *J* = 7.6 Hz, 2H), 2.41-2.44 (m, 2H), 2.81-2.87 (m, 2H), 3.04-3.09 (m, 2H), 3.11-3.19 (m, 6H), 3.25-3.30 (m, 1H), 3.39-3.44 (m,

1H), 3.66-3.75 (m, 2H), 3.86 (t, *J* = 6.4 Hz, 2H), 4.08-4.16 (m, 2H), 4.26-4.30 (m, 1H), 4.44-4.64 (m, 2H), 5.02 (s, 1H), 5.54 (d, *J* = 9.4 Hz, 1H), 6.64-6.68 (m, 2H), 6.75-6.80 (m, 2H), 6.82-6.86 (m, 1H), 6.96-7.00 (m, 2H), 7.17-7.23 (m, 2H), 7.24-7.29 (m, 4H), 7.95 (s, 1H). MS (LC-HRMS, ESI): *m/z* $[M+H]^+$ calcd for $[C_{48}H_{65}FN_{11}O_{11}]^+$ 990.4844, found: 990.4865. $C_{48}H_{64}FN_{11}O_{11} \times C_2HF_3O_2$ (1104.51).

N^1-(2-(2-(2-Aminoethoxy)ethoxy)ethyl)-*N*^{4}-(4-(3-((1*S*,4*R*)-4-((4-hydroxybenzyl)carbamoyl)-9-imino-2,11,16-trioxo-1-phenyl-3,8,10,12,15-pentaazaoctadecyl)phenoxy)butyl)succinamide bis(hydrotrifluoroacetate) (3.14)

A freshly prepared solution of 2,2-dimethyl-4,15-dioxo-3,8,11-trioxa-5,14-diazaoctadecan-18-oic acid (**3.13**, 7.3 mg, 20 µmol), HOBt (3.4 mg, 22 µmol), HBTU (8.3 mg, 22 µmol) and DIPEA (24.2 µL, 160 µmol) in DMF (200 µL) was stirred at rt for 5 min. (*S*,*R*)-**2.14** (18.8 mg, 20 µmol) was added and stirring was continued at rt for 16 h. The solvent was removed *in vacuo*, TFA/CH_2Cl_2 1:1 v/v (5 mL) was added and the mixture was stirred at rt for 1 h. The volatiles were removed *in vacuo*, 0.5% aq. TFA/acetonitrile 80:20 v/v (1 mL) was added and the mixture was subjected to preparative HPLC (system B, column: Gemini-NX C18, gradient: 0-40 min: C/B 85:15-70:30, t_R = 23 min) to yield **3.14** (11.9 mg, 10 µmol, 51%) as a white fluffy solid. ^{1}H-NMR (600 MHz, methanol-d_4): δ (ppm) 1.11 (t, *J* = 7.6 Hz, 3H), 1.52-1.76 (m, 4H), 1.68-1.79 (m, 3H), 1.81-1.89 (m, 1H), 2.20 (q, *J* = 7.6 Hz, 2H), 2.44-2.50 (m, 4H), 3.09-3.13 (m, 2H), 3.19-3.28 (m, 4H), 3.34-3.37 (m, 2H), 3.51-3.55 (m, 2H), 3.61-3.66 (m, 4H), 3.67-3.70 (m, 2H), 3.92-3.95 (m, 2H), 4.21-4.29 (m, 2H), 4.39-4.45 (m, 1H), 5.05 (s, 1H), 6.69-6.73 (m, 2H), 6.79-6.83 (m, 1H), 6.85-6.89 (m, 2H), 7.04-7.08 (m, 2H), 7.19-7.31 (m, 6H). Note: 4 ^{1}H signals were not apparent due to interference with the solvent residual peak at 3.27-3.34 ppm, as identified by ^{1}H-^{13}C HSQC. ^{13}C-NMR (150 M Hz, methanol-d_4): δ (ppm) 10.37, 25.78, 27.11, 27.72, 30.19, 30.32, 32.11, 32.15, 39.88, 40.13, 40.26, 40.53, 40.68, 41.76, 43.73, 54.33, 58.63, 67.87, 68.51, 70.61, 71.31, 71.35, 114.14, 116.32, 116.35, 122.25, 128.13, 129.51, 129.83, 129.97, 130.29, 130.54, 140.71, 142.30, 155.73 (2 merging carbon signals, as identified by ^{1}H-^{13}C HMBC), 157.85, 161.00, 162.60 (q, *J* = 35 Hz), 173.32, 174.58, 174.77, 174.85, 177.52. MS (LC-HRMS, ESI): *m/z* $[M+H]^+$ calcd for $[C_{47}H_{69}N_{10}O_{10}]^+$ 933.5193, found: 933.5190. $C_{47}H_{68}N_{10}O_{10} \times C_4H_2F_6O_4$ (1161.16).

N^1-(4-(3-((1*S*,4*R*)-4-((4-Hydroxybenzyl)carbamoyl)-9-imino-2,11,16-trioxo-1-phenyl-3,8,10,12,15-pentaazaoctadecyl)phenoxy)butyl)-*N*^{4}-(2-(2-(2-(pent-4-ynamido)ethoxy)ethoxy)ethyl)succinamide hydrotrifluoroacetate (3.15)

3.7 (3.0 mg, 15 µmol) was added to a solution of **3.14** (11.9 mg, 10 µmol) and DIPEA (7.8 µL, 60 µmol) in DMF (500 µL) and the mixture was stirred at rt for 1 h. 0.5% Aq. TFA/acetonitrile 80:20 v/v (2 mL) was added and the mixture was subjected to preparative HPLC (system B,

column: Gemini-NX C18, gradient: 0-20 min: C/B 85:15-70:40, t_R = 18 min) to yield **3.15** (7.6 mg, 7 µmol, 67%) as a white fluffy solid. ^{1}H-NMR (600 MHz, methanol-d_4): δ (ppm) 1.11 (t, *J* = 7.6 Hz, 3H), 1.51-1.76 (m, 4H), 1.69-1.79 (m, 3H), 1.81-1.88 (m, 1H), 2.19 (q, *J* = 7.6 Hz, 2H), 2.26 (t, *J* = 2.6 Hz, 1H), 2.36-2.41 (m, 2H), 2.43-2.50 (m, 6H), 3.12-3.38 (m, 10H), 3.50-3.55 (m, 4H), 3.57-3.62 (m, 4H), 3.93 (t, *J* = 6.3 Hz, 2H), 4.21-4.29 (m, 2H), 4.41-4.46 (m, 1H), 5.04 (s, 1H), 6.69-6.72 (m, 2H), 6.79-6.83 (m, 1H), 6.84-6.88 (m, 2H), 7.04-7.08 (m, 2H), 7.19-7.31 (m, 6H). Note: 2 ^{1}H signals were not apparent due to interference with the solvent residual peak at 3.29-3.33 ppm, as identified by ^{1}H-^{13}C HSQC. ^{13}C-NMR (150 MHz, methanol-d_4): δ (ppm) 10.39, 15.70, 25.77. 27.13, 27.69, 30.20, 30.39, 32.24, 32.30, 35.96, 39.88, 40.11, 40.38, 40.40, 40.63, 41.80, 43.74, 54.19, 58.64, 68.52, 70.33, 70.56, 70.60, 71.33 (2 merging carbon signals, as identified by ^{1}H-^{13}C HSQC), 83.54, 114.17, 116.32 (2 merging carbon signals, as identified by ^{1}H-^{13}C HSQC), 122.24, 128.14, 129.50, 129.83, 129.98, 130.28, 130.56, 140.67, 142.29, 155.66 (2 merging carbon signals, as identified by ^{1}H-^{13}C HMBC), 157.86, 160.60, 173.26, 174.12, 174.63, 174.78, 177.01, 177.54. MS (LC-HRMS, ESI): *m/z* $[M+H]^+$ calcd for $[C_{52}H_{73}N_{10}O_{11}]^+$ 1013.5455, found: 1013.5471. $C_{52}H_{72}N_{10}O_{11} \times C_2H_1F_3O_2$ (1127.23).

N^1-(2-(2-(2-(3-(1-(1,6-Bisdeoxy-6-fluoro-β-D-glucopyranos-1-yl)-1*H*-1,2,3-triazol-4-yl)propanamido)ethoxy)ethoxy)ethyl)-*N*^{4}-(4-(3-((1*S*,4*R*)-4-((4-hydroxybenzyl)carbamoyl)-9-imino-2,11,16-trioxo-1-phenyl-3,8,10,12,15-pentaazaoctadecyl)phenoxy)butyl)succinamide hydrotrifluoroacetate (3.16)

3.10 (1.5 mg, 7.1 µmol), a solution of $CuSO_4$ pentahydrate (10.7 µL of a 0.2 M solution in H_2O, 2.1 µmol) and a solution of sodium ascorbate (10.7 µL of a 0.6 M solution in H_2O, 6.4 µmol) were added to a solution of **3.15** (2.0 mg, 1.8 µmol) in 180 µL H_2O/ethanol 1:1 v/v (180 µL) and the mixture was stirred at rt for 1 h. 0.5% Aq. TFA/acetonitrile 80:20 v/v (500 µL) were added and the mixture was subjected to preparative HPLC (system B, column: Gemini-NX C18, gradient: 0-40 min: C/B 85:15-60:40, t_R = 23 min) to yield **3.16** (1.5 mg, 1.1 µmol, 62%) as a colorless hygroscopic resin. RP-HPLC (system A, 220 nm): 97%, t_R = 13.3 min, *k* = 4.1. ^{1}H-NMR (600 MHz, DMSO-d_6/D_2O 10:1 v/v): δ (ppm) 0.97 (t, *J* = 7.6 Hz, 3H), 1.38-1.53 (m, 5H), 1.60-1.69 (m, 3H), 2.06 (q, *J* = 7.6 Hz, 2H), 2.25-2.31 (m, 4H), 2.42-2.44 (m, 2H), 2.81-2.86 (m, 2H), 3.02-3.06 (m, 2H), 3.11-3.21 (m, 8H), 3.26-3.30 (m, 1H), 3.35-3.39 (m, 4H), 3.39-3.43 (m, 1H), 3.47 (s, 4H), 3.70-3.75 (m, 2H), 3.86 (t, *J* = 6.4 Hz, 2H), 4.08-4.16 (m, 2H), 4.26-4.30 (m, 1H), 4.45-4.62 (m, 2H), 5.02 (s, 1H), 5.54 (d, *J* = 9.4 Hz, 1H), 6.63-6.68 (m, 2H), 6.75-6.80 (m, 2H), 6.82-6.86 (m, 1H), 6.96-7.00 (m, 2H), 7.16-7.23 (m, 2H), 7.24-7.29 (m, 4H), 7.95 (s, 1H), 8.31-8.35 (m, 0.4H*), 8.41-8.45 (m, 0.4H*). *Residual NH proton signals due to incomplete deuterium/proton exchange. MS (LC-HRMS, ESI): *m/z* $[M+H]^+$ calcd for $[C_{58}H_{83}FN_{13}O_{15}]^+$ 1220.6110, found: 1220.6111. $C_{58}H_{82}FN_{13}O_{15} \times C_2HF_3O_2$ (1334.39).

(2*R*,3*R*,4*S*,5*R*,6*R*)-2-(Acetoxymethyl)-6-(((2*R*,3*R*,4*S*,5*R*,6*R*)-4,5-diacetoxy-2-(acetoxymethyl)-6-azidotetrahydro-2*H*-pyran-3-yl)oxy)tetrahydro-2*H*-pyran-3,4,5-triyl triacetate[39] (3.17)

33% HBr in acetic acid (2.5 mL) was added dropwise to a stirred solution of β-maltose peracetate (1.3 g, 1.9 mmol) in acetic acid (5 mL) and the mixture was stirred at rt for 3 h. CH_2Cl_2 (20 mL) was added and the mixture was poured into ice cold H_2O (20 mL). The organic phase was separated, washed with saturated $NaHCO_3$ (20 mL) and dried over Na_2SO_4. Removal of the solvent by rotary evaporation afforded the brominated intermediate, which was dissolved in chloroform (10 mL) followed by the addition of saturated $NaHCO_3$ (10 mL). NaN_3 (0.62 g, 9.5 mmol) and TBAHS (0.65 g, 1.9 mmol) were added to the vigorously stirred biphasic mixture and stirring was continued at rt for 16 h. The organic phase was separated, washed with saturated $NaHCO_3$ (2 × 10 mL) and 1 N aqueous HCl (1 × 10 mL), and the volatiles were removed *in vacuo* to yield **3.17** as a white solid (0.93 g, 1.4 mmol, 73%), which was used without further purification. ^{1}H-NMR (400 MHz, $CDCl_3$): δ (ppm) 1.98-2.06 (m, 15H), 2.10 (s, 3H), 2.15 (s, 3H), 3.73-3.81 (m, 1H), 3.90-3.97 (m, 1H), 3.98-4.07 (m, 2H), 4.20-4.27 (m, 2H), 4.50 (d, J_1 = 12.5 Hz, J_2 = 2.4 Hz, 1H), 4.70 (d, J = 8.8 Hz, 1H), 4.77 (t, J = 8.8 Hz, 1H), 4.85 (dd, J_1 = 10.5 Hz, J_2 = 4.1 Hz, 1H), 5.05 (t, J = 9.7 Hz, 1H), 5.25 (t, J = 8.8 Hz, 1H), 5.31-5.38 (m, 1H), 5.40 (d, J = 4.1 Hz, 1H). ^{13}C-NMR (100 MHz, $CDCl_3$): δ (ppm) 20.68, 20.69, 20.71, 20.73, 20.81, 20.91, 20.98, 61.58, 62.65, 68.10, 68.78, 69.40, 70.13, 71.64, 72.51, 74.40, 75.22, 87.61, 95.85, 169.54, 169.62, 170.06, 170.23, 170.54, 170.64, 171.55. MS (LC-HRMS, ESI): *m/z* $[M+NH_4]^+$ calcd for $[C_{26}H_{39}N_4O_{19}]^+$ 679.2304, found: 679.2312. $C_{26}H_{35}N_3O_{19}$ (661.57).

(*S*)-2-((tert-Butoxycarbonyl)amino)-3-(1-((2*R*,3*R*,4*S*,5*R*,6*R*)-3,4-diacetoxy-6-(acetoxymethyl)-5-(((2*R*,3*R*,4*S*,5*R*,6*R*)-3,4,5-triacetoxy-6-(acetoxymethyl)tetrahydro-2*H*-pyran-2-yl)oxy)tetrahydro-2*H*-pyran-2-yl)-1*H*-1,2,3-triazol-4-yl)propanoic acid (3.19)

3.17 (500 mg, 0.76 mmol) was added to a solution of (*S*)-2-((*tert*-butoxycarbonyl)amino)pent-4-ynoic acid (**3.18**, 135 mg, 0.63 mmol) in H_2O/ethanol 1:1 v/v (20 mL). A solution of $CuSO_4$ pentahydrate (157 mg, 0.63 mmol) and sodium ascorbate (374 mg, 1.89 mmol) in H_2O (2 mL) was added and the suspension was stirred at rt for 1 h. The suspension was treated with ethyl acetate (20 mL) and the organic phase was separated, dried over Na_2SO_4 and the solvent was removed by rotary evaporation. The crude product was subjected to column chromatography (light petroleum/ethyl acetate/acetic acid 50:50:1 v/v/v to light petroleum/ethyl acetate/acetic acid 25:75:1 v/v/v) to yield **3.19** as a white solid (168 mg, 0.19 mmol, 25%). TLC (light petroleum/ethyl acetate/acetic acid 50:50:1 v/v/v): R_f = 0.60. ^{1}H-NMR (400 MHz, DMSO-d_6): δ (ppm) 1.35 (s, 9H), 1.74 (s, 3H), 1.94-2.06 (m, 18H), 2.89-3.09 (m, 2H), 3.97-4.06 (m, 2H), 4.09-4.21 (m, 4H), 4.27-4.35 (m, 1H), 4.38-4.45 (m, 1H), 4.92 (dd, J_1 = 10.4 Hz, J_2 = 3.8 Hz, 1H), 5.01 (t, J = 9.8 Hz, 1H), 5.25 (dd, J_1 = 10.4 Hz, J_2 = 9.8 Hz, 1H), 5.36 (d, J = 3.8 Hz, 1H),

5.47 (t, *J* = 9.3 Hz, 1H), 5.56 (t, *J* = 9.2 Hz, 1H), 6.28 (d, *J* = 9.2 Hz, 1H), 7.02-7.12 (m, 1H), 7.98 (s, 1H), 12.61 (br s, 1H). ^{13}C-NMR (100 MHz, DMSO-d_6): δ (ppm) 19.99, 20.27, 20.33, 20.35, 20.43, 20.54, 20.57, 27.12, 28.13, 53.20, 61.38, 62.93, 67.99, 68.14, 68.93, 69.41, 70.50, 73.74, 73.86, 74.53, 78.16, 83.16, 95.79, 122.10, 135.69, 155.39, 168.60, 169.17, 169.52, 169.72, 169.85, 170.00, 170.12, 173.06. MS (LC-HRMS, ESI): *m/z* $[M+H]^+$ calcd for $[C_{36}H_{51}N_4O_{21}]^+$ 875.3040, found: 875.3056. $C_{36}H_{50}N_4O_{21}$ (874.80).

(2*R*,3*R*,4*S*,5*R*,6*R*)-2-(Acetoxymethyl)-6-(((2*R*,3*R*,4*S*,5*R*,6*R*)-4,5-diacetoxy-2-(acetoxymethyl)-6-(4-((*S*)-2-((tert-butoxycarbonyl)amino)-3-((4-(3-((1*S*,4*R*)-4-((4-hydroxybenzyl)carbamoyl)-9-imino-2,11,16-trioxo-1-phenyl-3,8,10,12,15-pentaazaoctadecyl)phenoxy)butyl)amino)-3-oxopropyl)-1*H*-1,2,3-triazol-1-yl)tetrahydro-2*H*-pyran-3-yl)oxy)tetrahydro-2*H*-pyran-3,4,5-triyl triacetate hydrotrifluoroacetate (3.20)

A freshly prepared solution of **3.19** (26.7 mg, 29 µmol), HOBt (4.4 mg, 29 µmol), HBTU (11.0 mg, 29 µmol) and DIPEA (20.0 µL, 116 µmol) in DMF (300 µL) was stirred at rt for 5 min. (*S*,*R*)-**2.14** (26.8 mg, 29 µmol) was added and stirring was continued at rt for 2 h. 0.5% Aq. TFA/acetonitrile 80:20 v/v (1 mL) was added and the mixture was subjected to preparative HPLC (system B, column: Gemini-NX C18, gradient: 0-30 min: C/B 82:18-40:60, t_R = 21 min) to yield **3.20** (14.0 mg, 9 µmol, 31%) as a white fluffy solid. ^{1}H-NMR (600 MHz, methanol-d_4): δ (ppm) 1.13 (t, *J* = 7.6 Hz, 3H), 1.42 (s, 9H), 1.56-1.65 (m, 4H), 1.67-1.78 (m, 3H), 1.82 (s, 3H), 1.84-1.89 (m, 1H), 2.01-2.03 (m, 6H), 2.04 (s, 3H), 2.05 (s, 3H), 2.07 (s, 3H), 2.08 (s, 3H), 2.21 (q, *J* = 7.6 Hz, 2H), 3.00-3.07 (m, 1H), 3.12-3.30 (m, 7H), 3.91-3.96 (m, 2H), 4.08-4.17 (m, 3H), 4.18-4.31 (m, 5H), 4.32-4.36 (m, 1H), 4.45-4.55 (m, 2H), 4.91 (dd, J_1 = 10.5 Hz, J_2 = 3.9 Hz, 1H), 5.05-5.11 (m, 2H), 5.38-5.43 (m, 1H), 5.46 (d, *J* = 3.9 Hz, 1H), 5.50 (t, *J* = 9.3 Hz, 1H), 5.59 (t, *J* = 9.3 Hz, 1H), 6.09 (d, *J* = 9.3 Hz, 1H), 6.71-6.74 (m, 2H), 6.82-6.85 (m, 1H), 6.86-6.90 (m, 2H), 7.06-7.09 (m, 2H), 7.23 (t, *J* = 7.9 Hz, 1H), 7.25-7.33 (m, 5H), 7.96 (s, 1H). Note: 2 ^{1}H signals were not apparent due to interference with the solvent residual peak at 3.31-3.35 ppm, as identified by ^{1}H-^{13}C HSQC. ^{13}C-NMR (150 MHz, methanol-d_4): δ (ppm) 10.40, 20.26, 20.53, 20.55, 20.64, 20.74, 20.76, 21.13, 25.78, 26.97, 27.47, 28.69, 29.25, 30.20, 30.36, 39.88, 39.98, 40.69, 41.85, 43.74, 54.23, 55.79, 58.64, 63.03, 64.16, 68.47, 69.66, 69.98, 70.71, 71.67, 72.48, 74.54, 76.41, 76.46, 80.89, 86.12, 97.40, 114.20, 116.33, 122.26, 123.63, 128.20, 129.56, 129.87, 129.98, 130.29, 130.59, 140.66, 142.37, 145.15, 155.65, 157.50, 157.85, 160.58, 161.44, 161.81, 170.66, 171.14, 171.59, 171.73, 171.96, 172.16, 172.28, 173.23, 173.56, 174.75, 177.55. MS (LC-HRMS, ESI): *m/z* $[M+2H]^{2+}$ calcd for $[C_{73}H_{100}N_{12}O_{26}]^{2+}$ 780.3430, found: 780.3451. $C_{73}H_{98}N_{12}O_{26} \times C_2HF_3O_2$ (1559.65).

_N_-((_S_)-3-(1-((2_R_,3_R_,4_R_,5_S_,6_R_)-3,4-Dihydroxy-6-(hydroxymethyl)-5-(((2_R_,3_R_,4_S_,5_S_,6_R_)-3,4,5-trihydroxy-6-(hydroxymethyl)tetrahydro-2_H_-pyran-2-yl)oxy)tetrahydro-2_H_-pyran-2-yl)-1_H_-1,2,3-triazol-4-yl)-1-((4-(3-((1_S_,4_R_)-4-((4-hydroxybenzyl)carbamoyl)-9-imino-2,11,16-trioxo-1-phenyl-3,8,10,12,15-pentaazaoctadecyl)phenoxy)butyl)amino)-1-oxopropan-2-yl)pent-4-ynamide hydrotrifluoroacetate (3.21)

TFA (500 µL) was added to a solution of **3.20** (14.0 mg, 8.4 µmol) in CH_2Cl_2 (500 µL) and the mixture was stirred at rt for 16 h. The solvent was removed by rotary evaporation and the oily residue was taken up in H_2O/acetonitrile 4:1 v/v (10 mL) followed by lyophilization. The resulting white solid was dissolved in DMF (1 mL) followed by the addition of DIPEA (8.6 µL, 50.3 µmol) and **3.7** (2.0 mg, 10.1 µmol). The mixture was stirred at rt for 1 h and H_2O/acetonitrile 4:1 v/v (10 mL) was added followed by lyophilization. The resulting white solid was dissolved in anhydrous methanol (1 mL) and sodium methoxide (2 µL of a 5.5 M stock solution in methanol, 11.0 µmol) was added. The mixture was stirred at rt for 30 min, the volatiles were removed *in vacuo* and the mixture was subjected to preparative HPLC (system B, column: Gemini-NX C18, gradient: 0-30 min: C/B 82:18-40:60, t_R = 21 min) to yield **3.21** (3.3 mg, 2.4 µmol, 29%) as a white fluffy solid. ^{1}H-NMR (600 MHz, methanol-d_4): δ (ppm) 1.10 (t, J = 7.7 Hz, 3H), 1.53-1.64 (m, 4H), 1.67-1.75 (m, 3H), 1.81-1.88 (m, 1H), 2.19 (q, J = 7.7 Hz, 2H), 2.29-2.31 (m, 1H), 2.41-2.46 (m, 4H), 3.08 (dd, J_1 = 14.9 Hz, J_2 = 7.8 Hz, 1H), 3.15-3.29 (m, 8H), 3.47 (dd, J_1 = 9.1 Hz, J_2 = 3.9 Hz, 1H), 3.62-3.74 (m, 5H), 3.80-3.86 (m, 4H), 3.90-3.95 (m, 3H), 4.22-4.30 (m, 2H), 4.42-4.49 (m, 1H), 4.62 (dd, J_1 = 6.4 Hz, J_2 = 7.8 Hz, 1H), 5.05 (s, 1H), 5.22 (d, J = 3.9 Hz, 1H), 5.58 (d, J = 9.1 Hz, 1H), 6.69-6.73 (m, 2H), 6.80-6.85 (m, 2H), 6.87-6.90 (m, 1H), 7.05-7.08 (m, 2H), 7.19-7.31 (m, 6H), 7.97 (s, 1H). Note: 2 ^{1}H signals were not apparent due to interference with the solvent residual peak at 3.29-3.33 ppm, as identified by ^{1}H-^{13}C HSQC. MS (LC-HRMS, ESI): *m/z* $[M+H]^+$ calcd for $[C_{59}H_{81}N_{12}O_{18}]^+$ 1245.5786, found: 1245.5809. $C_{59}H_{80}N_{12}O_{18} \times C_2HF_3O_2$ (1359.38).

(_R_)-2-((_S_)-2-(3-(4-((_S_)-3-(1-((2_R_,3_R_,4_R_,5_S_,6_R_)-3,4-Dihydroxy-6-(hydroxymethyl)-5-(((2_R_,3_R_,4_S_,5_S_,6_R_)-3,4,5-trihydroxy-6-(hydroxymethyl)tetrahydro-2_H_-pyran-2-yl)oxy)tetrahydro-2_H_-pyran-2-yl)-1_H_-1,2,3-triazol-4-yl)-2-(3-(1-(1,6-bisdeoxy-6-fluoro-β-D-glucopyranos-1-yl)-1_H_-1,2,3-triazol-4-yl)propanamido)propanamido)butoxy)phenyl)-2-phenylacetamido)-_N_-(4-hydroxybenzyl)-5-(3-((2-propionamidoethyl)carbamoyl)guanidino)pentanamide hydrotrifluoroacetate (3.22)

3.10 (41 µL of a 43 mM solution in H_2O, 1.8 µmol), sodium ascorbate (5.3 µL of a 0.6 M solution in H_2O) and $CuSO_4$ pentahydrate (5.5 µL of a 0.2 M solution in H_2O) were added to a solution of **3.21** (1.2 mg, 0.88 µmol) in H_2O/ethanol 1:1 v/v (250 µL) and the mixture was stirred at rt for 1 h. 1% Aq. TFA/acetonitrile 1:1 v/v (200 µL) was added and the mixture was subjected to preparative HPLC (system C, column: Gemini-NX C18, gradient: 0-35 min: C/B 83:17-60:40,

t_R = 15 min) yielding **3.22** (0.7 mg, 0.45 µmol, 51%) as a white, fluffy solid. RP-HPLC (system A, 220 nm): 99%, t_R = 12.3 min, k = 3.7. ^{1}H-NMR (600 MHz, DMSO-d_6/D_2O 10:1 v/v): δ (ppm) 0.97 (t, J = 7.6 Hz, 3H), 1.38-1.54 (m, 5H), 1.58-1.69 (m, 3H), 2.05 (q, J = 7.6 Hz, 2H), 2.42-2.47 (m, 2H), 2.79-2.85 (m, 2H), 2.85-2.90 (m, 1H), 3.03-3.10 (m, 4H), 3.11-3.19 (m, 6H), 3.25-3.30 (m, 2H), 3.37-3.46 (m, 3H), 3.47-3.53 (m, 2H), 3.55-3.82 (m, 9H), 3.85 (t, J = 6.4 Hz, 2H), 4.08-4.16 (m, 2H), 4.26-4.30 (m, 1H), 4.42-4.61 (m, 3H), 5.02 (s, 1H), 5.07 (d, J = 3.9 Hz, 1H), 5.53-5.56 (m, 2H), 6.63-6.68 (m, 2H), 6.76-6.80 (m, 2H), 6.83-6.86 (m, 1H), 6.96-7.00 (m, 2H), 7.16-7.23 (m, 2H), 7.24-7.29 (m, 4H), 7.95 (s, 1H), 8.00 (s, 1H). Note: Due to interference with the residual HDO signal (3.60-3.66 ppm), 8 ^{1}H-signals (3.55-3.82 ppm) were identified based on the ^{1}H-NMR spectrum acquired in neat DMSO-d_6 (resulting in a shift of the residual H_2O signal by ≈ 0.16 ppm), as demonstrated in the ^{1}H-NMR spectrum displayed in section A.2.6. MS (LC-HRMS, ESI): *m/z* $[M+H]^+$ calcd for $[C_{65}H_{91}FN_{15}O_{22}]^+$ 1452.6442, found: 1452.6456. $C_{65}H_{90}FN_{15}O_{22} \times C_2HF_3O_2$ (1566.54).

2,2',2''-(10-(2-((4-(3-((1*S*,4*R*)-4-((4-Hydroxybenzyl)carbamoyl)-9-imino-2,11,16-trioxo-1-phenyl-3,8,10,12,15-pentaazaoctadecyl)phenoxy)butyl)amino)-2-oxoethyl)-1,4,7,10-tetraazacyclododecane-1,4,7-triyl)triacetic acid bis(hydrotrifluoroacetate) (3.24)

3.23 (9.8 mg, 12.8 µmol) was added to a solution of (*S*,*R*)-**2.14** (12.0 mg, 12.8 µmol) and DIPEA (18.0 µL, 102 µmol) in DMF (500 µL) and the mixture was stirred at rt for 1 h. 0.5% Aq. TFA/acetonitrile 80:20 v/v (4 mL) was added and the mixture was subjected to preparative HPLC (system B, column: Gemini-NX C18, gradient: 0-20 min: C/B 85:15-70:30, t_R = 14 min) to yield **3.24** (9.0 mg, 6.8 µmol, 53%) as a white fluffy solid. ^{1}H-NMR (600 MHz, DMSO-d_6/D_2O 10:1 v/v): δ (ppm) 0.97 (t, J = 7.6 Hz, 3H), 1.36-1.56 (m, 5H), 1.62-1.70 (m, 3H), 2.06 (q, J = 7.6 Hz, 2H), 2.95-3.40 (m, 24H), 3.63-4.01 (m, 10H), 4.08-4.16 (m, 2H), 4.26-4.30 (m, 1H), 5.04 (s, 1H), 6.64-6.67 (m, 2H), 6.75-6.84 (m, 3H), 6.96-7.00 (m, 2H), 7.19 (t, J = 8.0 Hz, 1H), 7.21-7.24 (m, 1H), 7.25-7.30 (m, 4H). MS (LC-HRMS, ESI): *m/z* $[M+H]^+$ calcd for $[C_{53}H_{77}N_{12}O_{13}]^+$ 1089.5728, found: 1089.5738. $C_{53}H_{76}N_{12}O_{13} \times C_4H_2F_6O_4$ (1317.30).

(Gallium(III))-2,2',2''-(10-(2-((4-(3-((1*S*,4*R*)-4-((4-hydroxybenzyl)carbamoyl)-9-imino-2,11,16-trioxo-1-phenyl-3,8,10,12,15-pentaazaoctadecyl)phenoxy)butyl)amino)-2-oxoethyl)-1,4,7,10-tetraazacyclododecane-1,4,7-triyl)triacetic acid hydrotrifluoroacetate (3.25)

A solution of gallium(III) nitrate monohydrate in 10 mM aqueous HCl (83 µL, 83 µmol) was added to a solution of **3.24** (9.9 mg, 8.3 µmol) in HEPES buffer (0.2 M, pH 4.2, 1.05 mL) and the mixture was incubated at 100°C for 10 min. The mixture was subjected to preparative HPLC (system B, column: Gemini-NX C18, gradient: 0-20 min: C/B 85:15-70:30, t_R = 15 min) to yield **3.25** (3.5 mg, 2.8 µmol, 33%) as a white fluffy solid. RP-HPLC (system A, 220 nm):

99%, t_R = 12.4 min, k = 3.8. ^{1}H-NMR (600 MHz, DMSO-d_6/D_2O 10:1 v/v): δ (ppm) 0.97 (t, J = 7.6 Hz, 3H), 1.35-1.57 (m, 5H), 1.61-1.70 (m, 3H), 2.06 (q, J = 7.6 Hz, 2H), 3.07-3.33 (m, 20H), 3.46 (s, 2H), 3.57-3.63 (m, 4H), 3.67-3.77 (m, 6H), 3.86 (t, J = 6.3 Hz, 2H), 4.08-4.16 (m, 2H), 4.25-4.29 (m, 1H), 5.02 (s, 1H), 6.64-6.67 (m, 2H), 6.75-6.78 (m, 2H), 6.84-6.87 (m, 1H), 6.96-7.00 (m, 2H), 7.17-7.24 (m, 2H), 7.25-7.30 (m, 4H). ^{13}C-NMR (150 MHz, DMSO-d_6/D_2O 10:1 v/v): δ (ppm) 9.84, 24.60, 25.65, 26.18, 28.49, 29.36, 38.05, 38.16, 39.12 (interfering with the solvent residual signal, as identified by ^{1}H-^{13}C HSQC), 40.35, 41.62, 52.36, 53.93, 54.38, 55.80, 56.51, 56.57, 59.64, 60.51, 61.48, 66.86, 111.96, 115.00, 115.27, 116.52 (q, J = 296 Hz, TFA), 120.74, 126.62, 128.18, 128.42, 128.45, 129.11, 129.23, 140.17, 141.86, 153.56, 153.80, 156.26, 158.20 (TFA), 158.44, 166.33, 169.28, 169.98, 170.89, 170.95, 173.31. MS (LC-HRMS, ESI): *m/z* $[M+H]^+$ calcd for $[C_{53}H_{74}{}^{69}GaN_{12}O_{13}]^+$ 1155.4732, found: 1155.4749. $C_{53}H_{73}GaN_{12}O_{13} \times C_2HF_3O_2$ (1269.98).

3.4.3 CD spectroscopic analysis of (*S*,*R*)-3.6

CD and absorbance spectra of 0.2 mg/mL methanolic solutions of (*S*,*R*)-**3.6** and the *S*,*R*- and *R*,*R*-configured diastereomers of **2.14** were recorded in a 2 mm path length cuvette at 20 °C with a Jasco J-810 spectropolarimeter (Jasco, Tokyo, Japan) equipped with a PTC-423S Peltier temperature controller (Jasco). Instrumental parameters: spectral range, 200–500 nm, bandwidth, 1 nm, scanning speed, 500 nm/min. The CD spectra shown in Figure 3.3 represent the average of five measurements after solvent subtraction.

3.4.4 Investigation of the chemical stability of compounds 3.11, 3.12, 3.16, 3.22 and 3.25 in PBS

The chemical stability of **3.11**, **3.12**, **3.16**, **3.22** and **3.25** was investigated in PBS (pH 7.4) at 22 °C. Incubation was started by the addition of 2.5 µL of a 2 mM stock solution or 5 µL of a 1 mM stock solution (stock solutions prepared in DMSO) of the investigated compounds to 47.5 µL or 45 µL of PBS to give a final concentration of 100 µM. For each compound, this sample was prepared three times. Incubation was stopped by the addition of 50 µL 1% aq. TFA/acetonitrile 1:1 v/v after 0 min, 6 h and 24 h. 90 µL of the resulting solutions were analyzed by analytical RP-HPLC (system A) using the conditions (column, eluent, etc.) as described in section 3.4.1.

3.4.5 Cell culture

Cells were cultured in 75-cm^2 or 175-cm^2 flasks (Sarstedt, Nümbrecht, Germany) in a humidified atmosphere (95% air, 5% CO_2) at 37 °C. SK-N-MC neuroblastoma cells (obtained from the American Type Culture Collection, ATCC HTB-10) were maintained in Eagle's minimum essential medium (EMEM) (Sigma-Aldrich) containing 10% fetal calf serum (FCS) (Sigma-Aldrich). Human erythroleukemia (HEL) cells (HEL 92.1.7 from the American Type

Culture Collection, ATCC TIB-180) were maintained in RPMI (Sigma) supplemented with 6.5% FCS. MCF-7-Y_1 cells, a sub-cell line originating from MCF-7 cells (ATCC HTB 22) featuring increased Y_1R expression,[40] were cultivated in EMEM containing 5% FCS or in DMEM/Ham's F12 (1:1 v/v) (Sigma) containing 10% FCS. MDA-MB-231 mammary carcinoma cells were maintained in DMEM containing 10% FCS. CHO-hY_2R cells (obtained from PerkinElmer, Rodgau, Germany) were cultured in Ham's F12 medium (Sigma) supplemented with 5% FCS and G418 (400 µg/mL) (Fisher Scientific). CHO-hY_4-Gqi5-mtAEQ cells[45] were cultured in Ham's F12 medium containing 10% FCS, G418 (400 µg/mL) (Sigma), hygromycin (400 µg/mL) (A.G. Scientific Inc, San Diego, CA, USA) and zeocin (250 µg/mL) (InvivoGen, San Diego, CA). HEC-1B-hY_5R cells[46] were maintained in EMEM containing 7.5% FCS and G418 (400 µg/mL). Murine P388 cells, previously treated with doxorubicin to induce P-gp expression,[38] were maintained as suspension cell culture in DMEM supplemented with 10 % FCS.

3.4.6 Radioligand competition binding

Y_1R binding: radioligand competition binding experiments at the hY_1R were performed at intact hY_1R-expressing SK-N-MC neuroblastoma cells at 22 ± 1 °C as previously described, using [^{3}H]**2.2** (c = 0.15 nM) as radioligand. Nonspecific binding was determined in the presence of BIBO3304 (75 nM). Y_2R binding: radioligand competition binding experiments at the hY_2R were performed at CHO-hY_2R cells (purchased from PerkinElmer, product no. ES352-C, lot no. 460-167-A) at 22 ± 1 °C as previously described, using [^{3}H]propionyl-pNPY (K_d = 0.14 nM, c = 0.5 nM) as radioligand.[27] Nonspecific binding was determined in the presence of BIIE0246 and JNJ31020028 (5 µM each). Y_4R binding: radioligand competition binding experiments at the hY_4R were performed at CHO-hY_4RG_{qi5}-mtAEQ cells at 22 ± 1 °C as previously described, using [^{3}H]UR-KK200 (K_d = 0.67 nM,[28] c = 1 nM) as radioligand.[47] Nonspecific binding was determined in the presence of hPP (1 µM). Y_5R binding: radioligand competition binding at the hY_5R was performed at intact HEC-1B-hY_5R cells at 22 ± 1 °C as previously described, using [^{3}H]propionyl-pNPY (K_d = 11 nM,[29] c = 5 nM) as radioligand.[28] Nonspecific binding was determined in the presence of pNPY (2 µM). For each compound and each receptor subtype, at least three individual experiments were performed in triplicate. For Y_1R binding, specific binding data (nonspecific binding subtracted from total binding) were normalized (100% = specifically bound radioligand in the absence of competitor), plotted as % over log(concentration of competitor) and analyzed by a four-parameter logistic equation (log(inhibitor) vs. response - variable slope, GraphPad Prism 9, GraphPad Software, San Diego, CA) to obtain pIC_{50} values, which were converted into pK_i values according to the Cheng-Prusoff equation (logarithmic form).[48] In the case of the Y_2R, Y_4R and Y_5R binding, for each studied compound, radioligand displacement was < 50% for the highest competitor concentration (3 or 10 µM), precluding a determination of pIC_{50} values.

3.4.7 Fura-2 Ca^{2+} assay

The Y_1R Fura-2 Ca^{2+} assay was performed at hY_1R-expressing HEL cells in antagonist mode at 22 ± 1 °C as previously described.[49] Ca^{2+} mobilization was induced by the addition of pNPY (pEC_{50} = 8.29,[23] final concentration = 10 nM) after preincubation of the cells with the antagonists **3.11**, **3.12**, **3.16**, **3.22** or **3.25** for 15 min. Net Ca^{2+} responses (basal cytosolic Ca^{2+} concentration subtracted from the measured peak Ca^{2+} concentration) were normalized (100% = Ca^{2+} response induced by 10 nM pNPY) and plotted against log(concentration of antagonist) followed by analysis according to a four-parameter logistic equation (log(inhibitor) vs response − variable slope, GraphPad Prism 9) to obtain pIC_{50} values.

3.4.8 Calcein-AM assay

P388 cells previously treated with doxorubicin (for induction of P-gp expression),[38] were harvested and washed once with PBS. The supernatant was discarded and the cells were resuspended in loading buffer (120 mM NaCl, 5 mM KCl, 2 mM $MgCl_2 \times 6\ H_2O$, 1.5 mM $CaCl_2 \times 2\ H_2O$, 25 mM HEPES, 10 mM glucose, pH 7.4) to give a density of 0.50 × 10^6 cells/mL. To this cell suspension, loading suspension (loading buffer, 20 mg/mL BSA, 5 µL/mL pluronic F127 (20 % in DMSO)) was added to reach a final density of 0.38 × 10^6 cells/mL. 200 µL of the cell suspension were added to the wells of a polypropylene round bottom 96 well plate (Brand, Wertheim, Germany) prefilled with 2 µL of solutions of tariquidar, **2.2**, **3.12** or **3.25** in DMSO (100-fold concentrated compared to the final compound concentration), and the plate was incubated at 37 °C under shaking in the dark for 15 min. A 40 µM solution of calcein-AM in DMSO/H_2O 1:3 (5 µL) was added to each well (giving a final calcein-AM concentration of 1 µM) and the plate was incubated at 37 °C (5% CO_2) in the dark for 10 min. The plates were centrifuged at 4 °C at 60 g for 5 min, the supernatants were carefully removed by suction, and the cells were washed once with ice cold PBS (200 µL) and resuspended in 125 µL loading buffer. Calcein fluorescence was determined with a FACSCantoII flow cytometer (Becton Dickinson, Heidelberg, Germany). The following gain settings for forward and sideward scatter were applied: FSC: 200 V, SSC: 220 V. Fluorescence was recorded using the following settings: excitation: 488 nm, emission: 530 ± 15 nm (FITC channel), gain: 230 V. The sample volume was 30 µL throughout, corresponding to 2000-3000 gated events. For each compound, four individual experiments were performed in triplicate. Fluorescence intensities (arithmetic mean) obtained for the reference compound tariquidar were plotted over log(concentration of tariquidar) and analyzed by a four-parameter logistic equation (log(inhibitor) vs. response - variable slope, GraphPad Prism 9, GraphPad Software, San Diego, CA) to obtain concentration-inhibition curves and pIC_{50} values. Fluorescence intensities obtained for tariquidar, **2.2**, **3.12** and **3.25** were normalized based on the concentration-inhibition curves of tariquidar (100% = “top” of the four-parameter logistic fit, corresponds to the maximal inhibition

of calcein efflux by tariquidar; 0% = “bottom” of the four-parameter logistic fit, corresponds to the basal fluorescence measured in the absence of tariquidar). For compounds **2.2**, **3.12** and **3.25**, no inhibition of the P-gp mediated efflux of calcein was observed for the studied concentration range (1-30 µM), i.e. pIC_{50} values could not be determined.

3.4.9 Radiosynthesis of [^{18}F]3.11, [^{18}F]3.12 and [^{68}Ga]3.25

Preparation of fluoroglycosyl azide [^{18}F]**3.10** and subsequent CuAAC, yielding [^{18}F]**3.11** and [^{18}F]**3.12** from the alkynylated precursor compounds **3.8** and **3.9**, respectively, were performed according to a previously described protocol with minor modifications:[50] Purification of [^{18}F]**3.11** and [^{18}F]**3.12** was performed by semipreparative HPLC (column: Kromasil C8, 125 x 8 (Nouryon, Amsterdam), gradient: 0-20 min: aq. TFA (0.1%)/acetonitrile with 0.1% TFA 80:20-50:50).

The preparation of [^{68}Ga]**3.25** for PET imaging and the determination of $logD_{7.4}$ coefficients was performed according to a previously described protocol.[51]

The preparation of [^{68}Ga]**3.25** for autoradiography and the determination of the stability in human plasma was performed on a Scintomics GRP ® synthesizer module (Scintomics GmbH, Fürstenfeldbruck, Germany) with the Scintomics Control Center software, the Reagent and Hardware Kit SC-01 and SC-01-H (ABX, Radeberg, Germany) and an Isomed 2010 activimeter (MED Nuklear-Medizintechnik, Dresden, Germany) for activity measurements. Crude [^{68}Ga]$GaCl_3$ was eluted from a GalliaPharm ^{68}Ge/^{68}Ga-generator (Eckert&Ziegler, Berlin, Germany) using 0.1 M HCl as eluent. Subsequent loading onto a cationic exchange resin (CHROMAFIX Clean-up-Cartridge PS-H$^+$, ABX, Radeberg, Germany), followed by elution using 5 M aqueous NaCl as eluent yielded purified [^{68}Ga]$GaCl_3$ (9-10 mL). Precursor compound **3.24** (0.18 mM in ultrapure H_2O (Merck), 100 µL, 18 nmol) was added to a HEPES buffer (ABX Kit, 1.5 M, pH 5.5, 3 mL) followed by the addition of the [^{68}Ga]$GaCl_3$ eluate. The mixture was incubated at 125 °C for 6 min, cooled down to approximately 120 °C and passed through a C18 cartridge (Sep-Pak C18 Plus Short Cartridge, 55-105 µm, Waters, Milford, MA, USA). [^{68}Ga]**3.25** was eluted from the cartridge with 2 mL EtOH/H_2O (1:1 v/v) and diluted with PBS to yield ≈ 17 mL “PBS stock” of [^{68}Ga]**3.25**. The quality control was performed on a 1100 series system from Agilent Technologies (Santa Clara, CA) consisting of a 1100 Series quaternary pump equipped with a 1260 Infinity degasser, a 1100 Series Autosampler, a 1100 Series Thermostated Column Compartment, a 1100 Series Diode Array Detector, and a GABI Star radiometric detector (Raytest Isotopenmessgeräte GmbH, Straubenhardt, Germany) was used. A Luna C18(2), 3 µm, 100 × 4.6 mm (Phenomenex) served as stationary phase. The flow rate was 0.95 mL min^{-1}, the oven temperature was set to 25 °C, and the injection volume was 20 µL. Mixtures of solvents C (0.04% aqueous TFA) and B (acetonitrile) were used as the

mobile phase. The following gradient was applied: 0-9 min: C/B 90:10 to 65:35, 9-12 min: 65:35 to 5:95, 12-16 min: 5:95 (isocratic). For UV detection, the wavelength was set to 220 nm. To prove the identity of [^{68}Ga]**3.25** in the plasma stability samples, **3.25** (50 µM) was co-injected (*cf*. section A.3.2). Activity yields of [^{18}F]**3.11**, [^{18}F]**3.12** and [^{68}Ga]**3.25** are provided in Table 3.2. An exemplary radiochromatogram (purity control) of [^{68}Ga]**3.25** is shown in section A.3.4.

3.4.10 Determination of the distribution coefficients $logD_{7.4}$ of [^{18}F]3.11, [^{18}F]3.12 and [^{68}Ga]3.25

The determination of the $logD_{7.4}$ values was performed according to a previously described procedure.[20]

3.4.11 Stability of [^{68}Ga]3.25 in human plasma

150 µL of the stock solution of [^{68}Ga]**3.25** in PBS (1.02 MBq) were added to a mixture of human plasma (150 µL) and PBS pH 7.4 (150 µL) and the sample was incubated at 37 °C. Aliquots of 100 µL were taken after 30, 90 and 180 min. Proteins were precipitated by the addition of EtOH/MeCN 1:1 v/v (200 µL) followed by vortexing. After centrifugation (20,000 g, 5 min), 240 µL of the supernatant were withdrawn and 5 µL aq. TFA (1%) were added. The volatiles were removed in a vacuum concentrator (Savant SpeedVac Plus SC110A, Thermo Fisher Scientific) at 40 °C, the residue was taken up in 0.04% aq. TFA/acetonitrile 90:10 v/v (50 µL) and 20 µL of this solution were analyzed by RP-HPLC using the LC system and conditions as for the quality control of [^{68}Ga]**3.25** (*cf.* section A.3.2). To prove the identity of [^{68}Ga]**3.25** in the plasma stability samples, **3.25** (50 µM) was co-injected (*cf*. section A.3.2).

3.4.12 Tumor models

All mouse experiments were approved by the local animal protection authorities (MCF-7/MDA-MB-231 xenograft tumor model: Government of Central Franconia, Germany, no. 55.2-2532-2-279; SK-N-MC xenograft tumor model: Anzeige von Eingriffen und Behandlungen an Tieren zu wissenschaftlichen Zwecken an die Regierung der Oberpfalz, Abteilung 621 - Veterinärwesen, 12.05.2011). Crl:NMRI-Foxn1nu mice (Charles River, 8-10 weeks old), used for the combined MCF-7/MDA-MB-231 xenograft tumor model, were kept as described previously.[50] Likewise, NMRI nude (nu/nu) mice (in-house breeding at the University of Regensburg[52]), used for the SK-N-MC xenograft tumor model, were kept as previously reported.[53] Mice used for the combined MDA-MB-231/MCF-7 xenograft model, were subcutaneously implanted with a 17β-estradiol pellet (0.72 mg per pellet, 3 mm diameter) with a 60-day release time (Innovative Research of America, Sarasota, FL, USA) on the back under isoflurane anesthesia 3-5 days prior to injection of the tumor cells. To establish subcutaneous MDA-MB-231 tumors and subcutaneous MCF-7 tumors in one animal, cell suspensions (MCF-7: 2×10^6 cells in 100 µL PBS, MDA-MB-231: 2×10^6 cells in 100 µL PBS) were injected in the

upper left and in the upper right flank, respectively. Subcutaneous SK-N-MC tumors for autoradiographic binding studies were established in 8-12 weeks old female NMRI (nu/nu) mice by subcutaneous injection (right flank) of a SK-N-MC cell suspension in culture medium without FCS (3×10^6 cells/100 µL).

3.4.13 Autoradiography with [^{68}Ga]3.25

Subcutaneously grown MCF-7 and SK-N-MC tumors (ca. 10 mm diameter) were taken from the mice, immediately frozen in Tissue-Tek with the help of dry ice and stored at −78 °C. Cryosections (12 µm) were obtained at −16 °C with a 2800 Frigocut E freezing microtome (Reichert-Jung/Leica, Germany). Three adjacent tissue sections were mounted on one microscopic slide (Superfrost Plus, 75 × 25 × 1 mm), and the slide was immediately put into a chamber of 100% humidity. After 1-2 min, the sections were carefully covered with binding buffer (HEPES (10 mM), NaCl (150 mM), KCl (5 mM), $CaCl_2$ dihydrate (2.5 mM), KH_2PO_4 (1.2 mM), Mg_2SO_4 heptahydrate (1.2 mM), and $NaHCO_3$ (25 mM), supplemented with bacitracin (100 µg/mL) and BSA (0.2%)). After 5-10 min, the binding buffer was removed by putting the slides uprightly on a paper towel (ca. 1 min). For the incubation of the tissue sections with [^{68}Ga]**3.25**, the stock solution of [^{68}Ga]**3.25** in PBS (*cf.* section 3.4.9) was 1:10 diluted with binding buffer, yielding an activity concentration of 0.97 MBq/mL (at the start of the incubation). For total binding, tissue sections were carefully covered with this solution (ca. 1000 µL for one slide). To determine nonspecific binding, the same solution was used, but supplemented with 15 µM **2.1**. The sections were incubated in a chamber of 100% humidity at rt for a period of 50 min. After incubation, the binding buffer was removed, the slides were immersed three times into PBS split to 3 vessels (4 °C, 10 s) and finally immersed in a vessel with distilled water (4 °C, 3 s). The slides were put uprightly on a paper towel for ca. 3 min and then dried for 15 min in horizontal position in a desiccator over P_4O_{10}. The slides were set in close contact with a gamma-sensitive phosphor screen (Super Sensitive Phosphor Screen, PerkinElmer) using an X-ray film cassette and stored in the dark overnight. The autoradiographic image was generated from the screen using a phosphorimager (Cyclone Storage Phosphor System, Packard).

3.4.14 Biodistribution in MCF-7 tumor-bearing nude mice

Biodistribution studies with [^{18}F]**3.11** and [^{18}F]**3.12** (each 3-5 MBq per animal in 100 µL 0.9% NaCl), using mice with a subcutaneous MCF-7 and a subcutaneous MDA-MB-231 tumor, were performed as described for previously reported Y_1R PET ligands.[20] The activities of blood samples and of the following organs were determined: lung, liver, heart, spleen, kidney, MCF-7 tumor, MDA-MB-231 tumor, brain, muscle and femur. Based on the injected activity, the decay-corrected organ activities and the organ masses %ID/g values were calculated.

3.4.15 Small-animal PET imaging

Dynamic PET imaging with [^{18}F]**3.11**, [^{18}F]**3.12** and [^{68}Ga]**3.25** (each 3-5 MBq, 100 µL), using mice with a subcutaneous MCF-7 and a subcutaneous MDA-MB-231 tumor, was performed on an Inveon microPET scanner following a protocol previously reported.[50] Note: Blocking experiments were not required as the Y_1R-negative MDA-MB-231 tumor served as a control. After iterative maximum a posteriori image reconstruction of the decay and attenuation-corrected images, regions of interest (ROIs) were drawn over the tumors using the software PMOD (PMOD Technologies LLC, Switzerland). The radioactivity concentration within the regions was obtained from the mean value within the multiple ROIs and then converted to percentage injected dose per gram organ (%ID/g).

3.5 References

(1) Herzog, H. Neuropeptide Y and energy homeostasis: Insights from Y receptor knockout models. *Eur. J. Pharmacol.* **2003**, 480, 21-29.

(2) Heilig, M. The NPY system in stress, anxiety and depression. *Neuropeptides* **2004**, 38, 213-224.

(3) Hirsch, D.; Zukowska, Z. NPY and stress 30 years later: The peripheral view. *Cell. Mol. Neurobiol.* **2012**, 32, 645-659.

(4) Robinson, S. L.; Thiele, T. E. The role of neuropeptide Y (NPY) in alcohol and drug abuse disorders. *Int. Rev. Neurobiol.* **2017**, 136, 177-197.

(5) Gøtzsche, C. R.; Woldbye, D. P. D. The role of NPY in learning and memory. *Neuropeptides* **2016**, 55, 79-89.

(6) Körner, M.; Waser, B.; Reubi, J. C. Neuropeptide Y receptor expression in human primary ovarian neoplasms. *Lab. Invest.* **2003**, 84, 71-80.

(7) Körner, M.; Waser, B.; Reubi, J. C. High Expression of Neuropeptide Y1 Receptors in Ewing Sarcoma Tumors. *Clin. Cancer. Res.* **2008**, 14, 5043-5049.

(8) Körner, M.; Waser, B.; Reubi, J. C. High Expression of Neuropeptide Y Receptors in Tumors of the Human Adrenal Gland and Extra-Adrenal Paraganglia. *Clin. Cancer. Res.* **2004**, 10, 8426-8433.

(9) Reubi, J. C.; Gugger, M.; Waser, B.; Schaer, J. C. Y_1-mediated effect of neuropeptide Y in cancer: Breast carcinomas as targets. *Cancer Res.* **2001**, 61, 4636-41.

(10) Ruscica, M.; Dozio, E.; Motta, M.; Magni, P. Relevance of the neuropeptide Y system in the biology of cancer progression. *Curr. Top. Med. Chem.* **2007**, 7, 1682-1691.

(11) Körner, M.; Reubi, J. C. NPY receptors in human cancer: A review of current knowledge. *Peptides* **2007**, 28, 419-425.

(12) Li, J.; Tian, Y.; Wu, A. Neuropeptide Y receptors: a promising target for cancer imaging and therapy. *Regenerative Biomaterials* **2015**, 2, 215-219.

(13) Reubi, J.; Gugger, M.; Waser, B. Co-expressed peptide receptors in breast cancer as a molecular basis for *in vivo* multireceptor tumour targeting. *Eur. J. Nucl. Med. Mol. Imag.* **2002**, 29, 855-862.

(14) Fonseca, I. C. F.; Castelo-Branco, M.; Cavadas, C.; Abrunhosa, A. J. PET Imaging of the neuropeptide Y system: A systematic review. *Molecules* **2022**, 27, 3726.

(15) Hofmann, S.; Maschauer, S.; Kuwert, T.; Beck-Sickinger, A. G.; Prante, O. Synthesis and *in vitro* and *in vivo* evaluation of an ^{18}F-labeled neuropeptide Y analogue for imaging of breast cancer by PET. *Mol. Pharm.* **2015**, 12, 1121-1130.

(16) Zhang, C.; Pan, J.; Lin, K.-S.; Dude, I.; Lau, J.; Zeisler, J.; Merkens, H.; Jenni, S.; Guérin, B.; Bénard, F. Targeting the neuropeptide Y_1 receptor for cancer imaging by positron emission tomography using novel truncated peptides. *Mol. Pharm.* **2016**, 13, 3657-3664.

(17) Kameda, M.; Ando, M.; Nakama, C.; Kobayashi, K.; Kawamoto, H.; Ito, S.; Suzuki, T.; Tani, T.; Ozaki, S.; Tokita, S.; Sato, N. Synthesis and evaluation of a series of 2,4-diaminopyridine derivatives as potential positron emission tomography tracers for neuropeptide Y Y_1 receptors. *Bioorg. Med. Chem. Lett.* **2009**, 19, 5124-5127.

(18) Hostetler, E. D.; Sanabria-Bohórquez, S.; Fan, H.; Zeng, Z.; Gantert, L.; Williams, M.; Miller, P.; O'Malley, S.; Kameda, M.; Ando, M.; Sato, N.; Ozaki, S.; Tokita, S.; Ohta, H.; Williams, D.; Sur, C.; Cook, J. J.; Burns, H. D.; Hargreaves, R. Synthesis, characterization, and monkey positron emission tomography (PET) studies of [^{18}F]Y1-973, a PET tracer for the neuropeptide Y Y_1 receptor. *NeuroImage* **2011**, 54, 2635-2642.

(19) Keller, M.; Maschauer, S.; Brennauer, A.; Tripal, P.; Koglin, N.; Dittrich, R.; Bernhardt, G.; Kuwert, T.; Wester, H.-J.; Buschauer, A.; Prante, O. Prototypic ^{18}F-labeled argininamide-type neuropeptide Y Y_1R antagonists as tracers for PET imaging of mammary carcinoma. *ACS Med. Chem. Lett.* **2017**, 8, 304-309.

(20) Maschauer, S.; Ott, J. J.; Bernhardt, G.; Kuwert, T.; Keller, M.; Prante, O. ^{18}F-Labelled triazolyl-linked argininamides targeting the neuropeptide Y Y_1R for PET imaging of mammary carcinoma. *Sci. Rep.* **2019**, 9.

(21) Yang, Z.; Han, S.; Keller, M.; Kaiser, A.; Bender, B. J.; Bosse, M.; Burkert, K.; Kögler, L. M.; Wifling, D.; Bernhardt, G.; Plank, N.; Littmann, T.; Schmidt, P.; Yi, C.; Li, B.; Ye, S.; Zhang, R.; Xu, B.; Larhammar, D.; Stevens, R. C.; Huster, D.; Meiler, J.; Zhao, Q.; Beck-Sickinger, A. G.; Buschauer, A.; Wu, B. Structural basis of ligand binding modes at the neuropeptide Y Y_1 receptor. *Nature* **2018**, 556, 520-524.

(22) Buschmann, J.; Seiler, T.; Bernhardt, G.; Keller, M.; Wifling, D. Argininamide-type neuropeptide Y Y_1 receptor antagonists: the nature of N^{ω}-carbamoyl substituents determines Y_1R binding mode and affinity. *RSC Med. Chem.* **2020**, 11, 274-282.

(23) Müller, C.; Gleixner, J.; Tahk, M.-J.; Kopanchuk, S.; Laasfeld, T.; Weinhart, M.; Schollmeyer, D.; Betschart, M. U.; Lüdeke, S.; Koch, P.; Rinken, A.; Keller, M. Structure-based design of high-affinity fluorescent probes for the neuropeptide Y Y_1 receptor. *J. Med. Chem.* **2022**, 65, 4832-4853.

(24) Keller, M.; Pop, N.; Hutzler, C.; Beck-Sickinger, A. G.; Bernhardt, G.; Buschauer, A. Guanidine−acylguanidine bioisosteric approach in the design of radioligands: synthesis of a tritium-labeled N^G-propionylargininamide ([^{3}H]-UR-MK114) as a highly potent and selective neuropeptide Y Y_1 receptor antagonist. *J. Med. Chem.* **2008**, 51, 8168-8172.

(25) Keller, M.; Weiss, S.; Hutzler, C.; Kuhn, K. K.; Mollereau, C.; Dukorn, S.; Schindler, L.; Bernhardt, G.; König, B.; Buschauer, A. N^{ω}-Carbamoylation of the argininamide moiety: An avenue to insurmountable NPY Y_1 receptor antagonists and a radiolabeled selective high-affinity molecular tool ([^{3}H]UR-MK299) with extended residence time. *J. Med. Chem.* **2015**, 58, 8834-8849.

(26) Maschauer, S.; Prante, O. A series of 2-O-trifluoromethylsulfonyl-D-mannopyranosides as precursors for concomitant ^{18}F-labeling and glycosylation by click chemistry. *Carbohydr. Res.* **2009**, 344, 753-761.

(27) Konieczny, A.; Braun, D.; Wifling, D.; Bernhardt, G.; Keller, M. Oligopeptides as neuropeptide Y Y_4 receptor ligands: identification of a high-affinity tetrapeptide agonist and a hexapeptide antagonist. *J. Med. Chem.* **2020**, 63, 8198-8215.

(28) Kuhn, K. K.; Ertl, T.; Dukorn, S.; Keller, M.; Bernhardt, G.; Reiser, O.; Buschauer, A. High affinity agonists of the neuropeptide Y (NPY) Y_4 receptor derived from the C-terminal pentapeptide of human pancreatic polypeptide (hPP): Synthesis, stereochemical discrimination, and radiolabeling. *J. Med. Chem.* **2016**, 59, 6045-6058.

(29) Dukorn, S.; Littmann, T.; Keller, M.; Kuhn, K.; Cabrele, C.; Baumeister, P.; Bernhardt, G.; Buschauer, A. Fluorescence- and radiolabeling of [Lys^4,Nle^{17,30}]hPP yields molecular tools for the NPY Y_4 receptor. *Bioconjugate Chem.* **2017**, 28, 1291-1304.

(30) Rudolf, K.; Eberlein, W.; Engel, W.; Wieland, H. A.; Willim, K. D.; Entzeroth, M.; Wienen, W.; Beck-Sickinger, A. G.; Doods, H. N. The first highly potent and selective nonpeptide neuropeptide Y Y_1 receptor antagonist: BIBP3226. *Eur. J. Pharmacol.* **1994**, 271, R11-R13.

(31) Keller, M.; Kaske, M.; Holzammer, T.; Bernhardt, G.; Buschauer, A. Dimeric argininamide-type neuropeptide Y receptor antagonists: Chiral discrimination between Y_1 and Y_4 receptors. *Biorg. Med. Chem.* **2013**, 21, 6303-6322.

(32) Hu, Y.; Bloomquist, B. T.; Cornfield, L. J.; DeCarr, L. B.; Flores-Riveros, J. R.; Friedman, L.; Jiang, P.; Lewis-Higgins, L.; Sadlowski, Y.; Schaefer, J.; Velazquez, N.; McCaleb, M. L. Identification of a novel hypothalamic neuropeptide Y receptor associated with feeding behavior. *J. Biol. Chem.* **1996**, 271, 26315-26319.

(33) Choi, Y.; Yu, A.-M. ABC transporters in multidrug resistance and pharmacokinetics, and strategies for drug development. *Curr. Pharm. Des.* **2014**, 20, 793-807.

(34) Kusuhara, H.; Suzuki, H.; Sugiyama, Y. The role of P-glycoprotein and canalicular multispecific organic anion transporter in the hepatobiliary excretion of drugs. *J. Pharm. Sci.* **1998**, 87, 1025-1040.

(35) Holló, Z.; Homolya, L.; Davis, C. W.; Sarkadi, B. Calcein accumulation as a fluorometric functional assay of the multidrug transporter. *Biochim. Biophys. Acta* **1994**, 1191, 384-388.

(36) Tiberghien, F.; Loor, F. Ranking of P-glycoprotein substrates and inhibitors by a calcein-AM fluorometry screening assay. *Anti-Cancer Drugs* **1996**, 7, 568-578.

(37) Keppler, D. Progress in the molecular characterization of hepatobiliary transporters. *Dig. Dis.* **2017**, 35, 197-202.

(38) Höcherl, P. New tariquidar-like ABCB1 modulators in cancer chemotherapy: Preclinical pharmacokinetic/pharmacodynamic investigations and computational studies Doctoral Thesis. University of Regensburg, Regensburg, **2010**, https://epub.uni-regensburg.de/15219/.

(39) Maschauer, S.; Haubner, R.; Kuwert, T.; Prante, O. ^{18}F-Glyco-RGD peptides for PET Imaging of integrin expression: Efficient radiosynthesis by click chemistry and modulation of biodistribution by glycosylation. *Mol. Pharm.* **2013**, 11, 505-515.

(40) Keller, M.; Bernhardt, G.; Buschauer, A. [^{3}H]UR-MK136: A highly potent and selective radioligand for neuropeptide Y Y_1 receptors. *ChemMedChem* **2011**, 6, 1566-1571.

(41) Memminger, M.; Keller, M.; Lopuch, M.; Pop, N.; Bernhardt, G.; von Angerer, E.; Buschauer, A. The neuropeptide Y Y receptor: a diagnostic marker? Expression in MCF-7 breast cancer cells is downregulated by antiestrogens *in vitro* and in xenografts. *PLoS One* **2012**, 7, e51032.

(42) Biselli, S.; Bresinsky, M.; Tropmann, K.; Forster, L.; Honisch, C.; Buschauer, A.; Bernhardt, G.; Pockes, S. Pharmacological characterization of a new series of carbamoylguanidines reveals potent agonism at the H_2R and D_3R. *Eur. J. Med. Chem.* **2021**, 214, 113190.

(43) Williams, D. B. G.; Lawton, M. Drying of organic solvents: Quantitative evaluation of the efficiency of several desiccants. *J. Org. Chem.* **2010**, 75, 8351-8354.

(44) Horatscheck, A.; Wagner, S.; Ortwein, J.; Kim, B. G.; Lisurek, M.; Beligny, S.; Schütz, A.; Rademann, J. Benzoylphosphonate-based photoactive phosphopeptide mimetics for modulation of protein tyrosine phosphatases and highly specific labeling of SH2 domains. *Angew. Chem. Int. Ed.* **2012**, 51, 9441-9447.

(45) Ziemek, R.; Schneider, E.; Kraus, A.; Cabrele, C.; Beck-Sickinger, A. G.; Bernhardt, G.; Buschauer, A. Determination of affinity and activity of ligands at the human

neuropeptide Y Y_4 receptor by flow cytometry and aequorin luminescence. *J. Recept. Signal Transduct.* **2007**, 27, 217-233.

(46) Moser, C.; Bernhardt, G.; Michel, J.; Schwarz, H.; Buschauer, A. Cloning and functional expression of the hNPY Y_5 receptor in human endometrial cancer (HEC-1B) cells. *Can. J. Physiol. Pharmacol.* **2000**, 78, 134-142.

(47) Konieczny, A.; Conrad, M.; Ertl, F. J.; Gleixner, J.; Gattor, A. O.; Grätz, L.; Schmidt, M. F.; Neu, E.; Horn, A. H. C.; Wifling, D.; Gmeiner, P.; Clark, T.; Sticht, H.; Keller, M. N-Terminus to arginine side-chain cyclization of linear peptidic neuropeptide Y Y_4 receptor ligands results in picomolar binding constants. *J. Med. Chem.* **2021**, 64, 16746-16769.

(48) Cheng, Y.-C.; Prusoff, W. H. Relationship between the inhibition constant (K_i) and the concentration of inhibitor which causes 50 per cent inhibition (IC_{50}) of an enzymatic reaction. *Biochem. Pharmacol.* **1973**, 22, 3099-3108.

(49) Müller, M.; Knieps, S.; Geßele, K.; Dove, S.; Bernhardt, G.; Buschauer, A. Synthesis and neuropeptide Y Y_1 receptor antagonistic activity of N,N-disubstituted ω-guanidino- and ω-aminoalkanoic acid amides. *Arch. Pharm.* **1997**, 330, 333-342.

(50) Schindler, L.; Wohlfahrt, K.; Gluhacevic von Krüchten, L.; Prante, O.; Keller, M.; Maschauer, S. Neurotensin analogs by fluoroglycosylation at N^{ω}-carbamoylated arginines for PET imaging of NTS1-positive tumors. *Sci. Rep.* **2022**, 12.

(51) Bäuerle, T.; Gupta, S.; Zheng, S.; Seyler, L.; Leporati, A.; Marosfoi, M.; Maschauer, S.; Prante, O.; Caravan, P.; Bogdanov, A. Multimodal bone metastasis-associated epidermal growth factor receptor imaging in an orthotopic rat model. *Radiol Imaging Cancer* **2021**, 3, e200069.

(52) Spruss, T.; Schlemmer, R.; Bernhardt, G.; Wiesenmeyer, F.; Baumann, O. Five-year breeding data, immunology, and tumor take rates of an NMRI nude mouse colony in *Immunodeficient Animals: Models for Cancer Research*, *Vol. 51*, Arnold, W.; Köpf-Maier, P.; Michael, B., Eds., Karger: Berlin, **1996**, pp. 12-18.

(53) Schindler, L.; Moosbauer, J.; Schmidt, D.; Spruss, T.; Grätz, L.; Lüdeke, S.; Hofheinz, F.; Meister, S.; Echtenacher, B.; Bernhardt, G.; Pietzsch, J.; Hellwig, D.; Keller, M. Development of a neurotensin-derived ^{68}Ga-labeled PET ligand with high *in vivo* stability for imaging of NTS_1 receptor-expressing tumors. *Cancers (Basel)* **2022**, 14, 4922.

Chapter 4

Homobivalent NPY Y_1R ligands as potential tools to examine Y_1R homodimerization

4.1 Introduction

Homo- and heterobivalent ligands targeting G protein-coupled receptors can potentially contribute to a better understanding of the physiological meaning of receptor homo- and heterodimerization, which have been reported for many of the class A of GPCRs.[1] Receptor dimerization can affect affinity and selectivity profiles of receptor ligands, influence receptor trafficking to the cell membrane and alter physiological functions.[2, 3] Therefore, understanding the functional role of GPCR dimers and oligomers can promote new therapeutic approaches to GPCR-mediated disorders.[3-5] Homobivalent GPCR ligands have been developed for opioid receptors,[6] serotonin receptors,[7-9] the dopamine D_2 receptor,[10-12] cannabinoid receptors,[13, 14] adrenergic receptors,[15, 16] and muscarinic receptors.[17] In theory, orthosteric binding of one pharmacophoric entity is expected to enhance association of the second one, given the small containment volume in case a second receptor is in close proximity as a consequence of receptor dimerization. This formation of a thermodynamically favored complex – compared to binding of two separate ligand molecules to the receptor dimer – should result in sigmoidal binding curves with increased slope, implying some extent of positive binding cooperativity, and potentially in increased binding affinities.[6, 13, 18] Indeed, significant increases in binding affinity over the monovalent ligand were rarely noticed for reported homobivalent ligands targeting GPCRs, which raises doubts about the hypothesized binding mode of these ligands, i.e. a sequential and cooperative occupation of the orthosteric binding sites of two potentially dimerized receptors. However, changes in subtype selectivity and ligand activity were stated in some cases, most likely involving additional allosteric interactions of the bivalent ligand within the same receptor protomer or the adjacent receptor in addition to orthosteric binding.[15-17, 19]

Interestingly, BRET and FRET studies demonstrated that all NPY receptor subtypes are in principle capable of forming homodimers in *in vitro* experimental setups.[20, 21] Additionally, the formation of Y_1R-Y_5R heterodimers was suggested, potentially altering the physiological functions compared to receptor monomers.[22, 23] However, no evidence for homodimerization of Y_1 receptors could be extracted from pharmacological approaches using homobivalent ligands as tools to investigate potential changes in receptor function and binding affinities. Previous studies on the synthesis and characterization of homobivalent NPY Y_1 receptor ligands were based on the connection of two entities of the argininamide-type antagonists BIBP3226 (**2.1**, Figure 4.1, panel A) and BIBO3304 (**4.1**, Figure 4.1, panel A) by attachment of a linker to the guanidino groups in **2.1**, either *via* N^{ω}-acylation (e.g. compound **4.2**,[24] Figure 4.1, panel A) or N^{ω}-carbamoylation (e.g. compounds **4.3** and **4.4**,[25] Figure 4.1, panel A). Overall, the bivalent ligands acted as antagonists and exhibited decreased binding affinities in comparison to the monovalent ligands, at least fivefold in the case of the homobivalent ligand

with the highest Y_1R binding affinity, compound **4.2** (pK_i = 8.07). Hence, the presented studies, which included the synthesis and characterization of homobivalent Y_1R antagonists, did not provide evidence for the formation of Y_1R homodimers.[24-26] Interestingly, whereas the monovalent ligands **2.1** and **4.1** did not exhibit any binding affinity for the Y_4R, some of the dimers displayed moderate Y_4R affinity, resulting in dimeric compounds with K_i values (Y_1R and Y_4R) in the two- and three-digit nanomolar range, respectively (**4.3**, Figure 4.1, panel A).

The recently reported crystal structure of the Y_1R in complex with argininamide **2.2** (UR-MK299), representing an N^{ω}-carbamoylated derivative of **2.1** (BIBP3226), revealed that the carbamoylated guanidino group of **2.2** is deeply buried in the orthosteric binding pocket of the Y_1R. Therefore, an attachment of the linker to the guanidino group as present in previously described bivalent Y_1R ligands derived from **2.1**. (e.g. **4.2** and **4.3**), might be disadvantageous with respect to a simultaneous occupation of the orthosteric binding pockets of a receptor dimer. The knowledge of the Y_1R binding mode of **2.2** enables a structure-aided design of bivalent Y_1R ligands derived from **2.2**. As a straightforward approach, (*S*,*R*)-**2.14**, an amine-functionalized derivative of **2.2** (Figure 4.1, panel A) used for the preparation of fluorescent Y_1R ligands (*cf*. Chapter 2), was dimerized *via* connection to spacer molecules with varying lengths (Figure 4.1, panel B). In order to implement the option of a convenient synthesis of labeled bivalent ligands (not carried out in this study), most of the linkers contained an amine-functionalized branch in the center of the molecule. The synthesized bivalent Y_1R ligands were compared to the monovalent analogues **2.2** (UR-MK299) and (*S*,*R*)-**2.14**, labeled monovalent ligands described in Chapters 2 and 3, as well as the previously described homobivalent ligands **4.2**-**4.4** with regard to Y_1R binding (pK_i values and shape of the sigmoidal radioligand displacement curves), potentially providing a hint for Y_1R homodimerization. Additionally, NPY receptor subtype selectivity, in particular regarding Y_4R binding, was investigated.

A

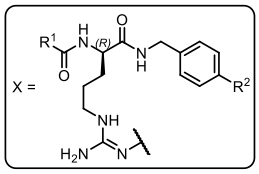

compd.	X	R^1	R^2	pK_i (hY_1R)	pK_i (hY_4R)
2.1 (BIBP3226)				8.80[b]	<5.30[c]
4.1 (BIBO3304)				9.60[d]	<5.30[c]
4.2	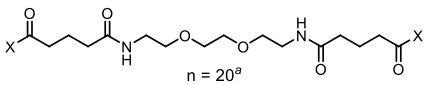 n = 20[a]			8.07[b]	5.62[b]
4.3	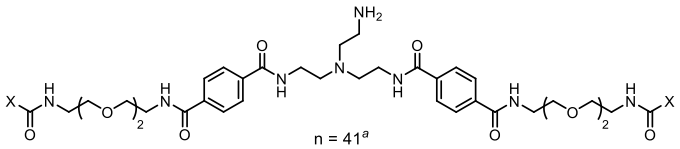 n = 41[a]			7.62[c]	6.92[c]
4.4	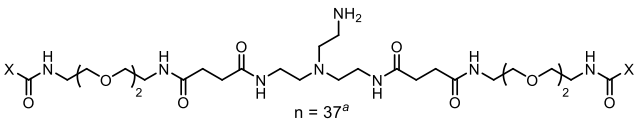 n = 37[a]			6.64[c]	6.54[c]
2.2 (UR-MK299)	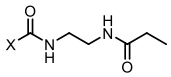			10.27[e]	<5[e]
(*S*,*R*)-**2.14**	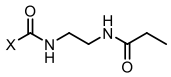	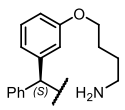		10.61[f]	<5[f]

B

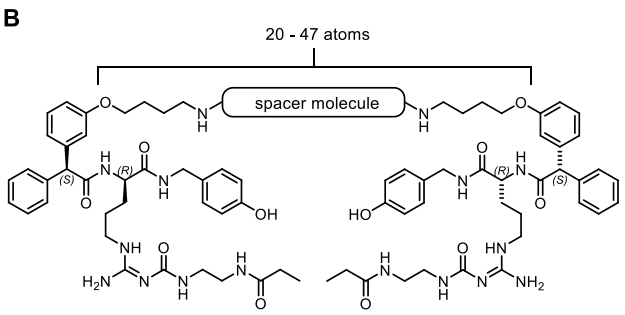

Figure 4.1. (A) Structures and Y_1R and Y_4R affinities (pK_i values) of BIBP3226 (**2.1**[27]), BIBO3304 (**4.1**[28]), UR-MK299 (**2.2**[29]), (*S*,*R*)-**2.14** and the previously reported homobivalent NPY Y_1R antagonists **4.2**,[24] **4.3**,[25] and **4.4**.[25] (B) Schematic approach to novel homobivalent ligands utilizing the amine-functionalized diphenylacetyl moiety in (*S*,*R*)-**2.14** to attach spacers with different lengths. [a]Number of atoms which determine the distance between the guanidine entities. [b]Keller *et al*.;[24] [c]Keller *et al*.;[25] [d]Keller *et al*.;[30] [e]Keller *et al*;[29] [f]Mueller *et al*.[31] Y_1R and Y_4R binding data of **2.1**, **2.2** and **4.1**-**4.4**, previously reported as K_i values, were converted to pK_i values.

4.2 Results and discussion

4.2.1 Synthesis of the symmetric spacers 4.13 and 4.14

The synthesis of novel homobivalent NPY Y_1R ligands required symmetrical spacer molecules with varying spacer lengths, which contained terminal carboxyl groups to enable amide bond formation between the respective spacer and two molecules of (*S*,*R*)-**2.14** (synthesis of (*S*,*R*)-**2.14** described in section 2.2.1). The synthesis of the spacer arms started with the treatment of benzyl 4-aminobutanoate tosylate **4.5** with succinic anhydride under basic conditions to afford benzyl ester **4.6** (Scheme 4.1). An analogue of **4.6**, extended by one GABA unit, was obtained by coupling of Boc-protected GABA to **4.5**, yielding compound **4.7**, which was converted to free amine **4.8** by acidic cleavage of the Boc protecting group. Treatment of **4.8** with succinic anhydride gave compound **4.9** in an overall yield of 34% over three steps (Scheme 4.1).

Mono-Boc-protected amine **4.10**[24] was coupled to **4.6** and **4.9** (used in excess, > 2eq) to afford the benzyl-protected dicarboxylic acids **4.11** and **4.12**, which were deprotected by hydrogenolysis to give the amine-functionalized symmetrical spacer molecules **4.13** and **4.14**, respectively (Scheme 4.1).

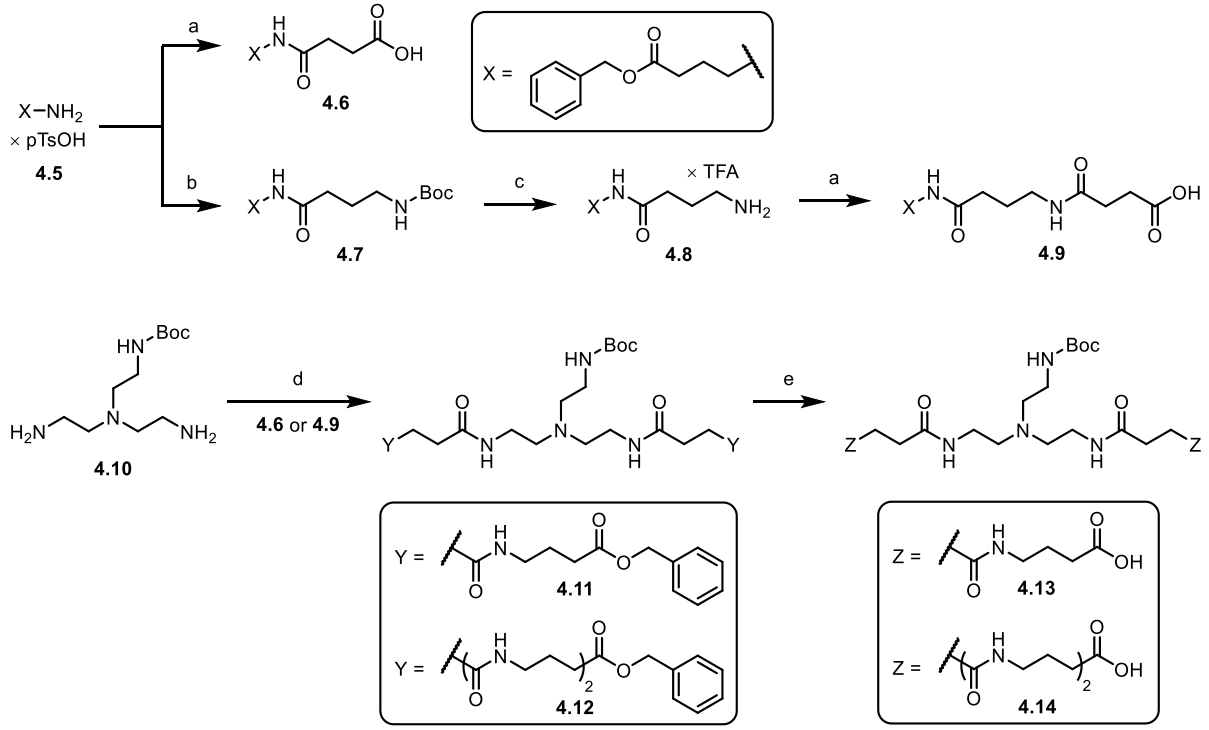

Scheme 4.1. Synthesis of the symmetrical spacer molecules **4.13** and **4.14**. Reagents and conditions: a) succinic anhydride, Et_3N, rt, 16 h, 77% (**4.6**), 80% (**4.9**); b) 4-(*tert*-butoxycarbonyl-amino)-butyric acid, HOBt, HBTU, DIPEA, DMF, rt, 1 h, 48%; c) TFA, CH_2Cl_2, rt, 16 h, 89%; d) EDC, DMAP, CH_2Cl_2, rt, 16 h, 55% (**4.11**), 26% (**4.12**); e) H_2, Pd/C, methanol, rt, 1 h, 56% (**4.13**), 41% (**4.14**).

4.2.2 Synthesis of the homobivalent NPY Y_1 antagonists 4.17-4.20

In addition to **4.13** and **4.14**, a nonfunctionalized spacer (**4.15**[24]) and the previously reported short linker **4.16**[25] were also used to bridge two molecules of (*S*,*R*)-**2.14**, leading to four homobivalent NPY Y_1R ligands, **4.17**-**4.20** (Scheme 4.2). **4.17** was synthesized by treatment of **4.15** with at least two equivalents of (*S*,*R*)-**2.14** in the presence of DIPEA (Scheme 4.2). **4.18**-**4.20** were synthesized from **4.16**, **4.13** and **4.14**, respectively, using HBTU/HOBt as coupling reagent, followed by acidic cleavage of the Boc protecting group at the branch in the center of the molecules (Scheme 4.2). Noteworthily, the use of the NHS ester of suberic acid **4.15**, led to **4.17** in moderate yield (49%), whereas the *in situ* activation of **4.13**, **4.14** and **4.16**, using HBTU followed by amide bond formation and Boc deprotection, gave the target compounds **4.18**-**4.20** in poor yields (22-29%). The resulting spacer components between the diphenylacetyl moieties in the homobivalent compounds contained 20 (**4.17**) to 47 atoms (**4.20**) (*cf.* Table 4.1), including the atoms of the 4-aminobutoxy moieties present in the precursor (*S*,*R*)-**2.14**.

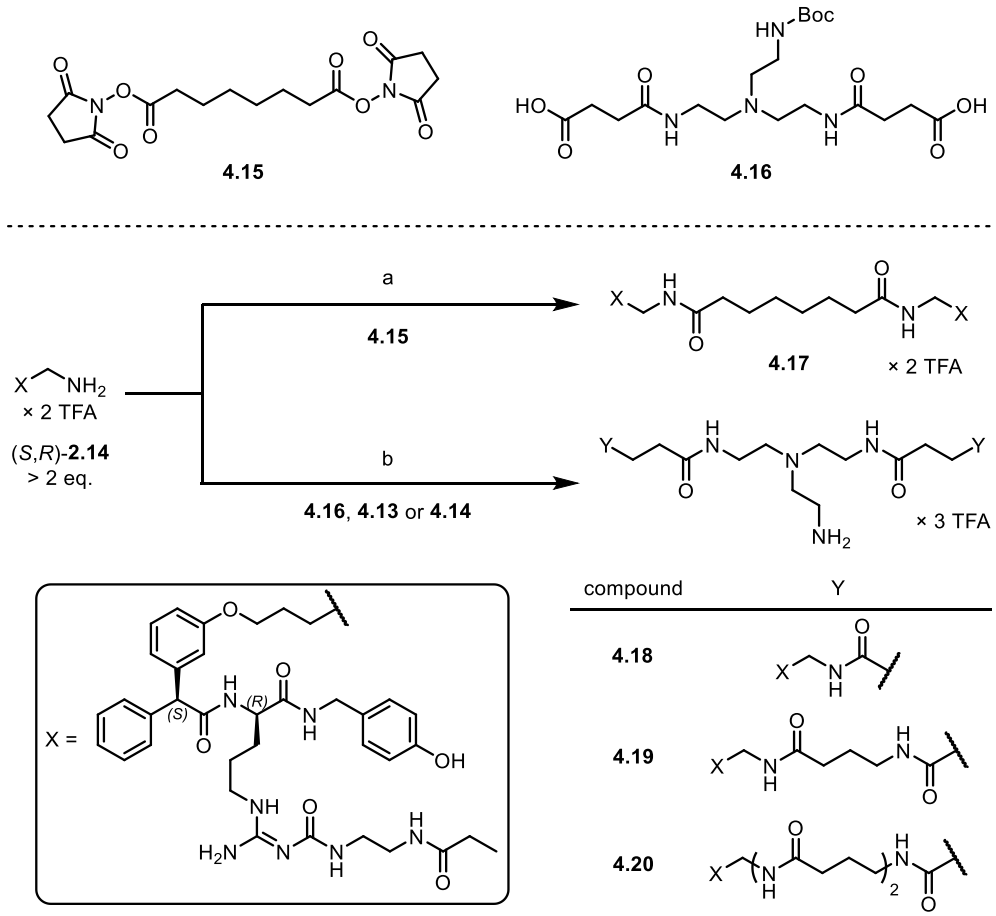

Scheme 4.2. Structures of compounds **4.15** and **4.16** and synthesis of the homobivalent NPY Y_1R antagonists **4.17**-**4.20**. Reagents and conditions: a) DIPEA, DMF, rt, 1 h, 49%; b) (1) HOBt, HBTU, DIPEA, DMF, rt, 1 h; (2) TFA, CH_2Cl_2, rt, 1 h, 26% (**4.18**), 29% (**4.19**), 22% (**4.20**).

4.2.3 Radioligand competition binding and Y_1R antagonism

In analogy to the characterization of the Y_1R ligands presented in section 2.2.4 and section 3.2.2, compounds **4.17**-**4.20** were analyzed with regard to Y_1R binding affinity at SK-N-MC cells using [^{3}H]**2.2** as the radioligand (Table 4.1, Figure 4.2). Compounds **4.18**-**4.20**, containing a primary amine group and several amide bonds between the two pharmacophores, exhibited high Y_1R affinities (pK_i = 10.01-10.13), which were only slightly lower compared to the amine-functionalized precursor (*S*,*R*)-**2.14** (pK_i = 10.61), and the parent compound **2.2** (pK_i = 10.27[29]). The Y_1R affinity of **4.17** (pK_i = 9.67) was lower by a factor of 2-3 compared to **4.18**-**4.20**, which could be attributed to the increased lipophilicity of the spacer entity, devoid of a primary amine group, or the decreased linker length. Hence, the at least five-fold drop in affinity compared to the respective monovalent ligand, which was observed for the reported homobivalent ligands **4.2**-**4.4**, was not apparent. Although not as pronounced as e.g. in the case of compound **4.3** (pK_i (Y_4R) = 6.92), compounds **4.18** and **4.19** displayed affinity for the Y_4R (pK_i = 5.79-5.98). It should be noted that the monovalent Y_1R ligands **2.2** and (*S*,*R*)-**2.14** did not bind to the Y_4R at concentrations as high as 10 µM (pK_i < 5). Interestingly, compounds **4.2** and **4.17**, containing a spacer devoid of a primary amine group, did not display any Y_4R affinity, suggesting a contribution of the amine group in the spacer entities of **4.3**, **4.4**, **4.18** and **4.19** to Y_4R binding. However, given the very high Y_1R affinities of **4.17**-**4.20**, the selectivity for the Y_1R over the other subtypes (Y_2, Y_4, Y_5) is still high (at least 11000-fold difference in binding affinity).

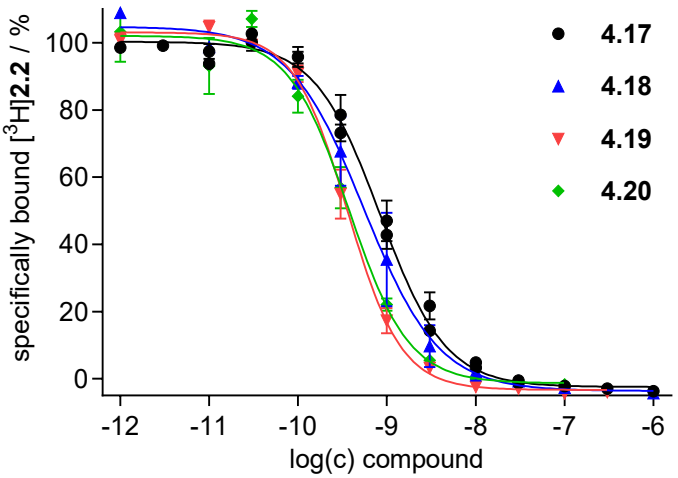

Figure 4.2. Radioligand displacement curves obtained from competition binding studies with [^{3}H]**2.2** (K_D = 0.044 nM, c = 0.15 nM)[29] and homobivalent ligands **4.17**-**4.20** performed at intact SK-N-MC neuroblastoma cells. Data represent mean values ± SEM from at least three independent experiments performed in triplicate.

When looking at the slope of competition binding curves, the slope is expected to be unity (−1) in the case that both labeled and competing ligand bind reversibly to the same binding site with a simple 1:1 stoichiometry (one pharmacophore addresses one binding site). A slope different

from unity can in theory be an indicator for cooperative effects as a consequence of receptor dimerization. Therefore, the slope of −1.50 ± 0.03 (mean ± SEM from four independent determinations) found for the bivalent ligand **4.19** should be emphasized (Table 4.1, Figure 4.2). However, while the slopes of most compounds included in Table 4.1 amounted to values close to unity, the amine-functionalized precursor compound (*S*,*R*)-**2.14** and the fluoroglycosylated argininamide **3.12** represent exceptions. The increased slope factors of (*S*,*R*)-**2.14** and **3.12** of −1.45 and −1.52, respectively, might be explained by allosteric interactions of the polar side chains, i.e. the 4-aminobutoxy group in (*S*,*R*)-**2.14** and the fluoroglycosyl moiety in **3.12**, with amino acids at the receptor surface outside the orthosteric binding pocket. It should be noted that in some cases (in particular compound (*S*,*R*)-**2.14**), the slopes from individual experiments deviated considerably, resulting in high SEM values, although the SEM of the respective mean pK_i value was low (Table 4.1).

All investigated compounds exhibited Y_1R antagonistic activities being able of fully inhibiting the increase in cytosolic Ca^{2+} elicited by the Y_1R agonist pNPY (Fura-2 calcium flux assay using Y_1R-expressing HEL cells).[32] The resulting pIC_{50} values, ranging from 9.86 to 10.21 (Figure 4.3) were in the same range as the pK_i values obtained from radioligand competition binding studies (Table 4.1).

Table 4.1. NPY receptor binding data of homobivalent ligands **4.2**-**4.4**, **4.17**-**4.20**, parent compounds **2.2** and (*S*,*R*)-**2.14**, fluorescent ligands **2.35**, **2.37**, **2.39** and "cold" PET-ligands **3.11**, **3.12** and **3.25**

compound	linker length[a]	pK_i ± SEM / K_i [nM][b]	hill slope[c]	pK_i ± SEM[b]		
		Y_1R[d]		Y_2R[e]	Y_4R[f]	Y_5R[g]
2.2 (UR-MK299)	-	10.27 ± 0.17 / 0.077[h]	-0.82 ± 0.04	<5.5[h]	<5[h]	<5[h]
(*S*,*R*)-**2.14**	-	10.61 ± 0.08 / 0.026	-1.45 ± 0.34	<5	<5	<5
4.2	20	8.07 / 8.6[i]	-1.06 ± 0.12[i]	5.89[i]	5.62[i]	5.63[i]
4.3	41	7.61 / 24[j]	-1.00 ± 0.18[j]	6.04[j]	6.92[j]	<5.3[j]
4.4	37	6.64 / 230[j]	-1.10 ± 0.12[j]	5.40[j]	6.54[j]	<5.3[j]
2.35	-	9.95 ± 0.01 / 0.11	-1.18 ± 0.02	<5.5	<5.5	6.38 ± 0.01
2.37	-	9.36 ± 0.06 / 0.44	-1.05 ± 0.10	<5.5	<5.5	<5.5
2.39	-	9.77 ± 0.12 / 0.19	-1.04 ± 0.06	<5.5	6.22 ± 0.15	<5.5
3.11	-	8.87 ± 0.02 / 1.30	-1.04 ± 0.15	<5.5	<5.5	<5.5
3.12	-	10.20 ± 0.06 / 0.065	-1.52 ± 0.16	<5.5	<5.5	<5.5
3.25	-	10.20 ± 0.05 / 0.060	-1.03 ± 0.03	<5.5	<5.5	<5.5
4.17	20	9.67 ± 0.10 / 0.22	-1.20 ± 0.03	<5.5	<5.5	<5.5
4.18	27	10.13 ± 0.08 / 0.076	-1.17 ± 0.15	<5.5	5.79 ± 0.06	<5.5
4.19	37	10.09 ± 0.08 / 0.087	-1.50 ± 0.03	<5.5	5.98 ± 0.13	<5.5
4.20	47	10.01 ± 0.13 / 0.110	-1.31 ± 0.13	<5.5	<5.5	<5.5

[a]Number of atoms which determine the distance between the guanidine entities (**4.2**-**4.4**) or the diphenylacetyl moieties (**4.17**-**4.20**). [b]Data represent mean pK_i values ± SEM (if available) or mean K_i values from at least three independent experiments performed in triplicate. [c]Hill slopes of the sigmoidal competition binding curves (determined with GraphPad Prism) as mean values ± SEM. [d]Determined by competition binding with [^{3}H]**2.2** (K_d = 0.044 nM,[22] c = 0.15 nM) at intact SK-N-MC neuroblastoma cells. [e]Determined by competition binding with [^{3}H]propionyl-pNPY (K_d = 0.14 nM,[33] c = 0.5 nM) at intact CHO-hY_2R cells. [f]Determined by competition binding with [^{3}H]UR-KK200 (K_d = 0.67 nM,[34] c = 1 nM) at intact CHO-hY_4-Gqi5-mtAEQ cells. [g]Determined by competition binding with [^{3}H]propionyl-pNPY (K_d = 11 nM,[35] c = 5 nM) at intact HEC-1B-hY_5 cells. [h]Keller *et al.*;[29] [i]Keller *et al.*;[24] [j]Keller *et al.*[25] (data, previously reported as K_i, were converted to pK_i values). Binding data of **2.2**, previously reported as K_i, were re-evaluated to obtain the pK_i values. Binding data of **4.2**-**4.4**, previously reported as K_i values, were converted to pK_i values.

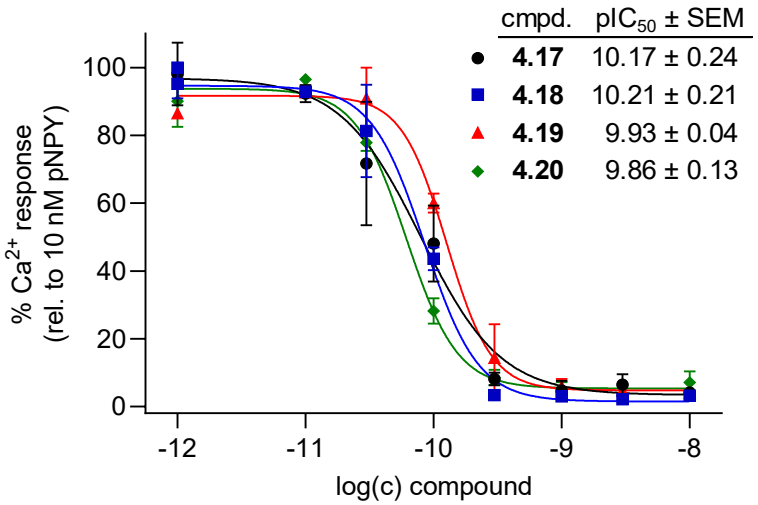

Figure 4.3. Investigation of the homobivalent Y_1R antagonists **4.17**-**4.20** in a Fura-2 Ca^{2+} assay using human erythroleukemia (HEL) cells. The inhibition curves resulted from the inhibition of the pNPY (10 nM)-induced intracellular Ca^{2+} mobilization by the antagonists. Data represent mean values ± SEM from three independent experiments.

4.2.4 Conclusion

Within the scope of this brief study, homobivalent NPY Y_1R antagonists (**4.17**-**4.20**), exhibiting subnanomolar binding affinity (pK_i = 9.67-10.13) and high subtype selectivity, were synthesized and characterized as potential tools to investigate the formation of NPY Y_1 receptor dimers. Y_1R binding data (pK_i values, curve slope factors) obtained from radiochemical competition binding studies were not markedly different from that of monovalent reference compounds, i.e. did not indicate the presence of Y_1R homodimers. To further investigate Y_1R homodimerization using bivalent ligands, **4.18**-**4.20**, bearing an amine group within the spacer moiety, can be used as precursors for the synthesis of fluorescently or radiolabeled bivalent molecular tools allowing a direct determination of ligand binding (saturation binding, association and dissociation kinetics). Noteworthily, a radiolabeled bivalent ligand bears the potential to quantify the ligand-receptor binding stoichiometry by direct comparison to binding of a monovalent radiolabeled analogue.

4.3 Experimental section

4.3.1 General experimental conditions

Chemicals. Standard chemicals, solvents, and buffer components were purchased from commercial suppliers (Sigma-Aldrich, München, Germany; Merck, Darmstadt, Germany; Fisher Scientific, Schwerte, Germany; TCI, Eschborn, Germany) and used without further purification. 4-(*tert*-Butoxycarbonyl-amino)-butyric acid was from ABCR, Karlsruhe, Germany. Gradient grade acetonitrile for HPLC was purchased from Sigma-Aldrich (München,

Germany). The preparations of compounds **4.10**[36], **4.15**,[24] and **4.16**[25] were described elsewhere. The preparation of [^{3}H]propionyl-pNPY was described in section 2.4.1. Purifications by column chromatography were carried out using technical grade solvents and Geduran Si 60 silica gel (pore size of 60 Å, particle size of 40-63 or 63-200 µm, Merck). Thin layer chromatography (TLC) was performed on ALUGRAM Xtra SIL G/UV254 TLC sheets from Macherey-Nagel GmbH & Co. KG (Düren, Germany).

NMR spectrometry. NMR spectra were recorded on a Bruker Avance 400 (^{1}H, 400 MHz, ^{13}C, 100 MHz) or an Avance 600 (^{1}H, 600 MHz) spectrometer (Bruker, Karlsruhe, Germany). The ^{1}H-NMR spectra of compounds **4.17**-**4.20** were recorded in methanol-d_4 resulting in a total H-D exchange of all phenolic OH protons and NH protons. Because only small amounts (< 0.6 µmol) of the bivalent ligands were used for ^{1}H-NMR spectroscopy, characteristic system signals were apparent in the ^{1}H-NMR (0.81-0.87 ppm and 1.20-1.30 ppm), most likely originating from impurities in the solvents used for preparative HPLC (*cf.* supplementary Figure A2.11 in section A.2.3).

Mass spectrometry. High-resolution mass spectrometry (HRMS) analysis was performed on an Agilent 6540 UHD AccurateMass Q-TOF LC/MS system coupled to an Agilent 1290 HPLC system (Agilent Technologies, Santa Clara, CA), using an ESI source. Analyses were performed using the following LC method: column: ZORBAX RRHD Eclipse Plus C18, 1.8 µm, 50 × 2.1 mm (Agilent Technologies, Santa Clara, CA), column temperature: 40 °C, flow: 0.6 mL/min, solvent/linear gradient: 0-4 min: 0.1% aqueous HCOOH/0.1% HCOOH in MeCN 95:5-2:98, 4-5 min: 2:98 (isocratic).

Analytical RP-HPLC. Reaction controls and purity controls were carried out by analytical HPLC (RP-HPLC) using an 1100 series system from Agilent Technologies (Santa Clara, CA) consisting of a degasser (G1379A), a binary pump (G1312A), a variable wavelength detector (G1314A), a thermostated column compartment (G1316A), and an autosampler (G1329A). This system is identical to system B, termed in section 2.4.1. A Kinetex XB-C18 100A (5 µm, 250 mm × 4.6 mm, Phenomenex, Aschaffenburg, Germany) was used as the stationary phase. The flow rate was 0.8 mL min^{-1}, the oven temperature was set to 30 °C, and the injection volume was 40 µL. Mixtures of solvents A (0.05% aqueous TFA) and B (acetonitrile) were used as the mobile phase. The following gradient was applied: 0-30 min: A/B 90:10 to 5:95, 30-40 min: A/B 5:95 (isocratic). The detection wavelength was set to 220 nm throughout. Retention factors k were calculated according to the following equation: $k = (t_R\text{-}t_0)/t_0$ (where t_0 is the dead time of 2.6 min). Chromatograms of the RP-HPLC purity controls of the target compounds **4.17**-**4.20** are provided in section A.4.1. The purities of these compounds were >95%.

Preparative HPLC. Purifications by preparative HPLC were performed with a system from Knauer (Berlin, Germany), composed of two K-1800 pumps and a K-2001 detector. A Gemini-NX C18 110A (5 µm, 250 mm × 21 mm, Phenomenex) was used as the stationary phase. The mobile phase was composed of solvents C (0.1% aqueous TFA with 5% acetonitrile) and B (acetonitrile). Lyophilization of the eluates containing the products was performed with a Scanvac CoolSafe 100-9 freeze-drying apparatus (Labogene, Allerød, Denmark) equipped with a RZ 6 rotary vane vacuum pump (Vacuubrand, Wertheim, Germany).

4.3.2 Experimental synthetic protocols and analytical data

Benzyl 4-aminobutanoate tosylate[37] (4.5)

A suspension of GABA (2.0 g, 18.3 mmol), benzyl alcohol (9.6 mL, 92 mmol) and 4-toluenesulfonic acid (5.3 g, 18.3 mmol) in toluene (20 mL) was refluxed for 5 h. The mixture was cooled to 4 °C and ice-cold ether (10 mL) was added. The precipitate was filtered off, washed with ice cold ether (20 mL) and dried *in vacuo* to yield **4.5** as a white solid (6.3 g, 17.2 mmol, 94%), which was used without further purification. ^{1}H-NMR (400 MHz, DMSO-d_6): δ (ppm) 1.76-1.85 (m, 2H), 2.29 (s, 3H), 2.45-2.48 (m, 2H), 2.77-2.87 (m, 2H), 5.10 (s, 2H), 7.09-7.15 (m, 2H), 7.30-7.41 (m, 5H), 7.46-7.51 (m, 2H), 7.69 (br s, 3H). ^{13}C-NMR (100 MHz, DMSO-d_6): δ (ppm) 20.78, 22.43, 30.25, 38.22, 65.62, 125.48, 128.01, 128.10, 128.47, 136.10, 137.74, 145.54, 172.04. MS (LC-HRMS, ESI): *m/z* $[M+H]^+$ calcd for $[C_{11}H_{16}NO_2]^+$ 194.1176, found 194.1175. $C_{11}H_{15}NO_5 \times C_7H_8SO_3$ (365.44).

4-((4-(Benzyloxy)-4-oxobutyl)amino)-4-oxobutanoic acid (4.6)

Succinic anhydride (0.26 g, 2.6 mmol) was added to a solution of **4.5** (0.60 g, 1.6 mmol) and Et_3N (0.90 mL, 3.3 mmol) in dichloromethane (30 mL) and the mixture was stirred at rt for 16 h. The solution was treated with 1 N HCl (30 mL), the organic phase was separated, dried over Na_2SO_4 and the volatiles were removed *in vacuo* to yield **4.6** as a white solid (0.37 g, 1.3 mmol, 77%), which was used without further purification. ^{1}H-NMR (400 MHz, DMSO-d_6): δ (ppm) 1.61-1.70 (m, 2H), 2.25-2.43 (m, 6H), 3.02-3.09 (m, 2H), 5.08 (s, 2H), 7.29-7.43 (m, 5H), 7.85 (t, J = 5.5 Hz, 1H). ^{13}C-NMR (100 MHz, DMSO-d_6): δ (ppm) 24.55, 29.15, 29.98, 30.88, 37.75, 65.37, 127.90, 127.96, 128.42, 136.24, 170.91, 172.54, 173.84. MS (LC-HRMS, ESI): *m/z* $[M+H]^+$ calcd for $[C_{15}H_{20}NO_5]^+$ 294.1336, found 294.1341. $C_{15}H_{19}NO_5$ (293.32).

Benzyl 4-(4-((tert-butoxycarbonyl)amino)butanamido)butanoate[38] (4.7)

HOBt (0.30 g, 2.0 mmol), HBTU (0.75 g, 2.0 mmol) and DIPEA (1.0 mL, 5.9 mmol) were added to a solution of 4-(*tert*-butoxycarbonyl-amino)-butyric acid (0.40 g, 2.0 mmol) in DMF (15 mL) and the mixture was stirred at rt for 5 min. A solution of **4.5** (0.72 g, 2.0 mmol) and DIPEA (1.0 mL, 5.9 mmol) in DMF (10 mL) was added and the mixture was stirred at rt for 1 h. H_2O (50 mL) was added and the mixture was treated with ethyl acetate (50 mL). The organic phase was

separated, washed with water (3 × 50 mL), dried over Na_2SO_4, and the solvent was removed by rotary evaporation. The crude product was subjected to column chromatography (ethyl acetate/light petroleum 2:1 v/v) to yield **4.7** as a colorless resin (0.36 g, 1.0 mmol, 48%). TLC (light petroleum/ethyl acetate 1:1 v/v): R_f = 0.15. ^{1}H-NMR (400 MHz, $CDCl_3$): δ (ppm) 1.42 (s, 9H), 1.72-1.80 (m, 2H), 1.81-1.89 (m, 2H), 2.13-2.19 (m, 2H), 2.38-2.44 (m, 2H), 3.07-3.17 (m, 2H), 3.24-3.31 (m, 2H), 4.84 (br s, 1H), 5.11 (s, 2H), 6.46 (br s, 1H), 7.27-7.39 (m, 5H). ^{13}C-NMR (100 MHz, $CDCl_3$): δ (ppm) 24.72, 26.50, 28.50, 31.84, 33.64, 39.03, 39.80, 66.48, 79.48, 128.31, 128.38, 128.68, 135.94, 156.67, 172.95, 173.32. MS (LC-HRMS, ESI): *m/z* $[M+H]^+$ calcd for $[C_{20}H_{31}N_2O_5]^+$ 379.2227, found 379.2232. $C_{20}H_{30}N_2O_5$ (378.47).

Benzyl 4-(4-aminobutanamido)butanoate hydrotrifluoroacetate (4.8)

TFA (10 mL) was added to a solution of **4.7** (0.36 g, 0.95 mmol) in dichloromethane (30 mL) and the mixture was stirred at rt for 16 h. The volatiles were removed *in vacuo* and the oily residue was emulsified in water (50 mL) followed by lyophilization to yield **4.8** as a colorless resin (0.33 g, 0.84 mmol, 89%), which was used without further purification. ^{1}H-NMR (400 MHz, DMSO-d_6): δ (ppm) 1.62-1.80 (m, 4H), 2.13-2.21 (m, 2H), 2.33-2.41 (m, 2H), 2.72-2.84 (m, 2H), 3.02-3.12 (m, 2H), 5.09 (s, 2H), 7.29-7.42 (m, 5H), 7.70 (br s, 3H), 7.89-7.98 (m, 1H). ^{13}C-NMR (100 MHz, DMSO-d_6): δ (ppm) 23.22, 24.52, 30.92, 31.97, 37.81, 38.65, 65.42, 127.03, 128.01, 128.44, 136.22, 171.21, 172.50. MS (LC-HRMS, ESI): *m/z* $[M+H]^+$ calcd for $[C_{15}H_{23}N_2O_3]^+$ 279.1703, found 279.1706. $C_{15}H_{22}N_2O_3 \times C_2F_3HO_2$ (392.16).

4-((4-((4-(Benzyloxy)-4-oxobutyl)amino)-4-oxobutyl)amino)-4-oxobutanoic acid (4.9)

Succinic anhydride (65 mg, 0.65 mmol) was added to a solution of **4.8** (170 mg, 0.43 mmol) and Et_3N (0.24 mL, 1.7 mmol) in dichloromethane (5 mL) and the mixture was stirred at rt for 16 h. The solution was treated with 1 N HCl (5 mL), the organic phase was separated, dried over Na_2SO_4 and the volatiles were removed *in vacuo* to yield **4.9** as a white solid (0.13 g, 0.34 mmol, 80%), which was used without further purification. ^{1}H-NMR (400 MHz, DMSO-d_6): δ (ppm) 1.54-1.70 (m, 4H), 2.01-2.07 (m, 2H), 2.26-2.31 (m, 2H), 2.34-2.43 (m, 4H), 2.96-3.08 (m, 4H), 5.08 (s, 2H), 7.30-7.41 (m, 5H), 7.75-7.85 (m, 2H), 12.09 (br s, 1H). ^{13}C-NMR (100 MHz, DMSO-d_6): δ (ppm) 24.56, 25.45, 28.77, 30.01, 30.92, 32.84, 37.72, 38.19, 65.39, 127.91, 127.98, 128.43, 136.24, 170.79, 171.73, 172.53, 173.86. MS (LC-HRMS, ESI): *m/z* $[M+H]^+$ calcd for $[C_{19}H_{27}N_2O_6]^+$ 397.1864, found 397.1881. $C_{19}H_{26}N_2O_6$ (378.43).

Dibenzyl 13-(2-((*tert*-butoxycarbonyl)amino)ethyl)-6,9,17,20-tetraoxo-5,10,13,16,21-pentaazapentacosanedioate (4.11)

EDC × HCl (73 mg, 0.38 mmol) was added to a solution of **4.6** (100 mg, 0.34 mmol), **4.10** (34 mg, 0.14 mmol) and DMAP (5.5 mg, 0.05 mmol) in dichloromethane (2.5 mL) and the mixture was stirred at rt for 16 h. The solvent was evaporated by rotary evaporation, the oily residue

was taken up in brine (3 mL) to yield a suspension, which was carefully acidified to pH 3 using 1 N aq. HCl followed by treatment with ethyl acetate (3 mL). The organic phase was separated, dried over Na_2SO_4 and the solvent was removed by rotary evaporation. The oily residue was subjected to column chromatography (ethyl acetate to ethyl acetate/methanol 2:1 v/v) to yield **4.11** as a pale-yellow resin (60 mg, 0.075 mmol, 55%). TLC (ethyl acetate/methanol 4:1 v/v): R_f = 0.3. ^{1}H-NMR (400 MHz, methanol-d_4): δ (ppm) 1.41 (s, 9H), 1.73-1.84 (m, 4H), 2.37-2.43 (m, 4H), 2.44-2.60 (m, 14H), 3.03-3.10 (m, 2H), 3.17-3.25 (m, 8H), 5.10 (s, 4H), 7.27-7.37 (m, 10H). ^{13}C-NMR (100 MHz, methanol-d_4): δ (ppm) 26.04, 28.81, 32.22, 32.34, 32.80, 38.28, 39.87, 39.95, 54.69, 54.81, 67.24, 80.24, 129.18, 129.21, 129.54, 137.63, 158.47, 174.65, 175.01, 177.61. MS (LC-HRMS, ESI): *m/z* $[M+H]^+$ calcd for $[C_{41}H_{61}N_6O_{10}]^+$ 797.4444, found 797.4471. $C_{41}H_{60}N_6O_{10}$ (796.44).

Dibenzyl 18-(2-((*tert*-butoxycarbonyl)amino)ethyl)-6,11,14,22,25,30-hexaoxo-5,10,15,18,21,26,31-heptaazapentatriacontanedioate (4.12)

EDC × HCl (43 mg, 220 µmol) was added to a solution of **4.9** (66 mg, 170 µmol), **4.10** (20 mg, 80 µmol) and DMAP (3.2 mg, 26 µmol) in dichloromethane/DMF 10:1 v/v (2 mL) and the mixture was stirred at rt for 16 h. The solvent was removed by rotary evaporation, the oily residue was taken up in brine (2 mL) yielding a suspension, which was carefully acidified to pH 3 using 1 N aq. HCl and treated with ethyl acetate (2 mL). The organic phase was separated, dried over Na_2SO_4 and the solvent was removed by rotary evaporation. The oily residue was subjected to column chromatography (ethyl acetate/methanol 4:1 v/v to ethyl acetate/methanol 2:1 v/v) to yield **4.12** as a pale-yellow resin (20 mg, 21 µmol, 26%). TLC (ethyl acetate/methanol 3:1 v/v): R_f = 0.6. ^{1}H-NMR (400 MHz, methanol-d_4): δ (ppm) 1.42 (s, 9H), 1.72-1.85 (m, 8H), 2.16-2.22 (m, 4H), 2.37-2.62 (m, 18H), 3.05-3.11 (m, 2H), 3.12-3.27 (m, 12H), 5.11 (s, 4H), 7.27-7.38 (m, 10H). ^{13}C-NMR (100 MHz, methanol-d_4): δ (ppm) 25.77, 26.83, 28.85, 32.24, 32.26, 32.35, 34.33, 38.67, 39.65, 39.83, 54.84, 55.04, 67.28, 80.14, 129.19, 129.22, 129.55, 137.66, 155.51, 174.55, 174.69, 174.78, 175.52. MS (LC-HRMS, ESI): *m/z* $[M+H]^+$ calcd for $[C_{49}H_{75}N_8O_{12}]^+$ 967.5499, found 967.5515. $C_{49}H_{74}N_8O_{12}$ (967.18).

13-(2-((*tert*-Butoxycarbonyl)amino)ethyl)-6,9,17,20-tetraoxo-5,10,13,16,21-pentaazapentacosanedioic acid (4.13)

Palladium on activated charcoal (10 wt %, 10 mg) was suspended in a stirred solution of **4.11** (60 mg, 75 µmol) in methanol (3 mL). The vigorously stirred mixture was set under an atmosphere of hydrogen (1 bar) at rt for 1 h. The charcoal was filtered off and the volatiles were removed *in vacuo* to yield **4.13** as a colorless resin (26 mg, 42 µmol, 56%), which was used without further purification. TLC (ethyl acetate/methanol 1:1 v/v): R_f = 0.2. ^{1}H-NMR (400 MHz, methanol-d_4): δ (ppm) 1.39 (s, 9H), 1.69-1.79 (m, 4H), 2.23-2.30 (m, 4H), 2.40-2.53

(m, 8H), 2.58-2.70 (m, 6H), 3.06-3.12 (m, 2H), 3.14-3.20 (m, 4H), 3.22-3.29 (m, 4H). ^{13}C-NMR (100 MHz, methanol-d_4): δ (ppm) 25.79, 28.83, 32.22, 32.29, 32.32, 38.60, 39.33, 39.64, 54.81, 54.92, 80.13, 158.42, 174.55, 174.65, 174.76. MS (LC-HRMS, ESI): *m/z* $[M+H]^+$ calcd for $[C_{27}H_{49}N_6O_{10}]^+$ 617.3505, found 617.3512. $C_{27}H_{48}N_6O_{10}$ (616.71).

18-(2-((*tert*-Butoxycarbonyl)amino)ethyl)-6,11,14,22,25,30-hexaoxo-5,10,15,18,21,26,31-heptaazapentatriacontanedioic acid (4.14)

Palladium on activated charcoal (10 wt %, 5 mg) was suspended in a stirred solution of **4.12** (20 mg, 21 µmol) in methanol (1.5 mL). The vigorously stirred mixture was set under an atmosphere of hydrogen (1 bar) at rt for 1 h. The charcoal was filtered off and the volatiles were removed *in vacuo* to yield **4.14** as a colorless resin (6.7 mg, 8.5 µmol, 41%), which was used without further purification. TLC (ethyl acetate/methanol 1:1 v/v): R_f = 0.15. ^{1}H-NMR (400 MHz, methanol-d_4): δ (ppm) 1.43 (s, 9H), 1.73-1.83 (m, 8H), 2.16-2.24 (m, 4H), 2.25-2.32 (m, 4H), 2.40-2.67 (m, 14H), 3.07-3.12 (m, 2H), 3.15-3.29 (m, 12H). MS (LC-HRMS, ESI): *m/z* $[M+H]^+$ calcd for $[C_{35}H_{63}N_8O_{12}]^+$ 787.4560, found 787.4572. $C_{35}H_{63}N_8O_{12}$ (786.93).

***N*^{1}-(4-(3-((1*R*,4*S*)-4-((4-Hydroxybenzyl)carbamoyl)-9-imino-2,11,16-trioxo-1-phenyl-3,8,10,12,15-pentaazaoctadecyl)phenoxy)butyl)-*N*^{8}-(4-(3-((1*S*,4*R*)-4-((4-hydroxybenzyl)carbamoyl)-9-imino-2,11,16-trioxo-1-phenyl-3,8,10,12,15-pentaazaoctadecyl)phenoxy)butyl)octanediamide bis(hydrotrifluoroacetate) (4.17)**

4.15 (0.6 mg, 1.7 µmol) was added to a solution of (*S*,*R*)-**2.14** (3.7 mg, 4.0 µmol) and DIPEA (2.8 µL, 16.7 µmol) in DMF (100 µL) and the mixture was stirred at rt for 1 h. Aq. TFA (0.05 %)/MeCN 19:1 v/v (1 mL) was added and the mixture was subjected to preparative HPLC (gradient: 0-30 min: C/B 85:15-55:45, t_R = 25 min) yielding **4.17** (1.4 mg, 0.8 µmol, 49%) as a white, fluffy solid. RP-HPLC (220 nm): 98%, t_R = 16.7 min, k = 5.4. ^{1}H-NMR (600 MHz, methanol-d_4): δ (ppm) 1.11 (t, J = 7.7 Hz, 6H), 1.32-1.36 (m, 4H), 1.55-1.66 (m, 12H), 1.69-1.77 (m, 6H), 1.80-1.88 (m, 2H), 2.13-2.22 (m, 8H), 3.19-3.26 (m, 8H), 3.92 (t, J = 6.4 Hz, 4H), 4.20-4.29 (m, 4H), 4.40-4.45 (m, 2H), 5.04 (s, 2H), 6.69-6.72 (m, 4H), 6.79-6.82 (m, 2H), 6.83-6.88 (m, 4H), 7.03-7.07 (m, 4H), 7.18-7.29 (m, 12H). Note: 8 ^{1}H signals were not apparent due to interference with the solvent residual peak at 3.28-3.33 ppm, as identified by ^{1}H-^{13}C HSQC. MS (LC-HRMS, ESI): *m/z* $[M+2H]^{2+}$ calcd for $[C_{82}H_{112}N_{16}O_{14}]^{2+}$ 772.4266, found 772.4277. $C_{82}H_{110}N_{16}O_{14} \times C_4H_2F_6O_4$ (1771.92).

N^1-(2-((2-Aminoethyl)(2-(4-((4-(3-((1*R*,4*S*)-4-((4-hydroxybenzyl)carbamoyl)-9-imino-2,11,16-trioxo-1-phenyl-3,8,10,12,15-pentaazaoctadecyl)phenoxy)butyl)amino)-4-oxobutanamido)ethyl)amino)ethyl)-N^4-(4-(3-((1*S*,4*R*)-4-((4-hydroxybenzyl)carbamoyl)-9-imino-2,11,16-trioxo-1-phenyl-3,8,10,12,15-pentaazaoctadecyl)phenoxy)butyl)succinamide tris(hydrotrifluoroacetate) (4.18)

HOBt (1.4 mg, 9.5 µmol), HBTU (3.6 mg, 9.5 µmol) and DIPEA (5.9 µL, 34.6 µmol) were added to a solution of **4.16** (2.0 mg, 4.3 µmol) in DMF (200 µL) and the mixture was stirred at rt for 5 min. A solution of (*S*,*R*)-**2.14** (8.8 mg, 9.5 µmol) in DMF (200 µL) was added and the mixture was stirred at rt for 1 h. Water/acetonitrile 4:1 v/v (5 mL) was added followed by lyophilization. The oily residue was dissolved in dichloromethane/TFA 1:1 v/v (500 µL) and the mixture was stirred at rt for 1 h. The volatiles were removed *in vacuo*, the residue was taken up in aq. TFA (0.05 %)/MeCN 4:1 v/v (1 mL) and the mixture was subjected to preparative HPLC (gradient: 0-30 min: C/B 85:15-60:40, t_R = 18 min) yielding **4.18** (2.3 mg, 1.1 µmol, 26%) as a white, fluffy solid. RP-HPLC (220 nm): 98%, t_R = 13.7 min, k = 4.3. ^{1}H-NMR (600 MHz, methanol-d_6): δ (ppm) 1.11 (t, J = 7.7 Hz, 6H), 1.53-1.64 (m, 8H), 1.67-1.76 (m, 6H), 1.80-1.87 (m, 2H), 2.19 (q, J = 7.7 Hz, 4H), 2.44-2.52 (m, 8H), 2.56-2.72 (m, 4H), 2.73-2.85 (m, 2H), 2.93-3.03 (m, 2H), 3.17-3.28 (m, 12H), 3.90 (t, J = 6.3 Hz, 4H), 4.20-4.29 (m, 4H), 4.38-4.44 (m, 2H), 5.05 (s, 2H), 6.69-6.72 (m, 4H), 6.77-6.81 (m, 2H), 6.82-6.88 (m, 4H), 7.03-7.07 (m, 4H), 7.18-7.29 (m, 12H). Note: 8 ^{1}H signals were not apparent due to interference with the solvent residual peak at 3.28-3.33 ppm, as identified by ^{1}H-^{13}C HSQC. MS (LC-HRMS, ESI): *m/z* $[M+3H]^{3+}$ calcd for $[C_{94}H_{128}N_{20}O_{22}]^{3+}$ 572.6522, found 572.6534. $C_{88}H_{122}N_{20}O_{16} \times C_6H_3F_9O_6$ (2058.14).

N^1-(3-(2-Aminoethyl)-20-(3-((1*R*,4*S*)-4-((4-hydroxybenzyl)carbamoyl)-9-imino-2,11,16-trioxo-1-phenyl-3,8,10,12,15-pentaazaoctadecyl)phenoxy)-7,10,15-trioxo-3,6,11,16-tetraazaicosyl)-N^4-(4-((4-(3-((1*S*,4*R*)-4-((4-hydroxybenzyl)carbamoyl)-9-imino-2,11,16-trioxo-1-phenyl-3,8,10,12,15-pentaazaoctadecyl)phenoxy)butyl)amino)-4-oxobutyl)succinamide tris(hydrotrifluoroacetate) (4.19)

HOBt (2.8 mg, 18.7 µmol), HBTU (7.1 mg, 18.7 µmol) and DIPEA (12.0 µL, 68 µmol) were added to a solution of **4.13** (5.0 mg, 8.1 µmol) in DMF (200 µL) and the mixture was stirred at rt for 5 min. A solution of (*S*,*R*)-**2.14** (17.4 mg, 18.7 µmol) in DMF (400 µL) was added and the mixture was stirred at rt for 1 h. Water/acetonitrile 4:1 v/v (5 mL) was added followed by lyophilization. The oily residue was dissolved in dichloromethane/TFA 1:1 v/v (500 µL) and the mixture was stirred at rt for 1 h. The volatiles were removed *in vacuo* and the mixture was subjected to preparative HPLC (gradient: 0-30 min: C/B 85:15-60:40, t_R = 17 min) yielding **4.19** (5.3 mg, 2.4 µmol, 29%) as a white, fluffy solid. RP-HPLC (220 nm): 98%, t_R = 13.7 min, k = 4.3. ^{1}H-NMR (600 MHz, methanol-d_6): δ (ppm) 1.11 (t, J = 7.7 Hz, 6H), 1.55-1.66 (m, 8H), 1.69-1.77 (m, 10H), 1.81-1.87 (m, 2H), 2.16-2.22 (m, 8H), 2.44-2.53 (m, 8H), 2.63-3.02 (m,

6H), 3.05-3.27 (m, 16H), 3.92 (t, *J* = 6.3 Hz, 4H), 4.21-4.30 (m, 4H), 4.39-4.44 (m, 2H), 5.05 (s, 2H), 6.69-6.72 (m, 4H), 6.79-6.82 (m, 2H), 6.83-6.89 (m, 4H), 7.04-7.08 (m, 4H), 7.18-7.30 (m, 12H). Note: 10 ^{1}H signals were not apparent due to interference with the solvent residual peak at 3.28-3.33 ppm, as identified by ^{1}H-^{13}C HSQC. MS (LC-HRMS, ESI): *m/z* $[M+3H]^{3+}$ calcd for $[C_{96}H_{139}N_{22}O_{18}]^{3+}$ 629.6885, found 629.6900. $C_{96}H_{136}N_{22}O_{18} \times C_6F_9H_3O_6$ (2228.34).

***N*^{1}-(3-(2-Aminoethyl)-25-(3-((1*R*,4*S*)-4-((4-hydroxybenzyl)carbamoyl)-9-imino-2,11,16-trioxo-1-phenyl-3,8,10,12,15-pentaazaoctadecyl)phenoxy)-7,10,15,20-tetraoxo-3,6,11,16,21-pentaazapentacosyl)-*N*^{4}-(4-((4-((4-(3-((1*S*,4*R*)-4-((4-hydroxybenzyl)carbamoyl)-9-imino-2,11,16-trioxo-1-phenyl-3,8,10,12,15-pentaazaoctadecyl)phenoxy)butyl)amino)-4-oxobutyl)amino)-4-oxobutyl)succinamide tris(hydrotrifluoroacetate) (4.20)**

HOBt (2.8 mg, 18.7 µmol), HBTU (7.1 mg, 18.7 µmol) and DIPEA (12.0 µL, 68 µmol) were added to a solution of **4.14** (6.7 mg, 8.5 µmol) in DMF (200 µL) and the mixture was stirred at rt for 5 min. A solution of (*S*,*R*)-**2.14** (17.4 mg, 18.7 µmol) in DMF (400 µL) was added and the mixture was stirred at rt for 1 h. Water/acetonitrile 4:1 v/v (5 mL) was added followed by lyophilization. The oily residue was dissolved in dichloromethane/TFA 1:1 v/v (500 µL) and the mixture was stirred at rt for 1 h. The volatiles were removed *in vacuo* and the mixture was subjected to preparative HPLC (gradient: 0-30 min: C/B 82:15-70:30, t_R = 23 min) yielding **4.20** (4.5 mg, 1.9 µmol, 22%) as a white, fluffy solid. RP-HPLC (220 nm): 96%, t_R = 13.7 min, *k* = 4.3. ^{1}H-NMR (600 MHz, methanol-d_6): δ (ppm) 1.11 (t, *J* = 7.7 Hz, 6H), 1.54-1.66 (m, 8H), 1.70-1.80 (m, 14H), 1.81-1.87 (m, 2H), 2.17-2.22 (m, 12H), 2.45-2.53 (m, 8H), 2.59-2.96 (m, 6H), 3.01-3.05 (m, 2H), 3.13-3.27 (m, 18H), 3.93 (t, *J* = 6.3 Hz, 4H), 4.21-4.30 (m, 4H), 4.40-4.45 (m, 2H), 5.04 (s, 2H), 6.69-6.72 (m, 4H), 6.79-6.82 (m, 2H), 6.83-6.88 (m, 4H), 7.04-7.08 (m, 4H), 7.19-7.30 (m, 12H). Note: 10 ^{1}H signals were not apparent due to interference with the solvent residual peak at 3.28-3.33 ppm, as identified by ^{1}H-^{13}C HSQC. MS (LC-HRMS, ESI): *m/z* $[M+3H]^{3+}$ calcd for $[C_{104}H_{153}N_{24}O_{20}]^{3+}$ 686.0559, found 686.0574. $C_{104}H_{150}N_{24}O_{20} \times C_6H_3F_9O_6$ (2398.55).

4.3.3 Cell culture

Cells used for radioligand competition binding assays (SK-N-MC (Y_1R), CHO-hY_2R (Y_2R), CHO-hY_4-Gqi5-mtAEQ (Y_4R) and HEC-1B-hY_5R (Y_5R)) and for the Fura-2 Ca^{2+} assay (HEL cells) were cultured as described in section 2.4.6.

4.3.4 Radioligand competition binding assay

Radioligand competition binding experiments at NPY receptors were performed as described in section 2.4.7, using [^{3}H]**2.2**[29] (Y_1R), [^{3}H]propionyl-pNPY[33, 34] (Y_2R and Y_5R) and [^{3}H]UR-KK200[34] (Y_4R) as radioligands. For Y_1R binding, specific binding data (nonspecific binding

subtracted from total binding) were normalized (100% = specifically bound radioligand in the absence of competitor), plotted as % over log(concentration of competitor) and analyzed by a four-parameter logistic equation (log(inhibitor) vs. response - variable slope, GraphPad Prism 9, GraphPad Software, San Diego, CA) to obtain pIC_{50} values, which were converted into pK_i values according to the Cheng-Prusoff equation (logarithmic form).[39] In the case of compounds **4.18** and **4.19** (Y_4R) radioligand displacement at the highest concentration of amounted to 60-80%. To obtain pIC_{50} values, log(B/(B_0 − B)) (Hill plot; B denotes specifically bound radioligand in the presence of competitor, B_0 = specifically bound radioligand in the absence of competitor (B_0 = 100%)) was plotted against log(competitor concentration) followed by linear regression (pIC_{50} corresponds to the intercept with the x-axis, log(B/(B_0 – B)) = 0). For the other compounds, investigated with respect to Y_2R, Y_4R and Y_5R binding, radioligand displacement was < 50% for the highest competitor concentration (3 µM), i.e. pIC_{50} values could not be determined.

4.3.5 Fura-2 Ca^{2+} assay

The Y_1R Fura-2 Ca^{2+} assay was performed at hY_1R-expressing HEL cells at 22 ± 1 °C as previously described.[40] In antagonist mode, Ca^{2+} mobilization was induced by the addition of pNPY (10 nM) after preincubation of the cells with the antagonists for 15 min. At least three independent experiments were performed in singlet. Net Ca^{2+} responses (basal cytosolic Ca^{2+} concentration subtracted from the measured peak Ca^{2+} concentration) obtained from the investigation of the antagonists **4.17**-**4.20** in antagonist mode (inhibition of the effect elicited by 10 nM pNPY) were normalized (100% = Ca^{2+} response in the absence of antagonist) and plotted against log(concentration of antagonist) followed by analysis according to a four-parameter logistic equation (log(inhibitor) vs response − variable slope, GraphPad Prism 9) to obtain pIC_{50} values.

4.4 References

(1) Faron-Górecka, A.; Szlachta, M.; Kolasa, M.; Solich, J.; Górecki, A.; Kuśmider, M.; Żurawek, D.; Dziedzicka-Wasylewska, M. Understanding GPCR dimerization. *Methods Cell Biol.* **2019**, 149, 155-178.

(2) Ugur, M.; Derouiche, L.; Massotte, D. Heteromerization modulates µ-opioid receptor functional properties *in vivo*. *Front. Pharmacol.* **2018**, 9.

(3) Sleno, R.; Hébert, T. E. The dynamics of GPCR oligomerization and their functional consequences in *Int. Rev. Cell Mol. Biol.*, *Vol. 338*, K., S. A., Eds., Academic Press, Elsevier: Amsterdam, **2018**, pp. 141-171.

(4) Wang, W.; Qiao, Y.; Li, Z. New insights into modes of GPCR activation. *Trends Pharmacol. Sci.* **2018**, 39, 367-386.

(5) Terrillon, S.; Bouvier, M. Roles of G-protein-coupled receptor dimerization. *EMBO reports* **2004**, 5, 30-34.

(6) Portoghese, P. S. From models to molecules: Opioid receptor dimers, bivalent ligands, and selective opioid receptor probes. *J. Med. Chem.* **2001**, 44, 2259-2269.

(7) Soulier, J.-L.; Russo, O.; Giner, M.; Rivail, L.; Berthouze, M.; Ongeri, S.; Maigret, B.; Fischmeister, R.; Lezoualc'h, F.; Sicsic, S.; Berque-Bestel, I. Design and synthesis of specific probes for human 5-HT_4 receptor dimerization studies. *J. Med. Chem.* **2005**, 48, 6220-6228.

(8) Cappelli, A.; Manini, M.; Paolino, M.; Gallelli, A.; Anzini, M.; Mennuni, L.; Del Cadia, M.; De Rienzo, F.; Menziani, M. C.; Vomero, S. Bivalent ligands for the serotonin 5-HT_3 receptor. *ACS Med. Chem. Lett.* **2011**, 2, 571-576.

(9) Soto, C. A.; Shashack, M. J.; Fox, R. G.; Bubar, M. J.; Rice, K. C.; Watson, C. S.; Cunningham, K. A.; Gilbertson, S. R.; Anastasio, N. C. Novel bivalent 5-HT_{2A} receptor antagonists exhibit high affinity and potency *in vitro* and efficacy *in vivo*. *ACS Chem. Neurosci.* **2017**, 9, 514-521.

(10) Kühhorn, J.; Götz, A.; Hübner, H.; Thompson, D.; Whistler, J.; Gmeiner, P. Development of a bivalent dopamine D_2 receptor agonist. *J. Med. Chem.* **2011**, 54, 7911-7919.

(11) McRobb, F. M.; Crosby, I. T.; Yuriev, E.; Lane, J. R.; Capuano, B. Homobivalent ligands of the atypical antipsychotic clozapine: Design, synthesis, and pharmacological evaluation. *J. Med. Chem.* **2012**, 55, 1622-1634.

(12) Ullmann, T.; Gienger, M.; Budzinski, J.; Hellmann, J.; Hübner, H.; Gmeiner, P.; Weikert, D. Homobivalent dopamine D_2 receptor ligands modulate the dynamic equilibrium of D_2 monomers and homo- and heterodimers. *ACS Chem. Biol.* **2021**, 16, 371-379.

(13) Zhang, Y.; Gilliam, A.; Maitra, R.; Damaj, M. I.; Tajuba, J. M.; Seltzman, H. H.; Thomas, B. F. Synthesis and biological evaluation of bivalent ligands for the cannabinoid 1 receptor. *J. Med. Chem.* **2010**, 53, 7048-7060.

(14) Morales, P.; Navarro, G.; Gómez-Autet, M.; Redondo, L.; Fernández-Ruiz, J.; Pérez-Benito, L.; Cordomí, A.; Pardo, L.; Franco, R.; Jagerovic, N. Discovery of homobivalent bitopic ligands of the cannabinoid CB_2 Receptor. *Chem. Eur. J* **2020**, 26, 15839-15842.

(15) Campbell, A. P.; Wakelin, L. P. G.; Denny, W. A.; Finch, A. M. Homobivalent conjugation increases the allosteric effect of 9-aminoacridine at the α_1-adrenergic receptors. *Mol. Pharmacol.* **2017**, 91, 135-144.

(16) Lalchandani, S. G.; Lei, L.; Zheng, W.; Suni, M. M.; Moore, B. M.; Liggett, S. B.; Miller, D. D.; Feller, D. R. Yohimbine dimers exhibiting selectivity for the human α_{2c}-adrenoceptor subtype. *J. Pharmacol. Exp. Ther.* **2002**, 303, 979-984.

(17) Matucci, R.; Nesi, M.; Martino, M. V.; Bellucci, C.; Manetti, D.; Ciuti, E.; Mazzolari, A.; Dei, S.; Guandalini, L.; Teodori, E.; Vistoli, G.; Romanelli, M. N. Carbachol dimers as homobivalent modulators of muscarinic receptors. *Biochem. Pharmacol.* **2016**, 108, 90-101.

(18) Mammen, M.; Choi, S.-K.; Whitesides, G. M. Polyvalent interactions in biological systems: Implications for design and use of multivalent ligands and inhibitors. *Angew. Chem. Int. Ed.* **1998**, 37, 2754-2794.

(19) Lane, J. R.; Sexton, P. M.; Christopoulos, A. Bridging the gap: Bitopic ligands of G protein-coupled receptors. *Trends Pharmacol. Sci.* **2013**, 34, 59-66.

(20) Dinger, M. C.; Bader, J. E.; Kóbor, A. D.; Kretzschmar, A. K.; Beck-Sickinger, A. G. Homodimerization of neuropeptide Y receptors investigated by fluorescence resonance energy transfer in living cells. *J. Biol. Chem.* **2003**, 278, 10562-10571.

(21) Berglund, M. M.; Schober, D. A.; Esterman, M. A.; Gehlert, D. R. Neuropeptide Y Y_4 receptor homodimers dissociate upon agonist stimulation. *J. Pharmacol. Exp. Ther.* **2003**, 307, 1120-1126.

(22) Gehlert, D. R.; Schober, D. A.; Morin, M.; Berglund, M. M. Co-expression of neuropeptide Y Y_1 and Y_5 receptors results in heterodimerization and altered functional properties. *Biochem. Pharmacol.* **2007**, 74, 1652-1664.

(23) Kilpatrick, L. E.; Humphrys, L. J.; Holliday, N. D. A G protein–coupled receptor dimer imaging assay reveals selectively modified pharmacology of neuropeptide Y Y_1/Y_5 receptor heterodimers. *Mol. Pharmacol.* **2015**, 87, 718-732.

(24) Keller, M.; Teng, S.; Bernhardt, G.; Buschauer, A. Bivalent argininamide-type neuropeptide Y Y_1 antagonists do not support the hypothesis of receptor dimerisation. *ChemMedChem* **2009**, 4, 1733-1745.

(25) Keller, M.; Kaske, M.; Holzammer, T.; Bernhardt, G.; Buschauer, A. Dimeric argininamide-type neuropeptide Y receptor antagonists: Chiral discrimination between Y_1 and Y_4 receptors. *Biorg. Med. Chem.* **2013**, 21, 6303-6322.

(26) Weiss, S.; Keller, M.; Bernhardt, G.; Buschauer, A.; König, B. Modular synthesis of nonpeptidic bivalent NPY Y_1 receptor antagonists. *Biorg. Med. Chem.* **2008**, 16, 9858-9866.

(27) Rudolf, K.; Eberlein, W.; Engel, W.; Wieland, H. A.; Willim, K. D.; Entzeroth, M.; Wienen, W.; Beck-Sickinger, A. G.; Doods, H. N. The first highly potent and selective nonpeptide neuropeptide Y Y_1 receptor antagonist: BIBP3226. *Eur. J. Pharmacol.* **1994**, 271, R11-R13.

(28) Wieland, H. A.; Engel, W.; Eberlein, W.; Rudolf, K.; Doods, H. N. Subtype selectivity of the novel nonpeptide neuropeptide Y Y_1 receptor antagonist BIBO3304 and its effect on feeding in rodents. *Br. J. Pharmacol.* **1998**, 125, 549-555.

(29) Keller, M.; Weiss, S.; Hutzler, C.; Kuhn, K. K.; Mollereau, C.; Dukorn, S.; Schindler, L.; Bernhardt, G.; König, B.; Buschauer, A. N^{ω}-Carbamoylation of the argininamide moiety: An avenue to insurmountable NPY Y_1 receptor antagonists and a radiolabeled selective high-affinity molecular tool ([^{3}H]UR-MK299) with extended residence time. *J. Med. Chem.* **2015**, 58, 8834-8849.

(30) Keller, M.; Erdmann, D.; Pop, N.; Pluym, N.; Teng, S.; Bernhardt, G.; Buschauer, A. Red-fluorescent argininamide-type NPY Y_1 receptor antagonists as pharmacological tools. *Biorg. Med. Chem.* **2011**, 19, 2859-2878.

(31) Müller, C.; Gleixner, J.; Tahk, M.-J.; Kopanchuk, S.; Laasfeld, T.; Weinhart, M.; Schollmeyer, D.; Betschart, M. U.; Lüdeke, S.; Koch, P.; Rinken, A.; Keller, M. Structure-based design of high-affinity fluorescent probes for the neuropeptide Y Y_1 receptor. *J. Med. Chem.* **2022**, 65, 4832-4853.

(32) Motulsky, H. J.; Michel, M. C. Neuropeptide Y mobilizes Ca^{2+} and inhibits adenylate cyclase in human erythroleukemia cells. *Am. J. Physiol. - Endocrinol. Metab.* **1988**, 255, E880-E885.

(33) Konieczny, A.; Braun, D.; Wifling, D.; Bernhardt, G.; Keller, M. Oligopeptides as neuropeptide Y Y_4 receptor ligands: identification of a high-affinity tetrapeptide agonist and a hexapeptide antagonist. *J. Med. Chem.* **2020**, 63, 8198-8215.

(34) Kuhn, K. K.; Ertl, T.; Dukorn, S.; Keller, M.; Bernhardt, G.; Reiser, O.; Buschauer, A. High affinity agonists of the neuropeptide Y (NPY) Y_4 receptor derived from the C-terminal pentapeptide of human pancreatic polypeptide (hPP): Synthesis, stereochemical discrimination, and radiolabeling. *J. Med. Chem.* **2016**, 59, 6045-6058.

(35) Dukorn, S.; Littmann, T.; Keller, M.; Kuhn, K.; Cabrele, C.; Baumeister, P.; Bernhardt, G.; Buschauer, A. Fluorescence- and radiolabeling of [Lys^4,Nle^{17,30}]hPP yields molecular tools for the NPY Y_4 receptor. *Bioconjugate Chem.* **2017**, 28, 1291-1304.

(36) Boon, J. M.; Lambert, T. N.; Smith, B. D.; Beatty, A. M.; Ugrinova, V.; Brown, S. N. Structure-activity study of tris(2-aminoethyl)amine-derived translocases for phosphatidylcholine. *J. Org. Chem.* **2002**, 67, 2168-2174.

(37) Hada, N.; Shida, Y.; Negishi, N.; Schweizer, F.; Takeda, T. Syntheses of glycoclusters containing a phosphocholine residue related to a glycosphingolipid from the earthworm pheretima hilgendorfi. *Chem. Pharm. Bull.* **2009**, 57, 1081-1088.

(38) Banasik, B. A. A pre-biotinylated linker assembly for single-step preparation of novel biosensors. *Org. Commun.* **2017**, 10, 40-45.

(39) Cheng, Y.-C.; Prusoff, W. H. Relationship between the inhibition constant (K_i) and the concentration of inhibitor which causes 50 per cent inhibition (IC_{50}) of an enzymatic reaction. *Biochem. Pharmacol.* **1973**, 22, 3099-3108.

(40) Müller, M.; Knieps, S.; Geßele, K.; Dove, S.; Bernhardt, G.; Buschauer, A. Synthesis and neuropeptide Y Y_1 receptor antagonistic activity of N,N-disubstituted ω-guanidino- and ω-aminoalkanoic acid amides. *Arch. Pharm.* **1997**, 330, 333-342.

Chapter 5

A synthetic approach towards argininamide-type Y_1 receptor radiohybrid ligands as potential theranostic agents

5.1 Introduction

In nuclear medicine, the term theranostics (alternatively also called theragnostics) describes the use of two almost identical radiopharmaceuticals for two purposes, cancer diagnosis and cancer therapy.[1] The most common pathway to gain access to a variety of potential theranostic agents is the attachment of bifunctional chelators to a bioactive carrier molecule, such as receptor ligands or enzyme inhibitors. The chelator allows the complexation of various radionuclides with distinct radioactive properties.[2, 3] Therefore, ^{68}Ga-labeled PET ligands, usually carrying the bifunctional chelator DOTA, naturally can be considered theranostic agents and are already established in nuclear medicine as valuable tools, for example ^{68}Ga-DOTATATE (**5.1a**), a PET tracer used to localize neuroendocrine tumors.[4] ^{68}Ga-DOTATATE is used as a diagnostic tracer, but can be transformed into the therapeutic agent ^{177}Lu-DOTATATE (**5.1b**, Lutathera®) when the β^- emitter ^{177}Lu is incorporated instead of the positron emitting ^{68}Ga (Figure 5.1, panel A).[5, 6] Provided that specificity and selectivity of the chelator-carrying radiopharmaceutical agent for the respective tumor marker are sufficiently high, ^{177}Lu-labeled analogues of ^{68}Ga-labeled PET tracers can be used as an effective cargo system to the tumor, thereby minimizing radiation exposure to healthy tissue.

The recently introduced concept of “radiohybrid” ligands has the potential to contribute theranostic agents with improved properties for PET imaging compared to ^{68}Ga/^{177}Lu-based agents.[7] Radiohybrid ligands can potentially contain two different radionuclides at separate sites, rather than only one exchangeable radiometal. The widespread use of ^{68}Ga in cancer diagnosis is mainly owed to its easy accessibility *via* ^{68}Ge/^{68}Ga generators and the straightforward one-step labeling procedure.[8] However, although the synthesis of ^{18}F-labeled tracers often involves laborious labeling reactions and manual purification steps, ^{18}F is commonly considered superior to ^{68}Ga due to its longer half-life and higher PET imaging resolution. Radiohybrid ligands bear the potential to combine ^{18}F-based PET imaging and radiotherapy using ^{177}Lu: Lately, a mild synthesis of the PSMA (prostate specific membrane antigen) PET ligand ^{18}F/^{175}Lu-rhPSMA-7.3 (**5.2a**) *via* silicon-fluoride acceptor (SiFA)-mediated ^{19}F-to-^{18}F nuclide exchange and its ^{177}Lu-containing radiochemical “twin”, ^{19}F/^{177}Lu-rhPSMA-7.3 (**5.2b**), was reported (Figure 5.1, panel B).[9] Administration of **5.2a** resulted in high-quality pretherapeutic PET images of C4-2 prostate tumor xenografts in nude mice, while administration of **5.2b** led to significant attenuation of tumor growth compared to control mice, confirming the promising concept of radiohybrid ligands as potential theranostic agents with improved PET imaging capabilities.[8, 10]

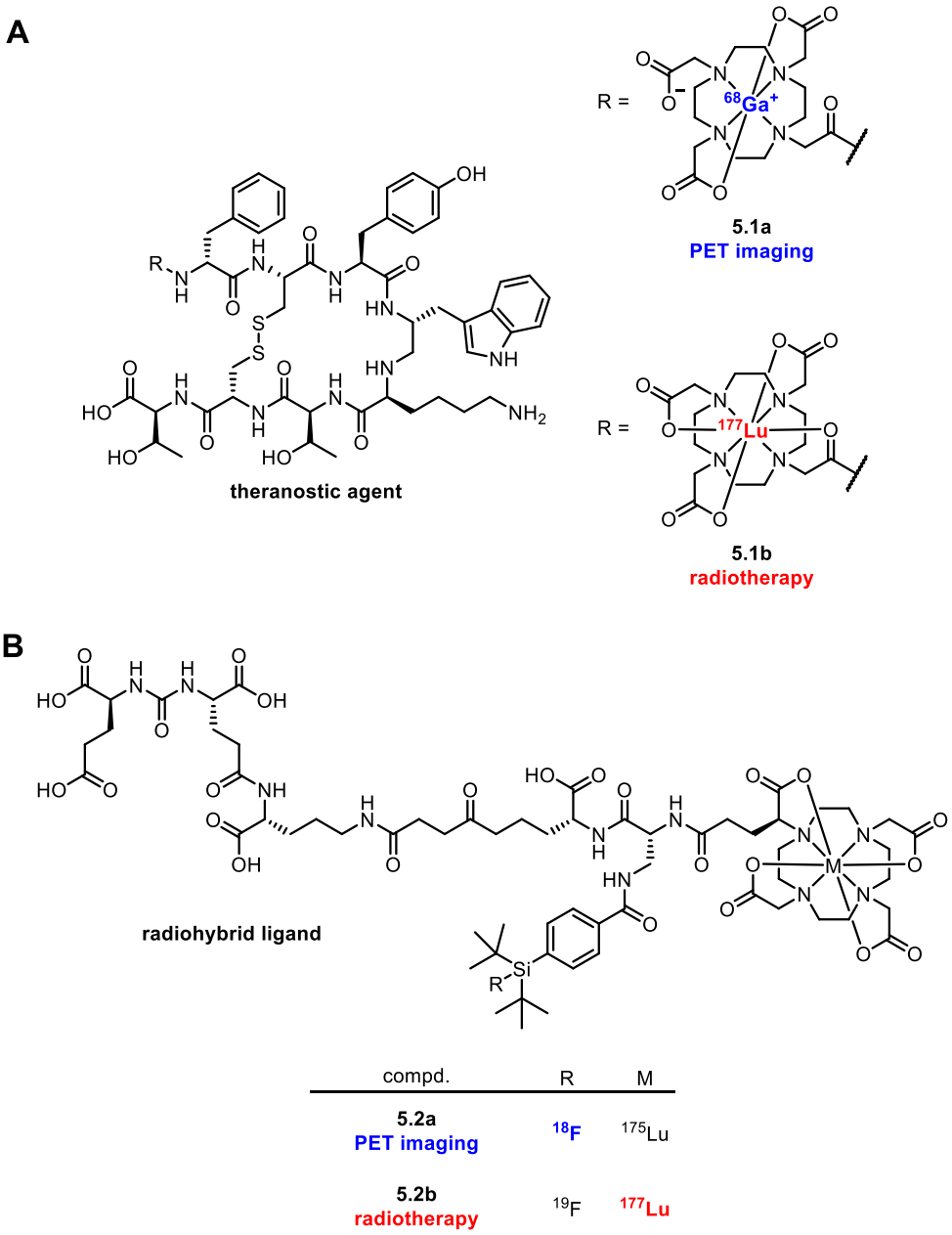

compd.	R	M
5.2a PET imaging	^{18}F	^{175}Lu
5.2b radiotherapy	^{19}F	^{177}Lu

Figure 5.1. (A) Structures of the somatostatin analogues ^{68}Ga-DOTATATE (**5.1a**) and ^{177}Lu-DOTATATE (**5.1b**), used as theranostic agents in diagnosis and radiotherapy of neuroendocrine tumors. (B) Structures of PSMA ligands ^{18}F/^{175}Lu-rhPSMA-7.3 (**5.2a**) and ^{19}F/^{177}Lu-rhPSMA-7.3 (**5.2b**), representing the concept of "radiohybrid" theranostics (Figure adapted from Yusufi *et al.*[10]).

In theory, radiohybrid ligands containing ^{18}F/^{19}F and a (radio)metal ion chelator also allow for an unbiased comparison of the PET imaging quality achieved with a ^{18}F-labeled and a ^{68}Ga-labeled tracer. As both radiolabeled variants exhibit identical physicochemical properties and consequently also identical systemic distribution, tumor uptake and clearance, differences, e.g. with respect to image resolution and sensitivity can only arise from the type of the positron emitting nuclide.

Prompted by the development of the promising ^{68}Ga- and ^{18}F-labeled Y_1R radioligands presented in Chapter 3, a synthetic route was worked out to gain access to high affinity potential “radiohybrid” Y_1R ligands. Precisely, a prototypic argininamide-type precursor for "radiohybrid" Y_1R ligands equipped with a bifunctional chelator for (radio)metal ion complexation and an alkyne functionality for conjugation to ^{18}F/^{19}F-fluoroglycosyl azides[11] was synthesized.

5.2 Results and discussion

5.2.1 Synthesis

To enable the synthesis of a PET tracer equipped with a complexed trivalent metal cation and a fluoroglycosyl residue, building block **5.3**, bearing a Boc-protected amine group and an alkyne group, was synthesized (Scheme 5.1). (*R*,*R*)-**2.14**, exhibiting identical Y_1R binding affinity compared to its epimer (*S*,*R*)-**2.14**, which was used as the amine precursor for the synthesis of fluorescent ligands (Chapter 2) and PET ligands (Chapter 3), was coupled to **5.3** using the coupling reagents HBTU and HOBt to afford amine **5.4** after TFA-mediated Boc deprotection (Scheme 5.1). Treatment of **5.4** with DOTA succinimidyl ester **3.23** under basic conditions gave the DOTA-conjugate **5.5**, which represents the precursor for the potential synthesis of a Y_1R radiohybrid ligand, obtainable by successive labeling of **5.5** with e.g. ^{177}Lu and/or a ^{18}F-containing residue, e.g. ^{18}F-fluoroglycosylazide [^{18}F]**3.10**. To synthesize the corresponding “cold” analogue, CuAAC-mediated glycosylation with **3.10** afforded compound **5.6**, which could, however, not be converted to target compound **5.7** under default reaction conditions for the incorporation of trivalent metal cations (in this study pursued with Ga^{3+}). Mass spectrometry analysis revealed an inclusion of Cu(II) in **5.6**, which most likely already occurred during the previous CuAAC (involving $CuSO_4$). Obviously, Cu^{2+} could not be displaced by Ga^{3+} (Scheme 5.1). Considering a putative complexation of trivalent lanthanide cations such as Lu^{3+}, which can in principle be coordinated by eight available donor atoms (*cf.* structures in Figure 5.1), the replacement of Cu^{2+} with Lu^{3+} under identical reaction conditions seems unlikely, as lanthanide(III)-DOTA complexes are considered less stable compared to octahedrally coordinated Cu^{2+}-DOTA and Ga^{3+}-DOTA complexes.[12, 13] Synthetic routes circumventing this issue (drawn in blue, Scheme 5.1), which were not pursued in this study, involve the incorporation of the trivalent cation prior to the exposure of **5.5** to Cu(II)-sulfate (Scheme 5.1). Alternatively, rather than using succinimidyl ester **3.23** (containing three carboxyl groups) for the conjugation of the DOTA to **5.4**, a *tert*-butyl-protected variant can be used (masked carboxyl groups) and can be deprotected after successful CuAAC-mediated fluoroglycosylation (Scheme 5.1). These synthetic approaches are subject of future studies.

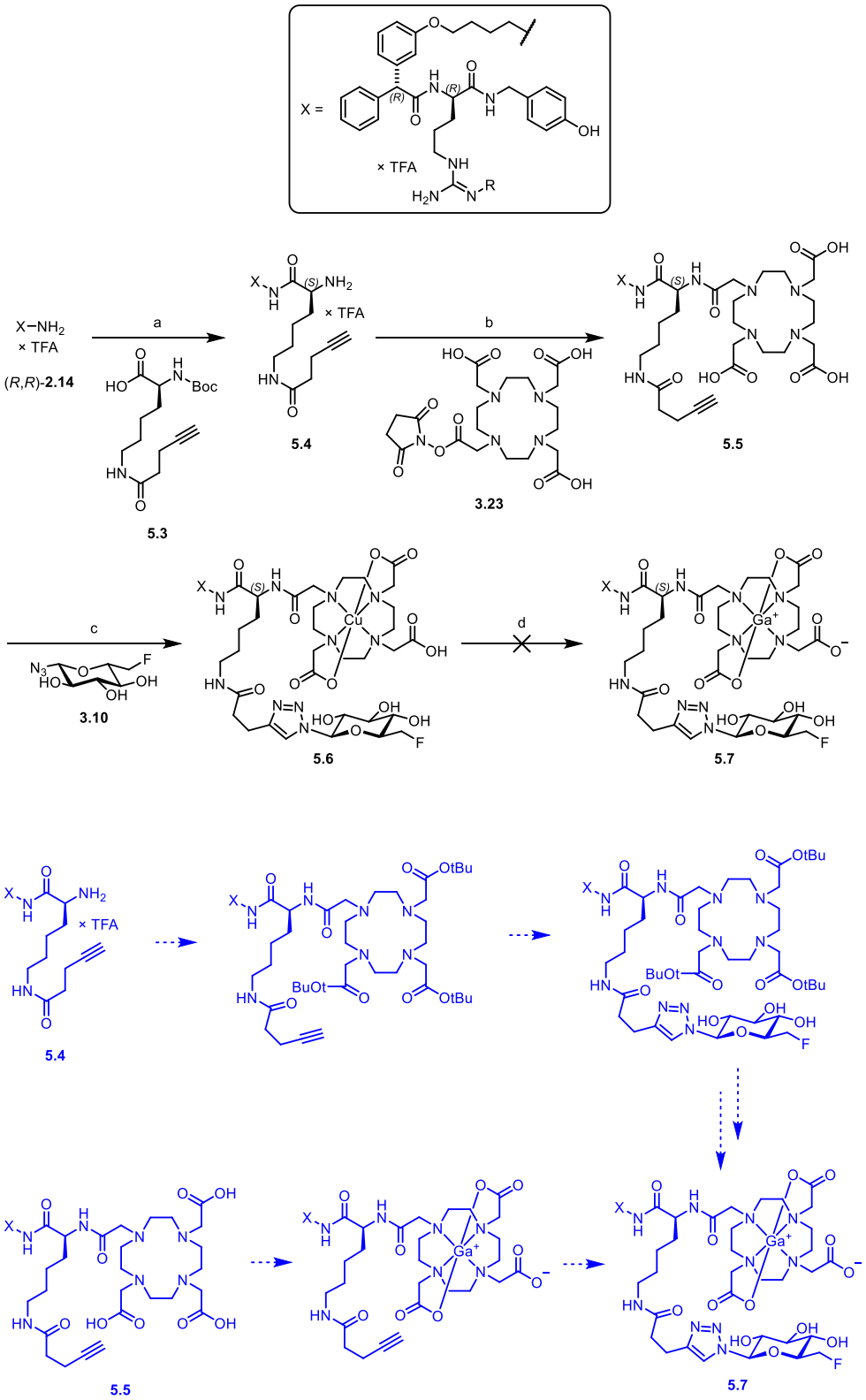

Scheme 5.1. Synthesis of compound **5.6**, unsuccessful conversion of **5.6** to target compound **5.7** (black), and putative alternative synthetic routes to compound **5.7** (blue). Reagents and conditions: a) (1) HBTU, HOBt, DIPEA, DMF, rt, 1 h; (2) TFA, CH_2Cl_2, 900 mbar, rt, 2 h, 85%; b) DIPEA, DMF, rt, 1 h, 35%; c) $CuSO_4$ × 5 H_2O, sodium ascorbate, H_2O/acetonitrile, rt, 1 h, 26%; d) $Ga(NO_3)_3$, HEPES pH 4.2, aq. HCl, 100 °C, 10 min, only the starting material **5.6** could be isolated.

5.3 Experimental section

5.3.1 General experimental conditions

Chemicals. Standard chemicals, solvents, and buffer components were purchased from commercial suppliers (Sigma-Aldrich, München, Germany; Merck, Darmstadt, Germany; Fisher Scientific, Schwerte, Germany; TCI, Eschborn, Germany) and used without further purification. Boc-L-Lys-OH was from Iris Biotech (Marktredwitz, Germany). **3.23** was from CheMatech (Dijon, France). The synthesis of **3.10** was described elsewhere.[11] Gradient grade acetonitrile for HPLC was purchased from Sigma-Aldrich (München, Germany). Purifications by column chromatography were carried out using technical grade solvents and Geduran Si 60 silica gel (pore size of 60 Å, particle size of 40-63 or 63-200 µm, Merck). Thin layer chromatography (TLC) was performed on ALUGRAM Xtra SIL G/UV254 TLC sheets from Macherey-Nagel GmbH & Co. KG (Düren, Germany).

NMR spectroscopy. NMR spectra were recorded on a Bruker Avance 400 (^{1}H, 400 MHz, ^{13}C, 100 MHz) or an Avance 600 (^{1}H, 600 MHz, ^{13}C, 150 MHz) spectrometer (Bruker, Karlsruhe, Germany). Note regarding the ^{1}H-NMR spectrum of compound **5.6**: Due to the presence of paramagnetic Cu(II), the resolution of the spectrum was markedly reduced.[14]

Mass spectrometry. High-resolution mass spectrometry (HRMS) analysis was performed on an Agilent 6540 UHD AccurateMass Q-TOF LC/MS system coupled to an Agilent 1290 HPLC system (Agilent Technologies, Santa Clara, CA), using an ESI source. Analyses were performed using the following LC method: column: ZORBAX RRHD Eclipse Plus C18, 1.8 µm, 50 × 2.1 mm (Agilent Technologies, Santa Clara, CA), column temperature: 40 °C, flow: 0.6 mL/min, solvent/linear gradient: 0-4 min: 0.1% aqueous HCOOH/0.1% HCOOH in MeCN 95:5-2:98, 4-5 min: 2:98.

Analytical RP-HPLC. Reaction controls were carried out by analytical HPLC (RP-HPLC) using an 1100 series system from Agilent Technologies (Santa Clara, CA) consisting of a degasser (G1379A), a binary pump (G1312A), a variable wavelength detector (G1314A), a thermostated column compartment (G1316A), and an autosampler (G1329A). This system is identical to system B, termed in section 2.4.1. A Kinetex XB-C18 100A (5 µm, 250 mm × 4.6 mm, Phenomenex, Aschaffenburg, Germany) was used as the stationary phase. The flow rate was 0.8 mL min^{-1}, the oven temperature was set to 30 °C, and the injection volume was 90 µL. Mixtures of solvents A (0.05% aqueous TFA) and B (acetonitrile) were used as the mobile phase. The following gradient was applied: 0-30 min: A/B 90:10 to 5:95, 30-40 min: A/B 5:95 (isocratic). The detection wavelength was set to 220 nm. Retention factors k were calculated according to $k = (t_R\text{-}t_0)/t_0$ (where t_0 is the dead time of 2.6 min).

Preparative HPLC. Purifications by preparative HPLC were performed with a Prep 150 LC system from Waters (Eschborn, Germany) consisting of a 2545 binary gradient module, a 2489 UV/visible detector and a Waters Fraction Collector III. A Gemini-NX C18 110A (5 µm, 250 mm × 21 mm, Phenomenex) was used as the stationary phase. The mobile phase was composed of solvents C (0.1% aqueous TFA with 5% acetonitrile) and B (acetonitrile). Lyophilization of the eluates containing the products was performed with a Scanvac CoolSafe 100-9 freeze-drying apparatus (Labogene, Allerød, Denmark) equipped with a RZ 6 rotary vane vacuum pump (Vacuubrand, Wertheim, Germany).

5.3.2 Experimental synthetic protocols and analytical data

(*S*)-2-((*tert*-Butoxycarbonyl)amino)-6-(pent-4-ynamido)hexanoic acid[15] (5.3)

A solution of 4-pentynoic acid (40 mg, 0.41 mmol), HOBt (64 mg, 0.41 mmol), HBTU (153 mg, 0.41 mmol) and DIPEA (280 µL, 1.64 mmol) in DMF (10 mL) was stirred at rt for 5 min. Boc-L-Lys-OH (100 mg, 0.41 mmol) was added and the suspension was stirred at rt for 16 h. H_2O (15 mL) was added, the mixture was carefully acidified to pH 3 by the addition of aqueous 1 N HCl, and was treated with ethyl acetate (30 mL). The organic layer was separated, washed with H_2O (3 × 20 mL), and dried over Na_2SO_4. The solvent was removed by rotary evaporation, and the product was purified by column chromatography (light petroleum/ethyl acetate 1:1 v/v to light petroleum/ethyl acetate/acetic acid 50:50:1 v/v/v) to yield **5.3** as a yellow resin (59 mg, 0.18 mmol, 45%). TLC (light petroleum/ethyl acetate/acetic acid 66:33:1 v/v/v): R_f = 0.25. ^{1}H-NMR (400 MHz, DMSO-d_6): δ (ppm) 1.21-1.29 (m, 2H), 1.34-1.57 (m, 12H), 1.62-1.70 (m, 1H), 2.20-2.26 (m, 2H), 2.30-2.36 (m, 2H), 2.74 (t, *J* = 2.5 Hz, 1H), 2.97-3.04 (m, 2H), 3.62-3.69 (m, 1H), 7.46-7.54 (m, 1H), 8.31-8.42 (m, 1H), 12.34 (br s, 1H). ^{13}C-NMR (100 MHz, DMSO-d_6): δ (ppm) 14.20, 21.63, 28.21, 28.31, 30.54, 34.15, 39.72 (interfering with the solvent residual signal, as identified by ^{1}H-^{13}C HSQC), 53.41, 70.54, 79.19, 82.29, 152.39, 171.02, 173.86. MS (LC-HRMS, ESI): *m/z* $[M+Na]^+$ calcd for $[C_{16}H_{26}NaN_2O_5]^+$ 349.1739, found: 349.1734. $C_{16}H_{26}N_2O_5$ (326.39).

(*S*)-2-Amino-N-(4-(3-((1*R*,4*R*,*Z*)-9-amino-4-((4-hydroxybenzyl)carbamoyl)-2,11,16-trioxo-1-phenyl-3,8,10,12,15-pentaazaoctadec-9-en-1-yl)phenoxy)butyl)-6-(pent-4-ynamido)hexanamide bis(hydrotrifluoroacetate) (5.4)

A solution of **5.3** (11.7 mg, 35.4 µmol), HOBt (5.5 mg, 35.4 µmol), HBTU (13.4 mg, 35.4 µmol) and DIPEA (33 µL, 250 µmol) in DMF (300 µL) was stirred at rt for 10 min. (*R*,*R*)-**2.14** (30.0 mg, 32.2 µmol) was added and stirring was continued at rt for 1 h. 0.5% Aq. TFA/acetonitrile 80:20 v/v (1 mL) was added and the mixture was subjected to preparative HPLC (gradient: 0-30 min: C/B 80:20-50:50, t_R = 20 min), the resulting white solid was dissolved in CH_2Cl_2 (2 mL) and TFA (500 µL) was added. The mixture was stirred at rt at 900 mbar for 2 h followed by rotary

evaporation of the volatiles to yield **5.4** (31 mg, 27.2 μmol, 85%) as a colorless resin. RP-HPLC (220 nm): t_R = 13.1 min, k = 4.0. ^{1}H-NMR (400 MHz, DMSO-d_6): δ (ppm) 0.98 (t, J = 7.8 Hz, 3H), 1.22-1.30 (m, 2H), 1.34-1.48 (m, 4H), 1.50-1.60 (m, 3H), 1.62-1.74 (m, 5H), 2,06 (q, J = 7.8 Hz, 2H), 2.21-2.27 (m, 2H), 2.31-2.37 (m, 2H), 2.72-2.76 (m, 1H), 2.97-3.05 (m, 2H), 3.10-3.23 (m, 8H), 3.62-3.70 (m, 1H), 3.87-3.94 (m, 2H), 4.09-4.19 (m, 2H), 4.29-4.35 (m, 1H), 5.08 (s, 1H), 6.64-6.69 (m, 2H), 6.76-6.87 (m, 3H), 6.96-7.03 (m, 2H), 7.15-7.33 (m, 6H), 7.47-7.54 (m, 1H), 7.78-7.89 (m, 2H), 8.02-8.18 (m, 3H), 8.33-8.51 (m, 6H), 8.97 (br s, 1H), 10.31 (br s, 1H). ^{13}C-NMR (100 MHz, DMSO-d_6): δ (ppm) 9.82, 14.26, 21.63, 24.61, 25.56, 26.11, 28.46, 28.64, 29.43, 30.77, 34.30, 38.04, 38.17, 38.38, 38.77, 40.32, 41.61, 52.26, 52.30, 55.78, 66.86, 71.24, 83.76, 112.01, 115.00, 115.10, 120.82, 126.64, 128.19, 128.39, 128.45, 129.08, 129.17, 140.31, 141.69, 153.64, 153.88, 156.25, 158.42, 168.33, 170.08, 170.91, 171.00, 173.29. MS (LC-HRMS, ESI): *m/z* $[M+H]^+$ calcd for $[C_{48}H_{67}N_{10}O_8]^+$ 911.5138, found 911.5147. $C_{48}H_{66}N_{10}O_8 \times C_4H_2F_6O_4$ (1139.16).

2,2',2''-(10-(2-(((*S*)-1-((4-(3-((1*R*,4*R*,*Z*)-9-Amino-4-((4-hydroxybenzyl)carbamoyl)-2,11,16-trioxo-1-phenyl-3,8,10,12,15-pentaazaoctadec-9-en-1-yl)phenoxy)butyl)amino)-1-oxo-6-(pent-4-ynamido)hexan-2-yl)amino)-2-oxoethyl)-1,4,7,10-tetraazacyclododecane-1,4,7-triyl)triacetic acid bis(hydrotrifluoroacetate) (5.5)

3.23 (17.0 mg, 22.5 μmol) was added to a solution of **5.4** (25.6 mg, 22.5 μmol) and DIPEA (98 μL, 180 μmol) in DMF (1 mL) and the mixture was stirred at rt for 1 h. 0.5% Aq. TFA/acetonitrile 80:20 v/v (1 mL) was added and the mixture was subjected to preparative HPLC (gradient: 0-20 min: C/B 85:15-70:30, t_R = 14 min) to yield **5.5** (12.0 mg, 7.9 μmol, 35%) as a white fluffy solid. RP-HPLC (220 nm): t_R = 12.6 min, k = 3.8. ^{1}H-NMR (600 MHz, D_2O): δ (ppm) 1.06 (t, J = 7.8 Hz, 3H), 1.25-1.36 (m, 2H), 1.40-1.88 (m, 12H), 2.21 (q, J = 7.8 Hz, 2H), 2.30-2.36 (m, 3H), 2.37-2.43 (m, 2H), 2.88-3.42 (m, 26H), 3.50-4.10 (m, 10H), 4.11-4.18 (m, 1H), 4.19-4.28 (m, 3H), 5.13 (s, 1H), 6.76-6.81 (m, 2H), 6.82-6.86 (m, 2H), 6.87-6.91 (m, 1H), 7.05-7.11 (m, 2H), 7.23-7.41 (m, 6H). MS (LC-HRMS, ESI): *m/z* $[M+2H]^{2+}$ calcd for $[C_{64}H_{94}N_{14}O_{15}]^{2+}$ 649.3506, found 649.3521. $C_{64}H_{92}N_{14}O_{15} \times C_4H_2F_6O_4$ (1525.56).

(Copper(II))-2,2'-(4-(2-((1-((4-(3-((1R,4R,Z)-9-amino-4-((4-hydroxybenzyl)carbamoyl)-2,11,16-trioxo-1-phenyl-3,8,10,12,15-pentaazaoctadec-9-en-1-yl)phenoxy)butyl)amino)-6-(3-(1-(1,6-bisdeoxy-6-fluoro-β-D-glucopyranos-1-yl)-1H-1,2,3-triazol-5-yl)propanamido)-1-oxohexan-2-yl)amino)-2-oxoethyl)-10-(carboxymethyl)-1,4,7,10-tetraazacyclododecane-1,7-diyl)diacetate hydrotrifluoroacetate (5.6)

A solution of deoxy-6-fluoro-β-D-glucopyranosyl azide (**3.10**, 3.5 mg, 17 μmol), $CuSO_4$ pentahydrate (1.3 mg, 5.0 μmol) and sodium ascorbate (3.0 mg, 15.1 μmol) in H_2O (500 μL) was added to a solution of **5.5** (6.0 mg, 3.9 μmol) in acetonitrile (500 μL) and the mixture was

stirred at rt for 1 h. 0.5% Aq. TFA/acetonitrile 80:20 v/v (1 mL) was added and the mixture was subjected to preparative HPLC (gradient: 0-20 min: C/B 85:15-75:25, t_R = 18 min) to yield **5.6** (1.6 mg, 1.0 µmol, 26%) as a light blue fluffy solid. RP-HPLC (220 nm): t_R = 12.1 min, k = 3.7. ^{1}H-NMR (600 MHz, DMSO-d_6/D_2O 10:1 v/v): δ (ppm) 0.90-0.98 (m, 3H), 1.18-1.24 (m, 2H), 1.27-1.84 (m, 12H), 1.98-2.07 (m, 2H), 2.38-2.45 (m, 2H), 2.78-2.87 (m, 2H), 2.94-3.47 (m, 12H), 3.68-3.75 (m, 2H), 3.85-4.00 (m, 2H), 4.05-4.17 (m, 2H), 4.19-4.30 (m, 1H), 4.43-4.62 (m, 2H), 4.93-5.05 (m, 1H), 5.49-5.59 (m, 1H), 6.59-6.70 (m, 2H), 6.73-6.90 (m, 3H), 6.91-7.03 (m, 2H), 7.08-7.34 (m, 6H), 7.86-8.02 (m, 1H). Note: 25 ^{1}H signals were not apparent due to interference with the residual peak of HDO (3.55-3.65 ppm). MS (LC-HRMS, ESI): *m/z* $[M+3H]^{3+}$ calcd for $[C_{70}H_{103}{}^{63}CuFN_{17}O_{19}]^{3+}$ 522.5627, found 522.5635. $C_{70}H_{100}CuFN_{17}O_{19} \times C_2HF_3O_2$ (1680.23).

5.4 References

(1) Langbein, T.; Weber, W. A.; Eiber, M. Future of theranostics: An outlook on precision oncology in nuclear medicine. *J. Nucl. Med.* **2019**, 60, 13S-19S.

(2) Holik, H. A.; Ibrahim, F. M.; Elaine, A. A.; Putra, B. D.; Achmad, A.; Kartamihardja, A. H. S. The chemical scaffold of theranostic radiopharmaceuticals: Radionuclide, bifunctional chelator, and pharmacokinetics modifying linker. *Molecules* **2022**, 27, 3062.

(3) White, J. M.; Escorcia, F. E.; Viola, N. T. Perspectives on metals-based radioimmunotherapy (RIT): Moving forward. *Theranostics* **2021**, 11, 6293-6314.

(4) Patel, M.; Tena, I.; Jha, A.; Taieb, D.; Pacak, K. Somatostatin receptors and analogs in pheochromocytoma and paraganglioma: Old players in a new precision medicine world. *Front. Endocrinol.* **2021**, 12.

(5) Strosberg, J.; El-Haddad, G.; Wolin, E.; Hendifar, A.; Yao, J.; Chasen, B.; Mittra, E.; Kunz, P. L.; Kulke, M. H.; Jacene, H.; Bushnell, D.; O'Dorisio, T. M.; Baum, R. P.; Kulkarni, H. R.; Caplin, M.; Lebtahi, R.; Hobday, T.; Delpassand, E.; Van Cutsem, E.; Benson, A.; Srirajaskanthan, R.; Pavel, M.; Mora, J.; Berlin, J.; Grande, E.; Reed, N.; Seregni, E.; Öberg, K.; Lopera Sierra, M.; Santoro, P.; Thevenet, T.; Erion, J. L.; Ruszniewski, P.; Kwekkeboom, D.; Krenning, E. Phase 3 trial of ^{177}Lu-DOTATATE for midgut neuroendocrine tumors. *New Engl. J. Med.* **2017**, 376, 125-135.

(6) Hennrich, U.; Kopka, K. Lutathera®: The first FDA- and EMA-approved radiopharmaceutical for peptide receptor radionuclide therapy. *Pharmaceuticals* **2019**, 12, 114.

(7) Piron, S.; Verhoeven, J.; Vanhove, C.; De Vos, F. Recent advancements in ^{18}F-labeled PSMA targeting PET radiopharmaceuticals. *Nucl. Med. Biol.* **2022**, 106-107, 29-51.

(8) Wurzer, A.; Di Carlo, D.; Schmidt, A.; Beck, R.; Eiber, M.; Schwaiger, M.; Wester, H.-J. Radiohybrid ligands: A novel tracer concept exemplified by ^{18}F- or ^{68}Ga-labeled rhPSMA inhibitors. *J. Nucl. Med.* **2020**, 61, 735-742.

(9) Wurzer, A.; Di Carlo, D.; Herz, M.; Richter, A.; Robu, S.; Schirrmacher, R.; Mascarin, A.; Weber, W.; Eiber, M.; Schwaiger, M.; Wester, H.-J. Automated synthesis of [^{18}F]Ga-rhPSMA-7/-7.3: Results, quality control and experience from more than 200 routine productions. *EJNMMI Radiopharmacy and Chemistry* **2021**, 6.

(10) Yusufi, N.; Wurzer, A.; Herz, M.; D'Alessandria, C.; Feuerecker, B.; Weber, W.; Wester, H.-J.; Nekolla, S.; Eiber, M. Comparative preclinical biodistribution, dosimetry, and endoradiotherapy in metastatic castration-resistant prostate cancer using ^{19}F/^{177}Lu-rhPSMA-7.3 and ^{177}Lu-PSMA I&T. *J. Nucl. Med.* **2021**, 62, 1106-1111.

(11) Maschauer, S.; Haubner, R.; Kuwert, T.; Prante, O. ^{18}F-Glyco-RGD peptides for PET Imaging of integrin expression: Efficient radiosynthesis by click chemistry and modulation of biodistribution by glycosylation. *Mol. Pharm.* **2013**, 11, 505-515.

(12) Anderegg, G.; Arnaud-Neu, F.; Delgado, R.; Felcman, J.; Popov, K. Critical evaluation of stability constants of metal complexes of complexones for biomedical and environmental applications (IUPAC Technical Report). *Pure Appl. Chem.* **2005**, 77, 1445-1495.

(13) Kubíček, V.; Havlíčková, J.; Kotek, J.; Tircsó, G.; Hermann, P.; Tóth, É.; Lukeš, I. Gallium(III) complexes of DOTA and DOTA−monoamide: kinetic and thermodynamic studies. *Inorg. Chem.* **2010**, 49, 10960-10969.

(14) Bertini, I.; Pierattelli, R. Copper(II) proteins are amenable for NMR investigations. *Pure Appl. Chem.* **2004**, 76, 321-333.

(15) Isidro-Llobet, A.; Hadje Georgiou, K.; Galloway, W. R. J. D.; Giacomini, E.; Hansen, M. R.; Méndez-Abt, G.; Tan, Y. S.; Carro, L.; Sore, H. F.; Spring, D. R. A diversity-oriented synthesis strategy enabling the combinatorial-type variation of macrocyclic peptidomimetic scaffolds. *Org. Biomol. Chem.* **2015**, 13, 4570-4580.

Summary

In humans, neuropeptide Y (NPY), a linear 36-amino acid peptide abundantly present in the CNS and PNS, is involved in the regulation of numerous physiological processes. NPY exerts its actions by activation of four G protein-coupled receptors constituting the neuropeptide Y receptor family (Y_1R, Y_2R, Y_4R, Y_5R). Several studies revealed an overexpression of Y_1Rs in different malignant tumors with the highest levels found in breast cancer tissue, suggesting the Y_1R as a potential target for tumor imaging and cancer therapy. Therefore, fluorescence and radiolabeled ligands with high selectivity and affinity for the Y_1R are needed as tool compounds for the development of functionalized Y_1R ligands to study Y_1R expression in cells and tissues, and as tumor imaging agents themselves.

This work focused on the design of novel molecular tools for the Y_1R with markedly improved binding affinity compared to previously reported ligands. The approach was guided by the reported X-ray crystal structure of the Y_1R in complex with the high-affinity Y_1R antagonist UR-MK299, which represents an N^{ω}-carbamoylated derivative of the argininamide BIBP3226. According to the crystal structure, the introduction of bulky substituents at the guanidino group in BIBP3226 is incompatible with the binding mode, but the attachment of large substituents to the diphenylacetyl moiety of the argininamides should be well tolerated. Therefore, derivatives of UR-MK299 (**2.14** and **2.30**) and BIBP3226 (**3.6**), containing a 4-aminobutoxy substituent at one of the phenyl rings, were synthesized and the absolute stereochemistry of the generated second chiral center was determined. The obtained amine precursors exhibited similar binding affinity (pK_i = 10.30-10.89) as UR-MK299 (pK_i = 10.11). Conjugation of (*S*,*R*)-**2.14** and (*R*,*R*)-**2.14** to different fluorophores yielded a set of fluorescently labeled Y_1R antagonists (**2.35**-**2.39**) with subnanomolar affinities (pK_i = 9.37-9.95) and excellent Y_1R selectivity (at least 1000-fold over Y_2R, Y_4R and Y_5R). Flow cytometric saturation binding assays performed with intact MCF-7-Y_1 mammary carcinoma cells afforded dissociation constants (pK_D = 9.57-9.87), which were in agreement with the pK_i values obtained from radioligand competition binding studies. The characterization of the 5'-TAMRA-labeled ligand **2.39** in fluorescence anisotropy-based binding assays, which take into account ligand depletion, suggested an even higher Y_1R affinity (pK_D = 11.02). The binding kinetics of the fluorescent probes at the Y_1R were also studied by flow cytometry (**2.35**, **2.37** and **2.39**) and fluorescence anisotropy (**2.39**). Furthermore, **2.37** and **2.39** were successfully used to visualize Y_1R receptors in the plasma membrane of live MCF-7-Y_1 cells using widefield and TIRF microscopy.

Prompted by the promising results of the fluorescent ligand approach, the amine-functionalized precursors were also used to synthesize potential Y_1R PET ligands, exhibiting higher Y_1R affinity and increased hydrophilicity than previously reported argininamide-type Y_1R PET ligands. The PET ligand candidates were obtained by attachment of a fluoroglycosyl moiety

via click chemistry (**3.11**, **3.12**, **3.19** and **3.22**) or by conjugation to a DOTA chelator and subsequent incorporation of Ga^{3+} (**3.25**). As anticipated, the potential PET ligands displayed high Y_1R binding (pK_i = 8.87-10.20). Radiosyntheses were performed to afford the PET-tracers [^{18}F]**3.11**, [^{18}F]**3.12** and [^{68}Ga]**3.25**, which were studied in nude mice with subcutaneous MCF-7-Y_1 tumors (PET imaging, biodistribution). All PET ligands enabled the imaging of the tumor by PET with [^{68}Ga]**3.25** representing the most promising tracer due to a pronounced renal clearance.

To obtain high-affinity homobivalent Y_1R antagonists (**4.17**-**4.20**, pK_i = 9.67-10.13) as potential tools to study receptor homodimerization, amine precursor (*S*,*R*)-**2.14** was dimerized by conjugation to spacers with varying lengths (8, 15, 25 and 37 atoms). Notably, the radioligand competition binding data, specifically the slopes of the sigmoidal displacement curves, did not indicate binding to Y_1R homodimers.

Finally, a synthetic route towards argininamide-type potential “radiohybrid” Y_1R ligands was explored, which will support the future development of theranostic agents targeting the Y_1R.

In conclusion, this work presents the structure-guided design of amine-functionalized argininamide-type Y_1R ligands that could be converted to fluorescently labeled ligands, PET ligands and homobivalent ligands displaying subnanomolar Y_1R affinity and excellent Y_1R selectivity. Based on the presented approach, a broad variety of specifically functionalized tools compounds for the Y_1R, including imaging agents for cancer diagnosis, will be accessible in future studies.

Appendix

Note: The section A.1 was omitted so that the numbering of the sections A.2-A.5 corresponds to the numbering of the respective Chapters 2-5.

A.2 Chapter 2

A.2.1 Supplementary Scheme A2.1 and description

Guanidinylation reagent **2.6**[1] was synthesized from amine **2.41** (prepared according to a reported protocol[2]) and isothiourea derivate **2.42** (synthesized according to a described procedure[3]). For this purpose, amine **2.41** was converted to an isocyanate by the aid of triphosgene followed by treatment with **2.42** (Scheme A2.1). For the synthesis of the diphenyl acetic acid derivatives **2.12** and **2.29**, benzophenones **2.43** and **2.44** were reduced to the secondary alcohols **2.45** and **2.46**, respectively, using sodium borohydride as reducing agent. The racemic alcohol **2.45** was converted to the chloride by the aid of thionyl chloride followed by the treatment with trimethylsilyl cyanide in the presence of perchlorostannane to afford the nitrile **2.15**. Noteworthily, for the conversion of racemic alcohol **2.46** to nitrile **2.47** under the same reaction conditions the formation of the chloride intermediate was not necessary. Cleavage of the methyl group in **2.15** and **2.47** and concomitant hydrolysis of the cyano group under strongly acidic conditions (47% aqueous HBr/glacial acidic acid 1:1 v/v) yielded the carboxylic acids **2.17** and **2.48**, respectively (Note: the synthesis of **2.17** from nitrile **2.15** is also shown in Scheme 2.2). Esterification of **2.17** and **2.48** with methanol gave compounds **2.49** and **2.50**, respectively. Alkylation of **2.49** and **2.50** at the phenolic hydroxy group by bromide **2.24** using Cs_2CO_3 as base yielded **2.51** and **2.52**, respectively, which were subjected to ester hydrolysis yielding **2.12** and **2.29**. Conversion of amine **2.53** to an isocyanate followed by the treatment of **2.42** yielded the guanidinylating reagent **2.54**. Compound **2.54** was used to prepare (*R*)-arginine derivative **2.56** from (*R*)-ornithine derivative **2.55** (synthesized according to a reported procedure[4]). Concomitant cleavage of the benzyl ester and removal of the Cbz group in **2.56** by hydrogenolysis followed by propionylation at the primary amino group using succinimidyl ester **2.8** yielded (*R*)-arginine derivative **2.28**.

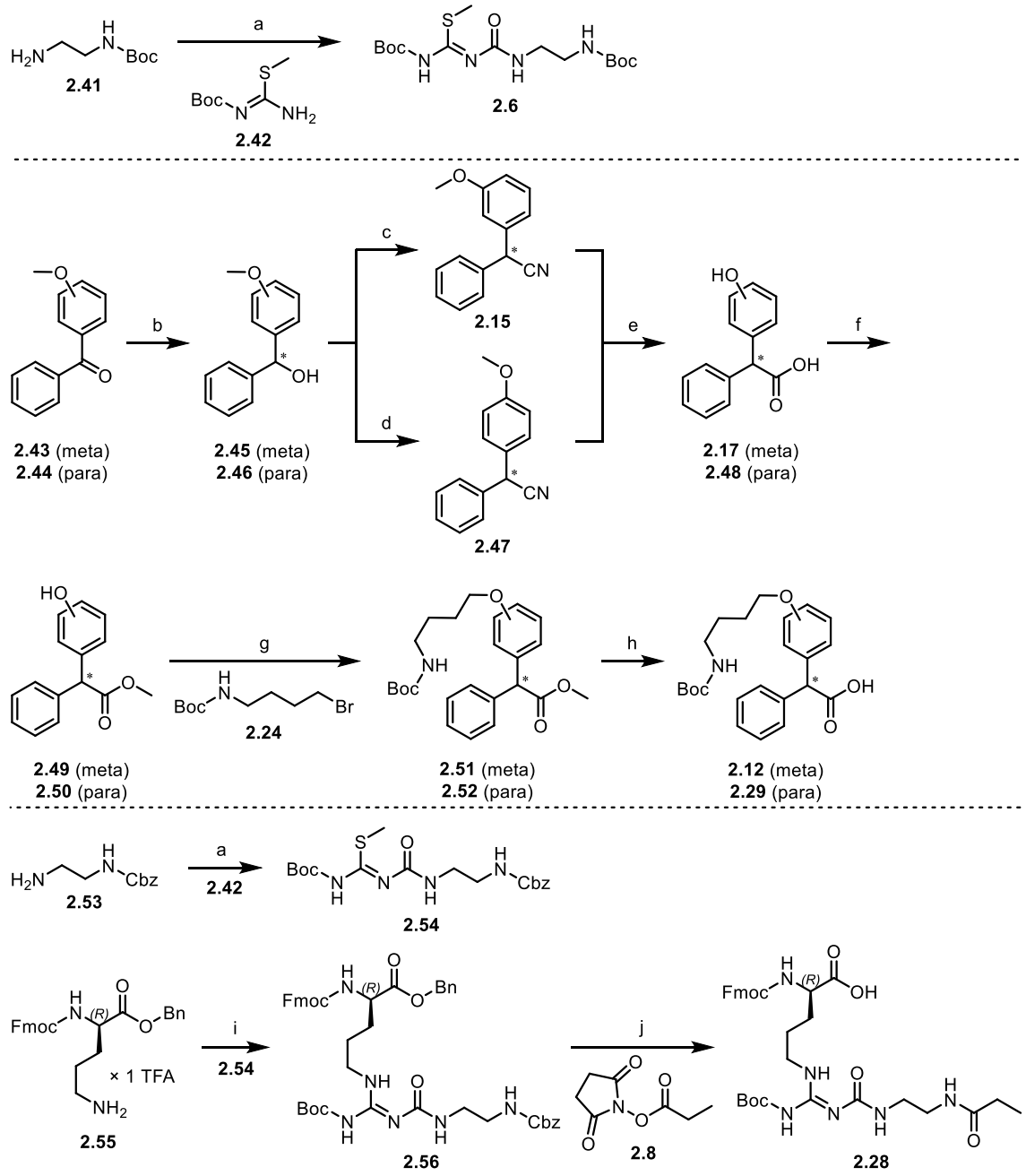

Scheme A2.1. Synthesis of compounds **2.6**, **2.12**, **2.15**, **2.28** and **2.29**. The asterisks in **2.12**, **2.15**, **2.17**, **2.29** and **2.45-2.52** indicate racemic mixtures. Reagents and conditions: a) (1) triphosgene, $NaHCO_3$, H_2O/CH_2Cl_2, 0 or 4 °C, 15 or 20 min; (2) DIPEA, rt, 15 min; 51% (**2.6**), 63% (**2.54**); b) $NaBH_4$, methanol, 0 °C, 10 or 90 min, 99% (**2.45**), 94% (**2.46**); c) (1) thionyl chloride, CH_2Cl_2, 0 °C, 3 h; (2) trimethylsilyl cyanide, $SnCl_4$, CH_2Cl_2, -10 °C to rt, 17 h, 54%; d) trimethylsilyl cyanide, $SnCl_4$, CH_2Cl_2, 0 °C, 2.5 h, 89%; e) aq. HBr (47%), glacial acetic acid, H_2O, reflux, 16 or 48 h, 75% (**2.17**), 55% (**2.48**); f) conc. H_2SO_4, methanol, reflux, 2 or 24 h, 96% (**2.49**), 89% (**2.50**); g) Cs_2CO_3, DMF, 2 or 24 h, rt; 64% (**2.51**), 79% (**2.52**); h) LiOH, methanol/H_2O, rt, 16 or 36 h, 84% (**2.12**), 85% (**2.29**); i) mercury(II) chloride, DIPEA, CH_2Cl_2, rt, 2 h, 84%; j) (1) H_2, Pd/C, trifluoroethanol, rt, 3 h; (2) DIPEA, rt, 1 h, 62%.

A.2.2 Synthesis procedures and analytical data of compounds 2.6, 2.12, 2.15, 2.28, 2.29, 2.43-2.54 and 2.56-2.58

N-*tert*-Butoxycarbonyl-*N'*-(2-(*tert*-butyloxycarbonylamino)ethyl)aminocarbonyl-*S*-methylisothiourea[1] (2.6)

The previously reported guanidinylation reagent **2.6**[1] was synthesized from amine **2.41** and isothiourea derivate **2.42** using an optimized procedure. A solution of $NaHCO_3$ (5.0 g, 59.5 mmol) in H_2O (50 mL) was added to a solution of **2.41** (2.7 g, 17.1 mmol) in CH_2Cl_2 (50 mL) and the biphasic mixture was cooled to 0 °C under vigorous stirring. Triphosgene (2.2 g, 7.5 mmol) was added and stirring was continued at 0 °C for 20 min. The organic layer was transferred into a round-bottom flask followed by the addition of **2.42** (4.2 g, 22.3 mmol) and DIPEA (2.9 mL, 17.1 mmol). Stirring was continued for 15 min at rt. The mixture was washed with H_2O (3 × 50 mL), the organic layer was dried over Na_2SO_4, and the solvent was removed by rotary evaporation. The crude product was purified by column chromatography (light petroleum/ethyl acetate 5:1 v/v to light petroleum/ethyl acetate 2:1 v/v) to yield **2.6** as a white solid (6.5 g, 8.7 mmol, 51%). TLC (light petroleum/ethyl acetate 2:1 v/v): R_f = 0.55. ^{1}H-NMR (400 MHz, DMSO-d_6): δ (ppm) 1.37 (s, 9H), 1.44 (s, 9H), 2.28 (s, 3H), 2.96-3.11 (m, 4H), 6.83 (t, *J* = 5.5, 1H), 7.74 (t, *J* = 5.3 Hz, 1H), 12.32 (br s, 1H). ^{13}C-NMR (100 MHz, DMSO-d_6): δ (ppm) 13.59, 27.59, 28.22, 39.34, 39.42, 77.66, 82.16, 150.19, 155.64, 161.59, 164.82. MS (LC-MS, ESI): *m/z* (%) 377.2 (100) $[M+H]^+$. $C_{15}H_{28}N_4O_5S$ (376.47).

(3-(4-((*tert*-Butoxycarbonyl)amino)butoxy)phenyl)(phenyl)acetic acid (2.12)

LiOH (960 mg, 40 mmol) was added to a stirred suspension of **2.51** (1.76 g, 4.0 mmol) in methanol (30 mL) and H_2O (30 mL) and the mixture was vigorously stirred at rt for 16 h. Methanol was removed by rotary evaporation and aqueous 1 N HCl was carefully added until precipitation of the product was completed. The product was extracted with ethyl acetate (150 mL), the organic layer was dried over Na_2SO_4, and the volatiles were removed *in vacuo* to yield **2.12** as a yellow solid (1.35 g, 3.4 mmol, 84%), which was used without further purification. TLC (light petroleum/ethyl acetate 2:1 v/v): R_f = 0.25. ^{1}H-NMR (400 MHz, DMSO-d_6): δ (ppm) 1.37 (s, 9H), 1.45-1.55 (m, 2H), 1.62-1.70 (m, 2H), 2.91-2.99 (m, 2H), 3.88-3.93 (m, 2H), 5.01 (s, 1H), 6.79-6.90 (m, 4H), 7.19-7.27 (m, 2H), 7.30-7.34 (m, 4H), 12.70 (br s, 1H). ^{13}C-NMR (100 MHz, DMSO-d_6): δ (ppm) 26.58, 26.61, 28.74, 40.00, 56.60, 67.62, 77.83, 112.79, 115.57, 121.07, 127.31, 128.82, 128.92, 129.88, 139.89, 141.37, 156.07, 159.04, 173.74. MS (LC-HRMS, ESI): *m/z* $[M+Na]^+$ calcd for $[C_{23}H_{29}NNaO_5]^+$ 422.1938, found 422.1939. $C_{23}H_{29}NO_5$ (399.49).

(3-Methoxyphenyl)(phenyl)acetonitrile[4] (2.15)

Under an atmosphere of dry nitrogen, a stirred solution of **2.45** (22.2 g, 106.3 mmol) in CH_2Cl_2 (250 mL) was cooled to 0 °C in an oven-dried Schlenk flask. Thionyl chloride (11.3 mL, 155.4 mmol) was added and the mixture was stirred at 0 °C for 3 h. The volatiles were removed *in vacuo*, the resulting red oil (crude 1-(chloro(phenyl)methyl)-3-methoxybenzene) was dissolved in anhydrous CH_2Cl_2 (250 mL) and the mixture was cooled to −10 °C. Trimethylsilyl cyanide (13.0 mL, 103.6 mmol) was added followed by the dropwise addition of a solution of $SnCl_4$ (6.1 mL, 51.8 mmol) in anhydrous CH_2Cl_2 (250 mL) over a period of 1 h. The dark red solution was allowed to warm up to rt and stirring was continued for 16 h. The reaction was quenched by the careful addition of methanol (20 mL) and the mixture was treated with H_2O (300 mL). The organic layer was separated, washed with H_2O (3 × 150 mL) and dried over Na_2SO_4. The solvent was removed by rotary evaporation. The product was purified by column chromatography (light petroleum/ethyl acetate 20:1 v/v) to yield **2.15** as a yellow oil (12.6 g, 56.2 mmol, 54%). TLC (light petroleum/ethyl acetate 4:1 v/v): R_f = 0.65. ^{1}H-NMR (300 MHz, DMSO-d_6): δ (ppm) 3.74 (s, 3H), 5.77 (s, 1H), 6.89-7.00 (m, 3H), 7.29-7.45 (m, 6H). ^{13}C-NMR (75 MHz, DMSO-d_6): δ (ppm) 40.70, 55.19, 113.17, 113.49, 119.54, 120.32, 127.45, 128.05, 129.20, 130.42, 136.56, 138.08, 159.64. MS (GC-MS, EI): *m/z* (%) 223.1 (100) $[M]^{+\cdot}$. $C_{15}H_{13}NO$ (223.28).

***N*$^{\alpha}$-Fluoren-9-ylmethoxycarbonyl-*N*$^{\omega}$-(2-(propionylamino)ethyl)aminocarbonyl-*N*$^{\omega'}$-*tert*-butoxycarbonyl-(*R*)-arginine (2.28)**

Palladium on activated charcoal (10 wt %, 200 mg) was added to a stirred solution of **2.56** (1.8 g, 2.3 mmol) in trifluoroethanol (50 mL). The mixture was vigorously stirred under an atmosphere of hydrogen (1 bar) at rt for 3 h. The catalyst was filtered off and washed with trifluoroethanol (2 × 20 mL). DIPEA (1.4 mL, 7.9 mmol) and **2.8** (0.42 mg, 2.26 mmol) were added and the mixture was stirred at rt for 1 h. The solvent was removed by rotary evaporation and the product was purified by column chromatography (acetonitrile/ethanol/acetic acid 2000:80:1 v/v/v to acetonitrile/ethanol/acetic acid 500:75:1 v/v/v). The eluate was concentrated to approx. 100 mL by rotary evaporation and H_2O (400 mL) was added. Lyophilisation yielded **2.28** as a white fluffy solid (0.89 g, 1.39 mmol, 62%). TLC (methanol/ethanol/acetic acid 50:5:1 v/v/v): R_f = 0.74. ^{1}H-NMR (400 MHz, $CDCl_3$): δ (ppm) 1.11 (t, *J* = 7.6 Hz, 3H), 1.49 (s, 9H), 1.69-1.88 (m, 3H), 1.93-2.05 (m, 1H), 2.23 (q, *J* = 7.6 Hz, 2H), 3.33-3.48 (m, 4H), 3.52-3.62 (m, 2H), 4.22 (t, *J* = 6.9 Hz, 1H), 4.27-4.46 (m, 3H), 5.98-6.04 (m, 1H), 6.69-6.78 (m, 1H), 6.79-6.87 (m, 1H), 7.30 (t, *J* = 7.5 Hz, 2H), 7.39 (t, *J* = 7.5 Hz, 2H), 7.57-7.64 (m, 2H), 7.75 (d, *J* = 7.5 Hz, 2H), 8.61 (s, 1H), 9.08 (s, 1H), 12.30 (br s, 1H). ^{13}C-NMR (100 MHz, $CDCl_3$): δ (ppm) 9.98, 25.42, 28.05, 28.09, 29.73, 39.19, 39.23, 40.48, 47.39, 54.21, 66.93, 77.37, 120.21,

125.27, 127.19, 127.84, 141.46, 144.13, 152.69, 153.81, 155.25, 156.33, 170.95, 175.37. MS (LC-MS, ESI): *m/z* (%) 639.3 (100) $[M+H]^+$. $C_{32}H_{42}N_6O_8$ (638.72).

(4-(4-((*tert*-Butoxycarbonyl)amino)butoxy)phenyl)(phenyl)acetic acid (2.29)

LiOH (185 mg, 7.7 mmol) was added to a suspension of **2.52** (1.1 g, 2.6 mmol) in methanol (50 mL) and H_2O (50 mL) and the reaction mixture was stirred at rt for 36 h. Methanol was removed by rotary evaporation and H_2O (100 mL) was added. Under stirring, the mixture was carefully acidified to pH 3 by the addition of aqueous 1 N HCl followed by treatment with ethyl acetate (3 × 30 mL). The combined organic layers were dried over Na_2SO_4, and the solvent was removed by rotary evaporation. H_2O (200 mL) and acetonitrile (50 mL) were added. Lyophilisation yielded **2.29** as a white solid (0.87 mg, 2.2 mmol, 85%). TLC (light petroleum/ethyl acetate 2:1 v/v): R_f = 0.20. ^{1}H-NMR (300 MHz, DMSO-d_6): δ (ppm) 1.36 (s, 9H), 1.43-1.55 (m, 2H), 1.60-1.71 (m, 2H), 2.90-2.99 (m, 2H), 3.91 (t, *J* = 6.3 Hz, 2H), 4.97 (s, 1H), 6.82-6.90 (m, 3H), 7.18-7.34 (m, 7H), 12.68 (br s, 1H). ^{13}C-NMR (75 MHz, DMSO-d_6): δ (ppm) 26.10, 26.18, 28.30, 39.54, 55.49, 67.12, 77.40, 114.28, 126.74, 128.36, 128.38, 129.55, 131.45, 140.00, 155.61, 157.49, 173.73. MS (LC-HRMS, ESI): *m/z* $[M+Na]^+$ calcd for $[C_{23}H_{29}NNaO_5]^+$ 422.1938, found 422.1937. $C_{23}H_{29}NO_5$ (399.49).

(3-Methoxyphenyl)(phenyl)methanone[5] (2.43)

A stirred solution of 3-methoxybenzoic acid (30.0 g, 197 mmol) and thionyl chloride (21.5 mL, 296 mmol) in a mixture of anhydrous DMF (1 mL, 13.0 mmol) and anhydrous CH_2Cl_2 (150 mL) was refluxed in an oven-dried Schlenk flask under an atmosphere of dry nitrogen for 3 h. The volatiles were removed *in vacuo*, the resulting yellow oil (crude 3-methoxybenzoyl chloride) was dissolved in anhydrous benzene (150 mL) and the mixture was cooled to 0 °C. Aluminum chloride (31.1 g, 256 mmol) was added in small portions over a period of 1 h. The stirred suspension was allowed to warm up to rt and stirring was continued for 16 h. The mixture was cooled to 0 °C and quenched by the careful addition of ice-cold H_2O (150 mL) followed by treatment with ethyl acetate (200 mL). The organic layer was washed with brine (200 mL), dried over Na_2SO_4, and the solvent was removed by rotary evaporation. The crude product was purified by column chromatography (light petroleum/ethyl acetate 12:1 v/v) to yield **2.43** as a yellow oil (31.4 g, 148 mmol, 75%). TLC (light petroleum/ethyl acetate 10:1 v/v): R_f = 0.55. ^{1}H-NMR (300 MHz, DMSO-d_6): δ (ppm) 3.86 (s, 3H), 7.22-7.28 (m, 3H), 7.44-7.51 (m, 1H), 7.53-7.60 (m, 2H), 7.65-7.77 (m, 3H). ^{13}C-NMR (75 MHz, DMSO-d_6): δ (ppm) 55.22, 113.99, 118.51, 122.08, 128.46, 129.50, 129.60, 132.64, 136.87, 138.27, 159.08, 195.42. MS (GC-MS, EI): *m/z* (%) 212.1 (100) $[M]^{+\cdot}$.$C_{14}H_{12}O_2$ (212.25).

(4-Methoxyphenyl)(phenyl)methanone[6] (2.44)

Under an atmosphere of dry nitrogen, a stirred solution of 4-methoxybenzoic acid (10.0 g, 66.0 mmol) in thionyl chloride (100 mL) and anhydrous DMF (1 mL, 13.0 mmol) was refluxed in an oven-dried Schlenk flask for 16 h. Excess thionyl chloride was removed by distillation under reduced pressure. The yellow residue (crude 4-methoxybenzoyl chloride) was suspended in anhydrous benzene (100 mL) and the mixture was cooled to 0 °C. Aluminum chloride (13.2 g, 99.0 mmol) was added in small portions, the suspension was allowed to warm up to rt and stirring was continued for 16 h. The mixture was cooled to 0 °C and the reaction was quenched by the careful addition of ice-cold H_2O (50 mL). The mixture was treated with ethyl acetate (2 × 200 mL), the combined organic layers were washed with saturated $NaHCO_3$ (200 mL) and dried over Na_2SO_4. The solvent was removed by rotary evaporation and the product was purified by column chromatography (light petroleum/ethyl acetate 9:1 v/v) to yield **2.44** as a white solid (7.8 g, 36.7 mmol, 56%). TLC (light petroleum/ethyl acetate 4:1 v/v): R_f = 0.55. ^{1}H-NMR (400 MHz, DMSO-d_6): δ (ppm) 3.86 (s, 3H), 7.07-7.12 (m, 2H), 7.52-7.58 (m, 2H), 7.63-7.70 (m, 3H), 7.73-7.77 (m, 2H). ^{13}C-NMR (100 MHz, DMSO-d_6): δ (ppm) 55.58, 113.92, 128.44, 129.23, 129.36, 132.08, 132.16, 137.76, 162.97, 194.42. MS (GC-MS, EI): *m/z* (%) 135.0 (100) $[M\text{-}C_6H_5]^+$, 212.1 (52) $[M]^{+\cdot}$. $C_{14}H_{12}O_2$ (212.25).

(3-Methoxyphenyl)(phenyl)methanol[7] (2.45)

A stirred solution of **2.43** (31.4 g, 148 mmol) in methanol (300 mL) was cooled to 0 °C and $NaBH_4$ (6.2 g, 163 mmol) was added in small portions over a period of 30 min. The mixture was allowed to warm up to rt and stirring was continued for 1 h. The solvent was removed by rotary evaporation, the residue was suspended in brine (300 mL) and the product was extracted with CH_2Cl_2 (2 × 300 mL). The combined organic layers were washed with H_2O (200 mL) and dried over Na_2SO_4. The volatiles were removed *in vacuo* to yield **2.45** as a yellow oil (31.5 g, 147 mmol, 99%), which was used without further purification. TLC (light petroleum/ethyl acetate 4:1 v/v): R_f = 0.45. ^{1}H-NMR (400 MHz, DMSO-d_6): δ (ppm) 3.72 (s, 3H), 5.67 (d, *J* = 3.8 Hz, 1H), 5.88 (d, *J* = 3.9 Hz, 1H), 6.74-6.79 (m, 1H), 6.90-6.95 (m, 1H), 6.96-6.98 (m, 1H), 7.17-7.24 (m, 2H), 7.26-7.32 (m, 2H), 7.35-7.40 (m, 2H). ^{13}C-NMR (100 MHz, DMSO-d_6): δ (ppm) 54.92, 74.13, 111.85, 111.88, 118.50, 126.21, 126.69, 128.02, 129.10, 145.60, 147.37, 159.12. MS (GC-MS, EI): *m/z* (%) 214.1 (100) $[M]^{+\cdot}$. $C_{14}H_{14}O_2$ (214.26).

(4-Methoxyphenyl)(phenyl)methanol[7] (2.46)

$NaBH_4$ (454 mg, 12.0 mmol) was added in small portions to a cooled (0 °C) stirred solution of **2.44** (4.0 g, 18.8 mmol) in methanol (100 mL) and the mixture was stirred at 0 °C for 10 min. The solvent was removed by rotary evaporation and the residue was suspended in brine

(100 mL) followed by treatment with ethyl acetate (2 × 100 mL). The combined organic layers were washed with brine (150 mL), dried over $MgSO_4$ and the volatiles were removed *in vacuo* to yield **2.46** as a white solid (3.8 g, 17.6 mmol, 94%), which was used without further purification. TLC (light petroleum/ethyl acetate 3:1 v/v): R_f = 0.50. ^{1}H-NMR (400 MHz, DMSO-d_6): δ (ppm) 3.71 (s, 3H), 5.64 (d, *J* = 4.1 Hz, 1H), 5.76 (d, *J* = 4.1 Hz, 1H), 6.83-6.87 (m, 2H), 7.16-7.21 (m, 1H), 7.24-7.32 (m, 4H), 7.32-7.37 (m, 2H). ^{13}C-NMR (100 MHz, DMSO-d_6): δ (ppm) 55.00, 73.78, 113.41, 126.11 126.52, 127.42, 127.97, 137.87, 146.00, 158.06. MS (GC-MS, EI): *m/z* (%) 109.1 (100), 135.0 (69) $[M-C_6H_7]^+$, 214.1 (48) $[M]^{+\cdot}$. $C_{14}H_{14}O_2$ (214.26).

(4-Methoxyphenyl)(phenyl)acetonitrile (2.47)

Under an atmosphere of dry nitrogen, a stirred solution of **2.46** (3.0 g, 14.0 mmol) in anhydrous CH_2Cl_2 (100 mL) was cooled to 0 °C in an oven-dried Schlenk flask. Trimethylsilyl cyanide (2.3 mL, 18.2 mol) was added followed by the dropwise addition of a solution of $SnCl_4$ (3.3 mL, 28.0 mmol) in anhydrous CH_2Cl_2 (100 mL) over a period of 1 h. The mixture was stirred at 0 °C for 1.5 h and then carefully quenched by the addition of methanol (10 mL) and ice-cold H_2O (100 mL). The organic layer was separated, dried over Na_2SO_4 and the solvent was removed *in vacuo* to yield **2.47** as a white solid (2.8 g, 12.4 mmol, 89%), which was used without further purification. TLC (light petroleum/ethyl acetate 3:1 v/v): R_f = 0.60. ^{1}H-NMR (400 MHz, DMSO-d_6): δ (ppm) 3.74 (s, 3H), 5.73 (s, 1H), 6.96-6.98 (m, 2H), 7.28-7.44 (m, 7H). ^{13}C-NMR (100 MHz, DMSO-d_6): δ (ppm) 39.97, 55.18, 114.53, 120.56, 127.31, 127.81, 128.56, 128.68, 137.00, 158.87. MS (GC-MS, EI): *m/z* (%) 223.1 (100) $[M]^{+\cdot}$. $C_{15}H_{13}NO$ (223.28).

(4-Hydroxyphenyl)(phenyl)acetic acid (2.48)

A suspension of **2.47** (2.1 g, 9.4 mmol) in acetic acid (30 mL) and aqueous HBr (47%, 30 mL) was refluxed for 48 h. After cooling (rt), the mixture was treated with CH_2Cl_2 (2 × 50 mL), the combined organic layers were dried over Na_2SO_4 and the volatiles were removed *in vacuo* to yield **2.48** as a red solid (1.3 g, 5.2 mmol, 55%), which was used without further purification. TLC (light petroleum/ethyl acetate/acetic acid 67:33:1 v/v/v): R_f = 0.35. ^{1}H-NMR (400 MHz, DMSO-d_6): δ (ppm) 4.91 (s, 1H), 6.65-6.73 (m, 2H), 7.06-7.35 (m, 7H), 9.33 (s, 1H), 12.54 (br s, 1H). ^{13}C-NMR (100 MHz, DMSO-d_6): δ (ppm) 55.23, 114.84, 126.37, 128.01, 128.08, 129.20, 129.65, 137.72, 156.92, 178.36. MS (LC-MS, ESI): *m/z* (%) 183.1 (100) $[M-H-CO_2]^-$, 197.1 (23), 455.2 (18) $[2M-H]^-$. $C_{14}H_{12}O_3$ (228.25).

(3-Hydroxyphenyl)(phenyl)acetic acid methyl ester (2.49)

A stirred solution of **2.17** (2.0 g, 8.6 mmol) in methanol (30 mL) and conc. H_2SO_4 (0.75 mL, 14.1 mmol) was refluxed for 2 h. The mixture was cooled to rt, diluted with H_2O (200 mL) and treated with CH_2Cl_2 (2 × 100 mL). The combined organic layers were washed with H_2O

(100 mL), dried over Na_2SO_4 and the volatiles were removed *in vacuo* to yield **2.49** as a brown oil (2.0 g, 8.2 mmol, 96%), which was used without further purification. TLC (light petroleum/ethyl acetate 3:1 v/v): R_f = 0.75. ^{1}H-NMR (400 MHz, DMSO-d_6): δ (ppm) 3.66 (s, 3H), 5.10 (s, 1H), 6.62-6.73 (m, 1H), 6.69-6.73 (m, 2H), 7.08-7.13 (m, 1H), 7.23-7.36 (m, 5H), 9.40 (s, 1H). ^{13}C-NMR (100 MHz, DMSO-d_6): δ (ppm) 52.03, 55.58, 114.04, 115.26, 118.99, 127.00, 128.40, 128.43, 129.42, 138.92, 140.16, 157.39, 172.39. MS (LC-MS, ESI): *m/z* (%) 183.1 (100) $[M+H-C_2H_4O_2]^+$, 260.1 (98) $[M+NH_4]^+$, 243.1 (82) $[M+H]^+$. $C_{15}H_{14}O_3$ (242.27).

(4-Hydroxyphenyl)(phenyl)acetic acid methyl ester (2.50)

A stirred solution of **2.48** (0.94 mg, 4.1 mmol) and conc. H_2SO_4 (1.0 mL, 18.8 mmol) in methanol (100 mL) was refluxed for 24 h. The solvent was removed by rotary evaporation, the residue was suspended in H_2O (100 mL) and the mixture was treated with ethyl acetate (2 × 80 mL). The combined organic layers were dried over Na_2SO_4, and the solvent was evaporated. The product was purified by column chromatography (light petroleum/ethyl acetate 4:1 v/v) to yield **2.50** as a yellow oil (1.2 g, 4.6 mmol, 89%). TLC (light petroleum/ethyl acetate 3:1 v/v): R_f = 0.35. ^{1}H-NMR (300 MHz, DMSO-d_6): δ (ppm) 3.64 (s, 3H), 5.06 (s, 1H), 6.67-6.73 (m, 2H), 7.06-7.12 (m, 2H), 7.20-7.35 (m, 5H), 9.40 (s, 1H). ^{13}C-NMR (75 MHz, DMSO-d_6): δ (ppm) 52.04, 54.94, 115.23, 126.60, 128.30, 128.45, 129.18, 129.46, 139.58, 156.46, 172.84. MS (FD-MS): *m/z* (%) 242.1 (100) $[M]^{+\cdot}$. $C_{15}H_{14}O_3$ (242.27).

(3-(4-((*tert*-Butoxycarbonyl)amino)butoxy)phenyl)(phenyl)acetic acid methyl ester (2.51)

2.24 (1.8 g, 7.0 mmol) was added to a stirred suspension of **2.49** (1.7 g, 7.0 mmol) and Cs_2CO_3 (3.4 g, 10.5 mmol) in DMF (15 mL) and the mixture was stirred at rt for 2 h. H_2O (200 mL) was added followed by the treatment with CH_2Cl_2 (100 mL). The organic layer was separated, washed with H_2O (3 × 100 mL) and dried over Na_2SO_4. The solvent was removed by rotary evaporation. The product was purified by column chromatography (light petroleum/ethyl acetate 5:1 v/v) to yield **2.51** as a yellow resin (1.78 g, 4.46 mmol, 64%). TLC (light petroleum/ethyl acetate/acetic acid 75:25:1 v/v/v): R_f = 0.70. ^{1}H-NMR (400 MHz, DMSO-d_6): δ (ppm) 1.37 (s, 9H), 1.45-1.55 (m, 2H), 1.62-1.71 (m, 2H), 2.92-3.00 (m, 2H), 3.66 (s, 3H), 3.88-3.94 (m, 2H), 5.16 (s, 1H), 6.79-6.89 (m, 4H), 7.20-7.36 (m, 6H). ^{13}C-NMR (100 MHz, DMSO-d_6): δ (ppm) 26.08, 26.12, 28.24, 40.20, 52.04. 55.56, 67.07, 77.34, 112.58, 115.01, 120.47, 127.05, 128.37, 128.46, 129.53, 138.86, 140.33, 155.60, 158.65, 172.30. MS (LC-HRMS, ESI): *m/z* $[M+Na]^+$ calcd for $[C_{24}H_{31}NNaO_5]^+$ 436.2094, found 436.2096. $C_{24}H_{31}NO_5$ (413.51).

(4-(4-((*tert*-Butoxycarbonyl)amino)butoxy)phenyl)(pheny)acetic acid methyl ester (2.52)

Under an atmosphere of dry nitrogen, Cs_2CO_3 (2.2 g, 6.8 mmol) was added to a stirred solution of **2.50** (0.84 mg, 3.3 mmol) in anhydrous DMF (25 mL) in an oven-dried Schlenk flask and the

mixture was stirred at rt for 10 min. A solution of **2.24** (0.83 mg, 3.3 mmol) in anhydrous DMF (5 mL) was added dropwise over a period of 20 min and stirring was continued at rt for 24 h. Brine (100 mL) was added, and the mixture was treated with ethyl acetate (3 × 20 mL). The combined organic layers were washed with H_2O (3 × 20 mL), dried over Na_2SO_4 and the solvent was removed by rotary evaporation. The crude product was purified by column chromatography (light petroleum/ethyl acetate 3:1 v/v) to yield **2.52** as a yellow oil (1.1 g, 2.6 mmol, 79%). TLC (light petroleum/ethyl acetate 3:1 v/v): R_f = 0.30. ^{1}H-NMR (400 MHz, DMSO-d_6): δ (ppm) 1.36 (ppm) (s, 9H), 1.45-1.55 (m, 2H), 1.61-1.70 (m, 2H), 2.91-2.99 (m, 2H), 3.65 (s, 3H), 3.93 (t, *J* = 6.4 Hz, 2H), 5.12 (s, 1H), 6.76-6.80 (m, 1H), 6.80-6.94 (m, 2H), 7.18-7.34 (m, 7H). ^{13}C-NMR (100 MHz, DMSO-d_6): δ (ppm) 26.06, 26.13, 28.25, 39.51, 52.03, 54.58, 67.12, 77.37, 114.38, 126.93, 128.26, 128.44, 129.47, 130.80, 139.38, 155.59, 157.63, 172.66. MS (LC-HRMS, ESI): *m/z* $[M+Na]^+$ calcd for $[C_{24}H_{31}NNaO_5]^+$ 436.2094, found 436.2098. $C_{24}H_{31}NO_5$ (413.51).

_N_-Benzyloxycarbonyl-1,2-diaminoethane[8] (2.53)

A solution of benzyl O-succinimidyl carbonate (8.7 g, 35.0 mmol) in chloroform (350 mL) was added dropwise to a stirred solution of ethylenediamine (28.0 mL, 420 mmol) in chloroform (600 mL) at 0 °C over a period of 1 h. The mixture was washed with brine and saturated aqueous Na_2CO_3 (200 mL each). The aqueous layers were combined and treated with chloroform (200 mL). The organic layer was dried over $MgSO_4$, and the solvent was removed by rotary evaporation. The crude product was purified by column chromatography (CH_2Cl_2/methanol/7 N ammonia in methanol 75:25:1 v/v/v) to yield **2.53** as a yellow oil (4.9 g, 23.2 mmol, 66%). TLC (CH_2Cl_2/methanol/7 N ammonia in methanol 75:25:1 v/v/v): R_f = 0.75. ^{1}H-NMR (400 MHz, DMSO-d_6): δ (ppm) 2.54-2.60 (m, 2H), 2.96-3.03 (m 2H), 5.02 (s, 2H), 7.17-7.25 (m, 1H), 7.28-7.40 (m, 7H). ^{13}C-NMR (100 MHz, DMSO-d_6): δ (ppm) 41.56, 44.05, 65.18, 127.74, 128.33, 128.35, 137.24, 156.24. MS (LC-MS, ESI): *m/z* (%) 195.1 (100) $[M+H]^+$. $C_{10}H_{14}N_2O_2$ (194.23).

N-tert-Butoxycarbonyl-_N'_-(2-(benzyloxycarbonylamino)ethyl)aminocarbonyl-_S_-methylisothiourea (2.54)

A solution of $NaHCO_3$ (4.6 g, 55.6 mmol) in H_2O (50 mL) was added to a solution of **2.53** (3.6 g, 18.6 mmol) in CH_2Cl_2 (50 mL) and the biphasic mixture was cooled to 0 °C under vigorous stirring. Triphosgene (4.4 g, 8.4 mmol) was added and stirring was continued at 0 °C for 15 min. The organic layer was transferred into a round-bottom flask, **2.42** (6.6 g, 37.2 mmol) and DIPEA (3.0 mL, 18.6 mmol) was added and stirring was continued at rt for 15 min. The mixture was washed with H_2O (3 × 50 mL), the organic layer was dried over Na_2SO_4, and the solvent was removed by rotary evaporation. The product was purified by column chromatography (light

petroleum/ethyl acetate 4:1 v/v to light petroleum/ethyl acetate 1:1 v/v) to yield **2.54** as a white solid (4.8 g, 11.7 mmol, 63%). TLC (light petroleum/ethyl acetate 2:1 v/v) R_f = 0.20. ^{1}H-NMR (400 MHz, DMSO-d_6): δ (ppm) 1.44 (s, 9H), 2.28 (s, 3H), 3.04-3.16 (m, 4H), 5.01 (s, 2H), 7.27-7.38 (m, 7H), 7.76-7.85 (m, 1H). ^{13}C-NMR (100 MHz, DMSO-d_6): δ (ppm) 13.62, 27.60, 39.41 (interfering with the solvent residual peak, as identified by ^{1}H-^{13}C HSQC), 39.87 (interfering with the solvent residual peak, as identified by ^{1}H-^{13}C HSQC), 65.25, 82.19, 127.73, 127.77, 128.34, 137.17, 150.19, 156.18, 161.60, 164.95. MS (LC-HRMS, ESI): *m/z* (%) 411.1764 (100) $[M+H]^+$, calcd for $[C_{18}H_{27}N_4O_5S]^+$ 411.1697. $C_{18}H_{26}N_4O_5S$ (410.49).

N^{ω}-(2-(Benzyloxycarbonylamino)ethyl)aminocarbonyl-N^{α}-fluoren-9-ylmethoxycarbonyl-$N^{\omega'}$-*tert*-butoxycarbonyl-(*R*)-arginine benzyl ester (2.56)

Mercury(II) chloride (3.5 g, 12.9 mmol) and DIPEA (4.4 mL, 25.8 mmol) were added to a stirred solution of **2.55** (5.3 g, 9.5 mmol) and **2.54** (3.5 g, 8.6 mmol) in CH_2Cl_2 (400 mL). The reaction mixture was stirred at rt for 2 h. The precipitate was filtered off and washed with CH_2Cl_2 (2 × 100 mL). The solvent was removed by rotary evaporation and the product was purified by column chromatography (light petroleum/ethyl acetate 3:1 v/v to light petroleum/ethyl acetate 1:1 v/v) to yield **2.56** as a white solid (5.9 g, 7.3 mmol, 84%). TLC (light petroleum/ethyl acetate 2:1 v/v): R_f = 0.48. ^{1}H-NMR (400 MHz, DMSO-d_6, at least two rotamers, resulting in signal splitting, were evident): δ (ppm) 1.39-1.48 (m, 9H), 1.52-1.79 (m, 4H), 3.03-3.15 (m, 4H), 3.23-3.31 (m, 2H), 4.09-4.18 (m, 1H), 4.19-4.25 (m, 1H), 4.27-4.35 (m, 2H), 5.00-5.04 (m, 2H), 5.13 (s, 2H), 6.91-7.00 (m, 1H), 7.26-7.37 (m, 12H), 7.38-7.45 (m, 2H), 7.68-7.74 (m, 2H), 7.82-7.85 (m, 1H), 7.87-7.91 (m, 2H), 7.92-7.96 (m, 1H), 8.19-8.25 (m, 1H), 9.09-9.17 (m, 1H). ^{13}C-NMR (100 MHz, DMSO-d_6, at least two rotamers, resulting in signal splitting, were evident): δ (ppm) 25.33, 27.69/28.09, 27.80, 39.10, 39.20, 39.60 (last three signals interfering with the solvent residual peak, as identified by ^{1}H-^{13}C HSQC), 46.72, 53.58, 65.22, 65.29, 65.71/65.96, 82.03, 120.13, 125.24, 127.07, 127.65, 127.73, 127.74, 127.77, 128.01, 128.33/128.35, 128.39, 135.95, 137.13/137.20, 140.75, 143.74/143.84, 152.37, 153.21, 154.73, 156.17/156.21, 164.48, 172.11/172.18. MS (LC-HRMS, ESI): *m/z* $[M+H]^+$ calcd for $[C_{44}H_{51}N_6O_9]^+$ 807.3712, found 807.3737. $C_{44}H_{50}N_6O_9$ (806.92).

4-((1*E*,3*E*)-4-(4-(Dimethylamino)phenyl)buta-1,3-dien-1-yl)-2,6-dimethyl-1-propylpyridin-1-ium trifluoroacetate (2.57)

A solution of **2.31** (2.0 mg, 6.0 µmol) in DMF (80 µL) was added to a mixture of DIPEA (2.4 µL, 18.0 µmol) and propylamine (1.1 µL, 18 µmol) and the mixture was stirred at rt for 30 min. The reaction was quenched by the addition of 10% aqueous TFA (40 µL, 41.0 µmol) and the product was purified by preparative HPLC (system D, column: Actus Triart C18, 600 nm, 0-30 min, C/B 80:20-20:80, t_R(**2.57**) = 10 min) to yield **2.57** (0.21 mg, 0.48 µmol, 8%) as a dark

orange resin, which was stored at -20 °C under protection from light. MS (LC-HRMS, ESI): *m/z* $[M]^+$ calcd for $[C_{22}H_{29}N_2]^+$ 321.2325, found 321.2327. $C_{22}H_{29}N_2^+ \times C_2F_3O_2^-$ (434.50).

2-(6-(Dimethylamino)-3-(dimethyliminio)-3*H*-xanthen-9-yl)-5-(propylcarbamoyl)benzoate (2.58)

A solution of **2.34** (3.0 mg, 6.0 µmol) in DMF (80 µL) was added to a mixture of DIPEA (2.4 µL, 18.0 µmol) and propylamine (1.1 µL, 18 µmol) and the mixture was stirred at rt for 30 min. The reaction was quenched by the addition of 10% aqueous TFA (40 µL, 41.0 µmol) and the product was purified by preparative HPLC (system D, column: Actus Triart C18, 550 nm, 0-30 min, C/B 75:25-50:50, t_R(**2.58**) = 16 min) to yield **2.58** (1.09 mg, 2.3 µmol, 39%) as a pink resin, which was stored at −20 °C under protection from light. MS (LC-HRMS, ESI): *m/z* $[M+H]^+$ calcd for $[C_{28}H_{30}N_3O_4]^+$ 472.2231, found 472.2235. $C_{28}H_{29}N_3O_4$ (471.56).

A.2.3 Figures A2.1-A2.11

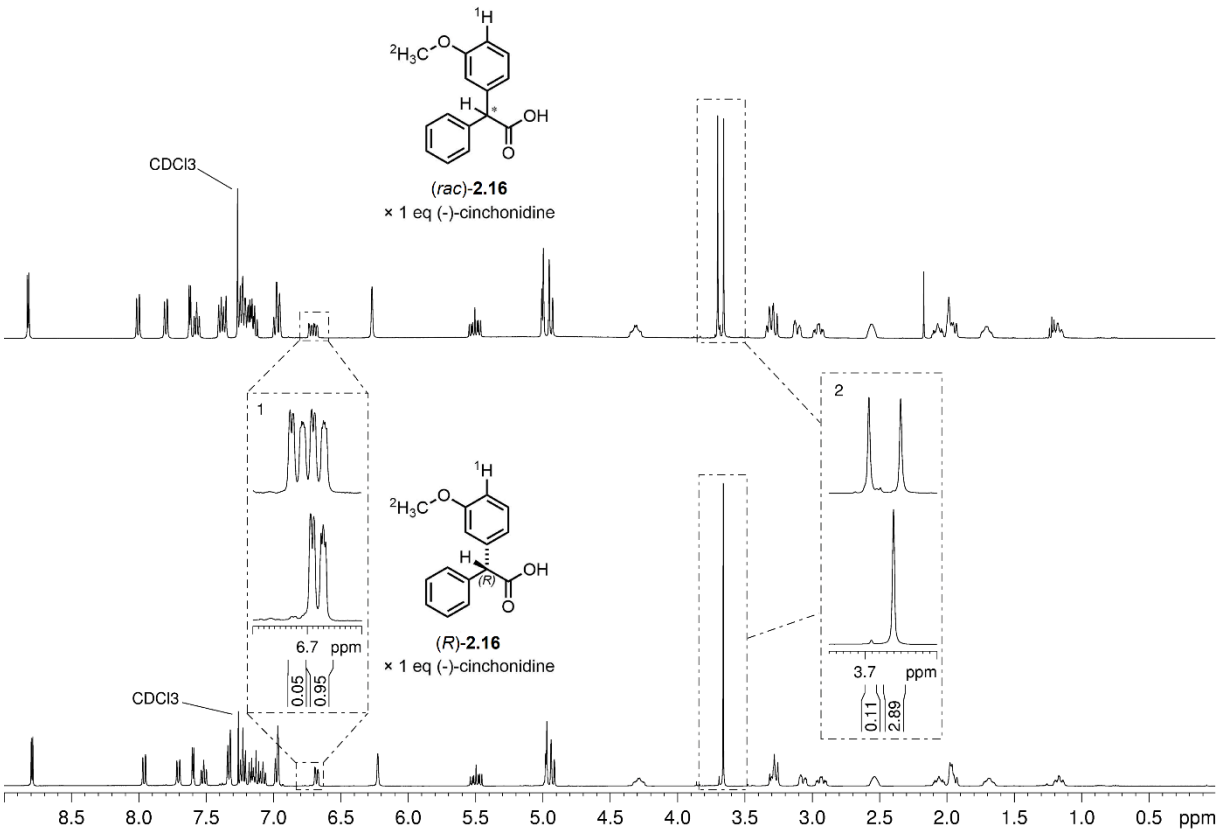

Figure A2.1. ^{1}H-NMR spectrum (400 MHz, $CDCl_3$) of enantiomerically pure (*R*)-**2.16** (bottom) in comparison to racemic **2.16** (top) each in the presence of 1 equivalent of (−)-cinchonidine. The presence of (−)-cinchonidine led to a separation of the denoted proton signals (1, 2) allowing the determination of an enantiomeric excess of 90% for (*R*)-**2.16**.

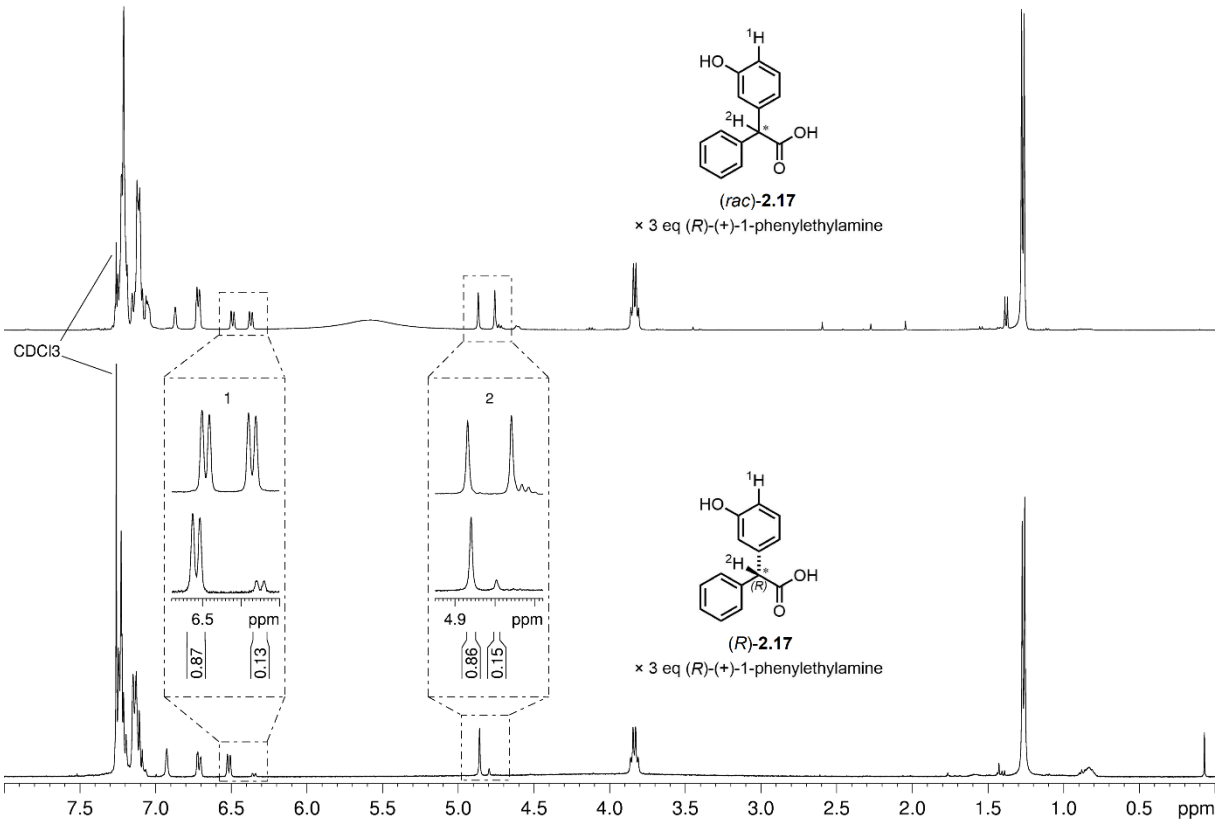

Figure A2.2. ^{1}H-NMR spectrum (400 MHz, $CDCl_3$) of (*R*)-**2.17**, obtained by treatment of (*R*)-**2.16** with BBr_3 (bottom), in comparison to racemic **2.17** (top) each in the presence of 3 equivalents of (*R*)-(+)-1-phenylethylamine. The presence of (*R*)-(+)-1-phenylethylamine led to a separation of the denoted proton signals (1, 2) revealing a decrease in enantiomeric purity from 90% *ee* ((*R*)-**2.16**) to 74% *ee* ((*R*)-**2.17**) caused by the BBr_3-mediated demethylation of (*R*)-**2.16**.

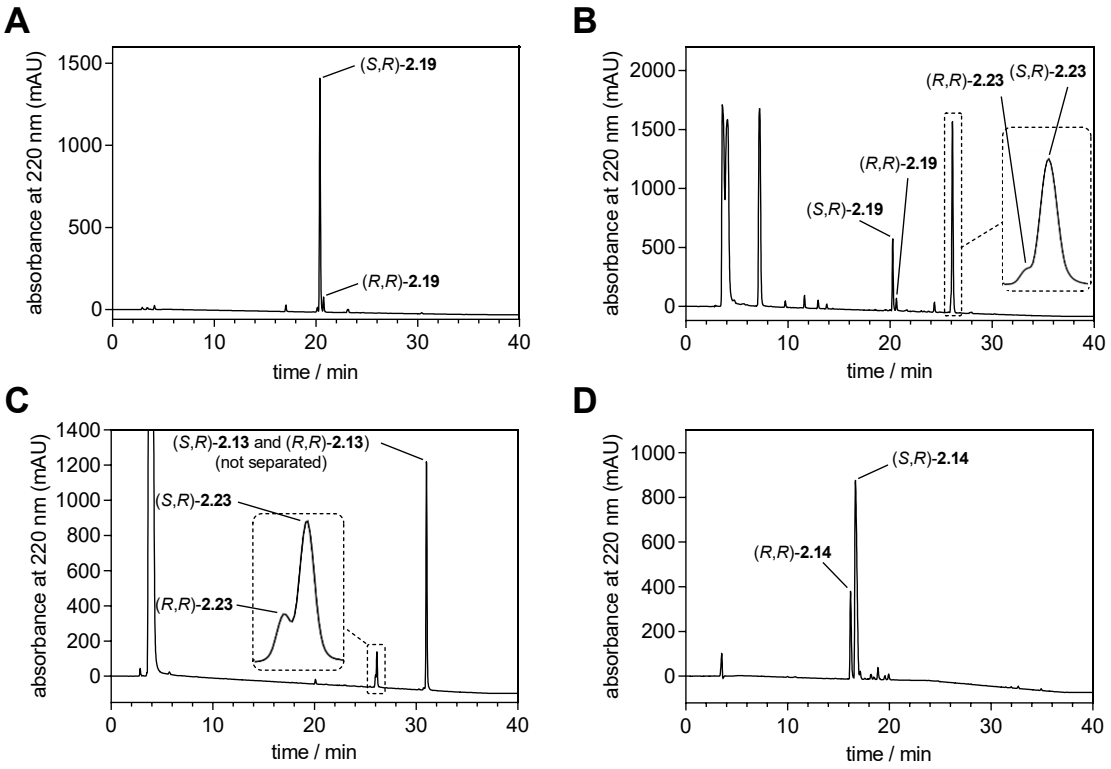

Figure A2.3. Chromatograms of the RP-HPLC analysis of (*S*,*R*)-**2.19**, **2.23**, (*S*,*R*)-**2.13** and (*S*,*R*)-**2.14**. (A) Chromatogram of the RP-HPLC analysis of (*S*,*R*)-**2.19** (90% de) used for the synthesis of (*S*,*R*)-**2.23** (step g in Scheme 2.2). (B) Chromatogram of the RP-HPLC analysis of crude (*S*,*R*)-**2.23** (prepared from (*S*,*R*)-**2.19** according to step g in Scheme 2.2) after a reaction time of 16 h, revealing epimerization at the methine carbon atom of the diphenyl acetyl moiety both in the starting material (*S*,*R*)-**2.19** and in the product (*S*,*R*)-**2.23**. (C) Chromatogram of the RP-HPLC analysis of crude (*S*,*R*)/(*R*,*R*)-**2.13** (prepared from (*S*,*R*)-**2.23** according to step h in Scheme 2.2) after a reaction time of 16 h, revealing ongoing epimerization of the remaining starting material (*S*,*R*)-**2.23**. Note: The diastereomers (*S*,*R*)-**2.13** and (*R*,*R*)-**2.13** could not be separated. (D) Chromatogram of the RP-HPLC analysis of crude (*S*,*R*)-**2.14** (prepared from (*S*,*R*)-**2.13** according to step j in Scheme 2.2) after a reaction time of 24 h, affording (*S*,*R*)-**2.14** and (*R*,*R*)-**2.14** in a diastereomeric ratio of 3:1 (50% de of (*S*,*R*)-**2.14** over (*R*,*R*)-**2.14**).

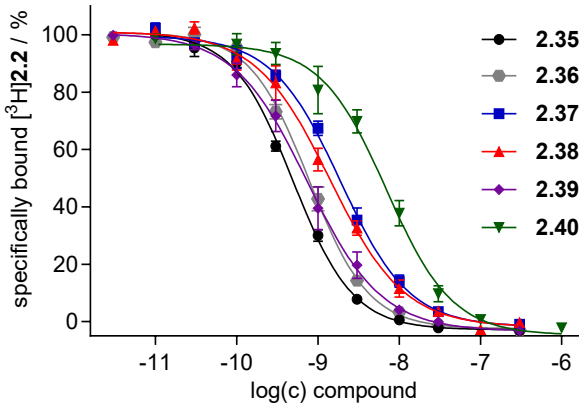

Figure A2.4. Radioligand displacement curves obtained from competition binding studies with [^{3}H]**2.2** (K_D = 0.044 nM, c = 0.15 nM)[1] and the fluorescent ligands **2.35-2.40** performed at intact SK-N-MC neuroblastoma cells. Data represent mean values ± SEM from at least three independent experiments performed in triplicate. The resulting pK_i values of **2.35-2.40** are presented in Table 2.1.

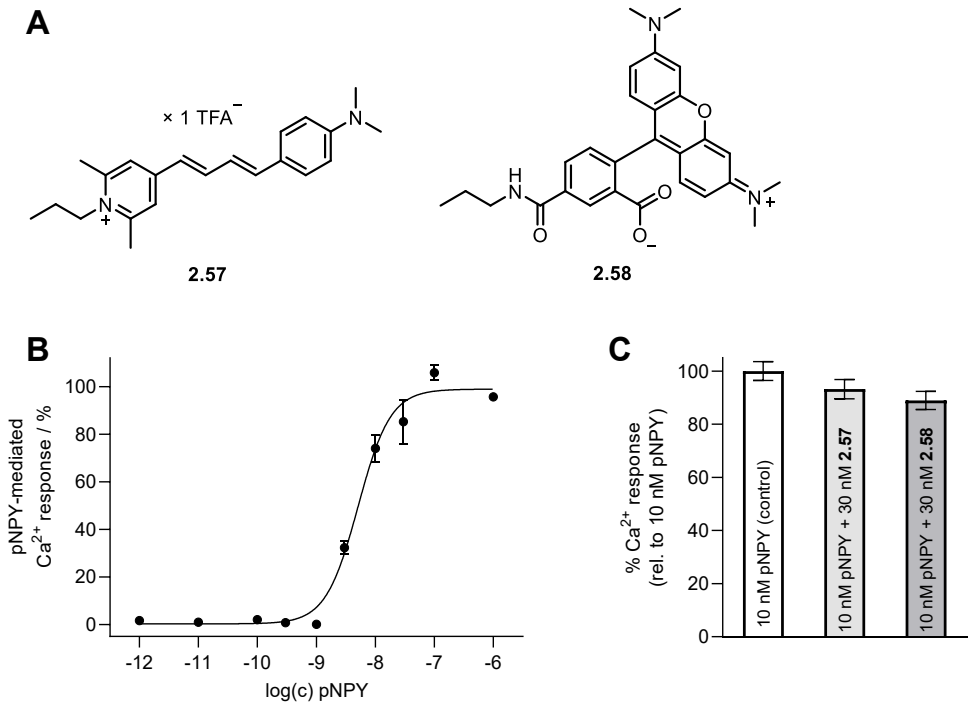

Figure A2.5. Y_1R Ca^{2+} assay: concentration-effect curve of pNPY and effect of 10 nM pNPY in the presence and absence of the fluorescent dummy ligands **2.57** and **2.58**. (A) Structures of the fluorescent dummy ligands **2.57** and **2.58**, representing the fluorescent moieties of the Py5-labeled fluorescent ligands **2.35** and **2.36**, and of the 5'-TAMRA-labeled fluorescent ligands **2.39** and **2.40**, respectively. (B) Concentration-effect curve of pNPY obtained from a Fura-2 Ca^{2+} assay using human erythroleukemia (HEL) cells (pEC_{50} = 8.29 ± 0.12, mean ± SEM from three individual experiments). (C) Comparison of the relative Ca^{2+} responses mediated by 10 nM pNPY in the absence (left bar, control experiment) and in the presence of **2.57** and **2.58** (30 nM each, central and right bar) (means ± SEM from six individual measurements). The presence of the dyes did not result in a significant change of the measured Ca^{2+} response (P > 0.4, Welch t-test), indicating that the optical readout of the assay (excitation: 340 or 380 nm, emission: 510 nm) was not impaired by the used dyes.

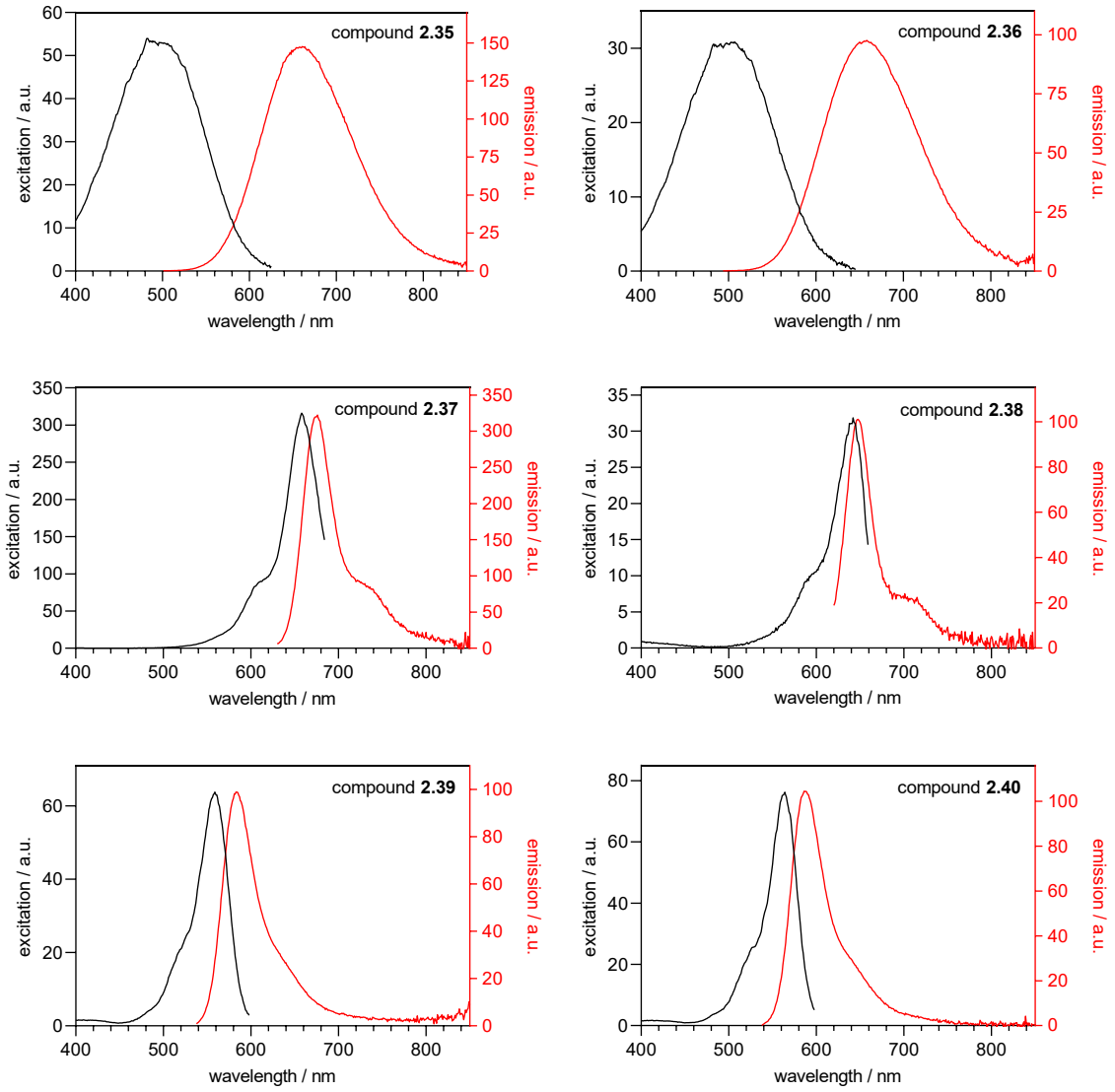

Figure A2.6. Excitation and corrected emission spectra of fluorescent ligands **2.35**-**2.40** recorded in PBS, pH 7.4, supplemented with 1% BSA, at 22 °C using fluorescent ligand concentrations of 6 µM (**2.35**, **2.36**) or 2 µM (**2.37**-**2.40**).

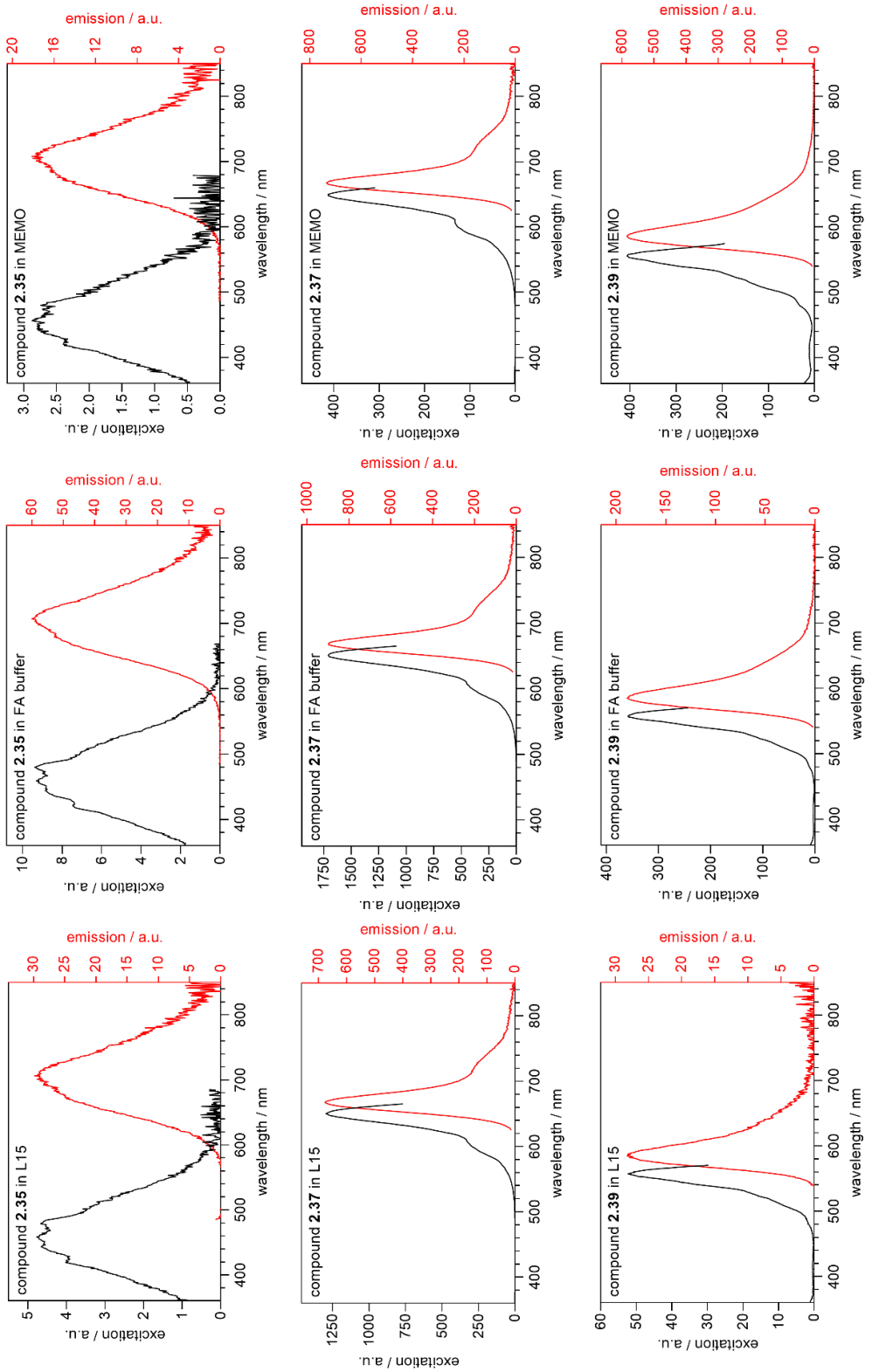

Figure A2.7. Excitation and corrected emission spectra of fluorescent ligands **2.35**, **2.37** and **2.39** recorded in L15, FA buffer (without protease inhibitor) and MEMO at 22 °C using fluorescent ligand concentrations of 6 µM (**2.35**), 2 µM (**2.37**) or 8 µM (**2.39**).

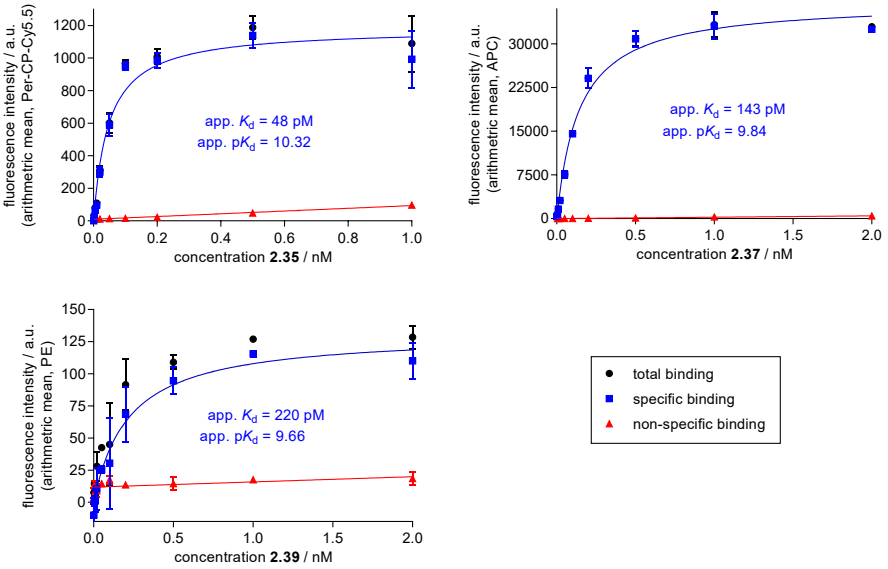

Figure A2.8. Representative Y_1R binding isotherms of the fluorescent ligands **2.35**, **2.37** and **2.39** obtained from flow cytometric saturation binding experiments (performed in duplicate at 22 °C) using intact human MCF-7-Y_1 mamma carcinoma cells (cell density: 1.0 × 10^5 cells/mL). Nonspecific binding was determined in the presence of **2.1** (10 µM). Total and nonspecific binding data represent mean values ± SEM. Specific binding data represent calculated values ± propagated error.

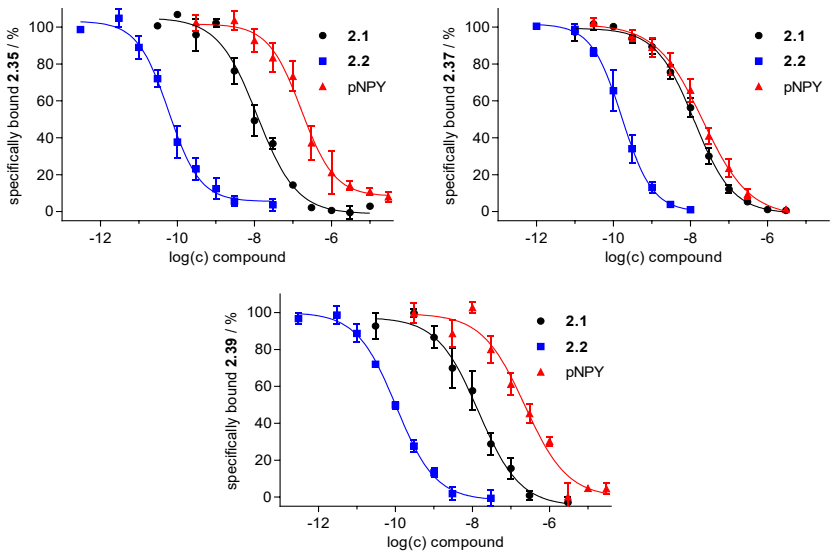

Figure A2.9. Displacement curves obtained from flow cytometric competition binding experiments performed at intact MCF-7-Y_1 cells with the fluorescent Y_1R ligands **2.35** (top left), **2.37** (top right) or **2.39** (bottom) displaced by **2.1** (black dots), **2.2** (blue squares) or pNPY (red triangles). Data represent mean values ± SEM from at least three independent experiments performed in duplicate. The concentrations of the probes were 0.25 nM (**2.35**) or 0.5 nM (**2.37**, **2.39**), and the cell density was 1.0 × 10^5 cells/mL. Cells were preincubated with the nonlabeled competing ligands for 10 min (**2.1**, **2.2**) or for 1 h (pNPY) before the addition of the fluorescent ligand. Incubations were performed at 22 °C in the dark for 2 h (**2.1**, **2.2**) or 4 h (pNPY). The resulting pK_i values of **2.1**, **2.2** and pNPY are presented in Table 2.4.

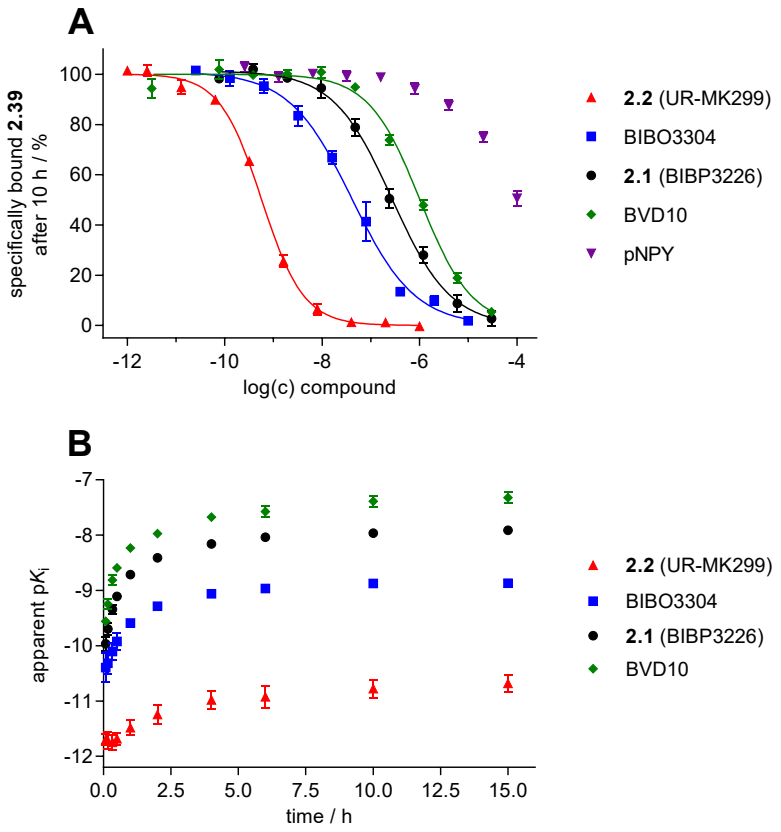

Figure A2.10. Fluorescent ligand displacement curves from fluorescence anisotropy-based Y_1R competition binding experiments performed with **2.39** and various Y_1R ligands at 26 °C using hY_1 receptor displaying BBV particles. (A) Displacement curves of **2.39** (0.1 nM) from competition binding experiments with **2.2** (red triangles), BIBO3304 (blue squares), **2.1** (black dots), BVD10 (green diamonds) and pNPY (purple triangles). Shown are data (mean values ± SEM from two independent experiments performed in duplicate) of snapshots at 10 h incubation from a total monitoring period of 15 h. The resulting pK_i values of **2.1**, **2.2**, BIBO3304 and BVD10 are presented in Table 2.4. The incomplete sigmoidal curve only allowed an estimation for the pK_i value of pNPY (< 6.0). (B) Time dependence of the pK_i values (calculated according to a previously described procedure[9]) obtained from the experiments described under A. Shown are mean values ± SEM from at least four independent experiments (performed in duplicate) carried out using a total fluorescent ligand concentration of 0.1 nM or 0.2 nM. After 10 h of incubation, no more change in pK_i was observed.

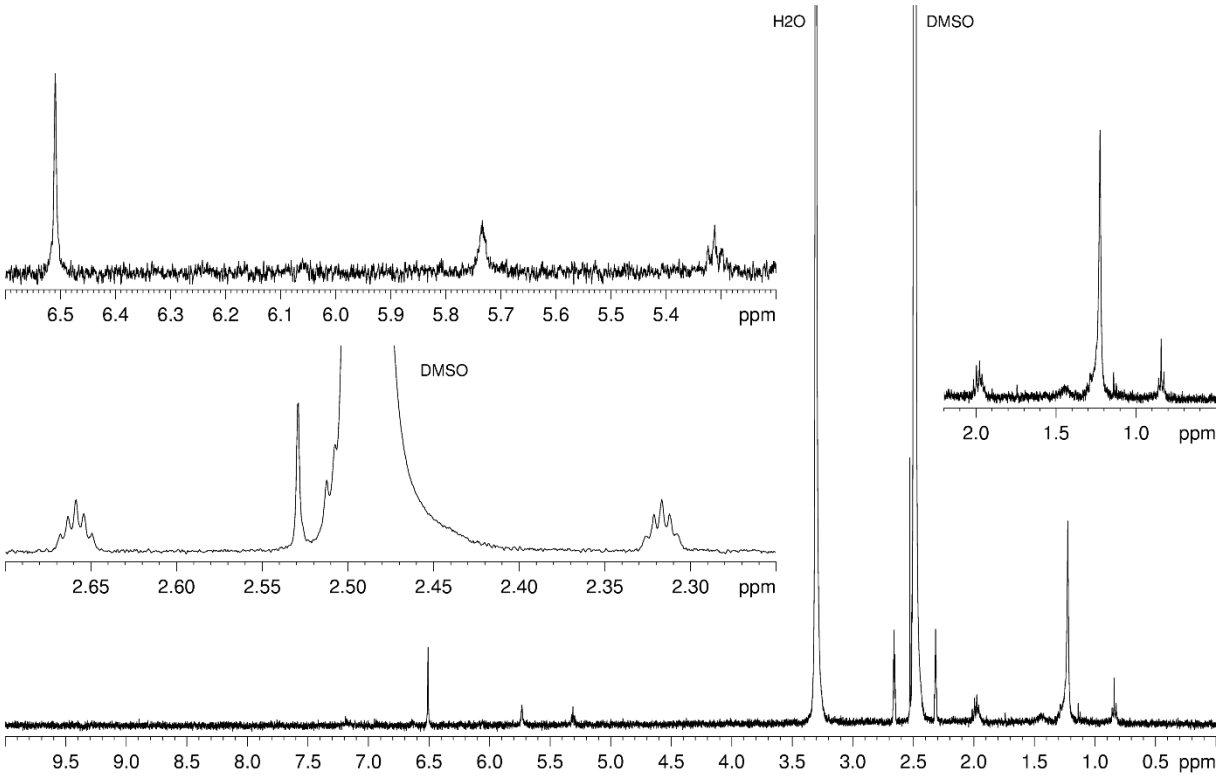

Figure A2.11. ^{1}H-NMR spectrum (400 MHz, DMSO-d_6) of a vehicle eluate from preparative HPLC (0.1% aq. TFA/acetonitrile ca. 40:60 v/v), which was processed (freeze drying, NMR sample preparation) as the eluates containing the fluorescent ligands. This control revealed characteristic system signals (0.81-0.87 ppm, 1.20-1.30 ppm), also present in the ^{1}H-NMR spectra of the fluorescent ligands.

A.2.4 X-ray crystallographic data of compound (*R*)-2.16

Selected crystallographic and refinement data for the X-ray crystal structure of compound (*R*)-**2.16**

Empirical formula	$C_{15}H_{14}O_3$
Formula weight	242.26
Crystal color / habit	colorless plate
T / K	100(2)
Crystal dimensions / mm^3	0.150 x 0.080 x 0.030
Crystal system	orthorhombic
Space group	$P\ 2_12_12_1$
a / Å	5.5437(2)
b / Å	8.4551(3)
c / Å	52.420(3)
V / $Å^3$	2457.05(17)
Z	8
F(000)	1024
Density (calcd) / g cm^{-1}	1.31
Absorption coefficient μ / mm^{-1}	739
Theta range / °	5.062 - 67.993
Index ranges	$-4 \leq h \leq 6$
	$-10 \leq k \leq 7$
	$-62 \leq l \leq 61$
Reflections collected	35814
Independent reflections	4448 (R_{int} = 0.0428)
Observed reflections	4448
Parameters/restraints	347/0
Goodness-of-fit	1.09
Largest difference peak and hole / e$Å^{-3}$	0.178 / -0.203
R1 (I>2σ(I))	0.0466
R1 (all data)	0.0520
wR2 (I>2σ(I))	0.1188
wR2 (all data)	0.1256
absolute structure parameter	-0.19(15)
corrected for absorption with	none
radiation	CuKα
wavelength	1.54178
collected with	STOE STADI VARI
CCDC Number	2095892

A.2.5 Chemical stability of the fluorescently labeled Y_1R ligands 2.35-2.40 in PBS

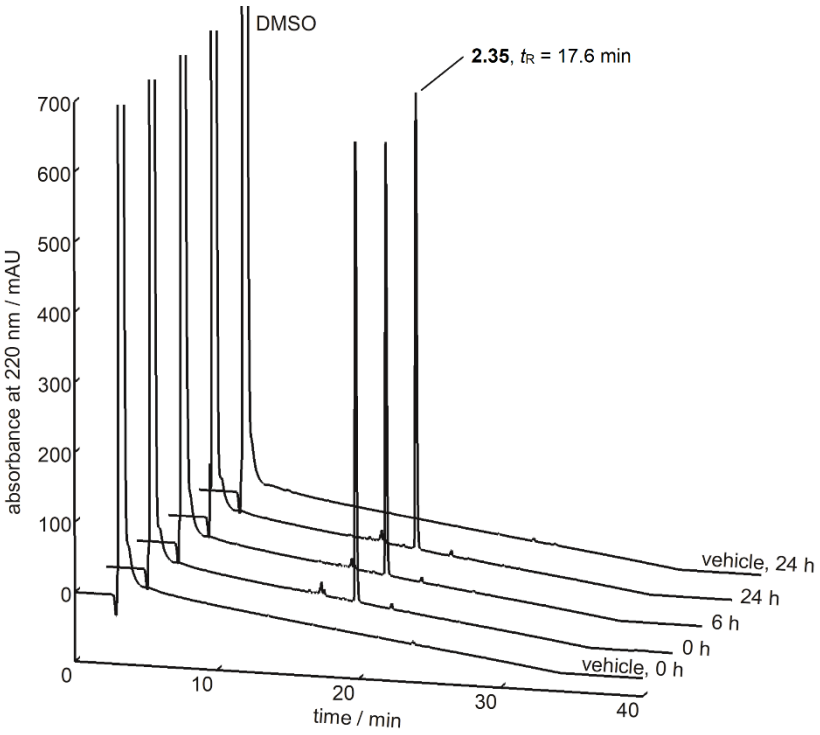

Chromatograms of the reversed-phase HPLC analysis of **2.35** after incubation in PBS pH 7.4 for up to 24 h. **2.35** showed no decomposition.

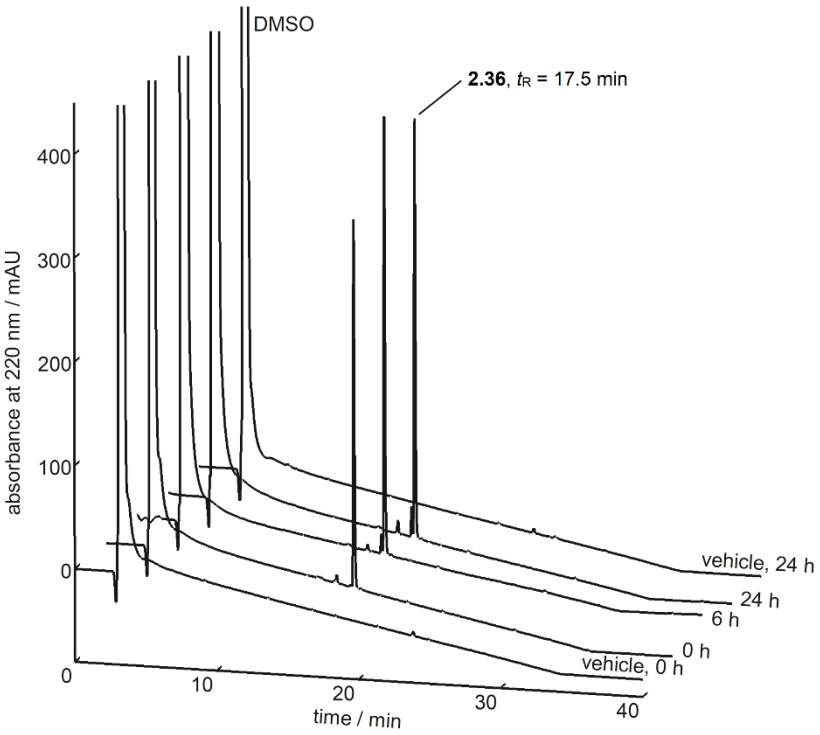

Chromatograms of the reversed-phase HPLC analysis of **2.36** after incubation in PBS pH 7.4 for up to 24 h. **2.36** showed slight decomposition.

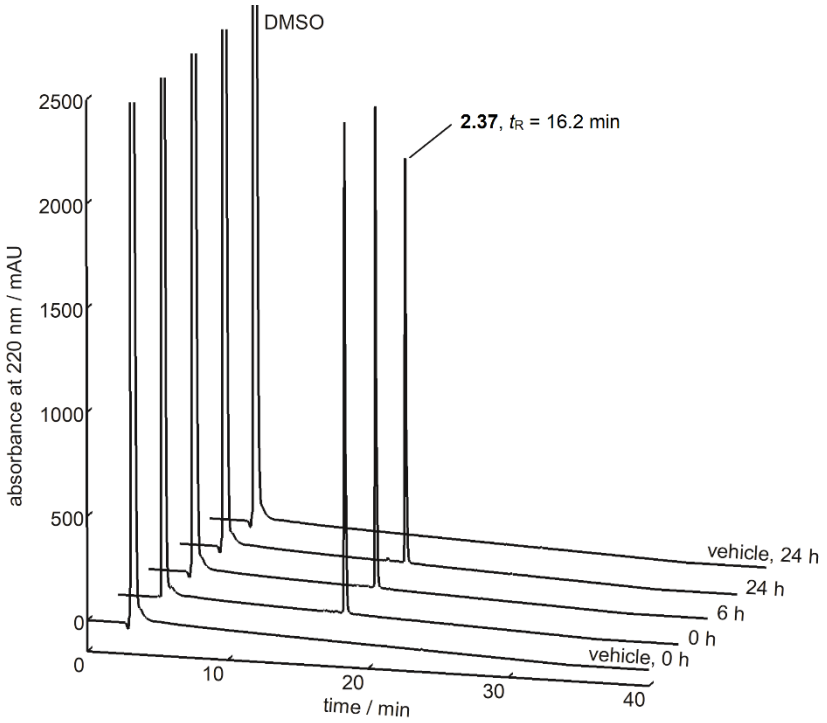

Chromatograms of the reversed-phase HPLC analysis of **2.37** after incubation in PBS pH 7.4 for up to 24 h. **2.37** showed no decomposition.

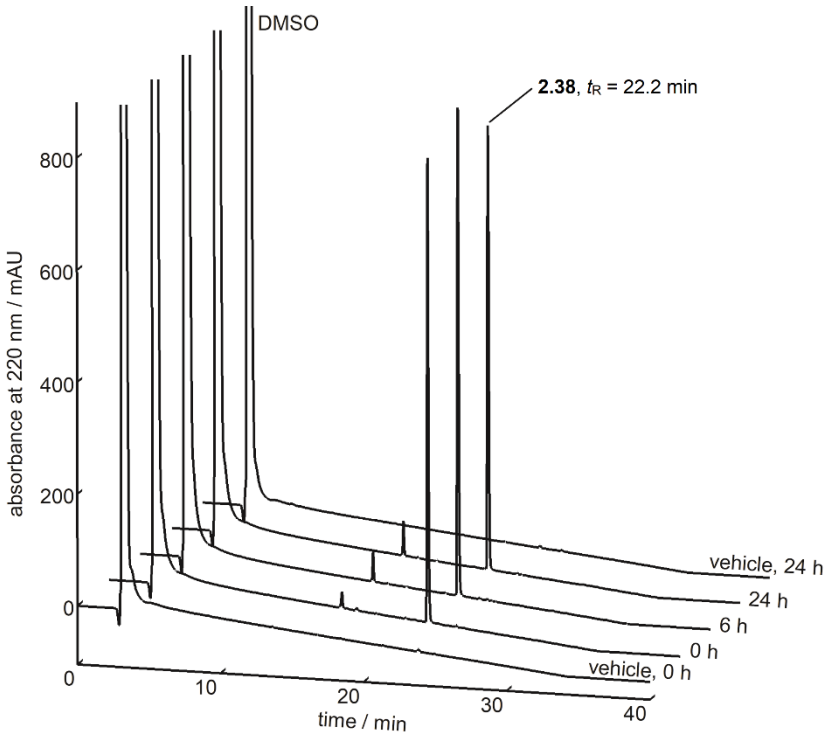

Chromatograms of the reversed-phase HPLC analysis of **2.38** after incubation in PBS pH 7.4 for up to 24 h. **2.38** showed slight decomposition.

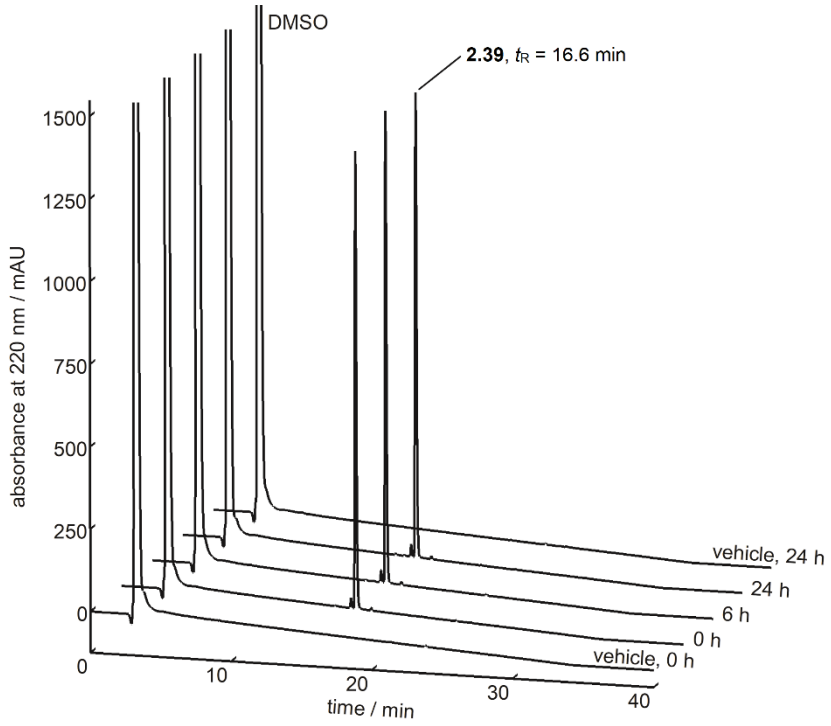

Chromatograms of the reversed-phase HPLC analysis of **2.39** after incubation in PBS pH 7.4 for up to 24 h. **2.39** showed no decomposition.

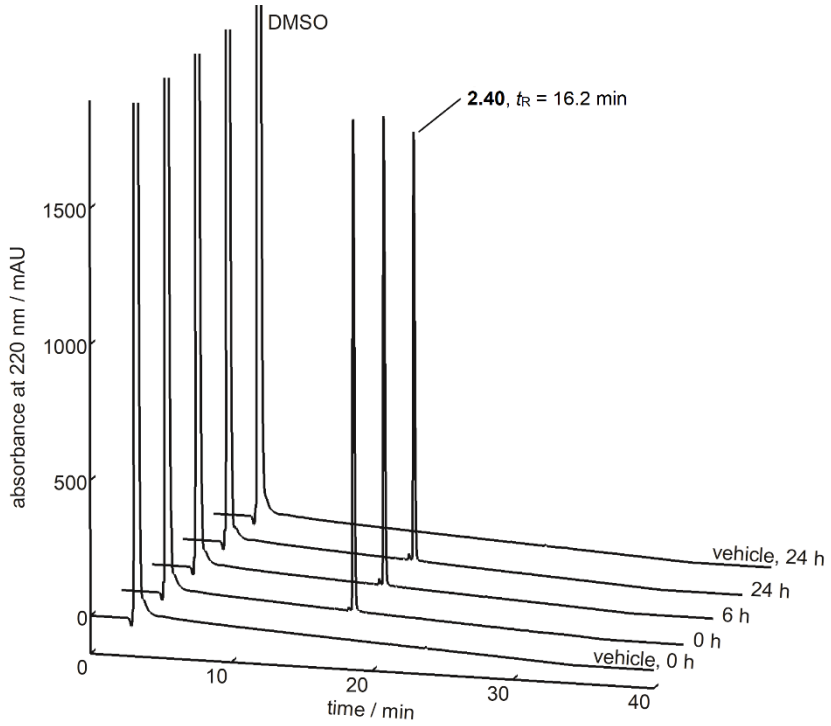

Chromatograms of the reversed-phase HPLC analysis of **2.40** after incubation in PBS pH 7.4 for up to 24 h. **2.40** showed no decomposition.

A.2.6 RP-HPLC chromatograms (purity controls) of (*S*,*R*)-2.14, (*R*,*R*)-2.14, (*S*,*R*)-2.30, (*R*,*R*)-2.30 and the fluorescently labeled compounds 2.35-2.40

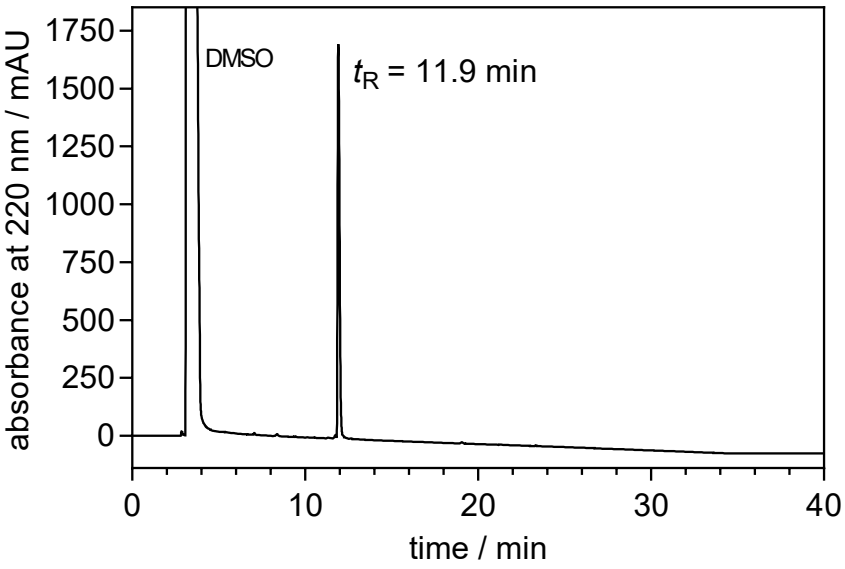

Chromatogram of the RP-HPLC analysis of (*S*,*R*)-**2.14**

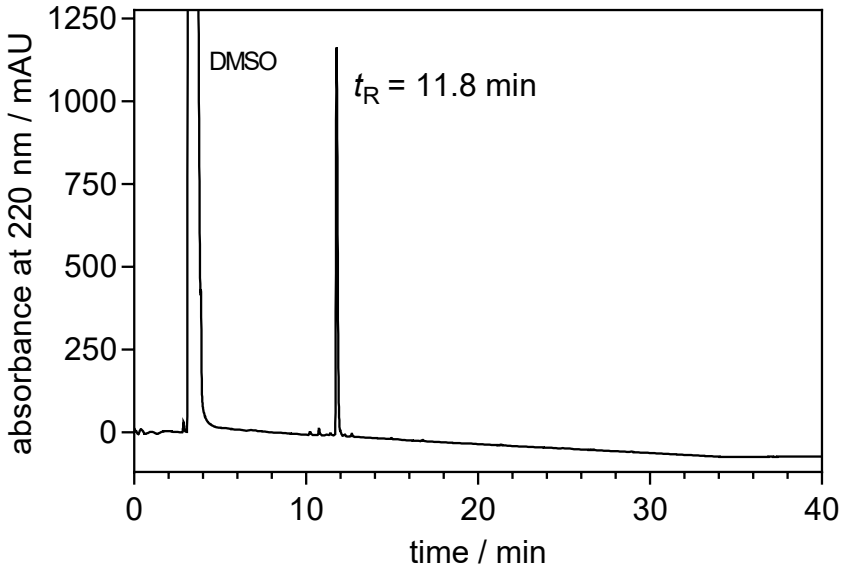

Chromatogram of the RP-HPLC analysis of (*R*,*R*)-**2.14**

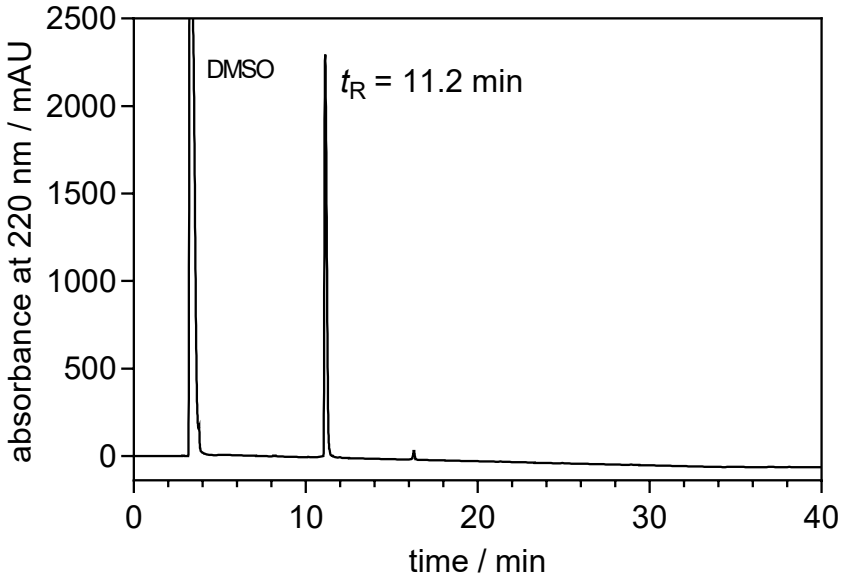

Chromatogram of the RP-HLPC analysis of (*S*,*R*)-**2.30**

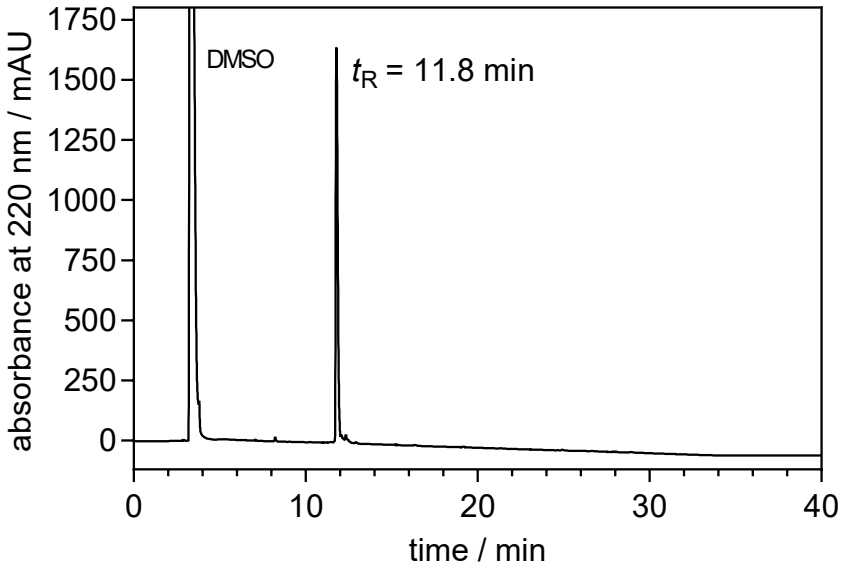

Chromatogram of the RP-HPLC analysis of (*R*,*R*)-**2.30**

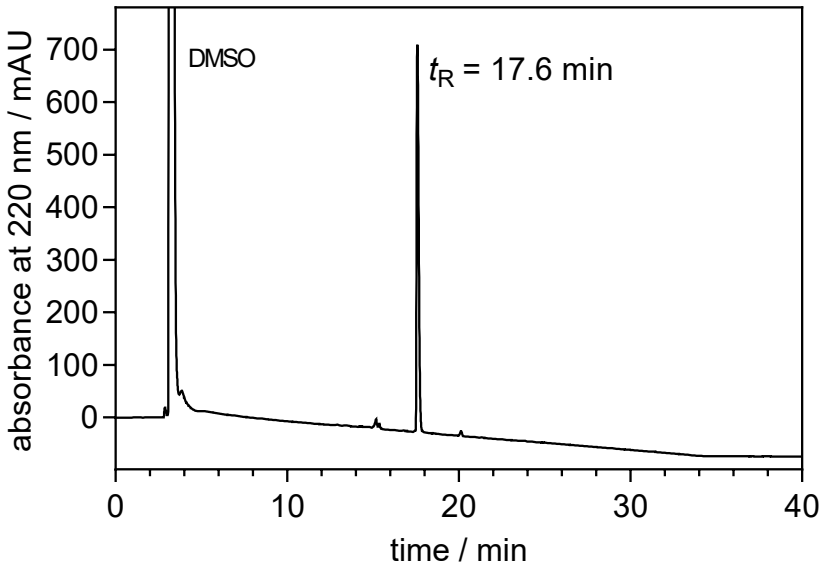

Chromatogram of the RP-HPLC analysis of **2.35**

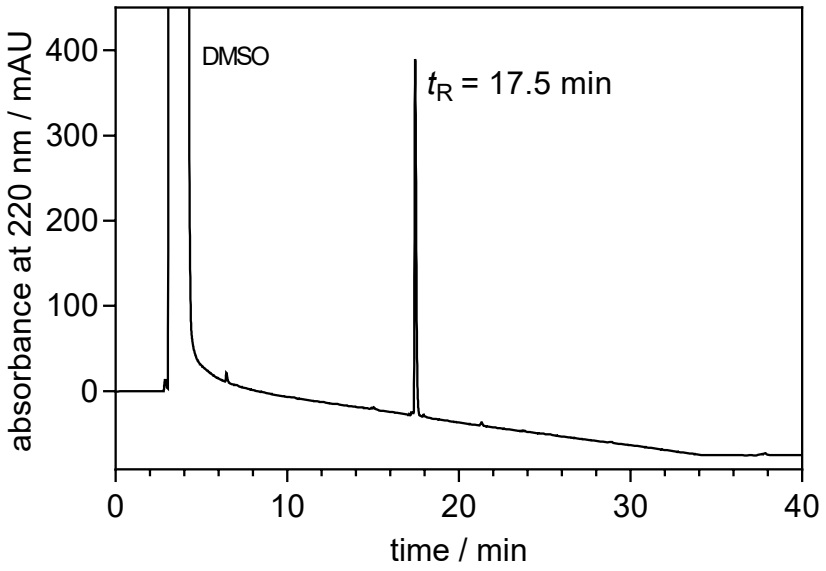

Chromatogram of the RP-HPLC analysis of **2.36**

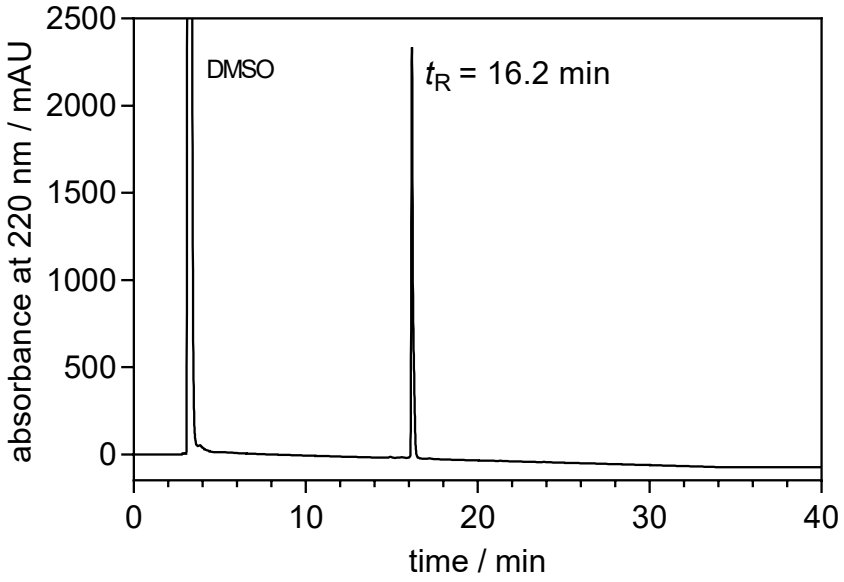

Chromatogram of the RP-HPLC analysis of **2.37**

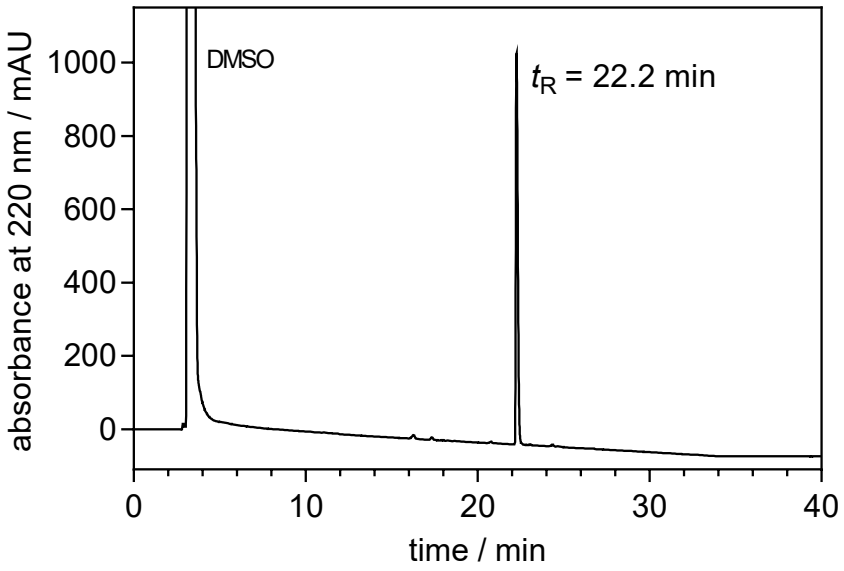

Chromatogram of the RP-HPLC analysis of **2.38**

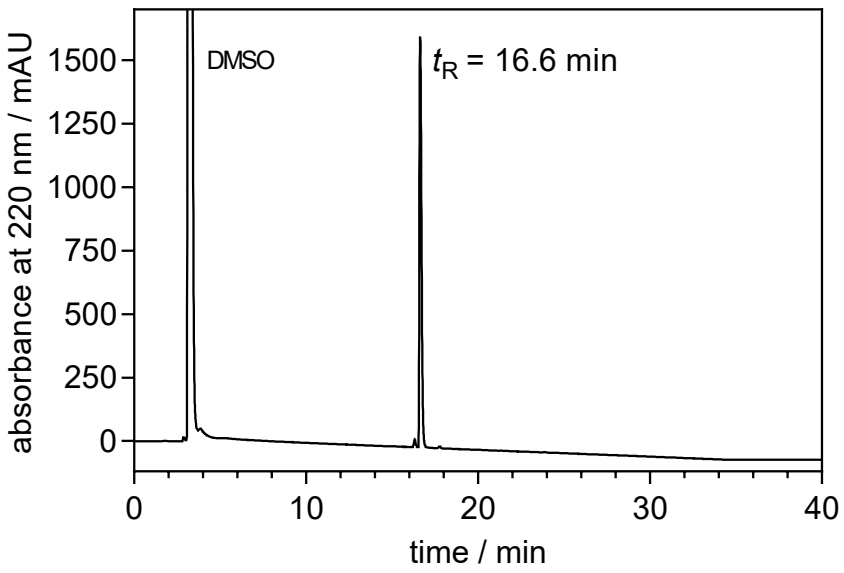

Chromatogram of the RP-HPLC analysis of **2.39**

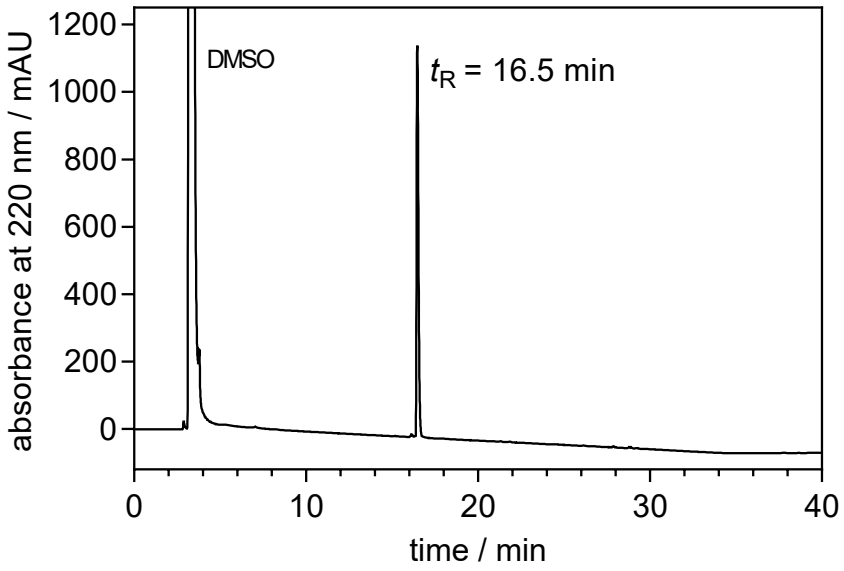

Chromatogram of the RP-HPLC analysis of **2.40**

A.2.7 ^{1}H-NMR and ^{13}C-NMR spectra of compounds 2.14, 2.19 and 2.30

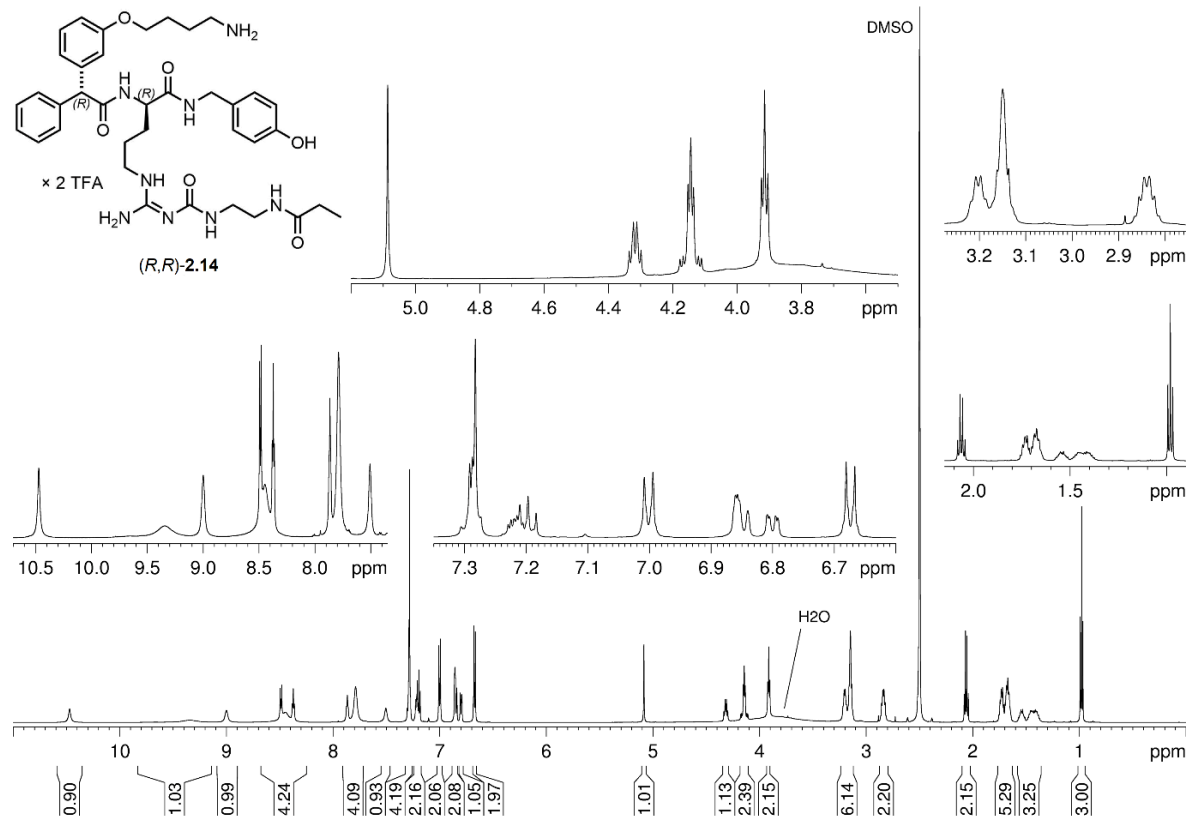

^{1}H-NMR spectrum (600 MHz, DMSO-d_6) of compound (*R*,*R*)-**2.14**

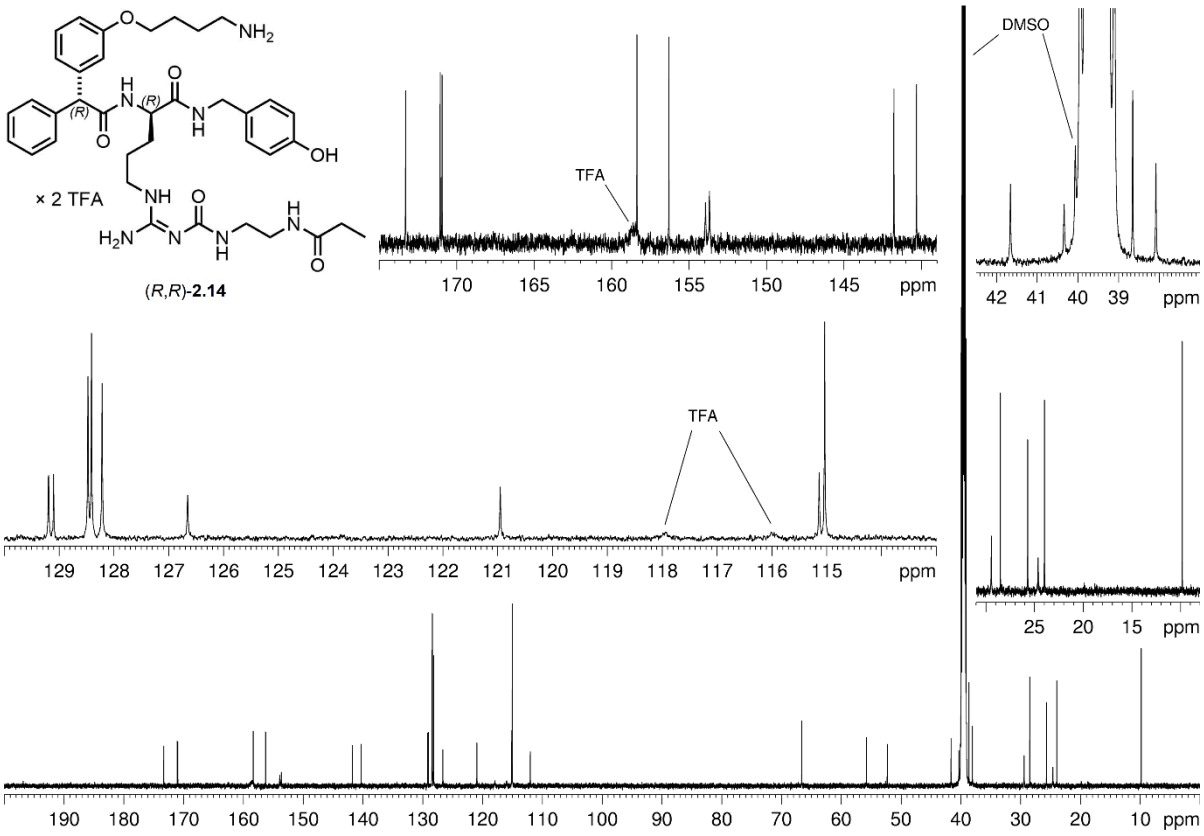

^{13}C-NMR spectrum (150 MHz, DMSO-d_6) of compound (*R*,*R*)-**2.14**

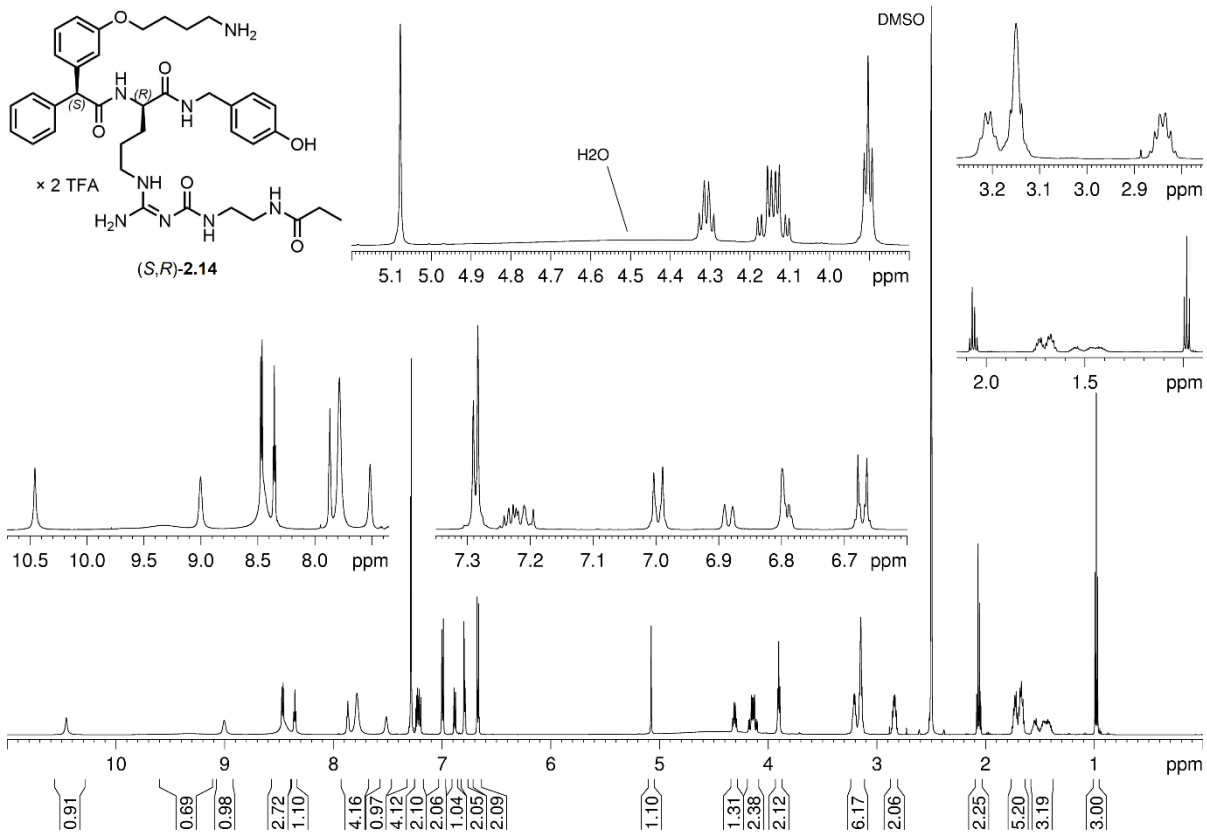

^{1}H-NMR spectrum (600 MHz, DMSO-d_6) of compound (*S*,*R*)-**2.14**

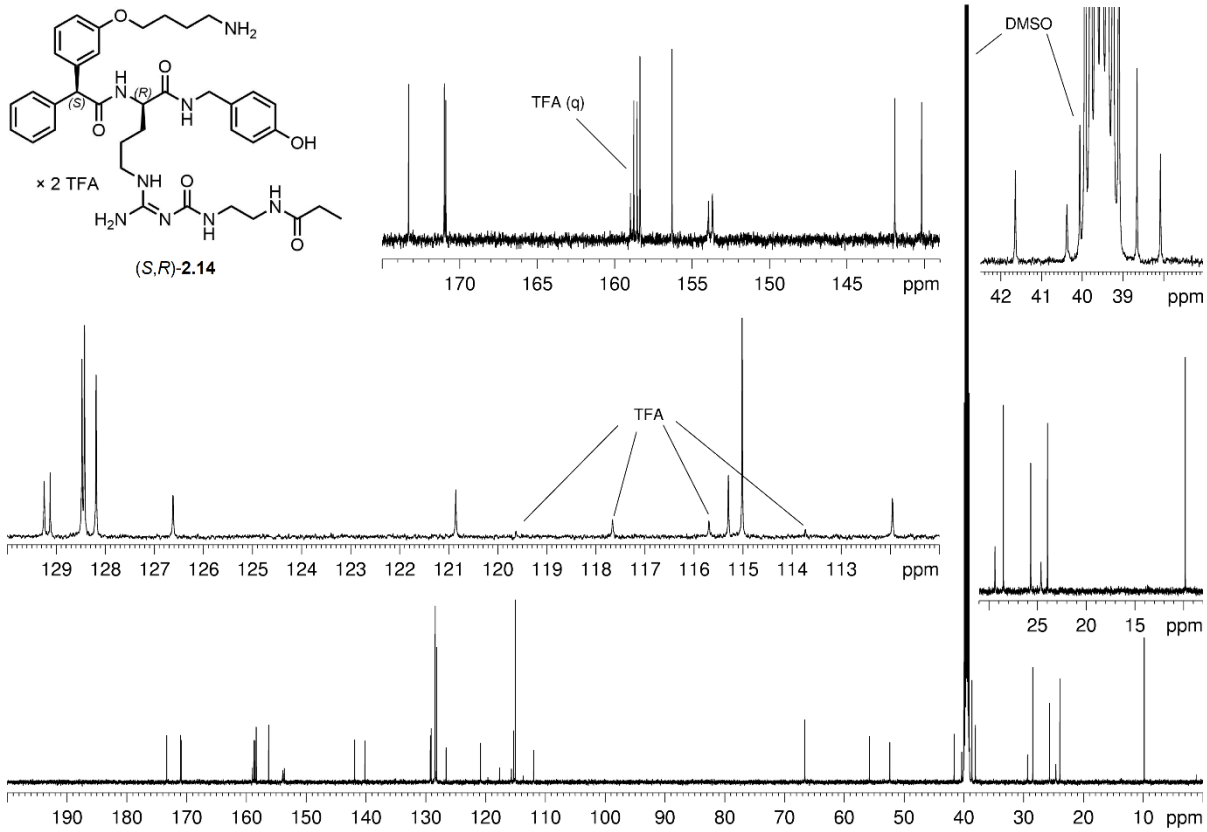

^{13}C-NMR spectrum (150 MHz, DMSO-d_6) of compound (*S*,*R*)-**2.14**

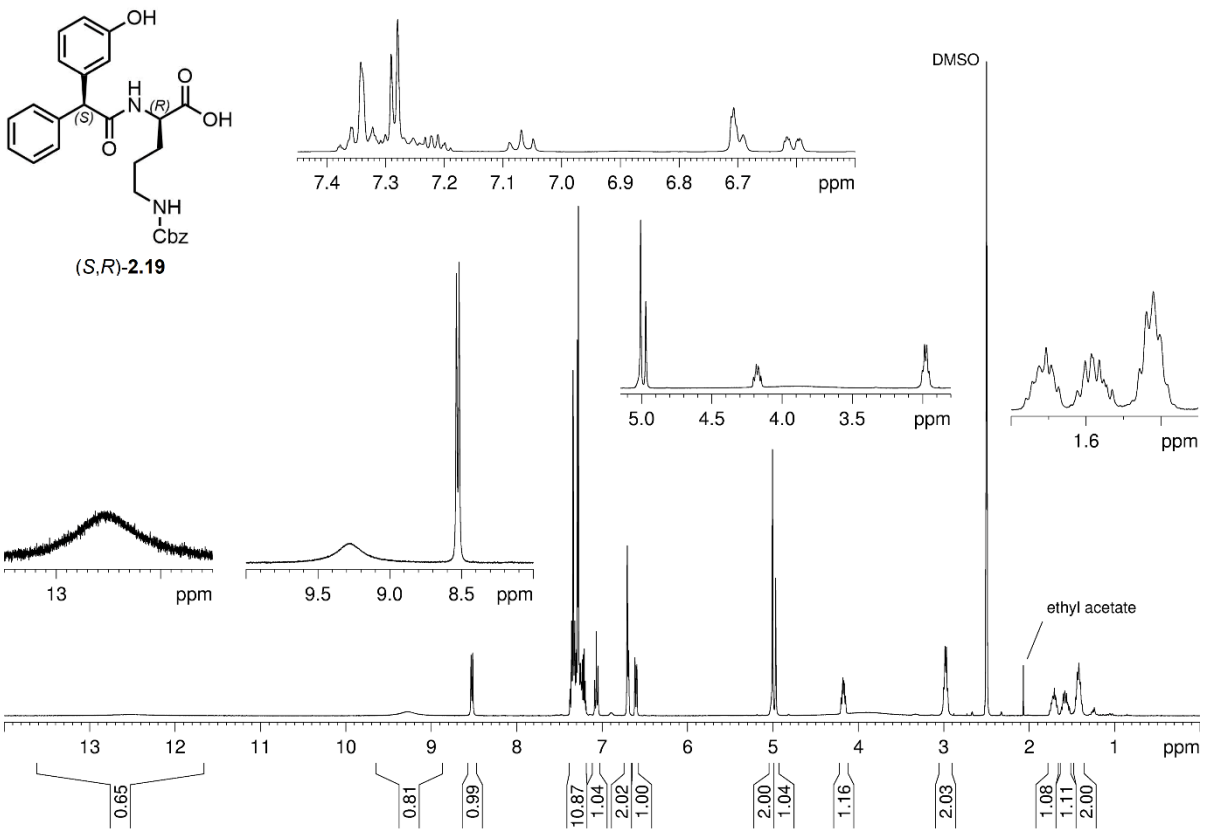

^{1}H-NMR spectrum (600 MHz, DMSO-d_6) of compound (*S*,*R*)-**2.19**

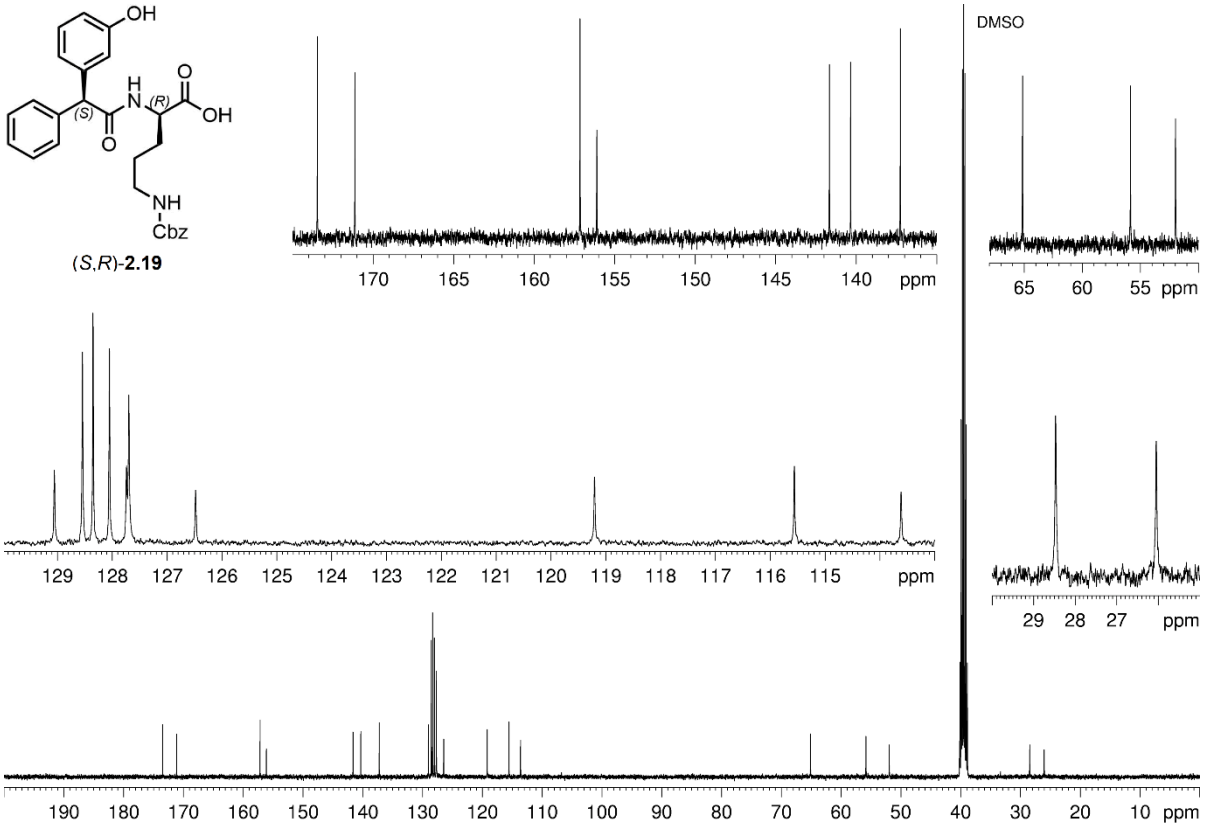

^{13}C-NMR spectrum (150 MHz, DMSO-d_6) of compound (*S*,*R*)-**2.19**

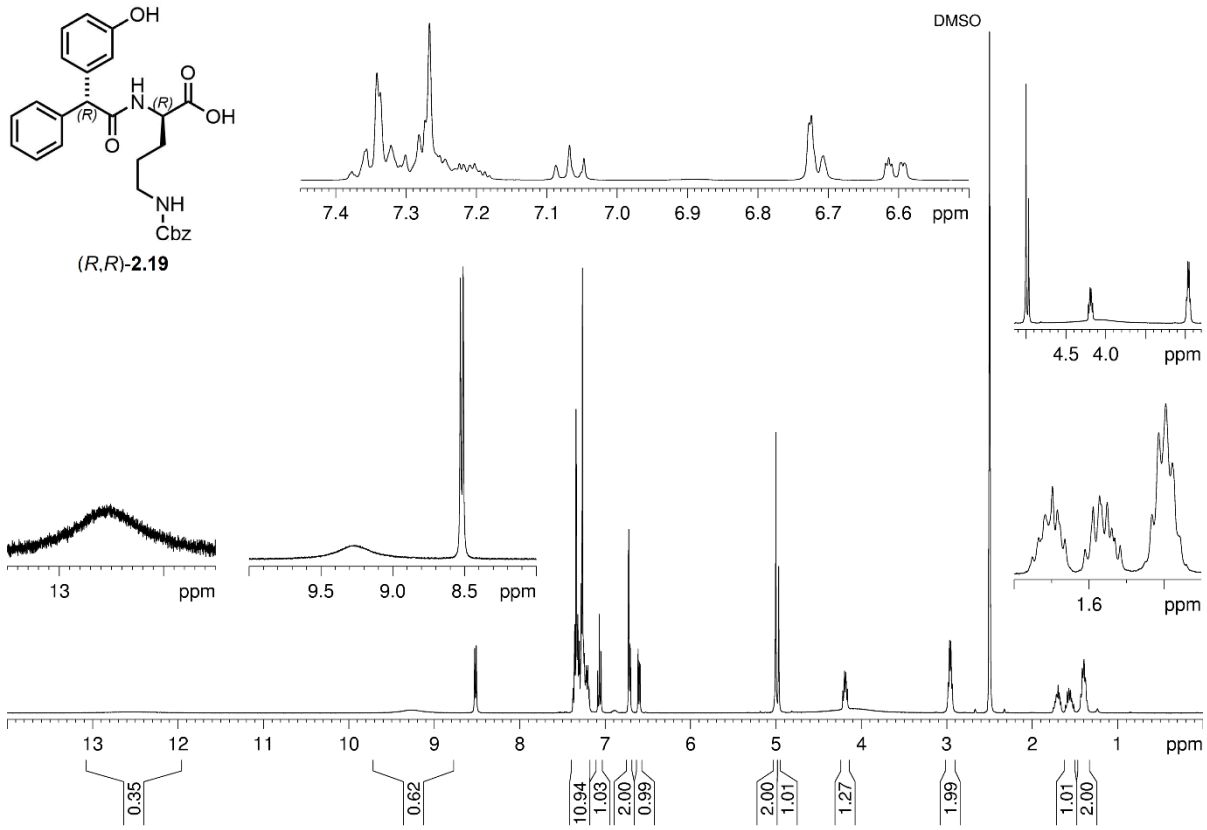

^{1}H-NMR spectrum (600 MHz, DMSO-d_6) of compound (*R*,*R*)-**2.19**

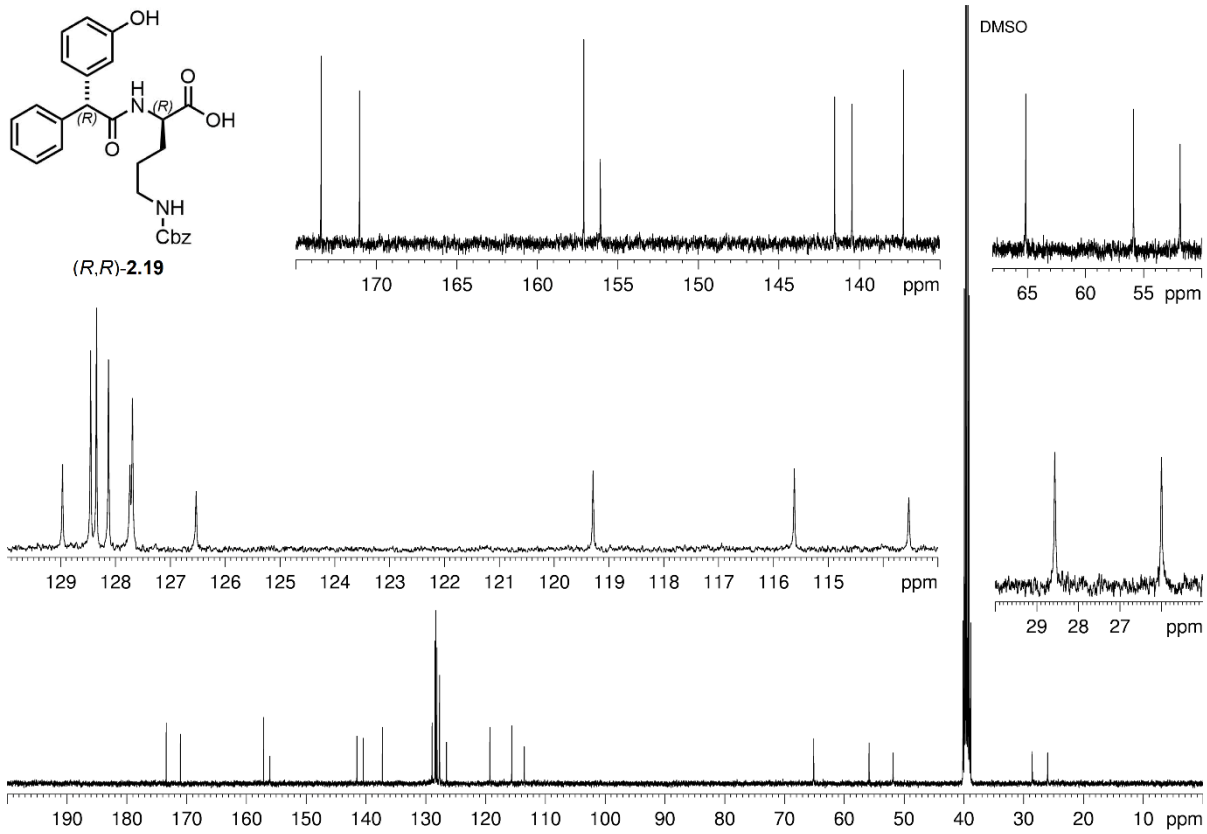

^{13}C-NMR spectrum (150 MHz, DMSO-d_6) of compound (*R*,*R*)-**2.19**

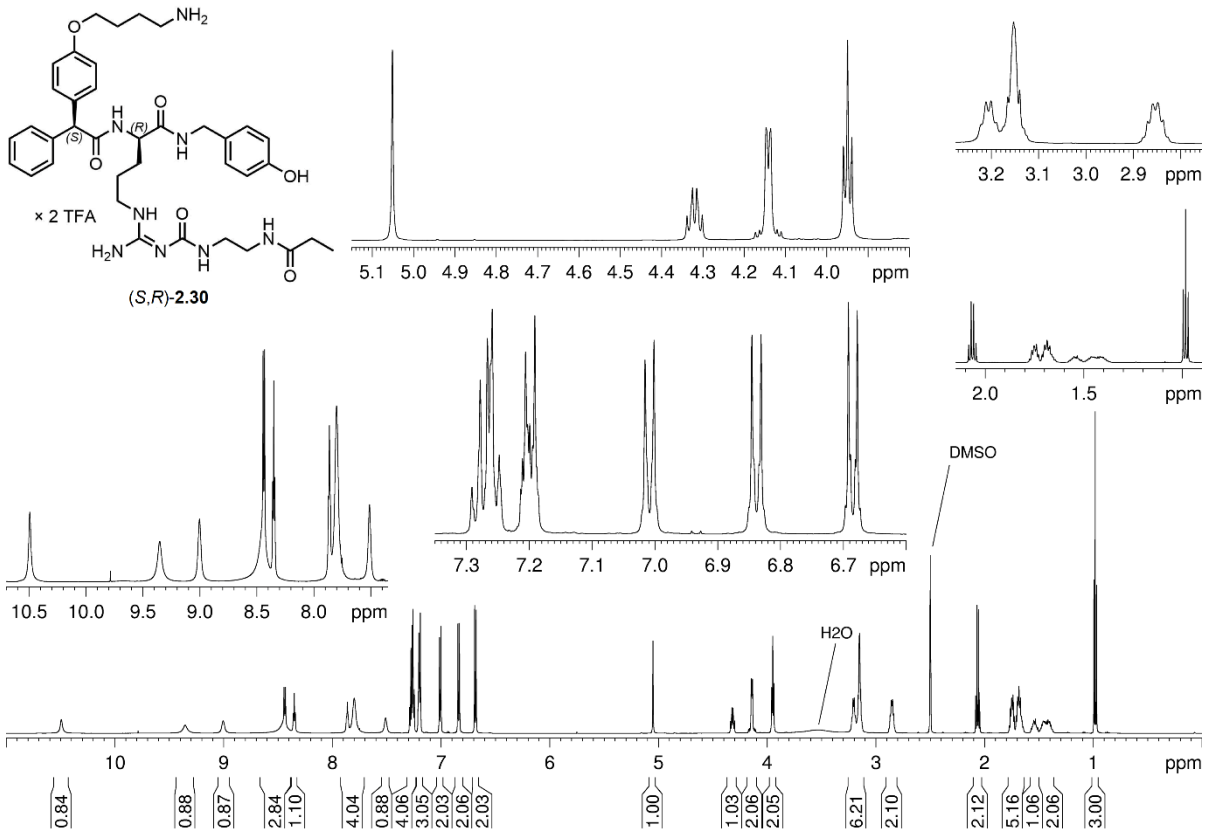

^{1}H-NMR spectrum (600 MHz, DMSO-d_6) of compound (*S*,*R*)-**2.30**

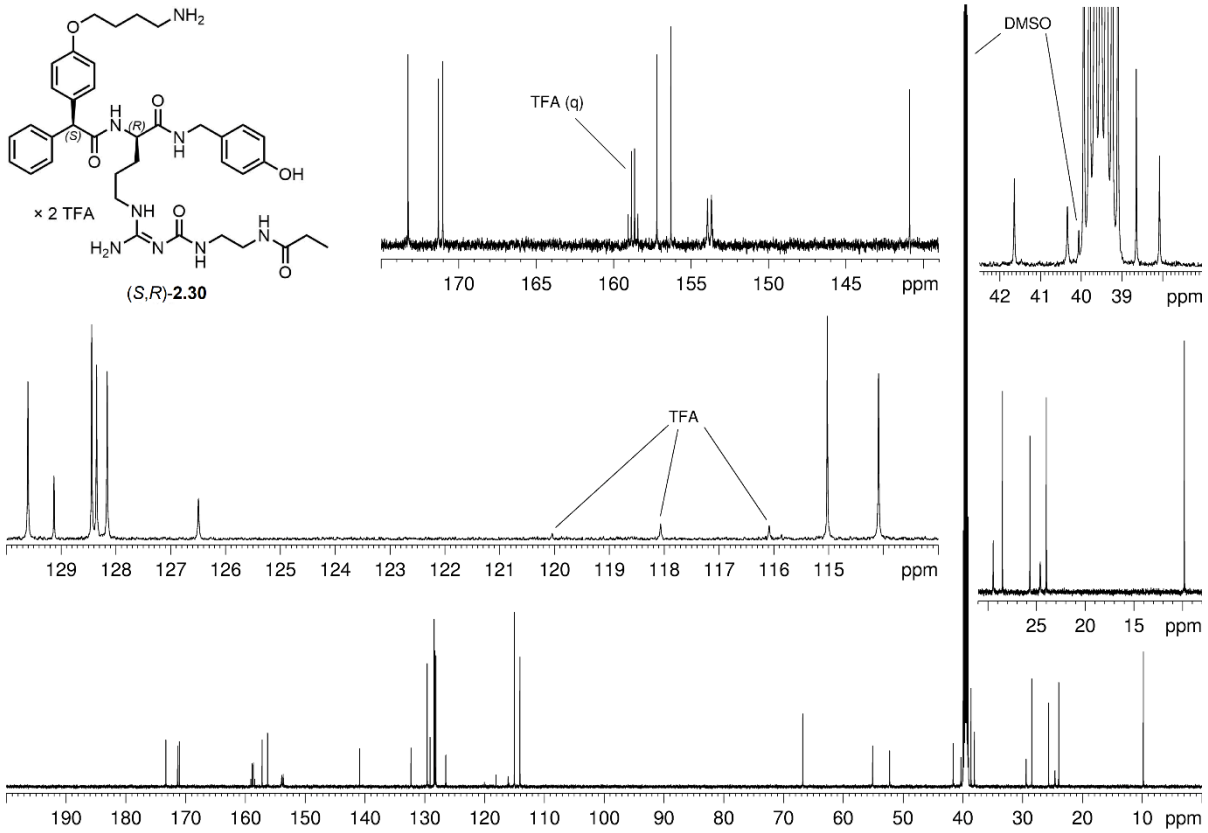

^{13}C-NMR spectrum (150 MHz, DMSO-d_6) of compound (*S*,*R*)-**2.30**

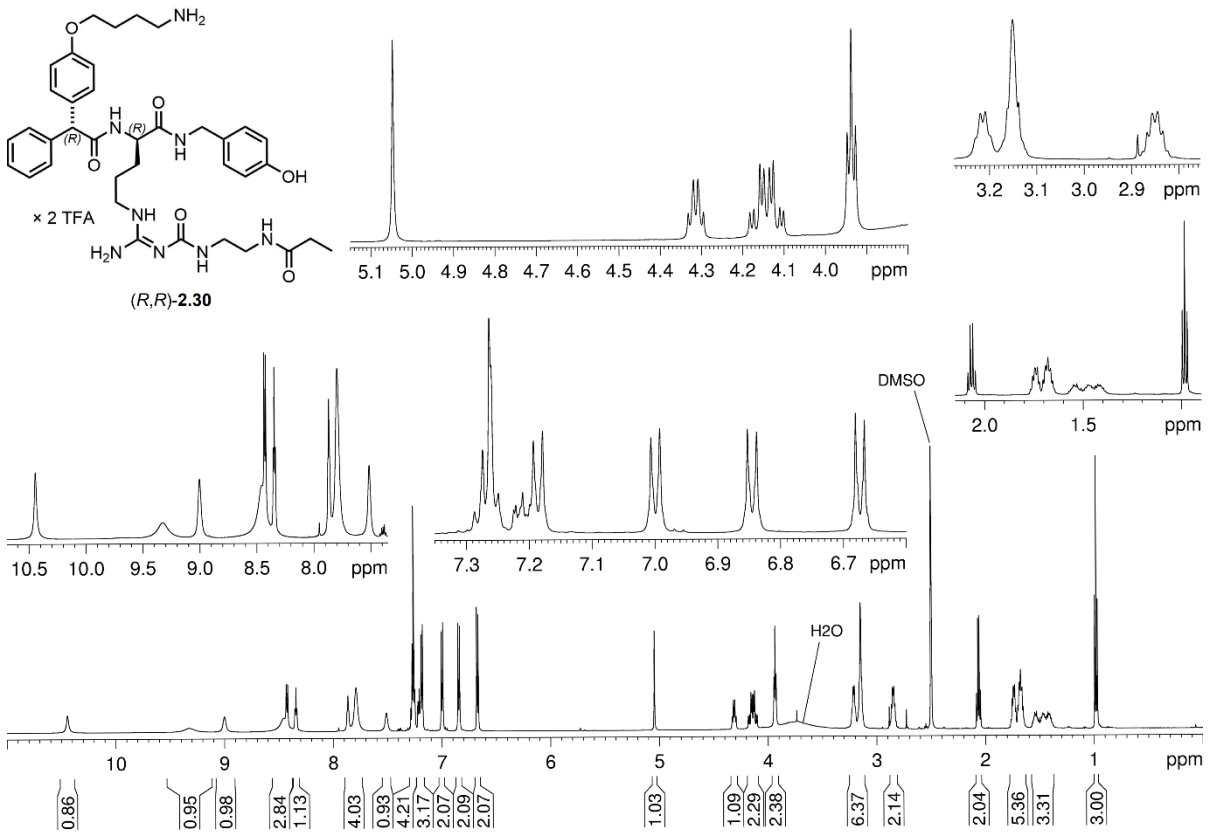

^{1}H-NMR spectrum (600 MHz, DMSO-d_6) of compound (*R*,*R*)-**2.30**

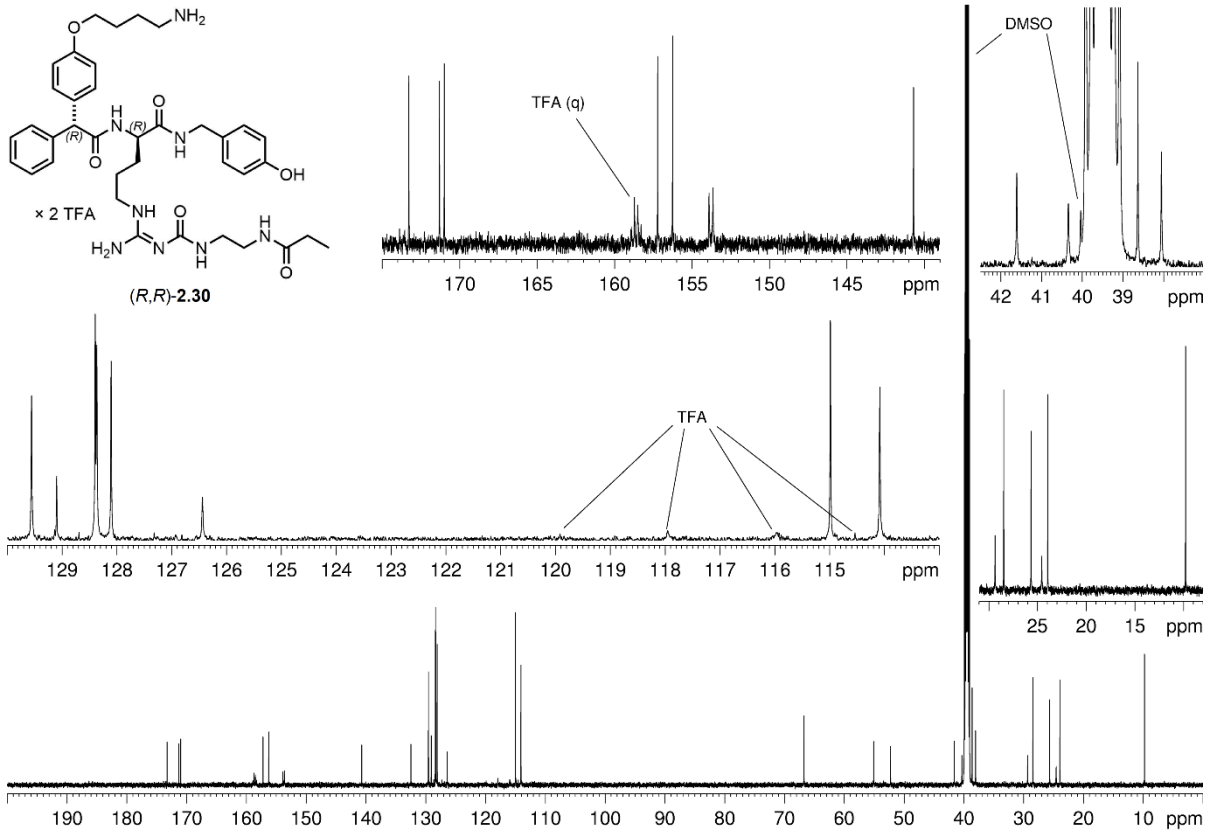

^{13}C-NMR spectrum (150 MHz, DMSO-d_6) of compound (*R*,*R*)-**2.30**

A.2.8 ^{1}H-NMR spectra of compounds 2.35-2.40

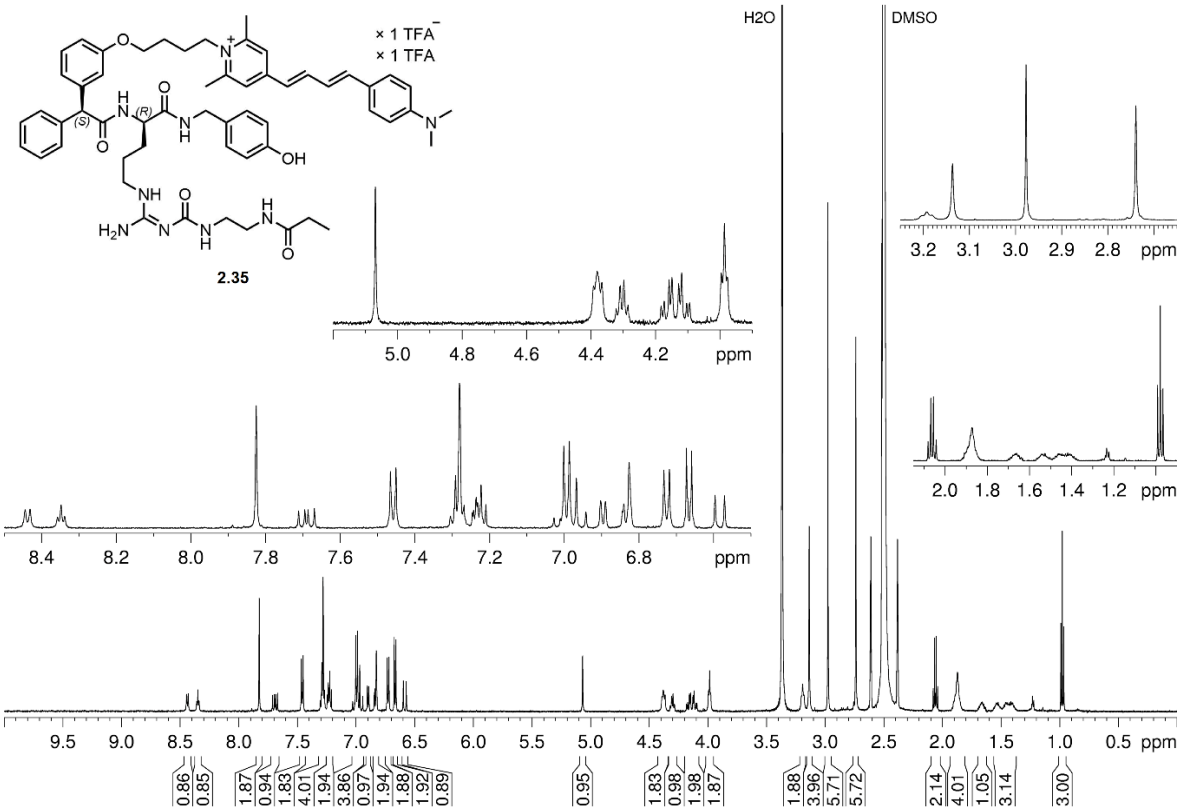

^{1}H-NMR spectrum (600 MHz, DMSO-d_6/D_2O 10:1) of compound **2.35**

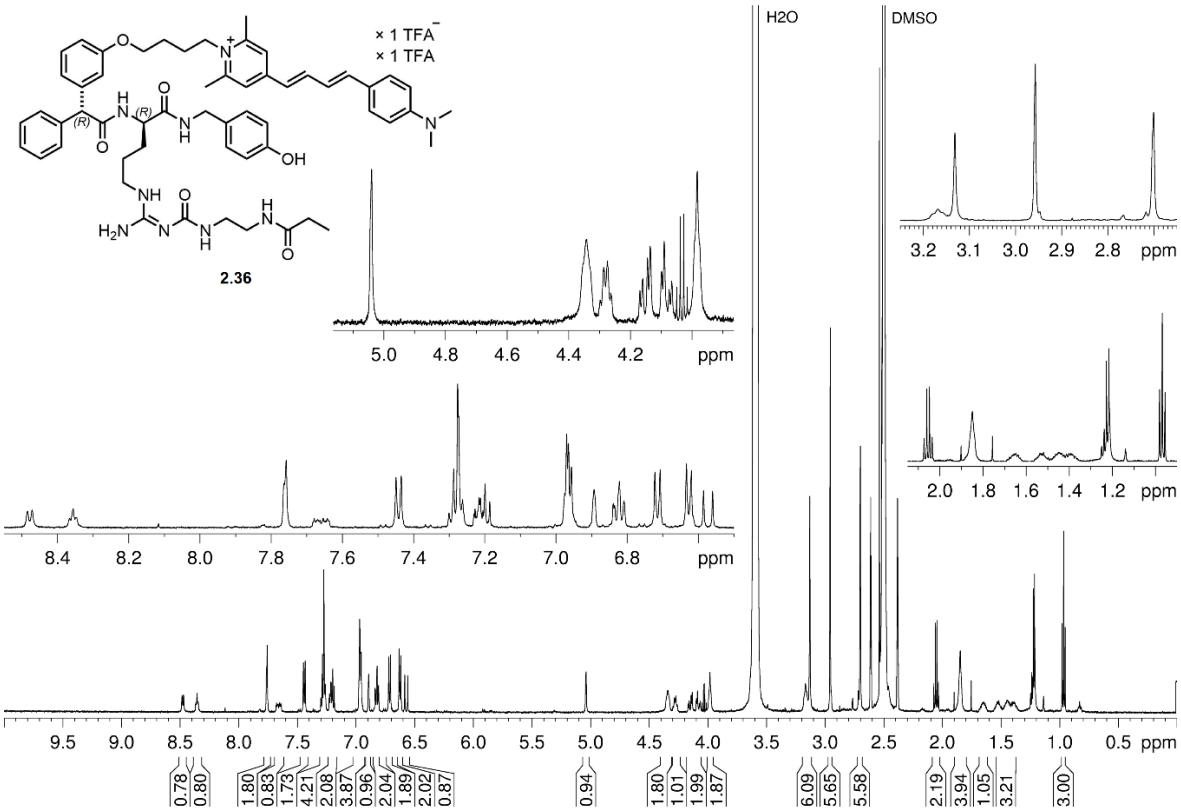

^{1}H-NMR spectrum (600 MHz, DMSO-d_6/D_2O 10:1) of compound **2.36**

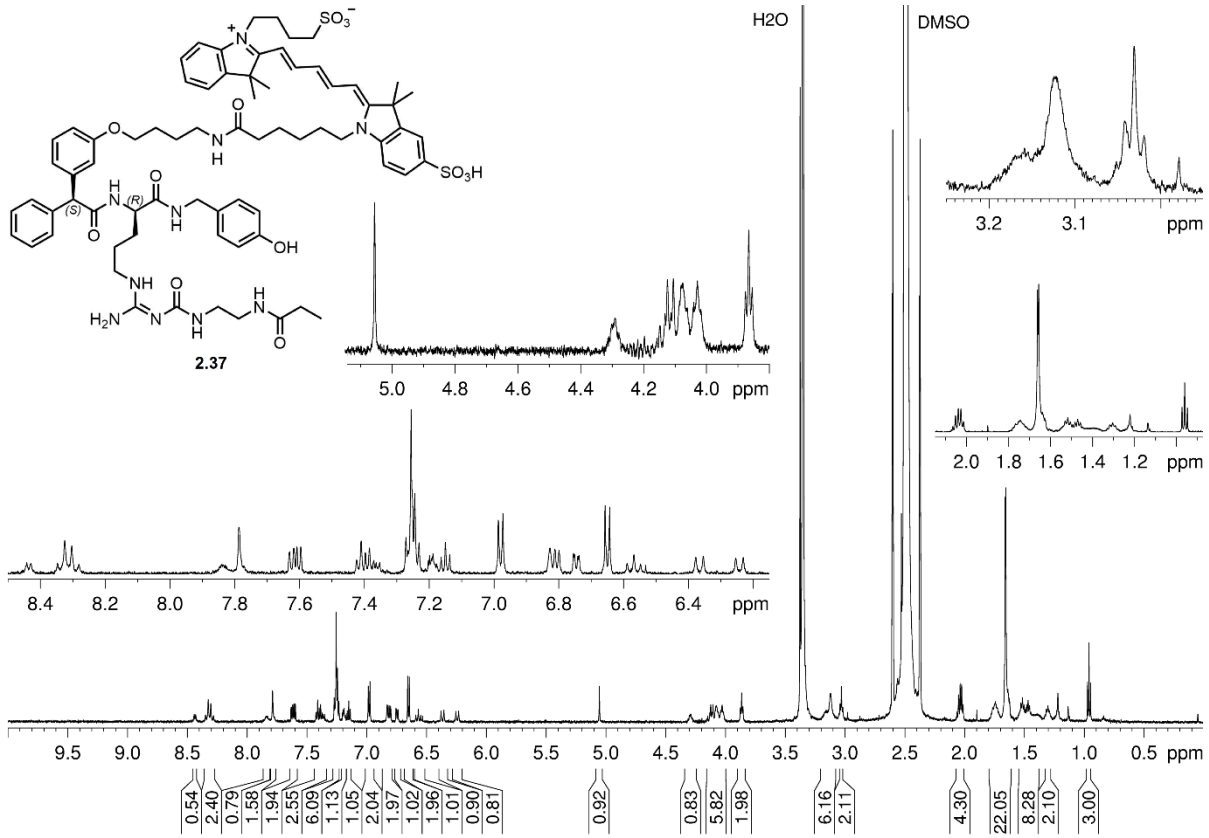

^{1}H-NMR spectrum (600 MHz, DMSO-d_6/D_2O 10:1) of compound **2.37**

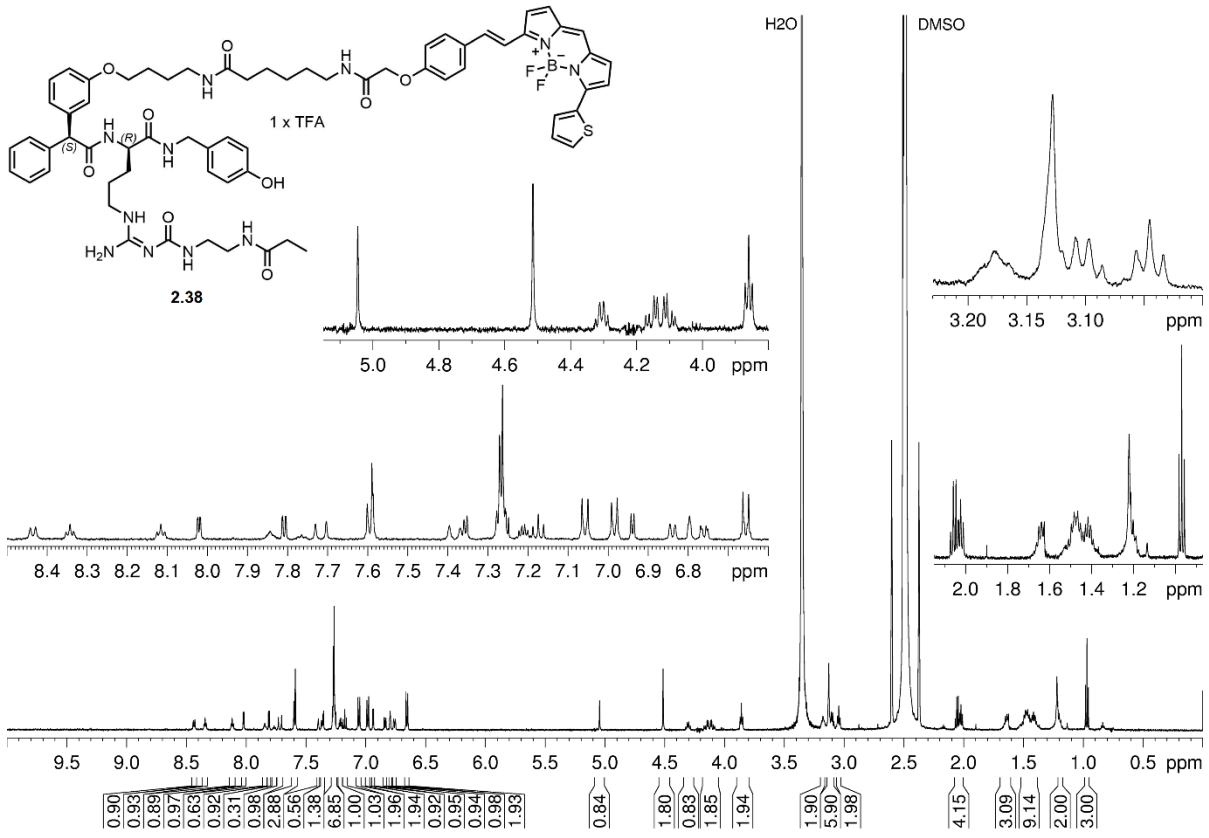

^{1}H-NMR spectrum (600 MHz, DMSO-d_6/D_2O 10:1) of compound **2.38**

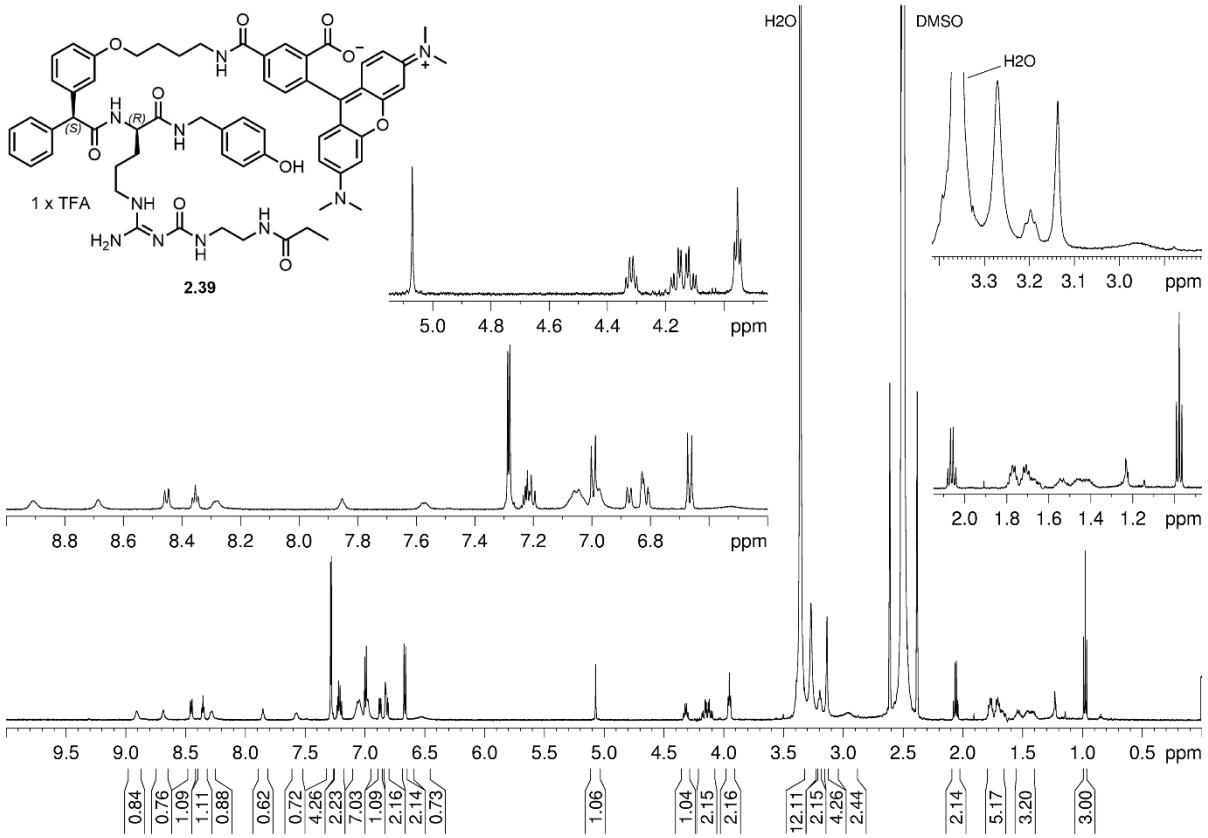

^{1}H-NMR spectrum (600 MHz, DMSO-d_6/D_2O 10:1) of compound **2.39**

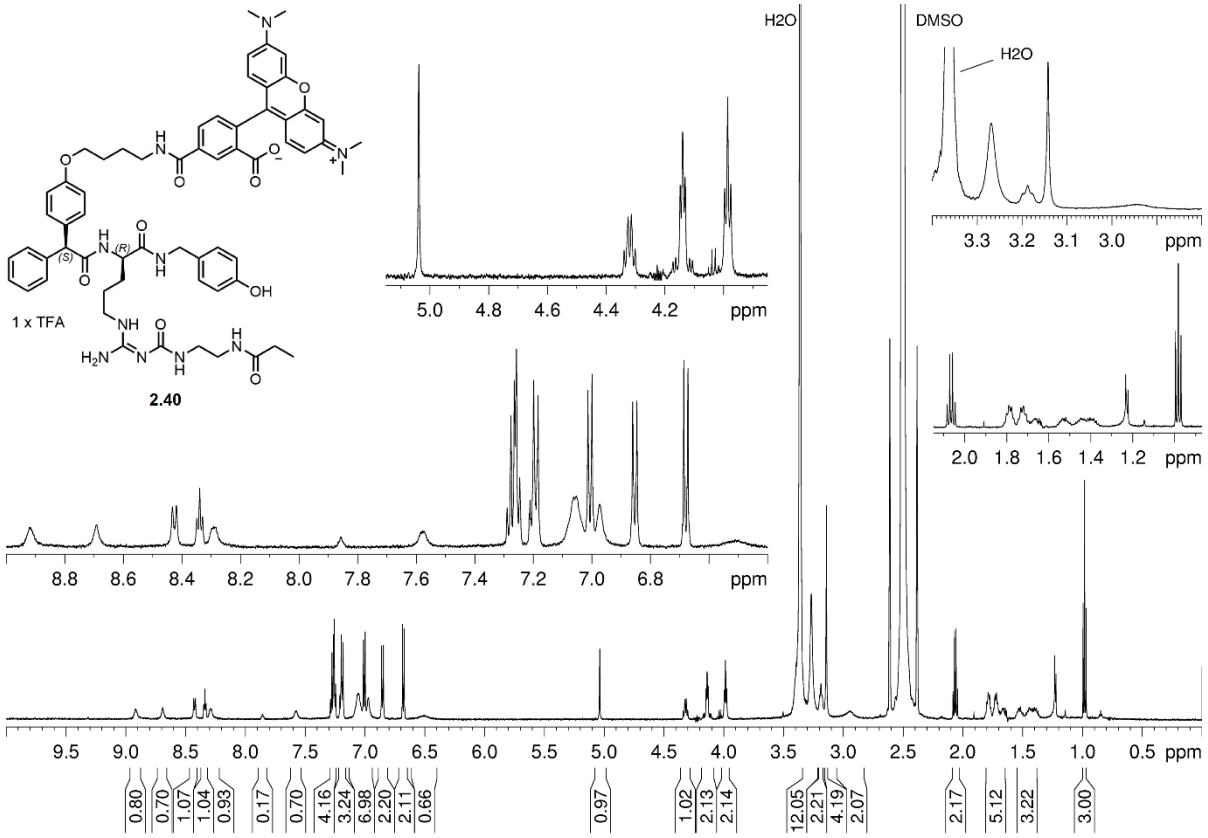

^{1}H-NMR spectrum (600 MHz, DMSO-d_6/D_2O 10:1) of compound **2.40**

A.2.9 References

(1) Keller, M.; Weiss, S.; Hutzler, C.; Kuhn, K. K.; Mollereau, C.; Dukorn, S.; Schindler, L.; Bernhardt, G.; König, B.; Buschauer, A. N^{ω}-Carbamoylation of the argininamide moiety: An avenue to insurmountable NPY Y_1 receptor antagonists and a radiolabeled selective high-affinity molecular tool ([^{3}H]UR-MK299) with extended residence time. *J. Med. Chem.* **2015**, 58, 8834-8849.

(2) Keller, M.; Erdmann, D.; Pop, N.; Pluym, N.; Teng, S.; Bernhardt, G.; Buschauer, A. Red-fluorescent argininamide-type NPY Y_1 receptor antagonists as pharmacological tools. *Biorg. Med. Chem.* **2011**, 19, 2859-2878.

(3) Kraus, A.; Ghorai, P.; Birnkammer, T.; Schnell, D.; Elz, S.; Seifert, R.; Dove, S.; Bernhardt, G.; Buschauer, A. N^G-Acylated aminothiazolylpropylguanidines as potent and selective histamine H_2 receptor agonists. *ChemMedChem* **2009**, 4, 232-240.

(4) Ji, Y.-H., C. Husfeld, C. Lange, R. Lee, Y. Mu. Preparation of (carbamoyldiphenylmethyl)methylpyrrolidinium derivatives for use as muscarinic receptor antagonists. WO 2008103426, **2008**.

(5) Liu, J.-K.; Gu, W.; Cheng, X.-R.; Cheng, J.-P.; Zhou, W.-X.; Nie, A.-H. Design and synthesis of cyclic acylguanidines as BACE1 inhibitors. *Chin. Chem. Lett.* **2015**, 26, 1327-1330.

(6) Gobbi, S.; Cavalli, A.; Negri, M.; Schewe, K. E.; Belluti, F.; Piazzi, L.; Hartmann, R. W.; Recanatini, M.; Bisi, A. Imidazolylmethylbenzophenones as highly potent aromatase inhibitors. *J. Med. Chem.* **2007**, 50, 3420-3422.

(7) Nikolova, S.; Kochovska, E.; Ivanov, I. Selective reduction of ortho-acylated β-enaminones of homoveratryamine and their cyclization to 1,2,3,4-tetrahydroisoquinolines with β-enaminone moiety. *Synth. Commun.* **2013**, 43, 326-336.

(8) López, A. M.; Scarel, F.; Carrero, N. R.; Vázquez, E.; Mateo-Alonso, A.; Ros, T. D.; Prato, M. Synthesis and characterization of highly water-soluble dendrofulleropyrrolidine bisadducts with DNA binding activity. *Org. Lett.* **2012**, 14, 4450-4453.

(9) Veiksina, S.; Kopanchuk, S.; Rinken, A. Budded baculoviruses as a tool for a homogeneous fluorescence anisotropy-based assay of ligand binding to G protein-coupled receptors: The case of melanocortin 4 receptors. *Biochim. Biophys. Acta* **2014**, 1838, 372-381.

A.3 Chapter 3

A.3.1 Chemical stability of compounds 3.11, 3.12, 3.16, 3.22 and 3.25 in PBS

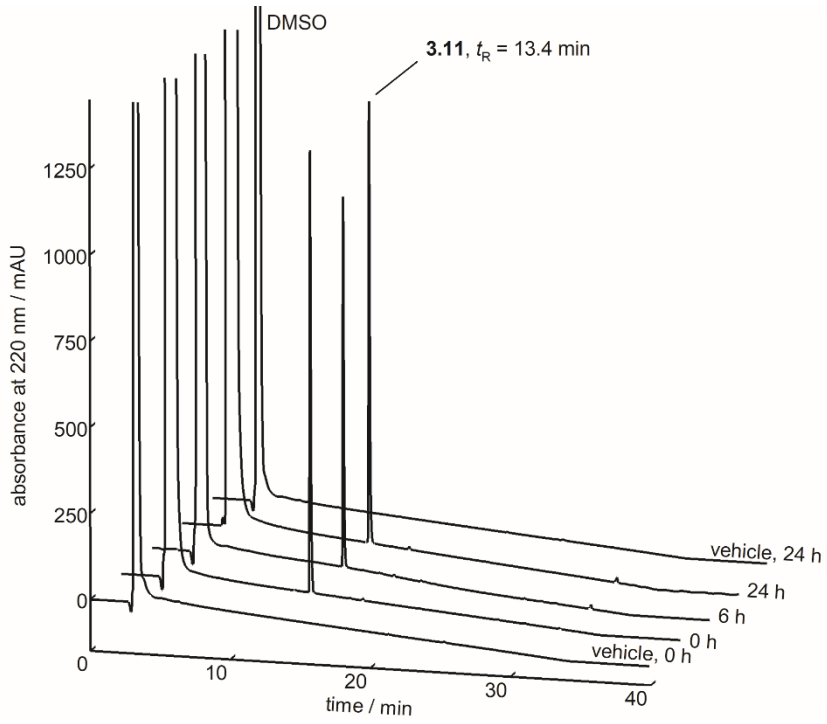

Chromatograms of the reversed-phase HPLC analysis of **3.11** after incubation in PBS pH 7.4 for up to 24 h. **3.11** showed no decomposition.

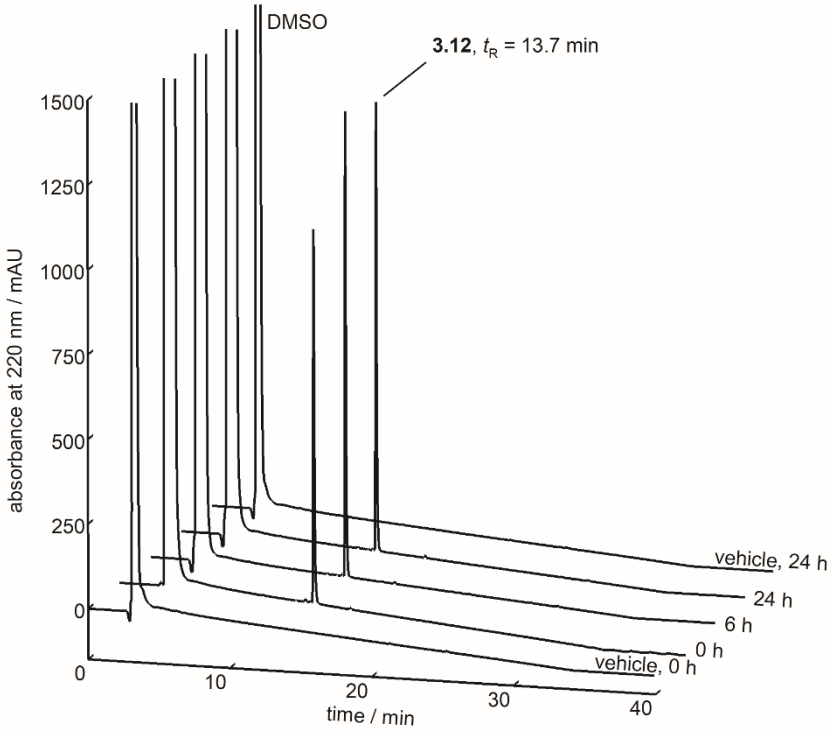

Chromatograms of the reversed-phase HPLC analysis of **3.12** after incubation in PBS pH 7.4 for up to 24 h. **3.12** showed no decomposition.

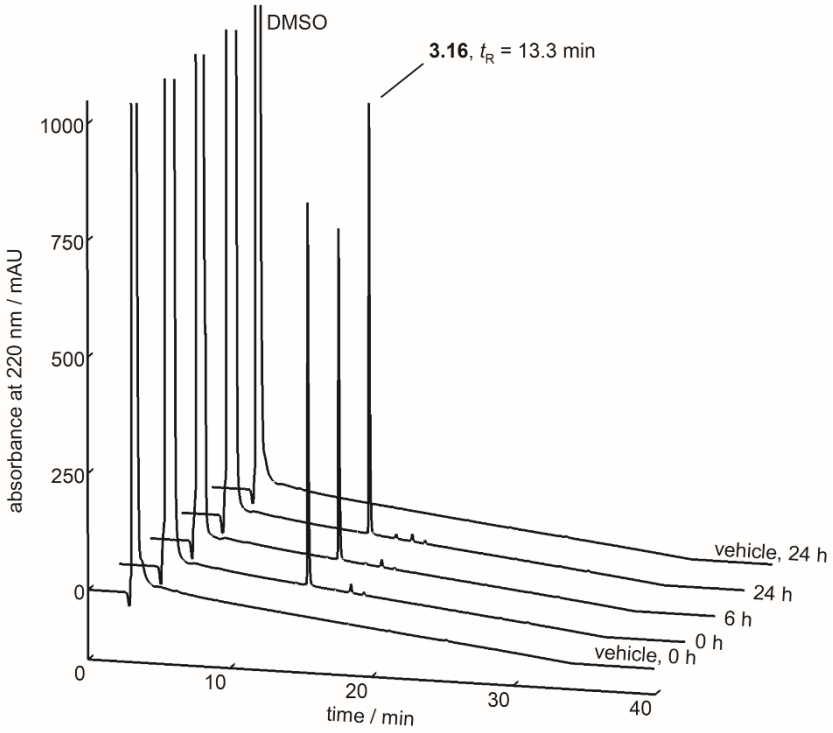

Chromatograms of the reversed-phase HPLC analysis of **3.16** after incubation in PBS pH 7.4 for up to 24 h. **3.16** showed no decomposition.

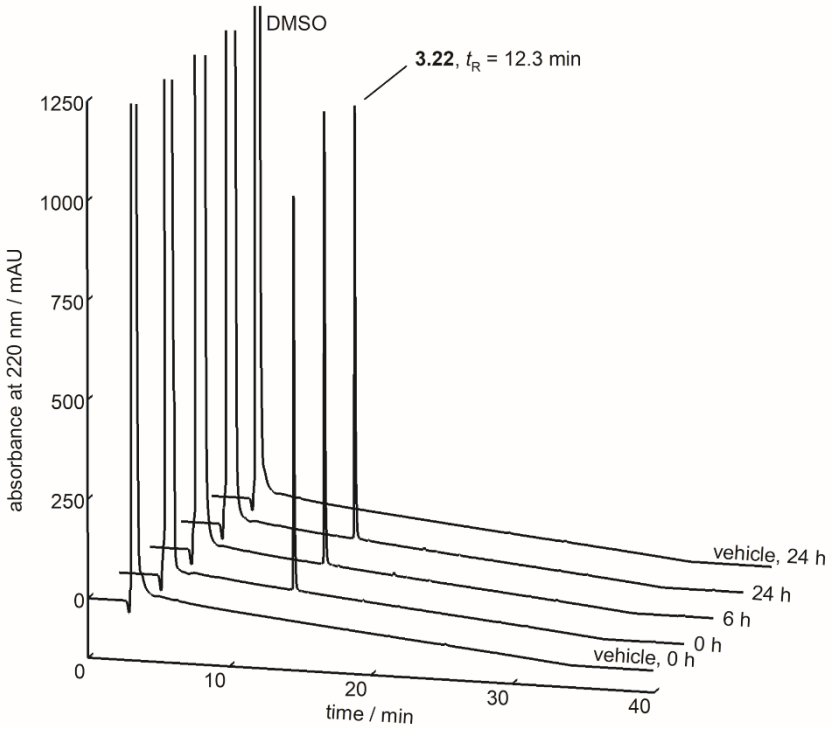

Chromatograms of the reversed-phase HPLC analysis of **3.22** after incubation in PBS pH 7.4 for up to 24 h. **3.22** showed no decomposition.

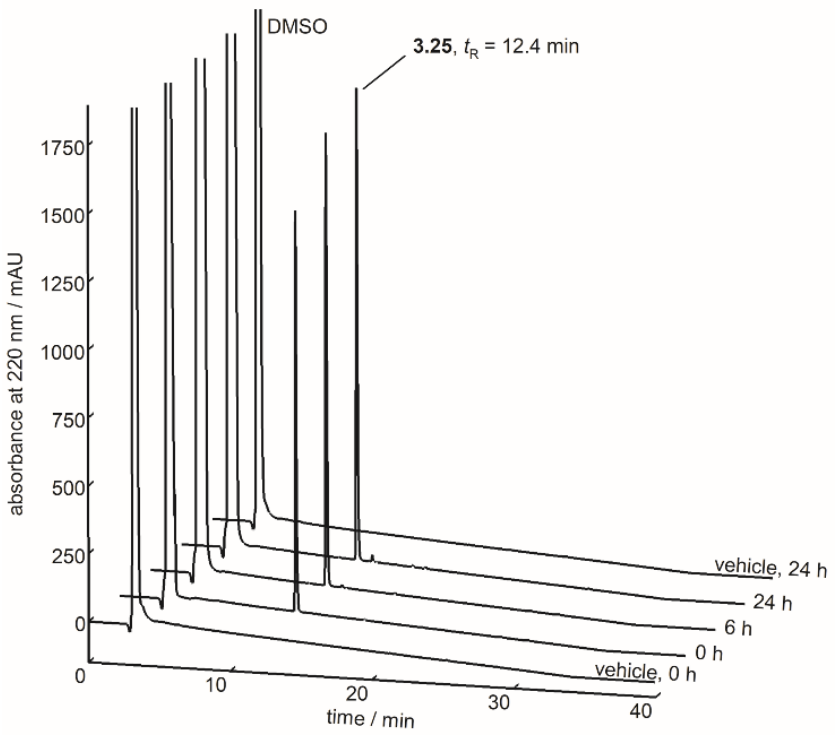

Chromatograms of the reversed-phase HPLC analysis of **3.25** after incubation in PBS pH 7.4 for up to 24 h. **3.25** showed no decomposition.

A.3.2 Chemical stability of compound [^{68}Ga]3.25 in human plasma

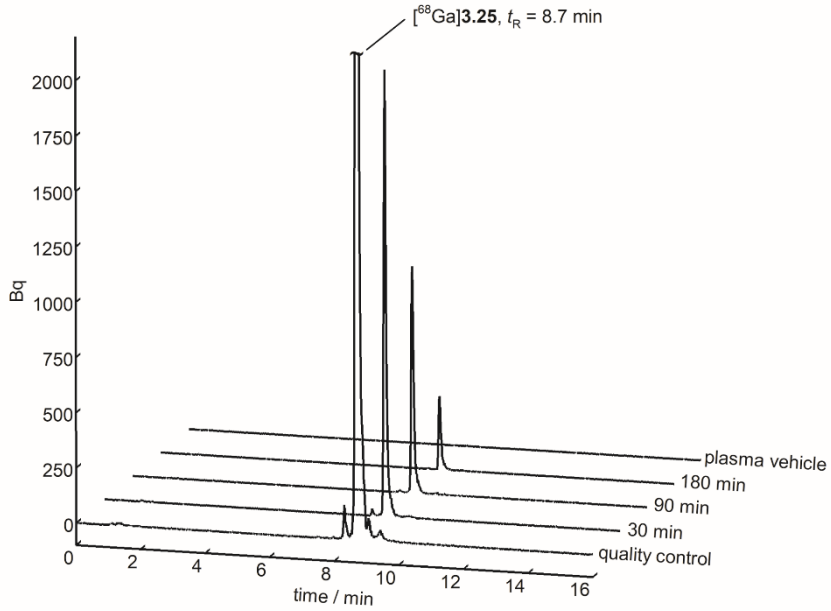

Radiochromatograms of the reversed-phase HPLC analysis of samples obtained from the investigation of the stability of [^{68}Ga]**3.25** in human plasma for up to 3 h. Degradation products of [^{68}Ga]**3.25** were not found. Note: the radiochromatogramm of the quality control is displayed in section A.3.4 with full Y-axis scaling.

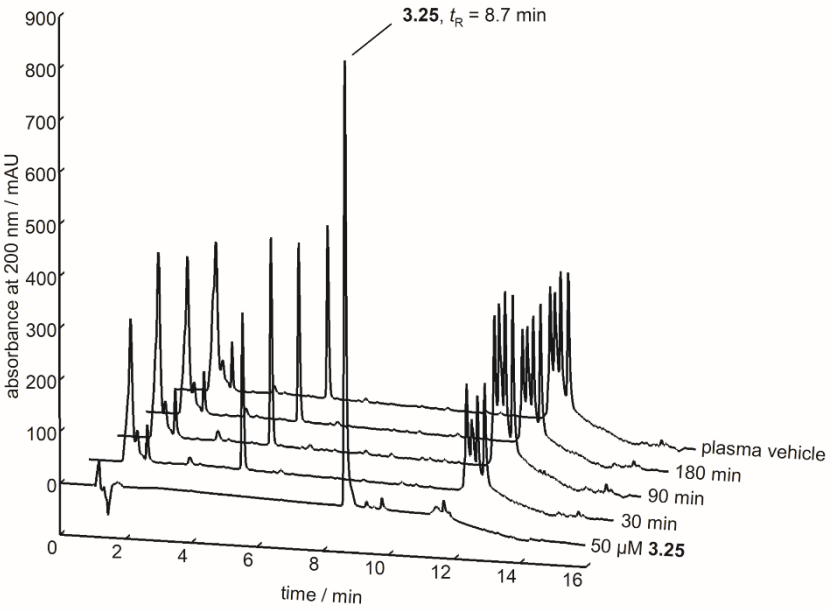

Chromatograms (UV detection) of the reversed-phase HPLC analysis of samples obtained from the investigation of the stability of [^{68}Ga]**3.25** in human plasma for up to 3 h (corresponding radiochromatograms are shown above).

A.3.3 RP-HPLC chromatograms (purity controls) of compounds (*S*,*R*)-3.6, (*R*,*R*)-3.6, 3.11, 3.12, 3.16, 3.22 and 3.25

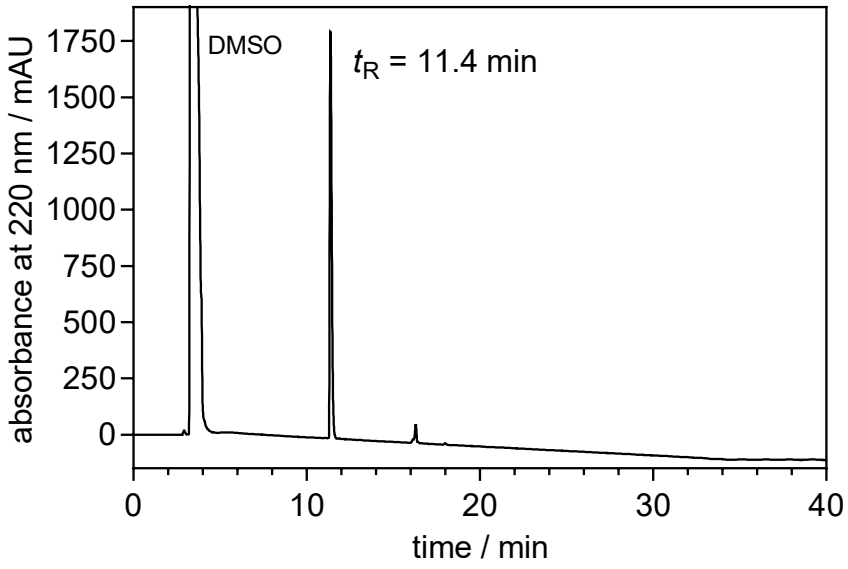

Chromatogram of the RP-HPLC analysis of (*R*,*R*)-**3.6**

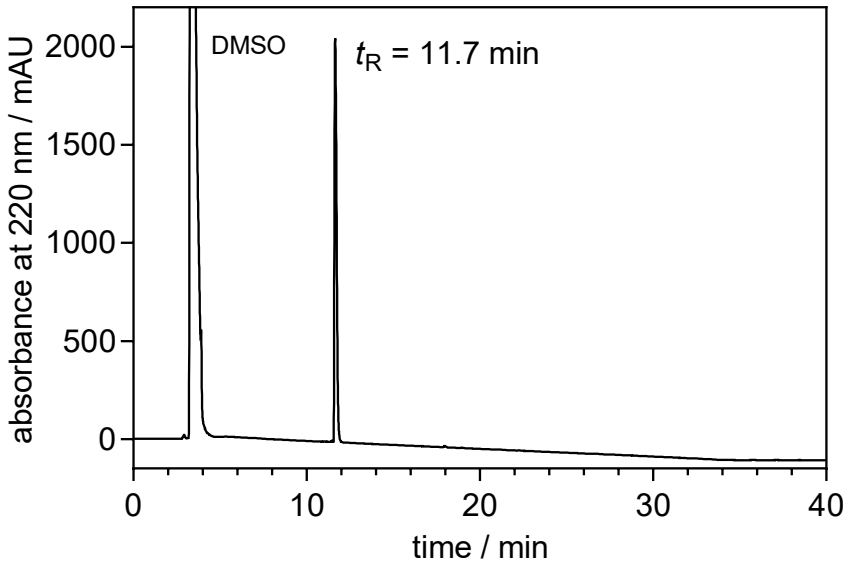

Chromatogram of the RP-HPLC analysis of (*S*,*R*)-**3.6**

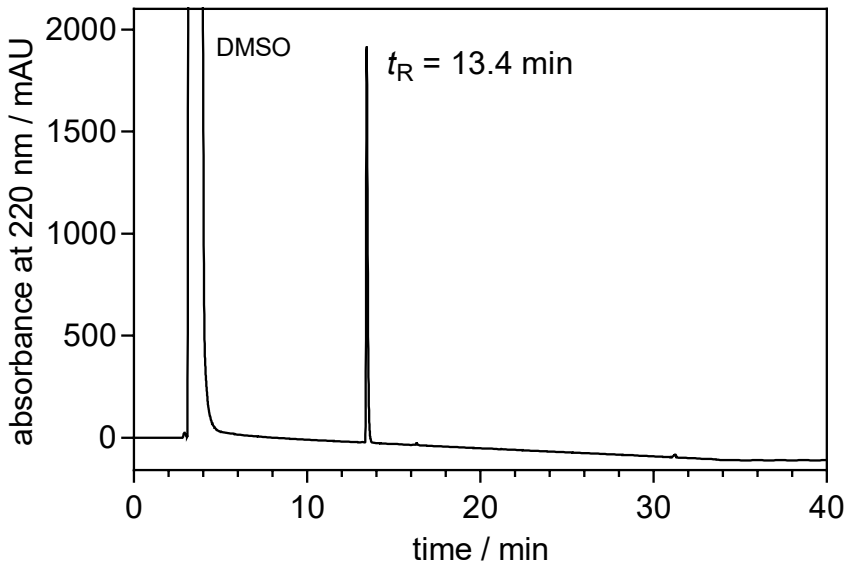

Chromatogram of the RP-HPLC analysis of **3.11**

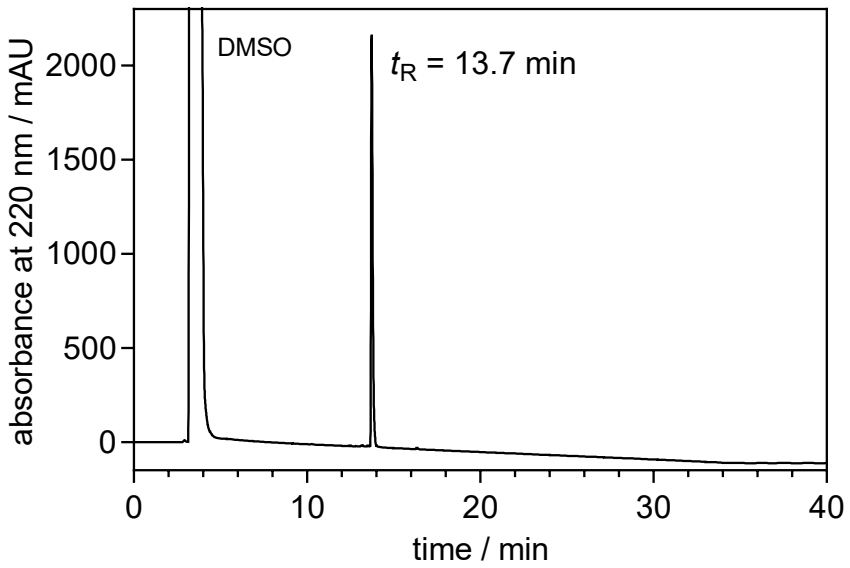

Chromatogram of the RP-HPLC analysis of **3.12**

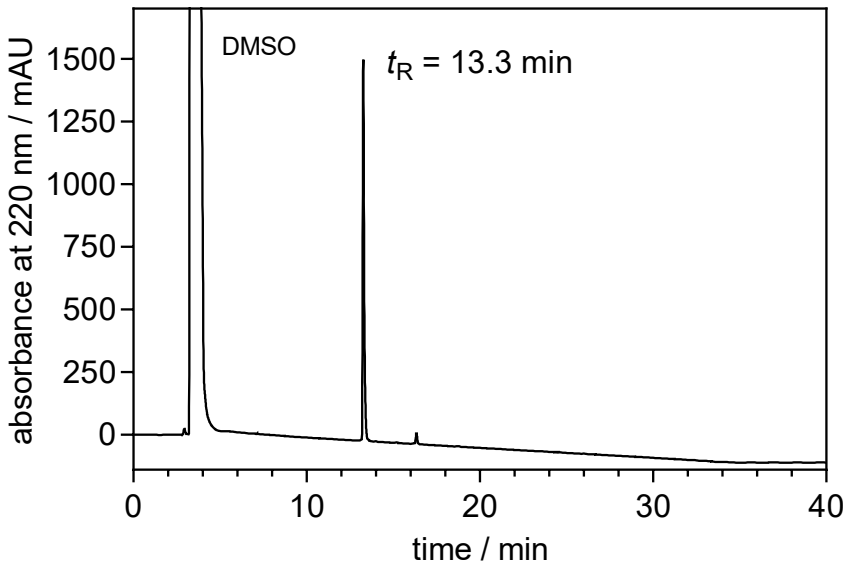

Chromatogram of the RP-HPLC analysis of **3.16**

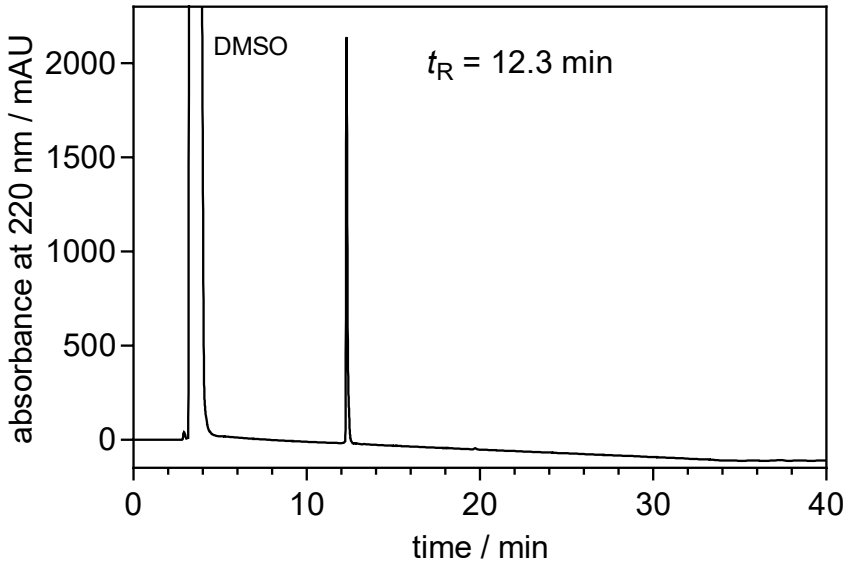

Chromatogram of the RP-HPLC analysis of **3.22**

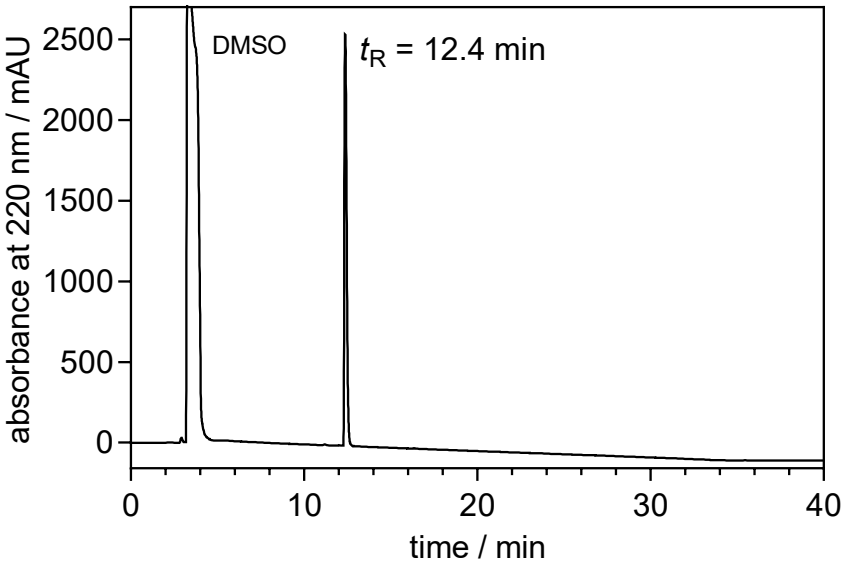

Chromatogram of the RP-HPLC analysis of **3.25**

A.3.4 RP-HPLC chromatogram (quality control) of radiolabeled compound [^{68}Ga]3.25

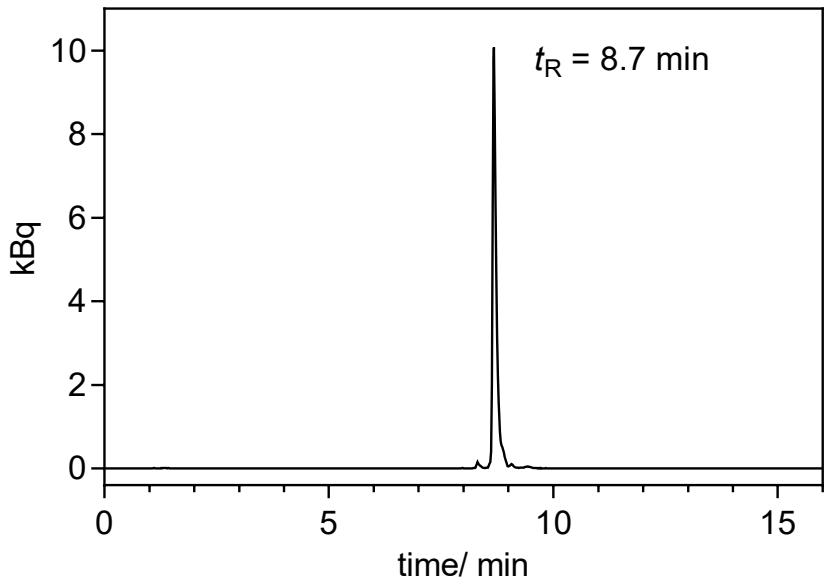

Radiochromatogram of the RP-HPLC analysis of [^{68}Ga]**3.25**

A.3.5 ^{1}H-NMR and ^{13}C-NMR spectra of compounds (*S*,*R*)-3.6, (*R*,*R*)-3.6 and 3.25

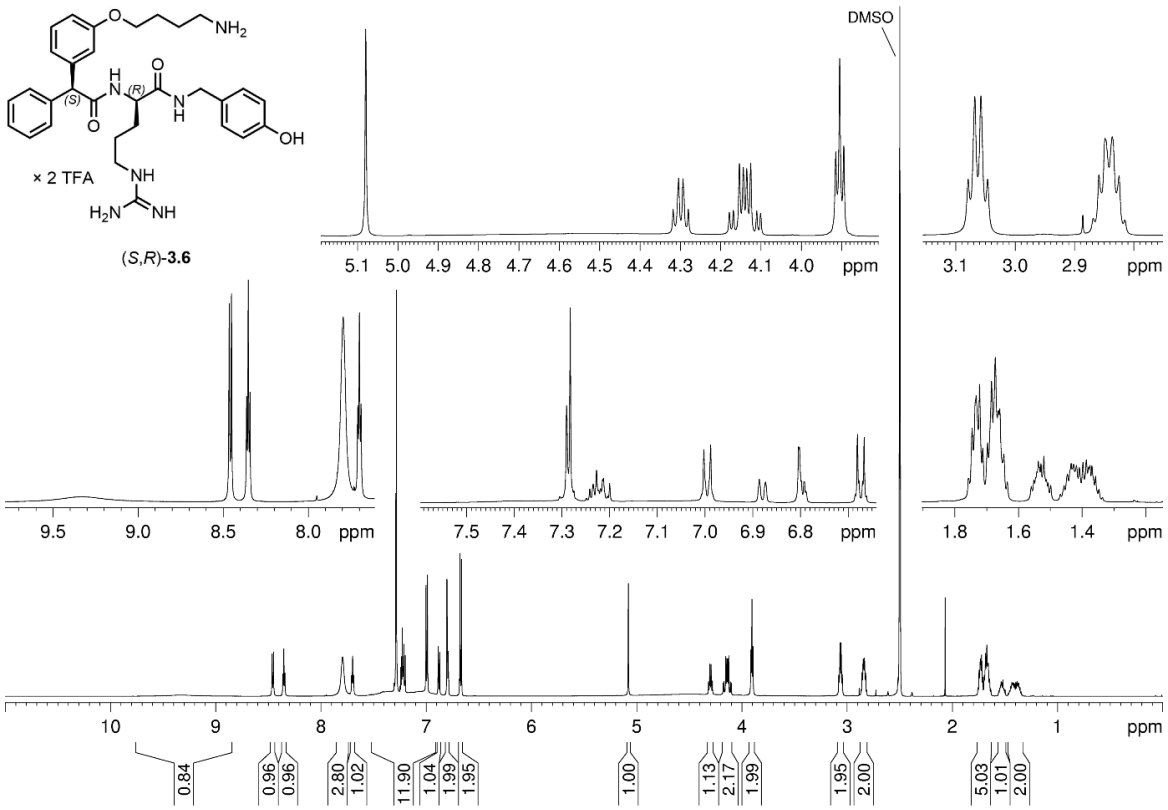

^{1}H-NMR spectrum (600 MHz, DMSO-d_6) of compound (*S*,*R*)-**3.6**

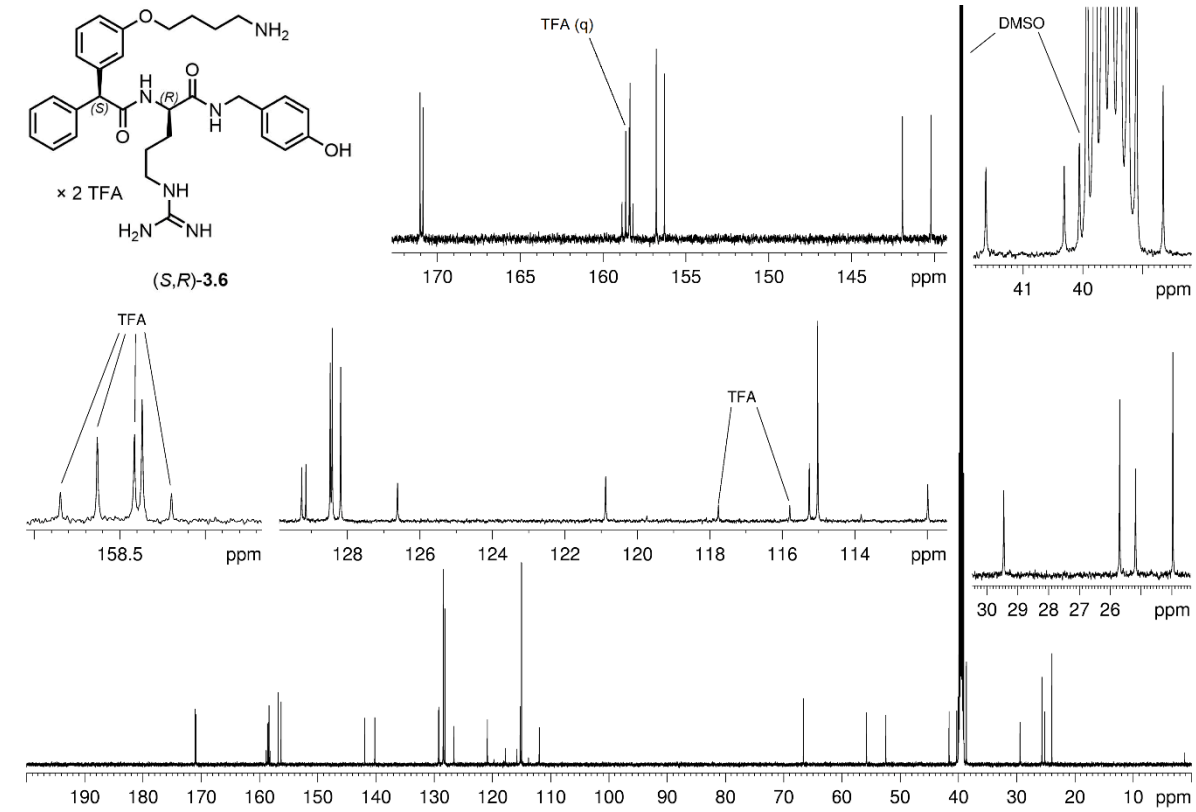

^{13}C-NMR spectrum (150 MHz, DMSO-d_6) of compound (*S*,*R*)-**3.6**

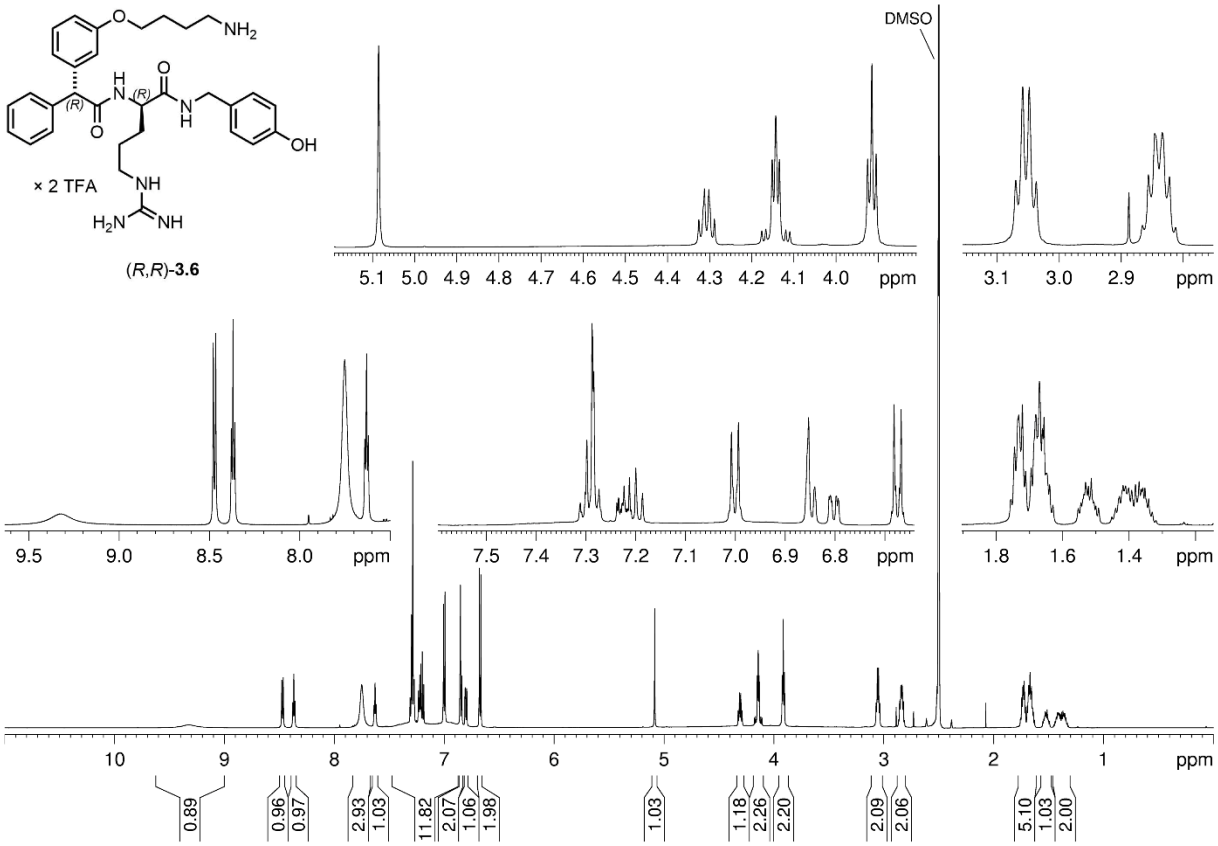

^{1}H-NMR spectrum (600 MHz, DMSO-d_6) of compound (*R*,*R*)-**3.6**

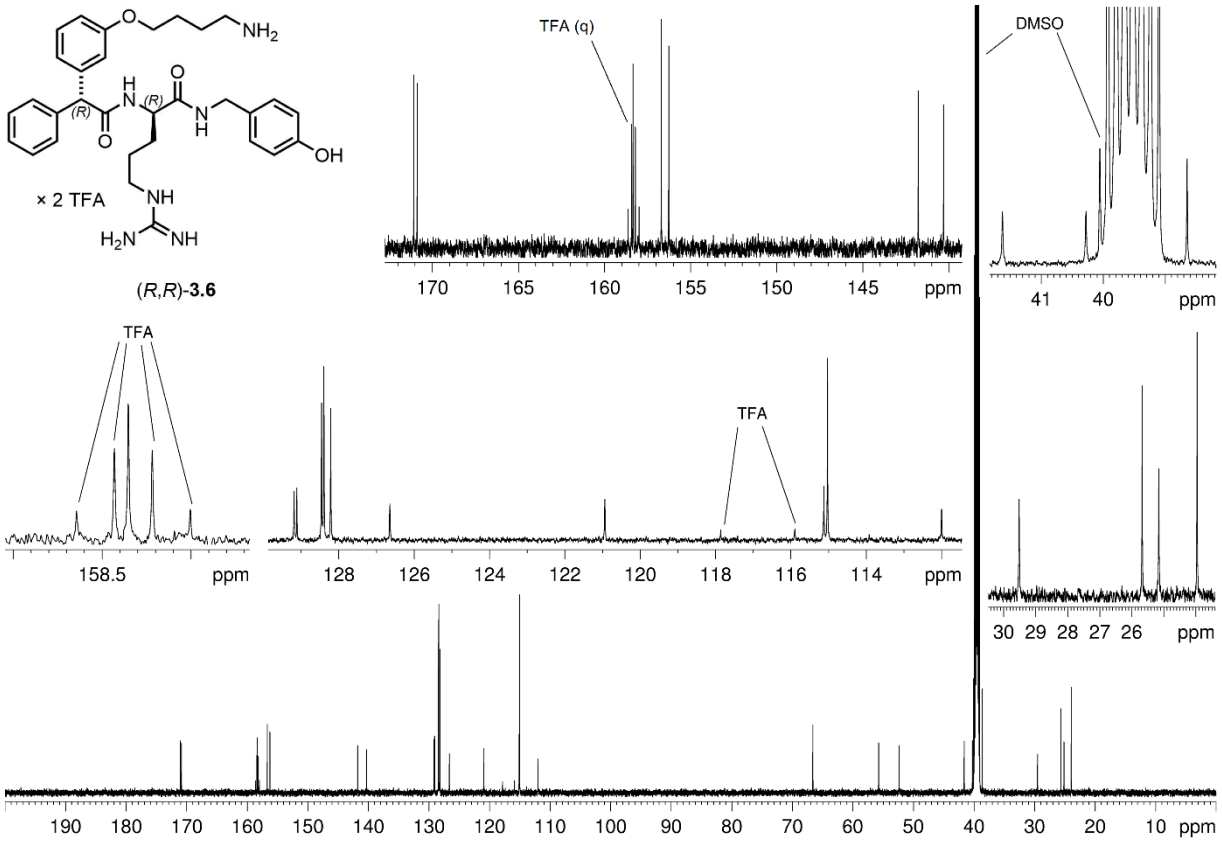

^{13}C-NMR spectrum (150 MHz, DMSO-d_6) of compound (*R*,*R*)-**3.6**

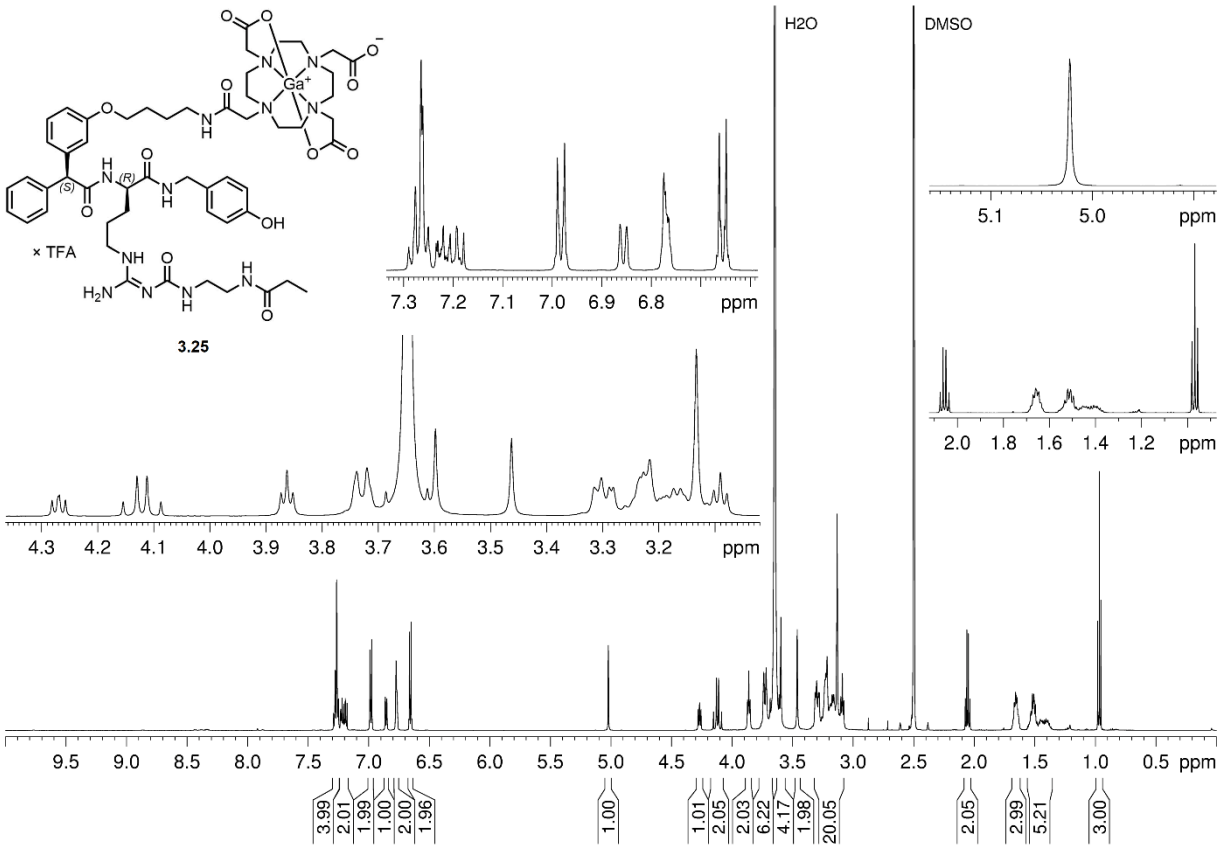

^{1}H-NMR spectrum (600 MHz, DMSO-d_6/D_2O 10:1) of compound **3.25**

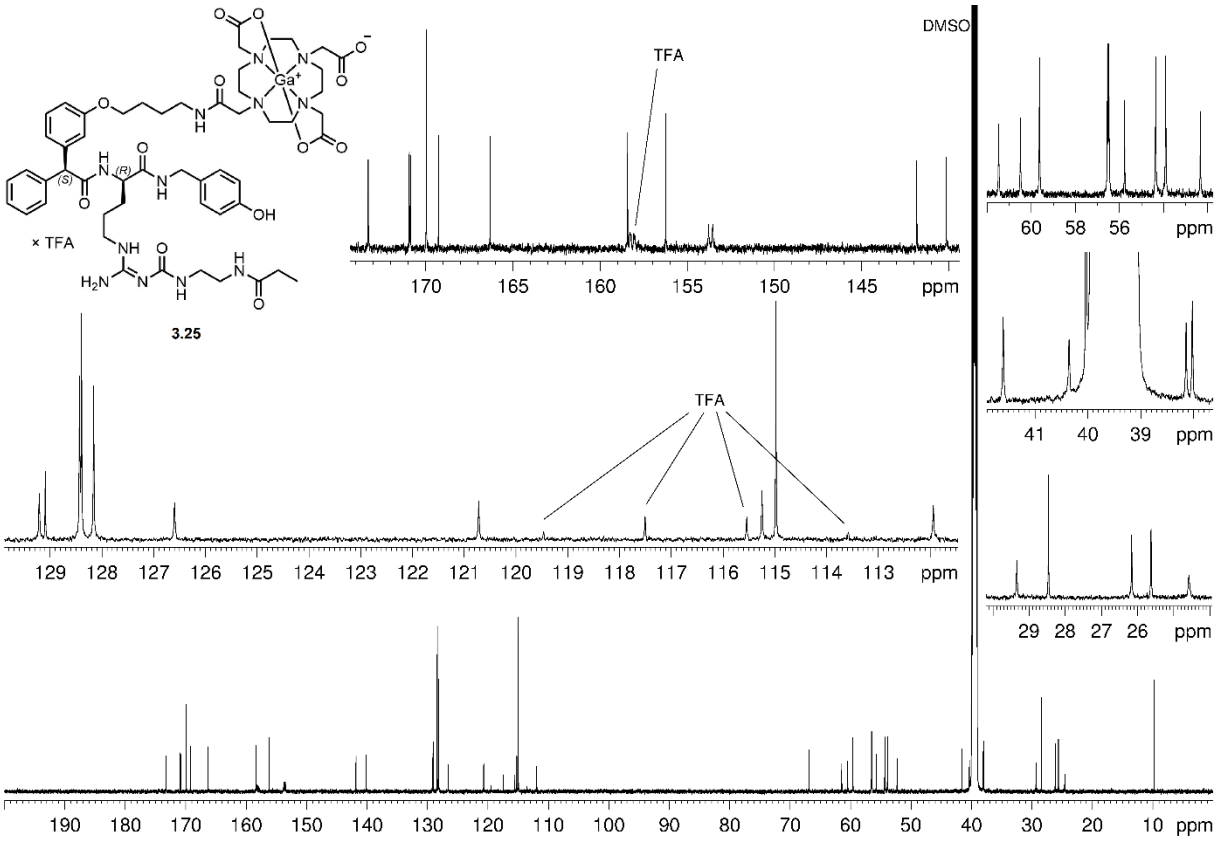

^{13}C-NMR spectrum (150 MHz, DMSO-d_6/D_2O 10:1) of compound **3.25**

A.3.6 ^{1}H-NMR spectra of compounds 3.11, 3.12, 3.16 and 3.22

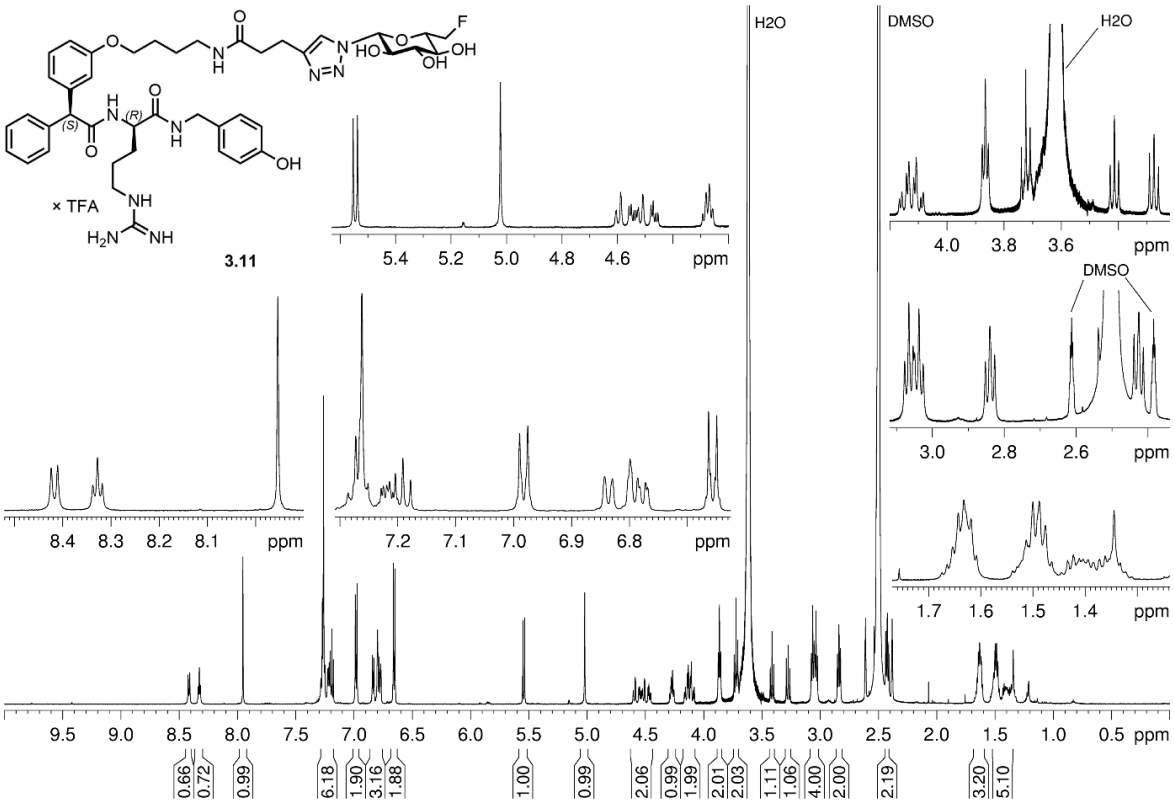

^{1}H-NMR spectrum (600 MHz, DMSO-d_6/D_2O 10:1) of compound **3.11**

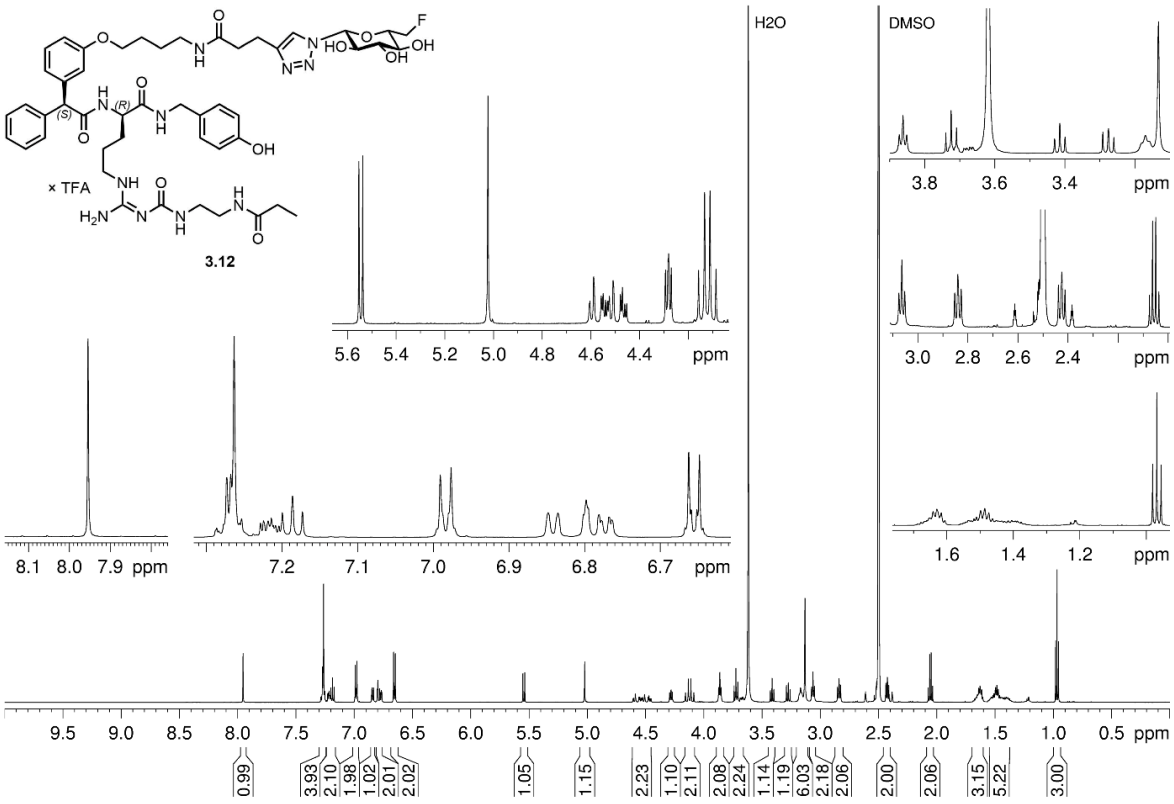

^{1}H-NMR spectrum (600 MHz, DMSO-d_6/D_2O 10:1) of compound **3.12**

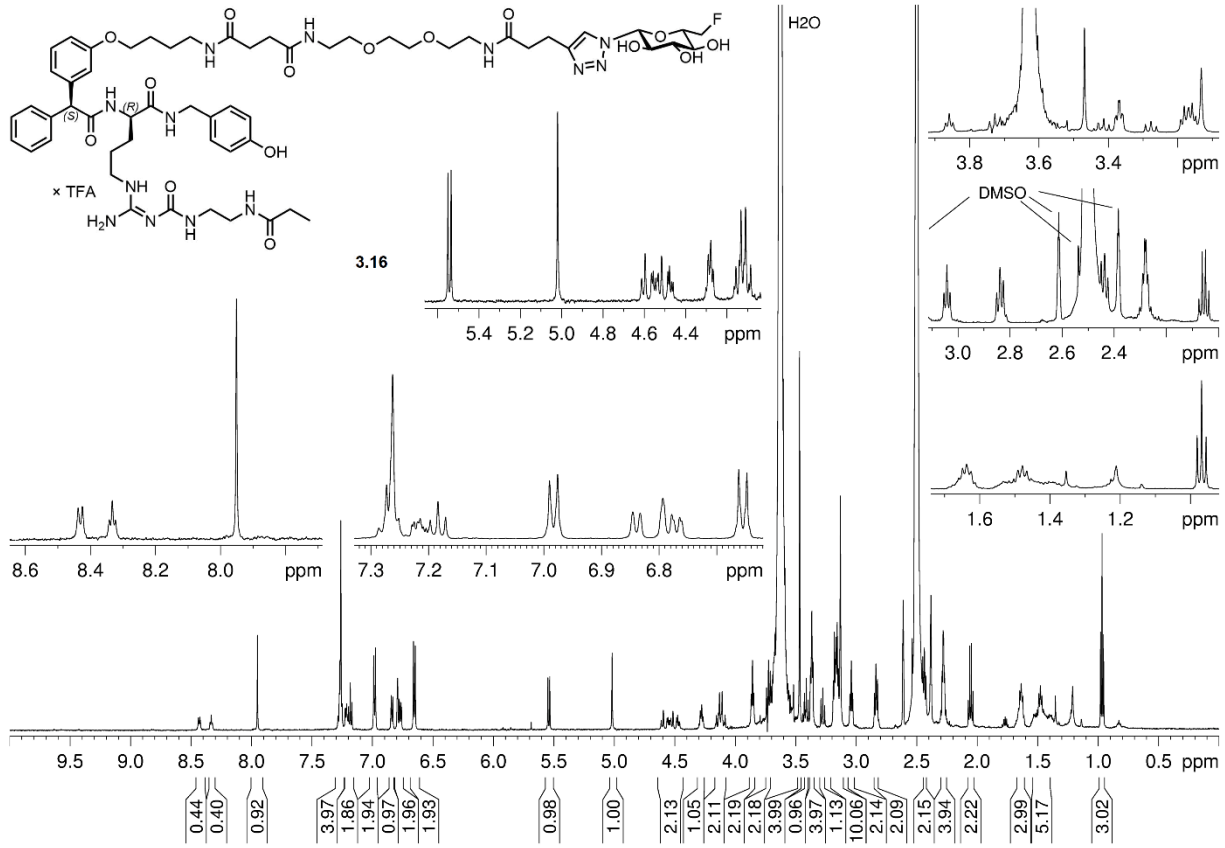

^{1}H-NMR spectrum (600 MHz, DMSO-d_6/D_2O 10:1) of compound **3.16**

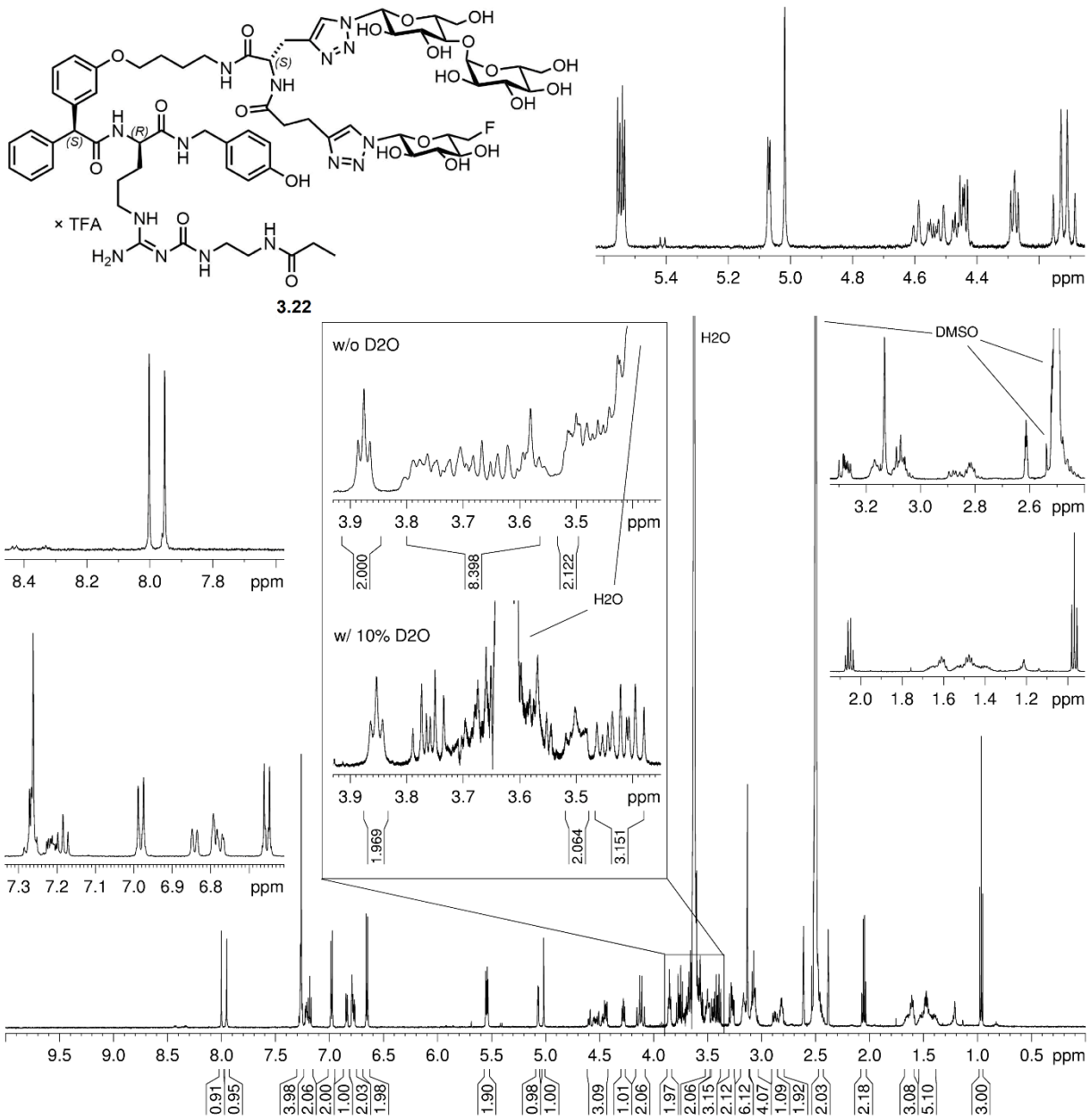

^{1}H-NMR spectrum (600 MHz, DMSO-d_6/D_2O 10:1) of compound **3.22**. In the top of the inset box, a section of an ^{1}H-NMR spectrum measured prior to the addition of D_2O (neat DMSO-d_6) is shown.

A.4 Chapter 4

A.4.1 RP-HPLC chromatograms (purity controls) of compounds 4.17-4.20

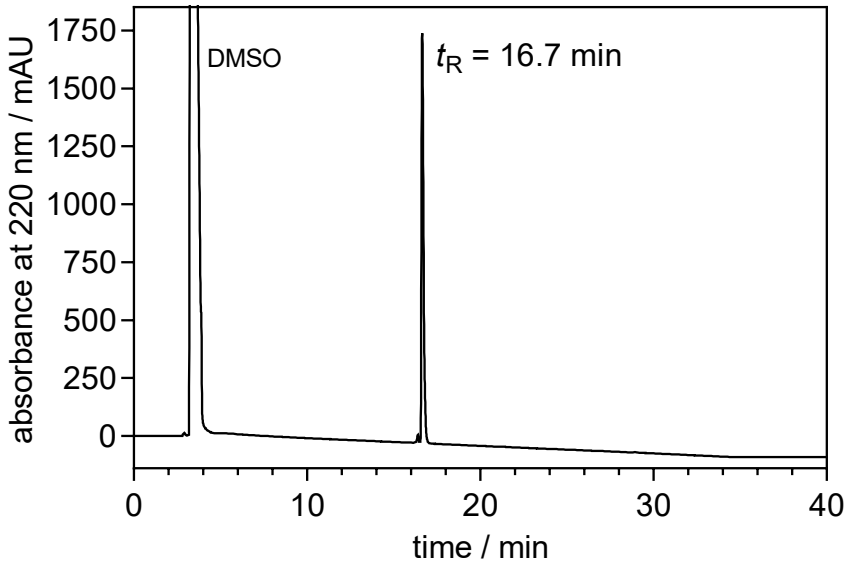

Chromatogram of the RP-HPLC analysis of **4.17**

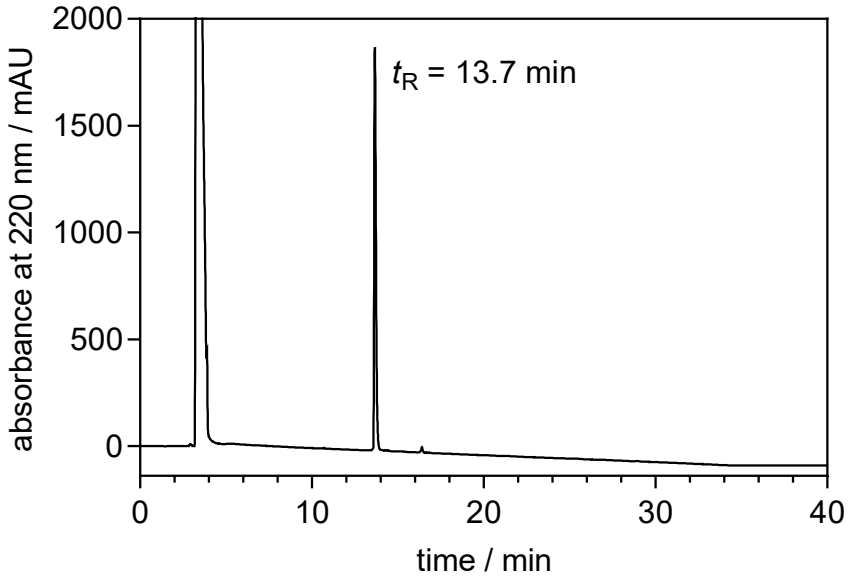

Chromatogram of the RP-HPLC analysis of **4.18**

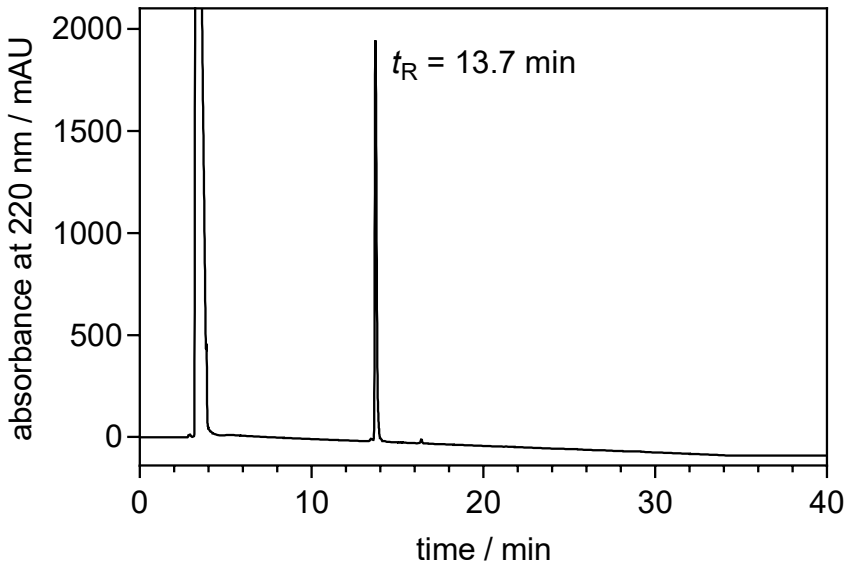

Chromatogram of the RP-HPLC analysis of **4.19**

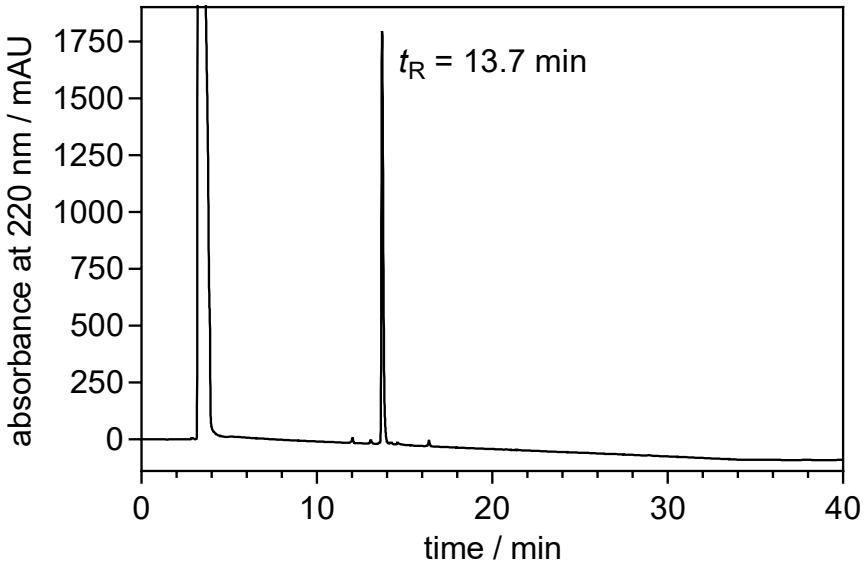

Chromatogram of the RP-HPLC analysis of **4.20**

A.4.2 ^{1}H-NMR spectra of compounds 4.17-4.20

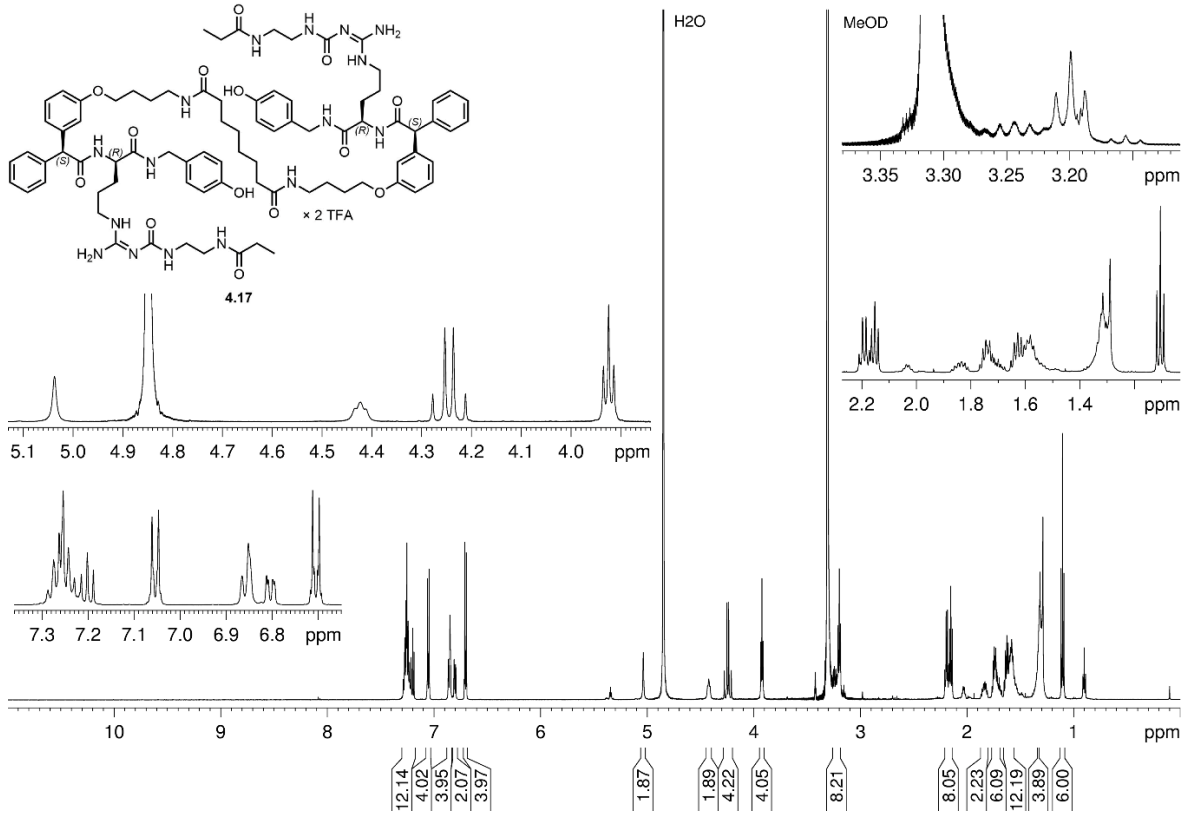

^{1}H-NMR spectrum (600 MHz, methanol-d_4) of compound **4.17**

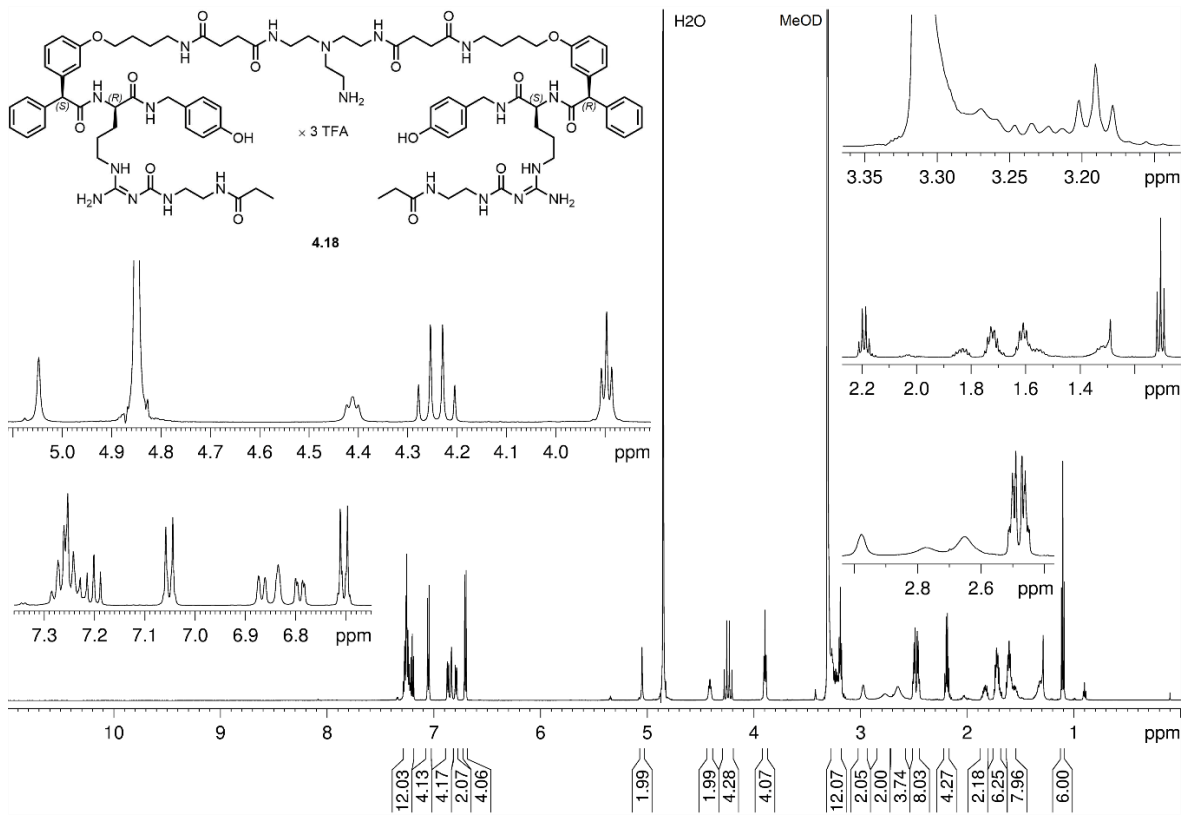

^{1}H-NMR spectrum (600 MHz, methanol-d_4) of compound **4.18**

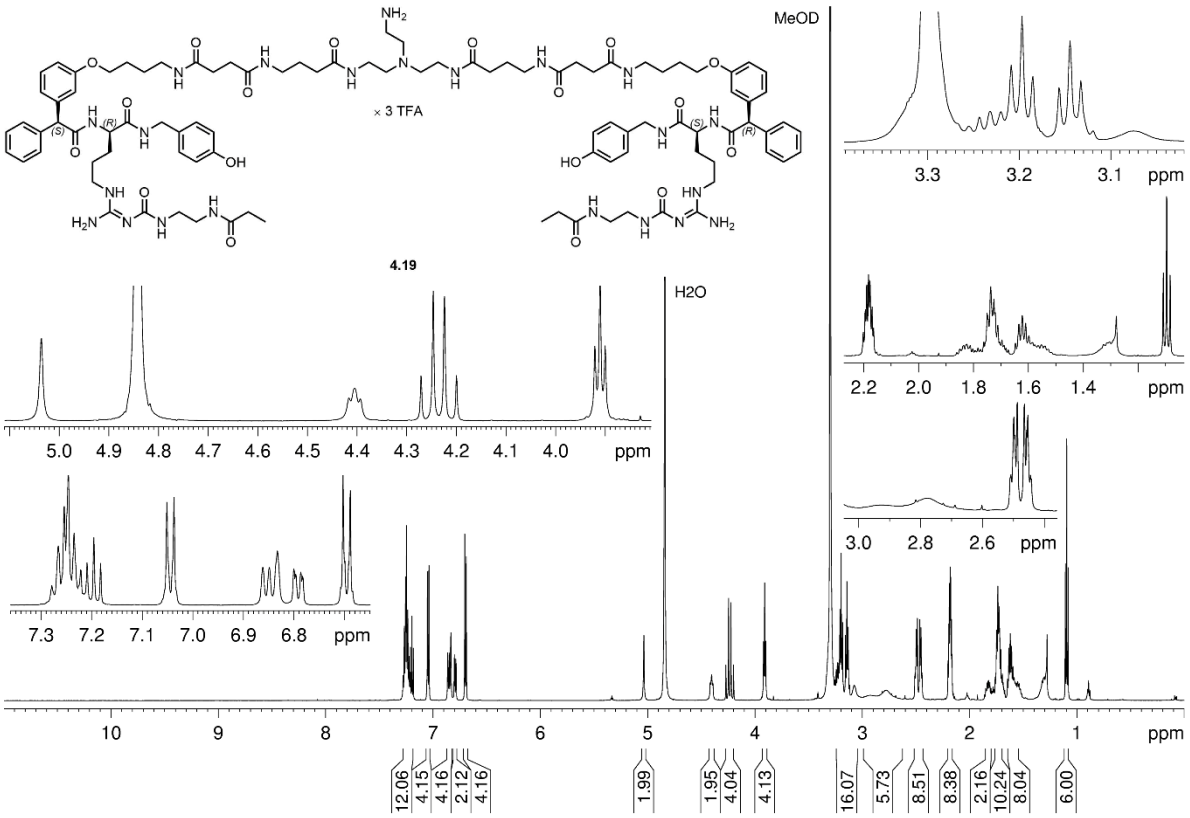

^{1}H-NMR spectrum (600 MHz, methanol-d_4) of compound **4.19**

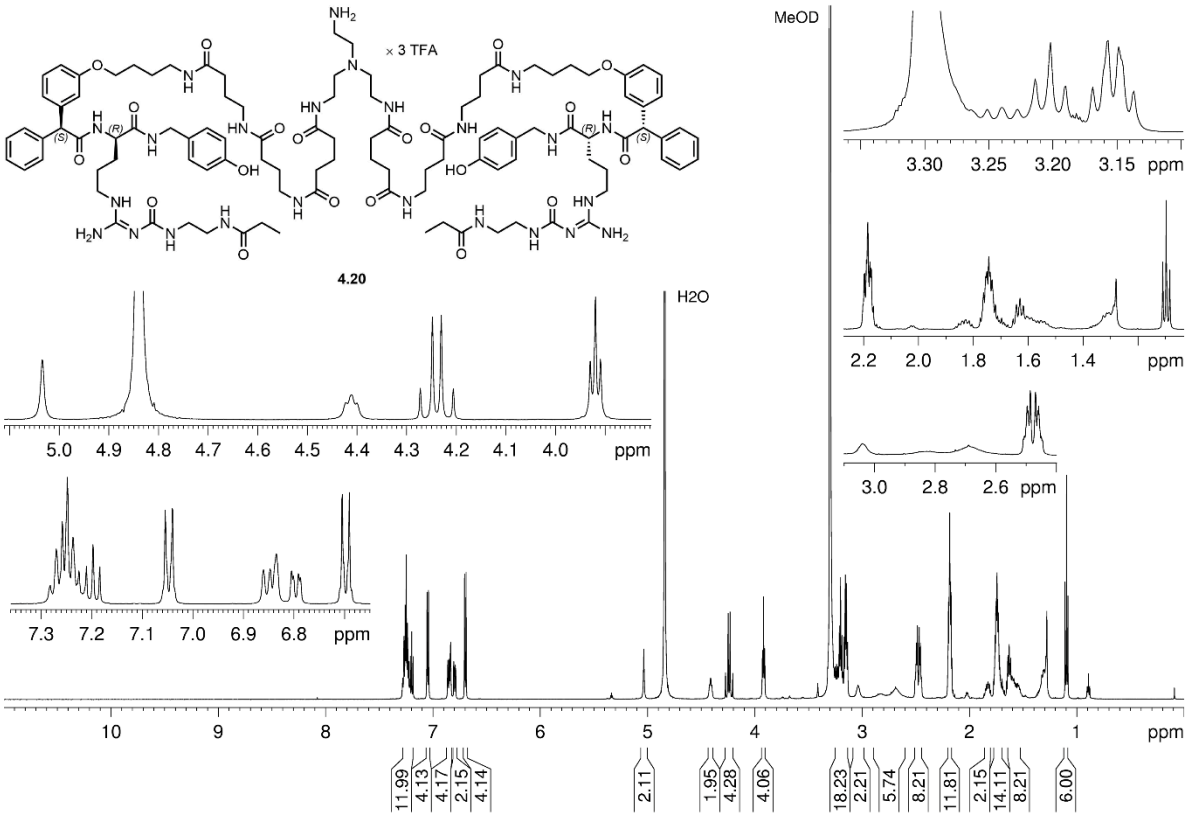

^{1}H-NMR spectrum (600 MHz, methanol-d_4) of compound **4.20**

A.5 Chapter 5

A.5.1 ^{1}H-NMR spectra of compounds 5.5 and 5.6

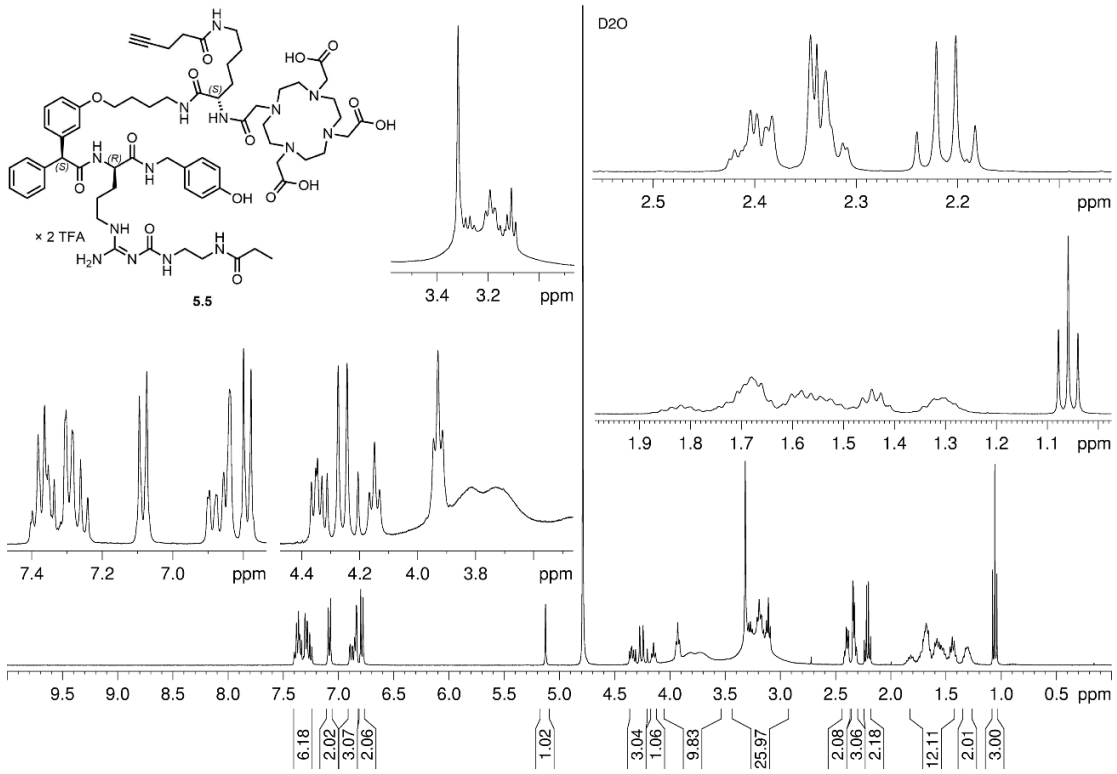

^{1}H-NMR spectrum (600 MHz, D_2O) of compound **5.5**

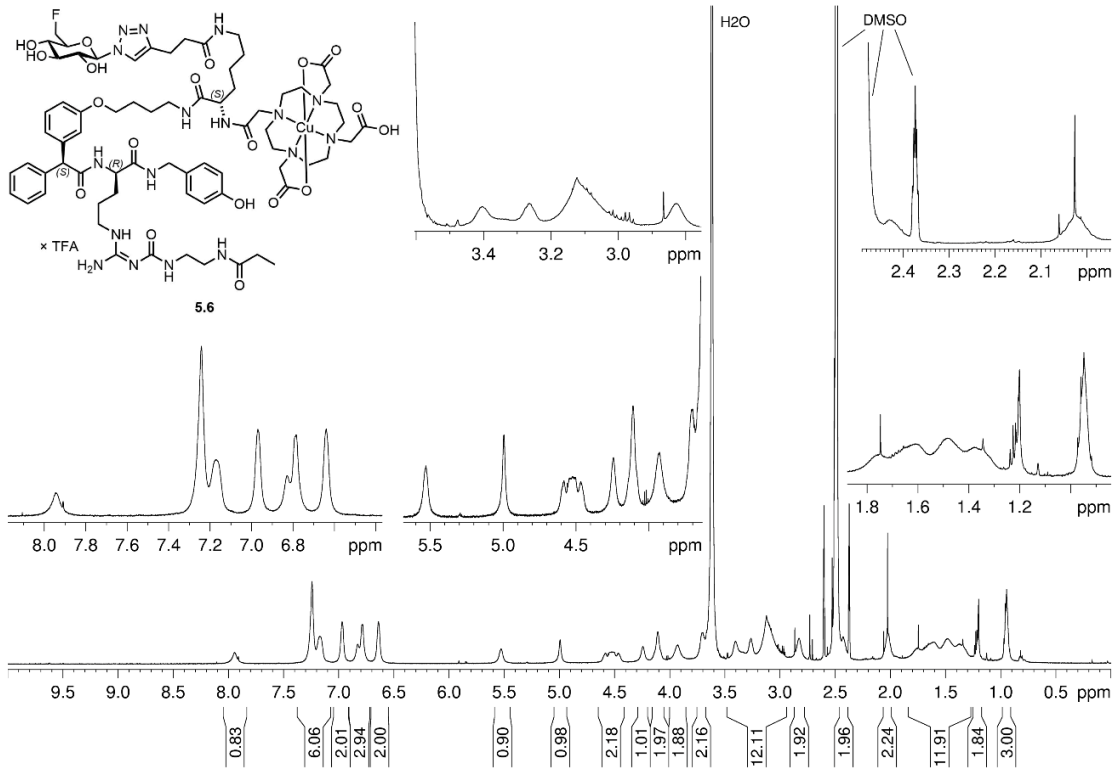

^{1}H-NMR spectrum (600 MHz, DMSO-d_6/D_2O 10:1) of compound **5.6**

A.6 Abbreviations

2-ClTrt	2-chlorotrityl
5-HT_{2A}R	serotonin 2A receptor
5`-TAMRA	5'-carboxy-tetramethylrhodamine
ATP	adenosine triphosphate
BBVs	budded baculovirus particles
Boc	*tert*-butyloxycarbonyl
BRET/FRET	bioluminescence-/fluorescence resonance energy transfer
cAMP	cyclic adenosine monophosphate
Cbz	benzyloxycarbonyl
CH_2Cl_2	dichloromethane
CH_3OTf	methyl trifluoromethanesulfonate (methyl triflate)
CHO cells	chinese hamster ovary cells
CNS	central nervous system
cpm	counts per minute
CuAAC	Cu(I)-catalyzed alkyne-azide cycloaddition
D_2R	dopamine D_2 receptor
DCC	*N*,*N*'-dicyclohexylcarbodiimide
DIPEA	*N*,*N*-diisopropylethylamine
DMAP	4-dimethylaminopyridine
DMF	*N*,*N*-dimethylformamide
DOTA	2,2′,2″,2‴-(1,4,7,10-tetraazacyclododecane-1,4,7,10-tetrayl)tetraacetic acid
DVB	divinylbenzene
EDC × HCl	1-(3-dimethylaminopropyl)-3-ethylcarbodiimide hydrochloride
EM	electron microscope
ER	endoplasmatic reticulum
Et_3N	triethylamine

FA	fluorescence anisotropy
FC	flow cytometry
Fmoc	fluorenylmethyloxycarbonyl
GABA	γ-aminobutyric acid
GPCR	G protein-coupled receptor
GRPR	gastrin-releasing peptide receptor
HBTU	*O*-(1*H*-benzotriazol-1-yl)-*N*,*N*,*N*′,*N*′-tetramethyluronium hexafluorophosphate
HEPES	4-(2-hydroxyethyl)-1-piperazineethanesulfonic acid
HOBt	1-hydroxybenzotriazole hydrate
hPP	human pancreatic polypeptide
(HR)MS	(high-resolution) mass spectrometry
hY_1R	human Y_1 receptor
%ID/g	injected dose per gram of tissue in percent
k	retention (or capacity) factor (HPLC)
K_d	dissociation constant obtained from a saturation binding experiment
K_i	dissociation constant obtained from a competition binding experiment
$logD_{7.4}$	n-octanol/PBS distribution coefficient at pH = 7.4
MCF-7	Michigan cell foundation-7
MOR	μ-opioid receptor
NHS	*N*-hydroxysuccinimide
NMR	nuclear magnetic resonance (spectroscopy)
(p)NPY	(porcine) NPY
PDB	protein data bank
pEC_{50}	negative logarithm of the half maximal effective concentration (in M)
PET	positron emission tomography

P-gp	P-glycoprotein
p.i.	post injection
pK_d	negative logarithm of the K_d (in M)
pK_i	negative decadic logarithm of the dissociation constant K_i (in M) obtained from a competition binding experiment
PNS	peripheral nervous system
(h)PP	(human) pancreatic polypeptide
PPh_3	triphenylphosphine
PSMA	prostate-specific membrane antigen
PTSD	post-traumatic stress disorder
RP	reversed phase
rt	room temperature
SD	standard deviation
SEM	standard error of the mean
SPECT	single-photon emission computed tomography
$SSTR_2$	somatostatin receptor 2
SVD	single value decomposition
TFA	trifluoroacetic acid
THF	tetrahydrofuran
THPTA	tris(3-hydroxypropyltriazolylmethyl)amine
TIRF microscopy	total internal reflection fluorescence microscopy
t_R	retention time
Y_xR	neuropeptide receptor subtype x (x = 1, 2, 4 or 5)

A.7 Overview of bold compound numerals and lab codes

compound	lab code	compound	lab code	compound	lab code
2.6	MC-128 MC-196 MC-231	**2.37**	CM-139	**3.17**	MC-246
2.7	MC-130	**2.38**	MC-150	**3.19**	MC-260
2.8	MC-029 MC-204	**2.39**	MC-159	**3.20**	MC-275
2.9	MC-135	**2.40**	MC-026	**3.21**	MC-278
2.10	MC-138 MC-214 MC-234	**2.41**	MC-211	**3.22**	MC-280
2.11	MC-200	**2.42**	MC-101	**3.24**	DB81 MC-235
2.12	MC-153 MC-240	**2.43**	MC-001	**3.25**	DB91
(*S*,*R*)-**2.13***l*(*S*,*R*)-**2.13** (1:1)	MC-207	**2.44**	CM-128 MC-019	**4.5**	MC-250
(*S*,*R*)-**2.13**	MC-137	**2.45**	MC-002 MC-276	**4.6**	MC-258
(*S*,*R*)-**2.14** (50% *de*)	MC-144	**2.46**	CM-129 MC-021 MC-037	**4.7**	MC-252
(*S*,*R*)-**2.14**	CM-123b (MC-215, MC-229)	**2.47**	CM-130	**4.8**	MC-255
(*R*,*R*)-**2.14**	CM-123a (MC-215, MC-229)	**2.48**	CM-131 MC-022 MC-038	**4.9**	MC-259
2.15	MC-004 MC-017 MC-032 MC-181 MC-277	**2.49**	MC-053 MC-179 MC-233	**4.10**	mk154
(*rac*)-**2.16**	MC-034	**2.50**	CM-132	**4.11**	MC-261
(*R*)-**2.16**	JG-008	**2.51**	MC-141 MC-239	**4.12**	MC-262
(*rac*)-**2.17**	CM-104 RUE-009 MC-044 MC-183	**2.52**	CM-133	**4.13**	MC-265
(*R*)-**2.17**	JG-009	**2.53**	RUE-004 MC-100 MC-211	**4.14**	MC-266
2.18	MC-155	**2.54**	RUE-005 MC-222	**4.15**	MC-244
(*S*,*R*)-**2.19**	MC-125a	**2.55**	CM-078	**4.16**	mk159
(*R*,*R*)-**2.19**	MC-125b	**2.56**	CM-096 MC-015	**4.17**	MC-247
(*R*,*R*)-**2.19** (56% *de*)	MC-284	**2.57**	MC-285	**4.18**	MC-251
2.20	MC-122	**2.58**	MC-286	**4.19**	MC-269
2.22	MC-051 MC-212	(*S*,*R*)-**3.6**	CM-122a	**4.20**	MC-270
(*S*,*R*)-**2.23**	MC-131	(*R*,*R*)-**3.6**	CM-122b	**5.3**	MC-287
2.24	MC-134 MC-158 MC-238	**3.7**	MC-162	**5.4**	MC-289
2.26	CM-021	**3.8**	MC-164	**5.5**	MC-290
2.27	CM-101	**3.9**	MC-165	**5.6**	MC-291
2.28	CM-097 MC-016	**3.11**	MC-167		
2.29	CM-134	**3.12**	MC-168		
(*S*,*R*)-**2.30**	CM-136a	**3.13**	MC-245		
(*S*,*R*)-**2.30**	CM-136b	**3.14**	MC-248		
2.35	CM-138	**3.15**	MC-263		
2.36	CM-137	**3.16**	MC-271		

Eidesstattliche Erklärung

Ich erkläre hiermit an Eides statt, dass ich die vorliegende Arbeit ohne unzulässige Hilfe Dritter und ohne Benutzung anderer als der angegebenen Hilfsmittel angefertigt habe. Die aus anderen Quellen direkt oder indirekt übernommenen Daten und Konzepte sind unter Angabe des Literaturzitats gekennzeichnet.

Einige der experimentellen Arbeiten wurden in Zusammenarbeit mit Personen von anderen wissenschaftlichen Instituten durchgeführt. Entsprechende Vermerke befinden sich zu Beginn der Kapitel 2 und 3.

Weitere Personen waren an der inhaltlich-materiellen Herstellung der vorliegenden Arbeit nicht beteiligt. Insbesondere habe ich hierfür nicht die entgeltliche Hilfe eines Promotionsberaters oder anderer Personen in Anspruch genommen. Niemand hat von mir weder unmittelbar noch mittelbar geldwerte Leistungen für Arbeiten erhalten, die im Zusammenhang mit dem Inhalt der vorgelegten Dissertation stehen.

Die Arbeit wurde bisher weder im In- noch im Ausland in gleicher oder ähnlicher Form einer anderen Prüfungsbehörde vorgelegt.

Regensburg, den 10.11.2022 _____

Christoph Müller